ANTARCTIC AND SOUTHERN OCEAN DUST TRANSPORT PATHWAYS: FORWARD-TRAJECTORY MODELING AND RARE EARTH ELEMENT SOURCE CONSTRAINTS FROM THE RICE ICE CORE

BY

PETER D. NEFF

A thesis submitted to the Victoria University of Wellington

in fulfillment of the requirements for the degree of

Doctor of Philosophy

in Geology

Victoria University of Wellington

(2015)

Abstract

Mineral dust fertilization of Southern Ocean surface waters, and mixing with Antarctic deep-water, influences oceanic uptake of carbon dioxide and draws down global atmospheric concentrations during glacial periods. Quantifying modern variability in dust source and transport strength, especially with respect to high- and low-latitude climate phenomena (e.g. the Southern Annular Mode, El Niño Southern Oscillation), will improve understanding of this important aspect of the global carbon cycle. Using high-order geochemical provenance techniques can also reveal in greater detail what aspects of dust transport are recorded in Antarctic ice core records, allowing for better interpretation of glacial-interglacial dust records at individual sites.

First, using forward trajectories and climate reanalysis data, this work explores modern variability (1979-2013) in atmospheric transport of mineral dust from Southern Hemisphere potential source areas (PSA)—primarily Australia, southern South America and southern Africa. Estimates of the relative source and transport strength of New Zealand are also discussed, and compared with other dust PSA to evaluate New Zealand's potential contribution to Southern Ocean and Antarctic dust deposition. Extra-Antarctic dust PSA distributions are detailed for individual ice core sites, including the newly recovered Roosevelt Island Climate Evolution (RICE) ice core (79.36ºS, 161.71ºW, 550 m a.s.l.). This approach—applicable to many types of aerosol—reveals persistent, strong transport from New Zealand and Patagonia to the southern high-latitudes during all seasons. It also demonstrates that southward transport of air masses from pan-Pacific dust sources is affected by circulation variability initiated in the central tropical Pacific Ocean.

High-resolution discrete sampling of the RICE core allows for unprecedented analysis of trace elements at sub-annual to annual scales. The rare earth elements (REE, lanthanide elements Lanthanum to Lutetium) can preserve the signature of their original source material and thus provide provenance constraints for dust preserved in Antarctic snow and ice. While challenging, measurements of REE concentration to the single femtogram per gram (10^{-15} g g^{-1}) level have been made by combining efficient sample introduction and a jet-interface sector-field inductively coupled plasma mass spectrometer. The methodology and fidelity of these measurements are presented, in addition to results for other low-concentration elements associated with natural and anthropogenic aerosols.

REE data from the RICE ice core are then used to explore possible modern sources of dust in the Ross Sea sector of Antarctica, testing hypothesized trajectory model distributions. Twentieth-century and late-Holocene (2.3 ka – present) REE data from the RICE ice core represent the first measurements of this kind from the Pacific sector of Antarctica. RICE data are compared with Holocene REE data from the Drønning Maud Land and Dome C ice cores, with consideration of REE signatures in dust samples from PSA. Data from the RICE ice core indicate fewer than 5% contributions of dust from South America, and show strong negative trends in crustal-normalized REE signatures suggesting contributions from local Antarctic dust.

Acknowledgements

Thank you very much to my supervisor, Nancy Bertler, who has provided endless support for all of us working on the RICE ice core project. Ross Edwards, your help and advice on trace-element laboratory work is second to none—you truly rescued this project and pushed us to raise the bar.

To Andrea Tuohy, my Ph.D. "twin," I feel lucky to have worked with you so closely for the past three years. How is it that we never had a disagreement? I wish you all the best and hope to share a trail somewhere soon with you and Ollie.

Alex Pyne and Darcy Mandeno have been very kind to include me as (what I consider) an honorary member of the Science Drilling Office. I have learned much from both of you. Darcy, our many therapy sessions on bikes, over beers and at Makara Beach have been indispensible and unforgettable. Huw Horgan, Ruzica Dadic and little Ivan have also been great supporters, neighbors and friends. The Antarctic Research Centre community is a true gem; thanks heaps to everyone.

I must thank my M.Sc. supervisor and friend Eric Steig for his enthusiasm, for continually including me in exciting ice core projects and engaging me as a colleague since I was a wee undergraduate. To all the University of Washington glaciologists, know that the foundation of knowledge that I gained (and continue to gain) through you has provided me with the confidence to tackle all things icy. Twit Conway especially has kept an eye on me since Glaciology 101 many years ago, and for that I am very grateful.

Of course, above all I wish to thank my constant partner (and sometimes office mate) in this adventure and this life, my fiancée, Heidi for her endless care and love. In a close second comes our shadow, Kuna, who has endured many days of insufficient ball-throwing during both of our Ph.D.'s. We have had amazing support and many great video calls with Connie and Peter (Blue) Roop. I can't wait to spend more time around the campfire with you two. My parents and family have of course always provided support and encouragement without question. Have fun reading this thesis, Mom.

Table of Contents

Foreword

One of the primary reasons that ice core projects produce such transformative scientific results, and why I find contributing to such projects so personally rewarding, is because they are highly interdisciplinary and require collaborative work at all stages. An ice core scientist must simultaneously be proficient at individual and team work, must be able to quickly understand information from diverse research fields, and be equally willing to shovel snow, write papers or design aircraft loads around getting many pounds of heavy cream to a remote drill site. My trace element work on the RICE ice core was particularly collaborative, requiring task sharing with fellow PhD candidate A. Tuohy at every step from sample preparation through to data interpretation. For these reasons, below are detailed my contributions to the RICE project over the last three years.

Field work

I participated in the 2012-2013 RICE field season as an assistant driller, helping to complete deep drilling from 130 m to 764 m. I undertook little additional science work because of drilling duties, but collected the 19.5 m “12/13 B” firn core with D. Mandeno and H. Berge, which was used in annual layer counting to connect the January 2013 snow surface with the top of the deep core (which begins at 8 m depth below the 2011-2012 snow surface due to trenching required for drill infrastructure).

Ice core processing

I assisted in ice core continuous flow analysis (CFA) campaigns during the austral winters of 2012, 2013 and 2014 (1-2 months each). During the latter two campaigns I led freezer sampling of the RICE ice core (40 m – 764 m), cutting samples for CFA and other analyses with the help of 2-3 assistants. I also made electrical conductivity measurements along the length of the core and recorded core quality. Electrical measurements were used to identify volcanic events, alerting CFA operators to remove these sections of ice from analysis (both for additional sampling and to protect CFA equipment from high particle concentrations in these layers).

Sample preparation

A. Tuohy and I shared many tasks in preparing trace element samples, including design and execution of an 8-week acid leaching experiment, transferring frozen samples between the freezer storage facility and the university, cleaning thousands of sample vials, and finally combining ~10,000 RICE samples into 621 approximately 3-year average samples. These 621 samples, an additional 784 from the top 40 m of the RICE ice core, and ~200 surface snow and snowpit samples were then acidified prior to analysis (and this over a very short period of time, splitting a 24-hour work schedule with A. Tuohy).

ICPMS analysis

Preliminary ICPMS work at Victoria University of Wellington involved setting up a new Element 2. Within a short span of time, we coordinated an in-lab course with a Thermo Scientific technician, purchased an autosampler, and following this I left for the RICE deep drilling season. A. Tuohy continued to work on instrumental development during this time. On my return we shared analytical duties, eventually measuring all samples at the Curtin University TRACE lab working around the clock for a three-week period.

Data calibration

Custom calibration of ICPMS trace element data was designed with A. Tuohy and R. Edwards. A. Tuohy completed the coding and quality assurance required for this step (while I was completing the 2014 RICE core processing line). Later iterations between A. Tuohy and myself resulted in the final version of these data to be published, with myself leading paper writing (Chapter 3).

Agescale development

Together with A. Tuohy and D. Emanuelsson I determined preliminary annual layer counts based on water stable isotopes and sulfur/sulfate in the 12/13B RICE firn core and the top 40 m of the deep RICE ice core (representing the 20th Century). These counts have since been refined by the RICE community and through further work by D. Emanuelsson.

Chapter 1: Introduction

1.1 The Roosevelt Island Climate Evolution (RICE) project

The RICE project is a recently completed Antarctic ice core drilling effort, which in December 2012 collected a 764 m long ice core from the summit of Roosevelt Island, a grounded ice dome at the northeastern margin of the Ross Ice Shelf (Figure 1). Roosevelt Island has been the site of glaciological research for more than 50 years, and is an ideal site for an ice core both due to its location within the Ross Ice Shelf and because of its stable ice flow geometry. Located near the Bay of Whales and Little America bases used by early Antarctic explorers, Roosevelt Island was the site of early glaciological investigations conducted during the International Geophysical Year [*Crary*, 1961; *Crary et al.*, 1962]. More recent work details ice flow geometry and heat flux at the site [*Thomas et al.*, 1980], with ice-penetrating radar data demonstrating long-term ice flow divide stability at the site and constraining the timing of Holocene retreat of the West Antarctic Ice Sheet (WAIS) [*Conway et al.*, 1999; *Martín et al.*, 2006]. Ice drilling at such a divide is ideal, as these flow conditions up-warp isochrones directly below, forming a "Raymond bump" which allows an ice core to capture older layers at shallower depths than would be possible at another site [*Nereson and Waddington*, 2002; *Raymond*, 1983].

Roosevelt Island is subject to the synoptic weather systems which characterize the Amundsen Sea Low (ASL), a center of low pressure affecting the Ross, Amundsen and Bellingshausen seas which efficiently advects marine air onto the WAIS—bringing with it moisture (e.g. latent heat) and aerosols [*Cohen et al.*, 2013; *Hosking et al.*, 2013; *Turner et al.*, 2013]. This strong southward moisture transport is seen in the mean (1979 – 2012) vertically-integrated moisture flux output of the European Centre for Medium-Range Weather Forecasts (ECMWF) ERA-Interim climate reanalysis dataset (Figure 1). This arrangement is in part caused by the relatively shallow slope of the WAIS and the axial asymmetry of the Antarctic continent, geographically offset from the South Pole by ~10º [*Lachlan‐Cope et al.*, 2001; *Nicolas and Bromwich*, 2011]. It is additionally significant that the Pacific Ocean basin lies to the north of this region, facilitating a unique teleconnection to the lower-latitudes which may be responsible for recent warming observed across the WAIS [*Bromwich et al.*, 2013; *Ding et al.*, 2011; *Nicolas and Bromwich*, 2014; *Steig et al.*, 2009; *Turner*, 2004].

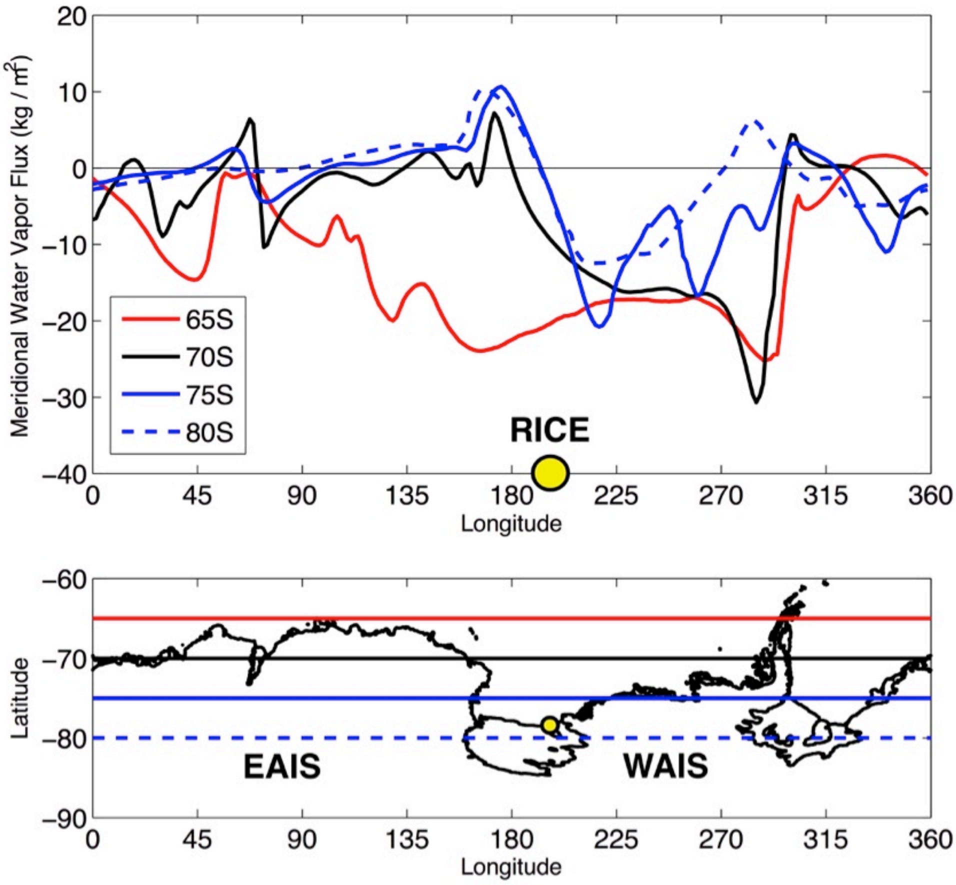

Figure 1. *ERA-Interim reanalysis 1979-2012 mean vertically-integrated meridional (northward positive, southward negative) water vapor flux (kg/m^2) at southern high-latitudes. Latitudes plotted in top panel are marked in bottom panel. Strongest southward (negative) flux south of 65^o latitude is seen in the vicinity of the WAIS.*

The RICE ice core thus lies at the intersection of two critical aspects of Antarctic glaciology and climate. Aspects of the ice core record may provide additional insight into rates of change characteristic of the Ross Ice Shelf, a major stabilizing feature of the marine WAIS, grounded below sea-level and possibly prone to collapse, as hypothesized by *Mercer* [1978]. Such collapse may already be underway in the Thwaites and Pine Island Glacier basins (~75ºS, 260ºE), where rapid glacier thinning and retreat has been observed in recent decades [*Joughin et al.*, 2014; *Pritchard et al.*, 2012; *Rignot et al.*, 2014]. The RICE ice core record is also well-positioned to contribute better understanding of tropical teleconnections affecting Antarctic climate variability, which are seen in comparisons of West Antarctic ice core records and meteorological data [*Kreutz et al.*, 2000; *Küttel et al.*, 2012; *Okumura et al.*, 2012; *Schneider et al.*, 2006], and are also implicated in recent glaciological change (e.g. *Dutrieux et al.* [2014]; *Steig et al.* [2012]).

1.2 Dust provenance in Antarctic ice cores

These same atmospheric transport mechanisms controlling advection of heat into West Antarctica are also of interest for their role in bringing terrestrial mineral particles (dust) from mid-latitude continents to the Southern Ocean and Antarctica. Antarctic ice core records show twenty- to thirty-fold increases in dust concentrations during cold glacial periods, suggesting large fluctuations in dust production, atmospheric loading and deposition [*Lambert et al.*, 2008; *Thompson and Mosley-Thompson*, 1981; *Wolff et al.*, 2010]. Dust exerts significant control on atmospheric radiative balance, as suspended insoluble particles both absorb and reflect incoming radiation, and fertilizing effects of dust deposited over remote ocean areas affects carbon uptake and atmospheric greenhouse gas concentrations (e.g. *Maher et al.* [2010] and references therein). This latter effect is of particular importance over areas of the Southern Ocean where downwelling Antarctic Bottom Water originates, facilitating atmosphere-ocean carbon exchange [*Orsi et al.*, 1999]. Antarctic ice core records of dust transported from Southern Hemisphere mid-latitude sources may therefore provide some constraint as to the timing and magnitude of this important aspect of the global carbon cycle. However, fluctuating dust concentrations preserved in Antarctic ice are possibly the result of environmental change at individual dust source regions or represent background dust loading of the atmosphere from multiple sources. Dust deposition is additionally affected by changing precipitation and wind patterns altering particle atmospheric lifetime [*Albani et al.*, 2012; *Mahowald et al.*, 1999].

Geochemical dust provenance efforts can elucidate additional details of these processes, reducing possible causes of fluctuating dust concentrations. Isotopic studies of Sr and Nd, as well as Pb suggest a coherent South American dust source during dusty glacial periods but analyses are challenged by low dust concentrations during interglacials [*Delmonte et al.*, 2008; *Delmonte et al.*, 2004; *Vallelonga et al.*, 2010]. Local Antarctic dust and volcanic input overprint extra-Antarctic source signals during interglacial periods of low dust input, but there is indication of greater input from additional Southern Hemisphere sources at these times (e.g. Australia, southern Africa, New Zealand [*Delmonte et al.*, 2010; *Revel-Rolland et al.*, 2006]). Advancements in the analysis of trace elemental species have spurred the development of new geochemical provenance tools, as sensitive measurements at sub picogram per gram (pg g^{-1}, part per trillion) concentrations can now be made simultaneously for many elements [*Barbante et al.*, 1997].

This thesis is designed to explore one such measure of Antarctic dust provenance, the Rare Earth Elements (REE). These fourteen elements (Lanthanum to Lutetium, atomic numbers 57-71) are abundant in crustal materials and inert through sedimentary processes, retaining the original REE abundance of parent rocks [*Cullers et al.*, 1987; *Gaiero et al.*, 2004; *Henderson*, 1984]. As such, the REE are an ideal system with a large number of variables to be used to identify individual dust sources from which Antarctic dust may originate. Work using this elemental system in Antarctic ice cores is in relatively early stages: *Gabrielli et al.* [2006] and *Gabrielli et al.* [2009] present the initial concept and analytical capabilities, with *Gabrielli et al.* [2010] developing interpretations from the European Project for Ice Coring in Antarctica (EPICA) Dome C ice core and forming a database of dust PSA signatures. Most recent work by *Wegner et al.* [2012] adds a glacial-interglacial REE sequence from the EPICA Drønning Maud Land ice core and collates additional dust PSA signatures. Once a dust potential source area (PSA) is suggested or positively identified in an ice core record, this better establishes the dust transport pathway from the location of emission to the ice core site, allowing further investigation through atmospheric modeling. Such an approach is taken in this thesis, although perhaps in the reverse direction, as detailed below.

1.3 Thesis outline

Chapters 2, 3 and 4 of this thesis are written as independent papers, the first two of which are currently in review for publication. The most recent work, Chapter 4, will undergo review by coauthors prior to submission to *Climate of the Past* in upcoming months. As these are stand-alone works, the reader should expect a certain amount of repetition in introductory material and motivation at the beginning of each chapter. Reference formatting and section structure varies depending on individual journal requirements. Appendix A is a published paper not strictly within the research themes of this thesis but highly relevant for development of future ice coring targets, especially coastal Antarctic sites similar to RICE. Appendix B contains all ICPMS trace element data discussed in Chapters 3 and 4. Below is a synopsis of each chapter, with explanation of specific motivation and detailing contributions from any co-authors in addition to the primary thesis supervisor.

Chapter 2: Trajectory modeling of modern dust transport to the Southern Ocean and Antarctica

***Neff, P. D.**, and N. A. N. Bertler (2015), Trajectory modeling of modern dust transport to the Southern Ocean and Antarctica, Journal of Geophysical Research: Atmospheres, doi:* 10.1002/2015JD023304.

This trajectory model study of daily 1979-2013 atmospheric transport from Southern Hemisphere dust sources explores seasonality and drivers of interannual variability in dust transport, as well as distribution across southern high-latitudes and at all Antarctic ice core sites. Specific consideration is given to potential dust sources in New Zealand, which are directly upwind from the RICE site in the circumpolar westerly circulation. Dust emissions from New Zealand are not well-quantified at present, but are regularly observed in glacial river valleys on either side of the New Zealand Southern Alps (see example photo, Figure 2). Especially during glacial periods, when ice was more extensive and glacial erosion more active in New Zealand, this area may represent a significant contributor to dust deposition especially over the South Pacific Ocean, as suggested by marine sediment core data [*Lamy et al.*, 2014]. Both high- and low-latitude climate patterns are seen to affect the southward extension of Southern Hemisphere dust transport pathways, illustrating the complexity of dust transport to the Antarctic.

***Figure 2.** Windblown dust over the Hopkins River near Lake Ohau, South Island, New Zealand. T. Baisden, photo.*

Chapter 3: Low-femtogram elemental analysis of Antarctic ice cores without preconcentration

***Neff, P. D.**, A. Tuohy, R. Edwards, and N. A. N. Bertler (in preparation), Low-femtogram elemental analysis of Antarctic ice cores without preconcentration.*

A detailed methodology for measurement of trace elements in the RICE ice core is presented, including tests for sample stability through acidification, with particular focus on quality of sub-pg g^{-1} species. This is only the second analytical setup specifically optimized for REE analysis, sensitive to single fg g^{-1} (part per quadrillion) concentrations. A. Tuohy shared in sample preparation, laboratory measurements, data calibration and provided comment on the manuscript. R. Edwards provided laboratory facilities, assisted and advised laboratory measurements, data calibration and presentation of results.

Chapter 4: Rare earth element dust signatures over the past two thousand years in the RICE ice core, Pacific sector, West Antarctica

***Neff, P. D.**, N. A. N. Bertler, A. Tuohy, R. Edwards, D. Emanuelsson, J. Lee, E. Brook, T. Blunier, and P. Mayewski (in preparation), Rare earth element dust signatures over the past two thousand years in the RICE ice core, Pacific sector, West Antarctica.*

Following the development of possible modern dust transport contributors to the RICE ice core and other sites (Chapter 2), possible rare earth element (REE) dust provenance is discussed for samples from the RICE ice core, measured using methods detailed in Chapter 3. Additional consideration is given to existing REE data from the Dome C and Drønning Maud Land ice cores, using dust PSA REE signatures presented by *Wegner et al.* [2012]. Because of considerable analytical uncertainties in Holocene samples with low dust concentrations, conservative interpretations of observed REE patterns are made, making use of large numbers samples achieved using this technique. A. Tuohy shared in sample preparation, laboratory measurements and data calibration. R. Edwards provided laboratory facilities, assisted and advised laboratory measurements and data calibration. D. Emanuelsson, J. Lee, E. Brook and T. Blunier provided age control points and otherwise assisted in developing the RICE 2k v1 agescale. P. Mayewski supported sampling of the RICE ice core for trace element analysis.

Appendix A: A review of the brittle ice zone in polar ice cores

Neff, P.D. *(2014). A review of the brittle ice zone in polar ice cores, Annals of Glaciology, 55(68), 72-82, doi: 10.3189/2014AoG68A023.*

This published manuscript collects all available information concerning the brittle ice zone of reduced ice core quality—a challenging aspect of deep/intermediate ice core drilling—and considers possible physical processes controlling onset and relief of this behavior. Initiated by experiences processing the RICE ice core, which exhibited damaging brittle behavior below 475 m, this paper is the result of a poster presented at the 7th International Workshop on Ice Drilling Technology. It is designed as a tool for the ice coring community as future ice core sites are selected to achieved targeted science goals, keeping in mind that at coastal Antarctic sites brittle behavior affects a large fraction of recovered ice core samples and >90% of dated ice core records.

Appendix B: RICE REE data

Concentration and relative standard deviation of all RICE trace element samples spanning 8 m to 320 m depth.

1.4 Selected conference presentations

Neff, P., A. Tuohy, N. Bertler, and R. Edwards. Antarctic and Southern Ocean Mineral Dust Aerosol Transport Pathways: Forward-Trajectory Modeling and Source Constraints Derived from the RICE Ice Core. (Poster) *American Geophysical Union Fall 2014 Meeting*, San Francisco, California, USA, December 15-19, 2014.

Kjær, H.A., P. Vallelonga, M. Simonsen, **P. Neff**, N. Bertler, A. Svensson and D. Dahl-Jensen. Initial Continuous Chemistry Results From The Roosevelt Island Ice Core (RICE). (Poster) *American Geophysical Union Fall 2014 Meeting*, San Francisco, California, USA, December 15-19, 2014.

Tuohy, A., **P. Neff**, N. Bertler, and R. Edwards. 1000 Year Record of Heavy Metal Contamination from the RICE Ice Core, Roosevelt Island, Antarctica. (Poster) *American Geophysical Union Fall 2014 Meeting*, San Francisco, California, USA, December 15-19, 2014.

Kjær, H.A., P. Vallelonga, M. Simonsen, **P. Neff,** N. Bertler, A. Svensson, I. Seierstad, P. Albert, and A. Bourne. Re-evaluating the 1257 AD eruption using annually-resolved ice core chemical analyses. (Poster) *American Geophysical Union Fall 2014 Meeting*, San Francisco, California, USA, December 15-19, 2014.

Neff, P., T. J. Fudge, B. Medley. Amundsen Sea coastal domes: high-resolution Holocene ice core sites. *Scientific Committee on Antarctic Research 2014 Open Science Conference*, Auckland, NZ, August 25-28, 2014.

Neff, P., A. Tuohy, N. Bertler, and R. Edwards. Exploring extra-Antarctic air transport pathways using Rare Earth Element concentrations in dust from the RICE ice core, Roosevelt Island, Ross Sea Sector. (Poster) *Scientific Committee on Antarctic Research 2014 Open Science Conference*, Auckland, NZ, August 25-28, 2014.

Neff, P., N. Bertler, R. Edwards, and A. Tuohy. Lanthanide element studies of aerosol particles in an ice core from Roosevelt Island, Antarctica. *New Zealand Snow and Ice Research Group Meeting*, Aoraki Mt. Cook National Park, NZ, July 2-4, 2014.

Neff, P., T.J. Fudge, B. Medley. Amundsen Sea coastal domes: high resolution Holocene ice core sites. *IDPO Community Workshop on Ice Coring*, Irvine, California, USA, February 26-27, 2014.

Neff, P., N. Bertler, and RICE Community. Roosevelt Island Climate Evolution (RICE) project update. (Poster) *2013 WAIS Divide Ice Core Science Meeting*, La Jolla, California, USA, September 24-25, 2013.

Neff, P., N. Bertler, A. Pyne, D. Mandeno, and RICE Community. Roosevelt Island Climate Evolution (RICE) project: ice core quality at an intermediate depth site. (Poster) *7th International Workshop on Ice Drilling Technology*, Madison, Wisconsin, USA, September 9-13, 2013.

Mandeno, D., A. Pyne, N. Bertler, and **P. Neff**. Ice coring at Roosevelt Island: Drill design, performance and refrigeration solutions at a low altitude “warm coastal” Antarctic location. *7th International Workshop on Ice Drilling Technology*, Madison, Wisconsin, USA, September 9-13, 2013.

1.5 References

Albani, S., N. M. Mahowald, B. Delmonte, V. Maggi, and G. Winckler (2012), Comparing modeled and observed changes in mineral dust transport and deposition to Antarctica between the Last Glacial Maximum and current climates, *Climate Dynamics*, *38*(9-10), 1731-1755, doi:10.1007/s00382-011-1139-5.

Barbante, C., T. Bellomi, G. Mezzadri, P. Cescon, G. Scarponi, C. Morel, S. Jay, K. van de Velde, C. Ferrari, and C. F. Boutron (1997), Direct determination of heavy metals at picogram per gram levels in Greenland and Antarctic snow by double focusing inductively coupled plasma mass spectrometry, *Journal of Analytical Atomic Spectrometry*, *12*(9), 925-931, doi:10.1039/A701686G.

Bromwich, D. H., J. P. Nicolas, A. J. Monaghan, M. A. Lazzara, L. M. Keller, G. A. Weidner, and A. B. Wilson (2013), Central West Antarctica among the most rapidly warming regions on Earth, *Nature Geoscience*, *6*(2), 139-145.

Cohen, L., S. Dean, and J. Renwick (2013), Synoptic weather types for the Ross Sea region, Antarctica, *Journal of Climate*, *26*(2), 636-649.

Conway, H., B. Hall, G. Denton, A. Gades, and E. Waddington (1999), Past and future grounding-line retreat of the West Antarctic ice sheet, *Science*, *286*(5438), 280-283.

Crary, A. (1961), Glaciological regime at Little America Station, Antarctica, *Journal of Geophysical Research*, *66*(3), 871-878.

Crary, A., E. S. Robinson, H. F. Bennett, and W. W. Boyd (1962), Glaciological regime of the Ross ice shelf, *Journal of Geophysical Research*, *67*(7), 2791-2807.

Cullers, R. L., T. Barrett, R. Carlson, and B. Robinson (1987), Rare-earth element and mineralogic changes in Holocene soil and stream sediment: a case study in the Wet Mountains, Colorado, USA, *Chemical Geology*, *63*(3), 275-297.

Delmonte, B., P. Andersson, M. Hansson, H. Schöberg, J. R. Petit, I. Basile‐Doelsch, and V. Maggi (2008), Aeolian dust in East Antarctica (EPICA‐Dome C and Vostok): Provenance during glacial ages over the last 800 kyr, *Geophysical Research Letters*, *35*(7), doi:10.1029/2008GL033382.

Delmonte, B., C. Baroni, P. S. Andersson, H. Schoberg, M. Hansson, S. Aciego, J. R. Petit, S. Albani, C. Mazzola, and V. Maggi (2010), Aeolian dust in the Talos Dome ice core (East Antarctica, Pacific/Ross Sea sector): Victoria Land versus remote sources over the last two climate cycles, *Journal of Quaternary Science*, *25*(8), 1327-1337, doi:10.1002/jqs.1418.

Delmonte, B., J. Petit, K. K. Andersen, I. Basile-Doelsch, V. Maggi, and V. Y. Lipenkov (2004), Dust size evidence for opposite regional atmospheric circulation changes over east Antarctica during the last climatic transition, *Climate Dynamics*, *23*(3-4), 427-438, doi:10.1007/s00382-004-0450-9.

Ding, Q., E. J. Steig, D. S. Battisti, and M. Küttel (2011), Winter warming in West Antarctica caused by central tropical Pacific warming, *Nature Geoscience*, *4*(6), 398-403, doi:10.1038/NGEO1129.

Dutrieux, P., J. De Rydt, A. Jenkins, P. R. Holland, H. K. Ha, S. H. Lee, E. J. Steig, Q. Ding, E. P. Abrahamsen, and M. Schröder (2014), Strong sensitivity of pine island ice-shelf melting to climatic variability, *Science*, *343*(6167), 174-178.

Gabrielli, P., C. Barbante, C. Turetta, A. Marteel, C. Boutron, G. Cozzi, W. Cairns, C. Ferrari, and P. Cescon (2006), Direct determination of rare earth elements at the subpicogram per gram level in antarctic ice by ICP-SFMS using a desolvation system, *Analytical Chemistry*, *78*(6), 1883-1889, doi:10.1021/ac0518957.

Gabrielli, P., F. Planchon, C. Barbante, C. F. Boutron, J. R. Petit, S. Bulat, S. Hong, G. Cozzi, and P. Cescon (2009), Ultra-low rare earth element content in accreted ice from sub-glacial Lake Vostok, Antarctica, *Geochimica et Cosmochimica Acta*, *73*(20), 5959-5974.

Gabrielli, P., A. Wegner, J. R. Petit, B. Delmonte, P. De Deckker, V. Gaspari, H. Fischer, U. Ruth, M. Kriews, and C. Boutron (2010), A major glacial-interglacial change in aeolian dust composition inferred from Rare Earth Elements in Antarctic ice, *Quaternary Science Reviews*, *29*(1), 265-273, doi:10.1016/j.quascirev.2009.09.002.

Gaiero, D. M., P. J. Depetris, J.-L. Probst, S. M. Bidart, and L. Leleyter (2004), The signature of river-and wind-borne materials exported from Patagonia to the southern latitudes: a view from REEs and implications for paleoclimatic interpretations, *Earth and Planetary Science Letters*, *219*(3), 357-376.

Henderson, P. (1984), *Rare earth element geochemistry*, Elsevier.

Hosking, J. S., A. Orr, G. J. Marshall, J. Turner, and T. Phillips (2013), The influence of the Amundsen–Bellingshausen Seas low on the climate of West Antarctica and its representation in coupled climate model simulations, *Journal of Climate*, *26*(17), 6633-6648.

Joughin, I., B. E. Smith, and B. Medley (2014), Marine ice sheet collapse potentially under way for the Thwaites Glacier Basin, West Antarctica, *Science*, *344*(6185), 735-738.

Kreutz, K., P. A. Mayewski, I. Pittalwala, L. Meeker, M. Twickler, and S. Whitlow (2000), Sea level pressure variability in the Amundsen Sea region inferred from a West Antarctic glaciochemical record, *Journal of Geophysical Research: Atmospheres (1984–2012)*, *105*(D3), 4047-4059.

Küttel, M., E. J. Steig, Q. Ding, A. J. Monaghan, and D. S. Battisti (2012), Seasonal climate information preserved in West Antarctic ice core water isotopes: Relationships to temperature, large-scale circulation, and sea ice, *Climate Dynamics*, *39*(7-8), 1841-1857, doi:10.1007/s00382-012-1460-7.

Lachlan‐Cope, T. A., W. M. Connolley, and J. Turner (2001), The role of the non‐axisymmetric antarctic orography in forcing the observed pattern of variability of the Antarctic climate, *Geophysical Research Letters*, *28*(21), 4111-4114.

Lambert, F., B. Delmonte, J.-R. Petit, M. Bigler, P. R. Kaufmann, M. A. Hutterli, T. F. Stocker, U. Ruth, J. P. Steffensen, and V. Maggi (2008), Dust-climate couplings over the past 800,000 years from the EPICA Dome C ice core, *Nature*, *452*(7187), 616-619, doi:10.1038/nature06763.

Lamy, F., R. Gersonde, G. Winckler, O. Esper, A. Jaeschke, G. Kuhn, J. Ullermann, A. Martínez-Garcia, F. Lambert, and R. Kilian (2014), Increased dust deposition in the Pacific Southern Ocean during glacial periods, *Science*, *343*(6169), 403-407, doi:10.1126/science.1245424.

Maher, B., J. Prospero, D. Mackie, D. Gaiero, P. Hesse, and Y. Balkanski (2010), Global connections between aeolian dust, climate and ocean biogeochemistry at the present day and at the last glacial maximum, *Earth-Science Reviews*, *99*(1), 61-97, doi:10.1016/j.earscirev.2009.12.001.

Mahowald, N., K. Kohfeld, M. Hansson, Y. Balkanski, S. P. Harrison, I. C. Prentice, M. Schulz, and H. Rodhe (1999), Dust sources and deposition during the last glacial maximum and current climate: A comparison of model results with paleodata from ice cores and marine sediments, *Journal of Geophysical Research: Atmospheres (1984–2012)*, *104*(D13), 15895-15916, doi:10.1029/1999JD900084.

Martín, C., R. C. Hindmarsh, and F. J. Navarro (2006), Dating ice flow change near the flow divide at Roosevelt Island, Antarctica, by using a thermomechanical model to predict radar stratigraphy, *Journal of Geophysical Research: Earth Surface (2003–2012)*, *111*(F1).

Mercer, J. H. (1978), West Antarctic ice sheet and CO 2 greenhouse effect- A threat of disaster, *Nature*, *271*(5643), 321-325.

Nereson, N. A., and E. D. Waddington (2002), Isochrones and isotherms beneath migrating ice divides, *Journal of Glaciology*, *48*(160), 95-108.

Nicolas, J. P., and D. H. Bromwich (2011), Climate of West Antarctica and influence of marine air intrusions, *Journal of Climate*, *24*(1), 49-67, doi:10.1175/2010JCLI3522.1.

Nicolas, J. P., and D. H. Bromwich (2014), New Reconstruction of Antarctic Near-Surface Temperatures: Multidecadal Trends and Reliability of Global Reanalyses, *Journal of Climate*, *27*(21), 8070-8093, doi:10.1175/JCLI-D-13-00733.1.

Okumura, Y. M., D. Schneider, C. Deser, and R. Wilson (2012), Decadal–interdecadal climate variability over Antarctica and linkages to the tropics: Analysis of ice core, instrumental, and tropical proxy data, *Journal of Climate*, *25*(21), 7421-7441.

Orsi, A., G. Johnson, and J. Bullister (1999), Circulation, mixing, and production of Antarctic Bottom Water, *Progress in Oceanography*, *43*(1), 55-109, doi:10.1016/S0079-6611(99)00004-X.

Pritchard, H., S. Ligtenberg, H. Fricker, D. Vaughan, M. Van den Broeke, and L. Padman (2012), Antarctic ice-sheet loss driven by basal melting of ice shelves, *Nature*, *484*(7395), 502-505.

Raymond, C. F. (1983), Deformation in the vicinity of ice divides, *Journal of Glaciology*, *29*(103), 357-373.

Revel-Rolland, M., P. De Deckker, B. Delmonte, P. Hesse, J. Magee, I. Basile-Doelsch, F. Grousset, and D. Bosch (2006), Eastern Australia: a possible source of dust in East Antarctica interglacial ice, *Earth and Planetary Science Letters*, *249*(1), 1-13, doi:10.1016/j.epsl.2006.06.028.

Rignot, E., J. Mouginot, M. Morlighem, H. Seroussi, and B. Scheuchl (2014), Widespread, rapid grounding line retreat of Pine Island, Thwaites, Smith, and Kohler glaciers, West Antarctica, from 1992 to 2011, *Geophysical Research Letters*, *41*(10), 3502-3509.

Schneider, D. P., E. J. Steig, T. D. van Ommen, D. A. Dixon, P. A. Mayewski, J. M. Jones, and C. M. Bitz (2006), Antarctic temperatures over the past two centuries from ice cores, *Geophysical Research Letters*, *33*(16).

Steig, E. J., Q. Ding, D. Battisti, and A. Jenkins (2012), Tropical forcing of Circumpolar Deep Water inflow and outlet glacier thinning in the Amundsen Sea Embayment, West Antarctica, *Annals of Glaciology*, *53*(60), 19-28, doi:10.3189/2012AoG60A110.

Steig, E. J., D. P. Schneider, S. D. Rutherford, M. E. Mann, J. C. Comiso, and D. T. Shindell (2009), Warming of the Antarctic ice-sheet surface since the 1957 International Geophysical Year, *Nature*, *457*(7228), 459-462.

Thomas, R. H., D. R. Macayeal, C. R. Bentley, and J. L. Clapp (1980), The creep of ice, geothermal heat flow, and Roosevelt Island, Antarctica, *Journal of Glaciology*, *25*, 47-60.

Thompson, L. G., and E. Mosley-Thompson (1981), Microparticle concentration variations linked with climatic change: evidence from polar ice cores, *Science*, *212*(4496), 812-815.

Turner, J. (2004), The El Niño–Southern Oscillation and Antarctica, *International Journal of Climatology*, *24*(1), 1-31, doi:10.1002/joc.965.

Turner, J., T. Phillips, J. S. Hosking, G. J. Marshall, and A. Orr (2013), The Amundsen Sea low, *International Journal of Climatology*, *33*(7), 1818-1829, doi:10.1002/joc.3558.

Vallelonga, P., P. Gabrielli, E. Balliana, A. Wegner, B. Delmonte, C. Turetta, G. Burton, F. Vanhaecke, K. Rosman, and S. Hong (2010), Lead isotopic compositions in the EPICA Dome C ice core and Southern Hemisphere Potential Source Areas, *Quaternary Science Reviews*, *29*(1), 247-255, doi:10.1016/j.quascirev.2009.06.019.

Wegner, A., P. Gabrielli, D. Wilhelms-Dick, U. Ruth, M. Kriews, P. De Deckker, C. Barbante, G. Cozzi, B. Delmonte, and H. Fischer (2012), Change in dust variability in the Atlantic sector of Antarctica at the end of the last deglaciation, *Climate of the Past*, *8*, 135-147, doi:10.5194/cp-8-135-2012.

Wolff, E., C. Barbante, S. Becagli, M. Bigler, C. Boutron, E. Castellano, M. De Angelis, U. Federer, H. Fischer, and F. Fundel (2010), Changes in environment over the last 800,000 years from chemical analysis of the EPICA Dome C ice core, *Quaternary Science Reviews*, *29*(1), 285-295, doi:10.1016/j.quascirev.20 09.06.013.

Chapter 2: Trajectory modeling of modern dust transport to the Southern Ocean and Antarctica

Abstract

Aerosol deposition over the Southern Ocean and Antarctica has the potential to alter marine productivity and thus ocean carbon uptake while also impacting radiative balance due to scattering and absorption from atmospheric particulates. Quantification of modern emission, transport and deposition of terrestrial dust and other airborne material from Southern Hemisphere sources is challenging due to low emission levels and poor detection from remote sensing platforms. Here, forward trajectory modeling is used to explore atmospheric transport, independent of deposition processes, from 1979 to 2013. Trajectories are initiated from known arid dust source areas in South America (Patagonia), Australia, and southern Africa, with detailed consideration of New Zealand as a potential source. Results suggest that Patagonian and New Zealand dust sources—and other aerosol emissions—share strong atmospheric transport during all seasons, allowing even potentially small New Zealand emissions to contribute significantly to Southern Ocean and Antarctic aerosol loading. We find that atmospheric dust transport controlling distribution of dust and other aerosols shows distinct spatial variability. New Zealand and Patagonia rapidly contribute a high proportion of trajectories to West Antarctica, while in interior East Antarctica source contributions are limited and highly mixed. The sensitivity of existing deep ice core sites to modern atmospheric transport is discussed. Finally, interannual variability of poleward trajectory extension over the Pacific and Atlantic sectors of the Southern Ocean highlights the association of both tropical Pacific sea-surface temperature and high-latitude wind variability (e.g. the Southern Annular Mode) with transport of dust and other aerosols to the Southern Ocean and Antarctica.

2.1 Introduction

Atmospheric suspension, transport and deposition of terrestrial mineral aerosols (dust) plays an important role in the climate system by directly affecting radiative balance, impacting cloud formation and structure, and fertilizing ocean areas characterised by high nutrient, low phytoplankton conditions due to a deficiency of bioavailable iron [*Mahowald et al.*, 2009; *Mahowald et al.*, 1999; *Miller and Tegen*, 1998]. The fertilization effect of terrestrial dust is especially significant in surface waters of the Southern Ocean (SO, ocean areas south of 50ºS), where phytoplankton blooms near areas of Antarctic Bottom Water formation can transfer atmospheric carbon into the deep ocean, potentially reducing atmospheric carbon dioxide concentrations [*Martin et al.*, 1990; *Martínez-Garcia et al.*, 2011; *Orsi et al.*, 1999; *Winton et al.*, 2014]. Marine sediment and Antarctic ice cores show large increases in dust flux during glacial periods—greater than twenty-fold in the Antarctic—in concert with temperature and atmospheric carbon dioxide decreases [*Lamy et al.*, 2014; *Petit et al.*, 1999; *Winckler et al.*, 2008; *Wolff et al.*, 2006]. While Holocene variability is less pronounced, ice core records from coastal sites in the Ross Sea region link an increase in dust loading during the Little Ice Age to stronger wind speed, leading to enhanced phytoplankton blooms and Antarctic Bottom Water formation [*Bertler et al.*, 2011; *Rhodes et al.*, 2012].

Primary contributions to SO and Antarctic dust deposition are thought to be from two dominant Southern Hemisphere (SH) dust Potential Source Areas (PSA): southern South America (Patagonia), due to its mid-latitude location and efficient transport, and Australia due to large dust emissions [*Albani et al.*, 2012; *Ginoux et al.*, 2012; *Li et al.*, 2008; 2010]. However, there is not consensus as to which of these PSA dominates modern or paleo dust deposition, particularly over Antarctica, nor how relative contributions vary regionally and temporally. Satellite observation platforms struggle to quantify modern concentrations of dust and other particulates in the SH atmosphere. This is in part due to low levels of emissions, poor detection of dust in cloudy conditions common in the mid-latitudes, and reduced measurement sensitivity for aerosols in the boundary layer [*Gassó and Stein*, 2007; *Maher et al.*, 2010; *Torres et al.*, 2002].

Modern general circulation model (GCM) experiments suggest large regional variation in PSA dust distribution over the SO and Antarctica, with largest contributions immediately downwind of PSA following circumpolar westerly winds. *Li et al.* [2008; 2010] and *Albani et al.* [2012] suggest that modern Australian dust dominates deposition over the Pacific SO and downwind coastal regions of Antarctica (e.g. Wilkes Land, Victoria Land, the Ross Ice Shelf and Marie Byrd Land), while Patagonian dust prevails over the Atlantic SO, the Antarctic Peninsula and much of the East Antarctic Ice Sheet (EAIS). Although southern Africa is a significant dust emission source, material from this location is deposited largely in the South Atlantic and Indian Oceans, contributing only ~5% of the total dust burden over the SO and Antarctica [*Albani et al.*, 2012; *Li et al.*, 2008]. However, modeled emission fluxes for SH dust PSA vary by as much as a factor of four, with estimates for Australia, for instance, ranging from 37 Tg a^{-1} (teragrams or 10^{12} grams per year) [*Zender et al.*, 2003] to 148 Tg a^{-1} [*Miller et al.*, 2004]. Relative contributions to the global dust budget are similarly inconsistent, with estimates for Australian contributions ranging from 2.5% to 15% [*Tanaka and Chiba*, 2006].

During the Last Glacial Maximum (LGM), GCM results suggest that Patagonian dust dominated deposition over Antarctica [*Albani et al.*, 2012] and large glacial outwash plains in Patagonia have been shown to activate coincident in time with dust peaks found in Antarctic ice cores [*Sugden et al.*, 2009]. Geochemical analyses of dust in Antarctic ice cores are consistent with dominance of Patagonian dust [*Basile et al.*, 1997; *Delmonte et al.*, 2008; *Delmonte et al.*, 2004a; *Delmonte et al.*, 2004b; *Gabrielli et al.*, 2010; *Gaiero*, 2007; *Vallelonga et al.*, 2010; *Vallelonga et al.*, 2005], but these studies stem exclusively from the EAIS and most samples are taken from glacial periods, when dust concentration is significantly enriched and provides enough sample for geochemical analyses. This bias in sample selection towards glacial samples from East Antarctica limits the representation of the actual spatial and temporal variability of Antarctic dust deposition. Recent progress in ultra-low-concentration (10^{-12} to 10^{-15} g/g) elemental analysis of small ice core samples and new ice core records outside the EAIS (e.g. WAIS Divide, RICE, Fletcher Promontory) provide an opportunity to improve the spatial and temporal representation of drivers and fluxes of dust deposition to Antarctica and the Southern Ocean.

Ocean sediment core data from the Pacific SO raise the consideration of New Zealand as a significant dust PSA for this region, possibly contributing to dust deposition three times larger during glacial periods than during interglacials [*Lamy et al.*, 2014]. New Zealand has also been specifically identified as a potential source of dust at two Antarctic ice core sites. Holocene-age samples from the European Project for Ice Coring in Antarctica (EPICA) Drønning Maud Land and Dome C ice cores in East Antarctica suggest multiple and more variable dust source contributions, possibly including Antarctic, Australian and New Zealand sources [*De Deckker et al.*, 2010; *Gabrielli et al.*, 2010; *Vallelonga et al.*, 2010; *Wegner et al.*, 2012]. A larger role for Australian dust during interglacial periods has also been interpreted from dust geochemistry in East Antarctic ice core samples [*Revel-Rolland et al.*, 2006].

Although New Zealand dust emissions are not quantified at present in GCM simulations, during the LGM the extensively-glaciated Southern Alps eroded large volumes of sediment due to efficient glacial action [*Hallet et al.*, 1996], and the resultant aggrading river floodplains supplied material forming extensive loess deposits [*Eden and Hammond*, 2003]. At this time the rivers of New Zealand's South Island also extended further east across a sparsely-vegetated coastal plain broadened by ~120 m eustatic sea level lowering, increasing the amount of sediment available for aeolian dispersal [*Alloway et al.*, 2007; *Carter et al.*, 2000]. Highly active mountain uplift and extreme erosion rates [*Adams*, 1980; *Koons*, 1990], in addition to ongoing lacustrine/riverine wind erosion and dust deposition make New Zealand a compelling region to consider as a contributor to the SH dust budget. This presents a challenge for model experiments, as New Zealand dust emissions occur in relatively narrow bands along river beds and glacial valleys, surrounded by often dense vegetation and with annual average precipitation rates above model thresholds for dust emission—all processes below grid resolution in many GCMs (i.e. 2º latitude × 2.5º longitude, Geophysical Fluid Dynamics Laboratory, GFDL AM2) [*Freidenreich et al.*, 2004]. Glaciogenic dust sources have been overlooked for these reasons, and considered insignificant because they are geographically restricted compared to regions of arid dust emission. However, glaciogenic dust deposition rates can be very high: deposition rates of ~250 g m^{-2} a^{-1} are observed in river valleys in the lee of the New Zealand Southern Alps, comparable to those observed in the Sahara Desert [*Bullard*, 2013; *McGowan et al.*, 1996].

The attribution of SH dust PSA is complicated by the interplay of source (emission), transport and sink (deposition) processes which are difficult to observe, quantify, and model. Here, we isolate modern atmospheric transport of air parcels from four SH dust PSA, using the HySPLIT model to calculate daily forward-trajectories from 1979 to 2013. This paper 1) highlights significant differences in transport between possible SH dust PSA, including New Zealand for the first time, 2) details regional distribution of modern forward trajectories from SH dust PSA over quadrants of the Southern Ocean and in the vicinity of all Antarctic ice core sites where continuous LGM-present dust records exist, and 3) explores modern interannual variability of atmospheric transport pathways from SH terrestrial dust sources to the southern high latitudes. While applicable to transport of many aerosol materials (e.g. anthropogenic pollutants and black carbon), this work focuses particularly on terrestrial dust for its considerable role in the carbon cycle, because dust modeling studies and ice core dust records exist against which to test this approach, and to inform expectations of possible dust source signatures present in the Roosevelt Island Climate Evolution (RICE) ice core recovered from Antarctica in 2013 (79.364 ºS, 161.706 ºW). This allows for generation of hypothetical modern dust source contributions to the site, which may be testable using geochemical provenance methods such as strontium/neodymium ratios and rare earth element signatures [*Delmonte et al.*, 2008; *Gabrielli et al.*, 2010; *Wegner et al.*, 2012].

2.2 Methods

The Hybrid Single-Particle Lagrangian Integrated Trajectory (HySPLIT) model is a free resource (*http://ready.arl.noaa.gov/HYSPLIT.php, National Oceanic and Atmospheric Administration Air Resources Laboratory, Silver Spring, MD, USA)* for calculating air parcel trajectories advected through three-dimensional National Centers for Environmental Prediction / National Center for Atmospheric Research (NCEP/NCAR) climate reanalysis data (hereafter NCEP1) [*Draxler and Hess*, 1998; *Kalnay et al.*, 1996]. Calculations include three-dimensional variables for geopotential height, temperature, zonal, meridional and vertical winds, and relative humidity. Surface temperature (2 m), 10 m zonal and meridional winds, and surface geopotential are also included. Performance of NCEP1 is robust for the SH from the beginning of the satellite era, 1979-present, with high correlations to high-latitude station measurements [*Bromwich and Fogt*, 2004; *Bromwich et al.*, 2007; *Renwick*, 2004]. Comparison of a number of reanalysis data sets, including the NCEP1 and European Centre for Medium Range Weather Forecasts ERA-40 and ERA-Interim (ERAi) reanalyses [*Dee et al.*, 2011], demonstrates that interannual to decadal variability of pressure fields is reproducible across datasets [*Bracegirdle*, 2013; *Bromwich et al.*, 2007]. Duplicating the HySPLIT results presented here using a five-year period of ERAi (2006-2010) yields very similar results to those obtained using NCEP1 data. As ERAi is the most recent and complete global climate reanalysis dataset, we use ERAi mean sea level pressure, geopotential height and sea-surface temperatures to investigate interannual variability observed in the NCEP1 trajectory results.

Here, ten-day forward trajectories are initiated from four SH terrestrial dust PSA, daily from January 1, 1979 to December 31, 2013. Ten days approximates the maximum lifetime of the smaller dust size fraction in model studies, particles from 0.1-2.5 μm in diameter, while larger particle lifetimes are only 1-3 days [*Luo et al.*, 2003; *Tanaka and Chiba*, 2006]. Particle lifetime in other studies, using 2.5 μm mass mean diameter, is approximately four days for both modern and LGM simulations [*Mahowald et al.*, 1999; *Tegen and Fung*, 1994]. In their modern GCM simulation, *Mahowald et al.* [1999] found dust particle lifetimes of eleven days due to wet deposition alone, reducing to nine days in LGM conditions (dry deposition lifetime was seven days in both simulated climates). Typical dust size distributions observed in Antarctic ice cores have mode diameters of 2-8 μm, with total size range from ~0.5-20 μm diameter (larger particles are likely from isolated Antarctic sources) [*Albani et al.*, 2012; *Delmonte et al.*, 2004b; *Koffman et al.*, 2014]. We suggest that ten days is a suitable length of time for considering transport of smaller size fractions of dust (as well as other aerosols), while transport of larger particles is likely restricted to the first several days of the forward trajectories considered here.

PSA trajectory initiation points were chosen near largest regional dust sources identified using satellite remote sensing techniques [*Ginoux et al.*, 2012]. This "point-source" approach is justifiable for the SH, as dust sources on the southern continents have relatively more concentrated areas of emission compared to the Northern Hemisphere, which is characterized by large, geographically extensive dust sources. In Australia (AUS) a point near the large ephemeral Lake Eyre is chosen, 29ºS, 137.5ºE, to be representative of this very active dust storm region and an area between the split dust transport pathways previously identified for Australia [*Bowler*, 1976; *McGowan and Clark*, 2008; *Revel-Rolland et al.*, 2006]. Patagonia (PAT) is responsible for perhaps 75% of dust emitted from South America [*Li et al.*, 2008], and the point 49ºS, 69ºW is used to initiate trajectories. This location in the center of the Santa Cruz province, San Julian's Great Depression, is in the lee of the Patagonian Andes and characterized by arid to semiarid drainages rich in glaciogenic sediment supplied by the erosive power of Andean glaciers [*Gaiero*, 2007; *Li et al.*, 2010]. In southern Africa (SAF) emissions are concentrated in arid regions near the border of Namibia and South Africa, 28ºS, 21ºE [*Ginoux et al.*, 2012; *Li et al.*, 2008]. An additional dust PSA in New Zealand (NZ), is considered here for the first time, 43.5ºS, 172ºE, chosen to be representative of the eastern drainages of the Southern Alps, which cut through extensive loess deposits (e.g. the Waitaki, Rangitata, Rakaia, Waimakariri rivers). The locations of trajectory initiation points have been chosen such that they lie near the center of the PSA. Synoptic surface wind conditions in the vicinity of all four chosen points are consistent across surrounding regions of elevated dust emission, with zonal and meridional correlation-distances extending for hundreds of kilometers or more (not shown). This suggests limited sensitivity of model results to the idealized dust PSA trajectory initiation points used here. Trajectories were initiated at 100 m to capture near-surface wind, model height was set to 20 km and the data-based vertical motion method used.

Forward-trajectory modeling has previously been used to investigate dust transport from source areas including those in Australia [*McGowan and Clark*, 2008], Patagonia [*Gassó and Stein*, 2007; *Li et al.*, 2010] and Asia [*Creamean et al.*, 2014; *Uno et al.*, 2009] and to track large dust plumes from exceptional events [*Gassó and Stein*, 2007; *Wang et al.*, 2011]. While this approach is limited by lack of constraints on dust emission and deposition schemes, the latter of which likely results in the calculations here representing an upper bound with respect to dust transport, it nonetheless provides an opportunity to investigate the characteristics and drivers of atmospheric transport controlling dust distribution (especially those considered as long-term averages). Dust emission, transport and deposition processes are complex, and while empirical and model data constrain some aspects of these processes, long-range transport of dust remains poorly understood [*Betzer et al.*, 1988; *Maher et al.*, 2010]. As we do not prescribe rates of dust emission and deposition, forward trajectory modeling is a computationally inexpensive way to explore aspects of atmospheric transport in isolation from these processes.

2.3 Results

2.3.1 Trajectory Distribution

Atmospheric transport to the SO and Antarctica is dominated by the influence of persistent mid-latitude circumpolar westerly winds, more specifically transient low-pressure systems traveling eastward over the SO [*Hoskins and Hodges*, 2005]. This is especially relevant for dust PSA in Patagonia and New Zealand for their more southerly location in latitudes of peak wind speed. Figures 1 and 2 display five-day forward trajectory endpoints for each SH dust PSA (one endpoint for each trajectory initiated daily from 1979 to 2013). Five days is the minimum time in which trajectories from all four dust PSA reach Antarctica, and also represents a more conservative mean particle lifetime, keeping in mind deposition processes as discussed above.

Persistent southeastward transport from higher-latitude PAT and NZ is observed, with dominant particle transport in the boundary-layer extending ~30º south and ~90º east of trajectory initiation points after five days (Figure 2). Lower-latitude dust PSA in SAF and AUS, positioned equatorward of the strongest mid-latitude westerly winds, exhibit both a northwest and southeast pathway and transport more trajectories in the mid-troposphere than PAT and NZ (Figure 2). This result agrees well with the 1979-1998 mean distribution observed by *Li et al. [2008]* using a GCM (GFDL-AM2) approach, which also located South American and Australian dust transport in the boundary layer and mid-troposphere, respectively.

2.3.2 Trajectory Seasonality

Strength of atmospheric transport from PSA to the SO and Antarctica shows limited seasonality, although greatest southward transport from AUS and to a lesser extent SAF occurs during austral winter months (Figure 3). *Lunt and Valdes [2001]* explored thirty-day backward trajectories from the Dome C, Antarctica ice core site to SH dust PSA and found similar seasonality. SAF and AUS trajectories also extend further eastward during winter and spring (Figure 3). NZ and PAT trajectories show limited seasonality, with generally strong south and eastward transport all year. Transport from higher-latitude PSA (NZ and PAT) is consistently in the boundary layer, while monthly mean pressure of lower-latitude SAF and AUS trajectories exhibits strong seasonality with transport in the boundary layer during austral winter and in the mid-troposphere during summer (Figure 3). Full-resolution 35-year timeseries of trajectory latitude, longitude and pressure are presented in Figures S1-S3.

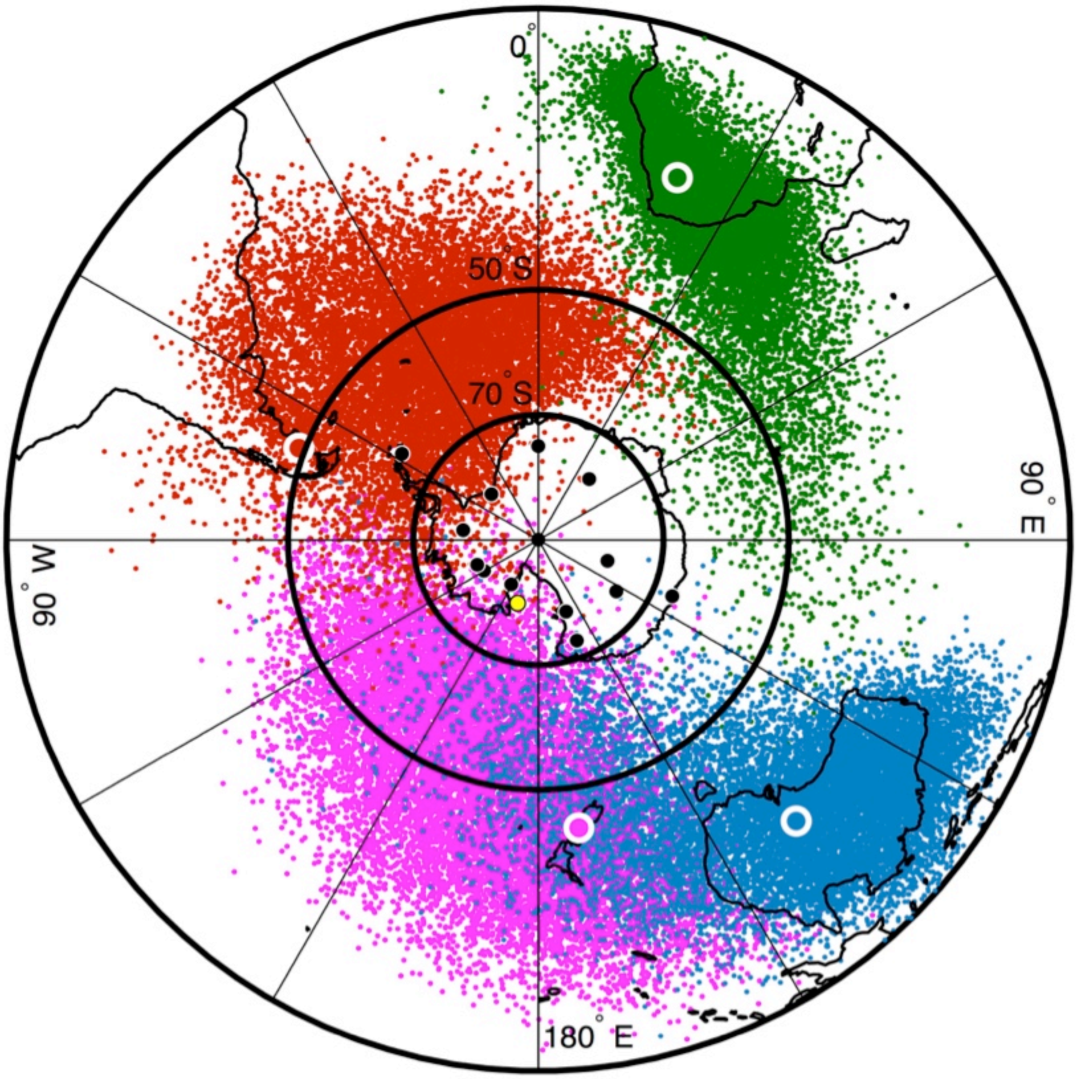

Figure 1. *Five-day HySPLIT forward trajectory endpoints, initiated every day from 1979-2013 for each dust PSA: New Zealand (magenta), Patagonia (orange), southern Africa (green) and Australia (cyan). Larger colored circles denote trajectory initiation points (dust PSA); black circles mark Antarctic ice core sites, with the yellow circle marking the RICE ice core site. Bold parallels mark northern boundaries of the Southern Ocean (50ºS) and Antarctica (70ºS) as considered in Figures 4 and 5.*

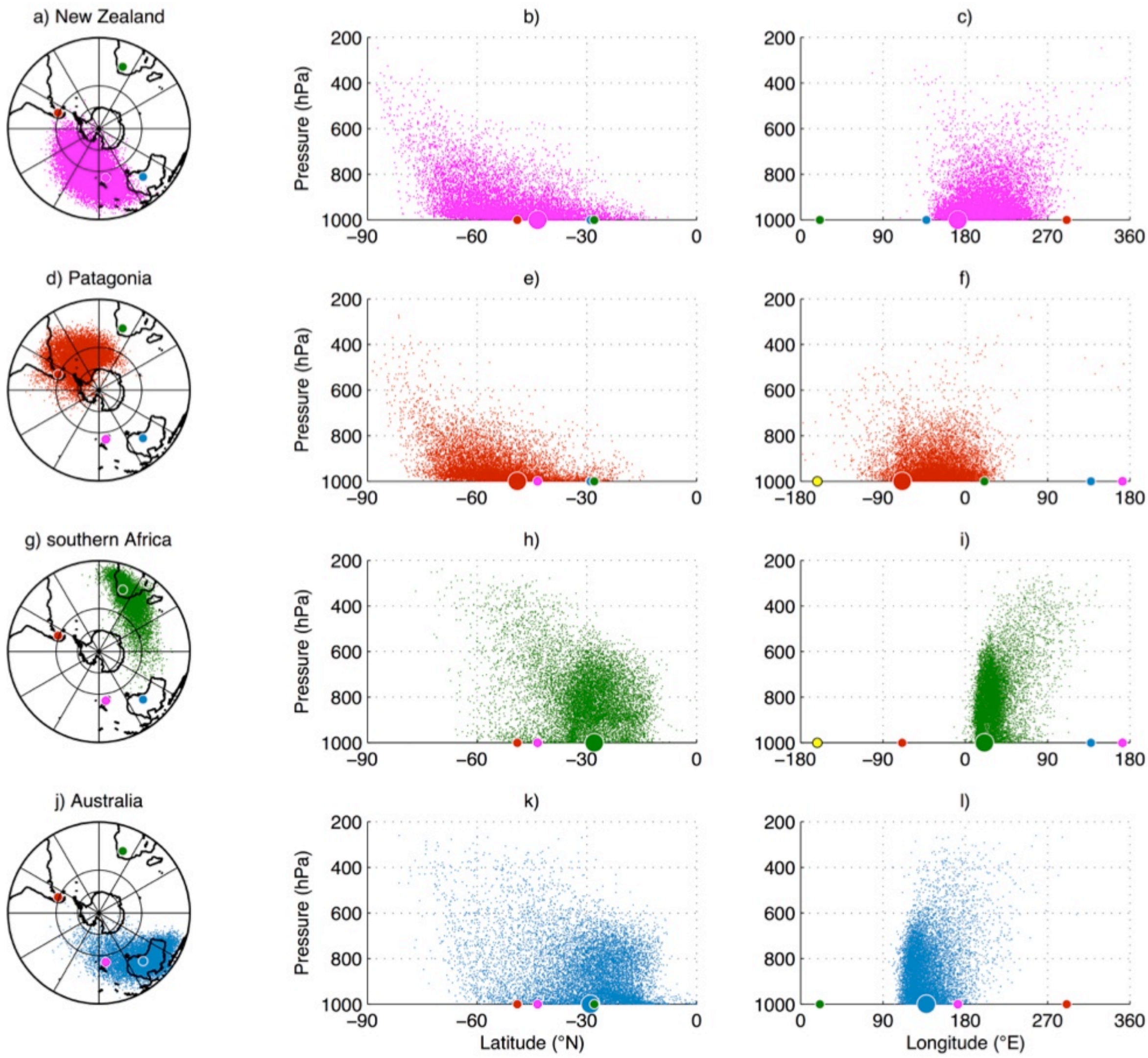

Figure 2. *Five-day HySPLIT forward trajectory endpoints calculated daily from 1979-2013 for dust PSA: New Zealand (a, b, c, magenta), Patagonia (d, e, f, orange), southern Africa (g, h, i, green) and Australia (j, k, l, cyan). Trajectory data are displayed in map view (a, d, g, j), degrees of latitude versus atmospheric pressure (hPa; b, e, h, k) and longitude versus atmospheric pressure (c, f, i, l). Larger colored circles denote trajectory initiation points (dust PSA). Note changes in x-axis of longitude plots to center data: centered on 0º longitude for Patagonia and southern Africa, and centered on 180º longitude for Australia and New Zealand.*

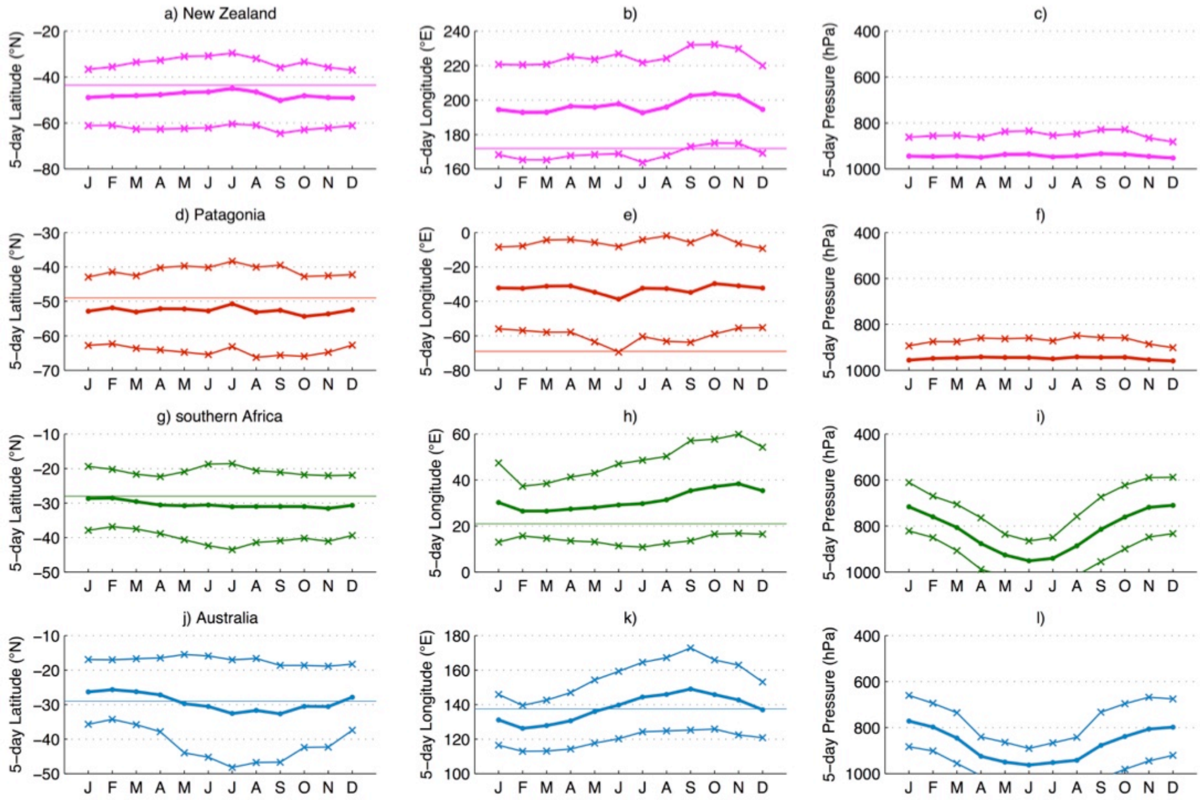

Figure 3. *Monthly means (bold line, circles) and one standard deviation (x's) of daily 1979-2013 five-day forward trajectory latitude, longitude and pressure (hPa) from PSAs. New Zealand (a, b, c, magenta), Patagonia (d, e, f, orange), southern Africa (g, h, i, green) and Australia (j, k, l, cyan). Horizontal lines mark trajectory initiation latitude or longitude.*

2.3.3 Ten-Day Trajectory Evolution

During the 35-year period considered here, higher-latitude PSA contribute a significant proportion of trajectories to the SO within 1-2 days (Figure 4a), with trajectories arriving over Antarctica (>70ºS, here) after 2-3 days (Figure 4b). Sixty percent of PAT trajectories pass over the SO after only three days, as the PAT initiation point is very near the SO, and the PAT contribution remains at this level through the ten-day model time. Transport from NZ rises more gradually over the ten days, after which nearly 50% of NZ trajectories have passed over the SO. More than 5% of trajectories from both PAT and NZ move over Antarctica after five days, rising to a maximum of approximately 8% of PAT trajectories after seven days and >10% of NZ trajectories after eight days.

Far fewer trajectories from low-latitude PSA extend within ten days to the SO and Antarctica. Five-day transport from AUS and SAF to the SO represents an approximately 2σ event (i.e. two standard deviations, 7.6% and 4.1% of all AUS and SAF trajectories, respectively). At the end of the ten-day model runtime, low-latitude PSA only transport 13% (SAF) and 16% (AUS) of trajectories over the SO, and a correspondingly low percentage of transport from low-latitude PSA ends in the Antarctic. Initial trajectories from SAF and AUS arrive over Antarctica after four days (Figure 4b), with a maximum of 2.4% of all AUS trajectories traveling to the Antarctic and slightly less than 1% of all SAF trajectories.

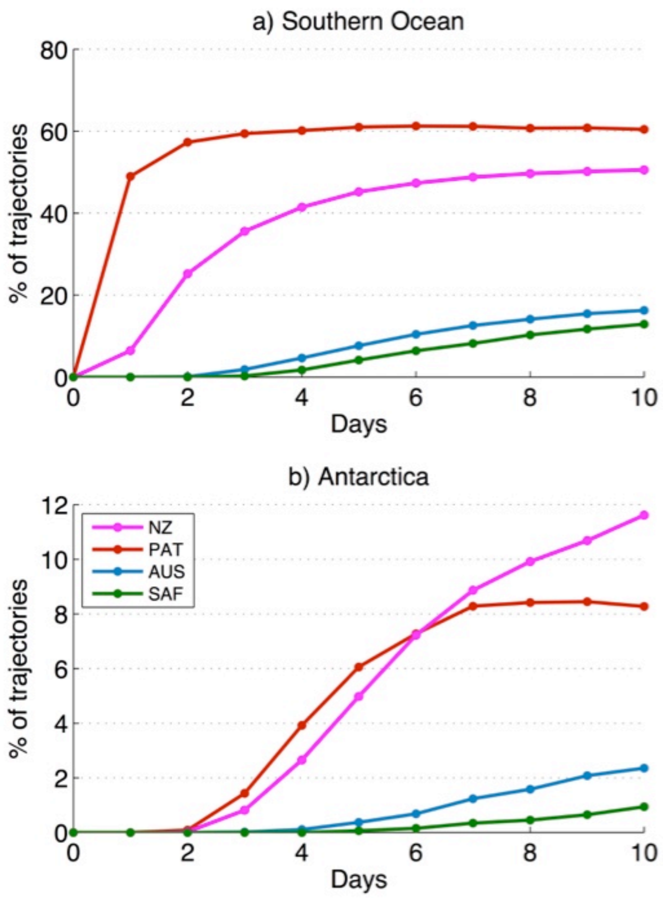

Figure 4. *Percent of 1979-2013 daily forward-trajectories (12,775 total) passing over a) the Southern Ocean (trajectories ending south of 50ºS) and b) Antarctica (trajectories ending south of 70ºS) at daily increments for all PSA.*

2.4 Discussion

2.4.1 Source Strength and Transport Efficiency

Due to stronger southward atmospheric transport in the SH mid-latitudes and shorter transport distance, atmospheric pathways for terrestrial aerosols from higher-latitude PSA (NZ and PAT) deliver three to four times more trajectories to the SO and Antarctica than lower-latitude PSA (SAF and AUS, Figure 4). While AUS and PAT are considered the primary contributors of dust aerosol to the SO and Antarctica [*Albani et al.*, 2012; *Li et al.*, 2008], these results demonstrate that unquantified dust emissions from NZ sources are transported southward with efficiency comparable to that of PAT. Air parcels leaving SAF are least efficiently transported southward, and similarly to the GCM results of *Li et al.* [2008] and *Albani et al.* [2012], this work suggests very limited influence of SAF dust on the SO and Antarctica (with the possible exception of coastal regions in the Indian Ocean sector of Antarctica, discussed below).

An estimation of relative dust source contributions can be made by taking into account atmospheric transport as modeled here, and applying linear weighting according to modeled dust emission rates. Model dust emission estimates are wide-ranging, as mentioned above, but we choose to use the emission rates of *Li et al.* [2008] because of their efforts to specifically investigate modern (1979-1998) dust transport to the SO and Antarctica. To explore possible contribution of New Zealand dust, a range of annual dust emissions are used to weight NZ trajectories: 10 Tg a^{-1}, 20 Tg a^{-1} and 30 Tg a^{-1}. While the upper limit of this range likely exceeds modern emissions from New Zealand, which are not observed by remote sensing techniques or modeled in GCM studies, it facilitates consideration of the potential relative strength of a NZ dust source. This simple linear approach ignores dust deposition due to gravitational settling and precipitation, and assumes all emissions come from a single point source. However, estimates of relative dust PSA contributions to the Antarctic are comparable to computationally-expensive GCM results.

Table 1 compares SH dust PSA percent contributions to regional dust deposition calculated here with the GCM results of *Li et al.* [2008]. This is done for latitudinal zones as defined by *Li et al. [2008]*: the SO (50º – 75ºS) and "inland" Antarctica (75ºS – 90ºS). All emissions from South America, AUS and SAF in *Li et al.* [2008] are assumed to originate at the respective trajectory initiation point in this study. To facilitate this comparison, the weight of PAT trajectories is increased by 25% to include the full 50 Tg a^{-1} emitted by all South American dust sources (e.g. including the Atacama Desert, Bolivian Altiplano, etc.). This is required because *Li et al.* [2008] do not model Patagonian emissions in isolation. Weighting of PAT trajectories for figures and discussion below remains 38 Tg a^{-1}, a figure more appropriate for reflecting only Patagonian dust emissions in the vicinity of the trajectory initiation point.

Table 1. *PSA contribution to total dust deposition over the Southern Ocean (SO, 50º - 75ºS) and inland Antarctica (ANT, 75ºS - 90ºS)**

	% S. America, Li et al. (2008)	% PAT, this study, NZ 0	% PAT, this study, NZ 10	% PAT, this study, NZ 30	% AUS, Li et al. (2008)	% AUS, this study, NZ 0	% AUS, this study, NZ 10	% AUS, this study, NZ 30	% SAF Li et al. (2008)	% SAF, this study, NZ 0	% SAF, this study, NZ 10	% SAF, this study, NZ 30	% NZ, this study, NZ 10	% NZ, this study, NZ 30
SO	60	**55.8**	**51.0**	**43.6**	37	**36.1**	**33.0**	**28.2**	2	**8.1**	**7.4**	**6.3**	**8.5**	**21.9**
ANT	56	**58.5**	**50.5**	**39.7**	39	**38.1**	**32.9**	**25.9**	6	**3.4**	**2.9**	**2.3**	**13.7**	**32.2**

**Percent contributions from this study are calculated from the tenth day of source-weighted forward trajectories (1979-2013 mean, as in Figure 5). Percent contributions of total emissions for this study are calculated including NZ contributions of 0, 10 and 30 Tg a^{-1}. PAT percent contributions have the full weight of South American sources (50 Tg a^{-1}) identified in Li et al. (2008) to facilitate comparison, and percentages from Li et al. (2008) exclude the contribution from Northern Hemisphere dust sources (3% and 10% of dust deposition over the SO and Antarctica, respectively). Annual PSA emissions of Li et al. (2008) are: South America, 50 Tg a^{-1}; Patagonia, 38 Tg a^{-1}; Australia, 120 Tg a^{-1}; and southern Africa, 34 Tg a^{-1}.*

The results of this approach suggest that, even as the smallest dust source in the SH, NZ may contribute a significant fraction of total dust deposited over portions of the SO and Antarctica. With a very modest dust emission weight of 10 Tg a^{-1}, dust transported from NZ possibly contributes as much as 8.5% of total deposition over the SO, and 13.7% over interior Antarctica (Table 1). Increasing NZ dust emission weighting to 30 Tg a^{-1}, a high estimate of present conditions but perhaps analagous to LGM emission rates with New Zealand glacial systems activated in a manner similar to Patagonia (e.g *Sugden et al.* [2009]), brings the relative contribution of NZ to 21.9% of dust deposition over the SO and 32.2% over Antarctica (maintaining modern emission weighting for other PSA).

The weighted ten-day forward-trajectory evolution (Figure 5) illustrates the dominance of dust source-weighted PAT trajectories, likely due to a combination of proximity and direct, efficient transport despite relatively modest dust emissions (38 Tg a^{-1}). Although large AUS dust emissions (120 Tg a^{-1}) may be an overestimate, as dust is emitted over a broad region of central Australia and not only in the vicinity of the trajectory initiation point and Lake Eyre Basin, source-weighted trajectories from this PSA rise to levels similar to those of PAT after two additional days of transport. As suggested above, while the 34 Tg a^{-1} modeled modern SAF dust emission rate is essentially equal to PAT emissions (38 Tg a^{-1}) within reported model error of ± 2-3 Tg a^{-1}, inefficient transport and long transport distance relegate SAF to a more limited role in atmospheric transport of dust to the SO and Antarctica.

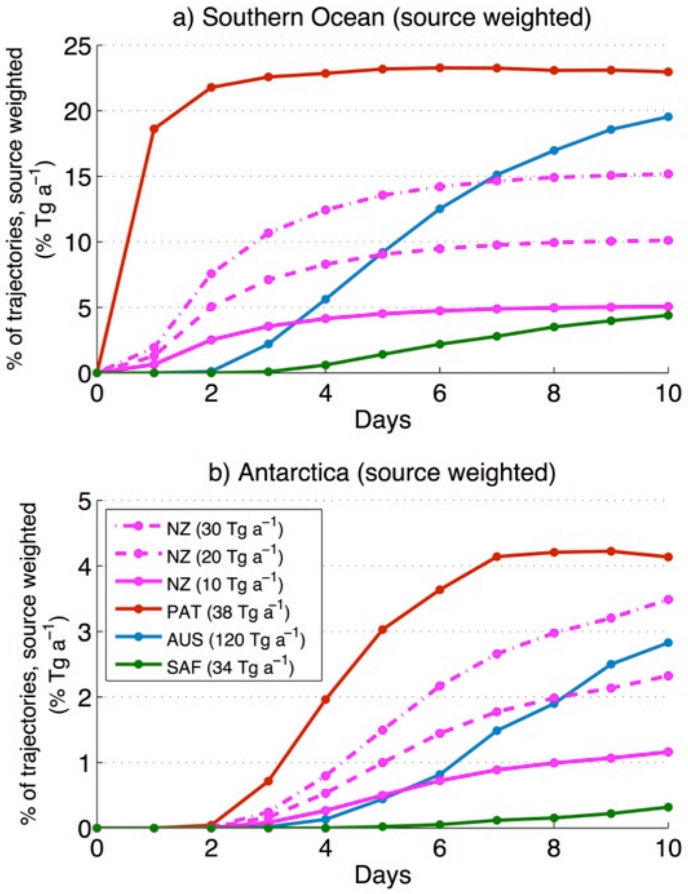

Figure 5. *Terrestrial dust emission-weighted percent (% Tg a^{-1}) of 1979-2013 daily forward-trajectories passing over a) the Southern Ocean (trajectories ending south of 50ºS) and b) Antarctica (trajectories ending south of 70ºS) at daily increments for all dust PSA. Emission estimates are as in Li et al. (2008), with a range of assumed emission rates for unquantified New Zealand dust sources.*

2.4.2 Southern Ocean Trajectory Distribution

In considering the distribution of trajectories from SH terrestrial dust PSA across more specific regions of the SO and at Antarctic ice core sites, both unweighted and dust emission-weighted trajectory distributions are of interest. The unweighted trajectories lend insight into relative atmospheric transport strength from SH terrestrial sources with respect to many types of aerosol, while the emission-weighting approach allows specific consideration of potential dust provenance across the SH high latitudes. Both approaches can aid interpretation of marine sediment and ice core records.

Figure 6 displays trajectory contributions over quadrants of the SO. As above, PSA trajectories dominate downwind areas of the SO. About 60% of all PAT trajectories move over the Atlantic SO after three days (Figure 6d), with 30% of trajectories continuing into the Indian Ocean sector of the SO after ten days, although likely depleted of larger dust and aerosol particles due to deposition (Figure 6a). Approximately 35% of NZ trajectories travel over the Pacific SO after five days (Figure 6c), with more than 20% continuing eastward to the Atlantic SO after ten days—albeit overshadowed by dominant PAT trajectories (Figure 6d). Far fewer trajectories from AUS and SAF travel south, but when weighted for dust emissions AUS is the largest contributor to SO areas south of Australia in the first 6-7 days of travel, as well as the Pacific SO after ten days (Figure 6f, g). SAF contributes a small fraction of trajectories to the SO, both unweighted and dust emission-weighted, but it does represent the second largest emission-weighted contribution to remote SO areas off the Antarctic coast near Wilkes Land (Figure 6f). It is significant that transport from these lower-latitude PSA is preferentially located in the mid-troposphere during austral spring and summer (Figure 3), as this may alleviate boundary-layer dust deposition during these seasons and promote further transport and deposition further from PSA. Such seasonality is not captured by the 35-year average transport results considered here.

Figure 6. (Following page) *Percent of 1979-2013 daily forward-trajectories, both unweighted (%, a – d) and terrestrial dust emission-weighted (% Tg* a^{-1}*, e – h), passing over quadrants of the Southern Ocean at daily increments for all Southern Hemisphere dust PSA. Maps of 1979-2013 trajectory endpoints after five days (i – l) detail areas considered in panels above, outlined by black boxes. Southern Ocean quadrants are 50º to 70ºS, 0 to 90ºE (a, e, i), 50º to 70ºS, 90 to 180ºE (b, f, j), 50º to 75ºS, -180 to -90ºE (c, g, k), and 50º to 75ºS, -90 to 0ºE (d, h, l). Emission estimates are as in Figure 5, taken from Li et al. (2008), with Patagonia emitting 38 Tg* a^{-1}*, Australia 120 Tg* a^{-1}*, southern Africa 34 Tg* a^{-1} *and a range of emission rates for unquantified New Zealand dust sources.*

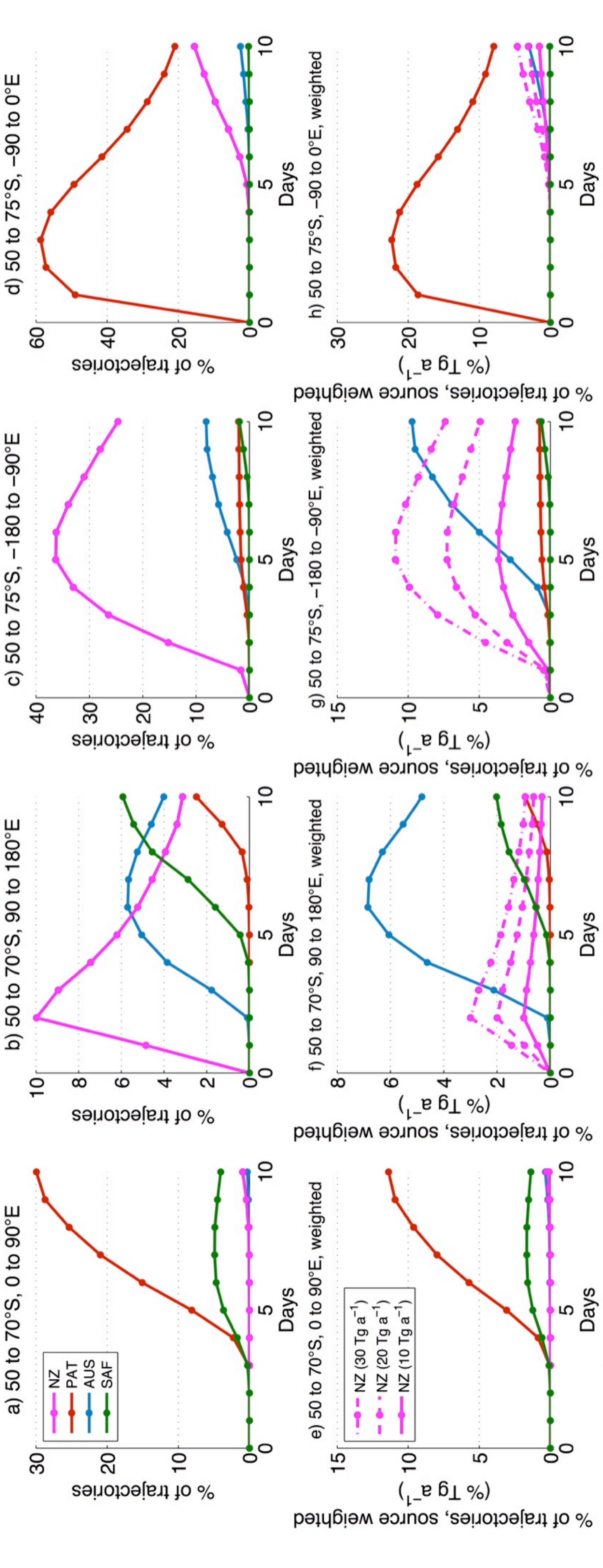

a) 50 to 70°S, 0 to 90°E
b) 50 to 70°S, 90 to 180°E
c) 50 to 75°S, −180 to −90°E
d) 50 to 75°S, −90 to 0°E
e) 50 to 70°S, 0 to 90°E, weighted
f) 50 to 70°S, 90 to 180°E, weighted
g) 50 to 75°S, −180 to −90°E, weighted
h) 50 to 75°S, −90 to 0°E, weighted
i) Day 5 snapshot
j) Day 5 snapshot
k) Day 5 snapshot
l) Day 5 snapshot
NZ
PAT
AUS
SAF
NZ (30 Tg a^{-1})
NZ (20 Tg a^{-1})
NZ (10 Tg a^{-1})
% of trajectories
% of trajectories, source weighted (% Tg a^{-1})
Days

2.4.3 Atmospheric Transport to Antarctic Ice Core Sites

Antarctic ice cores provide the opportunity to construct a record of dust transport to the SO and Antarctica where no observations exist, and also facilitate testing of model simulations of this process. To utilize these records fully, it is important to identify and quantify which one or several dust sources influences a particular ice core site. Dust records from Antarctic ice cores are likely to show significant differences both in their lithology and particle size distribution depending on which PSA the particular ice core site receives material from. The following sub-sections investigate aspects of modern dust transport possibly captured and recorded by deep Antarctic ice cores (Figures 7-10). During the thirty-five years considered here, fewer than 6% of all ten-day dust PSA forward trajectories reach the Antarctic continent, with less than 1% of trajectories traveling over any individual ice core site (excluding the Antarctic Peninsula, which receives up to 3% of PAT trajectories). Ice core sites on the high-elevation (~3000-4000 m) EAIS plateau are particularly isolated from extra-Antarctic dust sources, and GCM experiments struggle to reproduce dust concentrations measured in ice core samples [*Albani et al.*, 2012; *Li et al.*, 2008; *Mahowald et al.*, 1999].

2.4.3.1 Dust Transport to the East Antarctic Ice Sheet

The EAIS plateau ice core sites EPICA Drønning Maud Land (EDML), Dome Fuji, Vostok, South Pole, EPICA Dome C (EDC), Taylor Dome and Talos Dome (Figure 7 and 8) receive less than 0.15% of trajectories from any single PSA. This equates to approximately 20 of 12,775 daily trajectories spanning 1979 to 2013. However, there is considerable regional variability of relative dust PSA trajectory contributions.

The EDML ice core site, relatively coastal and downwind of the strong Patagonian dust source, is dominated by PAT trajectories by a factor of two, increasing to a factor of three to four when weighted for dust emissions (Figure 7). EDML dust provenance analysis, comparing rare earth element characteristics in ice core samples with those of dust samples taken directly from PSA, suggests a Holocene dust regime dominated by South American contributions but with larger AUS, NZ and local Antarctic contributions than during the LGM [*Wegner et al.*, 2012]. The modern dust-emission weighted and unweighted trajectory results here support this interpretation, with NZ contributing fewer trajectories than PAT, while a small AUS contribution is only observed on the tenth day of forward-trajectories.

Remote EAIS plateau ice core sites Dome Fuji, Vostok, South Pole, EDC and Taylor Dome (Figure 7 and 8) show mixed and very few dust PSA trajectory contributions, although source-weighted trajectories from the AUS dust PSA exhibit some dominance at Vostok, South Pole and especially the EDC ice core site. AUS trajectories arrive at EDC as soon as four days after initiation, while transport to Vostok and South Pole takes more than eight days. Australian dust contribution specifically from Lake Eyre to the EAIS has been suggested using strontium/neodymium isotope geochemistry in EDC and Vostok ice core samples [*Delmonte et al.*, 2004b; *Revel-Rolland et al.*, 2006]. Rare earth element studies of EDC ice core samples, similar to the EDML ice core, show a shift from dominant South American contributions during the LGM to a more mixed Holocene dust regime with possible contributions from Australia and New Zealand sources [*Gabrielli et al.*, 2010; *Wegner et al.*, 2012]. However, provenance work using all of these geochemical systems is complicated by low sample concentrations in interglacial ice, overprinting of local Antarctic dust and/or volcanic input during interglacial periods, and incomplete characterization of both Antarctic and extra-Antarctic dust PSA geochemical signatures [*Vallelonga*, 2015].

Figure 7. (Following page) *As in Figure 6, but for areas centered over Antarctic ice core sites EPICA Drønning Maud Land (EDML, a, e, i), Dome Fuji (b, f, j), Vostok (c, g, k) and South Pole (d, h, l). Areas considered extend 2.5º latitude to the north and south, and 10º longitude east and west of ice core sites (excluding South Pole, which includes the area south of 87.5ºS).*

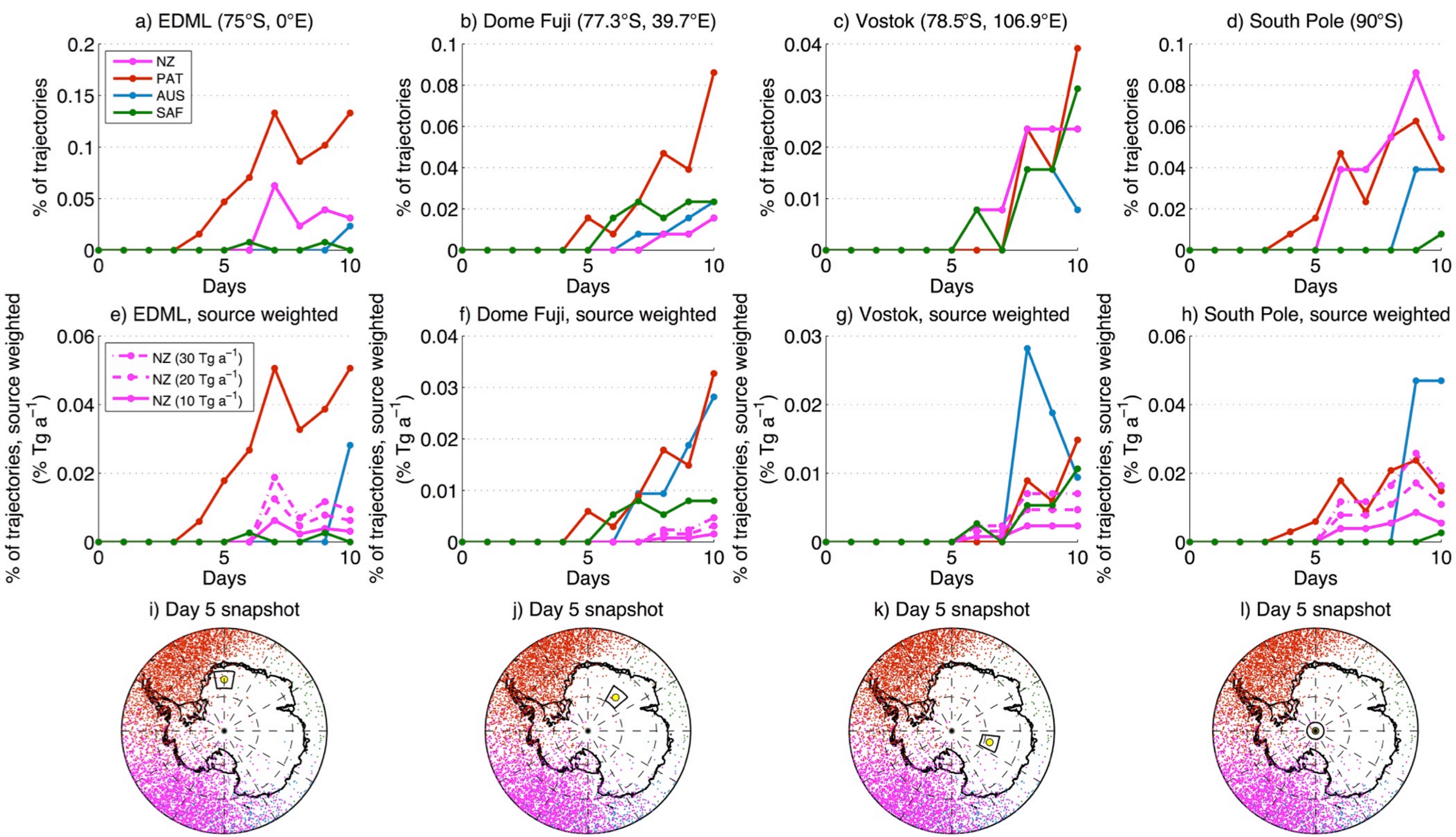
a) EDML (75°S, 0°E)
b) Dome Fuji (77.3°S, 39.7°E)
c) Vostok (78.5°S, 106.9°E)
d) South Pole (90°S)
NZ
PAT
AUS
SAF
% of trajectories
Days
e) EDML, source weighted
f) Dome Fuji, source weighted
g) Vostok, source weighted
h) South Pole, source weighted
NZ (30 Tg a^{-1})
NZ (20 Tg a^{-1})
NZ (10 Tg a^{-1})
% of trajectories, source weighted (% Tg a^{-1})
i) Day 5 snapshot
j) Day 5 snapshot
k) Day 5 snapshot
l) Day 5 snapshot

Coastal EAIS ice core sites at Law Dome and Talos Dome (Figure 8) also show dust PSA trajectory distributions with large AUS contributions as well as a significant SAF component at Law Dome. Lead (Pb) isotope studies in the Law Dome ice core provide additional evidence for modern atmospheric transport of pollutants from Australia to coastal regions of the EAIS, as the isotopic signature of Broken Hill Pb from Australian mining activity was identified in 20th century ice core samples [*Vallelonga et al.*, 2002]. At Talos Dome, similar to EDML and EDC, South American dust strontium-neodymium signatures are dominant during the LGM, while during the Holocene strontium-neodymium ratios of dust from proximal ice-free areas upwind of the ice core site match the signature observed in ice core samples [*Delmonte et al.*, 2010]. The NZ dust PSA is the most dominant source of unweighted trajectories arriving Talos Dome, suggesting that NZ should be considered as a potential contributor to the dust and additional aerosol budgets in the Victoria and Wilkes Land regions of East Antarctica.

Figure 8. (Following page) *As in Figure 7 but for Law Dome (a, e, i), EPICA Dome C (b, f, j), Taylor Dome (c, g, k) and Talos Dome (d, h, l).*

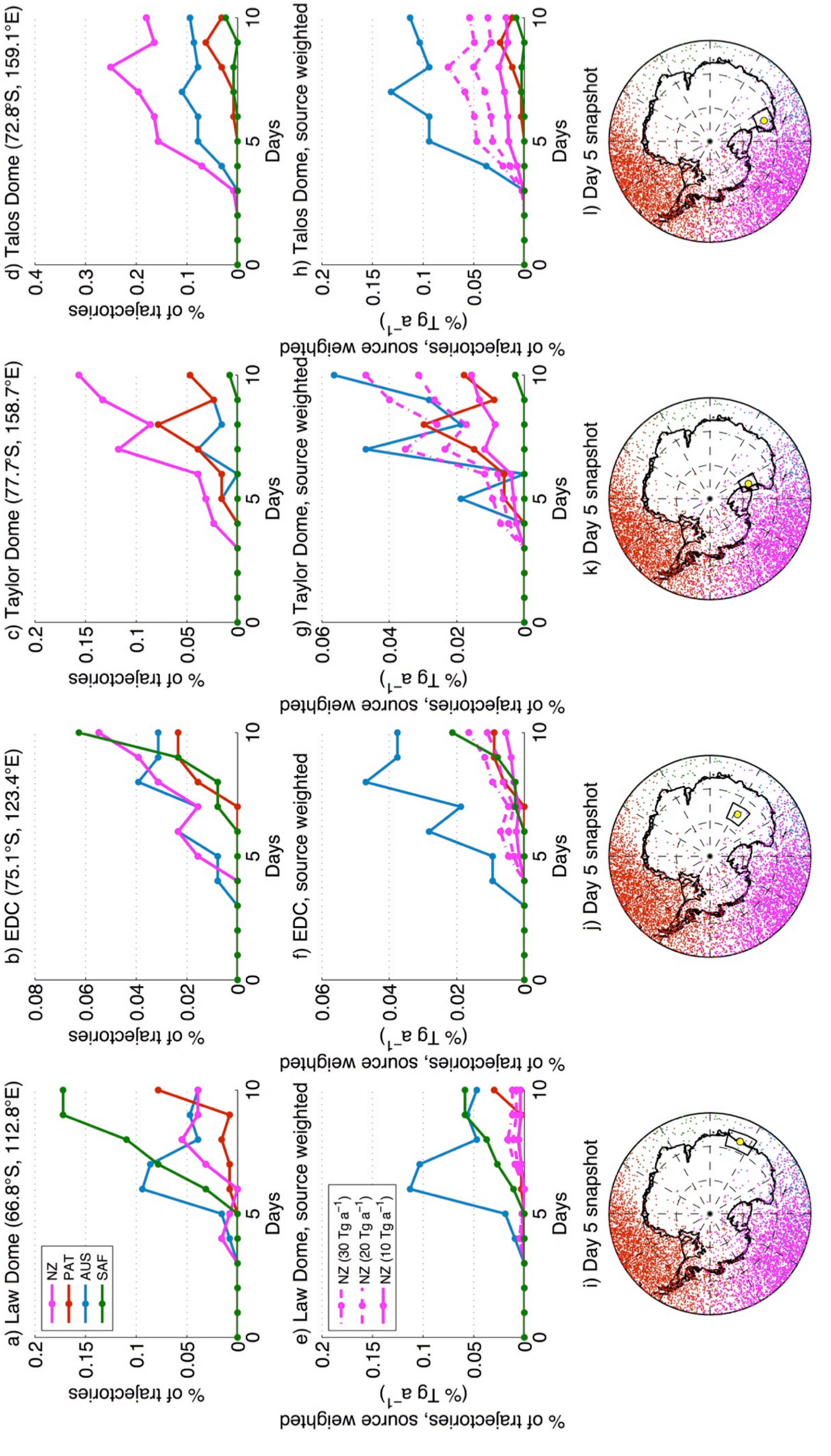

a) Law Dome (66.8°S, 112.8°E)
b) EDC (75.1°S, 123.4°E)
c) Taylor Dome (77.7°S, 158.7°E)
d) Talos Dome (72.8°S, 159.1°E)
NZ
PAT
AUS
SAF
% of trajectories
e) Law Dome, source weighted
f) EDC, source weighted
g) Taylor Dome, source weighted
h) Talos Dome, source weighted
NZ (30 Tg a⁻¹)
NZ (20 Tg a⁻¹)
NZ (10 Tg a⁻¹)
% of trajectories, source weighted (% Tg a⁻¹)
Days
i) Day 5 snapshot
j) Day 5 snapshot
k) Day 5 snapshot
l) Day 5 snapshot

2.4.3.2 Dust Transport to the West Antarctic Ice Sheet

The lower-elevation, marine-influenced West Antarctic Ice Sheet (WAIS) [*Nicolas and Bromwich*, 2011] receives two- to four-times more trajectories from dust PSA than the EAIS, particularly from NZ in the Ross and Amundsen Sea sectors and from PAT across the Antarctic Peninsula and Weddell Sea region (Figure 9, 10). More efficient transport of dust onto the WAIS, and local dust input from rock outcrops (e.g. Executive Committee Range, Ford Ranges, etc.), likely are the causes of higher dust concentrations and larger particle sizes observed in modern ice core samples from the WAIS Divide ice core compared to those from East Antarctic ice cores [*Koffman et al.*, 2014]. Few geochemical provenance studies have been undertaken using West Antarctic ice core samples, but this work is currently being undertaken using 20th century samples from the RICE ice core. Higher concentrations of terrestrial minerals (e.g. dust) and marine salts are both observed and modeled at lower-elevation sites and across the inland WAIS than at higher elevations on the EAIS plateau, and lower concentrations of dust should be expected in regions most distal from extra-Antarctic dust sources [*Bertler et al.*, 2005; *Li et al.*, 2008].

At the RICE and Siple Dome ice core sites (Figure 9) in the vicinity of the Ross Ice Shelf, NZ trajectories (unweighted) dominate by up to five times more than the next largest PAT contribution. Even when the NZ dust PSA is weighted by dust source emissions as low as 10 Tg a^{-1}, it contributes equally to the potential dust distribution at these coastal WAIS sites. Similar prevalence of NZ trajectories remains at the Byrd and WAIS Divide ice core sites (Figure 9) near the highest-elevation WAIS ice flow divide, although PAT trajectories become more common. Weighted for dust source emissions, NZ trajectories contribute with nearly equal strength to those from the more heavily-weighted PAT and AUS trajectories at Byrd and WAIS Divide.

Figure 9. (Following page) *As in Figure 8 but for RICE (a, e, i), Siple Dome (b, f, j), Byrd Station (c, g, k) and WAIS Divide (d, h, l).*

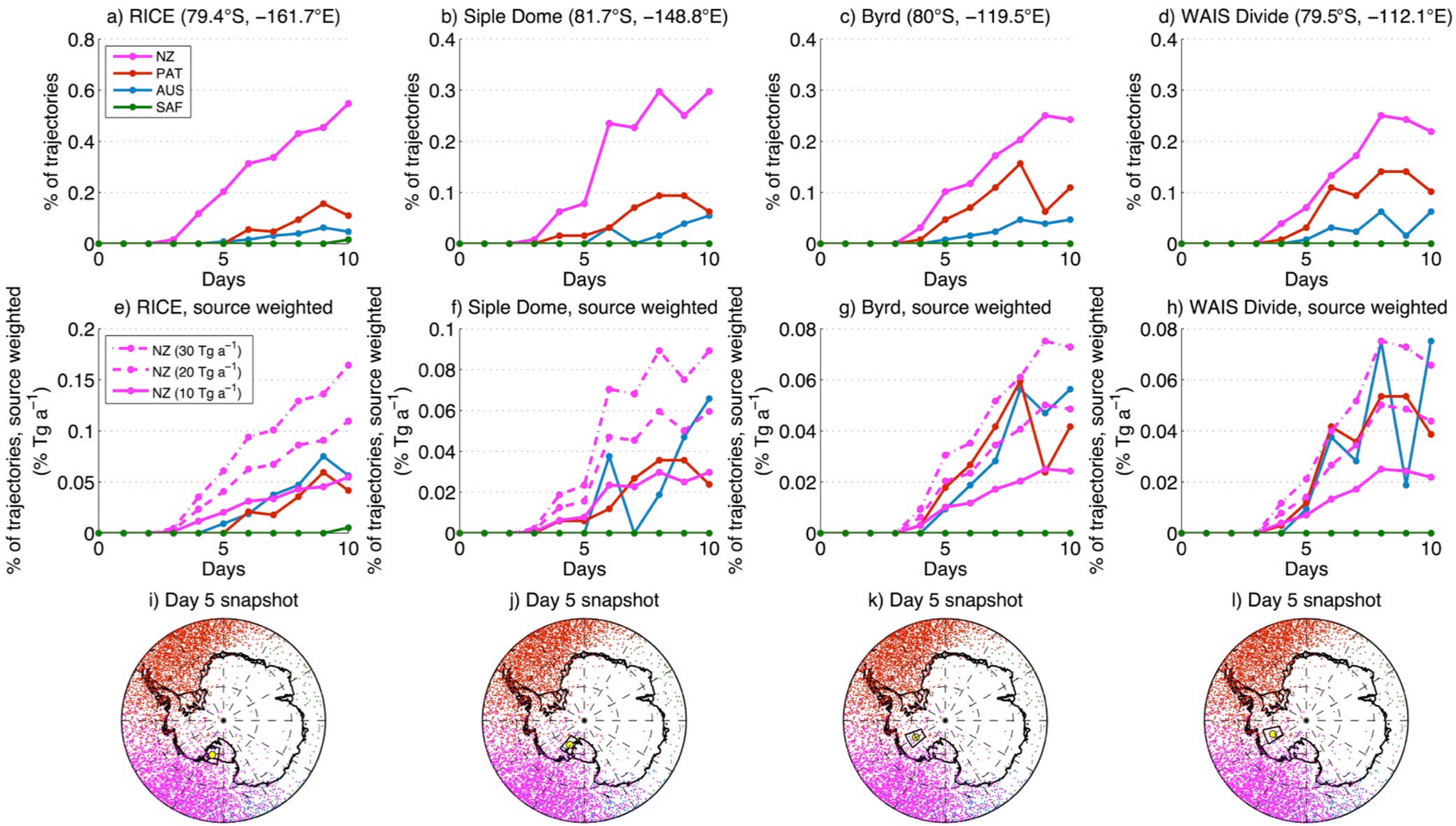

a) RICE (79.4°S, −161.7°E)
b) Siple Dome (81.7°S, −148.8°E)
c) Byrd (80°S, −119.5°E)
d) WAIS Divide (79.5°S, −112.1°E)
NZ
PAT
AUS
SAF
% of trajectories
Days
e) RICE, source weighted
f) Siple Dome, source weighted
g) Byrd, source weighted
h) WAIS Divide, source weighted
NZ (30 Tg a^{-1})
NZ (20 Tg a^{-1})
NZ (10 Tg a^{-1})
% of trajectories, source weighted (% Tg a^{-1})
i) Day 5 snapshot
j) Day 5 snapshot
k) Day 5 snapshot
l) Day 5 snapshot

Ice core sites on the Antarctic Peninsula and in the Weddell Sea sector of the WAIS (Figure 10) are dominated by PAT trajectories, with NZ nearing equal proportions only at Fletcher Promontory. James Ross Island is relatively close to PAT dust sources (~1,800 km), resulting in a strong dominance of PAT dust PSA trajectories which peak after three days of transport as trajectories pass over the site. Many PAT trajectories continue south, and Berkner Island shows highest PAT trajectory percentage after six to eight days but with approximately one tenth as many trajectories as the number traveling over the Antarctic Peninsula. A study of strontium/neodymium isotopes in snowpit samples at Berkner Island spanning the years 2002-2003 provided mixed provenance signatures, suggesting local Antarctic sources of dust in addition to PAT and AUS contributions [*Bory et al.*, 2010].

The trajectory results discussed here provide a unique framework for considering atmospheric transport from SH dust PSA likely contributing to SO and Antarctic dust distribution. As this approach is exclusive of deposition processes, we caution that our results represent an idealized maximum transport efficiency with respect to atmospheric dust and other aerosols originating at SH PSA. Despite this limitation, regional variations observed in trajectory distribution from individual dust PSA provide new insight into the possible spatial variability of dust provenance in Antarctica. This simple approach also highlights the competing roles of emission strength versus efficiency of atmospheric transport, the latter of which can also be investigated for dominant modes of variability associated with synoptic climate.

Figure 10. (Following page) *As in Figure 9 but for Fletcher Promontory (a, d, g), James Ross Island (b, e, h), and Berkner Island (c, f, i).*

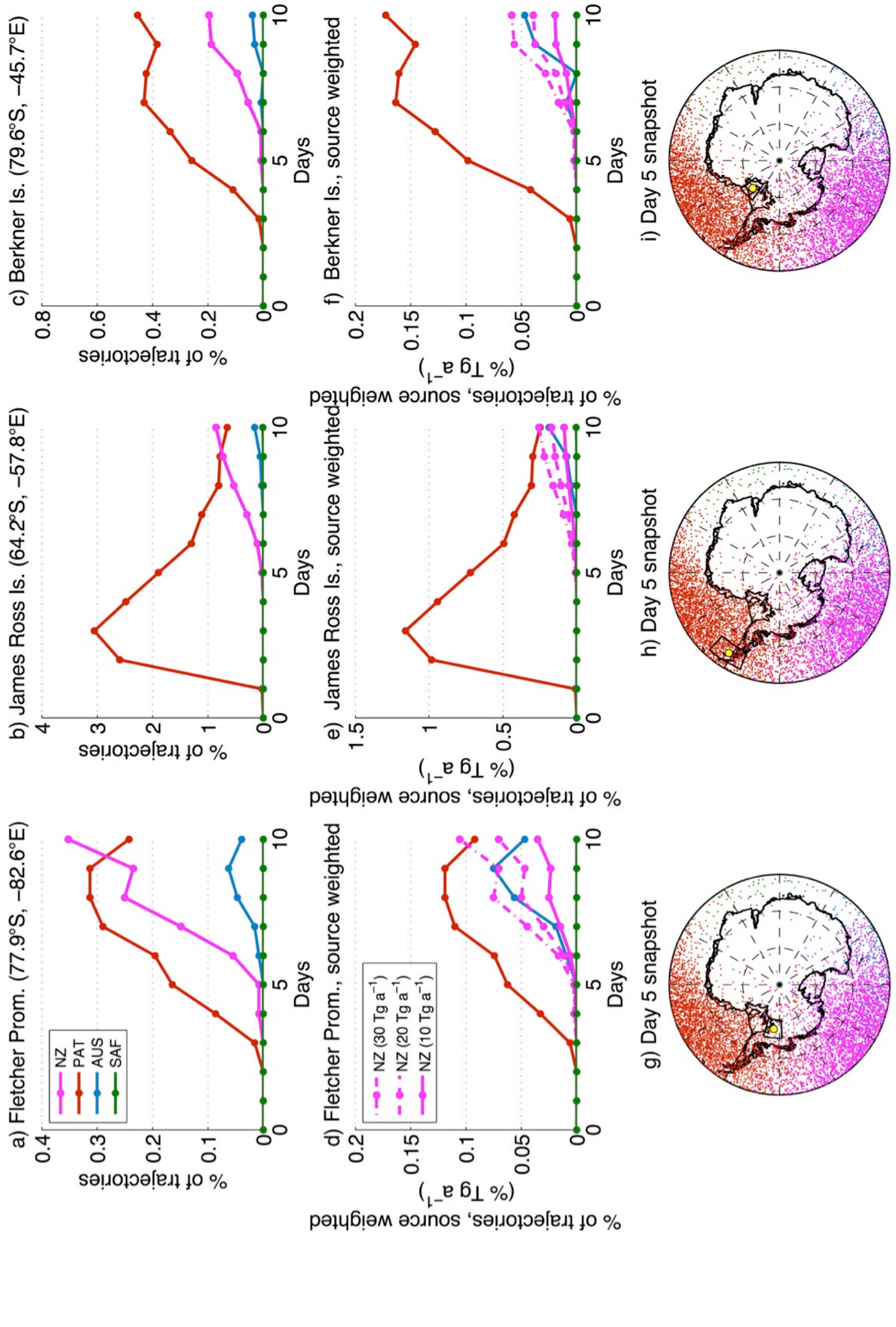

a) Fletcher Prom. (77.9°S, −82.6°E)
b) James Ross Is. (64.2°S, −57.8°E)
c) Berkner Is. (79.6°S, −45.7°E)
d) Fletcher Prom., source weighted
e) James Ross Is., source weighted
f) Berkner Is., source weighted
g) Day 5 snapshot
h) Day 5 snapshot
i) Day 5 snapshot
% of trajectories
% of trajectories, source weighted (% Tg a−1)
Days
NZ
PAT
AUS
SAF
NZ (30 Tg a−1)
NZ (20 Tg a−1)
NZ (10 Tg a−1)

2.4.4 Drivers of Interannual Transport Variability

Large dust sources in Patagonia and Australia, as well as transport-efficient New Zealand, are geographically situated on either side of the South Pacific Ocean basin. This suggests that regional atmospheric circulation—and hence transport of dust and other aerosols—should be moderated by well-known Pacific ocean-atmosphere dynamics. Variability in tropical Pacific sea-surface temperatures, commonly characterized by the El Niño-Southern Oscillation (ENSO), influences atmospheric circulation in the South Pacific with effects extending into Antarctica [*Bromwich et al.*, 2004; *Karoly*, 1989; *Turner*, 2004]. Sea-surface temperature anomalies in the central tropical Pacific Ocean—outside specific El Niño regions where strongest anomalies are observed—strongly affect deep convection associated with divergence high in the atmosphere [*Lachlan‐Cope and Connolley*, 2006]. Resultant atmospheric Rossby wave trains influence atmospheric circulation at mid- to high-latitudes in both hemispheres, characterized as the Pacific-North America and Pacific-South America modes (i.e. leading empirical orthogonal functions of 500 hPa height) [*Mo and Paegle*, 2001]. This relationship is demonstrated in Figure 11, annually and for three-month seasonal means, by regressing ERAi central tropical Pacific (CTP, 20ºN – 20ºS, 180º - 240ºE) sea-surface temperature (SST) against 500 hPa geopotential height. The same is done for CTP SST versus ERAi 10-meter zonal and meridional wind in Figures S4 and S5 to illustrate relationships directly with wind fields. The Pacific-South America pattern is seen in this way as anti-correlations between CTP SST and 500 hPa geopotential height across the SH mid-latitudes, and positive correlation over the Pacific SO. This relationship is statistically significant (>95% confidence) both for annual and seasonal correlations.

In the Pacific sector of the SO, specifically the Amundsen and Bellingshausen Seas, the additional impacts of both forced and possibly intrinsic variability in the Southern Annular Mode (SAM), a zonally-symmetric dipole in wind strength observed between the southern hemisphere mid- and high-latitudes, are intertwined with the meridional teleconnections initiated in the central tropical Pacific [*Ding et al.*, 2012; *Kidson*, 1988; *Thompson and Wallace*, 2000]. The *Marshall* [2003] SAM index (difference between observed zonal mean sea level pressures at 40ºS and 65ºS, http://www.antarctica.ac.uk/met/gjma/sam.html) is regressed against ERAi 500 hPa geopotential height in Figure S6 for reference. Climate in the Pacific SO is dominated by the Amundsen Sea Low (ASL, 60º - 75ºS, 170º - 290ºE), defined as in *Hosking et al.* [2013], an area of highly active transient synoptic- and smaller-scale low pressure systems which exerts strong control on the meridional component of atmospheric transport into West Antarctica and the Ross and Amundsen seas [*Hosking et al.*, 2013; *Hoskins and Hodges*, 2005; *Küttel et al.*, 2012; *Markle et al.*, 2012; *Nicolas and Bromwich*, 2011].

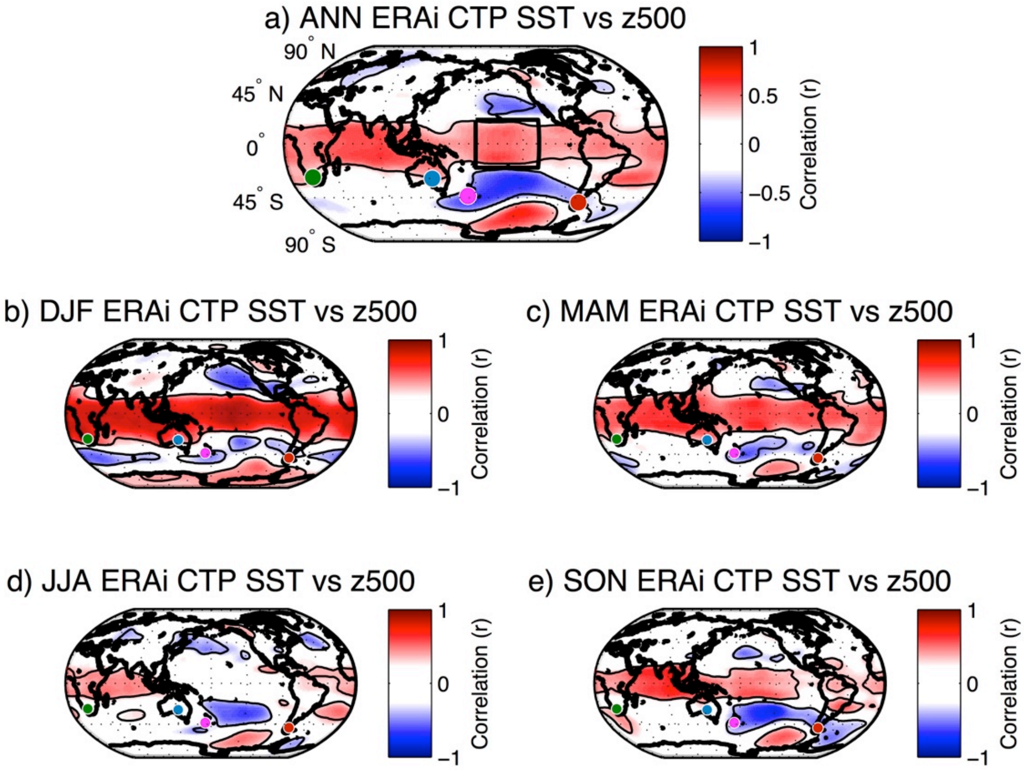

Figure 11. *Spatial correlation of 1979-2013 ERA-Interim reanalysis central tropical Pacific sea-surface temperature (CTP SST, 20ºN – 20ºS, 180ºE – 240ºE) versus 500 hPa geopotential height. Mean annual relationsip (ANN, a), December-January-February (DJF, b), March-April-May (MAM, c), June-July-August (JJA, d), and September-October-November (SON, e). Dust PSA are marked by colored circles, New Zealand (magenta), Patagonia (orange), southern Africa (green) and Australia (cyan). Black contour indicates >95% significance.*

With respect to atmospheric transport of terrestrial dust and other aerosols, the influences of tropical Pacific SST and SAM can be considered by comparison with the mean annual minimum latitude of five-day forward trajectories (i.e. only southward-moving trajectories, negative degrees latitude in the SH) from New Zealand, Patagonia and Australia. Detrending these 1979-2013 timeseries focuses investigation on natural interannual variability, removing decadal trends caused by additional dynamics (e.g. the impact of strengthening circumpolar westerly winds, which is outside the scope of this work). Typical interannual variability in mean annual five-day trajectory minimum latitudes for all PSA is one to two degrees latitude. When compared to the detrended annual and seasonal mean sea level pressure (MSLP) in the ASL region (ERAi data, collated by *Hosking et al. [2013]*, available at http://www.antarctica.ac.uk/data/absl/), statistically significant correlations are found between mean annual five-day minimum trajectory latitude from these three dust PSA and both CTP SST and ASL MSLP (Figure 12). Some limited, less significant relationships exist with the SAM and the latitudinal and longitudinal position of the ASL (as isolated by *Hosking et al.* [2013]). Full correlation statistics are displayed in Figure 13.

Southward trajectories from NZ correlate positively with ASL MSLP during December-January-February (DJF, austral summer), with $r = 0.40$ and $p < 0.05$ (Figure 12a, Figure 13). Southward trajectories from PAT are anti-correlated with ASL MSLP during September-October-November (SON, austral spring), $r = 0.41$, $p < 0.05$ (Figure 12b, Figure 13). Annual AUS southward trajectories do not show significant correlation with ASL MSLP directly, only weak positive correlation of low significance during austral autumn, March-April-May (MAM), $r = 0.28$, $p < 0.12$ (Figure 13). However, AUS southward trajectories are strongly positively correlated with CTP SST both annually and during austral autumn and winter, March-April-May (MAM) and June-July-August (JJA), with an annual correlation of $r = 0.43$ ($p < 0.01$), and seasonal correlations of $r = 0.51$ ($p < 0.01$) during MAM and $r = 0.35$ ($p < 0.05$) during JJA (Figure 12c, Figure 13). ERAi CTP SST (Figure 12d, dashed black) is strongly correlated with ASL MSLP in both ERAi ($r = 0.57$, $p < 0.001$, Figure 12d, solid black) and NCEP1 ($r = 0.55$, $p < 0.001$, Figure 12d, red). No statistically significant relationships are observed between SAF dust PSA southward trajectories and either CTP SST or ASL MSLP (Figure 13). The lack of correlations is perhaps not surprising as downwind areas over the Indian Ocean only show significant correlation between atmospheric circulation and CTP SST during DJF (Figure 11) and SAF trajectory distributions are far removed from the ASL region. However, some correlation between SAF trajectory southward latitude and the Marshall SAM index is observed during DJF and discussed below.

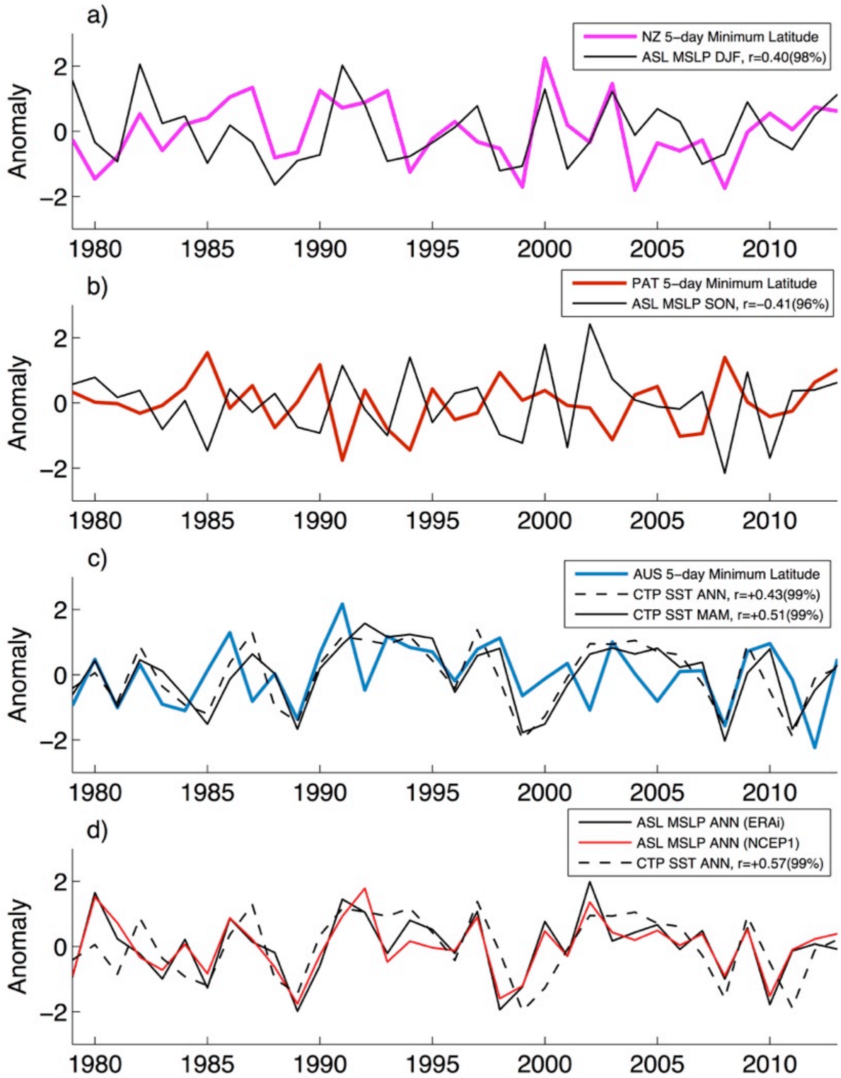

Figure 12. *Normalized timeseries of detrended 1979-2013 mean annual minimum latitude of 5-day forward trajectories, compared with detrended seasonal ERA-Interim Amundsen Sea Low (ASL) mean sea level pressure (MSLP, 60º – 75ºS , 170º – 290ºE; as in Hosking et al., 2013) and central tropical Pacific (20º – 20ºS, 180º – 240ºE) sea surface temperature (CTP SST). NZ versus DJF ASL MSLP (a), PAT versus SON ASL MSLP (b), AUS versus MAM and annual CTPSST (c) and ASL MSLP from both ERA-Interim and NCEP/NCAR reanalyses versus ERA-Interim CTP SST (d).*

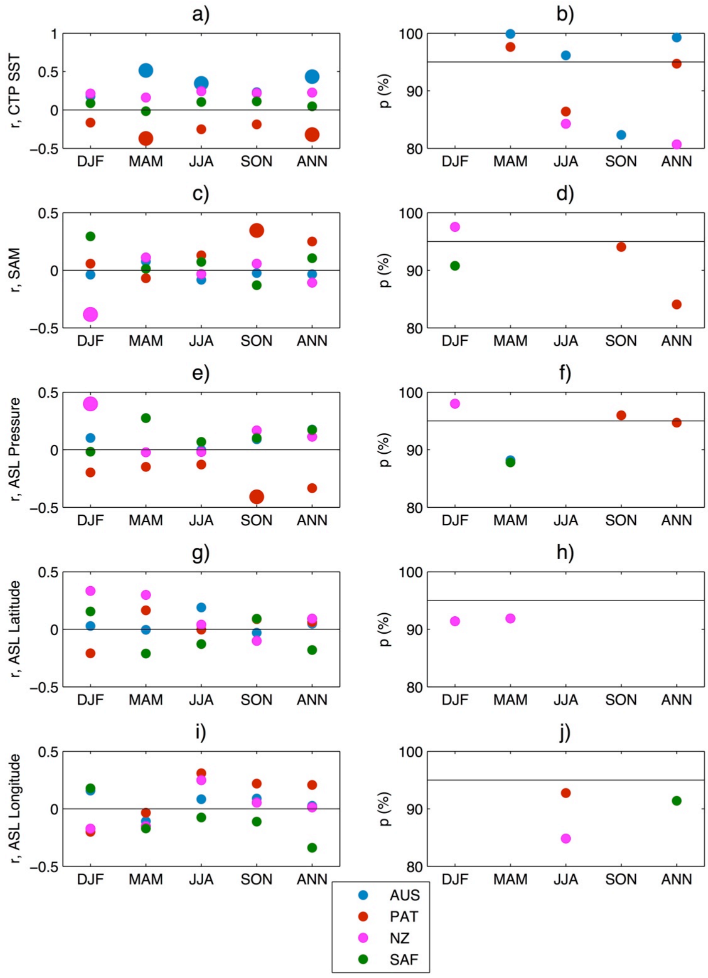

Figure 13. *Correlation statistics for annual 1979-2013 5-day trajectory minimum latitude (southward extent) versus annnual and seasonal averages of central tropical Pacific sea-surface temperature (CTP SST, a, b), the Marshall Southern Annular Mode index (SAM, c, d), and the Amundsen Sea Low (ASL) region mean sea level pressure (ASL Pressure, e, f), mean ASL latitude (ASL Latitude, g, h) and mean ASL longitude (ASL Longitude, i, j). Larger circles mark r values with high significance (~p < 0.05). ASL pressure and latitudinal and longitudinal position are taken from Hosking et al. [2013].*

For annual values, as well as during all seasons except DJF (Figure 11), tropical Pacific teleconnections in the SH are confined primarily to the South Pacific basin with some extension into the South Atlantic. During DJF there is a zonally-symmetric anti-correlation between CTP SST and mid-latitude SH circulation. This zonal symmetry is reminiscent of the SAM (Figure S6), which exhibits particularly significant relationships with CTP SST during DJF [*Ding et al.*, 2012; *L'Hereux and Thompson*, 2006]. This likely explains the positive correlation between NZ southward trajectories and ASL MSLP during DJF (lower

ASL MSLP, more southerly mean trajectory latitude, Figure 12). Indeed, NZ southward trajectories anti-correlate with the Marshall SAM index during DJF (1979-2012, $r = -0.38$, $p < 0.05$, Figure 13), with NZ trajectories extending further south in the positive SAM phase when the circumpolar westerly winds contract towards Antarctica. SAF southward trajectories also correlate with the SAM during DJF, although with low significance ($r = 0.29$, $p < 0.1$, Figure 13), indicating possible southward extension of SAF trajectories during SAM negative conditions when westerly winds reach further into the mid-latitudes.

During SON, southward trajectories from PAT are significantly anti-correlated with ASL MSLP (lower ASL MSLP, more northerly mean trajectory latitude, Figure 12, Figure 13). Tropical Pacific teleconnections are strong across the south Pacific basin during SON, and are particularly focused in the ASL region (Figure 11), which is one extreme of a regional dipole in the relationship between CTP SST and atmospheric circulation. Positive correlations between CTP SST and 500 hPa geopotential height in SON center over the ASL region (Figure 11e), with negative correlations to the East, over the Weddell Sea and Atlantic Southern Ocean (described as the Antarctic Oscillation with respect to its influence on sea-ice [*Renwick and Revell*, 1999; Yuan *and Martinson*, 2000]). This arrangement results in positive correlation between CTP SST and northward meridional winds in the region between this dipole (Figure S5), from the Bellingshausen Sea east across the Antarctic Peninsula to the western Weddell Sea, suggesting that southward transport of PAT trajectories in this region weakens during warm CTP SST conditions. PAT southward trajectory extent also positively correlates with the Marshall SAM index during SON, with significance slightly below 95%: $r = 0.35$, $p < 0.06$ (Figure 13). This suggests that PAT trajectories reach further south during negative SAM conditions, when circumpolar westerlies expand further into the mid-latitudes.

Southward transport of AUS trajectories is positively correlated with CTP SST as an annual average, strongly positively correlated during austral autumn (MAM), and shows additional correlation in winter (JJA, Figure 12c, Figure 13). We argue that the weak positive correlation between AUS southward trajectories and ASL MSLP during MAM is consistent with the relationship between CTP SST and ASL circulation (i.e. wave train seen in correlation between CTP SST and atmospheric circulation over both Australia and the ASL region, Figure 11c). The correlation with CTP SST likely reflects the large role that tropical variability plays in atmospheric circulation over Australia, seen in strong positive correlations with 500 hPa geopotential height over the continent (Figure 11).

These relationships between southward dust PSA trajectory extent and both tropical and high-latitude climate variability suggest that variability in atmospheric transport with respect to dust should be carefully considered in future model experiments. Additionally, these results can inform hypotheses with respect to past changes in dust transport, and thus atmospheric circulation, developed from ice core proxy records. For instance, *Koffman et al.* [2014] suggest poleward contraction of the circumpolar westerly winds from 1050 to 1400 Common Era (CE), based on a dust particle size record developed from the WAIS Divide ice core which demonstrates correlation with cyclonic activity in the ASL region. Although independent of deposition processes, our trajectory results suggest a possible mechanism explaining such a change in southward dust transport, and hence changing particle size observed in ice core records, with links to both tropical and high-latitude climate variability. This process warrants further study.

2.5 Conclusions

The dust flux to Antarctica and the SO is dependent on both the strength of the dust source and the competing mechanisms of transport and deposition. Here we focus strictly on the atmospheric transport component and investigate drivers behind observed spatial and temporal variability of SH dust distribution. Examination of modern atmospheric transport from four SH dust PSA to areas of the SO and Antarctica, based on thirty-five years of daily HySPLIT forward trajectories, highlights important features of modern atmospheric transport. Transport from both Patagonian and New Zealand dust sources to the southern high-latitudes is highly efficient with >40% of trajectories passing over the SO within the first four days of transport, and >8% of trajectories arriving in Antarctica after eight days. Transport from lower-latitude sources in Australia and southern Africa is both less efficient and slower: <20% of trajectories from these PSA move over the SO and a maximum of ~2% arrive in Antarctica within ten days.

Poorly-quantified glaciogenic dust emissions from New Zealand, which were especially active during the LGM, are thus strongly connected to the southern high-latitudes and may play a significant role in fertilization of the SO and uptake of carbon on glacial-interglacial timescales. Linear dust-emission weighting of PSA trajectories provides estimates of SH dust deposition which compare well with independent estimates. This approach suggests that even with very modest dust emissions of 10 Tg a^{-1}, New Zealand may comprise 8.5% of dust from SH sources distributed over the SO, and 13.7% of dust transported to Antarctica. Efforts should be made to better quantify New Zealand and other glaciogenic dust contributions to atmospheric dust loading and deposition across the SH.

Regional contributions from dust PSA are remarkably distinct over the SO and at individual Antarctic ice core sites. The Pacific SO is dominated by New Zealand and Australian airmasses, while the Atlantic and Indian Ocean sectors of the SO are largely dominated by Patagonian trajectories with southern Africa playing a more limited role. Remote East Antarctic ice core sites show variable source contributions, with Patagonian trajectories playing a larger role nearer the Atlantic sector (EDML), limited and highly mixed contributions across the interior plateau of East Antarctica (Dome F, Vostok, South Pole, Taylor Dome), and Australian trajectories becoming more common in Wilkes and Victoria Land (EDC, Law Dome, Talos Dome). Trajectory distribution over West Antarctica is divided between dominance of the highly-efficient transport from New Zealand and Patagonia, followed by Australian trajectories. Considerable New Zealand contributions span the Ross Ice Shelf and Marie Byrd Land (RICE, Siple Dome, Byrd, WAIS Divide) while clear prevalence of Patagonian trajectories exists over Ellsworth Land, the Antarctic Peninsula and the Weddell Sea (Fletcher Promontory, James Ross Island, Berkner Island).

With respect to the RICE ice core from Roosevelt Island, an ice rise at the northern margin of the Ross Ice Shelf, direct transport from New Zealand is as much as five-times more efficient than transport from any other SH mid-latitude continental source of dust or other aerosol emissions. Source-weighted dust PSA trajectory contributions from Australia and Patagonia are essentially equal at RICE, suggesting that geochemical dust provenance studies undertaken on this core should expect mixed contributions from these large dust sources with some material supplied from yet unquantified New Zealand dust emissions. Dust emissions from Antarctic ice-free areas such as the McMurdo Dry Valleys are not accounted for here. While emissions from these sites are orders of magnitude lower than extra-Antarctic dust sources, transport distances are much shorter and may allow for local ice-free areas to supply significant amounts of dust to ice core sites [*Dunbar et al.*, 2009; *Rhodes et al.*, 2012; *Winton et al.*, 2014].

Finally, we find that the southward extension of trajectories from dust PSA fluctuates in association with both low- and high-latitude climate variability. To understand dust records preserved in ice cores or to quantify the potential near-future influence on the carbon cycle via the biological pump, it is important to identify contributing dust sources, transport pathways and deposition processes to take into account their sensitivity to particular climate drivers. Strengthening of the circumpolar westerly winds (trend towards positive SAM) has been observed in recent decades, likely forced by anthropogenic changes in atmospheric ozone and greenhouse gas concentrations [*Arblaster and Meehl*, 2006; *Thompson and Solomon*, 2002]. Concomitant tropical warming will combine to alter high-latitude SH circulation [*Bracegirdle et al.*, 2008; *Timmermann et al.*, 1999], with impacts on dust transport to the SO and Antarctica that may affect the global carbon cycle. In addition to providing a mechanism possibly responsible for past dust particle size changes in Antarctic ice cores, this finding may also aid in anticipating future changes in high-latitude SH circulation and dust distribution over the SO.

Our analysis suggests that a strengthening of the ASL leads to southward extension of New Zealand trajectories during austral summer—when sea ice is reduced and phytoplankton blooms occur—while Patagonian trajectories remain further north when the ASL is strong during austral spring, reducing the transport efficiency of dust to the Atlantic sector of the SO at this time. Moreover, it is well known that the strength of the ASL is coupled with central tropical Pacific SST, promoting a deeper low (decreased pressure) during periods of cooler tropical SST. Southward extent of trajectories originating from Australia are positively correlated with central tropical Pacific SST, with cooler tropical SST and a deepening ASL coinciding with enhanced southward trajectories. This suggests that atmospheric transport affecting dust deposition in three known areas of Antarctic Bottom Water formation (Ross Sea, Weddell Sea, and Mertz Polynya, *Orsi et al.* [1999]) may be sensitive to distinct dust sources and potentially experience independent fluctuations in dust transport and deposition.

Acknowledgements

PSA trajectory datasets are available from the corresponding author upon request. The authors appreciate free access to software and data: HySPLIT software was retrieved from the NOAA Air Resources Laboratory (http://ready.arl.noaa.gov/HYSPLIT.php), NCEP1 data were downloaded from the NOAA Earth System Research Laboratory – Physical Sciences Division (http://www.esrl.noaa.gov/psd/data/gridded/data.ncep.reanalysis.html), and ERAi data from the ECMWF (http://apps.ecmwf.int/datasets/data/interim_full_daily/). We thank E. Steig and P. Vallelonga for fruitful discussion of the manuscript. This work is a contribution to the Roosevelt Island Climate Evolution (RICE) Programme, funded by national contributions from New Zealand, Australia, Denmark, Germany, Italy, the People's Republic of China, Sweden, United Kingdom, and the United States of America. P.D.N and N.A.N.B were funded by the New Zealand Ministry of Business, Innovation, and Employment Grants through Victoria University of Wellington (RDF-VUW-1103) and GNS Science (540GCT32).

2.6 References

Adams, J. (1980), Contemporary uplift and erosion of the Southern Alps, New Zealand, *Geological Society of America Bulletin*, *91*(1 Part II), 1-114, doi:10.1130/GSAB-P2-91-1.

Albani, S., N. M. Mahowald, B. Delmonte, V. Maggi, and G. Winckler (2012), Comparing modeled and observed changes in mineral dust transport and deposition to Antarctica between the Last Glacial Maximum and current climates, *Climate dynamics*, *38*(9-10), 1731-1755, doi:10.1007/s00382-011-1139-5.

Alloway, B. V., D. J. Lowe, D. J. Barrell, R. M. Newnham, P. C. Almond, P. C. Augustinus, N. A. Bertler, L. Carter, N. J. Litchfield, and M. S. McGlone (2007), Towards a climate event stratigraphy for New Zealand over the past 30 000 years (NZ ‐ INTIMATE project), *Journal of Quaternary Science*, *22*(1), 9-35, doi:10.1002/jqs.1079.

Arblaster, J. M., and G. A. Meehl (2006), Contributions of external forcings to southern annular mode trends, *Journal of climate*, *19*(12), 2896-2905, doi:10.1175/JCLI3774.1.

Basile, I., F. E. Grousset, M. Revel, J. R. Petit, P. E. Biscaye, and N. I. Barkov (1997), Patagonian origin of glacial dust deposited in East Antarctica (Vostok and Dome C) during glacial stages 2, 4 and 6, *Earth and Planetary Science Letters*, *146*(3), 573-589, doi: doi:10.1016/S0012-821X(96)00255-5.

Bertler, N., P. Mayewski, and L. Carter (2011), Cold conditions in Antarctica during the Little Ice Age—Implications for abrupt climate change mechanisms, *Earth and Planetary Science Letters*, *308*(1), 41-51, doi:10.1016/j.epsl.2011.05.021.

Bertler, N., P. A. Mayewski, A. Aristarain, P. Barrett, S. Becagli, R. T. Bernardo, X. Cunde, M. Curran, Q. Dahe, and D. Dixon (2005), Snow Chemistry Across Antarctica, *Annals of Glaciology*, *41*, 167, doi:10.3189/172756405781813320.

Betzer, P., K. Carder, R. Duce, J. Merrill, N. Tindale, M. Uematsu, D. Costello, R. Young, R. Feely, and J. Breland (1988), Long–range transport of giant mineral aerosol particles, *Nature*, *336*, 568-571, doi:10.1038/336568a0.

Bory, A., E. Wolff, R. Mulvaney, E. Jagoutz, A. Wegner, U. Ruth, and H. Elderfield (2010), Multiple sources supply eolian mineral dust to the Atlantic sector of coastal Antarctica: Evidence from recent snow layers at the top of Berkner Island ice sheet, *Earth and Planetary Science Letters*, *291*(1), 138-148, doi:10.1016/j.epsl.2010.01.006.

Bowler, J. (1976), Aridity in Australia: age, origins and expression in aeolian landforms and sediments, *Earth-Science Reviews*, *12*(2), 279-310, doi:Bowler, J. (1976). "Aridity in Australia: age, origins and expression in aeolian landforms and sediments." Earth-Science Reviews 12(2): 279-310.

Bracegirdle, T. J. (2013), Climatology and recent increase of westerly winds over the Amundsen Sea derived from six reanalyses, *International Journal of Climatology*, *33*(4), 843-851, doi:10.1002/joc.3473.

Bracegirdle, T. J., W. M. Connolley, and J. Turner (2008), Antarctic climate change over the twenty first century, *Journal of Geophysical Research: Atmospheres (1984–2012)*, *113*(D3), doi:10.1029/2007JD008933.

Bromwich, D. H., and R. L. Fogt (2004), Strong Trends in the Skill of the ERA-40 and NCEP-NCAR Reanalyses in the High and Midlatitudes of the Southern Hemisphere, 1958-2001*, *Journal of Climate*, *17*(23), 4603-4619, doi:10.1175/3241.1.

Bromwich, D. H., R. L. Fogt, K. I. Hodges, and J. E. Walsh (2007), A tropospheric assessment of the ERA‐40, NCEP, and JRA‐25 global reanalyses in the polar regions, *Journal of Geophysical Research: Atmospheres (1984‐2012)*, *112*(D10), doi:10.1029/2006JD007859.

Bromwich, D. H., A. J. Monaghan, and Z. Guo (2004), Modeling the ENSO Modulation of Antarctic Climate in the Late 1990s with the Polar MM5*, *Journal of climate*, *17*(1), 109-132, doi:10.1175/1520-0442(2004)017<0109:MTEMOA>2.0.CO;2.

Bullard, J. E. (2013), Contemporary glacigenic inputs to the dust cycle, *Earth Surface Processes and Landforms*, *38*(1), 71-89, doi:10.1002/esp.3315.

Carter, L., H. Neil, and I. McCave (2000), Glacial to interglacial changes in non-carbonate and carbonate accumulation in the SW Pacific Ocean, New Zealand, *Palaeogeography, Palaeoclimatology, Palaeoecology*, *162*(3), 333-356, doi:10.1016/S0031-0182(00)00137-1.

Creamean, J. M., J. R. Spackman, S. M. Davis, and A. B. White (2014), Climatology of long‐range transported Asian dust along the West Coast of the United States, *Journal of Geophysical Research: Atmospheres*, *119*(21), 12,171-112,185, doi:10.1002/2014JD021694.

De Deckker, P., M. Norman, I. D. Goodwin, A. Wain, and F. X. Gingele (2010), Lead isotopic evidence for an Australian source of aeolian dust to Antarctica at times over the last 170,000 years, *Palaeogeography, Palaeoclimatology, Palaeoecology*, *285*(3), 205-223, doi:10.1016/j.palaeo.2009.11.013.

Dee, D., S. Uppala, A. Simmons, P. Berrisford, P. Poli, S. Kobayashi, U. Andrae, M. Balmaseda, G. Balsamo, and P. Bauer (2011), The ERA‐Interim reanalysis: Configuration and performance of the data assimilation system, *Quarterly Journal of the Royal Meteorological Society*, *137*(656), 553-597, doi:10.1002/qj.828.

Delmonte, B., P. Andersson, M. Hansson, H. Schöberg, J. R. Petit, I. Basile‐Doelsch, and V. Maggi (2008), Aeolian dust in East Antarctica (EPICA‐Dome C and Vostok): Provenance during glacial ages over the last 800 kyr, *Geophysical Research Letters*, *35*(7), doi:10.1029/2008GL033382.

Delmonte, B., C. Baroni, P. S. Andersson, H. Schoberg, M. Hansson, S. Aciego, J. R. Petit, S. Albani, C. Mazzola, and V. Maggi (2010), Aeolian dust in the Talos Dome ice core (East Antarctica, Pacific/Ross Sea sector): Victoria Land versus remote sources over the last two climate cycles, *Journal of Quaternary Science*, *25*(8), 1327-1337, doi:10.1002/jqs.1418.

Delmonte, B., I. Basile-Doelsch, J.-R. Petit, V. Maggi, M. Revel-Rolland, A. Michard, E. Jagoutz, and F. Grousset (2004a), Comparing the Epica and Vostok dust records during the last 220,000 years: stratigraphical correlation and provenance in glacial periods, *Earth-Science Reviews*, *66*(1), 63-87, doi:10.1016/j.earscirev.2003.10.004.

Delmonte, B., J. Petit, K. K. Andersen, I. Basile-Doelsch, V. Maggi, and V. Y. Lipenkov (2004b), Dust size evidence for opposite regional atmospheric circulation changes over east Antarctica during the last climatic transition, *Climate Dynamics*, *23*(3-4), 427-438, doi:10.1007/s00382-004-0450-9.

Ding, Q., E. J. Steig, D. S. Battisti, and J. M. Wallace (2012), Influence of the tropics on the Southern Annular Mode, *Journal of Climate*, *25*(18), 6330-6348, doi:10.1175/JCLI-D-11-00523.1.

Draxler, R. R., and G. Hess (1998), An overview of the HYSPLIT_4 modelling system for trajectories, *Australian Meteorological Magazine*, *47*(4), 295-308.

Dunbar, G., N. Bertler, and R. McKay (2009), Sediment flux through the McMurdo Ice Shelf in Windless Bight, Antarctica, *Global and Planetary Change*, *69*(3), 87-93, doi:10.1016/j.gloplacha.2009.05.007.

Eden, D. N., and A. P. Hammond (2003), Dust accumulation in the New Zealand region since the last glacial maximum, *Quaternary Science Reviews*, *22*(18), 2037-2052, doi:10.1016/S0277-3791(03)00168-9.

Freidenreich, S. M., S. T. Garner, R. G. Gudgel, C. Gordon, and I. M. Held (2004), The new GFDL global atmosphere and land model AM2–LM2: Evaluation with prescribed SST simulations, *Journal of Climate*, *17*(24), 4641-4673, doi:10.1175/JCLI-3223.1.

Gabrielli, P., A. Wegner, J. R. Petit, B. Delmonte, P. De Deckker, V. Gaspari, H. Fischer, U. Ruth, M. Kriews, and C. Boutron (2010), A major glacial-interglacial change in aeolian dust composition inferred from Rare Earth Elements in Antarctic ice, *Quaternary Science Reviews*, *29*(1), 265-273, doi:10.1016/j.quascirev.2009.09.002.

Gaiero, D. M. (2007), Dust provenance in Antarctic ice during glacial periods: From where in southern South America?, *Geophysical Research Letters*, *34*(17), doi:10.1029/2007GL030520.

Gassó, S., and A. F. Stein (2007), Does dust from Patagonia reach the sub‐Antarctic Atlantic Ocean?, *Geophysical Research Letters*, *34*(1), doi:10.1029/2006GL027693.

Ginoux, P., J. M. Prospero, T. E. Gill, N. C. Hsu, and M. Zhao (2012), Global‐scale attribution of anthropogenic and natural dust sources and their emission rates based on MODIS Deep Blue aerosol products, *Reviews of Geophysics*, *50*(3), doi:10.1029/2012RG000388.

Hallet, B., L. Hunter, and J. Bogen (1996), Rates of erosion and sediment evacuation by glaciers: a review of field data and their implications, *Global and Planetary Change*, *12*(1), 213-235, doi:10.1016/0921-8181(95)00021-6.

Hosking, J. S., A. Orr, G. J. Marshall, J. Turner, and T. Phillips (2013), The influence of the Amundsen–Bellingshausen Seas low on the climate of West Antarctica and its representation in coupled climate model simulations, *Journal of Climate*, *26*(17), 6633-6648, doi:10.1175/JCLI-D-12-00813.1.

Hoskins, B. J., and K. I. Hodges (2005), A new perspective on Southern Hemisphere storm tracks, *Journal of Climate*, *18*(20), 4108-4129, doi:10.1175/JCLI3570.1.

Kalnay, E., M. Kanamitsu, R. Kistler, W. Collins, D. Deaven, L. Gandin, M. Iredell, S. Saha, G. White, and J. Woollen (1996), The NCEP/NCAR 40-year reanalysis project, *Bulletin of the American meteorological Society*, *77*(3), 437-471, doi:10.1175/1520-0477(1996)077<0437:TNYRP>2.0.CO;2.

Karoly, D. J. (1989), Southern hemisphere circulation features associated with El Niño-Southern Oscillation events, *Journal of Climate*, *2*(11), 1239-1252, doi:10.1175/1520-0442(1989)002<1239:SHCFAW>2.0.CO;2.

Kidson, J. W. (1988), Indices of the Southern Hemisphere zonal wind, *Journal of Climate*, *1*(2), 183-194, doi:10.1175/1520-0442(1988)001<0183:IOTSHZ>2.0.CO;2.

Koffman, B., K. Kreutz, D. Breton, E. Kane, D. Winski, S. Birkel, A. Kurbatov, and M. Handley (2014), Centennial-scale variability of the Southern Hemisphere westerly wind belt in the eastern Pacific over the past two millennia, *Climate of the Past*, *10*(3), 1125-1144, doi:10.5194/cp-10-1125-2014.

Koons, P. (1990), Two-sided orogen: collision and erosion from the sandbox to the Southern Alps, New Zealand, *Geology*, *18*(8), 679-682, doi:10.1130/0091-7613(1990) 018<0679:TSOCAE>2.3.CO;2

Küttel, M., E. J. Steig, Q. Ding, A. J. Monaghan, and D. S. Battisti (2012), Seasonal climate information preserved in West Antarctic ice core water isotopes: Relationships to temperature, large-scale circulation, and sea ice, *Climate Dynamics*, *39*(7-8), 1841-1857, doi:10.1007/s00382-012-1460-7.

Lachlan ‐ Cope, T., and W. Connolley (2006), Teleconnections between the tropical Pacific and the Amundsen ‐ Bellinghausens Sea: Role of the El Niño/Southern Oscillation, *Journal of Geophysical Research: Atmospheres (1984–2012)*, *111*(D23), doi:10.1029/2005JD006386.

Lamy, F., R. Gersonde, G. Winckler, O. Esper, A. Jaeschke, G. Kuhn, J. Ullermann, A. Martínez-Garcia, F. Lambert, and R. Kilian (2014), Increased dust deposition in the Pacific

Southern Ocean during glacial periods, *Science*, *343*(6169), 403-407, doi:10.1126/science.1245424.

L'Heureux, M. L. and D. W. Thompson (2006), Observed relationships between the El Niño-Southern Oscillation and the extratropical zonal-mean circulation, *Journal of Climate*, **19**(2), 276-287.

Li, F., P. Ginoux, and V. Ramaswamy (2008), Distribution, transport, and deposition of mineral dust in the Southern Ocean and Antarctica: Contribution of major sources, *Journal of Geophysical Research: Atmospheres (1984–2012)*, *113*(D10), doi:10.1029/2007JD009190.

Li, F., P. Ginoux, and V. Ramaswamy (2010), Transport of Patagonian dust to Antarctica, *Journal of Geophysical Research: Atmospheres (1984–2012)*, *115*(D18), doi:10.1029/2009JD012356.

Lunt, D. J., and P. J. Valdes (2001), Dust transport to Dome C, Antarctica, at the Last Glacial Maximum and present day, *Geophysical research letters*, *28*(2), 295-298, doi:10.1029/2000GL012170.

Luo, C., N. M. Mahowald, and J. Del Corral (2003), Sensitivity study of meteorological parameters on mineral aerosol mobilization, transport, and distribution, *Journal of Geophysical Research: Atmospheres (1984–2012)*, *108*(D15), doi:10.1029/2003JD003483.

Maher, B., J. Prospero, D. Mackie, D. Gaiero, P. Hesse, and Y. Balkanski (2010), Global connections between aeolian dust, climate and ocean biogeochemistry at the present day and at the last glacial maximum, *Earth-Science Reviews*, *99*(1), 61-97, doi:10.1016/j.earscirev.2009.12.001.

Mahowald, N., S. Engelstaedter, C. Luo, A. Sealy, P. Artaxo, C. Benitez-Nelson, S. Bonnet, Y. Chen, P. Y. Chuang, and D. D. Cohen (2009), Atmospheric iron deposition: Global distribution, variability, and human perturbations*, *Marine Science*, *1*, 245-278, doi:10.1146/annurev.marine.010908.163727.

Mahowald, N., K. Kohfeld, M. Hansson, Y. Balkanski, S. P. Harrison, I. C. Prentice, M. Schulz, and H. Rodhe (1999), Dust sources and deposition during the last glacial maximum and current climate: A comparison of model results with paleodata from ice cores and marine sediments, *Journal of Geophysical Research: Atmospheres (1984–2012)*, *104*(D13), 15895-15916, doi:10.1029/1999JD900084.

Markle, B., N. Bertler, K. Sinclair, and S. Sneed (2012), Synoptic variability in the Ross Sea region, Antarctica, as seen from back ‐ trajectory modeling and ice core analysis, *Journal of Geophysical Research: Atmospheres (1984‐2012)*, *117*(D2), doi:10.1029/2011JD016437.

Marshall, G. J. (2003), Trends in the Southern Annular Mode from observations and reanalyses, *Journal of Climate*, *16*(24), 4134-4143, doi:10.1175/1520-0442(2003)016<4134:TITSAM>2.0.CO;2.

Martin, J. H., R. M. Gordon, and S. E. Fitzwater (1990), Iron in Antarctic waters, *Nature*, *345*, 156-158.

Martínez-Garcia, A., A. Rosell-Melé, S. L. Jaccard, W. Geibert, D. M. Sigman, and G. H. Haug (2011), Southern Ocean dust-climate coupling over the past four million years, *Nature*, *476*(7360), 312-315, doi:10.1038/nature10310.

McGowan, H. A., and A. Clark (2008), Identification of dust transport pathways from Lake Eyre, Australia using Hysplit, *Atmospheric Environment*, *42*(29), 6915-6925, doi:10.1016/j.atmosenv.2008.05.053.

McGowan, H. A., A. P. Sturman, and I. F. Owens (1996), Aeolian dust transport and deposition by foehn winds in an alpine environment, Lake Tekapo, New Zealand, *Geomorphology*, *15*(2), 135-146, doi:10.1016/0169-555X(95)00123-M.

Miller, R., and I. Tegen (1998), Climate response to soil dust aerosols, *Journal of climate*, *11*(12), 3247-3267, doi:10.1175/1520-0442(1998)011<3247:CRTSDA>2.0.CO;2.

Miller, R., I. Tegen, and J. Perlwitz (2004), Surface radiative forcing by soil dust aerosols and the hydrologic cycle, *Journal of Geophysical Research: Atmospheres (1984–2012)*, *109*(D4), doi:10.1029/2003JD004085.

Mo, K. C., and J. N. Paegle (2001), The Pacific–South American modes and their downstream effects, *International Journal of Climatology*, *21*(10), 1211-1229, doi:10.1002/joc.685.

Nicolas, J. P., and D. H. Bromwich (2011), Climate of West Antarctica and influence of marine air intrusions*, *Journal of Climate*, *24*(1), 49-67, doi:10.1175/2010JCLI3522.1.

Orsi, A., G. Johnson, and J. Bullister (1999), Circulation, mixing, and production of Antarctic Bottom Water, *Progress in Oceanography*, *43*(1), 55-109, doi:10.1016/S0079-6611(99)00004-X.

Petit, J.-R., J. Jouzel, D. Raynaud, N. I. Barkov, J.-M. Barnola, I. Basile, M. Bender, J. Chappellaz, M. Davis, and G. Delaygue (1999), Climate and atmospheric history of the past 420,000 years from the Vostok ice core, Antarctica, *Nature*, *399*(6735), 429-436, doi:10.1038/20859.

Renwick, J. A. (2004), Trends in the Southern Hemisphere polar vortex in NCEP and ECMWF reanalyses, *Geophysical Research Letters*, *31*(7), L07209, doi:10.1029/2003GL019302.

Renwick, J. A. and M. J. Revell (1999), Blocking over the South Pacific and Rossby wave propagation, *Monthly Weather Review*, **127**(10), 2233-2247.

Revel-Rolland, M., P. De Deckker, B. Delmonte, P. Hesse, J. Magee, I. Basile-Doelsch, F. Grousset, and D. Bosch (2006), Eastern Australia: a possible source of dust in East Antarctica interglacial ice, *Earth and Planetary Science Letters*, *249*(1), 1-13, doi:10.1016/j.epsl.2006.06.028.

Rhodes, R., N. Bertler, J. Baker, H. C. Steen-Larsen, S. Sneed, U. Morgenstern, and S. J. Johnsen (2012), Little Ice Age climate and oceanic conditions of the Ross Sea, Antarctica from a coastal ice core record, *Climate of the Past*, *8*(4), 1223-1238, doi:10.5194/cp-8-1223-2012.

Sugden, D. E., R. D. McCulloch, A. J.-M. Bory, and A. S. Hein (2009), Influence of Patagonian glaciers on Antarctic dust deposition during the last glacial period, *Nature Geoscience*, *2*(4), 281-285, doi:10.1038/NGEO474.

Tanaka, T. Y., and M. Chiba (2006), A numerical study of the contributions of dust source regions to the global dust budget, *Global and Planetary Change*, *52*(1), 88-104, doi:10.1016/j.gloplacha.2006.02.002.

Tegen, I., and I. Fung (1994), Modeling of mineral dust in the atmosphere: Sources, transport, and optical thickness, *Journal of Geophysical Research: Atmospheres (1984–2012)*, *99*(D11), 22897-22914.

Thompson, D. W., and S. Solomon (2002), Interpretation of recent Southern Hemisphere climate change, *Science*, *296*(5569), 895-899, doi:10.1126/science.1069270.

Thompson, D. W., and J. M. Wallace (2000), Annular modes in the extratropical circulation. Part I: month-to-month variability*, *Journal of Climate*, *13*(5), 1000-1016, doi:10.1175/1520-0442(2000)013<1000:AMITEC>2.0.CO;2.

Timmermann, A., J. Oberhuber, A. Bacher, M. Esch, M. Latif, and E. Roeckner (1999), Increased El Niño frequency in a climate model forced by future greenhouse warming, *Nature*, *398*(6729), 694-697, doi:10.1038/19505.

Torres, O., P. Bhartia, J. Herman, A. Sinyuk, P. Ginoux, and B. Holben (2002), A long-term record of aerosol optical depth from TOMS observations and comparison to AERONET measurements, *Journal of the atmospheric sciences*, *59*(3), 398-413, doi:10.1175/1520-0469(2002)059<0398:ALTROA>2.0.CO;2.

Turner, J. (2004), The El Niño–Southern Oscillation and Antarctica, *International Journal of Climatology*, *24*(1), 1-31, doi:10.1002/joc.965.

Uno, I., K. Eguchi, K. Yumimoto, T. Takemura, A. Shimizu, M. Uematsu, Z. Liu, Z. Wang, Y. Hara, and N. Sugimoto (2009), Asian dust transported one full circuit around the globe, *Nature Geoscience*, *2*(8), 557-560, doi:10.1038/ngeo583.

Vallelonga, P. (2015), the enigma of dust provenance: where else does Antarctic dust come from?, *DUST*, *24*, 74.

Vallelonga, P., P. Gabrielli, E. Balliana, A. Wegner, B. Delmonte, C. Turetta, G. Burton, F. Vanhaecke, K. Rosman, and S. Hong (2010), Lead isotopic compositions in the EPICA Dome C ice core and Southern Hemisphere Potential Source Areas, *Quaternary Science Reviews*, *29*(1), 247-255, doi:10.1016/j.quascirev.2009.06.019.

Vallelonga, P., P. Gabrielli, K. Rosman, C. Barbante, and C. Boutron (2005), A 220 kyr record of Pb isotopes at Dome C Antarctica from analyses of the EPICA ice core, *Geophysical research letters*, *32*(1), doi:10.1029/2004GL021449.

Vallelonga, P., K. Van de Velde, J.-P. Candelone, V. Morgan, C. Boutron, and K. Rosman (2002), The lead pollution history of Law Dome, Antarctica, from isotopic measurements on ice cores: 1500 AD to 1989 AD, *Earth and Planetary Science Letters*, *204*(1), 291-306, doi:10.1016/S0012-821X(02)00983-4.

Wang, Y., A. F. Stein, R. R. Draxler, D. Jesús, and X. Zhang (2011), Global sand and dust storms in 2008: Observation and HYSPLIT model verification, *Atmospheric Environment*, *45*(35), 6368-6381, doi:10.1016/j.atmosenv.2011.08.035.

Wegner, A., P. Gabrielli, D. Wilhelms-Dick, U. Ruth, M. Kriews, P. De Deckker, C. Barbante, G. Cozzi, B. Delmonte, and H. Fischer (2012), Change in dust variability in the Atlantic sector of Antarctica at the end of the last deglaciation, *Climate of the Past*, *8*, 135-147, doi:10.5194/cp-8-135-2012.

Winckler, G., R. F. Anderson, M. Q. Fleisher, D. McGee, and N. Mahowald (2008), Covariant glacial-interglacial dust fluxes in the equatorial Pacific and Antarctica, *Science*, *320*(5872), 93-96, doi:10.1126/science.1150595.

Winton, V., G. Dunbar, N. Bertler, M. A. Millet, B. Delmonte, C. Atkins, J. Chewings, and P. Andersson (2014), The contribution of aeolian sand and dust to iron fertilization of phytoplankton blooms in southwestern Ross Sea, Antarctica, *Global Biogeochemical Cycles*, *28*(4), 423-436, doi:10.1002/2013GB004574.

Wolff, E. W., H. Fischer, F. Fundel, U. Ruth, B. Twarloh, G. C. Littot, R. Mulvaney, R. Röthlisberger, M. De Angelis, and C. F. Boutron (2006), Southern Ocean sea-ice extent, productivity and iron flux over the past eight glacial cycles, *Nature*, *440*(7083), 491-496, doi:10.1038/nature04614.

Yuan, X., and D. G. Martinson (2000), Antarctic sea ice extent variability and its global connectivity*, *Journal of Climate*, *13*(10), 1697-1717, doi:10.1175/1520-0442(2000)013<1697:ASIEVA>2.0.CO;2.

Zender, C. S., H. Bian, and D. Newman (2003), Mineral Dust Entrainment and Deposition (DEAD) model: Description and 1990s dust climatology, *Journal of Geophysical Research: Atmospheres (1984–2012)*, *108*(D14), doi:10.1029/2002JD002775.

2.7 Supporting Figures

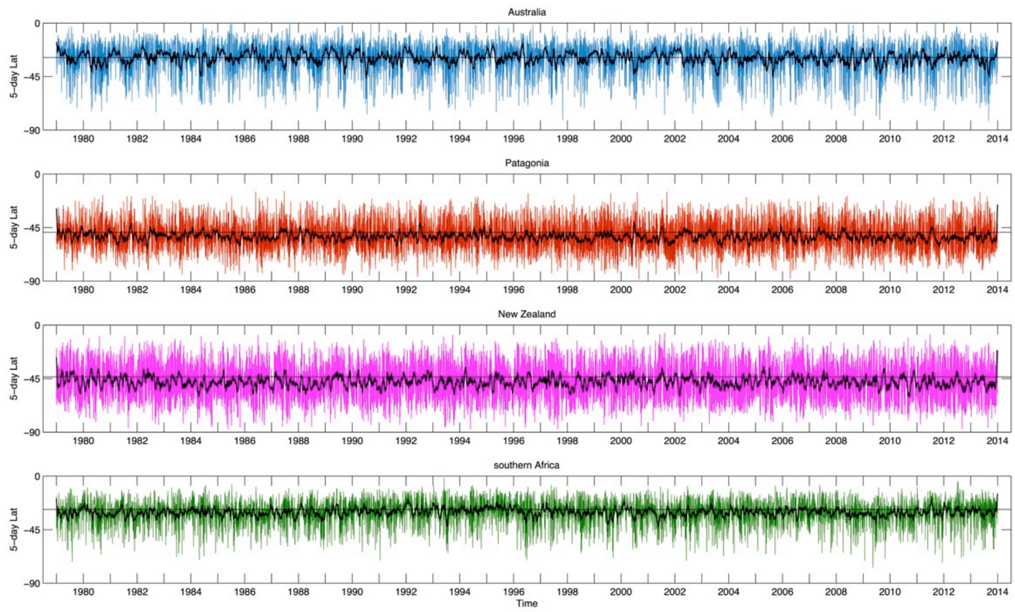

Figure S1. *5-day forward trajectory latitude for Australia (blue), Patagonia (orange), New Zealand (magenta) and southern Africa (green) dust PSA initiation points. Daily data is colored, solid black lines are a 30-point smooth, horizontal lines indicate latitude of trajectory initiation.*

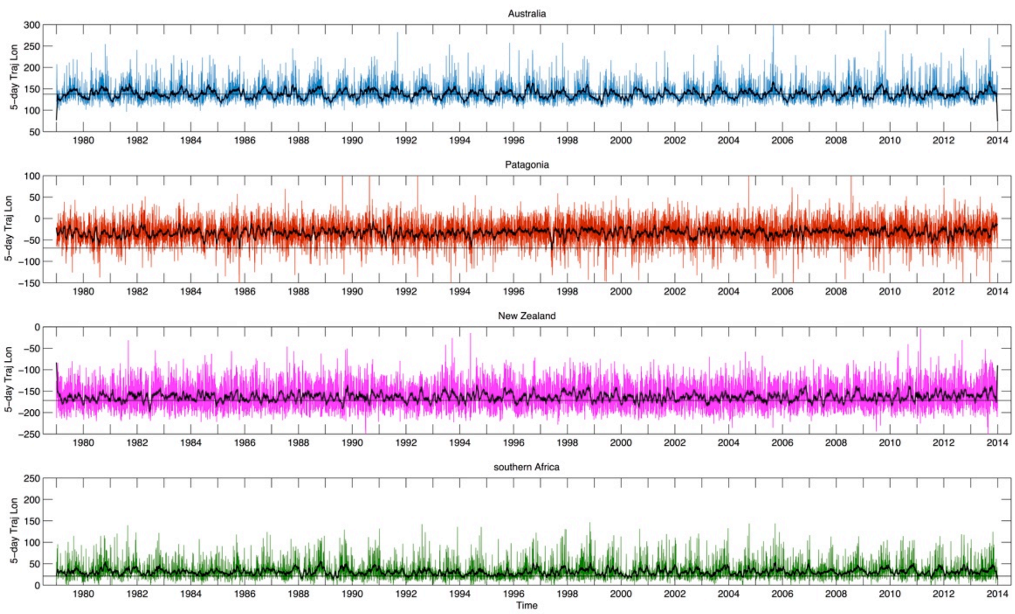

Figure S2. *5-day forward trajectory longitude for Australia (blue), Patagonia (orange), New Zealand (magenta) and southern Africa (green) dust PSA initiation points. Daily data is* *colored, solid black lines are a 30-point smooth, horizontal lines indicate longitude of trajectory initiation.*

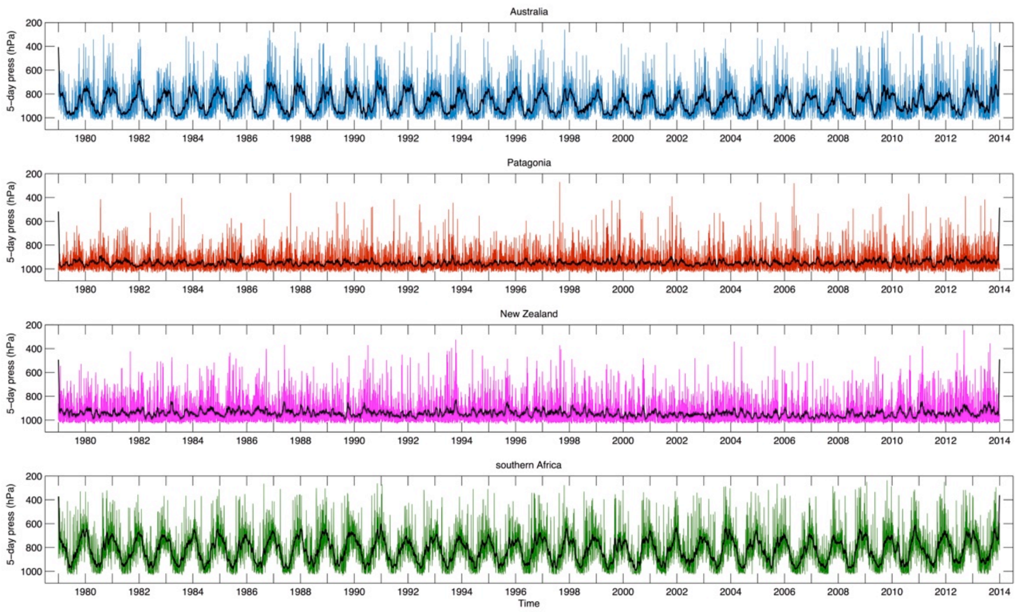

Figure S3. *5-day forward trajectory pressure (hPa) for Australia (blue), Patagonia (orange), New Zealand (magenta) and southern Africa (green) dust PSA initiation points. Daily data is colored, solid black lines are a 30-point smooth, horizontal lines indicate latitude of trajectory initiation.*

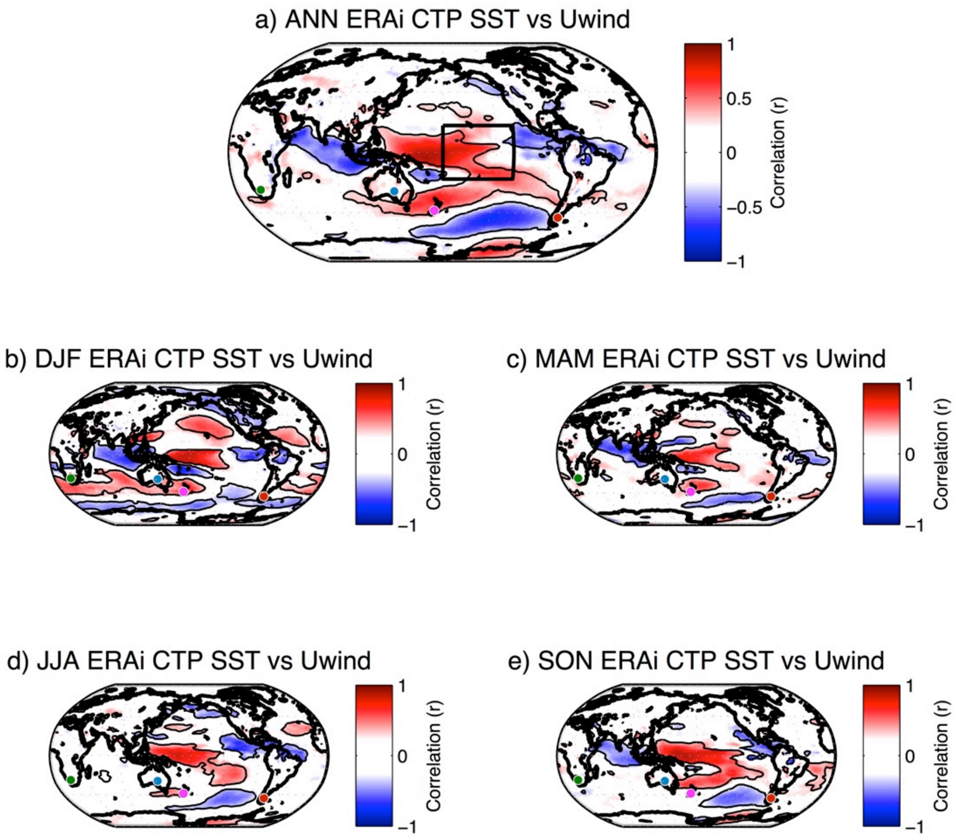

Figure S4. *Spatial correlation of 1979-2013 ERA-Interim reanalysis central tropical Pacific sea-surface temperature (CTP SST, 20ºN – 20ºS, 180ºE – 240ºE) versus 10 m eastward zonal (U) wind. Mean annual relationsip (ANN, a), December-January-February (DJF, b), March-April-May (MAM, c), June-July-August (JJA, d), and September-October-November (SON, e). Dust PSA are marked by colored circles, New Zealand (magenta), Patagonia (orange), southern Africa (green) and Australia (cyan). Black contour indicates >95% significance.*

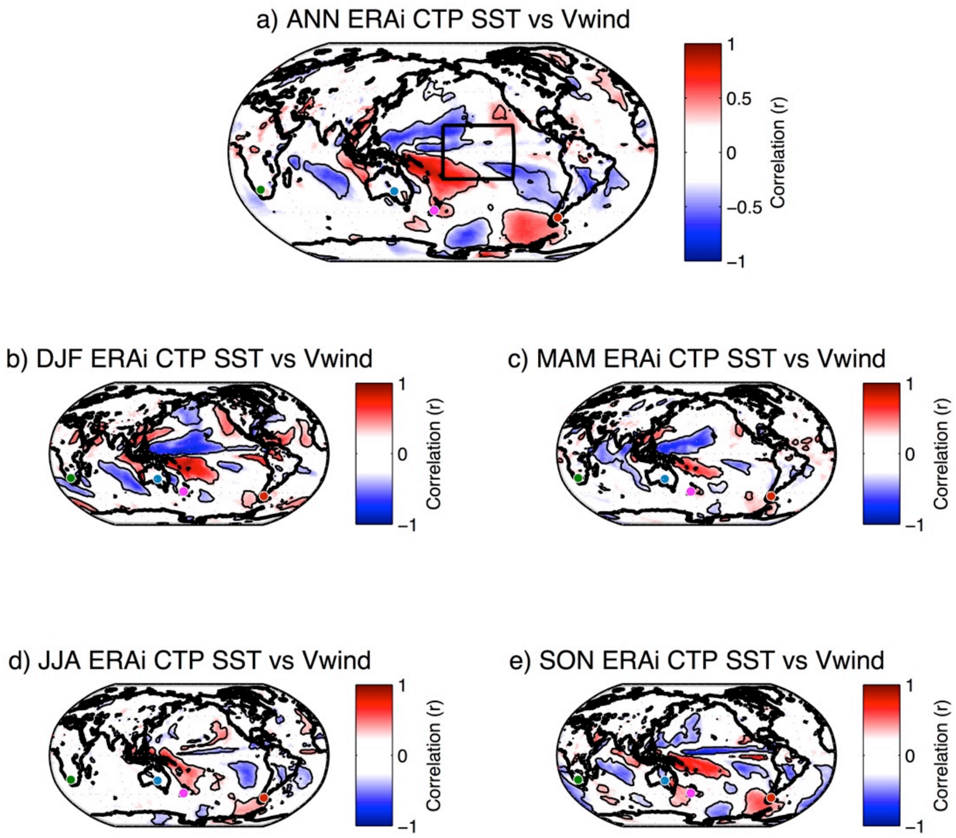

Figure S5. *Spatial correlation of 1979-2013 ERA-Interim reanalysis central tropical Pacific sea-surface temperature (CTP SST, 20ºN – 20ºS, 180ºE – 240ºE) versus 10 m northward meridional (V) wind. Mean annual relationsip (ANN, a), December-January-February (DJF, b), March-April-May (MAM, c), June-July-August (JJA, d), and September-October-November (SON, e). Dust PSA are marked by colored circles, New Zealand (magenta), Patagonia (orange), southern Africa (green) and Australia (cyan). Black contour indicates >95% significance.*

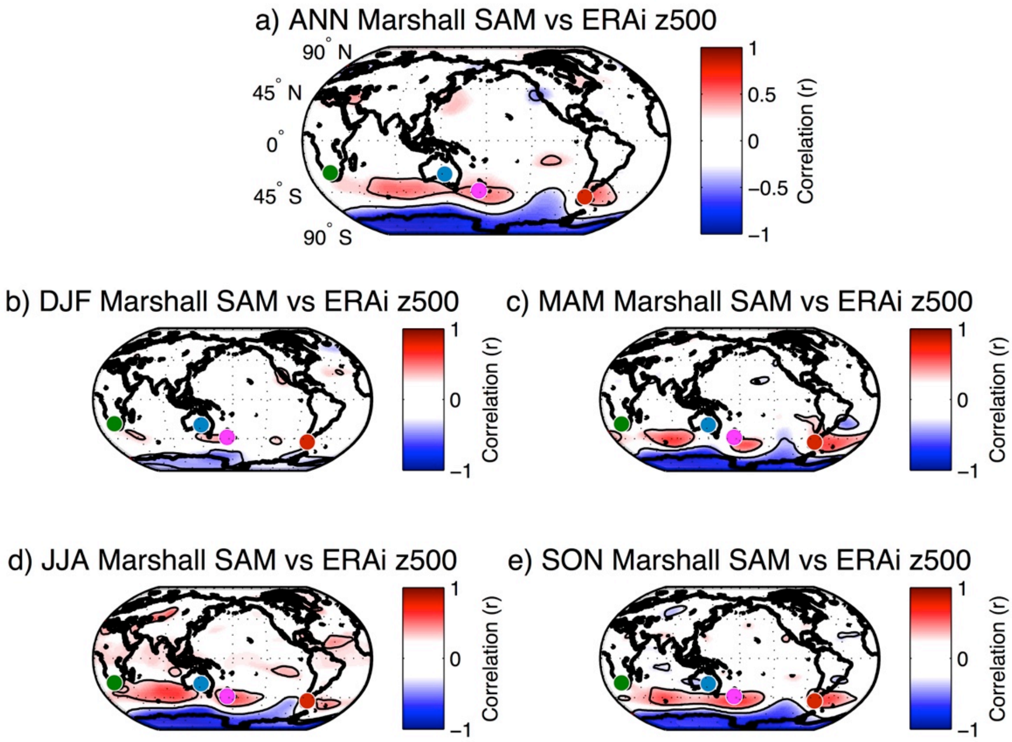

Figure S6. *Spatial correlation of the Marshall SAM index (difference between observed zonal mean sea level pressures at 40ºS and 65ºS, Marshall, 2003) versus 500 hPa geopotential height, plotted as in Figure 11. Mean annual relationsip (ANN, a), December-January-February (DJF, b), March-April-May (MAM, c), June-July-August (JJA, d), and September-October-November (SON, e). Dust PSA are marked by colored circles, New Zealand (magenta), Patagonia (orange), southern Africa (green) and Australia (cyan). Black contour indicates >95% significance.*

Chapter 3: Low-Femtogram Elemental Analysis of Antarctic Ice Cores without Preconcentration

Abstract

The Antarctic ice sheet preserves minute quantities of atmospheric material in a chronological sequence, providing an important historical record for bounding future changes in climate and atmospheric composition. Many chemical species in the ice are only present at the femtogram (fg g^{-1}, 10^{-15} g) level, and analysis of these species has accordingly required preconcentration and large sample volumes difficult to obtain from deep within the ice sheet. We report the elemental analysis of Antarctic ice at the low fg g^{-1} level using a sector-field inductively coupled plasma mass spectrometer enhanced with a jet interface (Jet-SF-ICPMS) and desolvation nebulizer without preconcentration. The study investigates rare earth elements (REE), transition and post-transition metals, actinide, metalloid, alkali and alkaline earth elements, presenting extremely low detection limits (< 10 fg g^{-1}) determined for many elements. Analytical background concentrations are essentially equal to these detection limits, suggesting that sample preparation methods and contamination levels are of primary importance in the pursuit of ultra-trace geochemical proxy information from polar ice cores.

3.1 Introduction

Polar ice cores provide records of past atmospheric composition and proxies of polar climate and that of teleconnected regions.[1,2] Chemical information preserved in layers of snow and ice takes the form of soluble and insoluble aerosols, gas phase species and the isotopic composition of both the ice and its impurities. Many of the impurities in Antarctic ice (e.g. mineral dust,[3,4] black carbon aerosols[5]) have few local sources and reflect trans-continental emissions and transport. Other species derive from regional marine emissions and reflect wind strength, sea-ice extent and biological productivity.[6-7] Large transient events such as volcanic eruptions,[8,9] and long-term changes in atmospheric pollution[10] are captured and allow a remote gauge of atmospheric change. Hence, well-dated glaciochemical time series can constrain the behavior of these processes on a range of spatial and temporal scales. Higher-order information from the records can be obtained through the disaggregation of chemical sources. The analysis of Pb[11,12] and Sr/Nd[13] isotope ratios and rare earth element (REE) abundance[14-15] has been used to identify major sources of mineral dust and anthropogenic pollutants.

Many of the chemical species in the Antarctic ice core record are present at extremely low concentrations ranging from a few femtograms (fg g^{-1}, 10^{-15}g) to the low picogram (pg g^{-1}, 10^{-12}g) level. While seemingly insignificant, measurements of REE concentration at the fg

g^{-1} level in Antarctic ice core samples provide insight into major climate and environmental changes. For example, at the Dome C[16] and Drønning Maud Land[15] sites in East Antarctica, a major shift in REE signatures suggests increased dust source variability beginning ~15 ka before present, during the transition from the last glacial period to the present interglacial. This work represents some of the lowest-concentration measurements of glaciochemical species, using sector-field inductively coupled plasma mass spectrometry (SF-ICPMS) for elemental analysis.[14] These instruments can detect multiple elements across a large range of concentrations, typically nanograms (ng g^{-1}, 10^{-9}g) to low pg g^{-1}, with high-sensitivity and small sample volumes (<5 mL). While the sensitivity of SF-ICPMS is already high, it can be increased further through the use of high-efficiency sample introduction systems[17] and by increasing ion transport into the mass analyser using a jet interface—a high capacity pump and large orifice cones.[18] Appropriate acid digestion and sample preparation schemes are also essential for reliable measurements of ice samples.[19-20] Acid leaching of mineral particles in these samples results in a rapid increase in lithogenic element concentration in the first hours after acidification, followed by continued increases for several weeks after acidification. The variability introduced by acidification schemes requires the establishment and reporting of consistent methodologies for interpreting ice core ICPMS trace-element data.

Here we report the analysis of ice core samples from Antarctica, collected as part of the Roosevelt Island Climate Evolution (RICE) project. Concentrations are quantified to the low fg g^{-1} level using a sector-field inductively coupled plasma mass spectrometer enhanced with a jet interface (Jet-SF-ICPMS) and desolvation nebulizer. This high transport-efficiency sample inlet system achieves reduced instrument backgrounds and improved instrument sensitivity and signal stability. This study focuses on thirty species, including REE, transition and post-transition metals, actinide, metalloid, alkali and alkaline earth elements—all at sub-ng concentrations. Extremely low detection limits (< 10 fg g^{-1}) are achieved for many elements without preconcentration, at or below levels of background contamination in the laboratory environment. To assess data quality, details of acidified sample stability, background contamination and instrumental limits are presented.

3.2 Experimental

3.2.1 Materials, Reagents and Standards

Optima™ (Fisher Scientific) HNO_3 and ultra-clean water (>18 MΩ) were used in cleaning of laboratory materials and acidification of samples at Victoria University of Wellington and GNS Science in New Zealand. Vials for ice core sampling were cleaned in a series of acid baths (1% HNO_3 v/v) of increasing purity. Sub-boiled double-distilled HNO_3

prepared in the Curtin University TRACE facility was used to clean vials and acidify blanks and standards used during ICPMS analysis. Standards, including quality control (QC) samples, were made from certified single- and multi-element stock solutions (Elemental Scientific).

3.2.2 Ice Core Sampling

The 763 m-long RICE ice core was drilled at Roosevelt Island, Antarctica (79.364 ºS, 161.706 ºW), a coastal ice dome at the margin of the Ross Ice Shelf. The core was cut into one-meter sections, packed into polyethylene bags and shipped frozen to New Zealand for sampling. Sticks of ice (~3.4 cm x 3.4 cm x 100 cm) were prepared and placed on a heated gold-plated copper melt-head, sectioned to isolate pristine interior ice and remove contaminated outer ice surfaces (Continuous Flow Analysis, CFA[21,22]). Water from the inner section of the melt-head was pumped to fraction collectors, located inside HEPA-filtered hoods, filling 10 mL sample vials with ~4 mL of water. Discussed here are 784 samples from the RICE ice core spanning 9 m to 40 m depth (dated using annual chemistry to approximately 1900 – 1990 CE). Procedural blanks were collected throughout ice core processing and at all stages of sample preparation to assess maximum contamination during preparatory stages. Sticks of frozen ultra-clean (>18 MΩ) water were prepared in the same way as ice core samples and passed through the CFA system. Measured concentrations in these blanks were in all instances significantly higher than any measured ice core sample concentrations, likely due to ultra-clean melt water scavenging trace material from CFA tubing walls. Because of this, these blanks are not considered further (i.e. are not subtracted from measured sample concentrations). All samples were stored frozen until acidification, and acidified samples were subsequently frozen only during shipment from New Zealand to Curtin University, Perth, Australia to prevent agitation and contact with vial caps known to contain barium (^{137}Ba is quantified here).

3.2.3 Sample Acidification

Aerosols contained in ice core samples exist in water-soluble and -insoluble mineralogical matrices. To recover total aerosol concentrations, the sample has to be acidified with the aim of complete digestion of particulates into a leachate. Ice core trace element analysis in an online CFA arrangement, where the sample is melted and water is immediately pumped away, acidified and injected directly into an ICPMS,[23] results in trace element concentrations that are representative of the water-soluble fraction (plus occasional mineral particles vaporized and ionized in the plasma). Ice core ICPMS analyses, as here, are also commonly performed on discrete samples taken in vials during ice core continuous flow sampling,[21] which are then acidified prior to analysis. Unless leaching rates are observed and quantified, comparison of ice core trace-element concentrations collected from online continuous flow analysis (water-soluble trace element fraction) and those from discrete samples (water-soluble plus partial digestion of particulate trace elements) proves challenging. For instance, *Edwards and Sedwick* (2001)[24] and *Edwards et al.* (2006)[19] reported that an extended leaching time (up to three months) was required for the analysis of lithogenic iron (Fe) in Antarctic ice and snow using a 0.1% hydrochloric acid acidification scheme.

Rhodes et al. (2011)[25] and *Koffman et al.* (2014b)[20] clearly demonstrate that acidification time and strength affect trace-element concentrations in ice core samples. Lithology and particle size also affect measured concentrations of many elements, suggesting that similar tests are required at individual ice core sites undergoing different aerosol transport regimes. In polar snow and ice, concentration changes over three months are limited for water-soluble elements such as Mg, S, K, Ca and Na, while elements associated with particulates, such as Al, Mn, Fe, La and Pb, change substantially. *Koffman et al.* (2014b)[20] note similar leaching behavior of Fe and Al, which continue to increase in concentration while most other particulate-associated elements cease changing significantly after one month. Both the *Rhodes*[25] and *Koffman*[20] studies conclude that ice core samples should be acidified (to 1% HNO_3) for at least one month prior to analysis to minimize these leaching effects.

To verify this behavior and determine acidification procedures for RICE ice core samples, we replicated the experiment of *Rhodes et al.* (2011)[25] using surface snow from Roosevelt Island. Solutions were prepared and the experiment undertaken in the same class 100 laboratory facilities as the original study. Snow from Roosevelt Island was collected during the 2010-2011 austral summer, placing freshly fallen snow into HNO_3-rinsed Nalgene bottles. These solutions were acidified to 1 % HNO_3 v/v and sampled at set times to allow for examination of changes in trace element concentration. Sampling was undertaken for eight weeks. The samples were analysed for a routine suite of trace elements using an Element 2 SF-ICPMS (Thermo Scientific) at Victoria University of Wellington. An SC-2 FAST autosampler (Elemental Scientific) coupled to a peristaltic pump was used for sample introduction, connected to a micro-flow Teflon nebuliser and a cooled double-bypass quartz spray chamber. Standard nickel sample and skimmer cones were used. Calibration was achieved using a set of eight dilutions of a certified multi-element standard (Inorganic Ventures). A run blank of ultra-pure water acidified to 1 % HNO_3 v/v and an external standard (SLRS-4 riverine water) bracketed every 9 samples, and were used to provide instrument background correction and to assess accuracy and reproducibility of analyses. Measured values of SLRS-4 for most analytes were within 5% of accepted values (i.e. GeoReM, http://georem.mpch-mainz.gwdg.de/). Considered below are well-quantified measurements of Fe (0.5% SLRS-4 accuracy), Mn (2.7%) and La (3%), representative of metal and REE acid-leaching behavior.

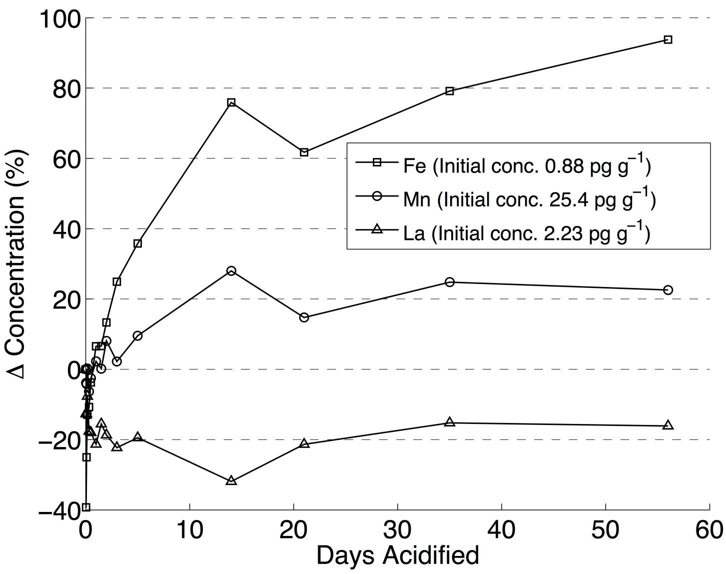

Figure 1. *Eight-week percent concentration change in acidified (1% HNO_3 v/v) RICE Antarctic snow sample, for Fe, Mn and La.*

In the RICE snow samples, these elements show significant concentration change over the 8-week sampling period (Figure 1), with rapid changes during the first 24 hours following acidification and continued large changes during the ensuing two weeks. Fe and Mn show the same pattern of concentration increase over time as the 1% HNO_3 v/v test in *Koffman et al.* (2014b),[20] rising by 20-80% in the first two weeks after acidification. La, in contrast, shows a small decrease in concentration. While other elements stabilize after 3 to 5 weeks, Fe continues to increase in concentration through the eighth week following acidification (Figure 1). This confirms that an acidification time longer than two months is necessary to allow all elements to stabilize to a point where leaching effects on measured sample concentration become negligible. RICE samples were acidified at the Victoria University of Wellington three months prior to analysis, in a class 100 clean room under laminar-flow hoods. Open vials of 1% HNO_3 v/v were placed in hoods for several hours during this process, and are presented below as procedural blanks quantifying maximum background contamination.

3.2.4 Analytical Environment

Ice core sample analysis and standard preparation was performed in the John de Laeter Centre Trace Research Advanced Clean Environment facility (TRACE) at Curtin University, Western Australia. The TRACE Facility is a unique, purpose-built, clean air environment designed for measuring extremely-low concentrations of chemical species. The laboratory consists of a large, class 100 clean air containment area, provided with air that has been passed through three stages of particulate filtration. The containment space houses five individual laboratory modules that provide an additional level of air filtration (class 10) and separation of activities. All cleaning procedures, sample and reagent preparation activities occurred in the laboratory modules. Analysis by SF-ICPMS occurred in the containment space.

3.2.5 Instrument Setup

Ice core sample analysis was performed using an Element XR (Thermo Scientific) SF-ICPMS with a jet interface (a high-capacity jet interface pump with nickel X-Skimmer and Jet-Sampler cones, Jet-SF-ICPMS). The ICPMS torch, auto-sampler and nebulizer desolvation system were all from Elemental Scientific Inc. (ESI). These included an enclosed (acrylic sample enclosure) seaFAST S2 high-purity syringe-pump auto-sampler (configured for direct injection), connected to an APEX-Q desolvation system (100°C / +2°C) fitted with a PFA-ST nebuliser. An additional gas (high purity nitrogen) was introduced to the APEX and adjusted for optimal response. The desolvation system was coupled to the ICPMS torch using a PFA aerosol focusing connector with an additional argon gas (Ar) of 0.350 L min^{-1}. The ICP torch Ar gas flow rates were: cool gas = 16 L min^{-1}; auxiliary gas 0.7 L min^{-1}, and sample gas flow ~ 0.8 L min^{-1} (tuned after every run ~32 hours). Instrument forward power was set 1248 W.

Ice core samples were introduced to the system at a flow rate of 200 µL min^{-1} using a 2 mL sample loop on the seaFAST2 injection valve and a syringe pumped carrier solution (1% HNO3 v/v). Internal standard (1.5 ng g^{-1} Indium, 1% HNO3 v/v, 100 µL min^{-1}) was mixed inline with the sample and carrier solutions using an internal tee built into the autosampler injection valve. In between samples, the sample probe was rinsed with ultrapure 1% HNO3 v/v. The total flow rate into the APEX-Q was 300 µL min^{-1}, resulting in a diluted internal standard concentration of 0.5 ng g^{-1} ^{115}In which gave a response of ~7 x 10^6 counts per second (equivalent to 14 x 10^6 counts per second for 1 ng g^{-1} ^{115}In) at low mass resolution. This high sensitivity was maintained throughout the analysis period.

3.2.6 Run Structure

Samples were analyzed in approximately 32 hour runs, structured with three calibrations of ten multi-element standards placed at the beginning, middle and end of the analytical sequence. Between calibrations, groups of ten samples were bracketed by an instrumental "run" blank and a QC sample (taken from middle-concentration standard; elemental concentrations detailed in Table 1). After every second group of ten samples an additional QC was analyzed as a duplicate to assess repeatability. A typical run consisted of 210 samples, with 59 additional analytes including standards, run blanks, QCs and duplicates.

3.2.7 Calibration

All ion intensities were normalized to the ^{115}In internal standard, with values calculated for a desired isotope, I, where:

$$I = I_{\text{meas}} \times \frac{c_{\text{IS}}}{I_{\text{IS}}}.$$

I_{meas} is the measured intensity of the desired isotope, c_{IS} is the concentration of the internal standard, and I_{IS} is the measured intensity of the internal standard. Normalized intensities were calibrated using ten external standards prepared from NIST traceable elemental standards (diluted in 1% HNO_3 v/v). Blank corrections were determined from the instrumental run blank concentrations. The run blank (average of 10 per ~32 hour run) was subtracted from all samples and calibration standards. Procedural blanks were determined and used to assess contamination of the samples from the acidification procedure. Linear equations were determined for the external calibrations using bi-square weighted robust linear regression[26]. The regression method was chosen to minimize the effect of outliers on the linear fit (i.e. points near the line get greater weight). A small number of outliers (>3σ) were manually removed from standard calibrations and a new regression calculated.

3.3 Results and Discussion

3.3.1 Quality Control Recoveries and Stability at the Low Pg g^{-1} to Fg g^{-1} Level

Elemental recoveries and instrument stability were assessed using the QC standards (run after every 10 samples). Statistics for the QCs determined over four individual ~32 hour run periods are shown in Table 1. Recoveries are between 95% and 100% for most elements analyzed. QC stability for selected elements is presented in Figure 2 for a 60-hour period of near-continuous analysis. QC stability and replication is excellent across this time period, with no evidence for significant memory effects, suggesting autosampler washout procedures are effective. Accuracy is > 95% for all transition- and post-transition metals, and measurements are precise to within 5% (Table 1). Additionally, measurements of actinides are excellent with a mean concentration of 100% for ^{232}Th, precise to within 4%, and a mean concentration of ^{238}U only 1% greater than the known QC concentration suggesting only limited $^{238}U^{16}O$ formation—and this at a very low concentration of 0.02 pg g^{-1}. ^{52}Cr and ^{75}As (Figure 2b) show 80% and 98% recovery of expected QC concentration, with 10% standard deviation at concentrations less than 5 pg g^{-1}.

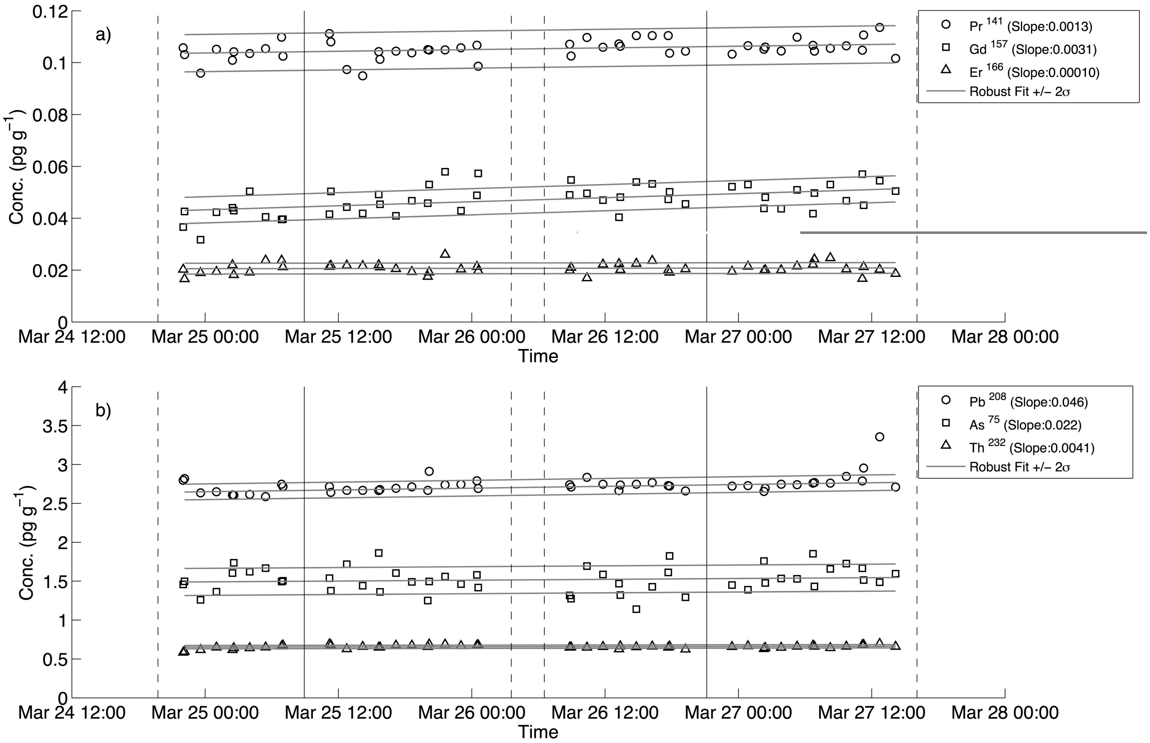

Figure 2. *Low-concentration QC stability through a ~60-hour analysis period for a) REE (Pr, Gd, Er) and b) Pb, As and Th. Robust linear fits (grey line) are plotted through QCs, with ± 2σ (dashed). Solid vertical lines mark standard calibrations used in final concentration calculations, dashed vertical lines mark additional calibrations.*

Measurements of REE, present in the QC at 1 pg g^{-1} and below—similar to levels in RICE Antarctic ice core samples—are excellent for the light REE (La, Ce, Pr, Nd) with measured QC concentrations averaging essentially 100% of known concentrations and standard deviation ≤ 4%. The lower-concentration medium REE (Sm, Eu, Gd, Tb, Dy, Ho) and heavy REE (Er, Tm, Yb, Lu) also accurately recover QC concentrations (>90%), with even the lowest mean QC concentration of 0.005 pg g^{-1} ^{175}Lu being 84% accurate, to within ~1 fg g^{-1}. Figure 2a demonstrates QC stability across the REE, showing results over ~60 hours for Pr, Gd and Er QCs. Measurements of medium and heavy REE are all precise to within ~5 fg g^{-1} or less.

3.3.2 Oxide formation

The instrument was set each run to minimize oxide formation, tuned for $^{238}U^{16}O$ production < 5% and including standard REE oxide corrections[27]. None of the REE exhibits appreciable additional recovery beyond the expected concentration of the QCs. As an additional test, REE-specific standards were prepared and measured in isolation, to observe whether oxide formation in mixed-element standards and QCs (which included ^{137}Ba) increased recovery of REE. No significant difference was observed.

3.3.3 Limits of Quantification and Concentration in Antarctic Ice Samples

Many ice core trace element studies report estimates of instrumental limits of detection as three times the standard deviation of limited measurements of an ultrapure acid solution.[14,20] While this is a critical measure, we provide a broader assessment to include all effects during analysis. Procedural and analytical background concentrations have the potential to limit quantification. Limits of detection for sector-field ICPMS instruments are expected in most cases to be well below blank concentrations due to background contamination during sampling procedures and laboratory analysis.[28] Means of analytical "run" blanks (n = 86) and procedural blanks (n = 13) are plotted in Figure 3a, as well as mean RICE Antarctic ice core sample concentration (n = 784) for comparison. Values are detailed in Table 2, including 3σ limits of detection. These values represent the long-term backgrounds associated with this analytical campaign. Within individual runs samples were corrected for the analytical blank of that run—that is, the mean value of 10 measured run blanks (excluding 3σ outliers). Mean sample relative standard deviation (RSD, sample standard deviation divided by mean concentration) for all isotopes is presented in Figure 3b as a measure of signal stability during analysis. RSD should not be confused with standard deviation of sample concentrations displayed in Table 2, which are included to demonstrate natural variability of concentrations in Antarctic ice samples.

Determinations of transition metals ^{55}Mn and ^{56}Fe are excellent (Figure 3a), with high accuracy and precision, low analytical and procedural blanks compared to concentrations found in ice core samples and sample RSD across all runs < 5% (Figure 3b). Both procedural and analytical blanks for ^{59}Co, however, are nearly identical to mean ice core sample concentration, and sample RSD is 11-13%. Although ^{52}Cr is well-determined, with low sample RSD (< 5%), blank concentrations are several times higher than mean ice core sample values (Figure 3a). ^{63}Cu procedural blanks are high due to the gold-plated copper melt-head used to sample ice cores. Barring this procedural contamination, determination of ^{63}Cu sampled in a different manner would be excellent using this ICPMS instrumentation, as sample RSD across all runs is only 2-3% and measurements are very accurate and precise (Table 1).

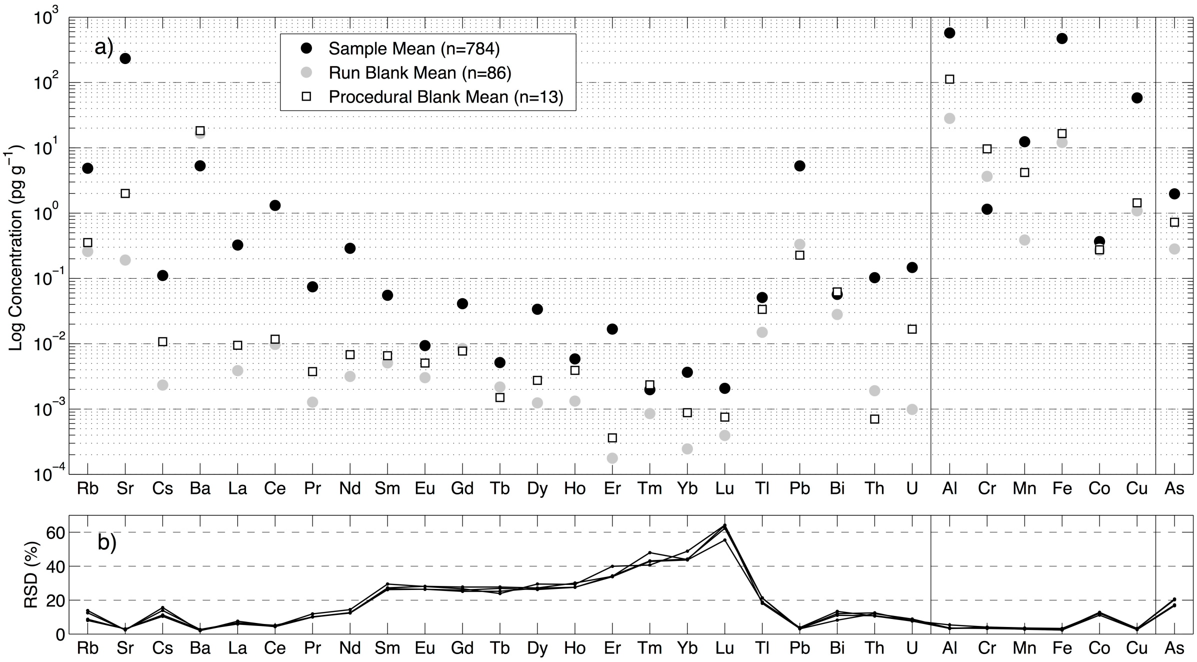

Figure 3. *(a) Sample (black circle), run blank (grey circle) and procedural blank (white square) mean concentrations (logarithmic scale) for all isotopes. Vertical lines separate isotopes analyzed at low, medium and high instrument resolution from left to right. (b) Sample relative standard deviation (RSD, %) for all isotopes, as an average of individual analytical runs; each run plotted as a black line.*

Post-transition metals ^{205}Tl and ^{209}Bi (Figure 3a) are quantifiable to concentrations as low as tens of fg g^{-1} (i.e. parts per quadrillion), with RICE ice core sample concentrations only slightly above these levels. Sample RSD are ~20% and ~10% across all runs for ^{205}Tl and ^{209}Bi, respectively (Figure 3b). However, ^{209}Bi procedural blanks are higher than mean ice core concentrations. ^{208}Pb and ^{27}Al have higher background concentrations due to greater natural abundances, but mean ice core sample concentrations remain well above both analytical and procedural blanks and sample RSD are also low. Actinides ^{232}Th and ^{238}U have very low background contamination, ^{232}Th at the single fg g^{-1} level and ^{238}U at tens of fg g^{-1}. Mean ice core sample values are well above blank levels for these analytes (Table 2). ^{75}As concentrations in ice core samples are on average only twice the concentration of procedural blanks, with sample RSD as high as 20%, while analytical blanks are approximately half again as low as procedural blanks.

REE, while present at low concentrations in Antarctic ice core samples, are similarly present at extremely low levels in the laboratory environment, as evidenced by the procedural and analytical blanks here (Figure 3a, Table 2). Analytical blank concentrations for light REE (La, Ce, Pr, Nd) are less than 2% of mean concentrations found in ice core samples, with procedural blanks concentrations less than 8% of the sample mean. Sample RSD for light REE are 5-13% (Figure 3b). Medium and heavy REE show significantly higher blank concentrations relative to single digit part per quadrillion concentrations in ice core samples, especially the alternating abundance of medium REE (Sm, Eu, Gd, Tb, Dy) and heavy REE (Ho, Er, Tm, Yb, Lu). At such low concentrations (single fg g^{-1}), sample RSD are relatively high, approximately 25% across the medium REE and rising in a linear fashion across the heavy REE to a maximum RSD of ~60% (Figure 3b). Tm is the only REE which shows a higher mean concentration in procedural blanks (Figure 3a), suggesting that laboratory contamination may render this element of limited use.

Our results suggest that detection limits of Jet-SF-ICPMS instrumentation are not the primary barrier to measuring low-fg g^{-1} concentration species in polar snow and ice. Instead, methodological contamination and associated uncertainties—for instance type and length of sample acidification—have the largest effect on the utility of trace element data for exploring paleoclimate information preserved in Antarctic snow and ice. International coordination and inter-laboratory comparisons, as called for by others,[20] would be of great utility to minimize methodological uncertainty and facilitate further development of trace-element ice core proxies, which contain higher-order information clarifying key aspects of climatic and environmental processes affecting myriad aspects of the earth system.

Tables

Table 1. *QC known concentration, mean of 96 QC measurements and standard deviation of 96 QC measurements.*

Isotope (resolution)	QC Concentration (pg g^{-1})	Mean of 96 QC measurements (% of known conc.)	RSD of 96 QC measurements (%)
Rb 85 (LR)	526.7	99	2
Sr 88 (LR)	105.3	99	2
Cs 133 (LR)	0.198	99	2
Ba 137 (LR)	26.3	95	9
La 139 (LR)	0.527	100	3
Ce 140 (LR)	1.053	100	4
Pr 141 (LR)	0.105	101	3
Nd 146 (LR)	0.527	101	3
Sm 147 (LR)	0.105	101	7
Eu 153 (LR)	0.021	96	8
Gd 157 (LR)	0.053	93	10
Tb 159 (LR)	0.011	93	13
Dy 163 (LR)	0.053	98	7
Ho 165 (LR)	0.011	94	8
Er 166 (LR)	0.021	98	7
Tm 169 (LR)	0.005	90	13
Yb 172 (LR)	0.021	101	6
Lu 175 (LR)	0.005	84	29
Tl 205 (LR)	0.658	99	2
Pb 208 (LR)	2.634	102	5
Bi 209 (LR)	0.237	97	6
Th 232 (LR)	0.658	100	3
U 238 (LR)	0.020	101	10
Al 27 (MR)	526.7	98	4
Cr 52 (MR)	3.292	80	10
Mn 55 (MR)	9.877	98	2
Fe 56 (MR)	526.7	98	2
Co 59 (MR)	1.053	96	5
Cu 63 (MR)	65.8	99	2
As 75 (HR)	1.646	89	10

Table 2. *Sample, analytical and procedural blanks (pg g^{-1}).*

Isotope (Resolution)	Sample mean, blank subtracted (n = 784)	Sample SD (n = 784)	Analytical Blank mean (n = 86)	Procedural Blank mean (n = 13)	LOD (3*SD Analytical Blank)
Rb 85 (LR)	4.864	3.031	0.259	0.354	0.239
Sr 88 (LR)	232	150	0.191	2.000	0.244
Cs 133 (LR)	0.111	0.115	0.002	0.011	0.002
Ba 137 (LR)	5.314	5.356	16.630	18.275	7.286
La 139 (LR)	0.324	0.385	0.004	0.009	0.004
Ce 140 (LR)	1.313	3.148	0.010	0.012	0.036
Pr 141 (LR)	0.074	0.090	0.001	0.004	0.001
Nd 146 (LR)	0.289	0.354	0.003	0.007	0.006
Sm 147 (LR)	0.055	0.066	0.005	0.007	0.007
Eu 153 (LR)	0.009	0.011	0.003	0.005	0.003
Gd 157 (LR)	0.041	0.050	0.008	0.008	0.012
Tb 159 (LR)	0.005	0.006	0.002	0.002	0.003
Dy 163 (LR)	0.034	0.034	0.001	0.003	0.003
Ho 165 (LR)	0.006	0.006	0.001	0.004	0.001
Er 166 (LR)	0.017	0.016	<0.001	<0.001	0.001
Tm 169 (LR)	0.002	0.002	0.001	0.002	0.002
Yb 172 (LR)	0.004	0.003	<0.001	0.001	<0.001
Lu 175 (LR)	0.002	0.006	<0.001	0.001	0.001
Tl 205 (LR)	0.051	0.047	0.015	0.034	0.007
Pb 208 (LR)	5.297	5.647	0.333	0.227	1.670
Bi 209 (LR)	0.057	0.093	0.028	0.062	0.051
Th 232 (LR)	0.103	0.192	0.002	0.001	0.008
U 238 (LR)	0.147	0.067	0.001	0.017	0.003
Al 27 (MR)	573	804	28.26	112	37.21
Cr 52 (MR)	1.147	3.8	3.652	9.654	2.157
Mn 55 (MR)	12.37	15.36	0.388	4.196	0.354
Fe 56 (MR)	472	1022	12.102	16.547	7.679
Co 59 (MR)	0.367	1.26	0.268	0.274	0.102
Cu 63 (MR)	58.23	92.87	1.084	1.436	0.959
As 75 (HR)	1.975	1.230	0.282	0.725	0.252

Author Contributions

The manuscript was written through contributions of all authors. PDN, AT, RE and NANB produced samples from the RICE ice core. PDN and AT conducted acidification experiments and prepared samples for analysis. PDN, AT and RE conducted ICPMS analysis, performed data calibration and assessed quality. All authors have given approval to the final version of the manuscript.

Acknowledgements

The authors are thankful for laboratory assistance at the National Ice Core Research Facility at GNS Science (R. Pyne) and the TRACE laboratory (A. Ellis, K. Jarrett, B. Proemse, H. Winton). This work is a contribution to the Roosevelt Island Climate Evolution (RICE) Program, funded by national contributions from New Zealand, Australia, Denmark, Germany, Italy, the People's Republic of China, Sweden, United Kingdom, and the United States of America. Logistic support for RICE was provided by Antarctica New Zealand and the United States Antarctic Program.

3.4 REFERENCES

1. Augustin, L.; Barbante, C.; Barnes, P. R.; Barnola, J. M.; Bigler, M.; Castellano, E.; Cattani, O.; Chappellaz, J.; Dahl-Jensen, D.; Delmonte, B., Eight glacial cycles from an Antarctic ice core. *Nature* 2004, *429*, (6992), 623-628.

2. Wolff, E.; Barbante, C.; Becagli, S.; Bigler, M.; Boutron, C.; Castellano, E.; De Angelis, M.; Federer, U.; Fischer, H.; Fundel, F., Changes in environment over the last 800,000 years from chemical analysis of the EPICA Dome C ice core. *Quaternary Science Reviews* 2010, *29*, (1), 285-295.

3. Dixon, D. A.; Mayewski, P. A.; Goodwin, I. D.; Marshall, G. J.; Freeman, R.; Maasch, K. A.; Sneed, S. B., An ice-core proxy for northerly air mass incursions into West Antarctica. *International Journal of Climatology* 2012, *32*, (10), 1455-1465.

4. Koffman, B.; Kreutz, K.; Breton, D.; Kane, E.; Winski, D.; Birkel, S.; Kurbatov, A.; Handley, M., Centennial-scale variability of the Southern Hemisphere westerly wind belt in the eastern Pacific over the past two millennia. *Climate of the Past* 2014, *10*, (3), 1125-1144.

5. Bisiaux, M.; Edwards, R.; McConnell, J.; Curran, M.; Van Ommen, T.; Smith, A.; Neumann, T.; Pasteris, D.; Penner, J.; Taylor, K., Changes in black carbon deposition to Antarctica from two high-resolution ice core records, 1850–2000 AD. *Atmospheric Chemistry and Physics* 2012, *12*, (9), 4107-4115.

6. Curran, M. A.; van Ommen, T. D.; Morgan, V. I.; Phillips, K. L.; Palmer, A. S., Ice core evidence for Antarctic sea ice decline since the 1950s. *Science* 2003, *302*, (5648), 1203-1206.

7. Criscitiello, A. S.; Das, S. B.; Evans, M. J.; Frey, K. E.; Conway, H.; Joughin, I.; Medley, B.; Steig, E. J., Ice sheet record of recent sea-ice behavior and polynya variability in the Amundsen Sea, West Antarctica. *Journal of Geophysical Research: Oceans* 2013, *118*, (1), 118-130.

8. Sigl, M.; McConnell, J. R.; Layman, L.; Maselli, O.; McGwire, K.; Pasteris, D.; Dahl-Jensen, D.; Steffensen, J. P.; Vinther, B.; Edwards, R., A new bipolar ice core record of volcanism from WAIS Divide and NEEM and implications for climate forcing of the last 2000 years. *Journal of Geophysical Research: Atmospheres* 2013, *118*, (3), 1151-1169.

9. Sigl, M.; McConnell, J. R.; Toohey, M.; Curran, M.; Das, S. B.; Edwards, R.; Isaksson, E.; Kawamura, K.; Kipfstuhl, S.; Krüger, K., Insights from Antarctica on volcanic forcing during the Common Era. *Nature Climate Change* 2014, *4*, (8), 693-697.

10. McConnell, J. R.; Maselli, O. J.; Sigl, M.; Vallelonga, P.; Neumann, T.; Anschütz, H.; Bales, R.; Curran, M.; Das, S. B.; Edwards, R., Antarctic-wide array of high-resolution ice core records reveals pervasive lead pollution began in 1889 and persists today. *Scientific Reports* 2014, *4*.

11. Barbante, C.; Bellomi, T.; Mezzadri, G.; Cescon, P.; Scarponi, G.; Morel, C.; Jay, S.; van de Velde, K.; Ferrari, C.; Boutron, C. F., Direct determination of heavy metals at picogram per gram levels in Greenland and Antarctic snow by double focusing inductively coupled plasma mass spectrometry. *Journal of Analytical Atomic Spectrometry* 1997, *12*, (9), 925-931.

12. Vallelonga, P.; Gabrielli, P.; Balliana, E.; Wegner, A.; Delmonte, B.; Turetta, C.; Burton, G.; Vanhaecke, F.; Rosman, K.; Hong, S., Lead isotopic compositions in the EPICA Dome C ice core and Southern Hemisphere Potential Source Areas. *Quaternary Science Reviews* 2010, *29*, (1), 247-255.

13. Delmonte, B.; Andersson, P.; Hansson, M.; Schöberg, H.; Petit, J. R.; Basile-Doelsch, I.; Maggi, V., Aeolian dust in East Antarctica (EPICA-Dome C and Vostok): Provenance during glacial ages over the last 800 kyr. *Geophysical Research Letters* 2008, *35*, (7).

14. Gabrielli, P.; Barbante, C.; Turetta, C.; Marteel, A.; Boutron, C.; Cozzi, G.; Cairns, W.; Ferrari, C.; Cescon, P., Direct determination of rare earth elements at the subpicogram per gram level in antarctic ice by ICP-SFMS using a desolvation system. *Analytical Chemistry* 2006, *78*, (6), 1883-1889.

15. Wegner, A.; Gabrielli, P.; Wilhelms-Dick, D.; Ruth, U.; Kriews, M.; De Deckker, P.; Barbante, C.; Cozzi, G.; Delmonte, B.; Fischer, H., Change in dust variability in the Atlantic sector of Antarctica at the end of the last deglaciation. *Climate of the Past* 2012, *8*, 135-147.

16. Gabrielli, P.; Wegner, A.; Petit, J. R.; Delmonte, B.; De Deckker, P.; Gaspari, V.; Fischer, H.; Ruth, U.; Kriews, M.; Boutron, C., A major glacial-interglacial change in aeolian dust composition inferred from Rare Earth Elements in Antarctic ice. *Quaternary Science Reviews* 2010, *29*, (1), 265-273.

17. Todolí, J. L.; Mermet, J. M., Sample introduction systems for the analysis of liquid microsamples by ICP-AES and ICP-MS. *Spectrochimica Acta Part B: Atomic Spectroscopy* 2006, *61*, (3), 239-283.

18. Russell, B. C.; Croudace, I. W.; Warwick, P. E.; Milton, J. A., Determination of Precise 135Cs/137Cs Ratio in Environmental Samples Using Sector Field Inductively Coupled Plasma Mass Spectrometry. *Analytical Chemistry* 2014, *86*, (17), 8719-8726.

19. Edwards, R.; Sedwick, P.; Morgan, V.; Boutron, C., Iron in ice cores from Law Dome: A record of atmospheric iron deposition for maritime East Antarctica during the Holocene and Last Glacial Maximum. *Geochemistry, Geophysics, Geosystems* 2006, *7*, (12).

20. Koffman, B. G.; Handley, M. J.; Osterberg, E. C.; Wells, M. L.; Kreutz, K. J., Dependence of ice-core relative trace-element concentration on acidification. *Journal of Glaciology* 2014, *60*, (219), 103-112.

21. Breton, D.; Koffman, B.; Kurbatov, A.; Kreutz, K.; Hamilton, G., Quantifying signal dispersion in a hybrid ice core melting system for geochemical and microparticle analysis, *Environmental Science &* Technology 2012, 46, (21), 11,922-11,928.

22. Bigler, M.; Svensson, A.; Kettner, E.; Vallelonga, P.; Nielsen, M. E.; Steffensen, J. P., Optimization of high-resolution continuous flow analysis for transient climate signals in ice cores. *Environmental Science & Technology* 2011, *45*, (10), 4483-4489.

23. McConnell, J. R.; Lamorey, G. W.; Lambert, S. W.; Taylor, K. C., Continuous ice-core chemical analyses using inductively coupled plasma mass spectrometry. *Environmental Science & Technology,* 2002, *36*, (1), 7-11.

24. Edwards, R.; Sedwick, P., Iron in East Antarctic snow: Implications for atmospheric iron deposition and algal production in Antarctic waters. *Geophysical Research Letters* 2001, *28*, (20), 3907-3910.

25. Rhodes, R. H.; Baker, J. A.; Millet, M.-A.; Bertler, N. A., Experimental investigation of the effects of mineral dust on the reproducibility and accuracy of ice core trace element analyses. *Chemical Geology* 2011, *286*, (3), 207-221.

26. Huber, P. J., *Robust Statistics*. Springer: 2011.

27. Aries, S.; Valladon, M.; Polvé, M.; Dupré, B., A Routine Method for Oxide and Hydroxide Interference Corrections in ICP-MS Chemical Analysis of Environmental and Geological Samples. *Geostandards Newsletter* 2000, *24*, (1), 19-31.

28. Rodushkin, I.; Engström, E.; Baxter, D. C., Sources of contamination and remedial strategies in the multi-elemental trace analysis laboratory. *Analytical and Bioanalytical Chemistry* 2010, *396*, (1), 365-377.

Chapter 4: Rare earth element dust signatures over the past two thousand years in the RICE ice core, Pacific sector, West Antarctica

Abstract

Concentrations of the Rare Earth Elements (REE) have been measured in the Roosevelt Island Climate Evolution (RICE) ice core, the first such measurements from the Pacific sector of Antarctica and the only REE data spanning the last two thousand years before present (ka BP). We find high variability in crustal-normalized REE measured as low as single fg g^{-1}, with persistent enrichment in the light REE and depletion in heavy REE. These data suggest 1) high variability in crustal-normalized REE signatures over the last 2 ka BP, similar to that seen in Holocene samples from the Drønning Maud Land and Dome C ice cores, 2) only 5% of all RICE samples indicate possible REE signatures of South American dust, and 3) suggest contributions from local Antarctic dust sources in ~40% of RICE samples showing strong negative trends across REE. These results are supported by trajectory modeling, which suggests that the RICE ice core site receives strongest transport from limited New Zealand dust sources, with lesser contributions and longer transport times from Patagonian and Australian dust sources.

4.1 Introduction

Terrestrial mineral aerosols (dust) have significant climatic effects, as a result of direct and indirect impacts on radiative forcing during atmospheric suspension [*Tegen et al.*, 1996], and through biogeochemical mechanisms when deposited over nutrient-rich, iron-deficient ocean areas [*Martínez-Garcia et al.*, 2011]. Records of dust deposition are preserved in glaciers and ice sheets, and have been used to infer past changes in regional and global dust regimes over the last 800,000 years [*EPICA*, 2004; *Fischer et al.*, 2007; *Wolff et al.*, 2010]. Dust flux in the European Project for Ice Coring in Antarctica (EPICA) Dome C, Antarctica ice core is 25-times greater during glacial periods than warmer interglacials [*Lambert et al.*, 2008], similar to other ice cores across the remote East Antarctic plateau [*Petit et al.*, 1999]. These fluctuations are the result of a complex mixture of environmental change in dust source regions [*Sugden et al.*, 2009], changing precipitation amounts and patterns affecting aerosol atmospheric lifetime [*Mahowald et al.*, 1999], and changing wind patterns and wind strength. Identifying which of these processes (or the combination of which) controls dust composition at ice core sites will allow for more accurate interpretation of these paleoclimate and paleoenvironmental records.

GCM results [*Li et al.*, 2008; *Mahowald et al.*, 2011] and ice core dust geochemical studies [*Delmonte et al.*, 2008; *Vallelonga et al.*, 2010] show some agreement that southern South American dust sources are the most dominant contributors to the Antarctic, particularly during glacial periods, with Australian dust emissions becoming of greater importance during interglacials and since the onset of the Holocene. Additional Southern Hemisphere dust sources exist in southern Africa and New Zealand, the latter of which may play a large role in dust deposition over and fertilization of the South Pacific Ocean during interglacial periods [*Lamy et al.*, 2014]. Ice core provenance studies, however, are restricted to the Atlantic and Indian Ocean sectors of the East Antarctic Ice Sheet (EAIS) and biased towards samples from dusty glacial periods, which contain enough material to allow for robust geochemical analysis.

The rare earth elements (REE, lanthanide elements Lanthanum to Lutetium) have been suggested as tracers to identify signatures of individual dust potential source areas (PSA) in small (< 5 mL), low-concentration (sub-pg g^{-1} to single fg g^{-1}) Antarctic ice core samples [*Gabrielli et al.*, 2010; *Wegner et al.*, 2012]. REE analysis requires no preconcentration or other laborious sample preparation, and although low concentrations in Holocene samples approach instrumental limits of detection this is mitigated by the large number of samples that can quickly be measured (e.g. *Gabrielli et al.* [2006] and *Neff et al.* [in review]). The REE are lithophilic elements abundant in the terrestrial crust [*Wedepohl*, 1995], and they are chemically conservative with low solubility and restricted mobility in terrestrial systems. They are not unlike isotopes, exhibiting slight differences in how they are included in crystal structures due to a small decrease in atomic radii with increasing atomic number (lanthanide contraction) [*Henderson*, 1984]. Because of their sedimentary conservatism, the relative amount of the fourteen REE measured in aeolian dust is thought to remain relatively stable and thus reflect the signature of their source. This may allow for dust provenance identification, or a reduction of possible sources, in Antarctic ice provided that the parent material has a unique, well-characterized REE signature, and that this signature is retained through atmospheric transport and deposition. However, analytical uncertainties including irregular dissolution of REE after sample acidification (e.g. *Rhodes et al.* [2011] and *Koffman et al.* [2014a]) and increased measurement uncertainty in low-concentration interglacial ice samples remain to be comprehensively addressed in consideration of REE as a paleoclimate tool.

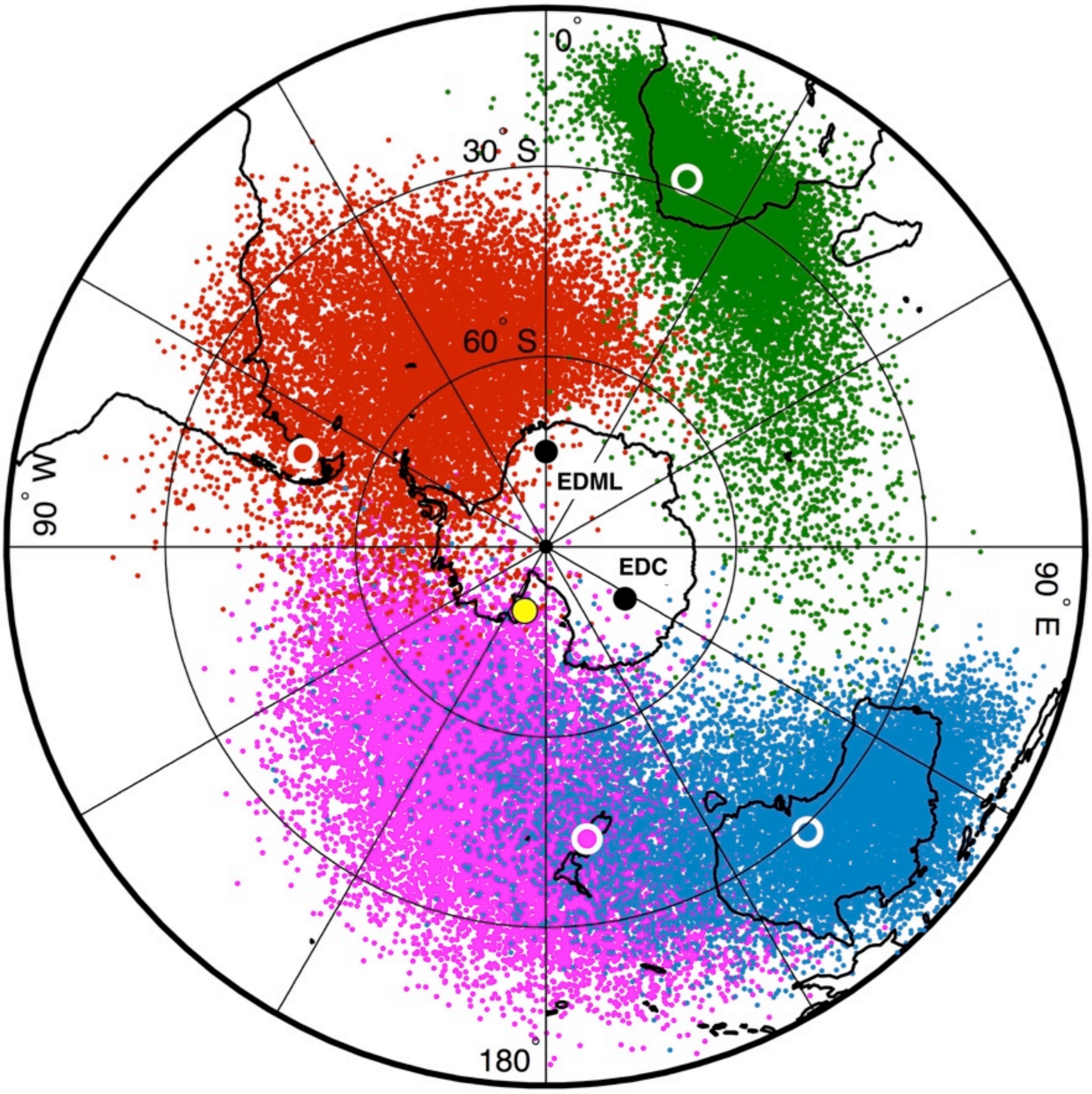

Figure 1. *RICE ice core site (yellow circle) relative to EDC and EDML (black circles) where other REE datasets are located. Small colored circles mark 5-day trajectory endpoints, initiated daily at dust potential source areas (PSA) from 1979-2013 (HySPLIT model, data from Neff and Bertler, in review). This outlines immediate transport pathways from extra-Antarctic dust PSA. PSA trajectory initiation points are indicated by large colored circles: New Zealand (magenta), Patagonia (orange), southern Africa (green) and Australia (blue).*

We present here the first ice core REE data from the Pacific Ocean sector of Antarctica. The Roosevelt Island Climate Evolution (RICE) ice core was drilled to bedrock (764 m) on Roosevelt Island, Antarctica (79.364 ºS, 161.706 ºW, Figure 1), located at the northern margin of the Ross Ice Shelf. REE measured in the RICE ice core are the only data spanning the 20th Century and the last two thousand years, and with higher-resolution than previous studies (sub-annual to three-year resolution). At this low-elevation (~550 m a.s.l.) site on the Ross Sea coast of the West Antarctic Ice Sheet (WAIS), trajectory modeling suggests strongest direct atmospheric transport from New Zealand, with lesser influence from potential dust-carrying Australian and Patagonian air masses [see data in Figure 1, from *Neff and Bertler, in review*]. RICE REE data are compared to the two existing ice core REE datasets from the EPICA Dome C (EDC, 75.1ºS, 123.4ºE, 3233 m a.s.l.) and EPICA Drønning Maud Land (EDML, 75ºS, 0ºE, 2892 m a.s.l.) ice cores.

In Section 2, we discuss sample preparation of RICE ice core samples and analytical methods employed to measure REE concentrations as low as single femtogram (10^{-15}g g^{-1}). Section 3 details the result of these analytical efforts, with comparison to measurements on the EDC and EDML ice cores. The discussion in Section 4 considers procedural and analytical challenges of this and previous work using REE to explore dust provenance, before commenting on possible advances in understanding of Antarctic dust gained from this new REE data from the RICE ice core. Conclusions are provided in Section 5, and suggestions are made for future steps to develop the REE as dust provenance indicators in polar ice core studies.

4.2 Methods

The detailed methodology for sample treatment and analysis is discussed at length in *Neff et al.* [in review], but is summarized here with additional details specific to REEs. Discrete samples were taken from the RICE ice core during a continuous flow analysis (CFA, e.g. *Bigler et al.* [2011]) campaign, melting in sequence 1 m-long rods cut from the interior of ice cores (~34 mm by 34 mm wide). Samples from the RICE ice core discussed here span depths from 8 m to 320 m below the 2011 snow surface (an 8 m deep trench was required to accommodate drill infrastructure). From 8 m to 40 m, mean sample depth-resolution is 4 cm (~4 mL liquid), with a total of 784 samples. Annual layer counting of sulfate and water stable isotopes in shallow firn cores and the RICE deep ice core dates ice at 8 m depth to 1993 CE (± 0.5 years) and 40 m depth to 1901 CE (± 1 year). Due to high loading of marine salts in the coastal RICE ice core, identification of known volcanic events has proven difficult and is ongoing. This agescale results in a mean sample age-resolution of ~0.13 years for 8 m – 40 m samples spanning the 20th Century (linear interpolation between annual layer determinations).

Below 40 m, individual samples were combined into approximately 3-year averages, estimated using a preliminary depth-age scale (*Dansgaard and Johnsen* [1969] ice flow model, T.J. Fudge, personal communication, 2014). Sampling was stopped at 320 m depth, determined to be approximately 2 ka BP using this initial age model. Aliquots were taken from every other sample (alternate samples were reserved for additional analyses) and pipetted into a single vial, combining samples spanning ~1 m depth at 40 m (14 individual samples combined into one), reducing to a ~0.2 m interval (4-5 samples into one) at 320 m for a total of 580 combined samples. Refinement of the RICE agescale since samples were prepared includes matching to high-resolution methane gas measurements from the RICE, WAIS Divide, and Law Dome ice cores, assuming a constant 150 year gas-age ice-age difference (Δage) at RICE. A volcanic tie point to the 1257 CE "unknown" eruption [*Sigl et al.*, 2013] also provides age control at 165 m depth (*A. Kurbatov*, personal communication 2015). The ice age at 320 m is approximately 2.3 ka BP. This increases mean sample age resolution for 40 m to 320 m combined samples to 3.6 years.

Preparatory work was conducted in a class-100 clean room under laminar flow hoods, and procedural blanks of ultrapure water (>18 MΩ) and 1% HNO_3 v/v (Optima^{TM}) were placed under hoods during this process to constrain maximum contamination levels (procedural blanks, mean concentrations in Table 1). All ice core samples were acidified to 1% HNO_3 v/v at least three months prior to analysis, allowing for extended solid-particle leaching and stable elemental concentrations (e.g. *Rhodes et al.* [2011], *Koffman et al.* [2014a]). Incongruent dissolution in acidified samples has considerable implications for elemental ratios with respect to crustal abundance, which is particularly important for REE dust provenance studies, and is discussed below. Trace element analysis was undertaken in the John de Laeter Centre Trace Research Advanced Clean Environment (TRACE) facility at Curtin University, Perth, Australia using a jet-interface sector-field inductively coupled plasma mass spectrometer (Jet-SF-ICPMS, Element XR, e.g. *Russell et al.* [2014]). A seaFAST S2 syringe-pump auto-sampler was coupled to a PFA-ST nebulizer and APEX-Q desolvation system (all Elemental Scientific, Inc.), with an additional flow of high-purity nitrogen to tune response. A 500 pg g^{-1} Indium (In) was mixed inline as an internal standard to correct for instrumental drift, with sensitivity of 14 x 10^6 counts per second per ng g^{-1} maintained through instrument tuning after every ~32 hour analytical session. Analytical blanks (1% HNO_3 v/v Optima^{TM}) and quality control samples (made from certified single- and multi-element stock solutions, Elemental Scientific, Inc.) were placed after every ten samples with duplicate quality controls run in every second grouping. Indium-normalized ion intensities were calibrated to ten external standards prepared from National Institute of Standards and Technology traceable elemental standards. Analytical blanks, an average of at least ten per ~32 hour analytical session, were subtracted from ice core sample concentrations (Table 1).

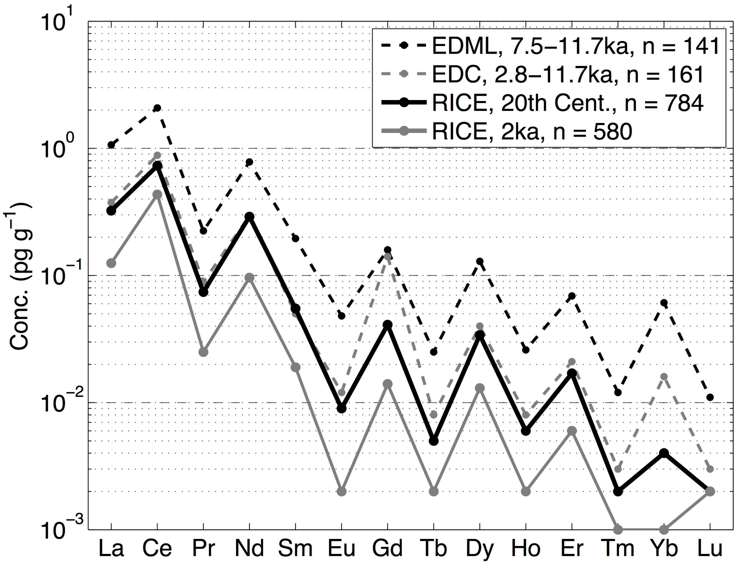

Figure 2. *Log concentration (pg g^{-1}) of mean REE in RICE ice core samples (20th Century, solid black; 2 ka BP, solid gray), and mean EDML (dashed black) and EDC (dashed gray) samples. EDML and EDC samples span the Holocene (beginning 11.7 ka BP) and extend to youngest measured samples (7.5 ka BP and 2.9 ka BP, respectively).*

4.3 Results

Mean RICE ice core REE concentrations, analytical and procedural blanks and limits of detection (LOD, three standard deviations, 3σ, of the analytical blank) are listed in Table 1. Modern RICE REE compare well to Holocene (beginning 11.7 ka BP) samples from EDC and EDML (Figure 2). Expected REE features are observed in RICE data: decreasing abundance with increasing atomic number (lanthanide contraction), a drop in concentration from Sm to Eu (Europium anomaly), and greater abundance of elements with even atomic numbers (Oddo-Harkins rule: paired protons of even atomic numbered elements enhance stability and hence natural abundance). Observed departures from expectations are as follows.

All RICE samples show low concentrations of Yb (Figure 2), which are not normally-distributed (see Figure S1 and S2) and thus excluded from further analysis. RICE samples also have very high concentrations of Ce near all breaks in the ice core (at least every 1 m), with concentrations >10 pg g^{-1}. This is removed by excluding all Ce values >1σ (3.2 pg g^{-1}, 49 samples), and the corrected mean is plotted in Figure 2. Despite this correction values for Ce remain anomalously high (especially in crustal ratios, see below), thus Ce is removed from calculations for all RICE samples and is interpreted with caution. RICE 40 m – 320 m combined samples have lower concentrations for all REE than 8 m – 40 m samples, particularly for Eu and Tm (see Table 1). This is likely due to particulate settling, as vials were not agitated prior to combination into 3-year averages. Tm is excluded from calculation of REE means for these samples. Certain REE are also excluded from consideration for EDC and EDML. Maximum Gd concentrations are reported for EDC samples due to spectral interferences during analysis, explaining anomalously high mean EDC Gd concentrations in Figure 1 [*Gabrielli et al.*, 2010]. Gd is not used further in calculations of means or consideration of REE patterns in EDC samples. High concentrations are observed in EDML samples for all REE, likely due to these data not being blank subtracted (see discussion in *Wegner et al.* [2012]). Tm was not considered by *Wegner et al.* [2012] due to likely spectral interferences and is similarly excluded here for EDML samples.

Mean REE concentrations for 8 m – 40 m samples are displayed in Table 1 both with and without samples below the LOD removed. We proceed with data analysis including all samples, bearing in mind this analytical limitation for very low-concentration HREE. Mean sample relative standard deviation (RSD) at sub-pg g^{-1} concentration is ~5-15% for light REE (LREE: La, Ce, Pr, Nd), 25-30% for medium REE (MREE: Sm, Eu, Gd, Tb, Dy) and rising from 30% to 60% for lowest-concentration heavy REE (HREE: Ho, Er, Tm, Yb, Lu). RICE REE measurement uncertainty at sub-pg g^{-1} (sub part per trillion) concentration compares favorably to that of EDC samples in *Gabrielli et al.* [2010], with consistent relationships between concentration and sample RSD (Figure 3). *Wegner et al.* [2012] did not publish RSD for EDML data, however since the same analytical method was used as *Gabrielli et al.* [2010], we assume similar sample RSD as for EDC samples. RICE 8 m to 40 m samples have similar concentration versus RSD trends to those of EDC measurements. One ICPMS analytical session, including combined samples from 40 m – 180 m, had reduced stability and high RSD and sample variability; this anomalous analytical performance is not included in Figure 3. The final ICPMS analytical session, samples spanning 180 m – 320 m, was very stable and showed limited increase in RSD even at single fg g^{-1} concentrations suggesting that with further optimization the method of *Neff et al.* (in review) may significantly reduce uncertainty in measurements of REE at these ultra-low concentrations (black x's, Figure 3).

All sample concentrations are normalized to upper continental crust (UCC) values as in *Wegner et al.* [2012]:

$$La^* = \frac{La_{ice}}{La_{UCC}}, \quad (1)$$

where La_{ice} is the La concentration in the ice sample (La used as an example), and La_{UCC} is the mean La concentration in the UCC [*Wedepohl*, 1995]. A further normalization step is made to remove the mean concentration of all REE from the ratio:

$$La_{norm} = \frac{La^*}{REE^*}, \qquad (2)$$

where REE^* is the mean normalized value of all REE as in Eq. 1 (excluding Ce and Yb for reasons stated above). Mean UCC-normalized REE concentrations (REE_{norm}) are presented in Table 2. $LREE_{norm}$, $MREE_{norm}$ and $HREE_{norm}$ are plotted in Figure 4 for RICE samples from 8 m to 40 m and 40 m to 320 m. $LREE_{norm}$ are consistently enriched by ~30%, with mean $MREE_{norm}$ enrichment of ~10% and $HREE_{norm}$ depletion of ~10%. Similar characteristics are observed in 3.6-year combined samples spanning 2 ka BP, although MREE are slightly less enriched due to anomalously low Eu concentration (with respect to sub-annual 8 m – 40 m samples). However, mean REE_{norm} values remain constant through samples measured during the unstable analytical session (40 m to 180 m samples, Figure 4), as do diagnostics discussed below, with some additional variability. No persistent shifts are observed in relative enrichment between REE groupings. Figure 4 illustrates the impact of increased sample resolution on variability in REE_{norm} groupings, which suggests caution in interpreting increased variability observed in Holocene REE trends relative to the LGS (Last Glacial Stage) as in *Gabrielli et al.* [2010] and *Wegner et al.* [2012]. Holocene samples from EDC and EDML are spaced more closely and span less time, reducing signal averaging as ice flow thinning effects progressively lessen and snow accumulation rates increase from LGS minima (e.g. *Cuffey and Paterson* [2010]). This is additionally complicated by the fact that EDC samples represent 2-3 to 4-5 years per samples (with large and inconsistent sample spacing), while EDML samples are 20 to 45 year averages (with samples more consistently spaced).

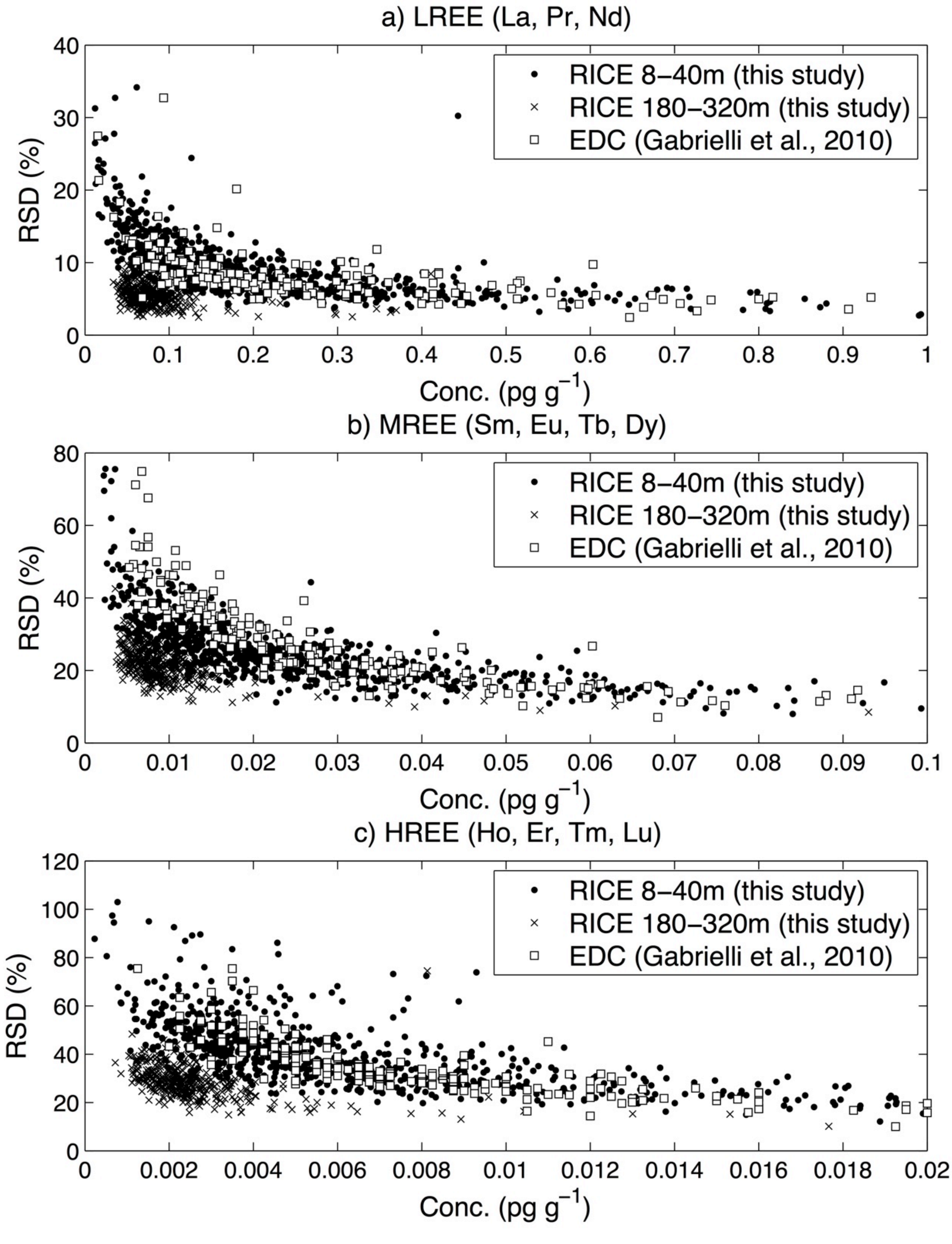

Figure 3. *Sub-pg g^{-1} concentration relative standard deviation (RSD, %) for a) LREE (excluding Ce), b) MREE (excluding Gd), and c) HREE (excluding Yb) in RICE (black circle and x) and EDC (white square) samples. RSD from unstable analytical session, samples from 40 m to 180 m, are not included.*

Table 1. *Concentration (pg g^{-1}) of 20th Century RICE REE sample mean, analytical blank mean, procedural blank mean and Limit of Detection (LOD)*

Isotope	8 m-40 m mean conc. (analytical blank subtracted, n = 784*)	8 m-40 m mean conc. (analytical blank subtracted, <LOD removed)	40 m-320 m mean conc. (analytical blank subtracted, n = 580)	Analytical blank mean (n = 86)	Procedural blank mean (n = 13)	LOD (3σ analytical blank)
^{139}La	0.324	0.324	0.125	0.004	0.009	0.004
^{140}Ce	0.730	0.737	0.433	0.010	0.012	0.036
^{141}Pr	0.074	0.074	0.025	0.001	0.004	0.001
^{146}Nd	0.290	0.290	0.096	0.003	0.007	0.006
^{147}Sm	0.055	0.057	0.019	0.005	0.007	0.007
^{153}Eu	0.009	0.011	0.002	0.003	0.005	0.003
^{157}Gd	0.041	0.047	0.014	0.008	0.008	0.012
^{159}Tb	0.005	0.008	0.002	0.002	0.002	0.003
^{163}Dy	0.034	0.034	0.013	0.001	0.003	0.003
^{165}Ho	0.006	0.006	0.002	0.001	0.004	0.001
^{166}Er	0.017	0.017	0.007	<0.001	<0.001	0.001
^{169}Tm	0.002	0.004	0.001	0.001	0.002	0.002
^{172}Yb	0.004	0.004	0.001	<0.001	0.001	<0.001
^{175}Lu	0.002	0.003	0.002	<0.001	0.001	0.001

**784 total RICE samples for all isotopes except Ce, for which n = 735 after removing contaminated samples (core breaks).*

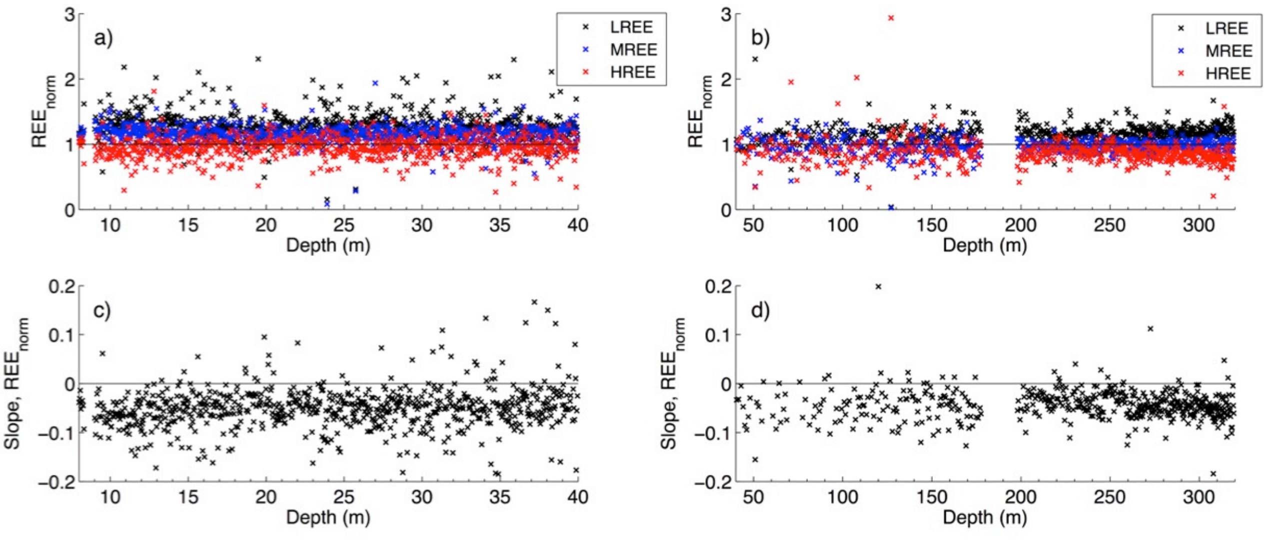

Figure 4. *REE$_{norm}$ for light (LREE, black), medium (MREE, blue) and heavy REE (HREE, red), a) 8 m to 40 m samples and b) 40 m to 320 m combined samples and corresponding REE$_{norm}$ slope in c) and d). The analytical run for samples from 40 m to 180 m depth (b) had reduced stability, explaining increased variability of these data.*

Sample distributions of all REE_{norm} for RICE, and Holocene EDC and EDML datasets (all normalized as in Eq. 1 and 2) are displayed in Figures S1-S4. We classify REE_{norm} patterns in samples by calculating the linear slope across all REE_{norm} concentrations to indicate relative enrichment of heavier REE (positive slope) versus enrichment of lighter REE (negative slope). This diagnostic has the advantage of taking into account all measured LREE and HREE isotopes, and not biasing interpretations towards individual elements or REE groupings (Figure 5). Although REE_{norm} slope is insensitive to less-variable MREE, this measure clearly captures strong trends across REE_{norm} (significant enrichment or depletion of the LREE and HREE), which are present in the most distinct and identifiable dust PSA signatures (see further discussion, Section 4.4). Ce and Yb are not considered in samples from the RICE ice core, Gd is excluded from consideration in EDC samples and Tm excluded in EDML samples, as above. REE_{norm} slope was not calculated for many samples from 40 m to 180 m depth, as many HREE concentrations were below blank levels; more variable but consistent slope values are maintained for calibrated samples through this analytical session (Figure 4d).

The slope from light to heavy elements across REE_{norm} in the RICE ice core is compared to existing data from the EDC and EDML ice cores in Figure 6 (mean and standard deviation detailed in Table 3). There is agreement between the two sample types from the RICE ice core, with a mean slope of -0.050 ± 0.049 (1σ) in 20th Century sub-annual samples from 8 m – 40 m and a slope of -0.043 ± 0.030 in 3.6-year combined samples from 40 m – 320 m extending from the late 19th Century to ~2 ka BP. Similar enrichment is seen in Holocene samples from EDC, while EDML REE_{norm} is essentially crustal in its mean signature (Figure 6, Table 3). Mean REE_{norm} slope and standard deviation for RICE samples and Holocene / Last Glacial Stage (LGS) EDC and EDML samples are presented in Table 3.

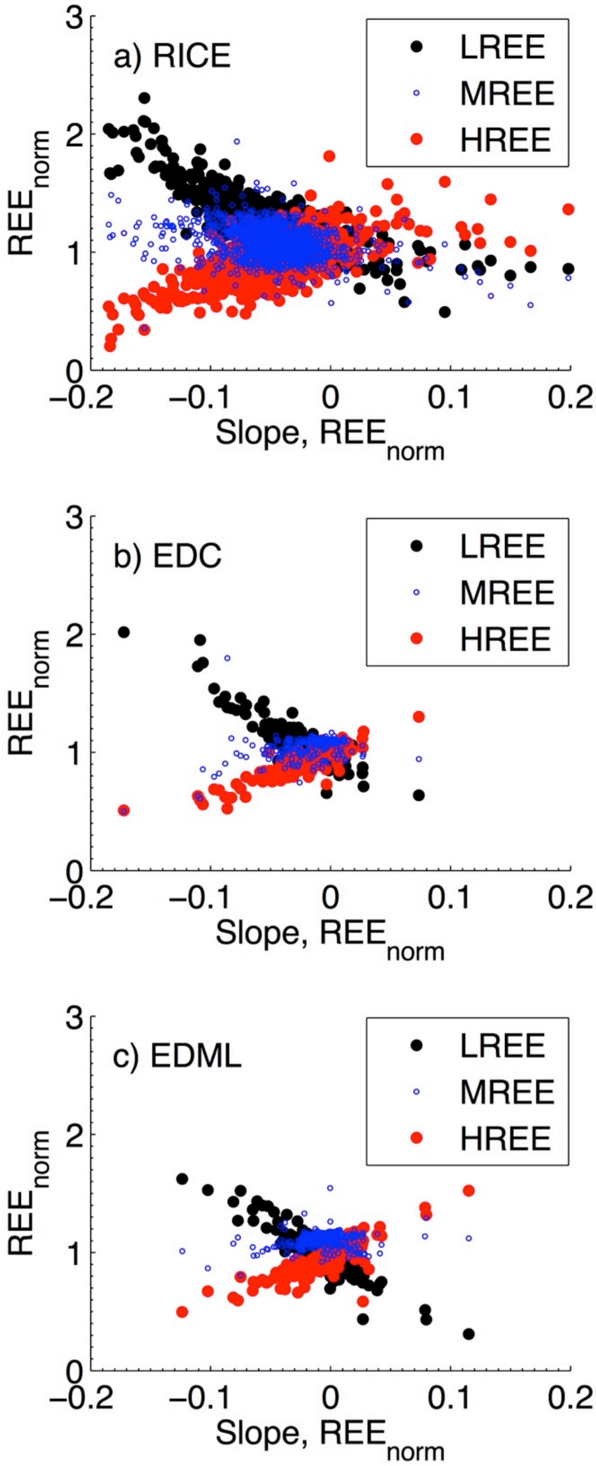

Figure 5. *REE_{norm} slope sensitivity to $LREE_{norm}$, $MREE_{norm}$ and $HREE_{norm}$ in a) RICE, b) EDC and c) EDML samples.*

Table 2. *Mean and standard deviation of UCC-normalized REE concentrations (REE_{norm}) in RICE samples and Holocene EDML and EDC ice core samples.*

Isotope	RICE 8-40m REE_{norm}	RICE 8-40m REE_{norm} (<LOD rem.)	RICE 8-40m STD	RICE 40-320m REE_{norm}	RICE 40-320m STD	EDC Holo. REE_{norm}	EDC Holo. STD	EDML Holo. REE_{norm}	EDML Holo. STD
^{139}La	**1.29**	1.29	0.26	**1.37**	0.19	**1.11**	0.34	**1.01**	0.20
^{140}Ce	**1.78**	1.55	1.21	**1.87**	0.50	**1.23**	0.45	**1.01**	0.25
^{141}Pr	**1.32**	1.31	0.22	**1.23**	0.19	**1.19**	0.26	**0.96**	0.15
^{146}Nd	**1.27**	1.27	0.19	**1.13**	0.27	**0.99**	0.16	**0.84**	0.12
^{147}Sm	**1.25**	1.24	0.27	**1.15**	0.26	**0.90**	0.18	**1.10**	0.15
^{153}Eu	**0.88**	0.88	0.23	**0.47**	0.26	**0.82**	0.22	**1.10**	0.55
^{157}Gd	**1.21**	1.24	0.25	**1.09**	0.25	**3.30**	2.77	**1.15**	0.11
^{159}Tb	**0.94**	0.98	0.26	**0.92**	0.28	**1.20**	0.19	**1.13**	0.10
^{163}Dy	**1.12**	1.09	0.20	**1.08**	0.21	**1.08**	0.16	**0.96**	0.12
^{165}Ho	**0.90**	0.92	0.21	**0.79**	0.31	**0.97**	0.16	**0.93**	0.12
^{166}Er	**1.03**	0.99	0.23	**1.03**	0.23	**1.01**	0.17	**0.92**	0.13
^{169}Tm	**0.84**	0.91	0.33	**0.90**	0.37	**0.98**	0.20	**1.17**	0.19
^{172}Yb	**0.24**	0.23	0.07	**0.21**	0.08	**0.73**	0.19	**0.86**	0.13
^{175}Lu	**0.72**	0.65	0.76	**0.74**	0.62	**0.77**	0.17	**0.87**	0.18

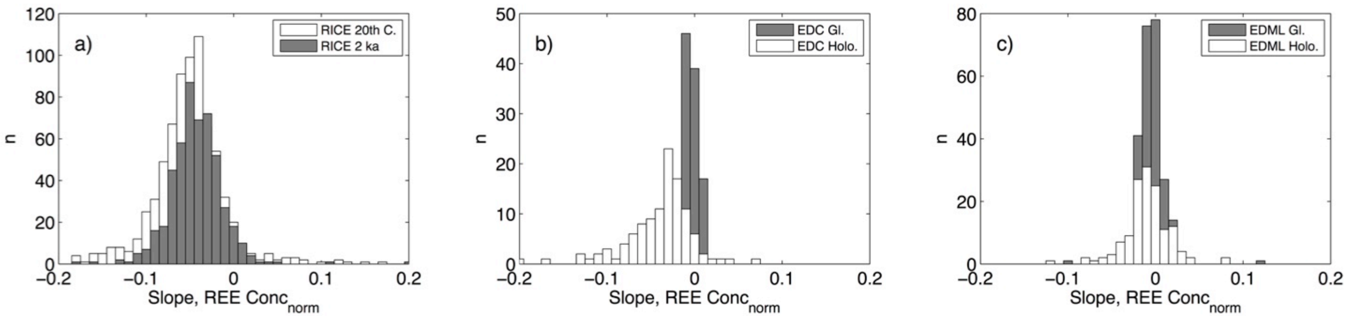

Figure 6. *Distribution (number of samples, n) of REE_{norm} slope in samples from a) RICE (20^{th} Century and 2 ka BP), b) EDC (LGS, 33.7 ka BP to 11.7 ka BP, n = 134; Holocene, 11.7 ka BP to 2.9 ka BP, n = 161) and c) EDML (LGS, 26.6 ka BP to 11.7 ka BP, n = 258; Holocene, 11.7 ka BP to 7.5 ka BP, n = 141). Positive slope indicates relative enrichment in $HREE_{norm}$ (depletion in LREE), negative slope indicates relative enrichment in $LREE_{norm}$ (depletion in HREE).*

Table 3. *Mean REE_{norm} slope and standard deviation in RICE, EDC and EDML samples spanning the Holocene and Last Glacial Stage*

Age	Mean RICE REE_{norm} slope	1σ	Mean EDC REE_{norm} slope	1σ	Mean EDML REE_{norm} slope	1σ
Holocene*	-0.050	0.049	-0.042	0.047	-0.010	0.026
LGS	-	-	-0.005	0.011	-0.006	0.022

* RICE samples are 8-40m (20th Century) samples

4.4 Discussion

4.4.1 Sample acidification biases towards LREE enrichment

Precaution must be taken during sample preparation in REE dust provenance studies, due to preferential leaching of lighter REE and incongruent leaching with respect to crustal values in acidified samples (required for ICPMS analysis). RICE samples show persistent enrichment in $LREE_{norm}$, which may be overestimated due to acid-leaching effects. When comparing lightly-acidified (1% HNO_3, as here) ice core sample REE recovery with that from a full acid digestion (HF and HNO_3), *Gabrielli et al.* [2010] found preferential enrichment of LREE—20% to 30% additional recovery relative to the HREE. An additional LREE bias was also observed in un-filtered samples with particle sizes larger than 0.2 μm, suggesting that larger particle sizes release more LREE after acidification. Preliminary particle size data from RICE surface snow (summer 2012) suggest a mode diameter of ~2 μm, but also indicate that particles > 5 μm diameter are present (*H. Winton and B. Delmonte,* unpublished data). In the WAIS Divide ice core (79.5ºS, 112.1ºW), located at the highest-elevation ice divide of the WAIS (1766 m a.s.l.), large mode particle diameters of ~5 μm are observed in Holocene samples [*Koffman et al.*, 2014b], compared to ~2 μm in EDC samples [*Delmonte et al.*, 2004]. Similar results suggesting incongruent REE dissolution were found by *Rhodes et al.* [2011], in acidification tests of rock standards diluted to approximate ice core dust concentrations. While we did not perform a similar experiment specifically for REE in RICE ice core samples, we assume that some preferential LREE enrichment may affect our samples. We suggest that a proportional correction to enriched RICE $LREE_{norm}$ data does not negate this observation and cannot explain $HREE_{norm}$ depletion prevalent in RICE samples.

4.4.2 RICE REE comparison to EDC and EDML

Two observations have resulted from previous REE dust provenance studies in ice cores. Firstly, REE in both the EDC and EDML ice cores display a persistent, approximately crustal-average REE_{norm} pattern in samples from the LGS [*Gabrielli et al.*, 2010; *Wegner et* *al.*, 2012]. Interpretation has been equivocal, suggesting that this stable signature either represents one dominant dust source or a consistent mix of many. The second observation is that REE_{norm} variability increases beginning ~15 ka BP. However, we caution that this change coincides with a twenty- to thirty-fold reduction in REE concentrations and dust mass, which continues through youngest available late-Holocene samples. This increase in variability is most pronounced in EDC samples, seen as a broadening of the Holocene normalized REE slope distribution in Figure 6b and Figure 7, with the mean REE_{norm} slope also shifting toward greater LREE enrichment (more negative REE_{norm} slope). EDML mean REE_{norm} trends do not change significantly, but show a small (~20%) increase in REE_{norm} slope variability from LGS to Holocene samples (Figure 6c, Table 3; this result is similar if data are partitioned at 15 ka BP as in *Wegner et al.* [2012]). Increased EDML REE_{norm} variably during the Holocene is not as well captured by our REE_{norm} slope diagnostic, as this measure is insensitive to fluctuations in $MREE_{norm}$ (Figure 5).

The role of increased measurement uncertainty in more variable Holocene REE_{norm} patterns must be carefully considered to evaluate REE as a tool to explore dust provenance during less dusty periods when the utility of other geochemical techniques are limited (e.g. Pb and Sr/Nd isotopes [*Delmonte et al.*, 2008; *Vallelonga et al.*, 2010]). Low REE concentrations during the Holocene incur greater relative measurement uncertainty, especially for MREE and HREE, which approach instrumental LODs. In EDC samples, RSD increases from <20% in LGS samples to 30-60% during the Holocene when many MREE and HREE concentrations are only several times greater than reported 3σ LODs (Figure 7, data from *Gabrielli et al.* [2010]). Holocene mean concentrations and LODs are presented in Table 4 for RICE, EDC and EDML. RICE REE have similar measurement uncertainty to EDC samples, as shown in Figure 3, but show slightly higher average errors due to lower concentrations especially in combined samples from 40 m to 320 m depth (Figure 7). While RSD representing uncertainties as small as single fg g^{-1} may seem insignificant, these relative uncertainties are propagated through crustal normalization, resulting in large uncertainties for $MREE_{norm}$ and $HREE_{norm}$ (uncertainties for $LREE_{norm}$ remain lower).

Table 4. *Mean Holocene REE concentrations (pg g^{-1}) and Limits of Detection (LOD) in RICE, EDC and EDML ice core samples*

	RICE 8-40m conc.	RICE LOD	**RICE conc./LOD**	EDC Holo. conc.	EDC LOD	**EDC conc./LOD**	EDML Holo. conc.	EDML LOD	**EDML conc./LOD***
^{139}La	0.324	0.004	**81**	0.375	0.004	**94**	1.066	0.027	**39**
^{140}Ce	0.730	0.036	**20**	0.882	0.004	**221**	2.078	0.160	**13**
^{141}Pr	0.074	0.001	**74**	0.089	0.002	**45**	0.224	0.050	**4.5**
^{146}Nd	0.290	0.006	**48**	0.294	0.008	**37**	0.781	0.010	**78**
LREE mean	0.355	0.012	**56**	0.410	0.005	**99**	1.037	0.062	**34**
^{147}Sm	0.055	0.007	**7.9**	0.050	0.008	**6.3**	0.195	0.012	**16**
^{153}Eu	0.009	0.003	**3.1**	0.012	0.003	**4.0**	0.048	0.005	**9.6**
^{157}Gd	0.041	0.012	**3.4**	0.141	0.030	**4.7**	0.159	0.003	**53**
^{159}Tb	0.005	0.003	**1.8**	0.008	0.002	**3.9**	0.025	0.002	**13**
^{163}Dy	0.034	0.003	**11**	0.040	0.003	**13**	0.129	0.002	**65**
MREE mean	0.029	0.006	**5.5**	0.050	0.009	**6.5**	0.111	0.005	**31**
^{165}Ho	0.006	0.001	**5.9**	0.008	0.001	**7.7**	0.026	0.001	**26**
^{166}Er	0.017	0.001	**17**	0.021	0.002	**11**	0.069	0.002	**35**
^{169}Tm	0.002	0.002	**1.0**	0.003	0.001	**3.0**	0.012	0.001	**12**
^{172}Yb	0.004	0.001	**3.7**	0.016	0.002	**8.0**	0.061	0.002	**30**
^{175}Lu	0.002	0.001	**2.1**	0.003	0.001	**2.7**	0.011	0.002	**5.3**
HREE mean	0.006	0.001	**5.9**	0.010	0.001	**6.4**	0.036	0.002	**22**

*EDML concentrations are not blank subtracted

Comparing observed trends across all REE (i.e. REE$_{norm}$ slope) in all ice core samples is the simplest method to reduce measurement uncertainty in Holocene samples, taking advantage of the large sample sizes achievable with REE analysis. In both RICE and Holocene EDC samples, REE$_{norm}$ slope is persistently negative, enriched in LREE and depleted in HREE relative to UCC (Figures 6 and 7, Table 3). The majority of EDML samples show limited change in REE$_{norm}$ slope from the LGS to the Holocene, exhibiting crustal LREE$_{norm}$ values, 10-15% enrichment in MREE$_{norm}$ and 10% depletion in HREE$_{norm}$ (Table 2). We proceed with an interpretation of this observed LREE$_{norm}$ enrichment and HREE$_{norm}$ depletion observed in Holocene ice from RICE and EDC, and a mean crustal REE$_{norm}$ signature at EDML. Yet, we do not treat these data as timeseries, acknowledging that understanding of signal-noise relationships has not been confidently demonstrated.

Figure 7. (Following page) *Characteristics of RICE and EDC ice core REE samples mean concentration (pg g^{-1}) of LREE, MREE and HREE (a, b), REE slope (c, d), and mean relative standard deviation (RSD; e, f). Vertical line marks the 15 ka BP transition discussed by Gabrielli et al. [2010] and Wegner et al. [2012].*

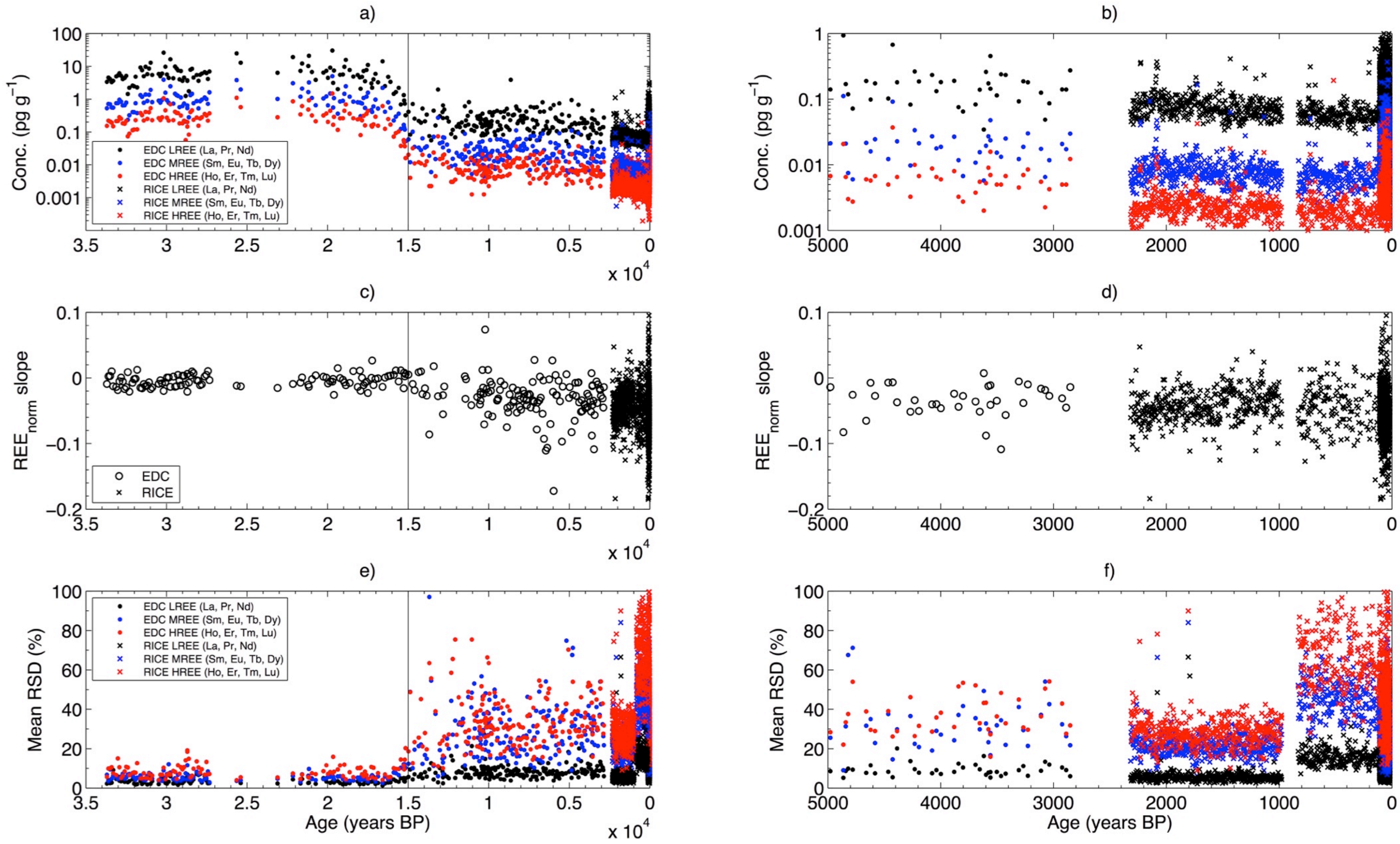
a)
b)
c)
d)
e)
f)
Conc. (pg g⁻¹)
REE norm slope
Mean RSD (%)
Age (years BP)
x 10⁴
EDC LREE (La, Pr, Nd)
EDC MREE (Sm, Eu, Tb, Dy)
EDC HREE (Ho, Er, Tm, Lu)
RICE LREE (La, Pr, Nd)
RICE MREE (Sm, Eu, Tb, Dy)
RICE HREE (Ho, Er, Tm, Lu)
EDC
RICE

4.4.3 Modern/Holocene dust PSA contributions to ice core sites

Prior to attributing the origin of REE signatures in ice core samples, likely PSA supplying dust to ice core sites are identified. We use the forward-trajectory data of *Neff and Bertler* (in review) to consider the modern atmospheric transport regimes at these sites (Figure 9), with additional consideration of independent local/regional geochemical and atmospheric model studies constraining dust sources for these sites. *Neff and Bertler* use the Hybrid Single Particle Lagrangian Integrated Trajectory model (HySPLIT, *http://ready.arl.noaa.gov/HYSPLIT.php, National Oceanic and Atmospheric Administration Air Resources Laboratory, Silver Spring, MD, USA;* [*Draxler and Hess*, 1998]) to explore atmospheric transport pathways from Southern Hemisphere dust PSA to Antarctica, calculating daily forward trajectories from 1979-2013 with a 10-day runtime. Daily trajectory endpoints (12,775 total) for each dust PSA are presented after 5 and 10 days, with an additional 15-day run time, in Figure S5. Trajectories become well-mixed after 15 days; this represents longer transport time than the average particle lifetime in either present or LGS model studies (e.g. *Mahowald et al.* [1999]) but is presented for reference.

4.4.3.1 RICE

RICE is a low-elevation, coastal site in the Pacific sector of Antarctica that is most directly downwind of Australian and New Zealand dust sources (Figure 1, Figure S5, *Neff and Bertler, in review*). This site and the WAIS is strongly influenced by synoptic storm activity associated with the Amundsen Sea Low [*Hosking et al.*, 2013; *Nicolas and Bromwich*, 2011], which brings airmasses from the Pacific sector of the Southern Ocean up the relatively shallow coastal gradient of the WAIS. Backward trajectories generated using the HySPLIT model demonstrate that in the 48-hours before arriving at Roosevelt Island, most daily trajectories over the four year period from 2010 to 2013 pass over the WAIS and specifically Marie Byrd Land (Figure 8).

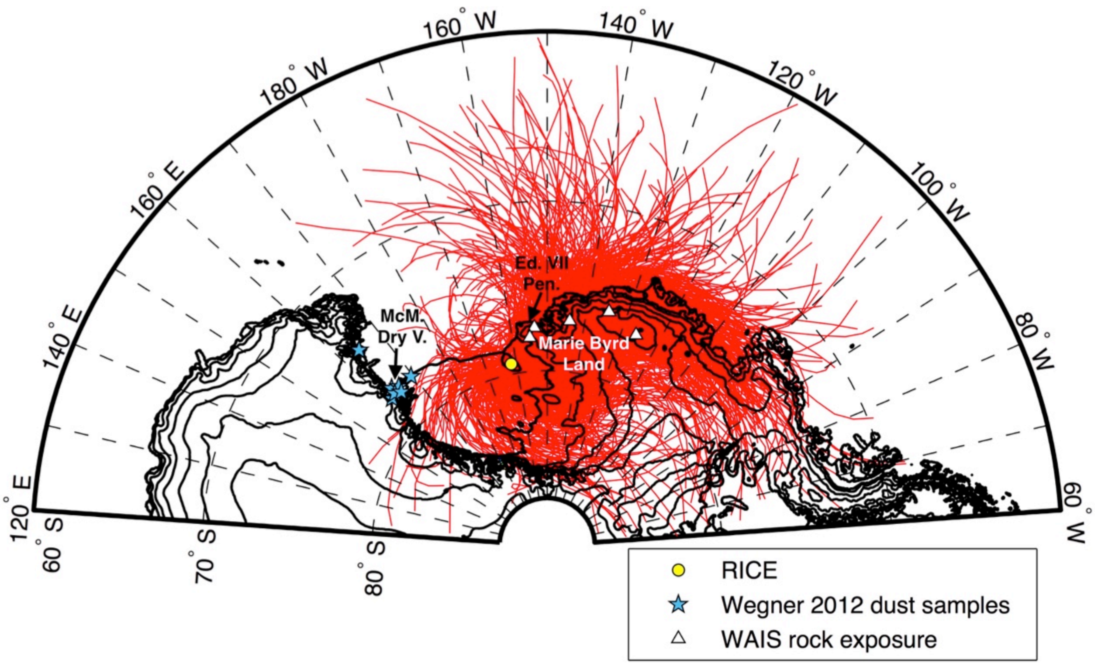

Figure 8. *2010-2013 daily 48-hour HySPLIT backward trajectories, initiated at the RICE ice core site (yellow circle), 100 m above ground level. The large ice-free McMurdo Dry Valleys are indicated, with dust samples from Wegner et al. [2012] marked (blue stars). Outcropping Marie Byrd Land mountain ranges, not sampled for REE, are marked (white triangles) and the location of King Edward VII Peninsula (Ed. VII Pen.) is indicated.*

Few high-order geochemical studies have been previously undertaken on West Antarctic ice cores, but large dust particle size distributions (5 – 8 µm mode diameter) in the WAIS Divide ice core, spanning the last 2.4 ka BP, suggest a possible local West Antarctic dust source in addition to extra-Antarctic PSA [*Koffman et al.*, 2014b]. While ice-free areas are not extensive cross the Marie Byrd land and the WAIS, a number of granitic, metamorphic and volcanic rock outcrops may contribute to local dust loading, indicated in Figure 8, including the Rockefeller and Alexandra Mountains (Edward VII Peninsula), Ford Ranges, Flood Range and Executive Committee Range in addition to regional volcanoes [*Luyendyk et al.*, 1996].

Neff and Bertler (in review) demonstrate that this sector of Antarctica, and the RICE ice core site, is subject to strong, direct atmospheric transport from New Zealand dust sources (Figure 9a, b). Over the last thirty-five years, fewer than of 12% of daily trajectories initiated at any Southern Hemisphere dust PSA reach the Antarctic continent (defined as areas south of 70ºS latitude). The number of New Zealand trajectories passing over the RICE ice core site within ten days is three to four times more than those from the Patagonian dust PSA (0.6

– 0.8% of all New Zealand trajectories pass over RICE, compared to 0.2% of all Patagonian trajectories). Half as many Australian dust PSA trajectories (0.1%) as those from Patagonia arrive in the vicinity of RICE within 10 days of transport time, and essentially no southern African trajectories arrive near RICE. While the differing trajectory contributions from these dust PSA trajectories seems small, the relative differences are significant as the represents a 35-year average of daily trajectory calculations. When trajectories are weighted by modeled dust emission rates from *Li et al.* [2008], contributions appear more mixed due to small but poorly quantified New Zealand dust emissions and large weighting given to Australian trajectories. Several independent GCM results also suggest that coastal Wilkes Land, Victoria Land and Marie Byrd Land are the most likely areas to be influenced by long-range mid-tropospheric transport of Australian dust [*Albani et al.*, 2012; *Krinner et al.*, 2010; *Li et al.*, 2008].

4.4.3.2 EDC

Isolated in the high interior of the EAIS plateau, EDC is removed from all dust sources. Katabatic airflow is persistent across Antarctica [*Parish and Bromwich*, 2007], restricting access of low-level airflow to interior areas of the continent—especially cutting off the high EAIS plateau and the EDC ice core site from extra-Antarctic atmospheric transport. As discussed above, geochemical studies from EDC and other EAIS ice cores favor South America as a dominant dust source (e.g. *Delmonte et al.* [2008]), especially during glacial periods when glaciogenic dust sources in Patagonia abruptly activate [*Sugden et al.*, 2009]. Transport of pollutants (Pb) from Australia is clearly observed in modern ice core samples from the coastal East Antarctic Law Dome ice core (66.8ºS, 112.8ºE) [*Vallelonga et al.*, 2002], confirming that Australian atmospheric transport is linked to this sector of the Antarctic and may also be an identifiable contributor to dust across coastal Wilkes Land and the EAIS during interglacial periods [*De Deckker et al.*, 2010; *Revel-Rolland et al.*, 2006]. Figure 9 (c, d) suggests highly mixed dust PSA contributions to the remote interior of the EAIS plateau, with very few trajectories initiated at dust PSA arriving over EDC in the thirty-five years considered by *Neff and Bertler* (in review). When weighted for dust PSA emissions, however, Australian dust contribution to EDC appears to be significantly greater than other PSA (Figure 9d).

4.4.3.3 EDML

EDML, located on the Atlantic margin of the EAIS plateau, is directly downwind of the significant Patagonian dust source (Figure 9). It is clearly subject to strong influence of this dust PSA, both at present and during the LGS, as indicated by model studies [*Albani et* *al.*, 2012; *Krinner and Genthon*, 2003; *Krinner et al.*, 2010; *Li et al.*, 2008; *Li et al.*, 2010b], and dust transport over the South Atlantic has been observed using remote sensing techniques [*Gassó and Stein*, 2007; *Li et al.*, 2010a]. The results of *Neff and Bertler* (in review) at EDML similarly suggest dominance of trajectories initiated near Patagonian dust sources (Figure 9e), followed by trajectories originating in New Zealand, although this dust source is clearly less influential as evidenced by dust emission-weighted trajectories (Figure 9f). Very little contribution from distant Australian and upwind southern African sources are seen in trajectory or other model results. Mineralogy of dust in LGS ice from EDML is similar to that of EDC, linking the strong Sr/Nd isotopic evidence for South American glacial dust composition at EDC to the dust budget of EDML [*Marino et al.*, 2009].

Figure 9. (Following page) *Percent of 1979-2013 daily forward-trajectories initiated at dust PSA, both unweighted (%, a, c, e) and terrestrial dust emission-weighted (% Tg a^{-1}, e – h), passing over Antarctic ice core sites at daily increments for all Southern Hemisphere dust PSA. Map of trajectory endpoints after 5 days (g) detail areas surrounding ice core sites considered in trajectory percentages (± 2.5° latitude for all sites; ± 10° longitude, EDC, EDML; ± 14° longitude, RICE; total area ~3.2×10^{5} km^{2} for all sites). Emission estimates are taken from Li et al. (2008), with Patagonia emitting 38 Tg a^{-1}, Australia 120 Tg a^{-1}, southern Africa 34 Tg $a^{-1}$and a 10-30 Tg a^{-1} range of emission rates for unquantified New Zealand dust sources.*

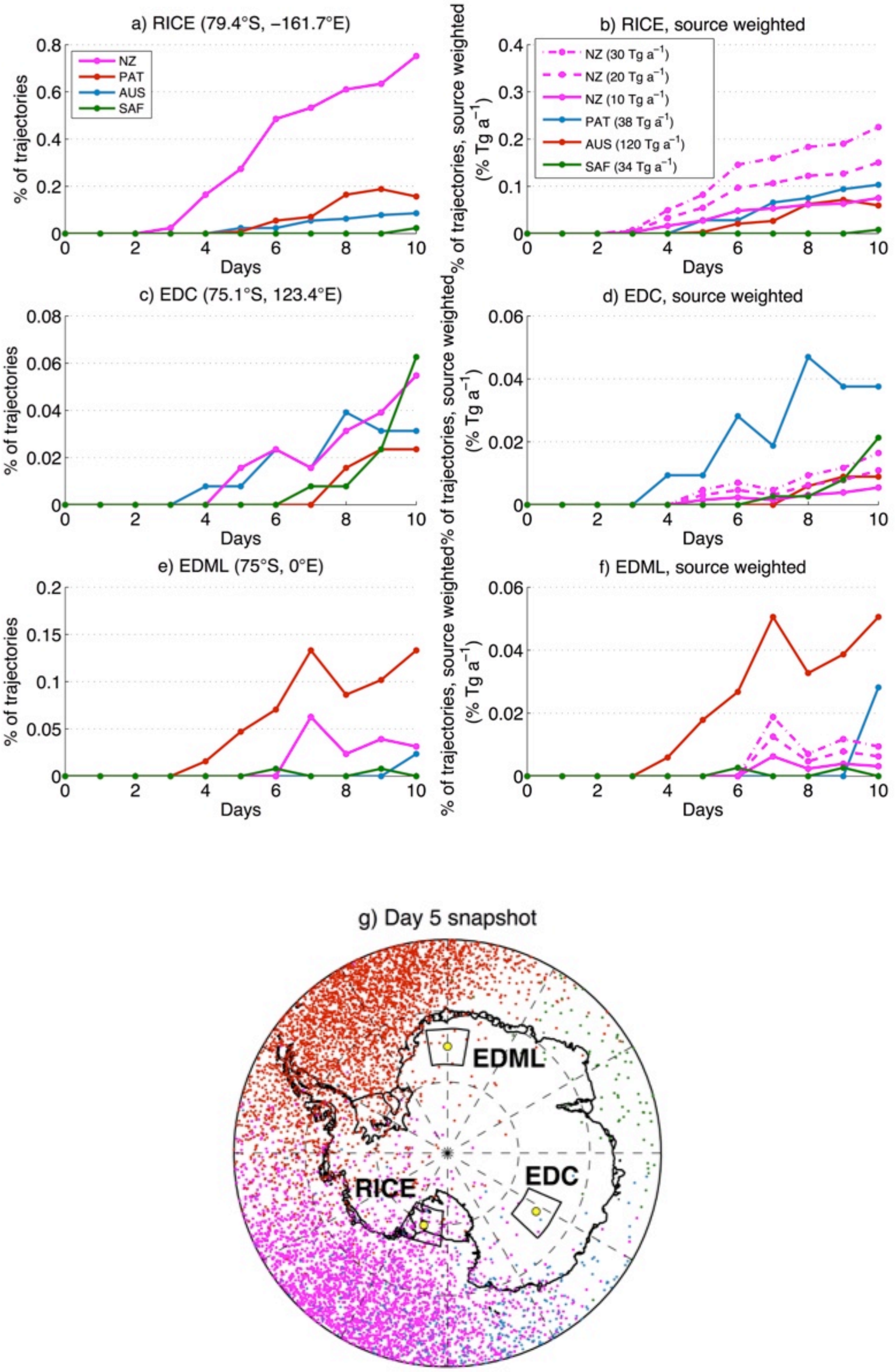

a) RICE (79.4°S, −161.7°E)
b) RICE, source weighted
c) EDC (75.1°S, 123.4°E)
d) EDC, source weighted
e) EDML (75°S, 0°E)
f) EDML, source weighted
% of trajectories
% of trajectories, source weighted (% Tg a^{-1})
Days
NZ
PAT
AUS
SAF
NZ (30 Tg a^{-1})
NZ (20 Tg a^{-1})
NZ (10 Tg a^{-1})
PAT (38 Tg a^{-1})
AUS (120 Tg a^{-1})
SAF (34 Tg a^{-1})
g) Day 5 snapshot
EDML
RICE
EDC

4.4.4 PSA REE signatures

The utility of the REE as a tool to identify dust provenance relies on thorough characterization of signatures in PSA dust, and that source REE signatures have unique distinguishing features. There is limited analytical uncertainty in determining REE signatures in highly concentrated dust samples, although REE_{norm} signatures are dependent on the dust size-fraction analyzed (e.g. *Gaiero et al.* [2004]; *Wegner et al.* [2012]). The compilation and measurement of REE in PSA samples by *Wegner et al.* [2012] is a significant advancement of this effort, however they note that these samples only “spotlight” regional REE patterns. We reproduce this compilation for reference in Figure 10. Australian PSA dust samples are primarily from the southeastern Murray-Darling region [*Marx et al.*, 2005] with few from the Lake Eyre region for which transport of dust emissions has been modeled [*McGowan and Clark*, 2008]. Five samples from southern Africa show large variability in REE signature, with three samples showing significant $MREE_{norm}$ enrichment and $HREE_{norm}$ depletion (Figure 10). Samples from New Zealand rivers and beaches show approximately crustal REE_{norm} except for two samples, which are depleted in $LREE_{norm}$ and have a large Eu anomaly.

Antarctic dust samples analyzed by *Wegner et al.* [2012] (locations marked in Figure 8) show distinct negative trends across REE_{norm} with strong enrichment in $LREE_{norm}$ and depletion in $HREE_{norm}$. While these few samples are primarily from the McMurdo Dry Valleys, the negative trend in REE_{norm} is consistent across all samples. The REE_{norm} signature of South American sediments and aeolian dust is particularly well characterized and REE_{norm} patterns are also quite distinct: South American REE_{norm} signatures show consistent depletion in $LREE_{norm}$ and enrichment in $HREE_{norm}$ across many samples (see *Gaiero et al.* [2004], *Smith et al.* [2003], data included in Figure 10). Southern African dust is highly unlikely to arrive at the RICE site in identifiable quantities, based on trajectory results and atmospheric modeling studies suggesting that southern African dust represents < 5% of the total Antarctic dust budget [*Li et al.*, 2008]. At this time, the dust PSA samples from Antarctica (Dry Valleys) and South America (Patagonia) show the most distinct REE signatures: both are easily distinguishable from the crustal mean and from each other. As with our examination of RICE REE data above, we choose to not rest conclusions on single elemental anomalies in dust PSA samples especially if anomalies are not consistent across many samples. For the RICE site, this unfortunately precludes consideration of New Zealand dust samples until they are better characterized and it is determined whether observed Europium anomalies present several New Zealand dust samples are truly representative of this PSA.

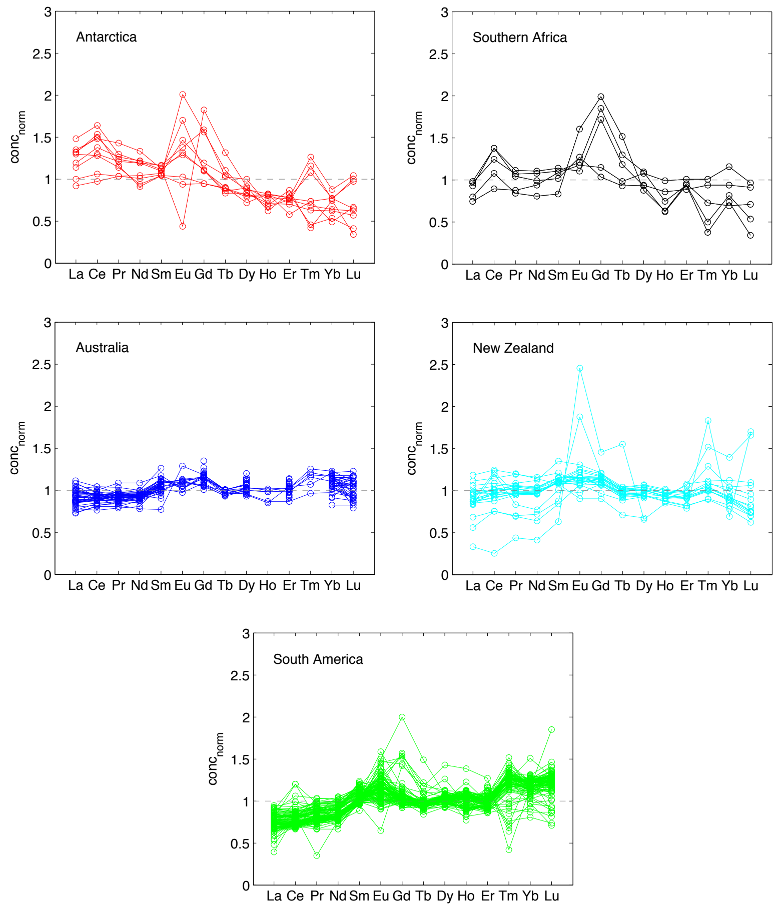

Figure 10. *REE_{norm} patterns in dust PSA samples, from Wegner et al. [2012].*

4.4.5 RICE ice core REE indications of dust provenance

RICE ice core samples show a consistent enrichment of $LREE_{norm}$ and depletion of $HREE_{norm}$ over the past 2.3 ka BP. Although REE characterization of Antarctic dust PSA is in early stages, we find it difficult to explain this negative REE_{norm} trend without a background dust source that is highly depleted in HREE. Several southern African samples show significant depletion in HREE, but these can be ruled out as a significant source of dust to the RICE ice core site, located on the opposite side of Antarctica from the African continent and shown to only weakly contribute to Antarctic dust loading. Considering the mean REE_{norm} slope of all RICE ice core samples spanning the last 2.3 ka BP, it also is difficult to explain such strong trends by invoking a mix of multiple dust sources, as this would likely result in a more closely crustal REE signature—as seen in glacial samples from both EDC and EDML.

South American dust samples show trends opposite to those most common in RICE samples; nearly all South American PSA samples have a positive REE_{norm} slope (Figure 11). While the South American dust sources are likely not the primary contributor of dust to the RICE ice core site, smaller contributions cannot be ruled out. Indeed, 71 samples measured here exhibit positive REE_{norm} slope (Figure 4, Figure 6a), suggesting by the most generous terms that South American REE signatures are represented in no more than 5% of all RICE samples spanning the last 2.3 ka. In contrast, strong negative REE_{norm} slope (< -0.05) is seen in 563 samples, 41% of those measured. As acknowledged previously, some of this tendency towards negative REE_{norm} slope may be due to preferential acid leaching of LREE during sample preparation, but this cannot explain the observed $HREE_{norm}$ depletion.

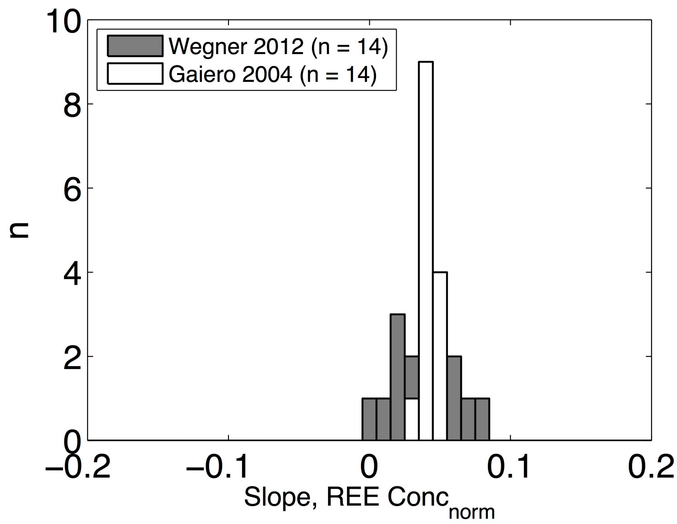

Figure 11. *REE_{norm} slope of dust samples taken from PSA in South America, from data published in Wegner et al. [2012] (all new South American samples) and Gaiero et al. [2004] (aeolian samples).*

If the Antarctic dust samples of *Wegner et al.* [2012] are representative of wider REE signatures present in dust originating in the Transantarctic Mountains and ranges in West Antarctica, data from the RICE ice core suggest a large overprinting of local dust onto extra-Antarctic REE signatures. Additional evidence for local dust contributions comes from preliminary characterization of RICE surface snow (summer 2012), which has $^{87}Sr/^{86}Sr$ ratios similar to those seen in low-grade metamorphic rocks from Mt. Nilsen located on King Edward VII Peninsula (indicated in Figure 8) [*Adams et al.*, 1995], one of several small outcropping peaks located only ~200 km in the upwind direction of the RICE site (see backward trajectories, Fig 8). Surface snow samples also include dust particles > 5 μm diameter which are unlikely to originate from extra-Antarctic dust PSA (*H. Winton and B. Delmonte*, personal communication 2015). While information about local dust could provide useful constraints on modern dust and wind activity within Antarctica, it likely obscures some REE signatures that would otherwise reveal details of wider Southern Hemisphere dust transport.

REE data from the East Antarctic EDC ice core become highly variable and trend towards negative REE_{norm} slope following the 15 ka BP transition from dusty LGS conditions into the Holocene (Figure 7). RICE data fill the gap from 2.5 ka BP to the present for which no previous REE data exist, and share the negative REE_{norm} slope of Holocene EDC samples. Although these sites experience very different climatological regimes—one is located on the Pacific margin of WAIS, the other on the central EAIS plateau—they are similarly removed geographically from South American dust PSA and likely only receive contributions from this source after extended periods of transport. Only 52 of 294 EDC samples, spanning 33.7 ka BP to 2.5 ka BP, have positive REE_{norm} slope (18%) and only 11 of those occur during the Holocene. The EDML ice core is more proximal to South America, causing Holocene REE at this site to be more influenced by the characteristic South American positive REE_{norm} trends. Samples with positive REE_{norm} slope represent 29% of those measured from EDML (representing 26.6 ka BP to 7.5 ka BP), rising slightly to 31% of Holocene samples. Although Holocene emissions of South American dust are lower than during the LGS, REE signatures confirm that this PSA represents a significant contributor to the dust loading observed in the EDML ice core.

4.5 Conclusions

REE patterns in the RICE ice core, located at the northeastern margin of the Ross Ice Shelf on the Pacific Ocean / Ross Sea margin of the WAIS, suggest a persistent local Antarctic dust contribution in both 3.6-year resolution and sub-annual samples spanning the last 2.3 ka BP. REE patterns suggest that the distinct South American dust source signature is present in fewer than 5% of all measured RICE ice core samples. Our diagnostic, REE_{norm} slope, and treatment of data as long-term averages also suggests that REE measured in Holocene samples from both RICE and the East Antarctic EDC ice core tend towards LREE enrichment and HREE depletion—a signature seen in dust samples from the largest ice-free area in Antarctica (McMurdo Dry Valleys). Although this treatment is conservative relative to the large number of elements (14 REE) and samples analyzed (minimum of 294, EDC, 31.2 ka total, *Gabrielli et al.* [2010]; maximum of 1364, 2.3 ka total; this study), we argue that this is the most constructive approach to interpret existing data and incorporate new information provided by the RICE ice core. RICE REE data are both the first from the Pacific sector of Antarctica, and the only existing REE data measured in samples younger than 2.5 ka BP, adding significantly to the spatial characterization of these signals in the Antarctic.

These data suggest that although South America is a dominant source of dust during the LGS, as evidenced by other dust provenance measures, at present its contribution varies regionally. Proximal EDML exhibits REE signatures with limited trends, possibly reflecting greater input of South American dust, which has characteristically positive REE trends. EDC is strongly isolated on the high EAIS plateau, and the RICE ice core site is located on the far side of the WAIS ice divide from South America. REE data from these sites suggests that local dust sources may have significant influence at these locations, although additional sources for which REE signatures are poorly characterized cannot be ruled out (e.g. Australia, New Zealand, southern Africa).

Future work developing the REE should focus on the following points, progressing through sample preparation, analysis and data interpretation.

1) Comprehensive evaluation of acid leaching effects on all REE for the particular matrix and insoluble particle characteristics at individual ice core sites, as previously recommended by *Rhodes et al.* [2011], with specific consideration of how the preferential LREE recovery observed by *Gabrielli et al.* [2010] affects REE crustal ratios.
2) Analysis of measurement uncertainty (e.g. RSD) effects on crust-normalized REE values, especially spanning the transition from the LGS to the Holocene. Consideration should also be given to changing sample resolution across measured time periods.
3) Development of a Southern Hemisphere dust PSA sample database, targeting samples from areas of known dust emission, spanning a range of particle sizes and measuring the REE, Pb- and Sr/Nd isotopic signatures and other parameters of relevance to dust provenance work. This work is highly relevant to international efforts, particularly several working groups of the Past Global Changes (PAGES) project (e.g. Dust Impact on Climate and Environment, Ocean Circulation and Carbon Cycling, International Partnerships in Ice Core Sciences).
4) Investigation into existing samples from Marie Byrd Land ice-free areas, which could be used to characterize small particle size fraction for Sr, Nd, Pb isotope ratios and REE concentrations.

Acknowledgements

We wish to thank P. Gabrielli and A. Wegner for making their ice core REE data easily accessible (EDC: doi:10.1016/j.quascirev.2009.09.002, EDML: doi:10.1594/PANGAEA.756834). EDC insoluble dust data was accessed from the US NOAA Paleoclimate Database (www.ncdc.noaa.gov/paleo, B. Delmonte, Data Contribution Series # 2004-040). The authors are thankful for assistance at the New Zealand National Ice Core Research Facility at GNS Science (R. Pyne), the TRACE laboratory (A. Ellis, K. Jarrett, B. Proemse, H. Winton), and VUW geochemistry laboratory (M. Handler, S. Lange, D. Sinclair). We thank all members of the RICE Community for their cooperation and support of this study. This work has been funded through the New Zealand Ministry for Business, Innovation, and Employment through contracts with Victoria University of Wellington (RDF-VUW-1103) and GNS Science (540-GCT-32). This work is a contribution to the Roosevelt Island Climate Evolution (RICE) Program, funded by national contributions from New Zealand, Australia, Denmark, Germany, Italy, the People's Republic of China, Sweden, United Kingdom, and the United States of America. Logistic support for RICE was provided by Antarctica New Zealand and the United States Antarctic Program.

4.6 References

Neff, P. D., and N. A. N. Bertler (2015, in review), Trajectory modeling of modern dust transport to the Southern Ocean and Antarctica, *Journal of Geophysical Research: Atmospheres*.

Neff, P. D., A. Tuohy, R. Edwards, and N. A. N. Bertler (2015, in review), Low-femtogram elemental analysis of Antarctic ice cores without preconcentration, *Environmental Science & Technology*.

Adams, C., D. Seward, and S. Weaver (1995), Geochronology of Cretaceous granites and metasedimentary basement on Edward VII Peninsula, Marie Byrd Land, West Antarctica, *Antarctic science*, *7*(03), 265-276.

Albani, S., N. M. Mahowald, B. Delmonte, V. Maggi, and G. Winckler (2012), Comparing modeled and observed changes in mineral dust transport and deposition to Antarctica between the Last Glacial Maximum and current climates, *Climate dynamics*, *38*(9-10), 1731-1755, doi:10.1007/s00382-011-1139-5.

Bigler, M., A. Svensson, E. Kettner, P. Vallelonga, M. E. Nielsen, and J. P. Steffensen (2011), Optimization of high-resolution continuous flow analysis for transient climate signals in ice cores, *Environmental science & technology*, *45*(10), 4483-4489, doi:10.1021/es200118j.

Cuffey, K. M., and W. S. B. Paterson (2010), *The physics of glaciers*, Academic Press.

Dansgaard, W., and S. Johnsen (1969), A flow model and a time scale for the ice core from Camp Century, Greenland, *Journal of Glaciology*, *8*, 215-223.

De Deckker, P., M. Norman, I. D. Goodwin, A. Wain, and F. X. Gingele (2010), Lead isotopic evidence for an Australian source of aeolian dust to Antarctica at times over the last 170,000 years, *Palaeogeography, Palaeoclimatology, Palaeoecology*, *285*(3), 205-223, doi:10.1016/j.palaeo.2009.11.013.

Delmonte, B., P. Andersson, M. Hansson, H. Schöberg, J. R. Petit, I. Basile-Doelsch, and V. Maggi (2008), Aeolian dust in East Antarctica (EPICA-Dome C and Vostok): Provenance during glacial ages over the last 800 kyr, *Geophysical Research Letters*, *35*(7), doi:10.1029/2008GL033382.

Delmonte, B., J. Petit, K. K. Andersen, I. Basile-Doelsch, V. Maggi, and V. Y. Lipenkov (2004), Dust size evidence for opposite regional atmospheric circulation changes over east Antarctica during the last climatic transition, *Climate Dynamics*, *23*(3-4), 427-438, doi:10.1007/s00382-004-0450-9.

Draxler, R. R., and G. Hess (1998), An overview of the HYSPLIT_4 modelling system for trajectories, *Australian Meteorological Magazine*, *47*(4), 295-308.

EPICA (2004), Eight glacial cycles from an Antarctic ice core, *Nature*, *429*(6992), 623-628, doi:10.1038/nature02599.

Fischer, H., M. L. Siggaard-Andersen, U. Ruth, R. Röthlisberger, and E. Wolff (2007), Glacial/interglacial changes in mineral dust and sea-salt records in polar ice cores: Sources, transport, and deposition, *Reviews of Geophysics*, *45*(1), doi:10.1029/2005RG000192.

Gabrielli, P., C. Barbante, C. Turetta, A. Marteel, C. Boutron, G. Cozzi, W. Cairns, C. Ferrari, and P. Cescon (2006), Direct determination of rare earth elements at the subpicogram per gram level in antarctic ice by ICP-SFMS using a desolvation system, *Analytical chemistry*, *78*(6), 1883-1889, doi:10.1021/ac0518957.

Gabrielli, P., A. Wegner, J. R. Petit, B. Delmonte, P. De Deckker, V. Gaspari, H. Fischer, U. Ruth, M. Kriews, and C. Boutron (2010), A major glacial-interglacial change in aeolian dust composition inferred from Rare Earth Elements in Antarctic ice, *Quaternary Science Reviews*, *29*(1), 265-273, doi:10.1016/j.quascirev.2009.09.002.

Gaiero, D. M., P. J. Depetris, J.-L. Probst, S. M. Bidart, and L. Leleyter (2004), The signature of river-and wind-borne materials exported from Patagonia to the southern latitudes: a view from REEs and implications for paleoclimatic interpretations, *Earth and Planetary Science Letters*, *219*(3), 357-376.

Gassó, S., and A. F. Stein (2007), Does dust from Patagonia reach the sub-Antarctic Atlantic Ocean?, *Geophysical Research Letters*, *34*(1), doi:10.1029/2006GL027693.

Henderson, P. (1984), *Rare earth element geochemistry*, Elsevier.

Hosking, J. S., A. Orr, G. J. Marshall, J. Turner, and T. Phillips (2013), The influence of the Amundsen–Bellingshausen Seas low on the climate of West Antarctica and its representation in coupled climate model simulations, *Journal of Climate*, *26*(17), 6633-6648, doi:10.1175/JCLI-D-12-00813.1.

Koffman, B. G., M. J. Handley, E. C. Osterberg, M. L. Wells, and K. J. Kreutz (2014a), Dependence of ice-core relative trace-element concentration on acidification, *Journal of Glaciology*, *60*(219), 103-112, doi:10.3189/2014JoG13J137.

Koffman, B. G., K. Kreutz, D. Breton, E. Kane, D. Winski, S. Birkel, A. Kurbatov, and M. Handley (2014b), Centennial-scale variability of the Southern Hemisphere westerly wind belt in the eastern Pacific over the past two millennia, *Climate of the Past*, *10*(3), 1125-1144, doi:10.5194/cp-10-1125-2014.

Krinner, G., and C. Genthon (2003), Tropospheric transport of continental tracers towards Antarctica under varying climatic conditions, *Tellus B*, *55*(1), 54-70.

Krinner, G., J.-R. Petit, and B. Delmonte (2010), Altitude of atmospheric tracer transport towards Antarctica inpresent and glacial climate, *Quaternary science reviews*, *29*(1), 274-284.

Lambert, F., B. Delmonte, J.-R. Petit, M. Bigler, P. R. Kaufmann, M. A. Hutterli, T. F. Stocker, U. Ruth, J. P. Steffensen, and V. Maggi (2008), Dust-climate couplings over the past 800,000 years from the EPICA Dome C ice core, *Nature*, *452*(7187), 616-619, doi:10.1038/nature06763.

Lamy, F., R. Gersonde, G. Winckler, O. Esper, A. Jaeschke, G. Kuhn, J. Ullermann, A. Martínez-Garcia, F. Lambert, and R. Kilian (2014), Increased dust deposition in the Pacific Southern Ocean during glacial periods, *Science*, *343*(6169), 403-407, doi:10.1126/science.1245424.

Li, F., P. Ginoux, and V. Ramaswamy (2008), Distribution, transport, and deposition of mineral dust in the Southern Ocean and Antarctica: Contribution of major sources, *Journal of Geophysical Research: Atmospheres (1984–2012)*, *113*(D10), doi:10.1029/2007JD009190.

Li, F., P. Ginoux, and V. Ramaswamy (2010a), Transport of Patagonian dust to Antarctica, *Journal of Geophysical Research: Atmospheres (1984–2012)*, *115*(D18), doi:10.1029/2009JD012356.

Li, F., V. Ramaswamy, P. Ginoux, A. J. Broccoli, T. Delworth, and F. Zeng (2010b), Toward understanding the dust deposition in Antarctica during the Last Glacial Maximum: Sensitivity studies on plausible causes, *Journal of Geophysical Research: Atmospheres (1984–2012)*, *115*(D24), doi:10.1029/2010JD014791.

Luyendyk, B., S. Cisowski, C. Smith, S. Richard, and D. Kimbrough (1996), Paleomagnetic study of the northern Ford Ranges, western Marie Byrd Land, West Antarctica: Motion between West and East Antarctica, *Tectonics*, *15*(1), 122-141.

Mahowald, N., S. Albani, S. Engelstaedter, G. Winckler, and M. Goman (2011), Model insight into glacial–interglacial paleodust records, *Quaternary Science Reviews*, *30*(7), 832-854, doi:10.1016/j.quascirev.2010.09.007.

Mahowald, N., K. Kohfeld, M. Hansson, Y. Balkanski, S. P. Harrison, I. C. Prentice, M. Schulz, and H. Rodhe (1999), Dust sources and deposition during the last glacial maximum and current climate: A comparison of model results with paleodata from ice cores and marine sediments, *Journal of Geophysical Research: Atmospheres (1984–2012)*, *104*(D13), 15895-15916, doi:10.1029/1999JD900084.

Marino, F., E. Castellano, S. Nava, M. Chiari, U. Ruth, A. Wegner, F. Lucarelli, R. Udisti, B. Delmonte, and V. Maggi (2009), Coherent composition of glacial dust on opposite sides of the East Antarctic Plateau inferred from the deep EPICA ice cores, *Geophysical research letters*, *36*(23).

Martínez-Garcia, A., A. Rosell-Melé, S. L. Jaccard, W. Geibert, D. M. Sigman, and G. H. Haug (2011), Southern Ocean dust-climate coupling over the past four million years, *Nature*, *476*(7360), 312-315, doi:10.1038/nature10310.

Marx, S. K., B. S. Kamber, and H. A. McGowan (2005), Provenance of long-travelled dust determined with ultra-trace-element composition: a pilot study with samples from New Zealand glaciers, *Earth Surface Processes and Landforms*, *30*(6), 699-716.

McGowan, H. A., and A. Clark (2008), Identification of dust transport pathways from Lake Eyre, Australia using Hysplit, *Atmospheric Environment*, *42*(29), 6915-6925, doi:10.1016/j.atmosenv.2008.05.053.

Nicolas, J. P., and D. H. Bromwich (2011), Climate of West Antarctica and influence of marine air intrusions, *Journal of Climate*, *24*(1), 49-67, doi:10.1175/2010JCLI3522.1.

Parish, T. R., and D. H. Bromwich (2007), Reexamination of the near-surface airflow over the Antarctic continent and implications on atmospheric circulations at high southern latitudes*, *Monthly Weather Review*, *135*(5), 1961-1973, doi:10.1175/MWR3374.1.

Petit, J.-R., J. Jouzel, D. Raynaud, N. I. Barkov, J.-M. Barnola, I. Basile, M. Bender, J. Chappellaz, M. Davis, and G. Delaygue (1999), Climate and atmospheric history of the past 420,000 years from the Vostok ice core, Antarctica, *Nature*, *399*(6735), 429-436, doi:10.1038/20859.

Revel-Rolland, M., P. De Deckker, B. Delmonte, P. Hesse, J. Magee, I. Basile-Doelsch, F. Grousset, and D. Bosch (2006), Eastern Australia: a possible source of dust in East Antarctica interglacial ice, *Earth and Planetary Science Letters*, *249*(1), 1-13, doi:10.1016/j.epsl.2006.06.028.

Rhodes, R. H., J. A. Baker, M.-A. Millet, and N. A. Bertler (2011), Experimental investigation of the effects of mineral dust on the reproducibility and accuracy of ice core trace element analyses, *Chemical Geology*, *286*(3), 207-221, doi:10.1016/j.chemgeo.2011.05.006.

Russell, B. C., I. W. Croudace, P. E. Warwick, and J. A. Milton (2014), Determination of Precise 135Cs/137Cs Ratio in Environmental Samples Using Sector Field Inductively Coupled Plasma Mass Spectrometry, *Analytical chemistry*, *86*(17), 8719-8726, doi:10.1021/ac501894a.

Sigl, M., J. R. McConnell, L. Layman, O. Maselli, K. McGwire, D. Pasteris, D. Dahl-Jensen, J. P. Steffensen, B. Vinther, and R. Edwards (2013), A new bipolar ice core record of volcanism from WAIS Divide and NEEM and implications for climate forcing of the last 2000 years, *Journal of Geophysical Research: Atmospheres*, *118*(3), 1151-1169, doi:10.1029/2012JD018603.

Smith, J., D. Vance, R. A. Kemp, C. Archer, P. Toms, M. King, and M. Zárate (2003), Isotopic constraints on the source of Argentinian loess–with implications for atmospheric circulation and the provenance of Antarctic dust during recent glacial maxima, *Earth and Planetary Science Letters*, *212*(1), 181-196.

Sugden, D. E., R. D. McCulloch, A. J.-M. Bory, and A. S. Hein (2009), Influence of Patagonian glaciers on Antarctic dust deposition during the last glacial period, *Nature Geoscience*, *2*(4), 281-285, doi:10.1038/NGEO474.

Tegen, I., A. A. Lacis, and I. Fung (1996), The influence on climate forcing of mineral aerosols from disturbed soils, *Nature*, *380*(6573), 419-422, doi:10.1038/380419a0.

Vallelonga, P., P. Gabrielli, E. Balliana, A. Wegner, B. Delmonte, C. Turetta, G. Burton, F. Vanhaecke, K. Rosman, and S. Hong (2010), Lead isotopic compositions in the EPICA Dome C ice core and Southern Hemisphere Potential Source Areas, *Quaternary Science Reviews*, *29*(1), 247-255, doi:10.1016/j.quascirev.2009.06.019.

Vallelonga, P., K. Van de Velde, J.-P. Candelone, V. Morgan, C. Boutron, and K. Rosman (2002), The lead pollution history of Law Dome, Antarctica, from isotopic measurements on ice cores: 1500 AD to 1989 AD, *Earth and Planetary Science Letters*, *204*(1), 291-306, doi:10.1016/S0012-821X(02)00983-4.

Wedepohl, K. H. (1995), The composition of the continental crust, *Geochimica et cosmochimica Acta*, *59*(7), 1217-1232, doi:10.1016/0016-7037(95)00038-2.

Wegner, A., P. Gabrielli, D. Wilhelms-Dick, U. Ruth, M. Kriews, P. De Deckker, C. Barbante, G. Cozzi, B. Delmonte, and H. Fischer (2012), Change in dust variability in the Atlantic sector of Antarctica at the end of the last deglaciation, *Climate of the Past*, *8*, 135-147, doi:10.5194/cp-8-135-2012.

Wolff, E., C. Barbante, S. Becagli, M. Bigler, C. Boutron, E. Castellano, M. De Angelis, U. Federer, H. Fischer, and F. Fundel (2010), Changes in environment over the last 800,000 years from chemical analysis of the EPICA Dome C ice core, *Quaternary Science Reviews*, *29*(1), 285-295, doi:10.1016/j.quascirev.20 09.06.013.

4.7 Supplementary Figures

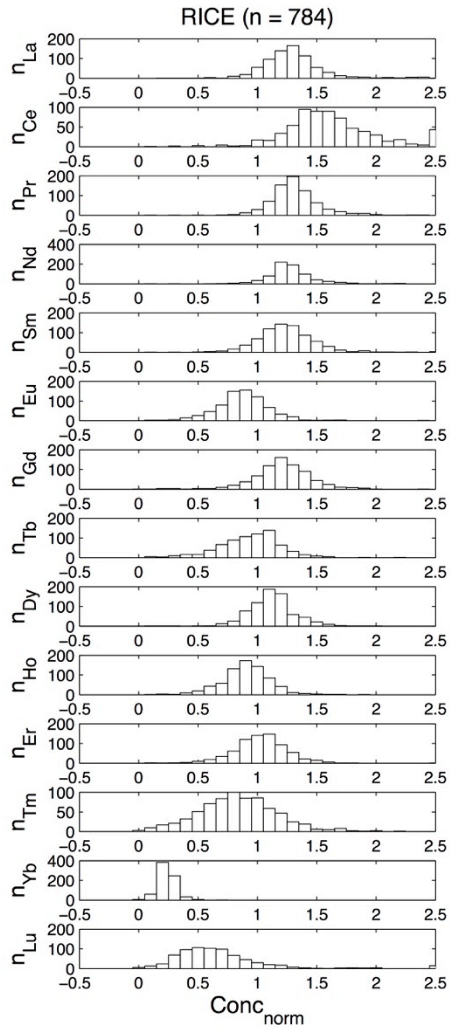

Figure S1. *UCC-normalized concentrations for all REE in 8 m – 40 m RICE ice core samples (n = 784).*

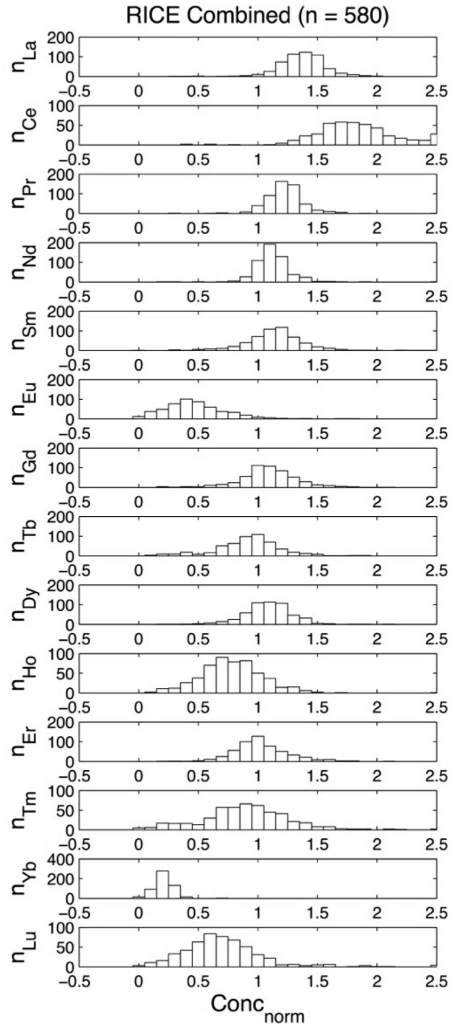

Figure S2. *UCC-normalized concentrations for all REE in 40 m – 320 m RICE ice core samples (n = 580).*

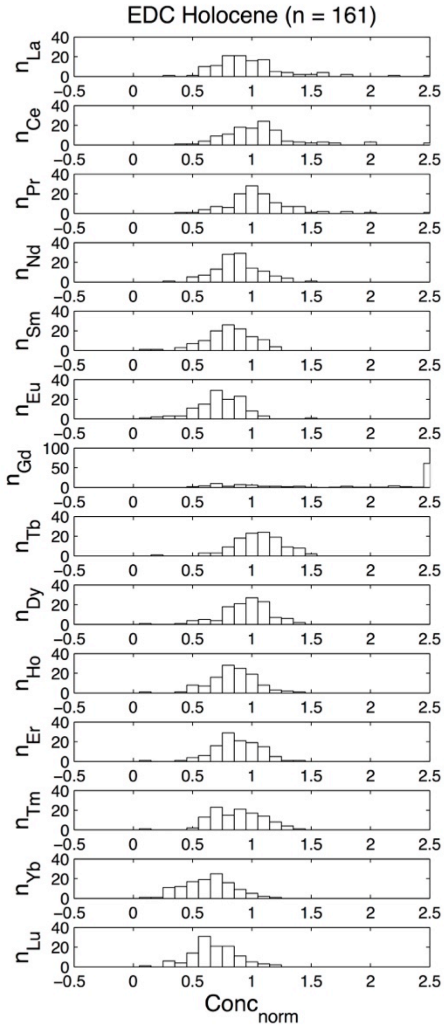

Figure S3. *UCC-normalized concentrations for all REE in Holocene EDC ice core samples (n = 161).*

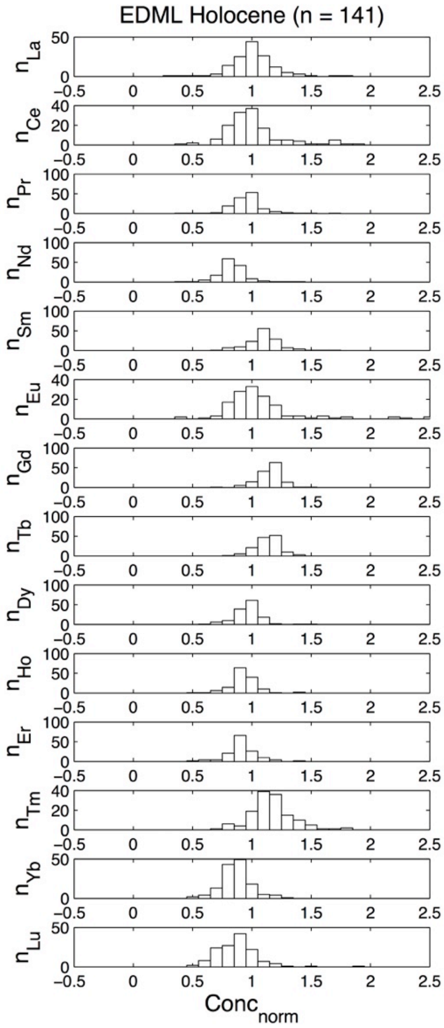

Figure S4. *UCC-normalized concentrations for all REE in Holocene EDML ice core samples (n = 141).*

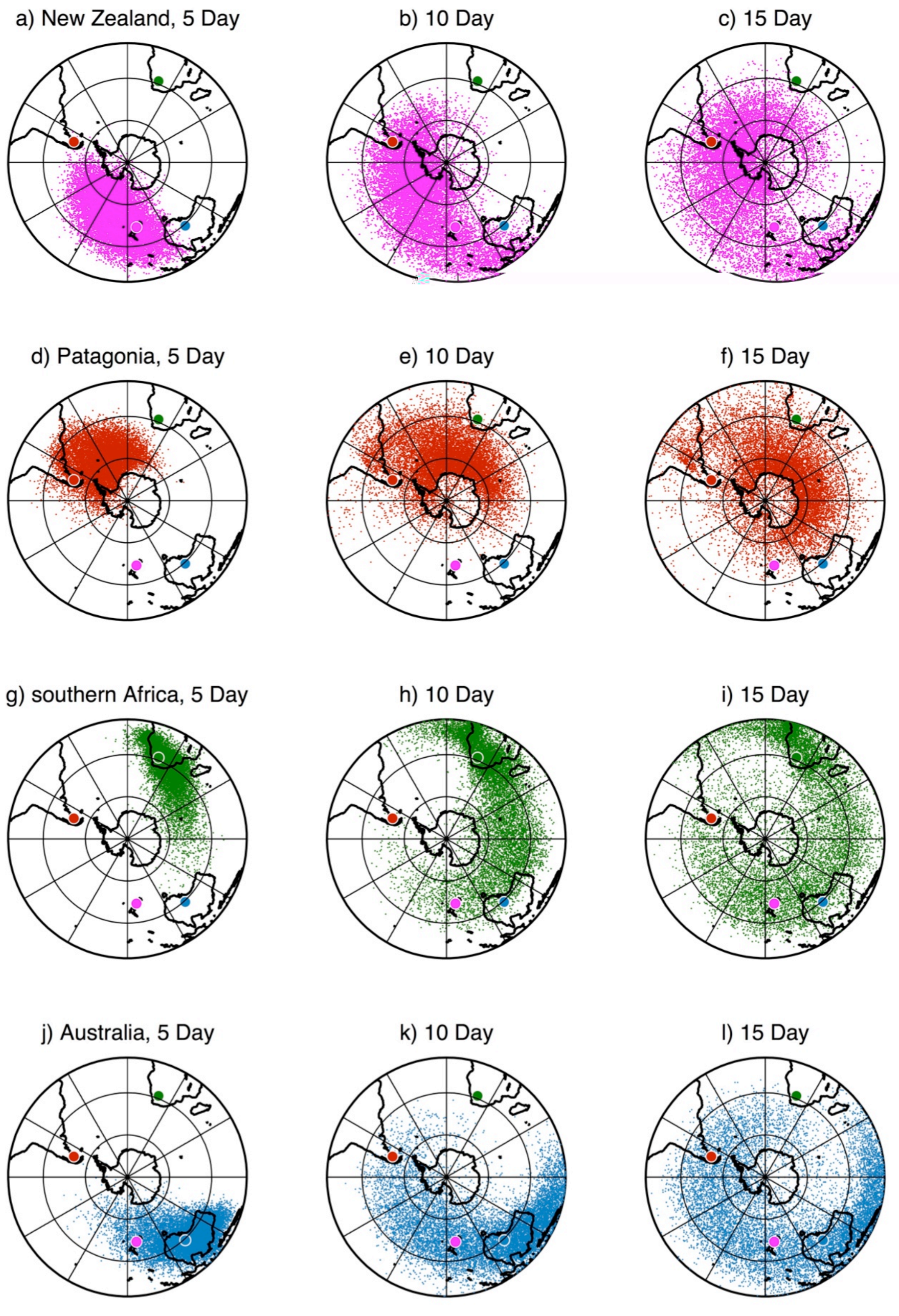

Figure S5. *Forward-trajectory endpoints from Neff and Bertler (in review), with 1979-2013 daily HySPLIT forward-trajectory endpoints displayed after 5, 10 and 15 days of runtime. Trajectories were initiated near New Zealand, Patagonia, southern Africa and Australia dust PSA.*

Chapter 5: Summary and future work

5.1 Project summary

The objective of this thesis was to develop better understanding of dust transport from Southern Hemisphere sources to the Antarctic, and ultimately explore the rare earth elements (REE) as an indicator of dust provenance in modern Antarctic ice. In working to achieve this objective, work progressed through three stages:

1) Trajectory analysis to determine likely distribution of extra-Antarctic dust potential source areas (PSA) across the Southern Ocean and at Antarctic ice core sites, while also exploring variability in atmospheric transport strength with respect to high- and low-latitude climate forcing.
2) Demonstration of analytical capability to quantify REE as low as single fg g^{-1} (10^{-15} g g^{-1}) concentrations, and measurement of RICE samples dating to ~2 ka BP.
3) Characterization and interpretation of REE signatures observed in the RICE ice core, combining dust PSA trajectory constraints with analytical understanding to reduce uncertainty associated with ice core and dust PSA REE data.

Conclusions made through these stages are as follows:

1) Trajectory modeling of Southern Hemisphere dust transport (Chapter 2)

Thirty-five year averages of daily forward trajectories from dust PSA, in the place of computationally expensive GCM simulations, demonstrate persistent, strong transport from Patagonia and New Zealand to the Southern Ocean and Antarctica. Even with New Zealand dust emission rates only one-third the size of any other dust PSA, this dust PSA may contribute more than 10% of the Antarctic dust budget. Seasonality, mode of atmospheric transport (e.g. altitude) and dust PSA trajectory distribution using this method agree well with previous studies, and reveal new associations between atmospheric transport strength and variability of both central Tropical Pacific sea surface temperature and state of the Southern Annular Mode.

2) Preparation and ICPMS analysis of REE in ice core samples (Chapter 3)

Examination of sample preparation methods and analytical performance suggests that Jet-SF-ICPMS instrumentation can ably measure a large number of analytes across a range of concentrations in ice core samples, with sensitivity not seen in other analytical arrangements.

Stability across extended analysis campaigns using this system allowed for accurate determination of >35 elements in >1400 samples from the RICE ice core. For many elements, limits of detection are below procedural blank concentrations, suggesting that sample preparation and contamination in the laboratory environment are the primary barriers to accurate determination of sub pg g^{-1} species.

3) REE as paleoclimate tools to identify dust provenance (Chapter 4)

RICE ice core REE measurements are both the first from the Pacific sector of Antarctica and the first spanning the last 2.3 ka BP. These measurements show strong trends across the REE (enrichment in light REE and depletion in heavy REE). This pattern is consistent through time, and is similar only to REE trends (slope) seen regularly in dust samples collected from Antarctic ice-free areas. Although the REE characterization of Antarctic dust is incomplete, this suggests significant contribution of local dust sources to RICE. REE signatures associated with South American dust, which is reliably enriched in heavy REE, are observed in less than 5% of RICE samples. Applying this same REE characterization method to the EPICA Dome C ice core suggests Holocene REE patterns similar to those of RICE, while the EPICA Drønning Maud Land site—closer to South American dust sources—exhibits a mean Holocene REE pattern likely more influenced by heavy REE enrichment seen in Patagonian dust samples. These results suggested significant overprinting of local Antarctic dust in Holocene ice core records, obscuring information about long range atmospheric transport from and environmental change at mid-latitude Southern Hemisphere dust sources.

5.2 Future work

When investigating any line of scientific inquiry, one undoubtedly produces as many questions as answers. Guided by the results of this thesis, we suggest the following points for further investigation.

1) Trajectory modeling

- Modern and last glacial stage emissions from New Zealand should be quantified, as strong connectivity between New Zealand and Antarctica (Chapter 2) suggests this dust PSA may influence dust records in West Antarctic ice cores and South Pacific marine sediment cores [e.g. *Lamy et al.*, 2014].

- These trajectory data can easily be adapted to consider transport of other aerosols to the Antarctic, including black carbon from fires and anthropogenic toxic heavy metal emissions [e.g. *Bisiaux et al.*, 2012; *McConnell et al.*, 2014].

2) Trace element sample preparation and analysis

- Strategies should be developed to use matrix-matched bulk waters (e.g. Antarctic snow-melt) to quantify trace element contamination from continuous flow analysis (CFA) systems, as >18 MΩ laboratory water blanks scour contaminants from CFA plumbing and are not representative of true background concentrations of trace elements (noted in Chapter 2 and mentioned by *Wegner et al.* [2012]).

- Prior to interpretation of REE dust provenance in ice cores, uncertainties associated with sample acidification, highlighted by *Rhodes et al.* [2011] and *Koffman et al.* [2014] and discussed in Chapters 3 and 4, must be constrained for individual ice core sites to account for any incongruent and artificial enrichment.

3) REE ice core dust provenance

- Across the last glacial transition, the effects of reduced REE concentrations, increased measurement uncertainty and decreased sample resolution on crustal-normalized REE trends must be quantified. Until this is done, interpretations of increased REE variability indicating changing dust sources across this period remain incomplete. To this end, detailed preparation and measurement methodologies quantifying uncertainties also must be reported to facilitate comparison of results produced by international laboratory facilities.

- Dust REE signatures of Southern Hemisphere dust potential source areas (PSA) are currently poorly characterized (with the possible exception of South America). Local expertise and existing samples should be utilized to build a database of measurements useful for Antarctic dust provenance work (e.g. Sr, Nd, Pb isotopes, REE).

- This work develops an array of Antarctic ice core REE records. Further REE measurements from ice cores at sites with dust regimes dominated by a single source could aid in evaluating the REE as a dust provenance tool. For instance, trajectory analysis (Chapter 2) suggests that the James Ross Island ice core is strongly influenced by South American atmospheric transport, while Law Dome is the only site possibly showing significant connection with southern Africa. REE measurements at these sites might more clearly reflect the signatures of these respective dust source areas and could further elucidate the fidelity of REE dust provenance identification.

5.3 References

Bisiaux, M., R. Edwards, J. McConnell, M. Curran, T. Van Ommen, A. Smith, T. Neumann, D. Pasteris, J. Penner, and K. Taylor (2012), Changes in black carbon deposition to Antarctica from two high-resolution ice core records, 1850–2000 AD, *Atmospheric Chemistry and Physics*, *12*(9), 4107-4115, doi:10.5194/acp-12-4107-2012.

Koffman, B. G., M. J. Handley, E. C. Osterberg, M. L. Wells, and K. J. Kreutz (2014), Dependence of ice-core relative trace-element concentration on acidification, *Journal of Glaciology*, *60*(219), 103-112, doi:10.3189/2014JoG13J137.

Lamy, F., R. Gersonde, G. Winckler, O. Esper, A. Jaeschke, G. Kuhn, J. Ullermann, A. Martínez-Garcia, F. Lambert, and R. Kilian (2014), Increased dust deposition in the Pacific Southern Ocean during glacial periods, *Science*, *343*(6169), 403-407, doi:10.1126/science.1245424.

McConnell, J. R., O. J. Maselli, M. Sigl, P. Vallelonga, T. Neumann, H. Anschütz, R. Bales, M. Curran, S. B. Das, and R. Edwards (2014), Antarctic-wide array of high-resolution ice core records reveals pervasive lead pollution began in 1889 and persists today, *Scientific reports*, *4*, doi:10.1038/srep05848.

Rhodes, R. H., J. A. Baker, M.-A. Millet, and N. A. Bertler (2011), Experimental investigation of the effects of mineral dust on the reproducibility and accuracy of ice core trace element analyses, *Chemical Geology*, *286*(3), 207-221, doi:10.1016/j.chemgeo.2011.05.006.

Wegner, A., P. Gabrielli, D. Wilhelms-Dick, U. Ruth, M. Kriews, P. De Deckker, C. Barbante, G. Cozzi, B. Delmonte, and H. Fischer (2012), Change in dust variability in the Atlantic sector of Antarctica at the end of the last deglaciation, *Climate of the Past*, *8*, 135-147, doi:10.5194/cp-8-135-2012.

Appendix A: A review of the brittle ice zone in polar ice cores

This appendix represents a published work:

Neff, P.D. (2014). A review of the brittle ice zone in polar ice cores, *Annals of Glaciology*, 55(68), 72-82, doi: 10.3189/2014AoG68A023.

Abstract

Maintaining ice core quality through the brittle ice zone (BIZ) remains challenging for polar ice core studies. At depth, increasing ice overburden pressurizes trapped air bubbles, causing fracture of cores upon exposure to atmospheric pressure. Fractured ice cores degrade analyses, reducing resolution and causing contamination. BIZ encounters at eighteen sites across the Greenland, West and East Antarctic ice sheets are documented. The BIZ begins at a mean depth of 545 ± 162 m (1 standard deviation), extending to depths where ductile clathrate-ice is reached: an average of 1132 ± 178 m depth. Ice ages in this zone vary with snow accumulation rate and ice thickness, beginning as young as 2 ka before present (BP) at Dye 3, Greenland, affecting ice >160 ka BP in age at Taylor Dome, Antarctica and compromising up to 90% of retrieved samples at intermediate-depth sites. Effects of pressure and temperature on the BIZ are explored using modeled firn-column overburden pressure and borehole temperatures, revealing complex associations between firn densification and BIZ depth, and qualitatively supporting expected thinning of the BIZ at low ice temperatures due to shallower clathrate stability. Mitigating techniques for drilling, transport, sampling and analysis of brittle ice cores are also discussed.

Introduction

Deep ice drilling at both poles reveals valuable climate records extending up to 800,000 years into the past (EPICA Community Members, 2004), in addition to unveiling much about the physical structure of the Greenland, West and East Antarctic ice sheets. In recent years, ice core drilling, transport, sampling, and analytical procedures have continually improved, spurred by the goal of providing continuous, high-resolution records of atmospheric greenhouse gases and climate and environmental proxies.

However, poor ice core quality in the so-called brittle ice zone (BIZ), where extensive fracturing of core samples is caused by rapid relaxation (decompression) of the ice (e.g. Gow, 1971), remains a technical challenge at all phases of intermediate-depth and deep ice core studies. At the drill site, mechanical stresses from drilling and logging the core can degrade initial core quality in this zone. Sampling at freezer facilities often induces further fracturing as individual brittle ice core samples are cut with bandsaws. Finally, brittle ice samples prove challenging for laboratory procedures such as continuous-flow analysis (e.g. Osterberg and others, 2006; Bigler and others, 2011), with fractures allowing drilling fluid required for deep ice drilling to penetrate into samples, contaminating major-ion chemistry, trace chemistry and gas measurements.

While at relatively high snow accumulation *deep* drill sites ice ages in the BIZ represent several thousand years of the Holocene, high snow accumulation *intermediate-depth* drill sites and low snow accumulation deep drill sites may place many thousands of years of transitional and/or glacial ice within this zone of compromised core quality. In the case of drill sites with intermediate ice-thickness, a large fraction (90% or more) of the dated ice core record will likely be placed within the BIZ. Brittle ice core quality, through recovery, transport, sampling and analysis, is one of the technical challenges identified by the International Partnerships in Ice Core Sciences (IPICS), with implications both for the "40k array" initiative to gather a spatially-distributed, bi-polar network of 40 ka ice core records, and any Antarctic "oldest ice" site chosen to retrieve a continuous 1.5 Ma record (IPICS, 2005; Brook and others, 2006).

The term "brittle ice" with respect to ice drilling originates in the description by *Gow and others* (1968) of highly fractured ice from depths between 400 m and 900 m in the Byrd Station ice core—the first drilled to bedrock in Antarctica. Investigation of ice relaxation by *Gow* (1968, 1971), also in the Byrd Station ice core, indicates that the linear increase in overburden pressure with depth accordingly increases the *in situ* pressure within air bubbles in the ice; once removed from this high-pressure environment, bubble pressure exceeds the tensile strength of the confining ice, causing cracking between bubbles and initiating widespread fracturing in ice cores (Uchida and others, 1994; IPICS, 2005). Immediately upon exposure at the surface, fracturing begins explosively, propagating across- and along-core on decimeter scales. Slower relaxation of ice cores over periods of months to years after drilling (also explored by *Gow*, 1971) may alleviate some or all remaining brittleness, however ice cores from Siple Dome, Antarctica remain brittle more than a decade after cores were retrieved (M. Twickler, personal communication). Brittle fracture in ice cores only fully diminishes at depths where air bubbles are absorbed into the ice, transitioning to air-hydrate crystals (clathrates). Here, the ice is more ductile as dissociation pressure and temperature is reached, incorporating gases into the crystal lattice (e.g. Miller, 1969; Shoji and Langway, 1982; Pauer and others, 1995; Kuhs and others, 2000; Lipenkov, 2000). This transition occurs gradually as bubble number-densities decrease and clathrates become dominant (e.g. Uchida and others, 1994; Kipfstuhl and others, 2001; Ueltzhöffer and others, 2010). It is expected that clathrate formation—and thus onset of ductile ice and improved ice core quality—occurs at shallower depths as ice temperature decreases (Miller, 1969).

The BIZ, though observed at all deep drilling sites, has seldom been specifically examined and is only approximately defined as a zone beginning several-hundred meters below the ice surface and extending to depths between 1000 m and 1500 m. This is in part due to the inherently qualitative definition of brittle ice, wide-ranging metrics for ice core quality, rounding of reported depths, and the entangled effects of ice physical properties and stresses (mechanical and thermal) induced during drilling, on-site handling and transport. BIZ depths collated here are likely accurate to ± 50 m. The first sustained decline in ice core quality should be reported—and is considered here—as the top depth of the BIZ, with the bottom depth marked by a return to consistently excellent ice core quality (e.g. Fig. 10 of *Souney and others*, this issue). This paper compiles reported information regarding the BIZ for eighteen deep (> 1500 m) and intermediate-depth (500 m to 1500 m) polar ice drilling projects (Figure 1a, b). Two effects are explored with possible controls on brittle ice onset and relief. First, the effect of varying firn-column thickness on overburden pressure at depth is considered using modeled firn-column densities at all sites. Second, reported brittle ice depths are examined with respect to clathrate stability using *in-situ* ice temperature from borehole measurements and modelled overburden pressures. Techniques are detailed that have been or could be employed in order to reduce brittle fracture in ice cores during drilling, transport and sampling, and challenges pertaining to analysis of brittle ice samples are also discussed.

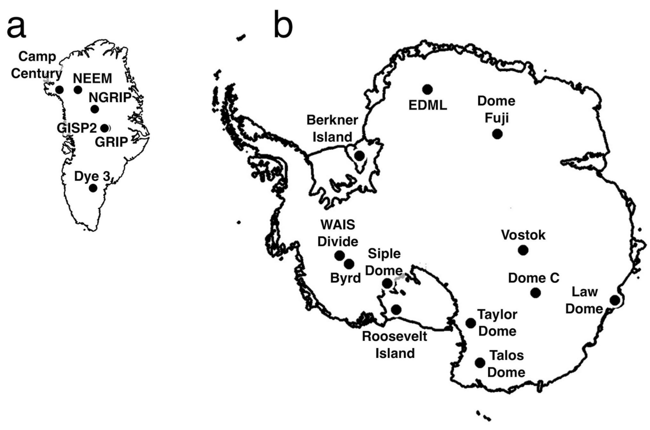

Figure 1. *Locations of polar drill sites in a) Greenland and b) Antarctica discussed in text. Map data from Timmerman and others (2011).*

***Table 1**: Site information, brittle ice zone (BIZ) depths, mean annual snow accumulation (m a^{-1} ice), mean surface air temperature (ºC), firn-ice transition depth (density 830 kg m^{-3} reached) and BIZ ice ages for Greenland Ice Sheet ice drilling sites.*

	Camp Century	Dye-3	GRIP	GISP2	NGRIP	NEEM
Coordinates	77.17° N, 61.13° W	65.18° N, 43.82° W	72.58° N, 37.63° W	72.60° N, 38.50° W	75.10° N, 42.32° W	77.45° N 51.60° W
Years drilled	1963–66[1]	1979–81[7]	1989–92[9]	1989–93[14]	1996–2004[9]	2008–12[19]
Surface elevation (m)	1887[2]	2490[7]	3238[11]	3200[14]	2917[9]	2450[19]
Drill depth (m)	1387[1]	2037[7]	3029[11]	3053[14]	3090[9]	2540[19]
Ice thickness (m)	1387[1]	2037[7]	3029[11]	3053[14]	3090[9]	2540[19]
BIZ top (m)	**600**[3]	**800**[8,9]	**800**[11]	**650**[15,16]	**790**[9]	**609**[20]
BIZ bottom (m)	**1150**[3]	**1200**[8,9]	**1300**[11,12]	**1400**[15,16]	**1200**[9]	**1281**[20]
BIZ thickness (m)	**550**	**400**	**500**	**750**	**410**	**671**
Snow accumulation (m ice a^{-1})	0.33[2]	0.56[9]	0.23[9]	0.22[9]	0.19[9]	0.22[19]
Mean air temperature (°C)	–24[4]	–20[9]	–32[9]	–32[4]	–32[9]	–29[19]
Firn/ice transition (m)	72[5]	67.5[4]	78[13]	77[4]	78[18]	78.8[21]
BIZ top age (ka BP)	2.3[6]	2[10]	4[9]	3[15,17]	4.7[9]	3[22]
BIZ bottom age (ka BP)	10[6]	3.8[10]	7.1[9]	8.3[15,17]	8[9]	9[22]

[1]Ueda and Garfield (1968); [2]Drinkwater and others (2001); [3]Shoji and Langway (1987); [4]Cuffey and Paterson (2010); [5]Kovacs and others (1969); [6]Dansgaard and others (1969); [7]Gundestrup and Hansen (1984); [8]Shoji and Langway (1982); [9]Vinther and others (2006); [10]Langway and others (1985); [11]Dansgaard and others (1993); [12]Pauer and others (1995); [13]Schwander and others (1993); [14]Alley and others (1993); [15]Gow and others (1997); [16]M. Twickler (personal communication, 2013); [17]The Greenland Summit Ice Cores CD-ROM (1997); [18]Martinerie and others (2009); [19]NEEM Community Members (2013); [20]Warming and others (2013); [21]Buizert and others (2012); [22]Rasmussen and others (2013).

Brittle ice zone depth

Reported BIZ depths and drill site conditions—snow accumulation rate, mean annual surface air temperature and firn-ice transition depth—are summarized in Tables 1, 2 and 3 for sites across the Greenland Ice Sheet (GIS), West Antarctic Ice Sheet (WAIS) and East Antarctic Ice Sheet (EAIS), respectively. BIZ top and bottom depths, as well as firn-ice transition (FIT) depth (assuming a density of 830 kg m^{-3}), are displayed for all sites in Figure 2. While intermediate-depth drilling projects at Siple Dome, Berkner Island, Roosevelt Island, Law Dome and Taylor Dome experienced brittle ice conditions, the ice-bed interface was encountered before reaching pressures and temperatures suitable for clathrate formation and the transition to ductile ice. Some ice core quality improvement was anecdotally observed in the final several meters of the Siple Dome, Berkner Island and Roosevelt Island ice cores, possibly due to warmer temperatures near the bed (Gow and Meese, 2007; Mulvaney and others, 2007; N. Bertler, personal communication).

Pressure and temperature effects I: brittle zone onset

Snow accumulation rate and surface air temperature are primary controls on the densification of polar firn (e.g. Herron and Langway, 1980; Ligtenberg and others, 2011), although the firnification process is not fully understood (Hörhold and others, 2011). Firn densification is relevant here for its role in isolating air bubbles from porous firn and because the thickness and density of the firn column controls the exact overburden pressure imposed on ice and air bubbles at depth. Overburden pressure may affect where brittle fracture of ice cores commences, as thin firn columns at warmer, higher snow accumulation sites should reach full ice density (920 kg m^{-3}) more rapidly and thus exert more overburden pressure on ice and air bubbles at depth, and vice versa. Additionally, overburden pressure and *in-situ* ice temperature control clathrate stability and are expected to affect the depth of the transition out of the bubbly, BIZ and into the bubble-free, ductile clathrate-ice zone below—with clathrates stabilizing at lower pressures when temperatures are low, and vice versa (e.g. Miller, 1969).

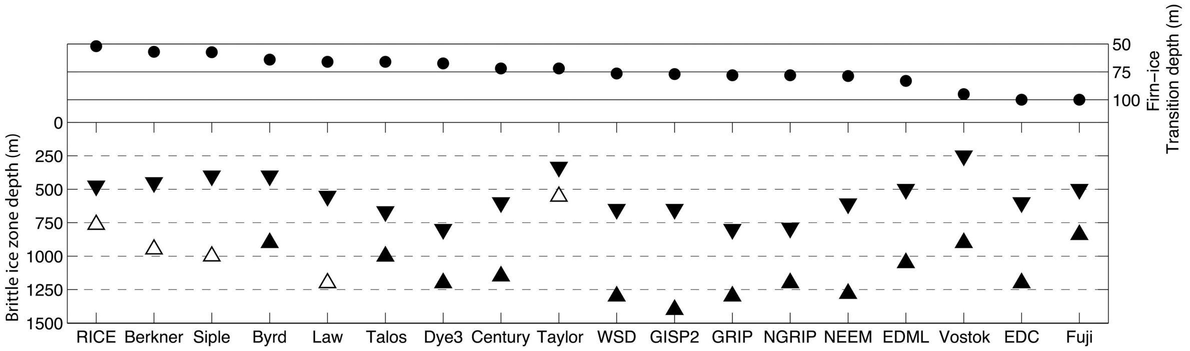

Figure 2. *Firn-ice transition (FIT, depth where density 830 kg m^{-3} reached, circles), BIZ top depths (inverted triangles) and BIZ bottom depths (triangles) at ice drilling sites, ordered by increasing FIT depth. Open triangles denote BIZ bottom depths which represent the ice-bed interface, rather than transition to the bubble-free, ductile ice zone. Abbreviated: WSD (WAIS Divide), RICE (Roosevelt Island Climate Evolution), EDC (EPICA Dome C), EDML (EPICA Drønning Maud Land).*

Table 2*: Site information, brittle ice zone (BIZ) depths, mean annual snow accumulation (m a^{-1} ice), mean surface air temperature (ºC), firn-ice transition depth (density 830 kg m^{-3} reached) and BIZ ice ages for West Antarctic Ice Sheet ice drilling sites.*

	Byrd Station	Siple Dome	Berkner Island	WAIS Divide	Roosevelt Island
Coordinates	80.02° S, 119.52° W	81.65° S, 148.81° W	79.55° S, 45.68° W	79.47° S, 112.09° W	79.36° S, 161.71° W
Years drilled	1966–68[1]	1997–99[5]	2003–05[7]	2006–11[10]	2011–12
Surface elevation (m)	1530[1]	620[5]	890[7]	1766[10]	550
Drill depth (m)	2164[1]	1004[5]	948[7]	3405[10]	764
Ice thickness (m)	2164[1]	1004[5]	948[7]	3455[10]	764
BIZ top (m)	**400**[1,2]	**400**[5]	**450**[7]	**650**[11]	**475**
BIZ bottom (m)	**900**[1,2]	**1000**[5]	**948**[7]	**1300**[11]	**764**
BIZ thickness (m)	**500**	**600**	**498**	**650**	**289**
Snow accumulation (m ice a^{-1})	0.14[3]	0.11[3]	0.13[7]	0.22[10]	0.23[13]
Mean air temperature (°C)	–28[3]	–25[3]	–26.5[7]	–30[10]	–23[13]
Firn/ice transition (m)	64[3]	57.5[3]	57[8]	76.5[12]	52[13]
BIZ top age (ka BP)	3.5[4]	5[6]	4.5[9]	2.7[10]	4[13]
BIZ bottom age (ka BP)	9.5[4]	57[6]	95[9]	6[10]	>40[13]

[1]Gow (1968); [2]Gow (1971); [3]Cuffey and Paterson (2010); [4]Blunier and Brook (2001); [5]Gow and Meese (2007); [6]Brook and others (2005); [7]Mulvaney and others (2007); [8]Gerland and others (1999); [9]R. Mulvaney (personal communication (2014); [10]WAIS Divide Project Members (2013); [11]Souney and others (2014); [12]Kreutz and others (2011); [13] N. Bertler (unpublished information).

***Table 3**: Site information, brittle ice zone (BIZ) depths, mean annual snow accumulation (m a^{-1} ice), mean surface air temperature (ºC), firn-ice transition depth (density 830 kg m^{-3} reached) and BIZ ice ages for East Antarctic Ice Sheet ice drilling sites.*

	Law Dome	Taylor Dome	Vostok station	EPICA Dome C	Dome Fuji	EPICA Dronning Maud Land	Talos Dome
Coordinates	66.77° S, 112.80° E	77.70° S, 159.07° E	78.47° S, 106.87° E	75.10° S, 123.35° E	77.32° S, 39.70° E	75° S, 0° E	72.78° S, 159.07° E
Years drilled	1991–93[1]	1993–94[4]	1990–98, 2005–12[7]	1999–2004[12]	1993–96,[15] 2003–07[16]	2000–06[20]	2005–07[25]
Surface elevation (m)	1370[1]	2375[5]	3488[8]	3233[13]	3810[15]	2892[21]	2318[26]
Drill depth (m)	1200[1]	554[4]	3769[9]	3260[12]	3035[16]	2774[20]	1620[26]
Ice thickness (m)	1220[1]	554[4]	3769[9]	3275[12]	3035[16]	2774[20]	1795[26]
BIZ top (m)	**552**[2]	**335**[4]	**250**[10]	**600**[14]	**500**[17]	**500**[22]	**667**[27,28]
BIZ bottom (m)	**1200**[2]	**554**[4]	**900**[10]	**1200**[14]	**840**[17]	**1050**[22]	**1002**[27,28]
BIZ thickness (m)	**648**	**291**	**650**	**600**	**340**	**550**	**334**
Snow accumulation (m ice a^{-1})	0.7[1]	0.06[5]	0.022[11]	0.036[11]	0.03[15]	0.064[21]	0.08[26]
Mean air temperature (°C)	–22[1]	–43[5]	–55[8]	–54[11]	–58[15]	–44[21]	–41[26]
Firn/ice transition (m)	66[3]	72[4]	95[11]	100[11]	100[18]	83[23]	66[27]
BIZ top age (ka BP)	0.9[1]	10[6]	10.5[8]	29[13]	19.3[19]	7.7[24]	11[26]
BIZ bottom age (ka BP)	20[1]	>160[6]	61.5[8]	80.5[13]	46[19]	24.3[24]	30[26]

[1]Morgan and others (1997); [2]Morgan and others (1994); [3]Etheridge and others (1996); [4]Fitzpatrick (1994); [5]Morse and others (1999); [6]Steig and others (2000); [7]Vasiliev and others (2011); [8]Petit and others (1999); [9]Jouzel (2013); [10]Uchida and others (1994); [11]Cuffey and Paterson (2010); [12]Parrenin and others (2007); [13]EPICA Community Members (2004); [14]Parrenin and others (2012); [15]Watanabe and others (1999); [16]Motoyama (2007); [17]Fujii and others (2002); [18]Hondoh and others (1999); [19]Kawamura and others (2007); [20]Severi and others (2007); [21]Ueltzhöffer and others (2010); [22]F. Wilhelms (personal communication, 2014); [23]Oerter and others (2004); [24]EPICA Community Members (2010); [25]TALDICE (Talos Dome Site Information; http://www.taldice.org/project/site/index.php); [26]Stenni and others (2011); [27]TALDICE, 2006/07 field season (http://www.taldice.org/site/0607/index.php); [28]Schilt and others (2010); [29]Frezzotti and others (2004).

To quantify the influence of firn column thickness on overburden pressure at depth, while also converting BIZ depths to equivalent overburden pressures, firn-column density is modeled using the University of Washington Firn Model Intercomparison Experiment online *Herron and Langway* (1980) model (FirnMICE, http://firny.ess.washington.edu/communityfirnmodel/). A surface snow density of 390 kg m^{-3} is assumed for all sites, and mean annual surface air temperature and snow accumulation rate (ice-equivalent) are input into the model to construct one-meter resolution depth-density profiles from the surface to 300 m for each site (Figure 3a). Constant ice density of 920 kg m^{-3} is assumed below 300 m, although for bubbly ice this may be an overestimate of several kilograms per cubic meter. Snow density measurements from Taylor Dome, Berkner Island and WAIS Divide agree well with model data generated for these sites (density measurements provided with the FirnMICE online model, not shown). Overburden pressure at a given depth is calculated as the sum of overlying snow and ice with density prescribed by the FirnMICE model output. One cubic meter of ice (density 920 kg m^{-3}) exerts 9.02×10^{-3} MPa overburden pressure (Figure 3b). Modeled overburden pressure at 300 m—the depth at which the thickest modeled firn column (Dome Fuji) reaches ice density of 920 kg m^{-3}—is presented in Figure 3c for all sites, plotted against modelled and observed FIT depths (830 kg m^{-3} density). The mean misfit between observed and modeled FIT depth is -4%, with minimum misfits of +1% and -2% (EPICA Dome C and WAIS Divide, respectively) and a maximum misfit of -25% (Siple Dome).

Across the 18 drill sites, 300 m overburden pressure varies from 2.36 MPa at Dome Fuji (modeled FIT depth 114 m, +12% misfit) to 2.56 MPa at Siple Dome (modeled FIT depth 46 m, -25% misfit; Figure 3b, c). Poor FIT depth reproduction for these end-member sites (Figure 3c) suggests an overestimate of the possible range of overburden pressures—more conservative is 2.4 MPa at EPICA Dome C (modeled FIT depth 101 m, +1% misfit) to 2.55 MPa at Berkner Island (modeled FIT depth 52 m, -10% misfit). This overburden pressure fluctuation at depth, a maximum difference of approximately 0.15 MPa to 0.2 MPa between the thickest firn column (slower firnification, lower overburden pressure at depth) to the thinnest (faster firnification, higher overburden pressure at depth), is equivalent to 16.5 m to 22.2 m of ice overburden. If the firn column is ignored and full ice density is assumed from the surface, overburden pressure at depth (2.7 MPa at 300 m) is overestimated by 0.14 MPa to 0.34 MPa or ~15.5 m to 37.7 m of ice (dashed line, Figure 3a, b). This results in an under-estimation of the depth for theoretical clathrate stability. The BIZ does generally occur at shallower depths where the firn-ice transition is shallower (e.g. Figure 2) and exerts greater overburden pressure at depth. This is most clearly observed at GIS and WAIS drill sites—although with low significance, as is expected due to low precision of reported BIZ depths and complex temperature and accumulation effects on firnification and clathrate formation processes. Reported BIZ top depths begin ~10 m deeper per 1 m thickening of the FIT at the eleven GIS and WAIS drill sites (regression of GIS and WAIS FIT depths and BIZ top depths gives R^2 = 0.54, not shown). As overburden pressure alone cannot explain such a deepening, this suggests that unidentified firnification processes likely exert significant control on BIZ onset depth. Proportional deepening of BIZ onset is not observed at all EAIS drill sites, especially not those on the EAIS plateau, perhaps because of increasing tensile strength of ice at smaller grain sizes and lower temperatures (e.g. Butkovich, 1954; Petrovic, 2003), as well as other unknown effects associated with extreme low-temperature and low-accumulation firn densification, grain growth and air-bubble formation.

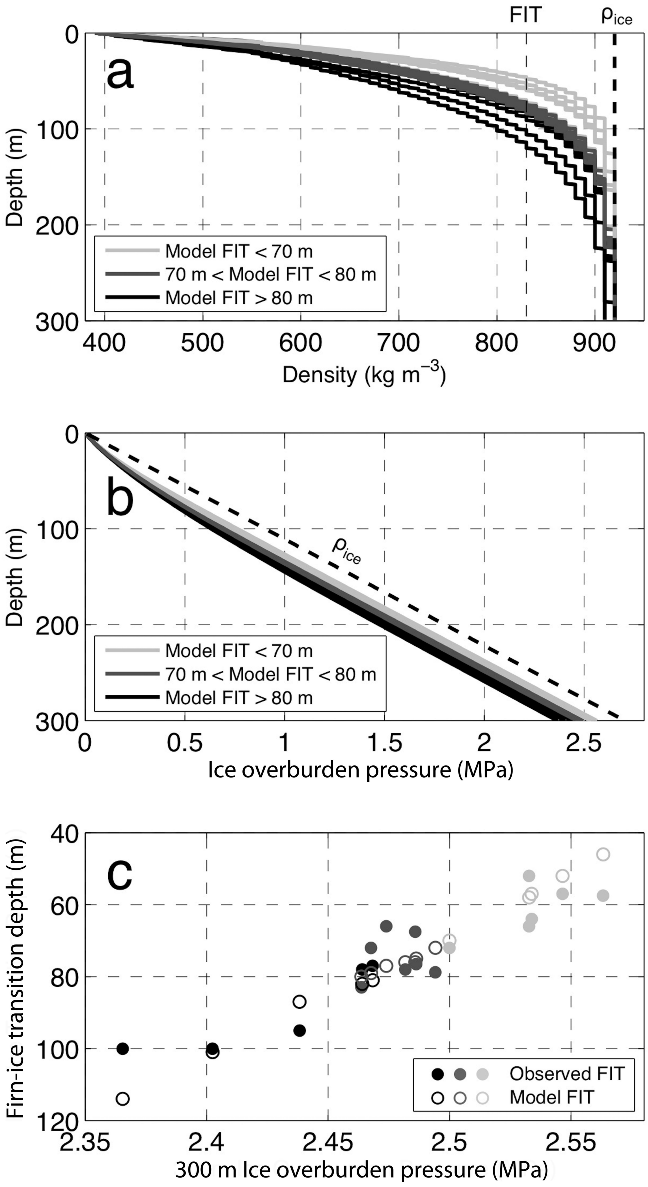

Figure 3. *Results of FirnMICE firn column density modeling (Herron and Langway, 1980 model) and overburden pressure calculations. a) Density-depth profiles generated for the 18 drill site temperature and snow accumulation regimes, shaded according to modeled firn-ice transition (FIT) depth (light grey, model FIT < 70 m; grey, 70 m < model FIT < 80 m; black, model FIT > 80 m); bold dashed line indicates ice density (920 kg m^{-3}). b) Ice overburden pressure versus depth in the firn column (0-300 m) for the 18 drill sites (light grey, model FIT < 70 m; grey, 70 m < model FIT < 80 m; black, model FIT > 80 m); bold dashed line indicates overburden pressure assuming constant ice density from the surface. c) 300 m-depth overburden pressure versus firn-ice transition (FIT) depth from modeled (open circles) and measured (filled circles) firn-column density data.*

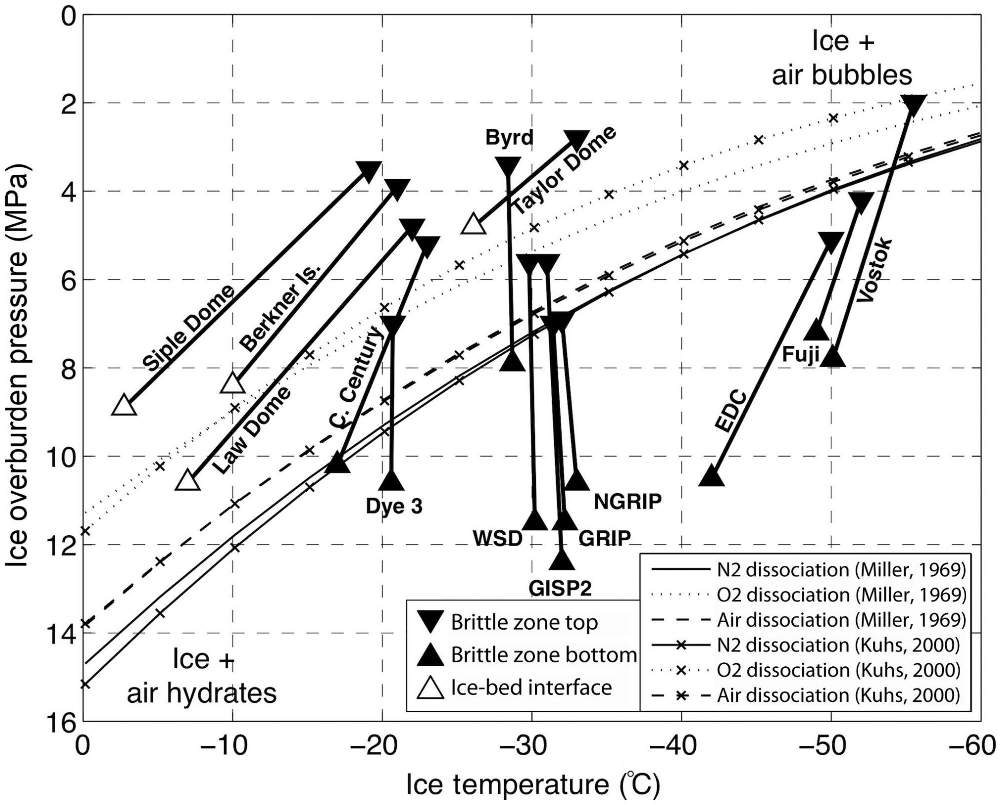

Figure 4. *BIZ top (inverted triangles) and bottom pressures (triangles) plotted at respective in-situ ice temperature from borehole temperature measurements (detailed in Table 4). Theoretical clathrate stability curves are plotted for N_2 (solid), O_2 (dotted), and air (dashed) hydrates (Miller, 1969; Kuhs and others, 2000). The stability curve of Kuhs and others (2000) is indicated with 'x'. Open triangles denote BIZ bottom pressures at the ice-bed interface, thus not the full transition from the bubbly, brittle-ice zone to the bubble-free, ductile ice zone below. Abbreviated: WSD (WAIS Divide), EDC (EPICA Dome C).*

Pressure and temperature effects II: brittle zone relief

In-situ ice temperature determines the depth (pressure) of clathrate stability and thus should affect the depth of the transition from bubbly, brittle ice to bubble-free, ductile ice. This is supported by observations of shallower appearance of clathrates and disappearance of air bubbles in ice cores at low-temperature sites (e.g. observations from Dye 3 and GRIP versus Vostok and Dome Fuji, Ikeda-Fukuzawa and others, 2001). While temperature effects controlling BIZ onset are less clear, it is expected that the BIZ will be relieved at shallower depths (lower pressures) where ice temperatures are lower. Using overburden pressure as calculated above, and borehole temperature data from selected drill sites (Table 4), the BIZ can be evaluated with respect to temperature and pressure and thus compared more accurately with theoretical clathrate stability (Figure 4). BIZ onset in many cases begins at pressures (depths) where clathrates should already begin to stabilize, but brittle fracture is not relieved until ductile conditions are reached as bubble number-densities become sufficiently low and clathrates dominate, strengthening ice cores. While it is tempting to suggest that BIZ bottom pressure indeed decreases with lower ice temperatures, this is not a statistically significant feature including all reported BIZ data (excluding intermediate-depth sites where clathrates do not stabilize before the ice-bed interface is reached). Certainly the BIZ in the Greenland summit ice cores and at WAIS Divide (1200 m to 1400 m BIZ bottom depths, ~5.5 MPa to 12.5 MPa) extends several hundred meters deeper than that of Dome Fuji, Vostok, EPICA Drønning Maud Land and Talos Dome (840 m to 1050 m BIZ bottom depths, 8.2 MPa to 9.2 MPa), but the EPICA Dome C ice core remained highly fractured to 1200 m depth (10.5 MPa). Additionally, the BIZ at Camp Century, Dye 3 and Byrd Station transitions to ductile ice at shallow depths—with pressures only 1 MPa to 2 MPa greater than that required for initial clathrate stability—while most sites transition out of the BIZ at pressures 3 MPa to 5 MPa in excess of requirements for theoretical onset of clathrate stability (Figure 4). This raises the interesting prospect that ice-flow advection of cold ice towards the surface at flank sites could encourage shallower formation of clathrates (e.g. Camp Century, Byrd Station; Shoji and Langway, 1987). However, without disentangling the effects of imprecise BIZ records, drill performance and ice core handling/transport, it is difficult to use reported brittle ice depths to further evaluate this correlation between clathrate stability and the bottom of the BIZ.

To improve understanding of the mechanisms involved in BIZ onset and relief, it may prove useful to investigate ice physical properties including bubble number-density, bubble size, micro-bubbles and ice fabric (e.g. grain size, crystal anisotropy). Take the anomalously shallow BIZ at Vostok, for example: *Uchida and others* (1994) observed a reduction of core quality caused by fractures as shallow as 100 m (likely linked to thermal drilling at Vostok), becoming heavily fractured from 250 m to 750 m with progressive improvement to 900 m where core quality again became excellent. This shallowest occurrence of the BIZ may be related to a rapid increase in bubble number-density (bubbles cm^{-3}) observed in the Vostok ice core beginning at approximately 300 m depth (increasing from ~400 to ~800 bubbles cm^{-3}; Uchida and others, 1994; Ueltzhöffer and others, 2010). Such an increase in bubble number-density may effectively reduce bubble pressures required for fracture propagation by narrowing interstitial ice between bubble cavities. Bubble number-densities reported in the BIZ at Byrd Station and WAIS Divide were relatively more constant at ~200 and ~450 bubbles cm^{-3}, respectively (Gow, 1971; Fitzpatrick et al., in press). Micro-bubbles formed through sublimation-condensation processes may also play a role at Vostok (e.g. Lipenkov, 2000), and are observed in the EPICA Dome C and Drønning Maud Land ice cores (Ueltzhöffer and others, 2010). The second shallowest occurrence of the BIZ, 335 m at Taylor Dome, may be anomalously shallow due to high strain rates at this site—elongated bubbles were observed from 360 to 390 m (Fitzpatrick, 1994).

Table 4: *In-situ ice temperature (borehole temperature) at brittle ice zone (BIZ) top and bottom depths (see Tables 1-3) for selected sites. Temperatures are ± 0.5 ºC, estimated from published graphical data where original datasets could not be accessed. Temperature data for Berkner Island is modeled.*

Drill site	Temperature BIZ top depth	BIZ bottom depth	Source
Camp Century	–23	–17	Shoji and Langway (1987)
Dye-3	–20.7	–20.6	Shoji and Langway (1987)
GRIP	–31.4	–32.2	The Greenland Summit Ice Cores CD-ROM (1997)
GISP2	–31	–32	The Greenland Summit Ice Cores CD-ROM (1997)
NorthGRIP	–32	–33	Dahl-Jensen and others (2003)
Byrd Station	–28.4	–28.7	Ueda and Garfield (1969), T.J. Fudge (personal communication, 2014)
Siple Dome	–19.1	–2.75	G. Clow (personal communication (2014)
Berkner Island	–21	–10	Mulvaney and others (2007)
WAIS Divide	–29.8	–30.2	Cuffey and Clow (2014)
Law Dome	–22	–7	Van Ommen and others (1999)
Taylor Dome	–33	–26.1	G. Clow (personal communication, 2014)
Vostok station	–55.5	–50.1	Salamatin and others (1994)
EPICA Dome C	–50	–42	Pol and others (2010)
Dome Fuji	–52	–49	Ikeda-Fukuzawa and others (2001)

Brittle ice zone age

Figure 5 displays observed BIZ top and bottom ages from published agescales developed for the eighteen drill sites discussed above (detailed ages in Tables 1, 2 and 3). At deep ice core sites where snow accumulation rates are relatively high (e.g. GIS and inland WAIS sites), the age of ice within the BIZ is relatively young, dating from the as few as 2 ka BP (Dye-3; Langway and others, 1985) to 9500 years BP (Byrd Station; Blunier and Brook, 2001). These ages represent approximately 10% or less of the age of dated ice core records developed from these sites. While the Holocene marks the beginning of relatively stable global climate, with the exception of the 8.2 ka BP event (e.g. Alley and others, 1997), continued emphasis on understanding natural climate variability precludes classifying ice of this age as scientifically less interesting than older transitional and glacial ice (e.g. Mayewski and others, 2004; Marcott and others, 2013; Steig and others, 2013).

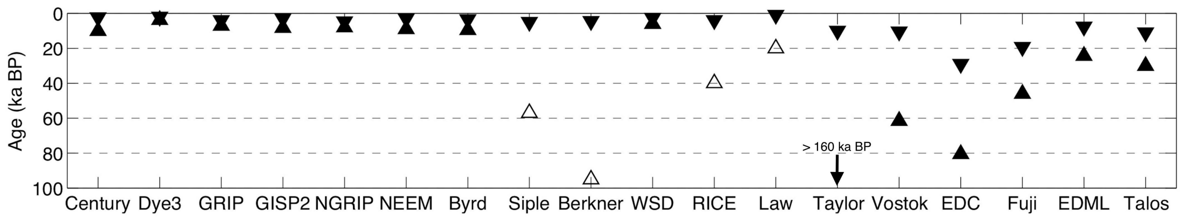

Figure 5. *BIZ top (inverted triangles) and bottom (triangles) age (kiloannum before present, BP) at drill sites, ordered by region and date of drilling. Open triangles denote BIZ bottom ages which represent the maximum dated age (~ice-bed interface) at these sites. Abbreviated: WSD (WAIS Divide), RICE (Roosevelt Island Climate Evolution), EDC (EPICA Dome C), EDML (EPICA Drønning Maud Land).*

A wide range of ice ages are found within the BIZ at deep ice core sites with low snow accumulation rates (e.g. EAIS plateau sites: Taylor Dome, Vostok, Dome C, Drønning Maud Land, Dome Fuji, Talos Dome), and intermediate-depth ice core sites with higher snow accumulation rates (e.g. coastal Antarctic sites: Siple Dome, Berkner Island, Roosevelt Island, Law Dome). In intermediate-depth ice core records (all at intermediate ice-thickness coastal Antarctic locations), ice at the top of the BIZ dates to between approximately 4 ka BP at Roosevelt Island (N. Bertler, personal communication) and 9 ka BP at Law Dome (Morgan and others, 1997). Ice at these coastal Antarctic sites remains brittle to the bed, dating to a minimum of ~40 ka BP (Roosevelt Island; N. Bertler, personal communication) and in all cases placing at least 90% of the dated ice core record within the BIZ. Brittle ice at EPICA Dome C dates from 29 ka BP to 80.5 ka BP (EPICA Community Members, 2004). While not a large fraction of the entire ice core record (~6% of the 800 ka record), this section of the Dome C ice core is highly detailed when compared to deeper ice where ice-flow thinning impairs resolution at this extremely low-accumulation site. From the surface to ~2000 m depth, 55 cm-long sections of the Dome C ice core exhibit temporal resolution of 50-100 years or less, while below 2000 m similar sections contain between 200-1000 years or more (Pol and others, 2010). Taylor Dome, a very shallow site, became brittle from a depth of 335 m, dated to 10 ka BP, remaining brittle to the bed and spanning ice ages in excess of 160 ka BP (Steig and others, 2000). Ice within the BIZ at these coastal Antarctic and EAIS plateau sites spans ages of fundamental interest to paleoclimate research, relevant to investigations into regional timing of the onset of deglaciation during the late-Pleistocene and rapid climate anomalies occurring during this transition (e.g. Younger Dryas, Antarctic Cold Reversal; Alley and others, 1993; WAIS Divide Project Members, 2013).

Mitigating brittle ice impacts

Drilling techniques

Currently, drilling through the BIZ produces ice core sections with several to many breaks, fractures and hairline cracks, commonly affecting more than half of recovered ice in the middle of this zone. Drilling fluid required at these depths pervades all cracks and fractures, contaminating many chemical analyses. At WAIS Divide, where BIZ core quality was the best of any recent United States led drilling project, 1 m-long core sections from 900 m to 1200 m were on average between "good" (containing zero to three breaks or 50% un-fractured) and "fair" quality (containing more than 10 cm of core length without fractures; Souney and others, this issue).

As the only step performed at *in situ* pressures within the ice sheet (minimum of 2.0 MPa, maximum 12.4 MPa in the BIZ), with the added benefit of damping effects associated with a liquid-filled borehole, the drilling process provides important opportunities to reduce the major component of brittle fracture in ice cores by performing mechanically severe steps that might damage cores if performed at surface pressures (~700 hPa, 0.07 MPa). For example, drilling at WAIS Divide employed a unique strategy specifically for brittle ice, performing three core-breaks per ~2.5 m drill run before returning the drill sonde to the surface (detailed in Souney and others, this issue). This technique of performing several core breaks per run at *in situ* pressure results in ice core sections that are ready to ship, without subjecting brittle ice cores at surface pressure to the vibration and high-stresses of making circular-saw section cuts. A similar down-hole technical innovation suggested by *Ueda* (2002) is the development of a drill sonde that captures and seals cores in a vessel at *in situ* pressures, potentially allowing for a more gradual transition to atmospheric pressure than the usual minutes- to hours-long transition as the drill sonde is brought to the surface. Slowing the pressure and temperature transition by hoisting brittle ice drill runs slowly to the surface, reducing drill penetration rate, and considering drill fluid pressure balance have also been proposed (see the discussion by J. Schwander and others in IPICS, 2005).

Maintaining temperatures within drilling and on-site storage structures similar to those at depth in the borehole is a commonly-practiced technique in ice drilling (e.g. Souney and others, this issue). At Roosevelt Island, an actively-cooled storage cave kept ice at -23 ºC despite surface temperatures reaching as much as -5 ºC (D. Mandeno, personal communication). Temperature gradients may reach several tens of degrees between *in-situ* ice temperature and surface drill structure temperatures, which will cause differential heating of ice cores brought to the surface, inducing temperature and stress gradients as the ice core surface warms (and expands) more quickly than the interior. However, it is difficult to overstate the primary impact of the pressure gradient between the BIZ and the surface, which, as a ratio, is a minimum of 30:1 at the shallowest observed BIZ onset (Vostok: 2.0 MPa at 250 m, ~0.07 MPa surface air pressure) and grows to more than a 100:1 ratio at most ice core drill sites (reaching a maximum BIZ bottom to surface pressure ratio of 177:1 at the bottom of the GISP2 BIZ: 1400 m depth, 12.4 MPa).

Transport techniques

Reduction of mechanical shock during core transport from the drill site to laboratories has been achieved primarily by sheathing brittle ice cores in tight-fitting nylon netting immediately upon removal from the drill, and delaying shipment of brittle ice for as long as logistically possible to allow for maximum relaxation. Use of netting was innovated at Berkner Island (Mulvaney and others, 2007), and the same was used successfully at WAIS Divide (Souney and others, this issue) and Roosevelt Island (N. Bertler, personal communication). While itself not preventing initial fracture of brittle ice cores, nylon netting holds badly fragmented sections in place, preventing any loss of stratigraphic order, and protects cores from further damage due to vibration during shipment.

Relaxation of ice cores after drilling is examined thoroughly by *Gow* (1971), measuring significant post-drilling volume expansion (density reduction) at all depths in the Byrd Station ice core. Cores from the BIZ around 800 m depth exhibit greatest expansion: ~0.2% (0.002 kg m^{-3} density decrease) after 8 months, ~0.4% (0.004 kg m^{-3} decrease) after 16 months, and up to ~0.6% (0.006 kg m^{-3} decrease) after 27 months (see Fig. 2 of *Gow*, 1971). Cores from other depths expanded by an average of ~0.2% (0.002 kg m^{-3} decrease) after 27 months. Nearly identical relaxation characteristics were observed in the GISP2 ice core (Gow and others, 1997). Ice cores retrieved using a hot-water drill at Siple Dome relaxed very quickly, likely due to the thermal drilling technique but cores were also stored at relatively warm surface temperatures after drilling (Engelhardt and others, 2000; Gow and Meese, 2007). Ice cores retrieved by PICO (Polar Ice Coring Office) mechanical drilling at

Siple Dome showed very little relaxation, and remain brittle to date (Gow and Meese, 2007; M. Twickler, personal communication).

Much of this relaxation in brittle ice is attributed to slow dilation of highly-pressurized bubbles abundant in this zone. This lends support to the practice of over-wintering brittle ice, most recently performed at WAIS Divide (Souney and others, this issue). At Roosevelt Island, ~2 m long drill runs were sheathed in netting and stored in a refrigerated snow cave for up to 14 days before making 1 m section cuts for shipment. Improvements were noted in band saw cuts after even this short period of relaxation, although some propensity for fracturing remained (N. Bertler, personal communication). It is important to note that over-wintering or long-term storage of brittle ice cores delays sampling and analysis of this section of ice. While this delay is less significant on the timeframe of a multi-year deep drilling project, for smaller endeavors, especially at intermediate-depth coastal sites where a significant portion of the dated ice core record lies within the BIZ, delaying shipment and/or sampling of ice cores is more challenging.

Sampling techniques

Ice core sampling is commonly performed at -20 to -25 ºC, making preliminary longitudinal cuts using a horizontal band saw and subsequent sampling with common vertical band saws. While a simple tool, the band saw applies consistent force at the cutting teeth, especially if tracking of the saw along-core is automated to steadily move the saw blade through the ice. After sufficient relaxation—allowing for slow dilation of air bubbles long after initial violent cracking and fracturing observed immediately after drilling—brittle ice may feed through a band saw with little additional fracturing. Brittle ice below depths of 475 m from Roosevelt Island proved prohibitively brittle after 6 months stored at -30 ºC, with several instances of near-catastrophic fracturing during horizontal cutting due to vibration from the saw blade. At this depth, a conventional vertical band saw used to make ~0.035 x 0.035 x 1.0 m rods of ice also began to add many fractures to previously flawless ice core samples, which had immediately prior been cut into ~0.1 x 0.035 x 1.0 m slabs without damage. Core sampling was halted at 500 m and the remaining ice stored at -18 ºC for an additional year, after which cutting proceeded without significant challenges.

Other cutting instruments may prove more conducive to processing brittle ice core samples. *Tison* (1994) describes the use of a diamond wire-saw for preparing thin sections of debris-rich or brittle ice, an option attractive for its reduced vibration levels. However, with slow cutting rates and high cost of diamond wires, this option may require significant development before being applicable to high-volume ice core sample processing.

Analytical techniques

Many analyses performed in polar ice core studies depend on relatively unbroken samples to prevent contaminants altering original paleoclimate or paleoenvironmental signals. Measurements of atmospheric gases preserved in bubbles ideally require avoidance of section cuts and other breaks present in ice core samples, in order to exclude modern atmospheric gases from analysis. Major-ion and trace chemistry, analyzed in longitudinal samples from the center of ice cores in order to avoid modern contaminants imparted during drilling, shipment and sampling, requires removal of outer sample surfaces and cleaning of any exposed surfaces including section cuts and fractures. Drilling fluid pervades all fractures in ice core samples—especially fluids with low volatility, such as Estisol-240 (Dow Haltermann, Germany) coconut oil extract used at NEEM and Roosevelt Island—rendering chemical analyses extremely difficult, especially in ice from the BIZ.

Continuous-flow analysis (CFA) systems gravity-feed longitudinal ice samples through a sectioned heating plate, pumping meltwater directly into on-line instruments and/or fraction collectors to create discrete sub-samples (e.g. Osterberg and others, 2006; Bigler and others, 2011). When analyzing highly-fractured samples in CFA systems, contamination does not only affect fractured core sections, but also subsequent ice as relatively high-concentration contaminants wash out of sample lines and instruments. Additionally, vertical guide systems for gravity-feeding samples struggle to accommodate ice samples containing fractures, especially high-angle longitudinal fractures, which commonly wedge against plastic guides, disrupting sample flow and accurate depth logging.

Fractured sample sections are commonly removed entirely from CFA campaigns, such that continuous-flow analysis for major-ion chemistry of brittle ice from the WAIS Divide ice core only processed ~62% of ice from the depths of 577 m to 1300 m (D. Ferris, personal communication). An optical drill fluid detection system identified 27 instances of drill fluid contamination in CFA tubing while analyzing 175 m of brittle ice from the NEEM ice core (Warming and others, 2013). Using this detection system, particular negative impacts were noted for dust, conductivity, ammonium, hydrogen peroxide and sulfate datasets in brittle ice from the NEEM ice core. While technically challenging, feasible solutions have been developed for analyzing brittle ice core samples with little sample loss, such as the high-resolution CFA water stable-isotope analysis of 13mm x 13mm x 1.0 m rods of ice from the WAIS Divide ice core (B. Vaughn, V. Morris, T. Jones and J. White, unpublished). This approach used tightly fitting square acrylic tubes to protect the fragile ice rods during shipment, and also support them vertically in a sample rack during analysis—

while light vibration successfully prevented wedging against the acrylic tubing during melting, even in highly-fractured brittle ice (B. Vaughn, personal communication).

Conclusion

At eighteen intermediate-depth and deep polar ice core drilling sites across the Greenland Ice Sheet and West and East Antarctic ice sheets, the brittle ice zone of poor-quality, highly-fractured ice cores extends from a mean top depth of 545 ± 162 m to a mean bottom depth of 1132 ± 178 m (excluding intermediate-depth sites where the ice-bed interface is reached before the transition to ductile ice).

Firn-column thickness, controlled primarily by site temperature and snow accumulation rate, determines the precise overburden pressure at depth, quantified here to demonstrate that thicker firn columns apply less pressure at depth and vice versa. Both reported BIZ top and bottom depths at GIS and WAIS sites are in fact deeper where FIT depth is similarly deep, as could expected due to fluctuating overburden pressure, however the deepening of the BIZ is greater than can be explained from overburden pressure alone. Additionally, the absence of this relationship at extremely cold, dry EAIS plateau sites suggests that other factors associated with firn densification and grain growth, affecting eventual clathrate formation and stability, are likely involved. While it is expected, due to pressure and temperature controls on clathrate stability, that the BIZ should transition to ductile, bubble-free ice at lower pressures (shallower depths) when ice temperatures are lower, this is not a quantitative feature of reported BIZ bottom depths including all deep drill sites. Although shallower stability of clathrates and shallower disappearance of air bubbles is observed in ice cores from colder sites, BIZ bottom depths do not clearly behave similarly. This is likely due to imprecision in reported BIZ depths, as well as the convolution of ice core fracture caused purely by physical properties during relaxation and fracture due to additional stresses induced during retrieval (e.g. drill performance, handling techniques).

Consideration of this 531 ± 138 m thick zone (mean BIZ top minus bottom depth excluding intermediate-depth sites), where pressurized air bubbles and ice relaxation upon retrieval of cores causes extensive and sometimes explosive fracturing, is pertinent to all projects developing records from ice cores recovered at depths greater than approximately 400 m (i.e. mean BIZ top depth, 545 m, less one standard deviation, 162 m, gives 383 m). Relatively high snow accumulation rates and thick ice ensures that ice from the BIZ at inland GIS and WAIS sites is restricted to Holocene ages, and spans less than 10% of the completed ice core records. EAIS plateau and coastal Antarctic drill sites, however, place a considerably larger amount of dated ice core records in the BIZ. Low snow accumulation rates and large ice thicknesses at EAIS plateau sites place 20,000 to 50,000 years of glacial ice from these ice core records in the BIZ, affecting the resolution of these valuable records which are already challenged by low snow accumulation rates. Conversely, high snow accumulation rates and limited ice thickness at coastal Antarctic drill sites place the majority of recovered ice and dated ice core records within the BIZ—at least 90% of the records at all coastal Antarctic drill sites.

Innovative drilling and transport strategies have had recent successes in minimizing fracturing in ice cores from the BIZ, including the WAIS Divide brittle-ice drilling technique, netting core after removing from the drill, and relaxing ice prior to shipment and/or sampling. However, comparatively little has been done to develop better sampling methods and techniques for analyzing highly fractured ice core samples. Consideration of mitigating strategies at any stage can have beneficial impacts on downstream work phases, most importantly potentially improving final scientific results. Targeting of ice core sites is increasingly focused by refined scientific questions, specific research interests, and desire to infill areas of sparse geographical coverage. Advancing understanding of the physical mechanisms controlling the BIZ has the potential to significantly improve the continuous recovery and development of ice core paleoclimate and environmental records, as this zone affects samples of ages spanning periods of fundamental scientific interest at many potential drill sites.

Acknowledgements

The author thanks R. Dadic and N. Bertler for thoughtful discussion of the manuscript. Thorough critique, discussion and encouragement from two anonymous reviewers significantly improved on the original text. The online University of Washington FirnMICE model (http://firny.ess.washington.edu/communityfirnmodel/) was used to model firn density and estimate overburden pressures. The author has been funded by the New Zealand Ministry of Business, Innovation, and Employment Grants (RDF-VUW-1103, CO5X0202), Victoria University and GNS Science. This work is a contribution to the Roosevelt Island Climate Evolution (RICE) Programme, funded by national contributions from New Zealand, Australia, Denmark, Germany, Italy, the People's Republic of China, Sweden, United Kingdom, and the United States of America. The main logistic support for RICE was provided by Antarctica New Zealand (K049) and the US Antarctic Program (I-209M).

References

Alley RB, Meese DA, Shuman CA and 8 others (1993). Abrupt increase in Greenland snow accumulation at the end of the Younger Dryas event. *Nature*, 362, 527-529.

Alley RB, Mayewski PA, Sowers T and 3 others (1997). Holocene climate instability: A prominent, widespread event 8200 yr ago. *Geology*, 25(6), 483.

Bigler M, Svensson A, Kettner E and 3 others (2011). Optimization of high-resolution continuous flow analysis for transient climate signals in ice cores. *Environ. Sci. Technol.*, 45, 4483-4489.

Blunier T and Brook E (2001). Timing of millennial-scale climate change in Antarctica and Greenland during the last glacial period. *Science*, 291, 109-112.

Brook EJ, White JWC, Schilla ASM and 6 others (2005). Timing of millennial-scale climate change at Siple Dome, West Antarctica, during the last glacial period. *Quaternary Sci. Rev.*, Vol. 24, pp. 1333-1343. doi:10.1016/j.quascirev.2005.02.002.

Brook EJ, Wolff E, Dahl-Jensen D, Fischer H, Steig EJ (2006). The future of ice coring: International Partnerships in Ice Core Sciences (IPICS), *PAGES News*, Volume 14(1), 6-9.

Buizert C, Martinerie P, Petrenko VV and 23 others (2012). Gas transport in firn: multiple-tracer characterization and model intercomparison for NEEM, Northern Greenland. *Atmos. Chem. Phys.*, 12, 4259-4277, doi:10.5194/acp-12-4259-2012.

Butkovich TR (1954). *Ultimate strength of ice*. Snow Ice and Permafrost Research Establishment Research Paper 11, U.S. Army Corps of Engineers.

Cuffey KM and Clow G (2014). Temperature Profile of the West Antarctic Ice Sheet Divide Deep Borehole. Boulder, Colorado USA: National Snow and Ice Data Center. http://dx.doi.org/10.7265/N5V69GJW.

Cuffey KM and Paterson WSB (2010). *The Physics of Glaciers*, 4th edn. Elsevier, Oxford.

Dahl-Jensen D, Gundestrup N, Gogineni SP and Miller H (2003). Basal melt at NorthGRIP modeled from borehole, ice-core and radio-echo sounder observations. *Ann. Glaciol.*, 37, 207-212.

Dansgaard W, Johnsen SJ, Møller J and Langway CC Jr (1969). One thousand centuries of climate record from Camp Century on the Greenland Ice Sheet. *Science*, Vol. 166(3903), 377-381.

Dansgaard W, Johnsen SJ, Clausen HB and 8 others (1993). Evidence for general instability of past climate from a 250-kyr ice-core record. *Nature*, 364, 218-220.

Drinkwater MR, Long DG and Bingham AW (2001). Greenland snow accumulation estimates from satellite radar scatterometer data. *J. Geophys. Res.*, 101(D24), 33,935-33,950.

EPICA community members (2004). Eight glacial cycles from an Antarctic ice core. *Nature*, 429, 623-628.

EPICA Community Members (2010). Stable oxygen isotopes of ice core EDML. doi:10.1594/PANGAEA.754444

Engelhardt H, Kamb B and Bolsey R (2000). A hot-water ice-coring drill. *J. Glaciol.*, 46(153), 341-345.

Etheridge DM, Steele LP, Langenfelds RL and 3 others (1996). Natural and anthropogenic changes in atmospheric CO_2 over the last 1000 years from air in Antarctic ice and firn. *J. Geophys. Res.*, 101(D2), 4115-4128.

Fitzpatrick JJ (1994). Preliminary report on the physical and stratigraphic properties of the Taylor Dome ice core. *Antarctic Journal of the United States*, 29(5), 84-86.

Fitzpatrick JJ, Voigt DE, Fegyveresi JM and 9 others (in press). Physical properties of the WAIS Divide ice core. *J. Glaciol.*

Frezzotti M, Bitelli G, De Michelis P and 10 others (2004). Geophysical survey at Talos Dome, East Antarctica: the search for a new deep-drilling site. *Ann. Glaciol.*, 39, 423-432.

Fujii Y, Azuma N, Tanaka Y and 23 others (2002). Deep ice core drilling to 2503 m depth at Dome Fuji, Antarctica. *Memoirs of National Institute of Polar Research*, Special Issue No. 56.

Gerland S, Oerter H, Kipfstuhl J and 6 others (1999). Density log of a 181 m long ice core from Berkner Island, Antarctica. *Ann. Glaciol.*, 29, 215-219.

Gow AJ, Ueda HT and Garfield DE (1968). Antarctic Ice Sheet: preliminary results of the first core hole to bedrock. *Science*, v. 161, p. 1011-1013.

Gow AJ (1968). Bubbles and bubble pressures in Antarctic glacier ice. *J. Glaciol.*, 7(50), 167-182.

Gow AJ (1971). Relaxation of ice in deep drill cores from Antarctica. *J. Geophys. Res.*, Vol. 76, 2533-2541.

Gow AJ, Meese DA, Alley RB and 4 others (1997). Physical and structural properties of the Greenland Ice Sheet Project 2 ice core: A review. *J. Geophys. Res.*, 102(C12), 26,559-26,575.

Gow AJ and Meese DA (2007). Physical properties, crystalline textures and *c*-axis fabrics of the Siple Dome (Antarctica) ice core. *J. Glaciol.*, 53(183), 573-584.

Gundestrup NS and Hansen BL (1984). Bore-hole survey at Dye 3, South Greenland. *J. Glaciol.*, 30(106), 282-288.

Herron MM and Langway CC Jr (1980). Firn densification: and empirical model. *J. Glaciol.*, 25(93), 373-385.

Hörhold MW, Kipfstuhl S, Wilhelms F and 2 others (2011). The densification of layered polar firn. *J. Geophys. Res.*, 116, F01001, doi:10.1029/2009JF001630.

Hondoh T, Narita H, Hori A and 13 others (1999). Basic analyses of Dome Fuji deep ice core Part 2: physical properties. *Polar Meterol. Glaciol.*, 13, 90-98.

Ikeda-Fukazawa, T., T. Hondoh, T. Fukumura, H. Fukazawa, and S. Mae (2001). Variation in N2/O2 ratio of occluded air in Dome Fuji antarctic ice, *J. Geophys. Res.,* 106(D16), 17799–17810, doi:10.1029/2000JD000104.

International Partnerships in Ice Core Sciences (2005). IPICS 2004 Workshop Report. http://www.icedrill.org/documents/view.shtml?id=38, accessed 30 July, 2014.

Kawamura K, Parrenin F, Lisiecki L and 15 others (2007). Northern Hemisphere forcing of climatic cycles in Antarctica over the past 360,000 years. *Nature*, 448, 912-916. doi:10.1038/nature06015.

Kipfstuhl S, Pauer F, Kuhs WH and Shoji H (2001). Air bubbles and clathrate hydrates in the transition zone of the NGRIP deep ice core. *Geophys. Res. Lett.*, Vol. 28, No. 4, 591-594.

Kovacs A, Weeks WF and Michitti, F (1969). Variation of some mechanical properties of polar snow, Camp Century, Greenland. *U.S. Army Cold Regions Research and Engineering Laboratory, Research Rep. 276*.

Kreutz K, Koffman B, Breton D and Hamilton G (2011). *Microparticle, Conductivity, and Density Measurements from the WAIS Divide Deep Ice Core, Antarctica*. Boulder, Colorado USA: National Snow and Ice Data Center. http://dx.doi.org/10.7265/N5K07264.

Kuhs WF, Klapproth A and Chazallon B (2000). Chemical physics of air clathrate hydrates. *In* “Physics of Ice Core Records,” T. Hondoh (ed.), Hokkaido Univ. Press, 2000, Sapporo.

Langway CC Jr, Oeschger H and Dansgaard W *eds.* (1985). Greenland ice core: Geophysics, geochemistry and environment: Geophysical Monographs, v. 33, American Geophysical Union, Washington D.C.

Ligtenberg SRM, Helsen MM and van den Broeke MR (2011). An improved semi-empirical model for the densification of Antarctic firn. *The Cryosphere*, 5, 809-819. doi:10.5194/tc-5-809-2011.

Lipenkov V (2000). Air bubbles and air-hydrate cyrstals in the Vostok ice core. *In* “Physics of Ice Core Records,” T. Hondoh (ed.), Hokkaido Univ. Press, 2000, Sapporo.
Lipenkov V, Vasiliev N, Ekaykin A and 2 others (2013). What have we learned from the first unsealing of Lake Vostok? *7th International Workshop on Ice Drilling Technology*, September 9-13, 2013, Madison, WI, USA.

Marcott SA, Shakun JD, Clark PU and Mix AC (2013). A reconstruction of regional and global temperature for the past 11,300 years. *Science*, 339, 1198-1201.

Martinerie P, Nourtier-Mazaurie E, Barnola J-M and 6 others (2009). Long-lived halocarbon trends and budgets from atmospheric chemistry modelling constrained with measurements in polar firn. *Atmos. Chem. Phys.*, 9, 3911-3934.

Mayewski PA, Rohling EE, Stager JC and 12 others (2004). Holocene climate variability. *Quaternary Res.*, *62*(3), 243-255.

Miller SL (1969). Clathrate hydrates of air in Antarctic ice. *Science*, Vol. 165, 489-490.

Morgan V, Wehrle E, Fleming A and 3 others (1994). Technical aspects of deep ice drilling on Law Dome, *Memoirs of National Institute of Polar Research, Special Issue No. 49*, Pages 78-86.

Morgan VI, Wookey CW, van Ommen T and 2 others (1997). Site information and initial results from deep ice drilling on Law Dome, Antarctica. *J. Glaciol.*, 43(143), 3-10.

Morse DL, Waddington ED, Marshall H-P and 5 others (1999). Accumulation rate measurements at Taylor Dome, East Antarctica: techniques and strategies for mass balance measurements in polar environments. *Geog. Ann.*, 81A, 683-694.

Motoyama H (2007). The second deep ice coring project at Dome Fuji, Antarctica. *Scientific Drilling*, 5, 41–43.

Mulvaney R, Alemany O and Possenti P (2007). The Berkner Island (Antarctica) ice-core drilling project. *Ann. Glaciol.*, 47 (1), 115-124.

NEEM community members (2013). Eemian interglacial reconstructed from a Greenland folded ice core, *Nature*, 493, 489-494, doi:10.1038/nature11789.

Oerter H, Graf W, Meyer H and Wilhelms F (2004). The EPICA ice core from Drønning Maud Land: first results from stable-isotope measurements. *Ann. Glaciol.,* 39(1), 307-312.
van Ommen TD, Morgan VI, Jacka TH and 2 others (1999). Near-surface temperatures in the Dome Summit South (Law Dome, East Antarctica) borehole. *Ann. Glaciol.*, 29(1), 141-144.

Osterberg EC, Handley MJ, Sneed SB, Mayewski PA and Kreutz KJ (2006). Continuous ice core melter system with discrete sampling for major ion, trace element, and stable isotope analysis. *Environ. Sci. Technol.*, 40, 3355-3361.

Parrenin F, Barnola J-M, Beer J and 24 others (2007). The EDC3 chronology for the EPICA Dome C ice core. *Clim. Past*, 3, 485-597.

Parrenin F, Petit J-R, Masson-Delmotte V and 10 others (2012). Volcanic synchronization between the EPICA Dome C and Vostok ice cores (Antarctica) 0-145 kyr BP. *Climate of the Past*, 8, 1031-1045.

Pauer F, Kipfstuhl J and Kuhs WF (1995). Raman spectroscopic study on the nitrogen/oxygen ratio in natural ice clathrates in the GRIP ice core. *Geophys. Res. Lett.*, 22(8), 969-971.

Petit JR, Jouzel J, Raynaud D and 16 others (1999). Climate and atmospheric history of the past 420,000 years from the Vostok ice core, Antarctica. *Nature* 399: 429-436.

Petrovic JJ (2003). Review: mechanical properties of ice and snow. *J. Materials Sci.*, 38, 1-6.

Pol K, Masson-Delmotte V, Johnsen S and 10 others (2010). New MIS 19 EPICA Dome C high resolution deuterium data: hints for a problematic preservation of climate variability at sub-millennial scale in the "oldest ice." *Earth and Planetary Sci. Lett.*, 298, 95-103.

Rasmussen SO, Abbott P, Blunier T and 21 others (2013). A first chronology for the NEEM ice core. *Clim. Past Discuss.*, 9, 2967-3013.

Salamatin AN, Lipenkov Vya and Blinov KV (1994). Vostok (Antarctica) climate record time-scale deduced from the analysis of a borehole-temperature profile. *Ann. Glaciol.*, 20, 207-214

Schilt A, Baumgartner M, Schwander J and 8 others (2010). Atmospheric nitrous oxide during the last 140,000 years. *Earth and Planetary Sci. Lett.*, 300, 33-43, doi:10.1016/j.epsl.2010.09.027.

Schwander J, Barnola JM, Andrié C and 4 others (1993). The age of the air in the firn and the ice at Summit, Greenland. *J. Geophys. Res.*, 98(D2), 2831-2838.

Severi M, Becagli S, Castellano E and 11 others (2007). Syncronization of the EDML and EDC ice cores for the last 52 kyr by volcanic signature matching. *Clim. Past.*, 3, 367-374.

Shoji H and Langway CC Jr (1982). Air hydrate inclusions in fresh ice core. *Nature*, 298, 548-550.

Shoji H and Langway CC Jr (1987). Microscopic observations of the air hydrate-bubble transformation process in glacier ice. *Journal de Physique*, 48(C1), 551-556.

Souney JM, Twickler MS, Hargreaves GM and 13 others (in press). Core handling and processing for the WAIS Divide ice-core project. *Ann. Glaciol.*, 55(68).

Steig EJ, Ding Q, White JWC and 19 others (2013). Recent climate and ice-sheet change in West Antarctica compared to the past 2000 years. *Nature Geoscience*, 6, 372-375.

Steig EJ, Morse DL, Waddington ED and 5 others (2000). Wisconsinan and Holocene climate history from an ice core at Taylor Dome, western Ross Embayment, Antarctica. *Geog. Ann.*, 82A, 213-235.

Stenni B, Buiron D, Frezzotti M and 37 others (2010). Expression of the bipolar see-saw in Antarctic climate records during the last deglaciation. *Nature Geoscience*, Vol. 4, No. 1, 46-49, doi: 10.1038/NGEO1026.

TALDICE, 2006-2007 Field season, http://www.taldice.org/site/0607/index.php, accessed 13 November, 2013.

TALDICE, Talos Dome Site Information, http://www.taldice.org/project/site/index.php, accessed 13 November 2013.

The Greenland Summit Ice Cores CD-ROM (1997). Available from the National Snow and Ice Data Center, University of Colorado at Boulder, and the World Data Center-A for Paleoclimatology, National Geophysical Data Center, Boulder, Colorado.

Timmerman R, LeBrocq AM, Deen TJ and 17 others (2011). A consistent dataset of Antarctic ice sheet topography, cavity geometry, and global bathymetry. *Earth System Science Data*, **2(2)**, 261-273, doi:10.5194/essd-2-261-2010.

Tison J-L (1994). Diamond wire-saw cutting technique for investigating textures and fabrics of debris-laden and brittle ice. *J. Glaciol.*, 40(135), 410-414.

Uchida T, Duval P, Lipenkov V and 3 others (1994). Brittle zone and air-hydrate formation in polar ice sheets. *Memoirs of the National Institute of Polar Research*, Special Issue No. 49.
Ueda HT and Garfield DE (1968). *Drilling through the Greenland Ice Sheet*. U.S. Army Cold Region Research and Engineering Laboratory (CRREL) Spec. Rep. 126.

Ueda HT and Garfield DE (1969). *Drilling through the Antarctic Ice Sheet*. U.S. Army Cold Region Research and Engineering Laboratory (CRREL) Tech. Rep. 231.

Ueda HT (2002). Some thoughts on deep core drilling systems design. *Mem. National Institute of Polar Res.*, Special Issue No. 56, 126-135.

Ueltzhöffer KJ, Bendel V, Freitag J and 4 others (2010). Distribution of air bubbles in the EDML and EDC (Antarctica) ice cores, using a new method of automatic image analysis. *J. Glaciol.*, 56(196), 339-348.

Vasiliev N, Talalay P, and Vostok Deep Ice Core Drilling Parties (2011). Twenty years of drilling the deepest hole in ice. *Scientific* Drilling, 11, 41-45, doi:10.2204/iodp.sd.11.05.2011.

Vinther BM, Clausen HB, Johnsen SJ and 10 others (2006). A synchronized dating of three Greenland ice cores throughout the Holocene. *J. Geophys. Res.*, 111(D13), D13102.

WAIS Divide Project Members (2013). Onset of deglacial warming in West Antarctica driven by local orbital forcing, *Nature*, 500, 440-444,doi: 10.1038/nature12376.

Warming E, Svensson A, Vallelonga P and Bigler M (2013). A technique for continuous detection of drill liquid in ice cores. *J. Glaciol.*, 59(215), 503-506.

Watanabe O, Kamiyama K, Motoyama H and 3 others (1999). The paleoclimate record in the ice core at Dome Fuji station, East Antarctica. *Ann. Glaciol.*, 29(1), 176.

Appendix B: RICE REE data

RICE deep core 8m to 40m samples, from the 2013 core processing campaign. Recalibrated using MATLAB 'robustfit' (bisquare) method; analytical blank corrected. All concentrations in pg g^{-1}.

Vial #	Top Depth (m)	La139	Ce140	Pr141	Nd146	Sm147	Eu153	Gd157	Tb159	Dy163	Ho165	Er166	Tm169	Yb172	Lu175
1	8.00	0.743	1.887	0.164	0.646	0.121	0.027	0.106	0.016	0.090	0.016	0.052	0.006	0.012	0.003
2	8.05	0.782	1.925	0.193	0.780	0.132	0.030	0.121	0.017	0.106	0.019	0.056	0.008	0.013	0.004
3	8.09	0.260	0.621	0.061	0.276	0.056	0.011	0.038	0.005	0.038	0.007	0.021	0.003	0.005	0.002
4	8.13	0.593	1.255	0.132	0.548	0.102	0.017	0.113	0.009	0.067	0.010	0.038	0.005	0.010	0.003
5	8.17	0.159	0.352	0.037	0.139	0.024	0.005	0.024	0.004	0.020	0.003	0.013	0.001	0.002	<0.001
6	8.22	0.068	0.164	0.015	0.061	0.010	0.003	0.011	0.001	0.007	0.001	0.005	<0.001	0.001	0.001
7	8.27	0.079	0.183	0.018	0.079	0.016	0.004	0.009	0.002	0.010	0.002	0.005	0.001	0.001	<0.001
8	8.32	0.916	14.639	0.087	0.326	0.091	0.022	0.069	0.005	0.049	0.007	0.019	0.003	0.005	0.004
9	9.01	0.157	3.756	0.034	0.139	0.034	0.005	0.023	0.003	0.020	0.003	0.010	0.001	0.001	0.001
10	9.06	0.446	1.419	0.107	0.421	0.096	0.010	0.061	0.008	0.044	0.007	0.019	0.002	0.004	0.001
11	9.11	0.440	1.100	0.095	0.353	0.072	0.016	0.052	0.007	0.039	0.007	0.019	0.003	0.004	0.001
12	9.16	0.447	1.122	0.107	0.439	0.088	0.016	0.079	0.006	0.067	0.011	0.037	0.005	0.008	0.003
13	9.21	0.279	0.734	0.068	0.268	0.063	0.007	0.035	0.005	0.036	0.005	0.016	0.003	0.004	0.001
14	9.27	0.622	1.592	0.139	0.561	0.113	0.018	0.110	0.014	0.087	0.017	0.052	0.008	0.013	0.003
15	9.32	0.192	0.501	0.045	0.164	0.029	0.005	0.024	0.003	0.026	0.004	0.009	0.001	0.003	<0.001
16	9.37	0.179	0.370	0.031	0.128	0.027	0.003	0.016	0.001	0.015	0.002	0.008	<0.001	0.001	<0.001
17	9.42	0.135	0.332	0.036	0.165	0.040	0.009	0.044	0.004	0.026	0.005	0.011	0.001	0.002	0.001
18	9.46	0.130	0.262	0.030	0.113	0.024	0.003	0.009	0.002	0.013	0.001	0.006	0.001	0.002	0.001
19	9.51	0.242	0.568	0.079	0.319	0.097	0.005	0.092	0.018	0.122	0.022	0.049	0.008	0.010	0.003
20	9.55	0.546	1.355	0.122	0.478	0.113	0.019	0.091	0.009	0.067	0.013	0.030	0.004	0.006	0.004
21	9.60	0.306	0.916	0.069	0.266	0.062	0.011	0.045	0.006	0.036	0.006	0.020	0.002	0.003	0.001
22	9.65	0.118	0.277	0.024	0.095	0.014	0.002	0.013	0.002	0.009	0.002	0.006	0.001	0.001	<0.001
23	9.69	0.062	0.154	0.014	0.051	0.011	0.002	0.006	0.002	0.005	0.001	0.004	<0.001	0.001	<0.001
24	9.73	0.102	0.223	0.023	0.088	0.010	0.001	0.009	-0.001	0.009	0.002	0.005	<0.001	0.001	<0.001
25	9.77	0.096	0.209	0.019	0.083	0.016	0.002	0.015	0.002	0.011	0.002	0.003	0.001	0.001	<0.001
26	9.81	0.148	0.338	0.028	0.108	0.019	0.003	0.023	0.002	0.012	0.003	0.007	0.001	0.002	<0.001
27	9.86	0.348	0.956	0.078	0.308	0.074	0.009	0.052	0.006	0.037	0.006	0.019	0.003	0.005	0.001
28	9.90	1.180	1.469	0.249	0.999	0.149	0.015	0.106	0.008	0.078	0.015	0.036	0.005	0.007	0.004
29	9.95	0.820	44.050	0.165	0.618	0.195	0.022	0.159	0.014	0.086	0.013	0.041	0.006	0.009	0.003
30	9.99	0.544	11.624	0.106	0.407	0.187	0.015	0.081	0.010	0.062	0.011	0.028	0.005	0.008	0.002
31	10.04	0.281	1.539	0.065	0.262	0.062	0.008	0.035	0.005	0.030	0.004	0.013	0.001	0.003	0.001
32	10.08	0.223	0.775	0.045	0.182	0.025	0.004	0.022	0.002	0.015	0.003	0.010	0.001	0.003	0.001
33	10.13	0.228	0.559	0.047	0.191	0.035	0.006	0.027	0.004	0.024	0.003	0.012	0.002	0.002	0.001
34	10.17	0.205	0.527	0.045	0.177	0.033	0.006	0.031	0.004	0.023	0.004	0.010	0.001	0.003	0.001
35	10.21	0.117	0.263	0.025	0.110	0.017	0.004	0.019	0.002	0.017	0.002	0.009	0.001	0.002	<0.001
36	10.25	0.204	2.450	0.036	0.139	0.028	0.003	0.019	0.001	0.020	0.003	0.010	<0.001	0.002	0.002
37	10.29	0.184	0.489	0.041	0.150	0.038	0.005	0.020	0.003	0.020	0.004	0.009	0.001	0.003	0.001
38	10.33	0.278	0.859	0.068	0.280	0.052	0.008	0.037	0.005	0.035	0.005	0.014	0.002	0.004	0.001
39	10.37	0.452	1.127	0.100	0.401	0.072	0.012	0.067	0.007	0.051	0.007	0.027	0.003	0.006	0.003
40	10.41	0.416	0.903	0.098	0.389	0.077	0.010	0.040	0.005	0.047	0.006	0.016	0.004	0.003	0.002
41	10.44	0.582	1.166	0.123	0.487	0.093	0.018	0.077	0.009	0.068	0.013	0.034	0.005	0.009	0.002
42	10.48	0.243	0.516	0.049	0.224	0.038	0.006	0.033	0.004	0.027	0.005	0.011	0.002	0.003	0.001
43	10.52	0.181	0.410	0.041	0.169	0.031	0.006	0.018	0.004	0.023	0.003	0.009	0.001	0.002	0.001
44	10.56	0.154	0.343	0.038	0.177	0.034	0.002	0.032	0.002	0.023	0.003	0.009	<0.001	0.002	0.001
45	10.60	0.175	0.392	0.042	0.156	0.033	0.005	0.020	0.003	0.020	0.003	0.010	0.001	0.002	0.001
46	10.63	0.279	0.586	0.063	0.224	0.046	0.009	0.032	0.004	0.023	0.004	0.013	0.002	0.003	0.001
47	10.67	0.388	1.076	0.088	0.354	0.062	0.012	0.053	0.007	0.044	0.007	0.019	0.003	0.004	0.001
48	10.70	0.339	0.762	0.071	0.276	0.053	0.009	0.026	0.004	0.029	0.005	0.018	0.002	0.004	0.002
49	10.74	0.269	0.508	0.052	0.210	0.038	0.008	0.029	0.004	0.028	0.005	0.015	0.003	0.002	0.001
50	10.78	0.138	0.272	0.027	0.104	0.018	0.005	0.016	0.003	0.016	0.002	0.005	0.001	0.001	0.001
51	10.82	0.145	0.303	0.032	0.137	0.022	0.008	0.022	0.003	0.021	0.003	0.007	0.001	0.001	0.001
52	10.85	0.221	0.484	0.051	0.195	0.050	0.004	0.025	0.001	0.018	0.004	0.010	0.001	0.002	<0.001
53	10.89	3.699	8.206	0.934	3.515	0.577	0.010	0.384	0.038	0.160	0.021	0.037	0.002	0.005	0.001
54	10.94	0.166	2.314	0.038	0.153	0.025	0.006	0.025	0.003	0.025	0.003	0.010	0.001	0.002	0.001
55	10.98	0.231	9.384	0.050	0.195	0.058	0.008	0.038	0.005	0.030	0.006	0.018	0.002	0.003	0.001
56	11.02	0.246	2.194	0.052	0.218	0.043	0.006	0.028	0.004	0.025	0.003	0.011	0.002	0.003	0.001
57	11.06	0.407	1.308	0.089	0.348	0.073	0.012	0.054	0.005	0.037	0.006	0.012	0.002	0.003	0.001
58	11.10	0.441	1.054	0.095	0.365	0.069	0.013	0.052	0.008	0.040	0.007	0.020	0.002	0.004	0.001
59	11.14	0.133	0.341	0.030	0.115	0.028	0.004	0.014	0.003	0.019	0.003	0.010	0.001	0.002	0.001
60	11.18	0.145	0.286	0.034	0.133	0.017	0.005	0.015	0.001	0.014	0.003	0.011	<0.001	0.002	<0.001
61	11.22	0.223	0.535	0.054	0.192	0.040	0.003	0.031	0.004	0.022	0.003	0.011	0.001	0.002	<0.001
62	11.26	1.455	3.940	0.317	1.199	0.212	0.011	0.176	0.026	0.159	0.029	0.073	0.011	0.014	0.004
63	11.30	0.140	0.292	0.032	0.121	0.021	0.004	0.015	0.002	0.013	0.002	0.010	0.001	0.001	<0.001
64	11.34	0.037	0.088	0.008	0.020	0.002	<0.001	0.002	<0.001	0.005	0.001	0.002	<0.001	0.001	<0.001
65	11.38	0.117	0.236	0.032	0.110	0.022	0.002	0.011	0.002	0.009	0.001	0.003	<0.001	<0.001	<0.001
66	11.42	0.231	0.506	0.057	0.219	0.040	0.008	0.031	0.004	0.022	0.004	0.010	0.001	0.003	0.001
67	11.45	0.181	0.526	0.041	0.164	0.038	0.005	0.030	0.004	0.027	0.004	0.011	0.001	0.003	0.001
68	11.50	0.234	0.668	0.050	0.181	0.040	0.004	0.021	0.002	0.025	0.005	0.010	0.001	0.002	0.001

69	11.54	0.289	0.729	0.066	0.277	0.059	0.007	0.044	0.006	0.028	0.005	0.018	0.003	0.004	0.001
70	11.57	0.459	0.979	0.100	0.394	0.079	0.014	0.075	0.007	0.045	0.008	0.024	0.003	0.006	0.002
71	11.61	0.894	2.113	0.223	0.820	0.145	0.013	0.107	0.013	0.068	0.008	0.025	0.002	0.004	0.002
72	11.64	0.167	0.391	0.035	0.138	0.028	0.003	0.012	0.001	0.016	0.003	0.008	0.001	0.002	0.001
73	11.68	0.060	0.147	0.015	0.061	0.016	0.003	0.010	0.002	0.009	0.001	0.005	<0.001	0.002	<0.001
74	11.71	0.153	0.370	0.036	0.148	0.028	0.005	0.018	0.004	0.013	0.001	0.006	0.001	0.001	0.001
75	11.75	0.103	0.221	0.022	0.099	0.019	0.005	0.013	0.002	0.011	0.002	0.006	0.001	0.002	0.001
76	11.78	0.107	0.267	0.025	0.089	0.025	0.003	0.006	<0.001	0.014	0.002	0.004	<0.001	0.002	<0.001
77	11.81	0.128	0.352	0.028	0.111	0.028	0.005	0.021	0.003	0.018	0.003	0.009	0.002	0.002	0.001
78	11.85	0.115	0.294	0.029	0.123	0.027	0.005	0.016	0.002	0.016	0.002	0.007	0.001	0.001	0.001
79	11.88	0.257	0.542	0.054	0.210	0.037	0.007	0.031	0.005	0.034	0.005	0.017	0.002	0.003	0.001
80	11.91	0.310	0.587	0.062	0.254	0.036	0.007	0.036	0.003	0.031	0.005	0.017	0.001	0.003	0.001
81	11.94	0.370	0.681	0.079	0.305	0.054	0.007	0.037	0.006	0.040	0.006	0.016	0.003	0.004	0.002
82	11.98	4.903	16.298	0.926	3.476	0.622	0.115	0.482	0.057	0.338	0.064	0.160	0.023	0.036	0.015
83	12.02	0.469	1.524	0.108	0.388	0.077	0.011	0.061	0.006	0.037	0.007	0.017	0.003	0.003	0.001
84	12.05	0.414	1.010	0.092	0.359	0.083	0.008	0.054	0.005	0.046	0.008	0.024	0.001	0.006	0.002
85	12.07	1.252	1.958	0.288	1.101	0.217	0.034	0.159	0.019	0.127	0.021	0.055	0.008	0.013	0.003
86	12.10	0.310	1.116	0.067	0.265	0.067	0.009	0.043	0.006	0.028	0.006	0.017	0.002	0.003	0.001
87	12.15	0.232	0.560	0.050	0.204	0.046	0.006	0.035	0.003	0.031	0.006	0.014	0.003	0.004	0.001
88	12.18	0.187	0.448	0.038	0.137	0.033	0.003	0.013	0.001	0.020	0.002	0.008	<0.001	0.003	0.001
89	12.22	0.300	0.578	0.061	0.240	0.045	0.008	0.035	0.005	0.031	0.005	0.017	0.002	0.004	0.001
90	12.26	0.982	1.861	0.202	0.719	0.132	0.014	0.094	0.010	0.066	0.010	0.024	0.004	0.005	0.002
91	12.30	0.230	0.455	0.047	0.177	0.032	0.003	0.024	0.003	0.017	0.003	0.010	0.001	0.002	0.003
92	12.34	0.090	0.337	0.019	0.077	0.013	0.002	0.004	<0.001	0.012	0.002	0.006	<0.001	0.001	<0.001
93	12.38	0.091	0.180	0.018	0.078	0.012	0.003	0.004	0.002	0.012	0.002	0.008	0.001	0.002	0.001
94	12.42	0.114	0.301	0.025	0.094	0.022	0.002	0.018	0.003	0.013	0.003	0.009	0.001	0.001	<0.001
95	12.46	0.124	0.338	0.030	0.122	0.027	0.003	0.014	0.002	0.015	0.003	0.008	0.001	0.002	<0.001
96	12.50	0.178	0.641	0.040	0.163	0.041	0.004	0.025	0.002	0.020	0.005	0.015	0.001	0.004	0.001
97	12.54	0.145	0.437	0.036	0.135	0.026	0.003	0.015	0.003	0.018	0.002	0.008	0.001	0.001	<0.001
98	12.58	0.120	0.332	0.028	0.113	0.021	0.002	0.014	0.001	0.010	0.001	0.006	<0.001	0.001	<0.001
99	12.62	0.251	0.558	0.066	0.269	0.050	0.009	0.041	0.005	0.036	0.005	0.018	0.002	0.004	0.001
100	12.66	0.160	0.346	0.040	0.146	0.017	0.005	0.011	0.001	0.017	0.003	0.010	<0.001	0.002	0.001
101	12.69	0.104	0.255	0.026	0.091	0.027	0.003	0.015	0.002	0.011	0.002	0.009	0.001	0.001	<0.001
102	12.73	0.137	0.274	0.029	0.129	0.022	0.004	0.018	0.003	0.017	0.003	0.010	0.001	0.002	0.001
103	12.77	0.211	0.338	0.046	0.182	0.029	0.008	0.025	0.004	0.021	0.003	0.011	0.001	0.002	0.001
104	12.81	0.134	0.280	0.031	0.134	0.024	0.005	0.028	0.002	0.027	0.005	0.025	<0.001	0.004	0.001
105	12.84	0.063	0.133	0.015	0.050	0.008	0.002	0.006	0.001	0.010	0.001	0.004	<0.001	0.002	<0.001
106	12.88	0.080	0.156	0.018	0.076	0.013	0.003	0.009	0.001	0.011	0.001	0.006	<0.001	0.001	<0.001
107	12.93	0.381	6.624	0.072	0.257	0.049	0.004	0.025	0.003	0.015	0.003	0.008	0.001	0.001	<0.001
108	12.97	0.373	8.335	0.083	0.308	0.111	0.012	0.062	0.002	0.040	0.007	0.021	0.002	0.005	0.001
109	13.02	0.174	1.058	0.032	0.148	0.038	0.004	0.020	0.003	0.023	0.003	0.009	0.001	0.002	0.001
110	13.06	0.099	0.537	0.022	0.087	0.015	0.002	0.012	0.002	0.013	0.002	0.004	0.001	0.002	<0.001
111	13.10	0.098	0.374	0.023	0.107	0.023	0.002	0.012	0.003	0.014	0.003	0.009	0.001	0.001	<0.001
112	13.14	0.090	0.275	0.020	0.076	0.026	0.003	0.006	<0.001	0.012	0.002	0.004	<0.001	0.001	<0.001
113	13.18	0.181	0.286	0.036	0.134	0.016	0.003	0.019	0.002	0.018	0.003	0.010	0.001	0.001	<0.001
114	13.22	0.241	0.511	0.054	0.197	0.044	0.006	0.034	0.004	0.024	0.004	0.011	0.002	0.002	0.001
115	13.26	0.165	0.342	0.035	0.129	0.034	0.005	0.022	0.003	0.017	0.004	0.010	0.001	0.002	<0.001
116	13.30	0.112	0.277	0.023	0.085	0.013	0.002	0.013	0.002	0.017	0.004	0.009	0.001	0.002	0.001
117	13.34	0.119	0.248	0.027	0.083	0.013	0.004	0.013	0.002	0.016	0.003	0.006	0.001	0.002	0.001
118	13.38	0.130	0.336	0.028	0.116	0.018	0.004	0.014	0.003	0.017	0.002	0.009	0.001	0.002	<0.001
119	13.42	0.245	0.684	0.057	0.216	0.051	0.007	0.035	0.004	0.033	0.005	0.012	0.002	0.004	0.001
120	13.46	0.221	0.716	0.051	0.207	0.042	0.006	0.027	0.002	0.024	0.004	0.012	0.001	0.004	0.001
121	13.50	0.229	0.531	0.054	0.205	0.039	0.006	0.032	0.006	0.024	0.005	0.012	0.003	0.003	0.001
122	13.54	0.303	0.551	0.054	0.188	0.038	0.008	0.036	0.005	0.025	0.005	0.013	0.002	0.002	0.001
123	13.58	0.081	0.174	0.018	0.078	0.013	0.002	0.008	0.001	0.011	0.002	0.005	0.001	0.001	<0.001
124	13.61	0.147	0.312	0.029	0.115	0.010	0.005	0.008	0.001	0.016	0.003	0.009	<0.001	0.002	0.001
125	13.65	0.693	1.418	0.175	0.700	0.139	0.032	0.140	0.018	0.114	0.020	0.059	0.009	0.013	0.004
126	13.69	0.118	0.263	0.027	0.107	0.015	0.004	0.016	0.002	0.011	0.001	0.007	0.001	0.002	<0.001
127	13.72	1.176	2.325	0.248	0.920	0.142	0.022	0.123	0.015	0.096	0.015	0.044	0.005	0.010	0.003
128	13.75	1.289	2.604	0.277	1.053	0.182	0.031	0.155	0.018	0.116	0.017	0.047	0.007	0.010	0.006
129	13.79	0.573	1.136	0.125	0.510	0.079	0.014	0.079	0.009	0.063	0.011	0.036	0.004	0.007	0.002
130	13.82	0.421	1.203	0.089	0.339	0.056	0.012	0.058	0.007	0.048	0.008	0.023	0.003	0.005	0.001
131	13.86	0.584	1.267	0.145	0.562	0.084	0.017	0.073	0.008	0.048	0.006	0.016	0.003	0.003	0.001
132	13.89	0.245	0.483	0.051	0.214	0.029	0.007	0.022	0.003	0.021	0.005	0.012	0.001	0.002	0.002
133	13.93	0.320	2.970	0.069	0.274	0.051	0.011	0.037	0.005	0.027	0.006	0.014	0.002	0.003	0.001
134	13.97	0.857	30.543	0.178	0.672	0.125	0.021	0.116	0.016	0.090	0.014	0.040	0.006	0.010	0.003
135	14.02	0.647	6.135	0.141	0.533	0.093	0.014	0.086	0.011	0.072	0.014	0.031	0.005	0.007	0.002
136	14.05	0.690	2.260	0.141	0.583	0.109	0.020	0.070	0.008	0.061	0.013	0.031	0.002	0.009	0.004
137	14.09	0.323	0.922	0.069	0.261	0.040	0.006	0.033	0.005	0.036	0.006	0.015	0.003	0.004	0.001
138	14.13	0.225	0.474	0.047	0.184	0.030	0.006	0.030	0.003	0.022	0.003	0.007	0.002	0.002	0.001
139	14.17	0.477	1.002	0.101	0.394	0.078	0.011	0.058	0.009	0.054	0.008	0.020	0.003	0.005	0.003
140	14.21	0.015	0.010	0.001	<0.001	-0.001	<0.001	0.006	<0.001	<0.001	-0.001	<0.001	0.001	<0.001	<0.001
141	14.24	0.430	1.076	0.100	0.396	0.079	0.013	0.057	0.010	0.051	0.009	0.026	0.004	0.006	0.001
142	14.28	0.256	0.654	0.068	0.290	0.048	0.010	0.046	0.007	0.040	0.007	0.017	0.003	0.004	0.002
143	14.32	0.103	0.266	0.028	0.116	0.021	0.004	0.018	0.002	0.010	0.002	0.005	<0.001	0.001	<0.001
144	14.36	0.086	0.204	0.021	0.069	0.012	0.002	0.016	0.002	0.009	0.001	0.004	<0.001	0.002	0.002
145	14.40	0.415	0.873	0.096	0.325	0.065	0.012	0.048	0.007	0.041	0.007	0.018	0.003	0.004	0.001

146	14.44	0.360	0.879	0.086	0.330	0.053	0.014	0.043	0.006	0.036	0.007	0.025	0.003	0.006	0.001
147	14.48	0.086	0.188	0.021	0.088	0.021	0.003	0.015	0.002	0.014	0.003	0.008	0.002	0.001	<0.001
148	14.51	0.052	0.135	0.010	0.047	0.001	0.002	0.012	<0.001	0.005	<0.001	0.001	0.001	<0.001	<0.001
149	14.55	0.093	0.153	0.020	0.078	0.009	0.003	0.006	0.001	0.010	0.001	0.003	0.001	0.001	0.001
150	14.59	0.315	0.674	0.072	0.270	0.048	0.008	0.031	0.003	0.019	0.004	0.008	0.001	0.002	0.001
151	14.63	0.398	0.886	0.089	0.349	0.069	0.013	0.064	0.008	0.036	0.006	0.022	0.003	0.004	0.001
152	14.66	0.368	0.787	0.077	0.297	0.052	0.009	0.041	0.004	0.036	0.006	0.019	0.003	0.005	0.002
153	14.70	0.180	0.381	0.039	0.158	0.030	0.006	0.023	0.003	0.020	0.003	0.010	0.001	0.002	0.001
154	14.73	0.155	0.348	0.038	0.164	0.048	0.007	0.053	0.007	0.052	0.009	0.021	0.003	0.005	0.001
155	14.77	0.205	0.412	0.044	0.167	0.039	0.004	0.023	0.004	0.023	0.004	0.012	0.002	0.002	0.001
156	14.81	0.242	0.504	0.052	0.200	0.042	0.008	0.024	0.002	0.021	0.004	0.011	0.002	0.004	0.001
157	14.84	0.113	0.260	0.024	0.122	0.026	0.004	0.020	0.003	0.017	0.003	0.008	0.001	0.003	0.001
158	14.88	0.282	0.683	0.067	0.280	0.054	0.010	0.052	0.006	0.039	0.006	0.017	0.002	0.003	0.001
159	14.93	0.241	0.574	0.056	0.237	0.039	0.009	0.035	0.005	0.032	0.007	0.017	0.002	0.003	0.001
160	14.97	2.050	14.427	0.484	1.886	0.409	0.074	0.346	0.037	0.252	0.043	0.131	0.015	0.026	0.013
161	15.01	0.155	3.599	0.037	0.131	0.040	0.006	0.030	0.003	0.018	0.004	0.012	0.002	0.003	0.001
162	15.05	0.423	1.341	0.081	0.300	0.046	0.007	0.036	0.004	0.024	0.004	0.012	0.001	0.003	0.001
163	15.09	0.153	0.487	0.034	0.134	0.023	0.004	0.020	0.003	0.017	0.003	0.008	0.001	0.002	0.001
164	15.13	0.192	0.601	0.045	0.167	0.046	0.006	0.027	0.004	0.021	0.004	0.010	0.002	0.004	0.003
165	15.17	0.141	0.294	0.030	0.116	0.025	0.005	0.022	0.001	0.011	0.002	0.007	0.001	0.001	<0.001
166	15.21	0.095	0.211	0.021	0.088	0.014	0.003	0.019	0.002	0.010	0.002	0.005	0.001	0.001	<0.001
167	15.25	0.050	0.393	0.011	0.041	0.009	0.001	0.001	0.001	0.007	0.001	0.003	0.001	0.001	<0.001
168	15.29	0.554	5.813	0.111	0.418	0.063	0.012	0.052	0.005	0.036	0.008	0.023	0.003	0.006	0.002
169	15.32	0.117	2.924	0.028	0.111	0.021	0.005	0.021	0.003	0.019	0.002	0.010	0.001	0.001	0.001
170	15.36	0.259	0.657	0.058	0.222	0.040	0.008	0.037	0.004	0.030	0.005	0.014	0.002	0.004	0.001
171	15.40	0.173	0.428	0.041	0.156	0.028	0.004	0.025	0.003	0.021	0.003	0.012	0.002	0.002	0.001
172	15.44	0.080	0.204	0.019	0.063	0.014	0.004	0.008	0.001	0.011	0.001	0.004	<0.001	0.001	<0.001
173	15.47	0.018	0.037	0.005	0.026	0.003	<0.001	0.006	0.001	0.005	<0.001	0.001	<0.001	<0.001	<0.001
174	15.51	0.023	0.027	0.004	0.022	0.005	0.002	0.001	0.001	0.002	<0.001	0.002	<0.001	<0.001	<0.001
175	15.55	0.036	0.063	0.008	0.035	0.009	0.001	0.009	<0.001	0.003	0.001	0.002	0.001	<0.001	<0.001
176	15.58	0.043	0.110	0.010	0.047	0.003	0.003	0.004	<0.001	0.007	0.001	0.003	0.001	<0.001	<0.001
177	15.62	0.033	0.046	0.008	0.038	0.004	0.001	0.009	0.001	0.007	0.001	0.004	0.001	0.001	<0.001
178	15.65	1.147	2.134	0.218	0.779	0.096	0.007	0.074	0.008	0.052	0.008	0.021	0.003	0.004	0.003
179	15.69	0.144	0.333	0.032	0.144	0.020	0.005	0.021	0.002	0.014	0.002	0.007	0.001	0.003	<0.001
180	15.72	0.128	0.379	0.033	0.125	0.027	0.006	0.020	0.002	0.015	0.004	0.007	0.001	0.002	0.001
181	15.76	0.157	0.460	0.037	0.151	0.029	0.005	0.020	0.003	0.026	0.004	0.010	0.001	0.003	0.001
182	15.79	0.136	0.412	0.033	0.127	0.035	0.004	0.022	0.003	0.017	0.002	0.009	0.001	0.002	<0.001
183	15.83	0.381	0.918	0.091	0.365	0.069	0.013	0.061	0.007	0.051	0.009	0.030	0.003	0.006	0.002
184	15.86	0.356	0.938	0.082	0.338	0.056	0.011	0.047	0.004	0.037	0.007	0.020	0.002	0.004	0.002
185	15.90	0.473	1.001	0.106	0.421	0.070	0.012	0.058	0.007	0.043	0.010	0.020	0.004	0.005	0.001
186	15.93	1.411	2.930	0.340	1.307	0.224	0.035	0.178	0.021	0.091	0.013	0.037	0.006	0.009	0.002
187	15.96	1.720	3.182	0.390	1.517	0.314	0.053	0.253	0.037	0.231	0.040	0.107	0.016	0.020	0.005
188	16.00	0.820	1.896	0.185	0.726	0.150	0.033	0.134	0.014	0.109	0.019	0.052	0.006	0.014	0.006
189	16.05	1.755	3.440	0.358	1.248	0.176	0.027	0.133	0.015	0.092	0.016	0.035	0.005	0.009	0.003
190	16.08	0.272	0.700	0.063	0.272	0.056	0.008	0.040	0.007	0.044	0.006	0.016	0.003	0.004	0.001
191	16.12	0.709	1.726	0.157	0.606	0.125	0.022	0.098	0.013	0.082	0.015	0.048	0.005	0.009	0.003
192	16.15	0.484	1.078	0.104	0.421	0.082	0.017	0.059	0.007	0.054	0.007	0.027	0.003	0.007	0.003
193	16.19	0.369	0.718	0.082	0.312	0.061	0.007	0.054	0.006	0.040	0.006	0.014	0.002	0.004	0.001
194	16.23	0.178	0.320	0.033	0.135	0.023	0.004	0.016	0.002	0.015	0.003	0.008	0.002	0.002	<0.001
195	16.27	0.108	0.506	0.027	0.129	0.021	0.004	0.020	0.003	0.018	0.003	0.013	0.001	0.003	0.001
196	16.31	0.060	0.150	0.013	0.051	0.007	0.003	0.012	<0.001	0.008	0.001	0.005	<0.001	0.001	<0.001
197	16.34	0.064	0.122	0.015	0.052	0.010	0.002	0.015	0.002	0.013	0.002	0.006	<0.001	0.001	<0.001
198	16.38	0.090	0.214	0.019	0.081	0.013	0.003	0.012	0.001	0.012	0.002	0.005	0.001	0.001	0.001
199	16.42	0.165	0.411	0.036	0.140	0.023	0.004	0.022	0.004	0.020	0.003	0.011	0.001	0.002	<0.001
200	16.46	0.013	0.012	0.001	<0.001	-0.002	0.002	0.001	<0.001	<0.001	<0.001	<0.001	<0.001	<0.001	<0.001
201	16.50	0.099	0.291	0.026	0.104	0.024	0.002	0.020	0.002	0.012	0.002	0.005	0.001	0.001	0.001
202	16.53	0.173	0.475	0.037	0.171	0.033	0.005	0.027	0.005	0.024	0.004	0.012	0.001	0.003	0.001
203	16.57	0.302	0.684	0.063	0.248	0.039	0.008	0.032	0.003	0.014	0.002	0.006	0.001	0.002	<0.001
204	16.62	0.100	0.277	0.021	0.097	0.012	0.005	0.014	<0.001	0.009	0.001	0.008	<0.001	0.001	0.001
205	16.66	0.185	0.429	0.042	0.177	0.033	0.005	0.030	0.004	0.026	0.004	0.013	0.001	0.003	0.001
206	16.69	0.193	0.399	0.046	0.160	0.040	0.005	0.025	0.003	0.027	0.003	0.014	0.002	0.003	0.001
207	16.73	0.048	0.100	0.012	0.052	0.008	0.003	0.007	0.002	0.009	0.001	0.005	0.001	0.001	<0.001
208	16.76	0.050	0.146	0.015	0.070	0.017	0.004	0.010	0.001	0.008	0.001	0.003	<0.001	<0.001	<0.001
209	16.80	0.102	0.285	0.024	0.108	0.023	0.003	0.020	0.002	0.010	0.002	0.006	0.002	0.002	<0.001
210	16.84	0.106	0.264	0.029	0.111	0.022	0.003	0.014	0.001	0.014	0.002	0.007	0.001	0.001	<0.001
211	16.88	0.156	0.334	0.037	0.149	0.022	0.005	0.020	0.004	0.018	0.003	0.008	0.002	0.001	0.001
212	16.91	0.632	1.079	0.155	0.550	0.102	0.019	0.063	0.007	0.044	0.006	0.021	0.002	0.005	0.002
213	16.95	0.585	37.910	0.099	0.392	0.100	0.011	0.093	0.010	0.055	0.009	0.031	0.004	0.006	0.001
214	16.99	0.737	12.453	0.168	0.670	0.138	0.026	0.108	0.014	0.090	0.016	0.043	0.007	0.008	0.003
215	17.04	0.302	0.825	0.067	0.239	0.043	0.007	0.045	0.006	0.040	0.008	0.019	0.003	0.005	0.001
216	17.08	0.429	0.945	0.093	0.342	0.061	0.013	0.047	0.006	0.042	0.006	0.019	0.002	0.004	0.003
217	17.13	0.262	0.653	0.059	0.231	0.033	0.009	0.032	0.005	0.039	0.006	0.015	0.002	0.003	0.001
218	17.17	0.451	0.969	0.093	0.355	0.064	0.011	0.061	0.008	0.053	0.008	0.026	0.002	0.005	0.001
219	17.21	0.511	1.128	0.115	0.429	0.090	0.015	0.064	0.009	0.061	0.010	0.029	0.004	0.006	0.002
220	17.25	4.069	8.966	1.063	4.357	0.855	0.123	0.754	0.075	0.419	0.073	0.165	0.016	0.028	0.014
221	17.30	0.108	0.409	0.028	0.099	0.020	0.005	0.014	0.003	0.019	0.003	0.008	0.001	0.002	<0.001
222	17.34	0.485	1.168	0.110	0.444	0.076	0.012	0.063	0.009	0.050	0.012	0.028	0.003	0.006	0.002

223	17.37	0.230	0.509	0.052	0.198	0.032	0.008	0.030	0.003	0.024	0.004	0.013	0.001	0.002	0.001
224	17.41	0.245	0.527	0.061	0.215	0.034	0.007	0.024	0.003	0.027	0.003	0.015	0.001	0.003	0.005
225	17.45	0.161	0.328	0.034	0.132	0.027	0.004	0.014	0.003	0.019	0.003	0.009	0.002	0.001	0.001
226	17.50	0.171	0.326	0.035	0.134	0.028	0.004	0.019	0.003	0.018	0.003	0.008	0.001	0.002	0.002
227	17.54	0.162	0.309	0.033	0.129	0.031	0.005	0.022	0.003	0.022	0.003	0.009	0.001	0.002	<0.001
228	17.58	0.096	0.238	0.022	0.086	0.012	0.001	0.004	<0.001	0.007	0.001	0.004	0.001	<0.001	0.001
229	17.62	0.127	0.184	0.018	0.069	0.010	0.003	0.009	0.001	0.005	0.001	0.003	<0.001	0.001	<0.001
230	17.66	0.079	0.131	0.018	0.076	0.015	0.002	0.007	0.001	0.012	0.002	0.006	0.001	0.001	<0.001
231	17.70	0.293	0.586	0.062	0.238	0.047	0.007	0.030	0.004	0.028	0.005	0.011	0.002	0.003	0.004
232	17.74	0.203	0.443	0.043	0.183	0.034	0.005	0.014	0.002	0.022	0.004	0.015	0.001	0.003	0.001
233	17.77	0.202	0.438	0.044	0.157	0.030	0.006	0.023	0.003	0.016	0.003	0.006	0.001	0.002	0.001
234	17.81	0.425	1.004	0.106	0.367	0.068	0.009	0.047	0.005	0.028	0.004	0.013	0.002	0.003	<0.001
235	17.85	0.243	0.545	0.054	0.211	0.037	0.007	0.034	0.005	0.024	0.004	0.015	0.002	0.003	0.001
236	17.89	0.087	0.214	0.022	0.075	0.011	0.002	0.006	0.001	0.010	0.002	0.005	<0.001	0.001	0.001
237	17.93	0.090	7.214	0.022	0.085	0.029	0.002	0.022	0.001	0.015	0.002	0.007	0.001	0.002	<0.001
238	17.97	0.165	14.557	0.030	0.119	0.036	0.005	0.033	0.003	0.016	0.004	0.008	0.002	0.002	0.001
239	18.02	0.161	1.949	0.040	0.155	0.025	0.004	0.015	0.002	0.016	0.003	0.007	0.001	0.001	<0.001
240	18.06	0.202	0.868	0.047	0.185	0.031	0.005	0.030	0.002	0.022	0.005	0.011	<0.001	0.002	0.001
241	18.10	0.100	0.290	0.021	0.086	0.020	0.003	0.010	0.002	0.016	0.002	0.008	0.001	0.002	<0.001
242	18.15	0.546	2.381	0.136	0.521	0.114	0.018	0.093	0.013	0.088	0.016	0.045	0.008	0.013	0.003
243	18.19	0.252	0.652	0.045	0.159	0.032	0.005	0.021	0.004	0.021	0.004	0.008	0.001	0.002	0.001
244	18.23	0.250	0.841	0.058	0.232	0.047	0.009	0.035	0.003	0.032	0.005	0.020	0.001	0.004	0.002
245	18.27	0.561	1.282	0.133	0.475	0.085	0.016	0.075	0.010	0.061	0.011	0.030	0.004	0.008	0.002
246	18.32	0.240	0.484	0.055	0.218	0.035	0.007	0.028	0.003	0.025	0.004	0.012	0.002	0.003	0.001
247	18.35	0.044	0.012	0.012	0.053	0.006	0.002	0.005	0.002	0.005	0.002	<0.001	<0.001	<0.001	<0.001
248	18.37	0.170	0.410	0.038	0.153	0.034	0.005	0.022	0.002	0.025	0.004	0.012	0.001	0.003	<0.001
249	18.45	0.036	0.051	0.011	0.030	0.007	0.002	0.003	<0.001	0.003	<0.001	0.001	<0.001	<0.001	0.001
250	18.49	0.016	0.011	0.004	0.016	0.004	0.001	0.001	<0.001	0.004	<0.001	0.001	<0.001	<0.001	<0.001
251	18.53	0.016	0.010	0.004	0.016	0.004	0.001	<0.001	<0.001	0.002	<0.001	<0.001	<0.001	<0.001	<0.001
252	18.57	0.025	0.071	0.003	0.017	0.002	<0.001	-0.003	<0.001	0.003	0.001	0.002	<0.001	<0.001	0.001
253	18.61	0.070	0.113	0.016	0.067	0.011	0.003	0.011	0.001	0.008	0.002	0.006	<0.001	0.002	<0.001
254	18.65	0.067	0.178	0.016	0.069	0.007	0.004	0.009	<0.001	0.013	0.001	0.006	0.001	0.001	0.001
255	18.69	0.110	0.294	0.026	0.093	0.020	0.007	0.022	0.003	0.020	0.003	0.008	0.002	0.001	0.001
256	18.73	0.491	1.315	0.119	0.500	0.099	0.020	0.072	0.009	0.057	0.011	0.031	0.003	0.006	0.003
257	18.77	0.296	0.991	0.065	0.245	0.047	0.009	0.047	0.005	0.029	0.006	0.017	0.002	0.004	0.001
258	18.80	0.171	0.496	0.038	0.150	0.021	0.005	0.022	0.003	0.022	0.003	0.012	0.002	0.003	0.001
259	18.84	0.298	0.650	0.068	0.255	0.046	0.010	0.036	0.005	0.026	0.004	0.017	0.002	0.004	0.001
260	18.89	0.218	0.536	0.044	0.178	0.024	0.006	0.026	0.003	0.016	0.005	0.010	<0.001	0.002	0.003
261	18.93	0.156	7.850	0.039	0.171	0.043	0.005	0.031	0.003	0.023	0.003	0.010	0.003	0.002	0.001
262	18.97	0.138	11.830	0.033	0.118	0.024	0.005	0.023	0.001	0.014	0.001	0.007	0.001	0.001	0.001
263	19.03	0.090	1.843	0.020	0.090	0.012	0.003	0.018	0.001	0.010	0.001	0.007	0.001	0.001	0.001
264	19.07	0.255	1.006	0.061	0.237	0.046	0.008	0.027	0.004	0.030	0.006	0.018	0.002	0.006	0.002
265	19.11	0.330	1.381	0.087	0.370	0.068	0.015	0.056	0.009	0.048	0.008	0.021	0.004	0.005	0.003
266	19.15	0.275	0.875	0.065	0.275	0.050	0.010	0.031	0.004	0.034	0.007	0.015	0.003	0.004	0.001
267	19.20	0.272	0.622	0.061	0.226	0.044	0.009	0.032	0.003	0.023	0.004	0.012	0.002	0.003	0.001
268	19.24	0.226	0.534	0.046	0.184	0.039	0.007	0.025	0.002	0.029	0.005	0.014	0.001	0.002	0.002
269	19.28	0.156	0.394	0.036	0.135	0.023	0.010	0.016	0.002	0.018	0.004	0.009	0.001	0.002	0.003
270	19.32	0.123	0.300	0.027	0.111	0.019	0.003	0.014	0.002	0.011	0.001	0.006	0.001	0.001	0.001
271	19.36	0.225	0.531	0.050	0.201	0.041	0.008	0.023	0.004	0.024	0.004	0.011	0.002	0.002	0.002
272	19.41	1.070	2.546	0.275	1.095	0.234	0.047	0.172	0.022	0.152	0.028	0.076	0.010	0.019	0.010
273	19.45	0.460	1.255	0.120	0.477	0.100	0.021	0.083	0.012	0.075	0.015	0.046	0.005	0.010	0.005
274	19.49	1.670	2.551	0.355	1.353	0.179	0.024	0.101	0.012	0.049	0.007	0.019	0.002	0.003	0.002
275	19.53	0.657	1.505	0.156	0.613	0.105	0.022	0.080	0.012	0.071	0.012	0.042	0.004	0.008	0.004
276	19.57	0.809	1.827	0.194	0.764	0.159	0.027	0.101	0.014	0.090	0.017	0.042	0.007	0.013	0.006
277	19.61	0.282	0.695	0.072	0.282	0.050	0.011	0.047	0.006	0.051	0.007	0.017	0.002	0.006	0.002
278	19.65	0.379	0.942	0.076	0.308	0.066	0.010	0.043	0.008	0.039	0.007	0.022	0.002	0.003	0.003
279	19.69	0.310	0.822	0.078	0.271	0.054	0.011	0.056	0.007	0.041	0.007	0.021	0.002	0.005	0.003
280	19.73	0.166	0.368	0.038	0.128	0.025	0.004	0.025	0.001	0.014	0.003	0.010	<0.001	0.002	0.001
281	19.77	0.059	0.165	0.018	0.060	0.014	0.004	0.006	0.001	0.008	<0.001	0.003	<0.001	<0.001	<0.001
282	19.80	0.035	0.092	0.009	0.028	0.007	0.002	-0.001	<0.001	0.006	<0.001	0.001	<0.001	<0.001	<0.001
283	19.84	0.058	0.141	0.013	0.062	0.006	0.002	0.007	<0.001	0.005	0.001	0.002	<0.001	0.001	<0.001
284	19.88	0.079	0.186	0.023	0.108	0.023	0.008	0.035	0.005	0.036	0.009	0.024	0.002	0.005	0.003
285	19.91	0.121	0.216	0.025	0.103	0.049	0.003	0.004	0.001	0.017	0.001	0.006	0.001	0.001	0.001
286	19.95	0.681	1.339	0.162	0.605	0.123	0.025	0.087	0.014	0.081	0.014	0.041	0.004	0.010	0.005
287	19.99	0.255	0.855	0.060	0.241	0.048	0.011	0.029	0.005	0.034	0.006	0.017	0.003	0.004	0.003
288	20.05	0.372	1.039	0.081	0.335	0.073	0.011	0.041	0.005	0.045	0.010	0.023	0.003	0.007	0.002
289	20.09	0.611	1.329	0.135	0.534	0.094	0.017	0.073	0.011	0.071	0.012	0.040	0.004	0.008	0.005
290	20.13	0.444	1.041	0.114	0.471	0.097	0.016	0.074	0.011	0.086	0.014	0.048	0.008	0.012	0.007
291	20.17	0.363	0.898	0.109	0.478	0.098	0.025	0.088	0.015	0.104	0.018	0.060	0.008	0.017	0.009
292	20.21	0.251	0.494	0.060	0.242	0.049	0.009	0.032	0.004	0.030	0.006	0.018	0.002	0.006	0.001
293	20.26	0.119	0.262	0.028	0.123	0.022	0.005	0.010	0.001	0.015	0.002	0.007	<0.001	0.002	0.001
294	20.30	0.118	0.285	0.030	0.110	0.024	0.004	0.025	0.002	0.022	0.003	0.011	0.001	0.002	0.001
295	20.34	0.466	1.236	0.124	0.552	0.099	0.025	0.087	0.014	0.079	0.014	0.042	0.006	0.010	0.005
296	20.39	0.347	0.970	0.078	0.332	0.068	0.012	0.054	0.006	0.038	0.008	0.023	0.002	0.004	0.002
297	20.43	0.353	0.852	0.085	0.383	0.086	0.014	0.050	0.008	0.042	0.006	0.020	0.002	0.004	0.002
298	20.47	0.183	0.392	0.043	0.182	0.039	0.006	0.030	0.004	0.031	0.006	0.019	0.003	0.003	0.002
299	20.51	0.239	0.524	0.057	0.236	0.047	0.007	0.033	0.005	0.038	0.006	0.017	0.001	0.003	0.001

300	20.55	0.417	0.880	0.088	0.363	0.069	0.011	0.036	0.005	0.038	0.007	0.018	0.001	0.004	0.002
301	20.59	0.134	0.290	0.029	0.132	0.019	0.003	0.013	0.001	0.016	0.002	0.007	<0.001	0.002	0.001
302	20.63	0.490	0.996	0.107	0.440	0.080	0.014	0.057	0.008	0.051	0.008	0.019	0.002	0.004	0.002
303	20.67	0.380	0.901	0.077	0.300	0.049	0.011	0.032	0.005	0.034	0.007	0.017	0.003	0.004	0.002
304	20.71	0.459	0.951	0.090	0.329	0.066	0.010	0.043	0.004	0.039	0.006	0.021	0.003	0.006	0.002
305	20.75	0.338	0.764	0.072	0.285	0.047	0.010	0.035	0.004	0.035	0.006	0.018	0.001	0.005	0.002
306	20.78	0.403	0.905	0.085	0.339	0.074	0.011	0.057	0.006	0.049	0.007	0.026	0.001	0.005	0.002
307	20.82	0.330	0.748	0.076	0.288	0.055	0.012	0.035	0.006	0.036	0.006	0.024	0.003	0.003	0.002
308	20.86	0.403	0.809	0.087	0.321	0.052	0.011	0.038	0.004	0.040	0.007	0.018	0.002	0.003	0.002
309	20.90	0.325	0.726	0.073	0.290	0.057	0.010	0.044	0.007	0.040	0.008	0.022	0.001	0.003	0.002
310	20.95	0.713	16.298	0.160	0.590	0.110	0.016	0.079	0.013	0.068	0.012	0.035	0.004	0.006	0.003
311	20.99	0.604	3.552	0.137	0.522	0.101	0.019	0.068	0.012	0.063	0.011	0.034	0.004	0.006	0.004
312	21.04	0.969	2.649	0.213	0.856	0.159	0.025	0.111	0.013	0.097	0.017	0.054	0.006	0.010	0.006
313	21.08	0.272	0.798	0.069	0.277	0.050	0.008	0.040	0.004	0.030	0.005	0.017	0.001	0.004	0.002
314	21.12	0.223	0.716	0.052	0.192	0.032	0.008	0.020	0.003	0.022	0.005	0.011	0.001	0.002	0.001
315	21.15	0.223	0.484	0.049	0.193	0.036	0.007	0.024	0.003	0.020	0.004	0.009	0.001	0.003	0.001
316	21.20	0.118	0.308	0.024	0.120	0.022	0.005	0.013	0.002	0.013	0.004	0.008	<0.001	0.002	<0.001
317	21.24	0.050	0.149	0.013	0.063	0.009	0.002	0.007	-0.001	0.005	<0.001	0.003	<0.001	0.001	0.001
318	21.28	0.052	0.152	0.013	0.057	0.006	0.003	<0.001	<0.001	0.007	0.001	0.003	<0.001	0.001	<0.001
319	21.32	0.091	0.280	0.027	0.104	0.016	0.002	0.008	0.001	0.011	0.001	0.005	<0.001	0.001	0.001
320	21.36	0.107	0.283	0.024	0.101	0.018	0.004	0.008	0.001	0.010	0.003	0.004	<0.001	0.001	<0.001
321	21.40	0.127	0.348	0.027	0.130	0.021	0.005	0.015	0.002	0.017	0.003	0.008	<0.001	0.002	0.001
322	21.44	0.237	0.567	0.050	0.214	0.045	0.006	0.021	0.003	0.026	0.004	0.015	0.002	0.003	0.001
323	21.48	0.455	1.180	0.111	0.469	0.097	0.019	0.066	0.011	0.070	0.009	0.032	0.004	0.006	0.003
324	21.52	0.607	1.338	0.140	0.517	0.107	0.016	0.075	0.009	0.076	0.017	0.038	0.005	0.010	0.005
325	21.56	0.376	0.720	0.078	0.347	0.066	0.013	0.051	0.007	0.051	0.009	0.026	0.004	0.008	0.003
326	21.61	0.628	1.514	0.143	0.565	0.105	0.016	0.092	0.012	0.067	0.012	0.029	0.003	0.007	0.004
327	21.64	0.774	1.874	0.189	0.719	0.137	0.025	0.096	0.012	0.084	0.014	0.038	0.004	0.008	0.004
328	21.68	0.491	1.244	0.111	0.437	0.097	0.017	0.081	0.007	0.048	0.012	0.032	0.005	0.006	0.004
329	21.72	0.418	0.979	0.098	0.389	0.077	0.015	0.052	0.006	0.049	0.009	0.023	0.003	0.006	0.002
330	21.76	0.281	0.681	0.065	0.265	0.049	0.009	0.027	0.005	0.041	0.006	0.023	0.002	0.005	0.003
331	21.80	0.289	0.790	0.064	0.264	0.055	0.013	0.046	0.005	0.039	0.006	0.021	0.002	0.004	0.002
332	21.84	0.205	0.649	0.052	0.205	0.039	0.007	0.041	0.002	0.020	0.004	0.017	0.002	0.004	0.002
333	21.88	0.170	0.549	0.040	0.164	0.028	0.007	0.025	0.004	0.026	0.004	0.009	0.001	0.002	0.002
334	21.92	0.161	6.022	0.034	0.128	0.031	0.005	0.016	0.002	0.018	0.003	0.011	0.001	0.002	0.001
335	21.96	0.183	10.180	0.039	0.166	0.030	0.005	0.031	0.003	0.028	0.003	0.014	0.001	0.003	0.001
336	22.02	0.262	1.703	0.062	0.234	0.047	0.011	0.033	0.003	0.021	0.004	0.011	0.001	0.002	0.013
337	22.06	0.446	1.316	0.104	0.418	0.086	0.015	0.050	0.010	0.062	0.011	0.035	0.003	0.007	0.004
338	22.10	1.599	3.830	0.332	1.264	0.226	0.044	0.165	0.024	0.149	0.027	0.081	0.011	0.018	0.010
339	22.14	0.554	1.734	0.126	0.526	0.106	0.018	0.076	0.009	0.072	0.012	0.040	0.003	0.008	0.005
340	22.17	0.817	1.893	0.172	0.630	0.123	0.017	0.100	0.011	0.079	0.018	0.049	0.005	0.009	0.005
341	22.22	0.077	0.223	0.015	0.066	0.009	0.002	0.005	<0.001	0.010	0.002	0.004	<0.001	0.001	<0.001
342	22.25	0.076	0.214	0.020	0.093	0.016	0.002	0.004	<0.001	0.008	0.001	0.003	<0.001	0.001	<0.001
343	22.30	0.084	0.229	0.022	0.076	0.013	0.003	0.006	0.002	0.012	0.002	0.006	<0.001	0.001	<0.001
344	22.33	0.091	0.472	0.021	0.078	0.023	0.002	0.015	<0.001	0.009	0.001	0.007	0.001	0.001	0.001
345	22.37	0.067	0.210	0.014	0.059	0.008	0.003	0.003	0.001	0.008	0.001	0.005	<0.001	0.002	<0.001
346	22.40	0.115	0.348	0.027	0.110	0.016	0.004	0.008	0.002	0.013	0.001	0.008	<0.001	0.001	0.001
347	22.44	0.231	0.658	0.050	0.204	0.039	0.009	0.030	0.005	0.030	0.006	0.016	0.002	0.005	0.002
348	22.49	0.370	0.856	0.080	0.311	0.067	0.009	0.041	0.005	0.032	0.008	0.015	0.002	0.004	0.006
349	22.53	0.228	0.493	0.045	0.186	0.027	0.003	0.021	0.002	0.019	0.003	0.009	0.001	0.002	0.001
350	22.56	0.140	0.315	0.029	0.119	0.013	0.004	0.015	0.002	0.011	0.003	0.007	<0.001	0.001	0.001
351	22.60	0.257	0.672	0.057	0.252	0.051	0.009	0.026	0.007	0.030	0.006	0.017	0.001	0.003	0.002
352	22.64	0.533	1.291	0.128	0.506	0.097	0.018	0.085	0.008	0.058	0.014	0.037	0.006	0.007	0.004
353	22.68	0.520	1.298	0.121	0.474	0.079	0.017	0.055	0.008	0.057	0.010	0.035	0.003	0.007	0.004
354	22.71	0.147	0.388	0.040	0.162	0.035	0.007	0.025	0.003	0.021	0.003	0.011	0.002	0.002	0.001
355	22.75	0.168	0.370	0.040	0.160	0.026	0.007	0.014	0.002	0.017	0.004	0.009	0.001	0.003	0.001
356	22.78	0.212	0.502	0.054	0.221	0.044	0.009	0.034	0.004	0.030	0.006	0.018	0.002	0.004	0.003
357	22.82	0.490	1.028	0.108	0.408	0.081	0.018	0.048	0.008	0.062	0.009	0.028	0.002	0.007	0.003
358	22.85	0.159	0.338	0.035	0.131	0.033	0.004	0.019	0.002	0.022	0.003	0.009	0.001	0.003	0.001
359	22.89	0.090	0.183	0.024	0.100	0.014	0.003	0.008	<0.001	0.009	0.002	0.005	<0.001	0.001	0.001
360	22.94	0.125	14.372	0.031	0.105	0.034	0.004	0.023	0.001	0.012	0.002	0.007	<0.001	0.002	0.001
361	22.99	0.577	2.904	0.119	0.460	0.075	0.012	0.038	0.004	0.024	0.004	0.012	0.001	0.002	0.002
362	23.04	0.135	0.411	0.028	0.116	0.019	0.004	0.016	0.002	0.021	0.003	0.008	<0.001	0.003	0.001
363	23.08	0.174	0.519	0.046	0.197	0.025	0.007	0.025	0.003	0.022	0.004	0.014	<0.001	0.003	0.002
364	23.12	0.116	0.327	0.027	0.104	0.022	0.003	0.014	0.001	0.011	0.002	0.007	0.001	0.002	0.001
365	23.16	0.132	0.303	0.031	0.105	0.016	0.004	0.009	0.001	0.017	0.002	0.007	0.001	0.001	0.001
366	23.21	0.178	0.364	0.034	0.125	0.030	0.003	0.009	0.001	0.008	0.002	0.006	<0.001	0.001	0.001
367	23.25	0.259	0.557	0.058	0.203	0.029	0.009	0.025	0.004	0.022	0.005	0.013	0.001	0.003	0.001
368	23.29	0.402	0.819	0.082	0.295	0.060	0.014	0.037	0.005	0.031	0.006	0.022	0.002	0.006	0.003
369	23.34	0.141	0.454	0.034	0.141	0.022	0.006	0.013	0.002	0.017	0.003	0.007	0.002	0.001	0.002
370	23.38	0.638	1.428	0.143	0.549	0.091	0.022	0.067	0.010	0.059	0.013	0.034	0.005	0.007	0.005
371	23.41	0.410	0.950	0.101	0.379	0.083	0.014	0.055	0.009	0.052	0.009	0.029	0.003	0.007	0.003
372	23.44	0.419	0.957	0.095	0.374	0.069	0.014	0.058	0.007	0.040	0.008	0.025	0.003	0.004	0.003
373	23.48	0.944	2.092	0.222	0.907	0.155	0.029	0.093	0.011	0.064	0.009	0.029	0.003	0.005	0.002
374	23.52	0.317	0.809	0.083	0.310	0.056	0.016	0.049	0.007	0.045	0.007	0.023	0.003	0.004	0.004
375	23.56	0.315	0.603	0.071	0.284	0.047	0.011	0.039	0.006	0.041	0.008	0.023	0.003	0.006	0.003
376	23.60	0.590	0.986	0.096	0.336	0.045	0.009	0.034	0.003	0.023	0.007	0.015	0.001	0.004	0.003

377	23.64	0.185	0.419	0.043	0.173	0.028	0.007	0.024	0.003	0.028	0.004	0.016	0.001	0.006	0.002
378	23.68	0.721	1.763	0.196	0.886	0.178	0.032	0.154	0.022	0.147	0.026	0.083	0.009	0.015	0.008
379	23.73	0.398	0.974	0.079	0.298	0.059	0.007	0.040	0.004	0.026	0.004	0.015	0.001	0.002	0.001
380	23.77	0.511	1.278	0.109	0.374	0.067	0.008	0.041	0.005	0.033	0.008	0.023	0.001	0.004	0.002
381	23.81	1.022	1.405	0.219	0.850	0.139	0.021	0.102	0.013	0.073	0.011	0.035	0.004	0.008	0.002
382	23.84	0.534	1.116	0.123	0.496	0.093	0.014	0.059	0.009	0.058	0.010	0.028	0.004	0.006	0.003
383	23.87	0.127	0.319	0.036	0.146	0.026	0.005	0.014	0.001	0.019	0.003	0.007	0.001	0.002	<0.001
384	23.91	0.157	0.534	0.029	0.109	0.018	0.003	0.008	0.002	0.007	0.002	0.005	<0.001	0.001	0.127
385	23.95	0.765	1.814	0.207	0.890	0.159	0.026	0.106	0.014	0.062	0.010	0.025	0.002	0.005	0.003
386	24.02	0.122	0.711	0.027	0.116	0.022	0.005	0.015	0.001	0.016	0.001	0.010	0.001	0.002	<0.001
387	24.06	0.112	0.363	0.026	0.112	0.014	0.004	0.015	0.002	0.016	0.002	0.010	0.001	0.001	0.001
388	24.10	0.257	0.529	0.054	0.207	0.040	0.006	0.028	0.003	0.022	0.006	0.014	0.002	0.004	0.003
389	24.14	0.133	0.360	0.030	0.125	0.023	0.005	0.013	0.002	0.016	0.002	0.007	0.001	0.001	0.001
390	24.18	0.658	1.461	0.156	0.653	0.104	0.015	0.067	0.012	0.052	0.008	0.019	0.002	0.004	0.002
391	24.21	0.265	0.631	0.060	0.229	0.046	0.007	0.028	0.003	0.026	0.005	0.015	0.001	0.004	0.002
392	24.25	0.117	2.699	0.026	0.109	0.023	0.003	0.015	0.002	0.012	0.004	0.009	<0.001	0.002	0.001
393	24.30	0.430	0.984	0.096	0.395	0.079	0.013	0.054	0.009	0.048	0.009	0.018	0.002	0.006	0.003
394	24.34	0.862	1.730	0.173	0.672	0.109	0.025	0.096	0.013	0.073	0.013	0.034	0.005	0.008	0.004
395	24.37	0.636	1.432	0.145	0.588	0.120	0.021	0.079	0.013	0.076	0.012	0.030	0.004	0.007	0.003
396	24.41	0.543	1.228	0.136	0.551	0.115	0.022	0.089	0.010	0.068	0.014	0.042	0.005	0.008	0.005
397	24.45	0.256	0.554	0.061	0.256	0.052	0.009	0.036	0.006	0.032	0.006	0.012	0.001	0.003	0.002
398	24.49	0.253	0.592	0.066	0.260	0.041	0.008	0.033	0.005	0.029	0.005	0.015	0.001	0.002	0.002
399	24.53	0.119	0.273	0.029	0.117	0.015	0.004	0.011	0.002	0.014	0.003	0.009	<0.001	0.002	0.001
400	24.56	0.141	0.311	0.030	0.128	0.036	0.004	0.010	0.002	0.010	0.003	0.007	<0.001	0.002	0.001
401	24.60	0.118	0.352	0.028	0.116	0.028	0.003	0.008	0.002	0.017	0.001	0.010	0.001	0.002	0.001
402	24.64	0.963	1.240	0.241	0.949	0.168	0.024	0.095	0.011	0.071	0.011	0.028	0.003	0.005	0.003
403	24.67	0.464	1.126	0.115	0.457	0.088	0.017	0.061	0.007	0.049	0.010	0.033	0.002	0.006	0.003
404	24.71	0.329	0.596	0.070	0.259	0.043	0.008	0.032	0.004	0.027	0.006	0.017	0.002	0.004	0.004
405	24.74	0.264	0.529	0.051	0.184	0.034	0.004	0.017	0.001	0.017	0.002	0.010	0.001	0.001	<0.001
406	24.78	0.053	0.167	0.012	0.043	0.020	0.002	<0.001	0.001	0.006	0.001	0.003	0.001	0.001	<0.001
407	24.81	0.114	0.249	0.024	0.115	0.020	0.006	0.014	0.003	0.020	0.001	0.009	0.001	0.002	0.001
408	24.85	0.091	0.216	0.023	0.105	0.016	0.003	0.015	0.001	0.011	0.001	0.006	<0.001	0.001	0.001
409	24.88	0.096	0.267	0.025	0.096	0.027	0.003	0.010	0.001	0.020	0.002	0.008	0.002	0.002	0.001
410	24.92	0.168	0.496	0.041	0.164	0.036	0.008	0.022	0.003	0.018	0.004	0.012	0.001	0.003	0.002
411	24.97	0.356	2.494	0.094	0.386	0.093	0.015	0.054	0.006	0.049	0.007	0.022	0.003	0.005	0.003
412	25.03	0.393	1.291	0.092	0.363	0.071	0.013	0.061	0.006	0.041	0.009	0.023	0.003	0.006	0.003
413	25.07	0.321	0.802	0.078	0.318	0.077	0.011	0.047	0.007	0.035	0.007	0.019	0.002	0.004	0.001
414	25.11	0.586	1.746	0.153	0.689	0.140	0.025	0.097	0.012	0.095	0.016	0.043	0.005	0.008	0.004
415	25.16	0.098	0.256	0.020	0.085	0.016	0.003	0.014	0.002	0.012	0.002	0.006	<0.001	0.002	<0.001
416	25.20	0.132	0.317	0.030	0.108	0.023	0.004	0.016	0.002	0.014	0.003	0.012	0.001	0.002	0.002
417	25.23	0.180	0.364	0.044	0.174	0.030	0.006	0.030	0.003	0.024	0.004	0.013	0.001	0.003	0.002
418	25.27	0.090	0.183	0.017	0.084	0.011	0.003	0.011	0.002	0.011	0.002	0.006	0.001	0.001	<0.001
419	25.31	0.030	0.078	0.007	0.021	0.009	0.002	0.001	<0.001	0.003	<0.001	0.002	0.001	0.001	<0.001
420	25.35	0.078	0.160	0.019	0.079	0.018	0.004	0.007	0.001	0.009	0.001	0.006	<0.001	0.001	0.001
421	25.39	0.140	0.339	0.037	0.152	0.030	0.005	0.018	0.003	0.019	0.002	0.008	0.001	0.003	0.002
422	25.43	0.471	1.072	0.106	0.450	0.067	0.011	0.049	0.005	0.041	0.009	0.016	0.002	0.002	0.002
423	25.48	0.193	0.409	0.036	0.121	0.027	0.003	0.013	0.002	0.020	0.003	0.007	0.002	0.002	0.002
424	25.52	0.491	1.368	0.103	0.403	0.071	0.015	0.055	0.006	0.050	0.009	0.025	0.003	0.004	0.004
425	25.55	0.131	0.355	0.030	0.132	0.019	0.005	0.015	0.001	0.014	0.002	0.007	<0.001	0.002	0.001
426	25.58	0.340	0.753	0.074	0.273	0.057	0.009	0.034	0.003	0.028	0.005	0.013	0.002	0.004	0.002
427	25.62	0.330	0.867	0.076	0.300	0.056	0.009	0.045	0.006	0.032	0.005	0.017	0.002	0.005	0.002
428	25.66	0.284	4.758	0.058	0.258	0.046	0.010	0.036	0.003	0.028	0.006	0.011	0.001	0.003	0.002
429	25.70	0.795	1.796	0.187	0.800	0.158	0.023	0.116	0.018	0.094	0.018	0.041	0.007	0.010	0.005
430	25.74	0.226	0.486	0.056	0.217	0.045	0.008	0.030	0.003	0.021	0.004	0.013	0.001	0.002	0.089
431	25.77	0.399	0.956	0.098	0.432	0.095	0.012	0.060	0.009	0.049	0.008	0.020	0.003	0.004	0.003
432	25.80	0.143	0.281	0.033	0.128	0.020	0.003	0.014	0.001	0.009	0.002	0.008	0.001	0.002	0.001
433	25.83	0.047	0.118	0.010	0.047	0.007	0.002	0.005	0.001	0.006	0.001	0.002	0.001	<0.001	<0.001
434	25.87	0.196	0.441	0.044	0.160	0.025	0.007	0.019	0.002	0.022	0.002	0.012	0.002	0.003	0.001
435	25.91	0.190	0.476	0.042	0.174	0.031	0.009	0.023	0.004	0.030	0.005	0.014	0.001	0.003	0.001
436	25.95	0.504	1.835	0.114	0.403	0.068	0.014	0.058	0.006	0.051	0.010	0.023	0.002	0.007	0.004
437	26.00	0.619	25.324	0.146	0.637	0.132	0.021	0.111	0.013	0.061	0.012	0.032	0.003	0.006	0.003
438	26.05	0.252	0.820	0.062	0.263	0.062	0.011	0.037	0.005	0.034	0.006	0.015	0.003	0.003	0.001
439	26.08	0.182	0.816	0.042	0.178	0.031	0.008	0.025	0.003	0.029	0.005	0.012	0.001	0.003	0.001
440	26.12	0.077	0.379	0.017	0.070	0.022	0.003	0.007	0.001	0.007	0.003	0.007	<0.001	0.002	0.001
441	26.16	0.266	0.816	0.056	0.239	0.047	0.008	0.035	0.006	0.030	0.005	0.017	0.002	0.005	0.002
442	26.21	0.331	1.605	0.074	0.296	0.064	0.009	0.046	0.006	0.044	0.006	0.020	0.003	0.004	0.002
443	26.26	0.420	1.628	0.101	0.408	0.083	0.011	0.054	0.008	0.039	0.008	0.024	0.002	0.005	0.002
444	26.30	0.292	0.953	0.068	0.272	0.053	0.010	0.049	0.004	0.035	0.006	0.018	0.002	0.004	0.002
445	26.32	0.268	0.755	0.059	0.249	0.041	0.010	0.029	0.003	0.025	0.004	0.013	0.001	0.003	0.002
446	26.36	0.100	0.394	0.023	0.107	0.022	0.005	0.013	0.002	0.014	0.002	0.006	<0.001	0.001	0.001
447	26.39	0.090	0.354	0.024	0.099	0.021	0.005	0.011	0.002	0.010	0.001	0.008	0.002	0.002	<0.001
448	26.43	0.203	0.551	0.043	0.175	0.032	0.006	0.031	0.002	0.018	0.003	0.010	0.001	0.002	0.002
449	26.47	0.306	0.897	0.066	0.264	0.045	0.009	0.037	0.006	0.034	0.005	0.019	0.001	0.004	0.002
450	26.51	0.502	1.235	0.098	0.416	0.077	0.011	0.055	0.007	0.037	0.007	0.018	0.002	0.004	0.002
451	26.55	0.118	0.500	0.024	0.106	0.011	0.003	0.019	0.002	0.013	0.003	0.010	0.001	0.001	<0.001
452	26.58	0.446	1.161	0.102	0.405	0.072	0.013	0.060	0.006	0.062	0.013	0.033	0.004	0.008	0.004
453	26.62	0.557	1.173	0.107	0.456	0.076	0.013	0.074	0.008	0.045	0.009	0.025	0.003	0.005	0.003

454	26.65	0.419	0.796	0.094	0.362	0.060	0.007	0.039	0.005	0.026	0.006	0.013	0.002	0.004	0.002
455	26.69	0.202	0.542	0.043	0.166	0.026	0.005	0.021	0.003	0.026	0.004	0.013	0.001	0.003	0.001
456	26.73	1.285	4.190	0.331	1.363	0.258	0.043	0.199	0.017	0.102	0.022	0.056	0.006	0.013	0.006
457	26.77	0.280	1.004	0.060	0.278	0.053	0.010	0.041	0.007	0.034	0.007	0.015	0.002	0.003	0.003
458	26.81	0.309	0.836	0.071	0.288	0.050	0.011	0.037	0.005	0.031	0.006	0.012	0.002	0.004	0.001
459	26.84	0.456	1.099	0.110	0.432	0.061	0.012	0.054	0.009	0.047	0.007	0.023	0.002	0.004	0.002
460	26.88	0.179	0.465	0.041	0.152	0.028	0.006	0.019	0.002	0.014	0.004	0.015	0.001	0.003	0.001
461	26.91	0.212	0.500	0.047	0.185	0.026	0.005	0.027	0.004	0.019	0.003	0.011	0.001	0.002	<0.001
462	26.95	0.440	7.767	0.087	0.363	0.085	0.011	0.054	0.007	0.032	0.006	0.016	0.002	0.004	0.002
463	26.99	0.086	4.662	0.018	0.064	0.063	0.002	0.010	0.001	0.009	0.002	0.008	<0.001	0.003	0.001
464	27.04	0.279	1.353	0.057	0.225	0.050	0.008	0.024	0.003	0.020	0.004	0.013	0.001	0.003	0.001
465	27.08	0.174	0.578	0.038	0.152	0.027	0.005	0.030	0.002	0.026	0.004	0.011	<0.001	0.003	0.002
466	27.13	0.241	0.732	0.052	0.222	0.041	0.009	0.037	0.003	0.022	0.004	0.013	0.001	0.004	0.001
467	27.17	0.187	0.569	0.043	0.175	0.044	0.007	0.027	0.004	0.026	0.005	0.016	0.001	0.002	0.001
468	27.21	0.284	0.710	0.059	0.262	0.048	0.007	0.031	0.003	0.031	0.006	0.017	0.001	0.004	0.002
469	27.25	0.243	0.645	0.063	0.244	0.039	0.009	0.027	0.002	0.027	0.004	0.011	0.001	0.003	0.001
470	27.28	0.139	0.398	0.030	0.120	0.021	0.006	0.025	0.002	0.012	0.002	0.006	0.001	0.002	<0.001
471	27.31	0.157	0.886	0.036	0.133	0.029	0.005	0.014	0.003	0.017	0.002	0.010	0.001	0.002	<0.001
472	27.35	0.265	0.564	0.056	0.209	0.045	0.007	0.028	0.003	0.021	0.006	0.014	0.002	0.003	0.002
473	27.39	0.126	0.484	0.029	0.135	0.023	0.003	0.016	0.003	0.015	0.002	0.005	0.001	<0.001	0.005
474	27.43	0.251	0.760	0.063	0.229	0.046	0.006	0.020	0.003	0.024	0.003	0.010	0.001	0.002	0.002
475	27.47	0.446	1.063	0.099	0.352	0.076	0.014	0.053	0.007	0.043	0.009	0.022	0.003	0.005	0.002
476	27.50	0.592	1.311	0.125	0.434	0.069	0.015	0.054	0.005	0.039	0.010	0.025	0.003	0.007	0.004
477	27.54	0.325	0.874	0.084	0.353	0.068	0.012	0.054	0.010	0.043	0.010	0.024	0.004	0.006	0.004
478	27.57	0.283	0.738	0.073	0.324	0.066	0.014	0.047	0.007	0.045	0.006	0.020	0.002	0.003	0.002
479	27.61	0.136	0.474	0.036	0.135	0.029	0.005	0.014	0.002	0.015	0.002	0.007	0.001	0.002	0.001
480	27.65	0.130	0.355	0.034	0.118	0.022	0.004	0.018	0.003	0.015	0.004	0.011	0.001	0.002	0.001
481	27.68	0.431	1.076	0.120	0.515	0.114	0.017	0.062	0.007	0.042	0.005	0.016	0.002	0.003	0.001
482	27.71	0.388	0.943	0.087	0.342	0.063	0.009	0.048	0.007	0.041	0.006	0.027	0.003	0.004	0.003
483	27.74	0.351	0.816	0.077	0.313	0.067	0.010	0.047	0.007	0.041	0.006	0.015	0.004	0.004	0.001
484	27.77	0.145	0.315	0.028	0.127	0.028	0.005	0.012	0.001	0.013	0.002	0.008	0.001	0.001	0.001
485	27.80	0.172	0.373	0.037	0.128	0.019	0.007	0.019	0.003	0.016	0.002	0.010	0.001	0.002	0.001
486	27.83	0.092	0.235	0.022	0.097	0.021	0.004	0.015	0.003	0.019	0.002	0.007	0.001	0.002	0.001
487	27.86	0.535	0.948	0.107	0.509	0.091	0.016	0.073	0.010	0.050	0.010	0.026	0.002	0.005	0.004
488	27.89	0.996	1.793	0.175	0.642	0.119	0.024	0.098	0.010	0.077	0.015	0.039	0.005	0.008	0.006
489	27.93	0.278	0.815	0.073	0.314	0.067	0.015	0.039	0.007	0.042	0.007	0.021	0.002	0.005	0.001
490	27.97	0.610	1.598	0.139	0.565	0.084	0.017	0.067	0.009	0.046	0.008	0.024	0.003	0.006	0.003
491	28.02	0.397	1.137	0.098	0.413	0.074	0.019	0.059	0.010	0.053	0.010	0.024	0.003	0.006	0.009
492	28.06	0.442	1.166	0.115	0.426	0.086	0.016	0.059	0.007	0.056	0.012	0.033	0.004	0.008	0.003
493	28.10	0.152	0.600	0.039	0.166	0.038	0.005	0.021	0.004	0.019	0.005	0.011	0.001	0.002	0.001
494	28.14	0.097	0.318	0.021	0.083	0.014	0.003	0.013	0.001	0.013	0.003	0.009	0.001	0.001	0.001
495	28.17	0.205	0.461	0.042	0.156	0.021	0.004	0.013	0.002	0.012	0.002	0.008	0.001	0.002	0.001
496	28.21	0.207	0.474	0.045	0.158	0.027	0.004	0.016	0.003	0.016	0.004	0.013	0.001	0.002	0.002
497	28.25	0.298	0.710	0.065	0.246	0.048	0.008	0.034	0.004	0.031	0.006	0.011	0.001	0.003	0.002
498	28.29	2.196	4.335	0.460	1.809	0.383	0.056	0.241	0.036	0.232	0.039	0.110	0.013	0.027	0.012
499	28.33	0.953	1.970	0.212	0.844	0.169	0.033	0.121	0.017	0.118	0.017	0.053	0.008	0.011	0.007
500	28.37	0.348	0.813	0.079	0.292	0.049	0.013	0.038	0.004	0.034	0.006	0.021	0.002	0.004	0.002
501	28.41	0.424	1.073	0.104	0.394	0.078	0.014	0.052	0.008	0.045	0.008	0.027	0.002	0.006	0.003
502	28.45	0.112	0.259	0.026	0.086	0.022	0.004	0.016	0.002	0.012	0.002	0.008	0.001	0.001	0.001
503	28.49	0.360	0.790	0.073	0.331	0.059	0.015	0.047	0.006	0.042	0.007	0.023	0.002	0.006	0.002
504	28.53	0.969	1.941	0.205	0.786	0.130	0.030	0.109	0.011	0.080	0.018	0.056	0.006	0.013	0.008
505	28.57	0.434	1.128	0.108	0.440	0.073	0.010	0.048	0.006	0.027	0.006	0.010	0.001	0.002	0.001
506	28.60	0.116	0.301	0.027	0.119	0.013	0.006	0.009	0.001	0.015	0.002	0.008	0.002	0.002	0.001
507	28.64	0.204	0.788	0.055	0.223	0.045	0.008	0.029	0.006	0.030	0.005	0.015	0.001	0.003	0.002
508	28.68	0.740	1.697	0.211	0.856	0.164	0.033	0.134	0.013	0.108	0.025	0.062	0.006	0.015	0.006
509	28.72	0.137	0.364	0.035	0.130	0.019	0.004	0.021	0.002	0.019	0.004	0.007	<0.001	0.001	<0.001
510	28.76	2.223	5.197	0.515	1.620	0.264	0.019	0.170	0.022	0.110	0.015	0.034	0.004	0.006	0.003
511	28.80	0.359	0.803	0.076	0.284	0.062	0.009	0.054	0.006	0.033	0.005	0.018	0.002	0.004	0.002
512	28.84	0.235	0.559	0.055	0.200	0.042	0.008	0.034	0.002	0.021	0.005	0.015	0.001	0.004	0.002
513	28.88	0.450	1.006	0.107	0.390	0.070	0.011	0.047	0.006	0.046	0.007	0.021	0.003	0.005	0.003
514	28.91	0.456	0.406	0.109	0.417	0.073	0.008	0.046	0.006	0.042	0.006	0.017	0.002	0.003	0.001
515	28.95	0.233	2.358	0.059	0.228	0.065	0.012	0.054	0.008	0.055	0.009	0.022	0.003	0.004	0.002
516	29.00	0.377	1.186	0.076	0.303	0.070	0.013	0.039	0.004	0.035	0.008	0.019	0.003	0.005	0.002
517	29.04	0.242	0.637	0.043	0.176	0.031	0.002	0.015	0.002	0.014	0.002	0.004	<0.001	0.001	0.001
518	29.09	0.106	0.331	0.027	0.101	0.019	0.003	0.018	0.001	0.011	0.004	0.006	0.001	0.002	<0.001
519	29.13	0.253	0.705	0.058	0.199	0.041	0.006	0.030	0.004	0.027	0.004	0.014	0.002	0.003	0.003
520	29.17	0.321	0.899	0.095	0.402	0.092	0.027	0.069	0.005	0.052	0.012	0.029	0.003	0.005	0.003
521	29.21	0.119	0.452	0.032	0.116	0.021	0.004	0.022	0.002	0.017	0.003	0.009	0.001	0.002	0.002
522	29.24	0.173	0.441	0.042	0.156	0.030	0.005	0.022	0.003	0.020	0.003	0.013	0.002	0.002	0.001
523	29.28	0.341	0.827	0.079	0.302	0.049	0.010	0.032	0.004	0.027	0.004	0.016	0.001	0.003	0.001
524	29.32	0.317	0.589	0.061	0.230	0.031	0.006	0.026	0.003	0.020	0.006	0.010	0.002	0.003	0.002
525	29.36	0.225	0.448	0.045	0.177	0.032	0.005	0.028	0.004	0.021	0.004	0.012	0.002	0.003	0.006
526	29.42	0.360	0.822	0.088	0.340	0.063	0.010	0.043	0.006	0.037	0.005	0.012	0.003	0.003	0.001
527	29.46	0.102	0.263	0.027	0.113	0.017	0.004	0.023	0.001	0.012	0.002	0.008	<0.001	0.001	0.001
528	29.50	0.160	0.431	0.042	0.156	0.026	0.006	0.028	0.002	0.022	0.004	0.012	0.001	0.003	0.001
529	29.54	0.489	1.192	0.117	0.460	0.071	0.016	0.057	0.008	0.056	0.010	0.026	0.003	0.006	0.003
530	29.58	0.165	0.450	0.042	0.163	0.031	0.005	0.022	0.003	0.020	0.003	0.010	0.001	0.002	0.002

531	29.61	0.247	0.565	0.058	0.216	0.042	0.008	0.038	0.004	0.043	0.006	0.015	0.002	0.003	0.002
532	29.65	0.808	1.663	0.148	0.476	0.064	0.010	0.044	0.004	0.031	0.007	0.016	0.002	0.004	0.002
533	29.70	0.284	0.725	0.070	0.273	0.051	0.016	0.035	0.006	0.034	0.007	0.014	0.002	0.003	0.002
534	29.74	0.637	1.553	0.154	0.590	0.113	0.020	0.088	0.012	0.065	0.011	0.029	0.004	0.007	0.003
535	29.78	0.796	1.987	0.226	0.866	0.187	0.034	0.147	0.019	0.094	0.018	0.051	0.007	0.010	0.006
536	29.82	0.527	1.293	0.142	0.583	0.129	0.023	0.081	0.012	0.074	0.015	0.037	0.004	0.009	0.004
537	29.85	0.002	0.016	0.003	0.009	0.013	0.004	0.001	0.011	0.006	0.004	0.001	0.001	<0.001	0.001
538	29.89	0.173	0.421	0.045	0.173	0.033	0.004	0.023	0.003	0.017	0.003	0.009	0.001	0.002	<0.001
539	29.93	0.103	2.957	0.017	0.065	0.011	0.001	0.012	0.001	0.010	0.002	0.005	<0.001	0.001	<0.001
540	29.97	0.168	6.755	0.020	0.080	0.022	0.004	0.010	<0.001	0.009	0.001	0.008	0.001	0.001	0.001
541	30.03	0.229	1.246	0.052	0.220	0.041	0.009	0.043	0.004	0.039	0.006	0.013	0.001	0.003	0.002
542	30.07	0.159	0.380	0.040	0.159	0.030	0.005	0.023	0.004	0.016	0.002	0.008	<0.001	0.002	0.001
543	30.11	1.246	2.792	0.289	1.028	0.197	0.030	0.136	0.016	0.094	0.016	0.040	0.005	0.009	0.006
544	30.15	0.447	1.101	0.107	0.397	0.088	0.017	0.062	0.007	0.049	0.012	0.033	0.006	0.007	0.003
545	30.19	0.230	0.582	0.053	0.204	0.038	0.004	0.028	0.003	0.027	0.004	0.016	0.002	0.003	0.001
546	30.23	0.348	0.779	0.079	0.329	0.053	0.013	0.039	0.005	0.035	0.006	0.020	0.002	0.003	0.003
547	30.28	0.213	0.490	0.047	0.185	0.029	0.006	0.020	0.002	0.020	0.003	0.007	0.001	0.003	0.001
548	30.32	0.271	0.590	0.060	0.253	0.051	0.008	0.026	0.003	0.025	0.004	0.011	0.001	0.002	0.002
549	30.37	0.153	0.553	0.038	0.156	0.026	0.005	0.025	0.003	0.022	0.004	0.009	0.001	0.002	0.001
550	30.41	0.297	0.736	0.065	0.244	0.056	0.009	0.052	0.007	0.041	0.007	0.017	0.003	0.007	0.004
551	30.45	1.132	2.476	0.256	0.982	0.180	0.033	0.116	0.018	0.098	0.017	0.050	0.006	0.010	0.004
552	30.49	0.246	0.620	0.059	0.221	0.048	0.009	0.027	0.003	0.028	0.005	0.012	0.002	0.003	0.003
553	30.53	0.160	0.324	0.038	0.129	0.022	0.005	0.017	0.001	0.014	0.003	0.008	0.001	0.002	<0.001
554	30.57	0.066	0.200	0.019	0.071	0.014	0.001	0.008	0.001	0.010	0.001	0.005	0.001	0.001	<0.001
555	30.61	0.130	0.340	0.030	0.097	0.026	0.004	0.015	0.001	0.013	0.002	0.009	<0.001	0.001	<0.001
556	30.65	0.428	1.323	0.100	0.357	0.052	0.013	0.038	0.004	0.028	0.005	0.015	0.001	0.002	0.002
557	30.69	0.057	0.164	0.013	0.056	0.005	0.002	0.002	0.001	0.005	0.001	0.004	0.001	0.001	0.001
558	30.73	0.172	0.547	0.045	0.150	0.026	0.004	0.022	0.003	0.024	0.003	0.010	0.001	0.002	0.001
559	30.76	0.512	1.360	0.139	0.556	0.123	0.018	0.089	0.014	0.085	0.015	0.041	0.006	0.010	0.007
560	30.80	0.098	0.280	0.025	0.088	0.019	0.003	0.014	0.001	0.013	0.001	0.007	0.001	0.002	0.001
561	30.84	0.206	0.588	0.050	0.207	0.039	0.009	0.034	0.003	0.022	0.004	0.013	0.002	0.003	0.001
562	30.87	0.520	1.141	0.118	0.453	0.089	0.020	0.076	0.008	0.055	0.009	0.030	0.004	0.005	0.002
563	30.91	0.288	0.699	0.072	0.274	0.064	0.012	0.055	0.005	0.036	0.005	0.017	0.003	0.004	0.001
564	30.95	0.215	9.702	0.044	0.160	0.057	0.007	0.030	0.003	0.021	0.005	0.014	0.002	0.004	0.002
565	30.99	0.263	2.401	0.066	0.253	0.062	0.009	0.042	0.005	0.030	0.004	0.018	0.002	0.004	0.002
566	31.04	1.087	3.099	0.280	1.073	0.213	0.039	0.166	0.022	0.145	0.024	0.068	0.008	0.015	0.007
567	31.08	0.633	1.966	0.176	0.684	0.138	0.030	0.125	0.018	0.101	0.017	0.050	0.007	0.010	0.007
568	31.13	0.221	0.546	0.049	0.201	0.039	0.006	0.024	0.002	0.024	0.003	0.011	0.001	0.002	0.002
569	31.17	0.136	0.336	0.035	0.117	0.026	0.002	0.015	0.003	0.016	0.003	0.009	0.001	0.002	0.001
570	31.21	0.198	0.539	0.051	0.191	0.040	0.005	0.032	0.004	0.034	0.005	0.016	0.002	0.003	0.002
571	31.26	0.074	0.220	0.017	0.072	0.013	0.002	0.009	0.001	0.010	0.002	0.005	<0.001	0.001	0.003
572	31.30	0.069	0.161	0.015	0.045	0.010	0.002	0.012	<0.001	0.006	0.001	0.005	<0.001	0.002	0.003
573	31.34	0.016	0.119	0.004	0.018	0.007	0.001	0.001	<0.001	0.002	<0.001	0.002	<0.001	<0.001	<0.001
574	31.38	0.037	0.190	0.011	0.032	0.007	<0.001	0.003	<0.001	0.006	0.001	0.003	<0.001	0.001	<0.001
575	31.42	0.151	0.534	0.037	0.142	0.029	0.004	0.021	0.003	0.019	0.001	0.008	<0.001	0.001	<0.001
576	31.45	0.354	0.821	0.076	0.275	0.055	0.009	0.036	0.003	0.022	0.005	0.018	0.002	0.004	0.003
577	31.49	0.100	0.375	0.024	0.092	0.015	0.002	0.017	0.002	0.013	0.002	0.005	<0.001	0.001	0.001
578	31.52	0.398	0.754	0.064	0.234	0.035	0.006	0.021	0.004	0.022	0.004	0.008	<0.001	0.003	0.001
579	31.57	0.199	0.512	0.048	0.176	0.035	0.005	0.022	0.004	0.024	0.003	0.013	0.001	0.002	0.001
580	31.61	0.304	0.771	0.062	0.261	0.056	0.009	0.036	0.004	0.030	0.007	0.020	0.003	0.004	0.002
581	31.65	0.199	0.515	0.044	0.171	0.038	0.006	0.026	0.002	0.017	0.004	0.010	<0.001	0.002	0.001
582	31.68	0.118	0.239	0.023	0.094	0.018	0.002	0.009	0.001	0.012	0.001	0.004	<0.001	0.001	0.001
583	31.71	0.053	0.152	0.013	0.048	0.012	0.001	0.005	<0.001	0.008	0.001	0.005	<0.001	0.001	0.001
584	31.75	0.086	0.182	0.017	0.077	0.014	0.002	0.010	<0.001	0.009	0.002	0.009	0.001	0.002	<0.001
585	31.79	0.134	0.367	0.033	0.126	0.028	0.003	0.018	0.003	0.019	0.003	0.010	0.001	0.002	0.001
586	31.82	0.112	0.330	0.026	0.109	0.024	0.005	0.017	0.002	0.013	0.003	0.007	<0.001	0.001	0.001
587	31.86	0.409	0.875	0.091	0.344	0.056	0.010	0.059	0.010	0.072	0.014	0.049	0.007	0.011	0.005
588	31.89	0.178	0.375	0.042	0.152	0.030	0.007	0.023	0.003	0.022	0.004	0.012	0.002	0.003	0.001
589	31.93	0.107	0.647	0.025	0.100	0.018	0.004	0.013	0.002	0.013	0.002	0.007	<0.001	0.002	0.001
590	31.97	1.092	2.733	0.241	0.826	0.153	0.019	0.112	0.014	0.063	0.009	0.021	0.003	0.005	0.003
591	32.04	0.076	0.247	0.019	0.070	0.011	<0.001	0.011	0.001	0.010	0.002	0.006	<0.001	0.001	<0.001
592	32.08	0.094	0.226	0.021	0.085	0.019	0.005	0.008	0.001	0.014	0.003	0.006	0.001	0.002	0.001
593	32.12	0.044	0.147	0.012	0.041	0.011	<0.001	0.006	0.001	0.008	0.001	0.003	<0.001	0.001	<0.001
594	32.16	0.145	0.395	0.037	0.147	0.035	0.007	0.026	0.003	0.023	0.004	0.011	0.001	0.003	0.001
595	32.20	0.300	0.808	0.071	0.262	0.051	0.010	0.029	0.004	0.034	0.005	0.013	0.003	0.003	0.001
596	32.24	0.283	0.595	0.064	0.226	0.047	0.008	0.031	0.003	0.022	0.004	0.014	0.002	0.003	0.002
597	32.28	0.201	0.588	0.046	0.183	0.033	0.005	0.021	0.004	0.025	0.004	0.011	0.001	0.002	0.001
598	32.33	0.402	1.129	0.097	0.368	0.062	0.011	0.053	0.007	0.039	0.006	0.016	0.001	0.003	0.002
599	32.37	0.200	0.750	0.053	0.204	0.052	0.007	0.032	0.004	0.031	0.006	0.012	0.002	0.004	0.001
600	32.41	0.175	0.543	0.040	0.151	0.026	0.005	0.024	0.002	0.020	0.002	0.011	0.002	0.002	0.001
601	32.46	0.211	0.533	0.047	0.175	0.033	0.004	0.025	0.003	0.021	0.003	0.012	0.002	0.001	0.001
602	32.50	0.089	0.234	0.021	0.082	0.014	0.002	0.010	0.001	0.009	0.002	0.004	0.001	0.001	<0.001
603	32.54	0.121	0.338	0.028	0.099	0.023	0.005	0.014	0.001	0.013	0.002	0.003	<0.001	0.001	<0.001
604	32.58	0.289	0.701	0.064	0.248	0.048	0.009	0.039	0.004	0.027	0.005	0.015	0.002	0.004	0.003
605	32.62	0.547	1.489	0.122	0.472	0.109	0.018	0.069	0.012	0.069	0.011	0.034	0.002	0.007	0.003
606	32.66	0.489	1.217	0.110	0.401	0.067	0.011	0.059	0.006	0.044	0.006	0.017	0.002	0.004	0.002
607	32.70	0.201	0.529	0.049	0.181	0.038	0.005	0.026	0.004	0.025	0.005	0.013	0.002	0.003	0.002

608	32.74	0.152	0.452	0.034	0.142	0.025	0.004	0.016	0.002	0.019	0.004	0.011	0.001	0.001	0.001
609	32.78	0.100	0.279	0.025	0.102	0.022	0.005	0.016	0.003	0.014	0.003	0.008	0.001	0.001	<0.001
610	32.84	0.129	0.394	0.028	0.108	0.019	0.002	0.021	0.002	0.015	0.003	0.009	0.001	0.002	0.001
611	32.88	0.066	0.164	0.013	0.050	0.007	0.001	0.004	<0.001	0.012	0.001	0.004	<0.001	0.001	0.001
612	32.92	0.193	0.286	0.045	0.157	0.031	0.007	0.020	0.002	0.018	0.003	0.007	0.001	0.001	0.001
613	32.96	0.291	3.956	0.069	0.264	0.050	0.008	0.048	0.006	0.038	0.006	0.016	0.003	0.004	0.003
614	33.01	0.391	4.280	0.090	0.323	0.074	0.009	0.050	0.007	0.046	0.008	0.022	0.002	0.005	0.002
615	33.05	0.182	0.492	0.042	0.169	0.032	0.006	0.025	0.004	0.021	0.002	0.010	0.001	0.003	0.002
616	33.10	0.161	0.367	0.035	0.137	0.025	0.005	0.021	0.002	0.017	0.003	0.009	0.001	0.002	0.001
617	33.14	0.080	0.203	0.020	0.064	0.008	0.001	0.008	0.001	0.012	0.001	0.006	<0.001	0.001	0.001
618	33.19	0.271	0.596	0.060	0.233	0.038	0.006	0.038	0.004	0.023	0.004	0.010	0.002	0.002	0.001
619	33.23	0.341	0.748	0.080	0.268	0.051	0.009	0.034	0.005	0.033	0.005	0.016	0.002	0.003	0.003
620	33.28	0.435	0.850	0.090	0.332	0.067	0.012	0.053	0.005	0.037	0.009	0.021	0.004	0.006	0.002
621	33.33	0.399	0.848	0.090	0.338	0.069	0.010	0.048	0.007	0.042	0.007	0.024	0.002	0.006	0.002
622	33.38	0.415	0.882	0.102	0.403	0.081	0.013	0.080	0.013	0.085	0.016	0.043	0.008	0.011	0.006
623	33.42	0.054	0.153	0.015	0.054	0.009	0.002	0.011	0.001	0.005	0.001	0.008	<0.001	0.001	<0.001
624	33.46	0.126	0.282	0.025	0.105	0.026	0.004	0.017	0.001	0.014	0.002	0.008	0.001	0.001	0.001
625	33.50	0.255	0.584	0.065	0.256	0.060	0.005	0.059	0.007	0.066	0.012	0.033	0.004	0.008	0.003
626	33.54	0.173	0.497	0.039	0.149	0.029	0.003	0.027	0.003	0.020	0.003	0.010	0.001	0.002	0.001
627	33.58	0.412	1.082	0.092	0.330	0.052	0.012	0.040	0.006	0.033	0.006	0.016	0.002	0.003	0.002
628	33.62	0.331	0.772	0.069	0.281	0.043	0.008	0.042	0.004	0.035	0.007	0.023	0.003	0.004	0.002
629	33.66	0.654	1.619	0.161	0.633	0.127	0.018	0.089	0.013	0.062	0.012	0.032	0.004	0.007	0.004
630	33.70	0.689	1.396	0.149	0.514	0.086	0.019	0.075	0.010	0.058	0.010	0.027	0.003	0.008	0.004
631	33.74	0.487	1.001	0.113	0.408	0.085	0.017	0.069	0.010	0.060	0.009	0.027	0.003	0.006	0.002
632	33.78	0.435	0.993	0.079	0.318	0.060	0.013	0.056	0.006	0.036	0.011	0.024	0.002	0.006	0.004
633	33.82	0.438	1.008	0.106	0.399	0.070	0.013	0.050	0.005	0.034	0.005	0.012	0.001	0.003	0.002
634	33.86	0.229	0.599	0.063	0.243	0.048	0.012	0.038	0.004	0.028	0.004	0.017	0.002	0.002	0.001
635	33.90	0.143	0.396	0.038	0.155	0.033	0.005	0.022	0.004	0.021	0.004	0.008	0.001	0.002	0.001
636	33.95	0.190	9.002	0.039	0.130	0.065	0.006	0.031	0.002	0.020	0.003	0.011	0.002	0.003	0.001
637	33.99	0.200	2.065	0.046	0.185	0.032	0.007	0.029	0.002	0.023	0.004	0.012	0.001	0.003	0.001
638	34.04	0.245	0.727	0.058	0.204	0.035	0.008	0.025	0.004	0.027	0.005	0.018	0.002	0.003	0.001
639	34.08	0.053	0.127	0.010	0.041	0.005	0.001	0.006	<0.001	0.005	0.002	0.004	0.001	0.001	0.002
640	34.13	1.054	1.889	0.224	0.897	0.193	0.038	0.169	0.021	0.158	0.039	0.099	0.010	0.019	0.009
641	34.17	0.257	0.600	0.061	0.212	0.037	0.006	0.030	0.005	0.026	0.004	0.013	0.002	0.003	0.001
642	34.22	0.159	0.401	0.039	0.152	0.032	0.006	0.016	0.003	0.017	0.003	0.008	0.001	0.001	<0.001
643	34.26	0.052	0.190	0.012	0.051	0.012	<0.001	0.008	0.001	0.007	0.001	0.002	<0.001	0.001	<0.001
644	34.30	0.166	0.342	0.037	0.135	0.022	0.005	0.021	0.002	0.019	0.003	0.011	0.001	0.002	0.002
645	34.33	0.258	0.601	0.056	0.202	0.044	0.005	0.035	0.005	0.030	0.004	0.015	0.002	0.002	0.001
646	34.37	0.395	0.974	0.092	0.362	0.063	0.010	0.048	0.006	0.036	0.006	0.019	0.002	0.003	0.002
647	34.41	1.275	2.678	0.262	0.888	0.137	0.011	0.082	0.010	0.060	0.009	0.025	0.003	0.005	0.002
648	34.45	0.179	0.420	0.045	0.178	0.029	0.006	0.026	0.003	0.026	0.004	0.015	0.002	0.002	0.002
649	34.49	0.041	0.151	0.011	0.047	0.004	0.001	0.010	0.001	0.008	<0.001	0.004	0.001	0.001	<0.001
650	34.53	0.046	0.155	0.018	0.043	0.007	0.001	0.009	<0.001	0.007	0.001	0.003	0.001	0.001	<0.001
651	34.58	0.082	0.190	0.016	0.065	0.015	0.001	0.007	0.001	0.008	0.002	0.006	<0.001	0.003	0.002
652	34.62	0.079	0.179	0.020	0.080	0.011	0.002	0.008	<0.001	0.010	0.002	0.006	0.001	0.002	0.001
653	34.67	0.089	0.230	0.022	0.084	0.012	0.003	0.011	0.002	0.009	0.001	0.006	0.001	0.001	0.002
654	34.71	1.714	4.306	0.572	2.546	0.470	0.093	0.306	0.031	0.121	0.013	0.027	0.002	0.003	0.001
655	34.76	0.132	0.319	0.030	0.114	0.026	0.004	0.018	0.002	0.016	0.002	0.006	0.001	0.001	0.002
656	34.80	0.114	0.248	0.024	0.085	0.019	0.003	0.016	0.002	0.013	0.002	0.004	0.001	0.001	0.001
657	34.84	0.166	0.388	0.038	0.131	0.022	0.005	0.017	0.003	0.018	0.004	0.006	0.002	0.001	0.001
658	34.88	0.312	0.591	0.076	0.280	0.051	0.002	0.023	0.002	0.016	0.002	0.007	0.001	0.001	<0.001
659	34.93	0.497	1.343	0.124	0.479	0.096	0.016	0.059	0.007	0.038	0.006	0.014	0.001	0.003	0.003
660	34.97	0.358	4.648	0.084	0.323	0.078	0.012	0.045	0.004	0.030	0.007	0.021	0.003	0.004	0.002
661	35.02	0.104	0.578	0.024	0.112	0.021	0.004	0.010	0.002	0.013	0.002	0.005	<0.001	0.002	<0.001
662	35.06	0.068	0.284	0.015	0.063	0.007	<0.001	0.011	0.001	0.008	0.001	0.004	<0.001	0.002	<0.001
663	35.10	0.237	0.738	0.057	0.216	0.042	0.006	0.032	0.004	0.023	0.005	0.013	0.001	0.003	0.001
664	35.15	0.370	0.879	0.081	0.313	0.057	0.010	0.035	0.004	0.032	0.006	0.018	0.003	0.006	0.010
665	35.19	0.451	1.026	0.104	0.363	0.070	0.010	0.053	0.008	0.051	0.009	0.021	0.003	0.005	0.002
666	35.23	0.252	0.657	0.064	0.235	0.038	0.005	0.036	0.004	0.029	0.005	0.012	0.002	0.003	0.002
667	35.27	0.451	8.556	0.101	0.367	0.058	0.015	0.052	0.006	0.053	0.007	0.021	0.003	0.006	0.002
668	35.31	0.376	0.901	0.086	0.348	0.059	0.010	0.046	0.005	0.043	0.006	0.017	0.003	0.004	0.002
669	35.35	0.549	1.234	0.130	0.482	0.085	0.016	0.075	0.010	0.061	0.011	0.029	0.004	0.006	0.004
670	35.39	0.207	0.484	0.046	0.177	0.035	0.005	0.026	0.003	0.023	0.003	0.011	0.001	0.002	0.001
671	35.43	0.217	0.502	0.043	0.166	0.027	0.006	0.021	0.003	0.024	0.004	0.014	0.002	0.002	0.001
672	35.47	0.145	0.294	0.032	0.136	0.020	0.003	0.023	0.001	0.017	0.001	0.009	0.001	0.001	0.001
673	35.51	0.211	0.529	0.046	0.186	0.043	0.005	0.027	0.003	0.024	0.003	0.012	<0.001	0.003	0.001
674	35.55	0.253	0.540	0.056	0.201	0.042	0.007	0.025	0.003	0.024	0.004	0.013	0.001	0.002	0.001
675	35.59	0.159	0.385	0.038	0.131	0.024	0.005	0.013	0.002	0.018	0.003	0.009	0.001	0.002	0.001
676	35.63	0.344	0.693	0.078	0.303	0.055	0.008	0.048	0.004	0.036	0.007	0.015	0.002	0.004	0.002
677	35.67	0.102	0.208	0.024	0.078	0.018	0.002	0.009	0.002	0.010	0.002	0.005	<0.001	0.002	<0.001
678	35.71	0.138	0.332	0.038	0.128	0.025	0.003	0.017	0.003	0.020	0.003	0.006	<0.001	0.001	<0.001
679	35.75	0.435	0.958	0.101	0.380	0.078	0.011	0.059	0.009	0.051	0.009	0.028	0.004	0.005	0.002
680	35.78	0.182	0.417	0.040	0.152	0.019	0.005	0.024	0.001	0.014	0.005	0.011	0.001	0.002	0.002
681	35.81	0.079	0.221	0.018	0.078	0.014	0.002	0.005	0.001	0.009	0.002	0.003	0.001	0.001	0.001
682	35.85	0.176	0.422	0.042	0.169	0.038	0.005	0.026	0.003	0.026	0.005	0.015	0.002	0.002	0.001
683	35.88	1.728	3.635	0.400	1.488	0.189	0.028	0.107	0.011	0.051	0.008	0.023	0.002	0.003	0.002
684	35.91	0.261	0.789	0.094	0.415	0.080	0.014	0.064	0.005	0.040	0.006	0.012	0.002	0.002	0.001

685	35.95	0.123	0.285	0.031	0.119	0.024	0.003	0.011	0.002	0.016	0.002	0.007	<0.001	0.001	0.001
686	35.98	0.415	0.997	0.093	0.328	0.055	0.013	0.037	0.006	0.041	0.007	0.014	0.002	0.005	0.001
687	36.05	0.219	0.518	0.052	0.173	0.033	0.005	0.019	0.003	0.013	0.003	0.008	0.001	0.002	0.001
688	36.08	0.257	0.597	0.061	0.239	0.048	0.009	0.027	0.004	0.032	0.006	0.013	0.004	0.003	0.002
689	36.12	0.130	0.367	0.034	0.113	0.023	0.002	0.015	0.003	0.015	0.002	0.008	0.001	0.001	0.001
690	36.16	0.201	0.498	0.041	0.151	0.026	0.002	0.020	0.003	0.017	0.004	0.009	<0.001	0.002	0.002
691	36.21	0.272	0.672	0.055	0.227	0.041	0.005	0.032	0.005	0.028	0.007	0.016	0.002	0.004	0.002
692	36.25	0.245	0.562	0.053	0.193	0.035	0.007	0.030	0.003	0.019	0.004	0.012	0.002	0.003	0.001
693	36.29	0.567	0.975	0.139	0.514	0.085	0.014	0.061	0.009	0.052	0.008	0.024	0.003	0.005	0.002
694	36.33	0.077	0.210	0.015	0.073	0.021	0.003	0.008	0.002	0.008	0.002	0.005	0.001	0.001	<0.001
695	36.37	0.206	0.491	0.048	0.175	0.027	0.004	0.021	0.004	0.020	0.002	0.008	0.001	0.002	0.001
696	36.41	0.157	0.331	0.033	0.145	0.023	0.004	0.017	0.002	0.013	0.004	0.010	0.002	0.002	0.001
697	36.45	0.065	0.235	0.015	0.066	0.015	0.003	0.005	0.002	0.015	0.002	0.007	<0.001	0.001	<0.001
698	36.49	0.059	0.197	0.017	0.077	0.024	0.006	0.031	0.003	0.014	0.002	0.008	<0.001	<0.001	0.001
699	36.52	0.093	0.248	0.025	0.088	0.025	0.002	0.012	0.003	0.015	0.002	0.006	0.001	0.002	<0.001
700	36.56	0.288	0.515	0.063	0.248	0.042	0.008	0.029	0.005	0.027	0.007	0.018	0.002	0.004	0.002
701	36.60	0.054	0.156	0.013	0.053	0.010	0.001	0.009	0.002	0.007	0.002	0.005	<0.001	<0.001	0.001
702	36.64	0.059	0.179	0.014	0.047	0.009	0.002	0.004	0.001	0.009	0.001	0.003	0.001	0.001	0.003
703	36.67	0.044	0.142	0.012	0.047	0.009	0.002	0.005	<0.001	0.007	0.001	0.003	0.001	0.001	<0.001
704	36.71	0.137	0.288	0.033	0.123	0.017	0.005	0.018	0.002	0.021	0.004	0.010	0.001	0.002	0.001
705	36.76	0.211	0.662	0.053	0.210	0.040	0.008	0.037	0.003	0.025	0.006	0.013	0.001	0.004	0.001
706	36.79	0.148	0.486	0.039	0.141	0.030	0.006	0.024	0.003	0.022	0.003	0.008	0.001	0.002	0.001
707	36.83	0.280	0.716	0.065	0.251	0.051	0.010	0.044	0.006	0.032	0.005	0.015	0.001	0.003	0.002
708	36.87	0.243	0.557	0.058	0.232	0.040	0.007	0.028	0.003	0.024	0.004	0.012	0.002	0.002	0.001
709	36.91	0.342	0.461	0.076	0.296	0.056	0.012	0.041	0.006	0.029	0.005	0.012	0.001	0.003	0.003
710	36.95	0.267	2.751	0.068	0.241	0.066	0.010	0.038	0.005	0.033	0.006	0.018	0.002	0.004	0.002
711	37.00	0.642	2.120	0.142	0.536	0.115	0.019	0.083	0.012	0.066	0.013	0.029	0.003	0.007	0.004
712	37.04	0.281	0.644	0.068	0.269	0.044	0.011	0.038	0.005	0.037	0.009	0.021	0.003	0.006	0.003
713	37.08	0.239	0.630	0.058	0.244	0.050	0.008	0.041	0.007	0.034	0.006	0.018	0.002	0.004	0.003
714	37.13	0.442	0.922	0.124	0.480	0.100	0.013	0.075	0.011	0.058	0.009	0.027	0.003	0.004	0.002
715	37.16	0.165	0.466	0.041	0.158	0.035	0.005	0.031	0.004	0.028	0.005	0.010	0.001	0.002	0.002
716	37.20	0.079	0.189	0.021	0.070	0.014	0.003	0.003	0.001	0.004	<0.001	0.003	0.001	<0.001	0.006
717	37.24	0.029	0.119	0.008	0.030	0.005	<0.001	0.004	0.001	0.007	0.001	0.002	<0.001	0.001	<0.001
718	37.28	0.024	0.097	0.007	0.030	0.003	0.001	0.003	<0.001	0.006	<0.001	0.002	<0.001	0.001	<0.001
719	37.32	0.049	0.643	0.013	0.033	0.007	0.001	0.006	0.001	0.007	0.001	0.001	<0.001	0.001	<0.001
720	37.35	0.229	0.318	0.044	0.170	0.020	0.007	0.020	0.003	0.022	0.004	0.012	0.002	0.003	0.002
721	37.39	0.312	0.878	0.075	0.303	0.059	0.011	0.041	0.006	0.036	0.006	0.021	0.003	0.004	0.003
722	37.43	0.422	1.179	0.097	0.376	0.075	0.015	0.063	0.010	0.054	0.008	0.022	0.002	0.006	0.002
723	37.46	0.332	0.840	0.082	0.312	0.051	0.009	0.040	0.006	0.031	0.006	0.018	0.002	0.005	0.002
724	37.50	0.627	1.355	0.145	0.575	0.123	0.025	0.111	0.014	0.100	0.019	0.054	0.006	0.013	0.005
725	37.54	0.543	1.228	0.136	0.499	0.102	0.009	0.077	0.010	0.056	0.009	0.027	0.003	0.005	0.002
726	37.58	0.080	0.215	0.019	0.072	0.016	0.002	0.016	0.002	0.010	0.002	0.006	<0.001	0.001	<0.001
727	37.61	0.063	0.194	0.014	0.061	0.014	0.002	0.008	0.001	0.007	0.002	0.006	0.001	0.001	<0.001
728	37.65	0.431	0.962	0.105	0.391	0.072	0.017	0.059	0.006	0.049	0.007	0.025	0.003	0.004	0.002
729	37.69	0.446	1.069	0.111	0.420	0.078	0.013	0.055	0.009	0.046	0.008	0.023	0.002	0.005	0.002
730	37.72	0.796	1.725	0.196	0.714	0.157	0.024	0.118	0.020	0.096	0.018	0.041	0.005	0.009	0.003
731	37.76	0.356	1.057	0.102	0.376	0.072	0.016	0.063	0.009	0.050	0.010	0.026	0.002	0.005	0.003
732	37.80	0.091	0.202	0.023	0.084	0.016	0.004	0.010	0.001	0.009	0.001	0.006	0.001	0.001	0.001
733	37.85	0.055	0.147	0.014	0.049	0.016	0.002	0.005	0.001	0.007	0.001	0.005	0.001	0.001	0.001
734	37.89	0.088	0.239	0.020	0.079	0.012	0.002	0.012	0.002	0.010	0.001	0.005	0.001	0.001	<0.001
735	37.93	0.188	0.462	0.047	0.163	0.034	0.006	0.025	0.002	0.018	0.002	0.009	0.001	0.002	0.001
736	37.97	0.418	16.994	0.094	0.382	0.095	0.017	0.069	0.007	0.049	0.012	0.030	0.002	0.007	0.002
737	38.01	0.149	0.739	0.040	0.152	0.025	0.004	0.018	0.003	0.018	0.003	0.009	0.002	0.002	0.001
738	38.05	0.207	0.515	0.048	0.175	0.026	0.005	0.030	0.004	0.025	0.004	0.012	0.002	0.002	0.014
739	38.09	0.214	0.543	0.047	0.177	0.026	0.004	0.024	0.005	0.021	0.004	0.010	0.002	0.003	0.001
740	38.13	0.141	0.315	0.034	0.126	0.017	0.007	0.021	0.001	0.014	0.002	0.006	0.001	0.001	0.002
741	38.17	0.082	0.242	0.020	0.069	0.011	0.003	0.008	0.001	0.014	0.001	0.005	<0.001	0.001	<0.001
742	38.21	0.355	0.736	0.076	0.274	0.058	0.009	0.042	0.006	0.036	0.006	0.013	0.001	0.003	0.004
743	38.25	0.310	0.790	0.081	0.306	0.056	0.011	0.046	0.006	0.037	0.005	0.018	0.002	0.005	0.002
744	38.29	1.291	0.854	0.233	0.871	0.105	0.020	0.071	0.006	0.051	0.009	0.026	0.003	0.006	0.004
745	38.33	1.137	1.569	0.132	0.452	0.078	0.015	0.066	0.010	0.055	0.009	0.037	0.003	0.006	0.004
746	38.37	0.633	1.403	0.148	0.640	0.116	0.022	0.106	0.014	0.083	0.015	0.048	0.005	0.009	0.005
747	38.40	0.538	1.180	0.127	0.482	0.108	0.017	0.082	0.012	0.065	0.015	0.036	0.006	0.008	0.005
748	38.44	0.433	0.968	0.108	0.427	0.072	0.017	0.057	0.009	0.056	0.012	0.029	0.004	0.007	0.004
749	38.48	0.180	0.497	0.042	0.157	0.028	0.003	0.026	0.003	0.022	0.003	0.012	0.002	0.003	0.001
750	38.52	0.209	0.656	0.050	0.182	0.032	0.006	0.028	0.005	0.024	0.005	0.010	0.001	0.002	0.002
751	38.55	0.087	0.370	0.021	0.095	0.017	0.003	0.009	0.002	0.014	0.001	0.009	<0.001	0.001	0.006
752	38.59	0.176	0.500	0.045	0.179	0.035	0.006	0.025	0.002	0.024	0.005	0.013	0.002	0.003	0.001
753	38.64	0.285	0.677	0.064	0.228	0.047	0.006	0.028	0.005	0.030	0.004	0.010	0.001	0.002	0.002
754	38.69	0.095	0.220	0.020	0.069	0.010	0.002	0.007	0.002	0.012	0.001	0.007	<0.001	0.001	0.001
755	38.74	0.085	0.218	0.020	0.081	0.016	0.001	0.020	0.004	0.014	0.002	0.006	0.001	0.002	0.002
756	38.79	0.103	0.345	0.028	0.102	0.014	0.003	0.019	0.001	0.013	0.002	0.006	0.001	0.001	0.001
757	38.83	0.265	0.567	0.054	0.201	0.044	0.005	0.033	0.004	0.020	0.003	0.011	0.002	0.003	0.001
758	38.86	0.596	1.229	0.145	0.533	0.098	0.013	0.057	0.007	0.032	0.005	0.010	0.001	0.002	0.002
759	38.91	0.064	0.214	0.018	0.070	0.012	0.002	0.013	0.001	0.011	0.002	0.004	0.001	0.001	0.001
760	38.95	0.139	8.858	0.031	0.122	0.036	0.005	0.019	0.002	0.014	0.002	0.009	0.001	0.001	0.002
761	38.99	0.155	3.098	0.031	0.118	0.032	0.002	0.018	0.003	0.020	0.003	0.008	0.001	0.002	0.001

762	39.04	0.136	0.518	0.029	0.108	0.018	0.002	0.019	0.003	0.019	0.003	0.010	0.001	0.003	0.001
763	39.09	0.141	0.452	0.038	0.149	0.031	0.003	0.022	0.003	0.020	0.002	0.008	0.001	0.003	0.001
764	39.13	0.215	0.652	0.047	0.179	0.029	0.007	0.031	0.001	0.018	0.004	0.013	0.001	0.003	0.002
765	39.18	0.246	0.659	0.057	0.227	0.048	0.005	0.035	0.005	0.035	0.005	0.014	0.002	0.003	0.001
766	39.22	0.238	0.711	0.056	0.221	0.049	0.005	0.028	0.004	0.030	0.005	0.010	0.002	0.003	0.002
767	39.26	0.246	0.674	0.060	0.232	0.049	0.009	0.043	0.006	0.029	0.006	0.013	0.002	0.004	0.003
768	39.31	0.096	0.228	0.025	0.085	0.020	0.003	0.014	0.001	0.016	0.002	0.006	0.001	0.001	<0.001
769	39.36	0.089	0.340	0.023	0.089	0.016	0.001	0.016	0.002	0.016	0.002	0.007	<0.001	0.001	<0.001
770	39.40	0.073	0.276	0.018	0.069	0.010	0.001	0.009	0.001	0.013	0.002	0.007	<0.001	0.001	0.001
771	39.44	0.129	0.406	0.031	0.125	0.026	0.004	0.019	0.003	0.019	0.004	0.008	0.001	0.002	0.001
772	39.48	0.194	0.454	0.041	0.149	0.019	0.007	0.018	0.003	0.018	0.003	0.010	0.001	0.002	0.001
773	39.52	0.148	0.443	0.045	0.196	0.054	0.007	0.035	0.006	0.033	0.005	0.013	0.001	0.003	0.002
774	39.57	0.055	0.180	0.015	0.049	0.008	0.001	0.011	0.001	0.007	0.001	0.003	<0.001	0.001	<0.001
775	39.61	0.052	0.260	0.011	0.047	0.006	<0.001	0.013	0.001	0.007	<0.001	0.003	<0.001	0.001	<0.001
776	39.65	0.242	0.620	0.056	0.217	0.037	0.009	0.036	0.003	0.028	0.005	0.015	0.002	0.002	<0.001
777	39.69	0.223	0.645	0.050	0.209	0.028	0.004	0.022	0.005	0.025	0.004	0.017	0.002	0.004	0.002
778	39.73	0.186	0.544	0.046	0.175	0.033	0.004	0.021	0.003	0.022	0.004	0.009	0.001	0.002	0.002
779	39.77	0.122	0.402	0.030	0.131	0.025	0.003	0.023	0.003	0.015	0.001	0.007	0.001	0.002	0.001
780	39.81	0.099	0.290	0.023	0.085	0.016	0.003	0.019	0.001	0.011	0.002	0.007	0.001	0.001	0.004
781	39.85	0.139	0.483	0.033	0.116	0.029	0.004	0.013	0.005	0.017	0.003	0.009	0.002	0.001	0.002
782	39.88	2.456	6.373	0.816	3.488	0.654	0.108	0.376	0.039	0.180	0.023	0.047	0.004	0.008	0.003
783	39.92	0.254	0.765	0.056	0.223	0.038	0.007	0.036	0.005	0.035	0.006	0.013	0.001	0.003	0.001
784	39.96	0.633	1.504	0.157	0.641	0.108	0.029	0.097	0.012	0.075	0.016	0.047	0.006	0.009	0.005

RICE deep core 8m to 40m samples, relative standard deviation (RSD, %).

Vial #	Top Depth (m)	La139	Ce140	Pr141	Nd146	Sm147	Eu153	Gd157	Tb159	Dy163	Ho165	Er166	Tm169	Yb172	Lu175
1	8.00	2.9	3.3	5.1	6.5	17.4	14.9	15.7	7.9	16.2	10.5	15.9	27.0	15.9	33.5
2	8.05	4.8	4.4	8.2	5.7	6.6	15.2	15.6	9.6	13.4	6.7	13.8	24.2	26.4	17.5
3	8.09	7.4	3.1	11.1	9.4	11.5	27.1	28.8	19.9	28.8	18.4	10.3	27.0	17.5	53.2
4	8.13	2.8	2.7	6.9	8.4	23.4	19.3	18.7	15.6	24.5	16.8	10.2	29.4	23.8	22.4
5	8.17	4.5	2.6	11.6	6.7	33.4	38.1	42.2	13.9	21.1	24.7	48.6	53.0	24.8	50.5
6	8.22	4.5	4.8	10.6	26.4	42.6	42.3	18.0	30.8	57.7	43.0	30.5	47.6	89.0	104.4
7	8.27	5.2	5.6	10.6	10.9	43.4	20.2	25.2	43.3	23.4	26.1	37.7	51.1	56.8	121.5
8	8.32	76.4	3.2	6.1	8.3	19.2	64.0	25.1	21.2	17.1	16.2	45.6	69.9	38.9	45.1
9	9.01	5.6	2.2	6.4	7.3	18.5	24.4	8.1	18.8	22.6	34.0	13.7	53.5	55.7	37.6
10	9.06	4.8	3.6	6.1	6.3	16.0	17.8	16.0	20.5	15.1	19.6	31.5	33.9	31.5	61.2
11	9.11	2.3	1.9	5.5	3.5	16.6	14.1	25.6	22.9	19.4	12.6	20.5	42.5	41.8	48.3
12	9.16	3.4	3.1	10.9	9.1	16.5	17.2	15.8	14.1	9.8	10.9	20.2	19.8	28.5	13.8
13	9.21	4.3	3.2	5.8	8.0	28.1	25.0	13.6	15.1	12.1	21.9	35.6	41.9	37.2	33.2
14	9.27	3.6	2.2	4.6	8.6	12.7	14.8	9.3	10.8	7.7	10.6	10.7	28.9	6.0	11.6
15	9.32	8.8	3.3	8.0	13.1	27.4	14.5	51.6	20.0	18.6	20.4	30.1	49.8	49.1	65.0
16	9.37	9.1	3.8	10.5	8.6	39.0	30.4	44.3	27.6	38.0	26.2	26.8	34.8	57.1	80.2
17	9.42	5.9	3.6	8.7	9.7	21.1	35.3	14.9	35.2	13.4	35.3	13.1	54.4	29.8	67.4
18	9.46	4.5	2.6	7.8	11.3	19.4	22.9	18.2	34.1	36.7	39.9	77.8	42.6	54.2	51.2
19	9.51	2.5	3.3	4.3	8.3	17.5	25.3	9.5	16.9	14.9	18.9	19.5	15.8	28.9	19.5
20	9.55	7.0	2.1	8.4	7.9	16.9	28.1	21.2	20.3	11.8	17.0	26.7	37.8	35.2	31.5
21	9.60	4.2	1.4	6.8	8.5	10.2	18.7	19.6	25.4	18.8	25.8	25.9	36.0	46.1	48.8
22	9.65	6.0	7.0	8.8	12.0	36.1	26.3	34.1	23.2	37.9	18.5	54.6	70.6	71.1	74.1
23	9.69	8.0	6.3	6.7	20.2	59.3	38.8	15.5	29.6	55.7	32.4	22.6	126.2	112.3	98.8
24	9.73	9.2	6.2	25.6	20.9	31.0	36.0	30.5	38.7	46.8	15.3	50.7	61.2	106.4	112.4
25	9.77	2.7	5.8	8.6	14.6	36.6	43.4	32.5	23.9	26.9	41.4	38.2	55.2	9.2	72.6
26	9.81	5.8	3.3	11.2	12.4	38.6	23.8	42.7	21.0	34.7	25.3	68.4	50.2	46.3	69.6
27	9.86	4.7	1.4	6.3	6.3	12.5	30.5	14.7	17.6	22.7	15.7	15.7	45.3	34.5	40.0
28	9.90	3.6	3.6	3.4	6.2	8.9	23.4	20.6	20.3	9.9	10.3	18.7	24.3	43.0	34.3
29	9.95	3.7	2.7	6.6	5.4	13.8	16.2	15.2	20.5	11.3	18.1	17.5	18.2	20.6	39.0
30	9.99	4.1	1.8	4.8	6.9	11.8	17.0	20.6	7.7	8.4	14.7	20.9	22.4	17.4	45.7
31	10.04	4.5	3.2	6.0	11.9	17.2	32.0	21.7	30.3	17.9	16.2	29.6	36.6	38.0	54.2
32	10.08	4.2	5.6	13.2	7.5	42.4	46.5	32.3	29.7	29.3	29.4	21.5	75.8	50.2	42.3
33	10.13	4.6	6.9	4.6	8.4	21.4	20.2	24.2	35.4	29.7	35.3	34.5	49.4	38.7	19.4
34	10.17	7.1	3.1	8.2	9.9	13.0	33.7	42.7	23.0	23.4	19.4	20.7	44.8	24.1	24.1
35	10.21	4.7	3.5	12.7	20.5	32.4	26.1	28.3	26.4	25.3	19.7	32.1	64.7	19.6	80.2
36	10.25	48.5	9.3	10.1	14.7	33.4	50.8	39.1	26.5	35.9	20.7	61.6	73.6	64.0	89.8
37	10.29	3.0	2.8	8.9	6.2	25.2	33.2	41.4	36.0	20.1	16.3	38.5	38.0	38.3	57.5
38	10.33	8.0	2.8	5.0	12.1	14.8	28.9	16.2	16.0	17.8	23.0	19.5	42.5	20.1	27.5
39	10.37	4.5	3.8	10.0	5.7	13.3	23.5	23.7	12.2	18.6	22.8	16.3	22.3	11.8	108.5
40	10.41	4.5	2.9	8.2	11.5	21.8	18.5	17.4	20.7	25.4	19.7	24.0	17.6	34.4	51.3
41	10.44	3.5	2.2	7.5	8.0	21.5	20.0	23.4	22.0	16.5	12.3	21.2	28.8	16.0	31.1
42	10.48	7.7	4.0	9.9	9.6	30.4	37.8	40.5	28.2	24.8	30.2	36.0	38.4	28.0	42.5
43	10.52	5.5	3.3	9.7	12.7	27.5	15.6	42.7	11.2	25.1	35.0	39.8	46.4	58.6	89.9
44	10.56	6.9	3.6	8.0	13.7	28.2	28.6	23.8	22.5	22.7	27.7	47.3	65.8	60.3	49.0
45	10.60	3.8	3.0	10.6	11.0	20.4	29.0	31.6	28.5	40.1	21.4	27.9	53.9	13.0	74.3
46	10.63	5.5	3.4	7.0	8.1	23.0	21.0	20.9	26.1	19.4	24.2	25.8	34.9	19.6	36.8
47	10.67	2.8	3.7	3.8	10.1	14.3	23.5	22.5	17.7	9.8	11.9	18.9	36.4	39.8	34.2
48	10.70	5.7	3.7	6.1	11.5	32.3	27.3	29.5	28.3	17.4	35.3	36.9	17.4	33.1	33.7
49	10.74	10.8	3.2	4.3	8.0	12.1	25.8	44.1	41.1	21.3	31.7	23.0	44.6	43.6	162.5

50	10.78	9.9	2.0	11.7	17.6	35.7	31.2	29.3	19.8	26.5	43.3	46.1	31.2	61.7	94.9
51	10.82	4.8	3.0	12.0	15.9	39.7	12.8	19.9	22.4	14.3	29.3	45.1	46.4	79.7	79.1
52	10.85	4.4	2.0	9.7	17.5	19.9	37.5	25.9	24.4	39.6	20.1	33.4	56.2	37.6	93.2
53	10.89	3.1	2.4	2.1	2.4	7.3	10.9	11.0	7.7	11.6	19.9	8.0	33.9	32.1	29.2
54	10.94	4.2	2.7	5.3	8.6	25.2	15.7	48.3	27.6	30.6	50.4	25.1	85.0	50.0	23.7
55	10.98	2.9	2.9	10.5	15.2	16.3	21.7	17.2	17.0	16.4	26.4	31.9	44.7	14.9	21.0
56	11.02	2.3	2.0	6.8	19.7	27.9	30.6	21.3	25.9	24.9	38.6	23.1	60.8	35.5	60.9
57	11.06	2.7	3.0	8.7	7.7	30.1	23.2	22.8	32.0	23.3	17.7	34.2	37.5	34.5	45.4
58	11.10	6.0	6.5	2.9	6.5	18.5	14.0	18.7	19.4	20.2	19.1	32.6	33.0	27.5	34.4
59	11.14	8.4	4.9	13.9	18.5	25.6	22.0	20.4	16.0	22.5	20.2	44.0	57.2	35.3	42.6
60	11.18	5.9	5.4	11.8	16.4	39.1	31.2	24.2	28.7	41.1	15.7	13.4	38.2	50.7	120.0
61	11.22	7.5	3.6	8.1	11.2	26.9	31.3	25.3	33.1	25.8	22.2	26.6	51.7	38.2	78.6
62	11.26	2.5	2.9	2.0	3.6	13.2	6.6	10.9	8.9	4.9	13.4	4.9	26.6	25.9	34.4
63	11.30	4.5	3.3	3.8	12.2	17.7	9.5	35.1	36.9	18.1	32.0	34.5	33.9	59.9	56.2
64	11.34	15.1	7.0	27.5	28.3	61.1	48.1	62.2	28.9	54.2	73.3	91.5	30.9	59.0	138.5
65	11.38	5.3	7.0	8.1	8.4	37.7	48.4	36.9	33.4	69.8	44.6	48.0	83.8	89.0	56.2
66	11.42	6.4	5.3	11.1	11.0	22.2	24.0	26.6	40.5	31.7	45.4	28.3	48.6	48.2	60.3
67	11.45	5.5	4.6	11.4	6.9	22.3	33.5	31.6	32.8	19.7	22.1	26.8	33.7	16.3	69.4
68	11.50	5.8	3.2	12.6	13.3	25.2	42.1	21.8	26.8	20.2	42.2	49.3	29.6	65.3	50.3
69	11.54	6.0	4.0	4.6	11.4	24.0	30.9	20.2	14.1	27.7	18.9	24.0	41.5	43.9	72.1
70	11.57	4.0	5.0	6.7	6.2	12.2	30.9	19.2	24.8	19.6	29.3	37.3	28.6	14.1	43.1
71	11.61	2.8	1.2	4.3	5.5	9.2	19.1	11.4	14.1	14.1	20.1	32.3	25.9	16.9	77.8
72	11.64	4.6	3.1	7.5	27.1	46.5	52.4	43.7	28.8	44.3	32.1	75.9	48.0	49.0	35.3
73	11.68	6.2	7.4	15.7	21.4	20.3	31.9	37.4	43.8	34.8	45.9	34.2	90.8	66.3	64.7
74	11.71	10.7	3.1	10.7	16.7	15.4	23.2	26.3	24.2	49.5	68.8	51.5	84.0	58.5	143.3
75	11.75	8.8	3.6	16.8	17.2	48.2	11.9	39.3	15.7	29.3	61.6	43.2	58.5	57.4	50.5
76	11.78	7.5	5.3	22.3	29.1	23.8	37.4	50.8	43.2	35.8	34.8	43.7	63.1	85.5	64.6
77	11.81	8.4	1.9	11.9	18.0	29.1	38.8	41.2	43.9	48.1	23.1	33.6	23.2	45.7	55.8
78	11.85	3.7	2.4	8.2	16.2	27.4	38.2	35.2	36.6	45.7	27.6	19.0	22.8	31.1	67.2
79	11.88	3.4	2.0	6.3	11.5	18.3	28.9	29.3	22.0	25.8	25.3	16.7	38.8	40.1	26.0
80	11.91	5.6	5.4	9.7	14.3	33.6	16.9	21.3	19.1	27.8	41.9	16.7	40.6	39.6	73.1
81	11.94	8.3	2.5	5.0	6.0	21.9	22.7	31.5	25.6	30.4	40.6	19.8	18.6	49.9	121.9
82	11.98	2.5	2.1	2.4	4.6	7.2	8.3	3.6	6.8	11.6	8.3	8.3	15.9	6.5	91.5
83	12.02	5.5	2.9	5.8	8.8	23.0	23.7	14.4	24.8	18.2	31.9	23.2	23.4	36.6	20.2
84	12.05	3.2	2.6	6.6	8.7	17.6	19.5	15.3	25.2	17.0	18.8	36.2	36.8	29.9	29.1
85	12.07	4.7	5.0	4.4	4.0	8.3	9.9	8.0	9.7	10.2	15.7	9.3	19.9	8.3	17.5
86	12.10	4.4	2.1	6.6	8.7	20.6	16.9	9.7	27.6	13.5	17.7	21.4	40.1	39.4	21.0
87	12.15	3.8	2.1	6.2	9.1	18.2	23.3	23.4	17.3	29.9	24.9	24.5	47.7	33.5	57.1
88	12.18	3.3	4.3	9.6	13.9	25.2	23.4	41.4	18.0	20.7	36.3	49.6	41.7	49.3	51.4
89	12.22	4.0	3.7	3.4	14.7	23.1	16.1	20.5	24.1	38.4	24.3	22.1	34.7	40.9	67.0
90	12.26	7.8	3.4	5.1	4.2	13.8	10.5	10.6	14.9	15.6	20.6	23.2	32.2	18.5	84.0
91	12.30	4.9	6.6	5.4	8.2	31.3	23.1	27.4	18.6	16.8	36.9	49.7	50.4	34.0	207.3
92	12.34	10.0	5.8	12.0	15.7	51.8	29.6	37.1	16.2	31.6	36.1	49.2	57.7	73.7	90.5
93	12.38	15.1	7.2	8.3	12.9	42.9	54.1	51.8	60.5	40.6	21.2	44.9	78.1	72.3	76.4
94	12.42	9.6	6.2	7.2	7.0	22.8	37.3	30.4	18.3	47.8	42.0	36.8	63.3	76.8	73.7
95	12.46	6.5	2.9	15.9	17.2	22.6	34.8	33.9	33.1	17.6	51.5	29.5	28.6	18.9	55.7
96	12.50	5.1	3.5	12.8	20.2	38.4	22.4	24.8	32.4	12.0	52.7	28.0	30.9	53.3	71.8
97	12.54	7.5	5.3	12.4	10.5	31.8	30.0	34.7	23.6	17.3	55.5	26.4	56.3	48.0	53.8
98	12.58	6.4	4.3	5.3	18.0	42.6	28.2	28.3	42.4	39.2	23.0	63.0	29.8	20.4	70.1
99	12.62	5.7	5.0	6.6	11.2	17.7	25.2	30.1	14.8	31.7	22.5	18.6	45.5	34.0	52.8
100	12.66	3.5	2.1	14.4	12.3	18.8	44.7	36.2	38.9	30.9	32.8	43.1	48.1	94.9	85.5
101	12.69	3.7	2.6	12.3	12.0	33.4	34.8	33.4	47.2	34.9	41.0	49.7	71.0	75.5	82.6
102	12.73	7.8	6.0	13.1	7.9	31.3	56.1	26.2	27.3	23.2	29.9	34.2	47.3	27.4	46.9
103	12.77	4.8	3.8	12.8	12.0	14.9	26.9	24.0	33.1	13.0	13.2	33.6	40.3	50.4	44.8
104	12.81	6.9	4.8	9.6	16.0	25.6	34.9	26.4	30.9	35.7	36.9	104.9	10.3	41.8	100.3
105	12.84	7.5	9.9	16.3	12.2	44.6	24.4	39.7	27.9	23.2	40.7	43.7	27.4	50.4	63.5
106	12.88	5.3	8.6	21.4	14.1	23.6	33.2	23.3	59.1	57.0	36.2	34.2	81.8	69.4	91.1
107	12.93	3.5	1.2	5.9	6.4	29.2	33.3	21.4	23.6	14.8	45.0	22.6	45.5	51.3	53.3
108	12.97	6.1	2.5	7.3	6.2	26.3	21.1	18.6	21.5	25.0	17.5	19.3	51.3	41.4	48.1
109	13.02	5.4	1.7	10.7	20.4	40.3	26.5	29.5	37.4	28.2	51.1	37.3	45.2	22.0	21.0
110	13.06	6.8	5.0	15.1	15.3	43.3	25.5	32.0	26.4	37.4	28.1	45.1	74.2	35.8	79.9
111	13.10	7.3	3.1	16.2	8.2	31.7	49.3	35.6	40.2	51.5	24.7	54.6	68.9	36.0	79.8
112	13.14	8.8	5.1	10.2	23.2	38.7	43.4	37.0	21.3	18.9	54.8	80.2	98.5	92.7	132.1
113	13.18	11.3	2.3	10.1	21.6	28.9	35.6	31.9	38.2	24.8	37.4	35.2	39.2	56.5	70.5
114	13.22	2.7	4.4	8.3	10.0	28.8	25.1	27.4	19.3	19.9	40.7	25.5	62.5	34.0	42.7
115	13.26	5.8	4.7	13.1	13.3	35.3	43.1	19.9	23.7	21.0	31.2	35.7	38.0	48.4	59.4
116	13.30	9.9	4.0	19.7	20.9	36.9	32.7	27.2	19.8	20.7	33.1	40.2	45.8	61.1	59.7
117	13.34	8.2	6.1	12.3	16.7	54.8	40.7	23.1	45.0	35.9	21.5	39.5	40.0	63.7	112.0
118	13.38	2.6	4.0	7.4	10.5	46.0	19.9	24.3	20.9	19.2	18.0	26.8	46.4	56.2	53.9
119	13.42	7.6	4.8	5.7	6.1	33.0	24.5	28.9	27.4	12.4	30.3	44.1	41.1	28.9	34.6
120	13.46	7.6	3.9	12.9	15.0	28.6	34.1	23.6	35.8	25.9	39.0	19.2	103.6	38.9	91.1
121	13.50	4.9	3.0	9.7	7.7	31.4	42.9	19.6	16.6	28.9	21.0	19.4	31.6	51.6	48.2
122	13.54	6.5	4.3	9.3	8.4	20.1	27.0	16.5	12.5	12.3	25.2	28.3	62.9	35.9	63.3
123	13.58	8.9	6.6	16.7	23.9	48.4	9.6	43.7	33.9	39.7	42.7	54.9	39.5	55.9	75.8
124	13.61	10.5	2.6	14.6	14.0	42.8	33.7	31.8	13.6	38.1	19.3	48.3	61.9	73.4	37.3
125	13.65	3.9	2.6	6.1	5.2	14.9	4.2	12.0	9.6	4.0	21.1	16.1	29.3	20.9	25.8
126	13.69	6.7	5.6	8.7	16.5	37.0	32.4	18.6	28.1	39.5	53.4	45.1	84.2	43.4	91.8

127	13.72	4.4	2.3	3.3	2.7	14.5	22.7	16.2	14.9	9.0	14.7	14.0	16.6	32.5	24.0
128	13.75	4.0	1.7	3.6	3.9	15.6	9.5	16.5	21.1	21.7	10.0	18.8	34.3	25.4	24.1
129	13.79	3.1	2.2	5.8	8.5	23.1	10.4	13.8	22.8	24.8	15.9	16.4	28.9	22.6	24.0
130	13.82	2.9	2.9	4.8	5.6	23.4	20.3	23.7	19.4	13.6	11.5	35.0	25.9	30.9	35.2
131	13.86	3.7	3.2	8.8	2.3	6.2	15.5	12.0	24.3	11.5	17.0	17.3	43.1	16.9	48.0
132	13.89	5.3	6.0	12.8	12.2	41.4	39.0	58.7	34.5	52.7	32.6	44.7	59.1	58.5	57.1
133	13.93	4.1	2.9	11.9	7.2	25.3	24.0	17.8	38.8	21.0	17.4	29.9	48.9	32.3	39.4
134	13.97	4.0	2.4	4.6	4.1	11.2	21.5	17.9	8.5	10.3	14.9	10.8	18.2	24.9	16.1
135	14.02	3.5	2.1	8.1	10.3	13.9	15.3	24.5	21.7	17.7	44.7	30.9	23.7	18.6	37.5
136	14.05	2.8	3.9	7.2	5.2	6.7	18.5	15.6	26.9	22.0	20.0	21.7	34.8	24.5	32.1
137	14.09	2.7	2.2	11.4	11.3	14.2	46.4	29.7	22.5	16.3	13.4	18.4	53.8	25.8	43.4
138	14.13	4.6	4.7	7.2	20.7	13.0	32.5	23.7	30.9	21.8	37.4	38.6	49.6	23.5	83.8
139	14.17	5.5	3.1	6.4	7.8	9.8	23.2	17.1	15.0	22.4	15.3	33.7	28.3	24.8	75.3
140	14.21	17.6	17.4	61.7	40.1	133.6	48.0	49.8	36.2	140.8	43.2	182.5	34.3	94.7	88.3
141	14.24	4.2	2.9	7.5	10.6	28.2	28.3	18.6	11.6	21.1	9.0	22.1	24.1	16.2	39.8
142	14.28	3.5	2.6	7.0	8.4	20.8	13.2	29.4	18.4	9.9	18.6	26.4	35.4	44.1	79.0
143	14.32	9.0	5.9	18.0	10.8	18.9	19.1	26.7	42.7	45.5	36.8	24.6	68.1	64.2	73.8
144	14.36	8.2	7.7	15.9	13.7	19.8	26.2	42.5	23.8	45.1	33.0	66.4	54.0	55.4	73.1
145	14.40	4.1	2.2	4.5	7.6	11.8	27.1	13.3	35.4	21.1	31.7	19.1	33.9	20.3	52.3
146	14.44	5.0	2.6	7.4	7.1	35.7	32.8	19.0	19.3	20.8	31.4	19.4	33.2	17.2	61.4
147	14.48	5.7	3.0	12.6	7.1	32.4	29.7	36.1	28.6	26.3	16.7	28.5	33.7	93.4	66.9
148	14.51	10.6	6.0	18.5	16.6	38.9	18.8	33.5	36.7	21.1	17.2	68.9	34.9	54.2	124.6
149	14.55	10.7	4.1	14.4	16.3	30.0	21.3	37.3	32.1	37.8	61.5	57.0	52.4	65.3	208.9
150	14.59	6.4	4.0	10.5	9.5	21.8	21.0	16.6	21.7	36.5	26.2	42.5	80.8	81.6	33.0
151	14.63	2.9	1.2	5.2	10.5	23.3	10.4	22.0	46.2	24.6	22.1	68.9	50.9	41.6	25.1
152	14.66	4.1	2.1	6.0	7.1	23.9	17.0	15.3	15.1	25.0	27.0	24.4	10.6	37.2	27.7
153	14.70	6.5	2.5	7.5	10.3	13.1	16.1	22.4	32.3	40.7	33.2	29.9	27.5	30.0	37.4
154	14.73	6.0	5.3	3.6	10.4	24.5	24.1	21.6	17.0	19.2	19.4	30.9	42.9	50.1	31.7
155	14.77	4.8	3.3	11.1	12.4	27.6	11.2	15.4	34.8	42.1	21.6	25.2	22.2	77.1	52.5
156	14.81	5.5	5.0	8.3	17.0	25.3	32.7	25.4	22.2	39.8	22.0	35.4	47.4	74.4	36.6
157	14.84	5.2	3.4	7.1	16.4	33.7	24.7	22.5	44.2	22.1	40.8	48.5	93.6	26.6	63.4
158	14.88	3.9	3.6	11.2	16.1	36.2	25.4	27.4	35.8	26.2	24.7	21.7	41.4	39.0	40.2
159	14.93	4.3	4.8	10.0	7.3	27.4	28.9	18.2	22.2	37.3	21.9	23.8	33.0	46.4	58.7
160	14.97	1.7	1.8	3.4	5.6	12.2	9.7	6.8	7.7	5.8	13.0	7.3	12.5	14.6	22.3
161	15.01	3.8	2.4	13.4	26.6	31.6	32.0	31.8	15.6	24.0	12.2	13.5	76.8	46.9	54.7
162	15.05	3.1	2.9	8.4	4.9	15.8	21.6	32.8	22.7	12.5	17.7	46.0	39.1	39.8	62.2
163	15.09	5.0	3.6	6.8	12.1	35.3	49.9	15.9	37.3	34.5	39.6	44.3	63.0	25.4	61.4
164	15.13	6.5	4.1	8.0	11.3	15.0	28.2	20.0	26.2	17.3	48.3	34.3	43.7	40.7	131.1
165	15.17	5.8	3.9	6.2	23.5	32.7	26.9	28.3	19.8	35.3	52.4	58.2	50.6	63.0	77.9
166	15.21	6.5	2.8	16.6	20.8	47.2	84.2	44.3	21.3	27.4	27.9	27.6	44.0	68.8	115.0
167	15.25	5.5	3.8	16.5	31.0	59.2	22.3	60.8	44.0	66.4	24.5	54.4	54.5	68.1	84.9
168	15.29	3.4	1.4	8.0	8.1	19.0	44.6	15.8	28.3	31.8	33.4	29.8	49.6	30.3	51.3
169	15.32	5.1	2.9	13.1	18.1	39.0	34.2	34.2	43.3	34.9	63.7	42.4	37.8	81.6	59.3
170	15.36	3.3	2.3	10.0	15.2	16.2	26.2	9.4	29.0	15.5	24.0	32.0	41.1	47.8	50.4
171	15.40	8.2	2.0	13.7	12.4	21.1	36.7	41.8	40.9	16.0	25.4	45.3	33.3	35.6	43.1
172	15.44	8.3	9.8	16.9	11.4	29.6	24.4	25.0	24.9	20.4	60.5	31.2	31.0	76.1	75.6
173	15.47	14.5	9.1	35.2	22.9	69.0	82.2	79.0	63.6	63.4	83.2	100.5	82.3	101.2	245.0
174	15.51	19.5	7.7	13.0	17.4	69.7	31.6	70.5	100.1	101.0	65.2	84.1	126.0	81.9	114.2
175	15.55	4.4	3.3	12.2	38.5	95.8	64.7	39.0	59.7	68.7	51.5	70.4	95.6	147.4	180.8
176	15.58	13.9	7.5	16.1	22.3	32.7	43.2	19.3	30.1	27.0	44.8	55.7	58.7	61.2	144.5
177	15.62	10.7	4.2	21.8	21.8	54.5	42.3	40.7	43.2	51.4	39.6	45.6	54.0	120.0	77.3
178	15.65	5.1	2.1	4.2	10.0	25.9	22.8	17.7	12.9	13.6	25.2	17.4	38.5	31.8	166.2
179	15.69	8.6	4.7	17.4	8.3	28.4	27.5	26.0	32.2	53.9	49.4	56.2	40.2	61.9	62.4
180	15.72	6.4	5.7	14.5	12.5	29.4	21.7	41.2	33.4	36.9	29.4	25.3	41.8	48.4	25.7
181	15.76	4.4	1.6	12.1	13.9	39.1	29.0	40.3	24.9	19.8	34.7	26.6	66.8	41.6	43.1
182	15.79	6.5	5.3	4.9	12.9	13.6	26.1	17.9	19.3	33.7	39.3	30.6	38.0	59.2	84.4
183	15.83	6.0	2.8	2.7	4.9	22.6	24.0	13.0	25.6	12.4	20.8	25.3	18.4	19.6	33.1
184	15.86	3.2	3.8	6.2	6.7	20.3	15.3	12.0	23.0	11.0	34.7	6.4	37.6	41.6	37.8
185	15.90	2.5	2.0	6.3	3.6	17.0	14.8	20.6	25.3	21.2	17.2	31.1	31.7	31.3	24.3
186	15.93	2.3	2.4	6.0	7.2	7.6	12.8	8.1	11.3	12.3	24.1	17.5	33.6	19.6	38.0
187	15.96	2.8	2.8	4.7	4.2	10.2	7.3	11.0	8.2	11.2	14.3	10.9	15.2	10.2	9.5
188	16.00	2.6	2.3	6.2	5.4	14.1	12.8	13.3	12.3	16.7	14.1	14.3	15.0	15.9	20.1
189	16.05	2.0	1.1	2.8	3.6	10.8	16.9	8.7	17.6	11.4	13.3	22.6	21.5	20.4	34.0
190	16.08	5.5	3.1	9.2	9.0	25.8	30.3	24.2	20.6	14.3	24.5	19.8	30.9	49.1	42.6
191	16.12	3.0	3.7	8.1	6.2	16.1	25.9	15.2	16.8	8.6	22.8	11.9	17.9	22.8	23.3
192	16.15	4.5	4.0	4.4	12.2	7.3	13.2	21.3	16.5	15.6	14.0	14.7	29.7	40.5	24.7
193	16.19	7.7	6.7	6.0	13.1	25.8	35.1	31.3	21.4	21.1	19.3	17.9	31.8	32.0	62.6
194	16.23	4.9	5.5	7.2	8.2	21.2	24.7	21.3	32.5	20.1	40.4	35.8	55.5	47.0	78.6
195	16.27	4.0	2.2	17.6	14.5	29.3	34.7	32.2	36.9	30.7	34.1	20.8	42.2	30.6	82.3
196	16.31	6.9	4.1	12.3	42.5	74.8	46.7	21.6	29.2	45.5	24.6	59.6	63.7	94.3	61.0
197	16.34	9.7	8.6	13.2	8.6	41.5	34.1	54.4	20.0	16.9	49.5	33.7	54.9	31.4	70.2
198	16.38	5.4	3.8	10.0	18.2	50.1	39.1	32.7	43.6	21.9	17.4	29.6	35.1	61.6	112.9
199	16.42	7.3	4.2	9.2	7.8	31.7	55.3	37.6	21.6	25.3	32.0	29.6	66.2	36.2	91.4
200	16.46	11.0	41.6	53.5	69.9	56.6	48.1	72.7	32.8	118.6	39.5	170.0	34.0	102.5	107.3
201	16.50	6.1	2.8	13.3	9.8	62.0	43.7	12.2	24.6	37.6	56.5	39.2	57.7	62.2	44.8
202	16.53	2.8	3.3	9.2	8.5	39.4	30.7	15.2	12.6	39.1	28.7	30.7	56.2	48.4	75.7
203	16.57	6.1	2.2	9.0	8.2	29.5	29.1	31.1	29.8	34.8	35.3	69.7	59.7	28.4	54.7

204	16.62	8.4	4.1	12.2	26.5	71.3	42.1	25.1	14.2	38.8	44.4	57.6	20.2	46.7	51.5
205	16.66	6.4	3.3	9.1	7.8	30.8	20.7	27.3	17.3	18.4	33.1	30.6	35.0	59.4	80.2
206	16.69	11.8	5.0	12.1	20.6	24.2	24.2	35.3	23.3	24.3	38.5	35.9	46.5	46.4	84.2
207	16.73	10.4	10.2	22.3	15.2	24.2	48.6	51.2	39.2	28.2	23.6	28.0	56.4	70.4	84.1
208	16.76	12.1	8.8	31.4	13.0	25.2	32.4	42.3	39.9	39.5	35.2	86.0	74.2	91.8	144.7
209	16.80	8.6	3.9	13.2	9.6	39.1	36.2	37.3	32.8	22.7	60.9	44.2	41.6	34.2	54.7
210	16.84	6.3	4.3	11.5	13.4	28.6	30.5	20.2	15.0	33.5	43.7	35.2	48.8	70.0	26.4
211	16.88	3.8	4.2	14.0	21.8	31.2	20.1	42.3	38.4	27.6	40.7	36.6	47.7	38.5	57.3
212	16.91	5.1	1.9	4.3	8.2	14.1	24.6	15.3	27.1	30.3	41.4	37.4	26.9	35.7	58.9
213	16.95	3.0	1.5	6.3	5.8	15.5	8.9	14.6	22.9	13.7	21.2	23.5	41.8	26.0	46.9
214	16.99	2.0	1.6	7.1	10.0	18.0	13.2	10.6	12.9	13.2	9.9	19.2	16.2	16.1	27.0
215	17.04	2.4	2.9	2.8	11.8	30.2	24.7	17.6	19.3	15.1	35.7	27.0	23.8	28.0	23.2
216	17.08	5.6	2.8	9.4	9.3	16.4	17.2	7.4	10.6	20.5	21.0	11.2	25.0	30.9	77.3
217	17.13	2.8	2.3	15.7	12.3	23.7	17.9	28.1	16.9	11.0	10.1	29.6	38.9	51.5	19.4
218	17.17	4.6	2.4	11.1	11.9	15.4	17.5	20.3	7.8	17.3	16.9	9.9	72.8	24.4	47.0
219	17.21	2.6	1.4	4.8	8.8	25.1	21.7	15.2	7.6	12.8	14.5	21.5	33.7	22.0	25.3
220	17.25	2.3	2.9	3.6	3.5	5.7	9.4	7.2	6.1	6.0	8.8	6.9	20.6	12.6	10.7
221	17.30	16.0	8.7	10.9	16.9	28.7	46.9	47.4	52.1	47.0	29.9	31.2	49.1	40.7	35.9
222	17.34	2.1	2.8	5.5	8.4	13.8	10.8	22.4	19.1	14.1	20.7	18.5	26.3	41.6	35.4
223	17.37	5.7	4.5	5.8	6.1	32.6	13.8	11.7	28.4	17.5	28.6	31.4	92.3	35.5	35.6
224	17.41	4.4	3.4	10.4	14.1	21.4	25.0	32.7	13.1	12.4	32.7	36.1	50.3	8.4	128.4
225	17.45	5.2	4.8	12.0	11.1	16.5	26.2	25.6	47.5	21.1	44.3	53.8	63.1	71.5	64.6
226	17.50	8.5	3.8	6.5	10.3	23.8	43.2	30.2	40.0	29.1	27.9	52.5	98.8	44.9	90.7
227	17.54	3.8	7.6	10.7	7.2	27.6	29.0	31.3	19.3	26.0	24.7	19.6	42.0	34.1	59.5
228	17.58	7.5	8.5	10.2	18.2	44.5	39.5	43.2	20.8	37.9	44.0	49.4	23.3	122.9	50.6
229	17.62	4.8	4.4	23.4	18.2	44.2	40.1	48.3	44.9	63.2	21.8	43.9	93.9	72.9	100.5
230	17.66	9.1	7.9	13.4	25.5	25.7	37.5	39.2	41.9	34.2	48.1	57.5	62.1	50.8	98.6
231	17.70	2.2	1.9	7.5	4.8	10.0	30.1	21.1	31.8	22.8	15.7	12.6	46.6	39.0	181.5
232	17.74	5.9	3.4	14.4	18.3	26.9	29.5	15.5	16.6	23.5	32.6	24.7	27.3	18.8	33.6
233	17.77	5.0	1.1	7.2	12.1	23.5	38.6	29.2	15.3	29.7	24.9	28.5	40.6	73.7	38.3
234	17.81	2.4	2.8	5.8	10.6	9.3	18.6	16.7	30.0	23.7	32.4	24.8	57.1	40.5	78.4
235	17.85	6.1	2.6	10.8	9.4	46.9	33.3	36.1	20.6	27.0	37.0	44.7	26.0	52.6	31.1
236	17.89	11.0	3.8	12.4	14.6	28.5	32.0	16.2	34.4	39.0	48.9	51.0	57.6	42.7	75.6
237	17.93	10.5	1.6	9.0	13.4	21.5	53.1	30.1	28.4	25.5	29.3	36.6	110.8	64.0	78.6
238	17.97	4.7	3.4	14.4	15.0	34.6	29.7	39.4	49.3	46.3	30.1	12.8	47.9	55.8	53.5
239	18.02	4.9	3.5	11.7	9.7	21.3	50.8	60.1	22.6	15.7	16.3	51.4	74.1	56.5	59.2
240	18.06	5.3	2.5	17.3	13.4	30.5	26.5	19.5	16.2	50.6	25.5	50.2	58.1	52.4	53.9
241	18.10	7.5	6.0	3.3	16.6	39.3	41.7	31.1	32.0	25.0	24.7	37.0	72.6	32.2	76.8
242	18.15	20.1	1.7	3.5	2.3	22.3	30.3	18.1	38.2	10.9	10.8	24.5	24.4	25.7	44.5
243	18.19	5.5	3.4	8.9	10.0	24.4	14.9	25.3	45.3	14.5	50.8	19.1	64.3	82.6	54.0
244	18.23	3.0	3.4	10.3	8.9	17.6	24.8	23.6	29.5	29.0	21.9	27.4	33.7	33.7	16.3
245	18.27	4.1	2.0	6.3	9.9	11.4	9.8	24.9	6.4	18.1	8.6	17.9	23.6	35.6	35.2
246	18.32	8.0	3.7	9.0	13.7	20.4	19.8	32.1	30.6	11.2	26.2	27.4	36.1	27.8	59.9
247	18.35	132.1	108.7	118.8	128.5	65.0	52.1	67.6	97.2	87.8	79.6	114.2	107.7	87.8	110.6
248	18.37	5.4	5.1	11.8	14.4	41.5	40.1	33.5	25.8	31.8	37.6	27.2	36.7	36.6	71.4
249	18.45	7.6	4.4	13.0	35.8	79.6	43.0	75.8	50.3	75.0	81.2	44.0	89.4	109.5	163.5
250	18.49	13.0	7.7	35.7	45.1	64.8	70.5	42.3	71.2	88.6	134.9	91.0	111.5	159.0	117.0
251	18.53	12.1	9.2	33.6	33.8	49.6	59.5	115.1	58.8	84.2	76.4	245.0	166.4	84.3	159.3
252	18.57	18.4	12.0	25.0	26.2	46.4	30.8	46.2	27.9	79.3	44.8	124.5	68.2	127.7	147.6
253	18.61	8.5	6.4	6.0	27.1	34.7	56.7	46.1	38.7	51.2	30.5	75.2	95.4	19.5	162.3
254	18.65	9.0	4.5	10.4	24.8	23.3	21.5	31.9	52.7	42.7	15.8	33.6	49.1	32.9	11.5
255	18.69	5.9	5.3	13.2	15.6	37.3	38.8	17.6	12.6	14.8	48.7	58.5	26.7	25.9	44.2
256	18.73	3.9	2.5	8.5	10.7	13.4	16.0	3.5	23.8	11.3	9.5	27.6	24.0	28.2	26.8
257	18.77	4.5	3.4	8.2	11.6	31.6	27.6	17.1	25.5	15.6	25.9	24.8	49.1	34.3	55.2
258	18.80	8.1	3.4	8.9	22.1	27.3	27.1	36.9	21.9	23.0	16.9	24.7	32.1	42.7	36.1
259	18.84	2.5	2.4	15.4	9.1	24.8	29.6	16.5	24.6	29.3	20.4	22.7	40.9	26.4	34.8
260	18.89	2.9	1.6	11.6	12.4	37.5	6.2	25.5	20.8	15.7	24.9	25.7	29.0	47.1	160.8
261	18.93	4.7	3.2	9.3	15.7	31.8	34.7	27.4	31.2	26.0	29.3	29.2	17.8	39.4	70.2
262	18.97	4.2	1.8	6.9	18.7	38.6	13.3	13.7	24.2	41.3	44.4	26.3	33.2	72.2	54.0
263	19.03	7.2	65.7	8.1	22.1	39.0	37.2	31.0	21.7	34.2	24.4	41.4	51.7	82.5	68.7
264	19.07	6.1	2.6	10.6	11.9	27.6	22.3	17.2	21.3	21.0	41.9	48.3	39.0	22.2	47.7
265	19.11	3.0	2.1	6.9	10.9	19.5	13.7	18.5	16.3	18.5	21.8	24.8	27.7	27.5	25.1
266	19.15	5.6	4.3	5.3	11.4	14.8	33.2	23.0	32.9	14.0	17.5	32.2	48.6	23.5	36.7
267	19.20	5.0	3.6	8.8	10.8	18.5	39.9	19.9	19.8	22.1	25.5	29.7	18.8	30.3	63.4
268	19.24	7.4	4.0	8.3	20.6	27.5	22.7	32.6	34.9	34.2	20.8	28.5	51.3	41.0	81.3
269	19.28	17.6	3.1	9.7	14.0	27.7	43.0	29.8	20.4	17.5	29.6	25.8	37.9	76.2	79.3
270	19.32	3.7	2.1	13.2	11.2	38.2	27.2	43.4	13.8	24.8	16.5	51.9	38.0	74.0	60.7
271	19.36	4.1	3.8	8.5	9.7	23.9	15.8	28.8	26.6	13.4	34.4	37.2	24.0	47.4	54.1
272	19.41	1.1	1.9	5.0	3.9	15.0	6.2	8.0	6.4	10.9	12.1	9.9	13.7	11.9	40.6
273	19.45	3.2	2.9	7.4	7.3	15.9	18.4	11.5	19.3	19.7	9.1	16.1	10.6	17.8	49.0
274	19.49	3.3	2.0	2.6	5.1	12.2	16.2	28.3	14.7	18.5	30.8	40.8	30.7	35.0	35.4
275	19.53	3.3	3.0	5.9	8.3	21.4	17.0	17.9	7.5	14.5	23.7	10.9	18.9	22.0	38.4
276	19.57	2.8	1.8	4.4	9.7	13.4	11.4	18.8	21.4	10.6	13.5	17.1	24.6	17.0	25.6
277	19.61	6.2	4.1	12.2	10.8	27.6	16.7	9.1	21.3	19.9	36.4	28.2	38.6	15.9	41.9
278	19.65	3.8	3.3	11.1	9.7	11.3	26.4	13.7	23.8	14.7	18.8	19.9	26.3	23.6	68.1
279	19.69	5.3	2.0	5.9	8.8	15.7	15.5	19.6	15.8	9.3	24.3	29.0	16.9	35.9	102.8
280	19.73	9.5	4.3	10.4	13.7	26.7	16.1	35.6	34.5	30.0	31.9	26.7	39.1	20.6	71.8

281	19.77	11.0	5.7	12.2	19.5	37.7	27.4	40.9	23.7	39.8	16.6	61.2	26.6	97.7	61.4
282	19.80	17.9	9.0	17.7	45.7	28.9	34.2	47.4	21.1	50.8	66.1	86.4	53.0	72.1	120.5
283	19.84	2.4	5.8	23.2	30.7	24.8	33.8	32.2	36.0	65.3	37.8	47.0	44.2	69.4	36.8
284	19.88	4.9	4.3	6.5	8.5	27.8	27.9	10.3	17.0	22.2	39.8	13.2	24.8	36.2	52.0
285	19.91	4.0	3.5	11.9	12.5	23.8	33.1	12.4	30.4	23.9	25.4	46.1	40.9	54.8	55.9
286	19.95	3.5	2.8	9.0	7.3	6.7	20.7	13.3	16.0	16.0	21.0	6.9	48.7	24.5	33.8
287	19.99	5.1	2.5	8.1	6.7	21.8	19.1	21.7	21.7	21.3	28.1	50.1	16.8	34.1	32.5
288	20.05	2.1	2.7	12.7	10.3	31.4	25.5	34.8	18.2	16.2	26.8	29.1	21.2	20.5	38.9
289	20.09	3.0	3.7	7.7	5.4	20.8	13.8	23.8	11.1	10.7	9.9	25.9	24.0	36.7	32.2
290	20.13	8.6	3.8	5.6	8.8	22.3	14.0	12.4	17.0	15.3	18.5	19.8	17.6	28.1	21.3
291	20.17	4.6	2.5	3.5	9.2	15.0	16.7	20.8	14.7	4.5	14.4	23.4	20.7	16.0	17.0
292	20.21	4.4	4.0	5.7	9.0	30.1	29.0	27.4	29.2	33.9	30.7	15.6	21.7	25.6	67.6
293	20.26	5.9	6.7	8.5	7.4	42.2	30.7	19.5	21.2	52.4	32.3	51.2	54.3	63.4	71.4
294	20.30	10.5	3.5	9.1	22.8	12.4	32.2	22.0	17.0	32.8	18.9	24.1	45.2	40.1	37.2
295	20.34	3.8	4.0	9.0	8.7	23.1	23.7	16.2	21.1	26.8	21.3	8.1	15.7	24.8	29.6
296	20.39	5.8	5.8	6.4	3.9	15.8	28.9	18.3	17.6	17.5	16.1	21.4	33.3	40.9	39.4
297	20.43	7.8	7.7	6.5	7.0	21.3	24.9	23.7	15.6	20.0	10.7	20.7	27.3	36.3	35.9
298	20.47	3.9	6.4	7.8	15.3	13.3	22.7	20.3	23.3	18.2	31.6	18.5	24.1	37.9	30.6
299	20.51	5.0	6.4	7.0	10.8	16.5	14.0	8.9	21.1	19.8	17.2	31.7	20.3	43.6	44.5
300	20.55	3.9	3.5	5.2	7.9	31.9	11.7	12.3	20.3	20.3	25.5	22.3	31.3	38.5	40.0
301	20.59	10.3	5.4	11.8	7.8	40.3	36.9	21.0	22.7	24.3	46.6	61.7	29.4	39.0	78.8
302	20.63	2.3	3.1	4.3	6.9	13.4	16.7	14.0	16.9	19.8	17.3	17.0	23.4	39.1	21.5
303	20.67	2.9	2.9	3.8	11.7	30.5	16.8	24.9	20.6	13.7	32.1	18.8	25.3	39.0	43.0
304	20.71	4.2	3.2	9.4	6.7	13.9	12.5	23.3	7.0	16.2	24.7	25.8	22.4	23.9	85.1
305	20.75	3.5	3.7	7.5	8.9	22.7	20.7	16.4	21.1	10.9	16.7	35.0	47.9	27.6	60.6
306	20.78	5.1	3.7	10.6	8.7	23.2	19.5	21.4	32.6	16.4	16.5	27.2	39.8	15.4	48.1
307	20.82	7.1	2.0	10.5	6.8	19.7	18.2	19.6	10.1	21.8	10.8	21.9	53.6	18.3	33.1
308	20.86	3.8	3.3	6.0	9.3	10.3	15.3	33.9	11.1	25.6	24.7	18.3	37.1	41.1	56.5
309	20.90	6.9	6.8	11.1	13.3	21.0	17.2	25.3	11.7	35.2	12.0	24.3	33.0	41.8	28.3
310	20.95	2.9	2.6	4.9	9.0	16.9	23.8	23.0	7.0	19.7	16.3	31.2	17.5	13.7	31.4
311	20.99	3.8	0.9	6.3	6.3	20.2	27.6	12.5	8.0	24.3	21.1	16.6	25.6	19.5	51.7
312	21.04	3.8	2.2	5.8	9.2	8.2	4.6	13.6	14.5	10.9	19.3	17.7	17.3	31.0	22.9
313	21.08	6.3	5.7	7.6	8.6	23.5	39.3	17.1	16.3	34.0	30.7	21.6	36.4	30.9	43.6
314	21.12	3.8	3.4	9.9	7.0	13.4	46.6	38.9	21.8	24.1	24.5	23.3	61.9	53.6	102.1
315	21.15	5.0	4.2	9.8	7.8	15.3	18.1	18.8	32.8	25.3	22.3	29.9	47.2	19.4	26.8
316	21.20	4.1	3.8	19.5	14.5	43.2	36.7	22.8	39.5	11.8	30.1	31.7	32.6	52.3	67.5
317	21.24	10.1	6.9	20.1	20.5	59.1	50.1	42.0	38.3	45.5	53.2	59.7	67.5	52.7	29.3
318	21.28	13.7	5.5	16.8	15.3	49.3	34.5	36.1	29.3	38.3	40.8	74.2	64.2	39.7	115.3
319	21.32	5.7	5.0	16.1	15.5	45.9	54.7	38.5	17.9	49.1	59.5	81.0	74.8	59.4	76.8
320	21.36	7.3	2.0	5.9	15.0	39.1	31.4	33.9	24.0	41.1	27.5	59.2	60.5	109.0	87.9
321	21.40	7.2	6.3	9.7	14.7	45.1	28.8	42.8	32.4	38.7	32.8	20.5	22.0	32.5	51.5
322	21.44	6.2	4.7	9.6	11.3	21.7	45.0	16.2	21.8	9.9	29.2	22.6	22.7	49.4	64.8
323	21.48	3.8	2.7	5.9	13.3	20.5	7.4	16.4	22.0	18.5	11.2	17.9	24.0	34.6	29.9
324	21.52	5.1	5.6	7.8	4.6	14.6	11.8	11.8	19.0	14.8	21.3	20.9	13.7	35.3	36.3
325	21.56	5.6	3.6	10.1	4.9	21.0	11.5	29.3	27.1	12.2	13.8	29.2	29.6	23.3	41.8
326	21.61	3.4	2.2	5.4	7.1	12.1	21.2	8.1	8.4	20.4	18.1	17.7	43.6	27.2	25.8
327	21.64	4.7	6.3	8.1	10.2	13.7	13.2	13.7	16.2	16.1	5.3	18.0	45.4	21.4	30.0
328	21.68	3.2	3.2	6.9	8.0	24.0	23.6	17.7	9.2	25.6	23.8	19.2	20.6	46.4	55.9
329	21.72	6.4	3.0	5.9	8.0	14.5	23.5	14.1	15.7	21.4	24.5	11.6	18.7	41.9	42.1
330	21.76	6.7	5.6	9.8	8.0	37.7	27.1	24.9	27.9	17.2	25.3	19.3	37.2	23.5	18.6
331	21.80	6.4	1.9	5.7	17.6	16.0	26.8	20.7	15.4	18.2	29.8	25.6	37.4	37.7	52.1
332	21.84	2.0	3.6	10.2	8.9	27.0	27.6	17.8	17.2	27.8	22.0	17.5	15.9	46.7	47.4
333	21.88	4.0	5.0	12.9	13.0	39.6	13.3	26.6	43.6	19.6	35.3	17.9	63.4	37.4	58.7
334	21.92	9.8	2.0	10.6	10.2	44.4	17.4	13.8	31.3	33.9	36.2	36.3	37.2	63.0	34.7
335	21.96	6.2	2.9	5.4	11.5	36.9	30.7	22.3	33.9	19.0	18.4	26.5	54.7	43.4	42.7
336	22.02	4.0	2.5	6.2	8.4	13.0	16.5	30.6	14.4	9.6	17.9	33.5	38.1	67.2	203.5
337	22.06	4.6	3.3	4.4	6.7	12.0	7.2	21.8	14.1	25.8	18.6	15.5	16.5	32.6	50.8
338	22.10	2.3	2.2	4.8	7.1	16.5	9.5	14.6	15.6	10.5	14.8	16.9	21.2	24.5	24.2
339	22.14	6.7	3.4	5.9	6.2	12.4	35.1	6.1	17.3	12.9	19.4	12.3	29.4	22.6	31.8
340	22.17	3.3	2.7	3.1	3.3	26.5	12.7	10.5	12.5	15.5	22.1	12.5	23.2	12.6	33.3
341	22.22	7.3	7.3	21.8	22.5	33.9	51.9	28.0	21.9	33.1	24.8	74.4	53.5	83.9	93.3
342	22.25	9.6	5.3	18.3	23.0	40.5	62.5	56.2	44.6	69.8	29.6	101.4	98.3	47.3	82.0
343	22.30	12.3	7.2	13.5	21.5	47.0	27.8	43.2	19.9	44.0	45.0	32.3	29.4	71.2	44.2
344	22.33	5.8	2.7	16.6	19.9	27.1	26.2	29.9	30.2	24.1	29.0	47.7	41.4	42.9	39.0
345	22.37	6.7	8.8	17.2	21.7	42.2	27.2	23.7	45.3	47.3	42.2	53.2	89.1	55.5	94.1
346	22.40	2.7	5.3	14.9	26.2	24.3	49.4	16.0	15.0	50.2	28.2	36.9	57.5	66.9	64.2
347	22.44	2.7	5.4	10.5	3.4	24.1	32.3	28.6	46.4	27.2	18.3	20.2	37.9	49.9	62.1
348	22.49	7.7	2.1	7.2	7.5	22.2	34.0	25.8	29.0	21.8	38.2	42.1	38.5	24.6	114.6
349	22.53	10.0	8.5	7.1	18.8	27.2	43.5	36.6	28.8	29.5	35.8	41.3	34.5	46.8	65.5
350	22.56	7.3	6.7	7.0	19.4	41.0	38.4	29.1	8.7	21.8	30.3	36.5	55.7	41.0	48.9
351	22.60	5.5	6.6	15.6	10.4	21.0	21.7	38.3	20.1	18.6	32.6	22.5	36.9	49.9	36.9
352	22.64	4.0	3.9	8.2	5.8	23.3	18.8	19.4	10.6	9.3	20.7	15.2	22.6	25.3	57.7
353	22.68	6.6	5.7	6.3	11.6	13.5	25.9	14.3	11.6	22.5	15.4	6.8	28.6	31.2	27.9
354	22.71	6.7	3.7	9.7	8.1	22.8	27.0	24.8	15.3	38.2	25.6	48.3	40.5	50.1	68.9
355	22.75	9.3	6.2	7.6	10.9	26.4	36.0	40.5	25.3	28.6	24.9	39.2	69.7	48.5	55.0
356	22.78	4.4	3.2	9.2	5.7	31.8	28.0	22.1	15.4	18.6	21.3	23.0	29.1	34.6	55.0
357	22.82	8.4	6.7	6.0	8.6	15.7	22.1	19.1	20.9	17.1	12.2	29.8	51.9	25.6	58.2

358	22.85	6.1	1.2	9.1	17.1	32.3	25.5	41.9	29.8	19.6	36.5	24.6	58.6	38.9	70.3
359	22.89	7.4	6.0	5.7	19.4	40.8	44.2	51.9	33.3	60.5	17.1	56.7	35.1	67.5	138.5
360	22.94	7.9	2.0	17.1	14.4	34.6	34.4	19.7	30.9	31.5	33.5	37.5	74.4	38.8	50.9
361	22.99	5.7	2.2	10.4	6.9	20.2	5.5	30.9	24.6	34.8	33.6	34.1	60.9	29.5	43.1
362	23.04	5.3	4.5	11.5	12.2	20.9	54.5	31.5	23.4	29.3	30.6	48.0	57.3	25.8	58.8
363	23.08	4.4	4.9	7.8	11.2	19.8	27.3	31.4	23.8	25.8	23.5	41.8	49.7	31.3	88.8
364	23.12	6.8	3.9	7.2	8.3	33.8	34.1	23.5	18.6	35.9	53.4	33.0	41.0	67.0	45.9
365	23.16	7.8	6.8	13.1	5.6	39.4	30.5	40.3	40.6	42.4	40.6	45.0	50.6	57.7	68.0
366	23.21	7.1	1.5	12.9	8.2	48.9	24.3	46.2	31.5	60.5	24.0	54.2	69.3	45.0	89.6
367	23.25	9.1	7.1	14.3	18.3	23.0	20.6	28.7	25.5	26.5	22.0	56.1	49.5	69.9	63.4
368	23.29	4.4	3.0	9.2	7.8	29.4	20.0	23.2	33.8	11.3	39.6	37.0	34.4	33.5	49.1
369	23.34	6.2	6.6	14.2	20.8	26.2	20.7	22.0	28.0	24.9	17.0	54.1	37.7	93.1	38.2
370	23.38	7.2	4.4	14.4	6.0	18.7	14.5	21.8	18.3	15.8	27.6	33.2	15.2	24.6	43.9
371	23.41	3.2	3.5	3.6	4.8	22.5	31.3	26.9	27.4	19.1	15.3	19.1	27.4	26.4	15.3
372	23.44	6.4	2.9	11.8	12.0	16.0	16.0	19.1	20.2	13.4	27.6	21.9	18.3	43.0	37.5
373	23.48	7.3	1.7	4.2	8.2	12.2	9.8	8.7	13.5	14.0	16.9	15.6	27.6	41.6	43.8
374	23.52	7.8	5.5	8.3	4.3	33.6	21.3	22.1	32.6	24.0	44.0	27.2	19.1	26.6	85.6
375	23.56	5.1	3.5	11.6	7.1	17.7	30.1	20.0	27.4	15.1	28.2	25.3	46.2	34.8	25.8
376	23.60	2.7	2.1	8.5	5.9	30.3	15.7	14.4	27.1	29.0	28.5	21.0	14.3	24.1	33.0
377	23.64	6.3	7.6	6.5	13.7	29.5	36.8	46.0	39.9	19.8	10.6	29.3	30.7	29.6	38.8
378	23.68	2.9	3.4	4.6	7.0	14.7	17.6	14.4	17.5	16.9	18.4	11.4	24.6	11.6	19.6
379	23.73	4.8	4.1	12.0	8.4	10.6	19.0	9.2	20.5	29.6	25.0	30.7	33.7	72.0	75.2
380	23.77	3.8	1.4	6.7	4.5	9.8	27.7	6.7	22.2	16.2	16.6	21.5	51.3	44.3	44.2
381	23.81	3.8	5.1	10.1	5.2	13.3	13.7	8.1	16.4	26.6	35.6	26.9	42.6	15.1	20.6
382	23.84	5.9	1.3	8.0	5.1	15.5	11.4	10.2	18.2	14.2	17.1	33.3	46.7	47.6	40.7
383	23.87	4.3	4.2	8.9	4.3	38.5	44.7	16.6	45.9	43.8	36.6	44.1	46.1	24.9	51.1
384	23.91	4.0	4.6	17.3	13.7	18.2	31.6	26.9	11.6	32.8	25.4	47.1	35.6	95.6	243.0
385	23.95	5.3	3.2	3.5	6.8	9.2	15.2	6.5	6.9	21.9	21.7	36.6	24.9	44.2	37.5
386	24.02	8.1	2.0	13.8	21.2	26.9	34.3	40.5	26.4	35.4	35.6	36.1	53.8	44.7	103.0
387	24.06	10.3	1.9	21.8	16.5	50.8	34.8	54.8	39.0	29.4	41.8	33.7	69.5	43.8	60.5
388	24.10	5.7	4.7	11.6	10.2	17.5	15.5	24.8	22.8	24.6	18.9	18.5	42.6	31.2	47.4
389	24.14	4.4	3.7	10.8	11.1	29.9	20.8	29.2	45.3	51.6	36.4	38.4	53.6	98.5	62.0
390	24.18	6.2	4.5	3.5	5.1	15.4	19.3	21.2	25.4	12.6	18.0	23.2	13.1	57.4	33.0
391	24.21	7.4	6.0	8.5	17.2	17.8	20.7	34.2	53.8	40.3	40.2	28.0	68.0	30.4	47.4
392	24.25	8.1	1.8	14.7	10.6	25.8	30.0	28.9	14.0	34.2	24.6	48.0	35.6	56.9	55.2
393	24.30	2.3	2.1	6.6	6.7	28.1	15.6	19.9	24.5	16.8	16.9	23.9	36.5	32.8	27.2
394	24.34	1.7	4.0	7.3	8.1	17.7	22.0	12.4	23.8	10.7	24.8	24.1	49.2	23.2	39.3
395	24.37	3.6	2.7	3.7	6.2	14.9	16.9	20.7	26.3	11.5	17.3	11.7	38.2	18.0	44.6
396	24.41	4.4	1.1	4.0	6.5	13.8	11.8	16.8	20.7	7.5	14.9	23.2	32.4	29.9	43.5
397	24.45	7.3	3.3	12.3	7.1	11.3	14.3	14.1	33.1	24.3	18.4	45.3	46.0	37.1	54.7
398	24.49	2.7	5.3	8.6	5.2	33.6	26.1	27.0	10.0	20.3	17.2	27.1	54.5	19.8	42.0
399	24.53	6.0	2.9	17.8	10.5	46.4	41.9	21.9	32.7	35.5	22.5	28.6	60.3	31.9	84.4
400	24.56	4.7	5.5	9.1	21.6	22.4	15.9	36.3	24.0	16.8	20.5	21.2	37.5	50.7	54.2
401	24.60	4.3	5.2	12.3	9.7	22.6	36.6	40.4	28.1	34.8	24.1	32.2	45.6	73.0	54.2
402	24.64	4.4	3.2	3.0	8.4	9.6	20.9	22.1	12.1	20.7	9.9	28.2	40.4	19.5	43.9
403	24.67	5.4	2.6	9.0	4.6	17.9	17.5	14.2	15.1	21.9	26.1	27.2	28.6	41.7	41.2
404	24.71	7.5	2.3	13.7	10.5	31.3	17.7	20.7	29.5	20.5	33.3	15.2	19.2	36.5	92.4
405	24.74	4.1	3.2	9.0	11.9	36.9	12.6	17.9	40.4	24.0	58.5	33.7	51.5	41.1	59.8
406	24.78	12.0	3.9	20.8	23.4	25.9	19.8	53.9	43.4	49.5	29.5	56.0	65.6	164.1	90.7
407	24.81	9.9	1.9	8.3	16.3	25.5	23.3	34.9	13.1	13.6	38.6	19.4	58.7	91.1	43.6
408	24.85	5.6	6.2	10.8	14.6	72.9	33.8	46.3	38.7	41.1	18.3	32.3	63.5	56.3	66.7
409	24.88	13.5	4.8	15.0	14.5	17.2	38.9	40.5	37.2	30.5	37.1	24.6	36.2	43.8	78.8
410	24.92	6.2	3.3	12.7	9.5	33.0	49.8	15.0	18.1	44.0	30.4	35.8	52.2	50.7	69.1
411	24.97	2.8	3.9	12.2	10.3	19.0	12.8	25.9	22.2	22.2	18.3	21.0	49.4	22.4	27.0
412	25.03	1.7	3.0	5.5	9.6	39.6	21.3	21.4	17.6	15.4	32.4	21.4	23.1	24.9	38.1
413	25.07	4.9	1.9	11.9	7.6	24.9	29.0	19.3	23.4	29.8	12.2	32.2	38.2	52.2	44.1
414	25.11	3.1	3.5	5.0	7.7	15.2	20.3	10.4	9.9	20.0	13.3	12.7	30.8	35.7	26.9
415	25.16	6.6	6.5	10.7	13.3	28.9	36.6	44.4	12.2	50.4	93.7	41.4	83.7	18.3	69.8
416	25.20	8.0	7.3	10.3	9.0	37.4	46.8	12.8	28.2	29.1	42.2	16.0	24.4	65.2	52.8
417	25.23	3.4	3.1	8.5	11.1	11.9	39.3	16.9	56.7	23.5	25.5	33.8	30.2	34.1	46.5
418	25.27	8.8	4.6	17.5	19.3	38.3	23.3	41.4	37.2	50.7	43.6	61.0	37.6	81.4	60.2
419	25.31	15.9	11.0	24.2	28.0	51.9	32.9	51.1	34.8	45.2	39.6	30.4	56.8	38.9	144.2
420	25.35	11.5	10.2	9.5	12.0	28.9	17.5	34.3	30.9	39.4	56.5	39.9	81.4	72.7	72.0
421	25.39	7.1	8.0	18.9	12.4	38.4	26.7	31.4	16.7	54.9	59.3	51.5	44.5	19.8	62.9
422	25.43	4.9	3.7	11.7	7.2	21.2	11.9	29.0	27.3	22.3	33.3	54.4	61.9	30.9	71.2
423	25.48	9.5	4.0	5.2	18.5	33.4	35.6	28.3	28.7	29.6	62.0	50.1	44.6	51.8	47.1
424	25.52	4.9	4.3	5.2	6.0	11.3	19.9	22.1	24.5	15.3	9.8	25.0	20.2	49.4	53.3
425	25.55	6.2	3.9	9.4	27.8	17.5	56.0	34.8	36.0	39.8	51.8	63.6	78.2	81.8	37.3
426	25.58	5.2	6.1	7.0	10.5	24.7	29.6	18.0	27.8	32.8	41.9	28.9	43.3	10.5	68.0
427	25.62	4.1	3.9	9.6	17.3	22.5	21.4	19.0	33.2	27.5	21.9	24.8	16.5	35.8	36.5
428	25.66	1.6	2.6	15.5	10.6	25.2	14.6	26.1	20.5	25.3	34.3	30.9	37.0	66.8	54.1
429	25.70	3.3	4.7	5.2	8.9	18.1	22.9	11.2	15.4	9.4	20.7	19.0	32.4	17.8	34.5
430	25.74	2.9	4.9	11.8	15.2	25.3	27.9	31.4	25.0	41.3	22.8	44.0	91.0	54.8	240.1
431	25.77	3.0	6.5	5.1	7.2	21.0	21.7	10.9	20.7	10.5	25.8	16.2	22.6	25.7	24.0
432	25.80	5.1	2.2	8.3	11.7	17.7	26.5	28.5	16.7	30.3	34.9	53.2	60.1	56.4	76.0
433	25.83	15.6	4.7	29.7	19.5	58.1	34.8	26.7	44.7	59.0	28.7	64.3	55.9	97.7	95.4
434	25.87	5.4	1.6	7.4	15.3	39.7	25.1	19.7	31.4	30.9	20.8	34.3	46.3	49.0	128.9

435	25.91	6.2	3.3	14.7	20.0	24.7	14.4	11.3	20.0	30.9	32.0	38.2	19.6	61.7	79.4
436	25.95	15.1	2.1	8.9	4.7	18.6	35.3	18.8	17.7	16.8	21.1	22.4	23.5	33.9	42.5
437	26.00	3.3	3.0	5.3	10.7	19.3	24.9	11.8	24.2	14.5	15.7	27.2	41.0	49.3	17.3
438	26.05	7.9	3.8	8.4	5.1	13.7	38.7	23.1	17.2	26.8	33.1	30.2	36.9	41.1	50.0
439	26.08	6.5	6.3	10.9	16.3	35.4	27.5	21.8	25.7	18.2	28.8	18.0	45.4	78.2	69.7
440	26.12	7.4	4.3	8.8	13.0	46.6	25.3	34.3	28.1	40.1	47.5	24.2	62.7	31.9	21.8
441	26.16	4.1	5.5	7.6	21.1	30.1	26.9	11.9	22.1	22.2	29.5	37.8	73.6	40.8	32.2
442	26.21	15.4	2.6	11.8	6.4	42.3	24.8	19.9	27.7	6.1	45.0	32.6	33.5	29.2	52.2
443	26.26	4.5	3.3	8.3	4.6	7.7	16.8	31.8	28.7	20.4	41.9	34.1	26.5	41.6	53.6
444	26.30	12.3	4.2	8.4	7.8	12.8	33.9	16.7	17.0	29.2	28.9	30.3	32.4	22.4	70.8
445	26.32	4.5	5.4	9.0	5.5	42.6	14.7	12.8	51.8	21.7	21.8	35.5	51.2	47.2	96.2
446	26.36	1.4	4.8	18.1	18.2	16.3	29.4	33.5	36.0	26.8	18.0	62.9	60.2	77.1	50.2
447	26.39	10.5	3.0	7.7	11.4	33.8	38.6	39.1	13.0	56.0	59.1	39.0	37.3	50.6	63.3
448	26.43	4.7	3.1	7.2	5.7	28.2	34.3	14.0	31.2	30.1	52.7	34.9	45.1	67.6	38.3
449	26.47	2.3	6.1	13.8	10.4	28.1	45.5	28.5	19.0	17.9	17.5	19.0	71.9	33.3	41.6
450	26.51	2.4	3.3	6.7	9.5	24.6	14.0	18.2	27.6	29.6	22.5	18.6	56.6	29.4	24.1
451	26.55	5.9	2.9	8.9	15.3	33.4	46.7	19.5	27.5	21.6	31.1	59.3	45.4	44.7	71.1
452	26.58	3.6	5.0	4.5	6.8	8.0	21.9	14.3	11.1	21.4	22.2	25.4	29.9	38.0	30.7
453	26.62	6.5	3.8	5.6	8.1	21.2	17.0	29.6	25.2	18.7	17.4	26.8	41.5	21.0	55.0
454	26.65	2.6	3.2	10.0	11.1	19.0	42.3	28.7	13.5	30.3	16.3	37.7	31.8	26.2	32.2
455	26.69	5.7	4.0	14.8	13.0	36.8	42.4	23.4	24.7	23.3	40.9	39.2	100.1	51.0	71.0
456	26.73	2.3	3.0	3.9	2.5	9.5	14.3	17.7	13.6	18.7	14.2	12.7	17.7	15.0	30.2
457	26.77	6.7	4.2	12.8	6.2	25.3	27.3	37.6	25.7	14.9	23.5	23.4	36.3	37.8	47.4
458	26.81	5.2	4.4	11.3	11.2	15.1	30.8	20.5	40.0	31.9	23.6	51.3	63.7	33.3	36.6
459	26.84	3.0	5.7	8.5	9.0	25.7	14.0	17.4	18.2	28.8	28.3	21.7	56.1	44.6	34.9
460	26.88	3.6	4.0	12.0	12.5	34.9	38.5	13.9	23.3	14.9	22.0	17.2	32.6	67.3	52.1
461	26.91	7.7	3.5	10.1	18.0	42.0	39.4	32.2	25.9	13.0	50.8	41.2	36.6	63.8	115.6
462	26.95	1.8	1.8	11.1	12.6	12.4	18.8	21.8	37.4	32.0	23.0	25.5	44.9	38.5	41.8
463	26.99	5.7	2.7	20.9	27.5	25.3	16.6	32.7	29.1	53.8	32.8	35.1	28.7	99.5	87.3
464	27.04	4.6	3.7	11.0	11.4	11.8	29.2	16.5	32.5	40.3	32.3	33.7	52.3	57.5	51.1
465	27.08	5.1	4.1	10.3	16.3	22.9	29.7	29.2	33.8	37.9	41.7	53.7	37.4	74.7	50.3
466	27.13	6.0	2.7	11.3	16.9	28.3	28.5	24.7	34.8	19.9	63.8	31.5	29.6	23.2	39.3
467	27.17	3.8	3.7	13.9	21.0	26.3	18.2	32.8	19.7	33.0	22.5	28.7	72.0	43.5	61.7
468	27.21	5.9	3.0	11.9	15.6	25.2	6.9	18.2	16.5	19.2	29.0	25.2	33.3	34.5	25.0
469	27.25	2.0	3.2	6.6	8.9	39.3	24.8	23.0	31.8	24.4	22.8	41.9	56.7	44.9	46.9
470	27.28	3.7	4.5	20.1	18.7	30.8	15.8	12.9	17.6	23.8	15.8	69.6	52.2	61.8	64.0
471	27.31	5.4	4.9	10.5	12.7	35.1	46.4	26.1	23.8	55.2	41.6	19.0	26.9	44.4	41.3
472	27.35	2.9	0.8	11.0	10.8	41.6	37.9	38.6	17.2	23.7	27.7	24.0	45.2	45.3	43.2
473	27.39	5.4	3.4	12.2	22.7	64.1	31.5	47.0	42.8	44.2	22.8	41.8	54.9	120.5	214.2
474	27.43	6.8	5.7	9.4	15.5	19.1	26.5	31.7	34.3	16.2	32.2	42.2	55.1	60.9	53.7
475	27.47	3.9	4.7	9.4	14.0	12.5	18.4	19.7	18.5	21.6	16.7	47.2	48.9	34.7	36.0
476	27.50	1.4	4.1	3.8	7.5	28.4	20.3	19.0	25.0	19.5	30.3	42.5	39.0	32.4	35.1
477	27.54	3.7	3.3	8.6	5.2	19.5	16.6	22.4	20.1	4.2	18.5	15.5	37.7	23.1	35.2
478	27.57	6.7	5.2	10.8	7.7	31.7	14.3	37.6	17.1	16.5	45.7	28.8	54.0	39.4	60.2
479	27.61	12.9	3.4	21.0	18.8	28.2	28.9	32.8	27.9	50.9	43.6	17.9	50.4	29.6	135.5
480	27.65	3.7	5.8	13.9	13.5	53.4	31.0	23.8	30.2	21.6	32.2	20.8	36.2	32.0	73.3
481	27.68	4.2	2.3	6.8	10.2	22.3	26.2	17.2	29.3	22.8	25.0	35.8	37.6	31.6	65.8
482	27.71	4.8	4.1	10.5	11.2	14.4	18.5	33.7	12.7	31.2	12.4	25.6	53.5	18.3	42.2
483	27.74	5.2	3.1	10.7	8.6	17.7	12.8	25.1	12.9	30.5	16.6	21.9	34.6	51.8	71.1
484	27.77	6.4	3.4	18.8	17.6	42.6	28.1	18.2	32.7	27.0	24.9	22.7	57.5	79.0	90.7
485	27.80	3.7	8.5	13.0	18.9	33.7	44.4	36.6	38.6	23.6	20.0	28.4	45.2	59.0	49.6
486	27.83	3.0	6.8	18.3	10.3	59.3	36.0	24.4	44.5	27.3	31.7	61.3	82.9	63.8	50.4
487	27.86	5.6	3.0	3.5	3.8	12.3	29.3	26.1	16.0	26.3	23.1	30.2	41.3	27.4	37.7
488	27.89	4.5	2.6	5.2	11.0	25.9	18.9	19.9	17.0	16.6	12.4	21.0	23.4	32.8	40.2
489	27.93	4.2	2.6	11.3	12.9	13.8	14.7	18.3	15.9	15.0	18.2	34.0	28.4	19.7	53.2
490	27.97	4.7	2.9	11.5	8.0	29.5	8.6	12.4	31.9	19.8	13.0	23.3	40.4	15.3	33.6
491	28.02	7.2	2.5	14.1	9.1	22.5	17.5	30.9	26.1	9.4	14.1	27.9	29.7	42.2	99.1
492	28.06	2.4	4.2	6.8	6.4	7.5	20.6	11.2	22.9	18.4	25.6	18.1	20.2	38.5	25.1
493	28.10	5.5	2.1	7.3	15.7	52.6	34.2	22.3	31.4	34.8	18.4	38.7	23.3	40.7	48.9
494	28.14	7.0	5.4	14.9	30.1	54.8	32.9	14.6	36.7	41.1	23.0	23.9	44.9	90.1	51.4
495	28.17	9.9	3.9	10.4	11.7	38.8	32.2	33.8	43.7	22.7	60.9	52.8	79.1	22.7	41.0
496	28.21	5.3	3.4	13.6	11.0	27.5	30.2	33.2	25.9	37.0	37.5	33.2	36.1	39.8	55.9
497	28.25	4.0	4.7	6.2	7.5	28.0	23.8	23.0	26.8	24.8	12.3	46.3	54.9	46.2	53.1
498	28.29	2.7	2.0	4.6	8.1	8.0	9.2	6.2	10.7	7.9	9.3	12.2	11.9	25.2	38.4
499	28.33	2.0	1.6	3.1	11.5	11.3	9.3	15.9	15.5	10.5	22.9	7.7	25.4	23.4	35.2
500	28.37	4.8	4.9	7.6	8.8	24.1	39.4	13.2	12.4	18.9	22.3	24.5	35.0	43.3	39.4
501	28.41	6.2	2.7	6.4	9.1	21.7	20.5	24.5	14.5	33.0	29.4	26.6	25.7	33.5	23.0
502	28.45	9.7	5.5	13.4	13.9	53.1	37.2	55.8	54.5	31.5	43.2	78.6	70.4	119.3	88.6
503	28.49	5.0	8.5	14.3	7.4	25.2	34.0	11.8	12.9	26.8	15.3	33.5	50.6	34.6	35.3
504	28.53	4.1	2.6	4.5	6.6	12.2	12.4	14.7	14.9	16.3	20.7	15.8	18.0	21.5	25.7
505	28.57	2.3	4.1	5.7	13.0	26.7	18.8	22.5	31.6	47.6	35.3	44.4	101.2	70.1	65.9
506	28.60	9.4	4.5	15.0	20.8	9.2	38.0	62.1	59.6	31.7	35.4	47.2	39.1	80.9	91.5
507	28.64	3.4	73.1	11.6	10.3	25.9	20.3	13.0	13.2	22.6	14.8	36.2	65.5	38.7	61.1
508	28.68	3.9	1.4	4.7	4.6	13.1	17.0	9.4	20.4	8.5	11.2	16.5	35.0	28.2	23.6
509	28.72	3.8	2.0	9.3	10.2	41.2	20.9	24.9	31.1	13.8	33.1	32.2	54.2	34.6	50.0
510	28.76	2.5	2.1	3.3	3.4	7.2	8.7	9.7	11.6	13.2	15.1	16.2	17.6	31.6	45.1
511	28.80	2.2	1.8	5.5	5.0	23.6	17.3	20.9	10.1	17.4	33.7	22.2	25.8	23.1	25.3

512	28.84	6.0	4.7	10.8	15.3	36.4	23.5	11.3	28.1	12.9	24.6	27.3	66.3	29.5	58.6
513	28.88	4.1	2.6	4.0	8.0	10.7	12.9	5.5	19.9	19.3	8.1	21.7	39.1	28.8	23.9
514	28.91	5.0	3.9	8.5	6.9	21.9	24.9	17.5	19.7	14.5	43.1	18.1	32.1	49.9	53.3
515	28.95	3.2	1.3	7.3	14.4	22.6	25.3	20.1	20.0	10.3	17.7	16.4	31.7	17.8	42.0
516	29.00	2.7	3.4	2.7	14.2	16.8	21.1	29.2	12.0	16.2	43.3	30.4	40.7	40.5	55.1
517	29.04	5.0	64.3	3.5	16.1	26.8	30.8	24.8	26.8	34.7	27.8	16.7	18.0	41.3	75.5
518	29.09	7.7	2.5	17.0	12.3	32.6	19.2	20.1	33.9	29.0	30.7	67.9	29.2	40.9	45.4
519	29.13	2.2	2.5	2.6	7.7	20.0	41.9	14.4	21.1	20.5	15.6	27.6	36.9	26.8	17.2
520	29.17	5.7	4.8	7.7	7.9	12.2	16.1	19.9	26.0	14.1	19.2	21.3	51.6	44.5	30.6
521	29.21	22.6	4.6	4.9	11.8	52.7	27.5	17.3	21.1	25.6	12.7	34.5	61.5	50.0	77.4
522	29.24	4.1	3.4	7.2	14.2	28.6	31.2	19.0	36.9	33.8	23.4	27.5	54.7	35.0	48.0
523	29.28	5.6	2.7	6.5	4.5	14.8	16.1	23.1	8.2	5.7	22.7	32.0	43.0	32.6	24.1
524	29.32	3.1	3.7	6.7	13.0	38.4	22.5	27.5	26.6	38.0	29.5	33.4	43.4	44.8	34.7
525	29.36	10.3	2.9	11.7	12.9	9.2	32.4	38.5	26.8	21.2	39.0	13.4	44.9	42.5	175.1
526	29.42	4.9	3.2	7.5	8.3	11.4	19.8	15.2	21.3	24.6	21.1	25.5	40.6	31.2	34.3
527	29.46	4.1	5.9	10.7	15.4	26.8	23.9	19.9	28.5	13.2	46.1	23.7	37.0	54.6	65.2
528	29.50	8.8	1.9	16.3	9.6	32.3	33.3	37.5	38.1	35.8	31.7	17.4	36.0	30.0	91.7
529	29.54	3.1	3.8	4.3	10.0	26.3	18.9	13.2	28.2	20.2	20.4	21.7	23.4	33.8	28.4
530	29.58	4.9	3.8	8.0	7.9	39.3	35.3	24.3	23.7	11.8	37.5	30.8	26.0	58.7	25.5
531	29.61	4.0	2.0	7.3	12.1	10.6	32.4	5.8	23.1	15.2	34.5	32.4	21.4	41.6	29.1
532	29.65	3.9	2.8	5.3	8.1	20.6	9.0	11.2	31.2	26.0	21.7	15.9	32.1	40.3	50.9
533	29.70	3.6	3.0	11.9	7.6	32.1	106.9	10.7	16.9	21.4	19.2	21.3	46.7	44.0	36.5
534	29.74	3.7	1.8	2.1	7.3	12.2	13.7	9.9	17.0	20.7	23.8	12.3	28.4	16.2	40.6
535	29.78	3.2	4.0	4.1	7.0	18.6	19.1	15.4	13.5	9.4	12.6	16.0	23.8	25.0	22.6
536	29.82	3.3	2.9	7.4	5.8	15.7	24.4	16.4	22.8	12.3	10.8	23.7	26.5	28.6	32.1
537	29.85	105.1	33.3	82.4	141.6	89.7	97.8	56.7	99.6	140.3	112.9	245.0	118.9	245.0	128.4
538	29.89	5.5	5.6	6.2	12.2	20.5	15.1	47.3	31.3	23.6	29.0	22.7	31.7	67.5	51.0
539	29.93	70.2	2.3	15.1	17.2	40.4	43.3	26.6	35.5	35.3	45.3	42.1	96.1	48.3	62.6
540	29.97	106.7	2.3	12.7	18.3	54.0	29.6	27.2	31.3	43.8	22.8	46.6	38.6	51.0	144.8
541	30.03	5.2	2.7	13.0	10.4	11.5	15.9	23.7	13.1	14.7	19.0	39.5	50.8	45.0	38.5
542	30.07	6.3	3.5	6.5	14.2	39.7	8.3	26.2	32.3	61.9	43.1	49.5	52.1	22.6	98.6
543	30.11	1.8	0.8	8.7	4.5	6.5	11.9	11.0	4.8	8.8	14.1	13.9	31.6	21.2	24.8
544	30.15	8.9	2.7	8.2	14.0	17.6	18.8	27.2	20.9	16.7	17.5	16.6	18.9	18.2	31.4
545	30.19	3.5	2.7	12.8	7.4	23.2	19.9	17.1	39.2	21.6	28.4	19.4	59.8	24.4	32.0
546	30.23	2.9	2.3	8.9	8.2	22.4	26.8	23.4	14.5	25.7	15.9	28.0	23.7	38.6	32.1
547	30.28	3.0	3.2	11.1	14.3	19.8	26.2	15.6	24.1	21.7	20.3	26.6	57.1	35.8	51.9
548	30.32	5.1	5.0	5.4	10.0	17.0	27.3	27.8	18.2	40.4	16.7	47.0	7.1	38.5	25.0
549	30.37	6.3	2.4	13.1	7.4	22.9	23.6	37.3	28.2	33.1	29.6	48.4	38.7	24.9	74.4
550	30.41	14.4	2.6	11.6	12.3	21.1	13.5	16.1	27.2	16.1	21.8	27.0	13.8	28.4	51.9
551	30.45	3.8	3.4	6.9	6.9	7.6	16.3	8.3	10.4	6.8	17.6	17.7	17.0	11.8	28.3
552	30.49	5.9	5.2	9.1	11.3	32.1	24.4	34.1	21.1	10.0	19.3	16.3	58.5	54.3	92.1
553	30.53	4.8	4.7	6.5	20.0	22.2	17.6	38.3	28.9	16.7	49.3	42.3	53.1	39.9	61.7
554	30.57	14.8	5.6	13.8	19.5	25.3	33.4	22.5	21.9	21.4	21.3	42.7	27.5	72.9	59.0
555	30.61	5.5	2.3	14.0	18.1	26.6	22.3	67.2	26.6	15.1	34.4	33.7	62.8	57.6	84.8
556	30.65	5.7	2.4	4.2	8.0	13.2	25.5	6.7	14.6	18.9	42.2	30.0	37.6	54.8	67.3
557	30.69	6.7	5.4	22.3	15.4	31.0	30.5	56.4	34.1	54.5	52.9	50.7	28.9	58.7	91.8
558	30.73	4.6	9.1	12.7	13.5	36.2	8.4	18.0	23.9	23.1	40.3	31.3	29.5	73.2	60.7
559	30.76	7.3	2.5	3.4	6.0	13.5	13.2	14.4	10.3	11.5	19.2	18.1	25.4	17.8	29.0
560	30.80	6.5	8.6	7.9	17.2	36.3	49.1	23.5	28.7	38.2	42.7	46.2	70.5	42.0	45.7
561	30.84	6.9	2.4	6.7	7.7	25.4	30.4	29.3	25.7	49.0	15.9	25.0	47.6	15.5	44.2
562	30.87	2.2	2.7	2.4	6.0	25.4	21.0	20.1	19.2	13.6	10.1	5.1	30.4	25.8	52.3
563	30.91	3.1	3.3	5.3	5.8	11.0	21.8	14.2	11.6	17.7	49.6	28.2	29.4	44.9	70.5
564	30.95	1.9	0.8	12.0	12.8	22.6	27.2	15.7	20.5	36.9	14.8	19.9	33.1	30.9	82.8
565	30.99	1.2	2.5	6.3	6.7	8.3	29.1	22.6	19.1	27.9	32.2	18.6	60.8	11.4	27.2
566	31.04	3.4	2.3	3.2	7.3	14.2	10.4	16.2	8.4	6.9	10.1	15.6	19.6	12.8	12.4
567	31.08	2.8	1.4	5.6	3.3	14.8	16.1	12.2	9.1	11.6	8.9	17.4	12.1	17.5	37.8
568	31.13	5.4	3.2	5.7	7.1	20.7	22.3	33.3	27.6	21.6	34.2	15.0	32.2	42.2	31.1
569	31.17	3.7	3.5	6.0	13.3	51.1	44.7	22.8	38.8	37.7	28.0	36.8	29.8	50.7	36.1
570	31.21	3.4	2.7	10.5	17.1	23.4	36.9	21.5	14.2	11.4	15.9	32.3	38.3	33.6	58.7
571	31.26	10.7	4.9	12.3	12.8	20.9	32.1	32.6	33.4	34.4	49.3	34.8	65.5	103.6	124.0
572	31.30	7.1	5.4	19.8	31.9	26.1	51.4	35.3	42.7	37.8	32.0	54.6	82.1	71.8	187.9
573	31.34	7.6	7.4	20.2	34.8	34.3	44.7	60.3	43.9	72.5	70.3	41.5	62.3	55.3	161.8
574	31.38	5.8	6.0	21.0	11.6	27.4	51.2	32.1	71.2	59.8	23.6	84.4	31.2	55.0	65.4
575	31.42	5.2	3.0	3.4	10.9	47.2	18.0	24.5	24.1	16.1	26.8	43.0	64.2	46.1	53.1
576	31.45	11.3	4.2	5.8	10.6	18.8	35.4	9.2	18.2	26.6	18.2	24.6	10.4	54.2	67.5
577	31.49	17.6	4.2	8.3	15.4	60.7	29.8	45.4	29.4	32.8	22.7	33.1	43.2	59.4	79.8
578	31.52	2.2	3.0	7.2	14.3	19.7	28.2	25.6	15.3	15.7	21.9	34.7	67.2	39.1	38.2
579	31.57	2.4	1.8	11.1	15.3	25.4	24.7	7.9	23.2	39.1	25.6	32.3	52.2	33.1	41.9
580	31.61	2.8	3.8	7.3	16.1	15.1	30.4	16.8	15.4	34.8	18.9	27.5	11.3	31.1	62.8
581	31.65	7.6	2.5	6.6	12.9	20.4	21.1	21.1	36.8	33.0	27.7	13.5	25.9	56.0	56.1
582	31.68	2.9	1.6	11.6	12.6	44.2	34.5	32.8	25.6	27.8	67.1	27.7	63.7	65.4	69.8
583	31.71	4.0	5.1	16.2	21.2	49.8	38.7	38.6	45.1	47.0	41.6	52.0	39.2	55.3	44.8
584	31.75	3.9	4.0	8.3	14.1	26.8	38.8	21.4	23.1	26.5	45.1	50.3	31.0	48.0	99.8
585	31.79	7.5	5.5	23.7	16.5	23.2	28.2	29.7	16.1	36.1	27.7	18.4	47.4	34.6	69.3
586	31.82	3.3	4.5	17.3	13.2	38.1	22.5	35.4	35.3	35.8	20.9	44.8	59.1	33.3	54.1
587	31.86	3.4	1.3	8.1	4.0	15.4	27.4	23.8	10.9	14.3	16.1	12.0	7.0	22.8	13.4
588	31.89	1.8	6.5	11.2	15.4	24.6	37.2	20.9	16.6	34.3	20.7	44.1	48.5	55.8	33.5

589	31.93	3.7	3.0	8.1	12.6	45.2	23.5	35.9	19.7	29.4	36.2	33.1	88.0	41.4	48.8
590	31.97	2.6	2.7	3.9	4.3	16.7	12.7	8.7	18.8	12.0	16.8	37.2	21.2	40.1	40.4
591	32.04	5.2	3.1	3.4	8.5	73.1	61.8	43.8	34.4	64.5	25.0	44.5	57.0	45.5	54.4
592	32.08	6.0	4.5	13.0	16.8	23.7	27.1	57.7	34.6	35.7	42.4	48.0	24.1	48.7	113.0
593	32.12	6.0	3.9	18.8	28.8	18.9	35.8	29.5	43.6	25.8	54.5	35.6	44.9	40.1	83.3
594	32.16	5.0	2.2	7.8	16.4	20.2	15.9	19.6	18.3	20.8	20.0	23.4	42.8	67.0	45.3
595	32.20	2.6	2.3	8.8	13.9	14.3	25.4	26.4	27.2	17.3	14.9	23.9	25.1	18.2	46.5
596	32.24	6.4	4.3	10.9	7.2	20.1	25.0	26.5	18.4	17.9	23.8	19.4	53.3	39.4	50.4
597	32.28	4.1	2.5	6.6	13.8	20.4	12.5	29.4	18.9	15.5	24.6	52.0	42.9	39.5	116.8
598	32.33	2.6	2.7	8.5	7.7	18.8	26.7	19.1	12.9	12.3	11.5	19.4	23.7	25.9	47.1
599	32.37	5.4	4.3	10.9	13.5	13.3	22.9	22.7	17.1	21.1	25.2	31.1	56.0	26.6	52.9
600	32.41	6.6	4.1	10.0	5.1	33.0	26.8	21.7	26.1	27.2	37.1	28.2	27.8	52.5	58.4
601	32.46	5.4	2.4	11.1	13.6	21.2	32.2	21.8	42.9	10.9	27.1	29.3	16.4	78.6	21.7
602	32.50	7.2	4.2	13.4	12.6	29.6	25.8	34.3	39.7	22.0	29.5	64.7	52.8	59.8	64.9
603	32.54	1.5	3.3	6.7	15.3	40.9	26.5	30.1	30.4	28.9	33.1	34.7	53.2	84.8	50.4
604	32.58	4.2	2.4	8.2	8.6	11.6	7.9	33.4	26.8	26.1	23.0	56.5	44.5	17.1	67.3
605	32.62	5.0	3.1	6.6	7.3	10.8	11.1	21.0	17.4	13.1	21.0	13.2	41.1	25.7	22.7
606	32.66	2.4	2.3	3.0	7.1	20.9	13.2	22.7	30.7	16.0	15.1	49.6	38.3	29.2	30.7
607	32.70	4.2	3.0	11.9	18.7	34.0	29.9	33.4	39.9	26.9	22.7	20.8	53.4	45.1	29.8
608	32.74	7.3	2.1	9.1	10.0	32.1	11.8	30.6	13.6	27.2	18.9	50.9	46.9	48.3	51.6
609	32.78	5.7	3.0	11.5	7.2	33.2	31.8	41.1	15.8	22.4	34.9	29.8	46.0	47.6	61.8
610	32.84	5.7	4.5	16.2	12.6	36.5	21.8	15.1	19.9	39.3	31.7	36.1	45.9	47.5	47.9
611	32.88	9.3	2.8	9.3	17.1	32.6	29.1	36.2	37.4	24.4	44.5	37.7	40.7	61.5	99.1
612	32.92	5.5	4.1	2.7	15.2	24.2	52.3	16.8	36.0	43.3	36.8	33.5	45.4	64.0	57.6
613	32.96	3.1	1.9	7.3	7.3	13.9	31.1	25.1	10.4	22.5	20.5	12.2	27.3	35.5	46.5
614	33.01	2.4	1.8	9.2	11.1	12.4	39.1	20.8	32.5	25.1	11.2	14.4	45.4	33.3	41.1
615	33.05	3.8	5.0	14.3	10.7	27.1	31.2	32.0	22.8	20.9	51.4	26.8	78.1	55.8	72.3
616	33.10	5.6	2.1	14.2	11.9	31.0	25.2	17.6	29.7	29.9	34.4	58.9	79.8	47.7	63.4
617	33.14	9.1	5.6	8.6	11.0	43.3	33.4	39.2	34.0	26.9	39.3	46.1	26.7	46.0	65.0
618	33.19	4.7	4.0	4.8	14.5	32.2	23.2	25.3	10.8	35.3	41.3	24.6	34.7	25.4	23.9
619	33.23	6.6	4.1	8.3	9.7	34.2	14.3	11.8	7.5	18.0	20.9	33.6	24.9	28.0	111.0
620	33.28	2.7	3.9	5.5	9.2	23.0	19.9	12.8	17.5	31.9	31.7	27.8	28.9	29.0	20.3
621	33.33	3.9	2.1	9.1	6.3	7.2	12.1	21.3	21.0	8.3	7.3	17.2	21.6	34.1	39.6
622	33.38	5.0	4.3	4.0	12.3	26.2	24.9	18.0	26.2	12.0	23.2	13.2	31.5	14.9	6.9
623	33.42	8.2	6.8	20.0	25.6	42.9	37.2	23.2	16.9	65.0	43.2	153.5	50.6	48.1	53.0
624	33.46	4.3	4.2	17.3	7.1	37.1	27.8	30.3	28.5	23.9	17.4	43.7	66.3	56.6	51.9
625	33.50	3.9	4.0	5.8	4.2	17.1	26.1	24.5	10.2	6.7	13.9	16.3	37.2	36.6	21.9
626	33.54	6.4	4.5	14.7	11.9	18.7	10.6	28.3	29.0	36.7	16.2	29.0	21.2	65.7	48.6
627	33.58	2.3	0.8	10.0	3.1	13.1	23.8	18.7	26.0	15.9	26.8	17.5	18.6	34.4	42.8
628	33.62	4.7	3.5	7.2	11.2	22.9	28.9	22.4	19.8	23.8	23.1	31.5	21.2	30.5	25.7
629	33.66	2.8	3.2	7.1	6.9	15.6	4.5	18.8	16.1	7.5	16.0	22.4	20.5	22.2	22.3
630	33.70	2.2	2.9	4.1	6.9	20.3	18.0	14.3	18.8	5.0	27.0	19.2	29.7	25.4	41.9
631	33.74	3.0	4.3	6.8	12.7	13.7	27.3	23.1	16.0	6.8	14.6	14.1	31.0	27.2	49.6
632	33.78	13.5	4.2	7.3	8.9	10.5	33.1	27.5	26.2	34.5	8.6	31.0	35.7	26.7	54.7
633	33.82	4.4	1.6	4.3	6.0	14.9	17.3	20.6	12.2	27.2	17.6	16.6	50.3	14.7	104.9
634	33.86	5.3	2.8	11.5	9.1	22.2	23.5	12.4	29.8	27.8	17.1	30.2	28.4	61.8	73.3
635	33.90	5.4	4.2	6.5	9.8	36.8	24.9	21.6	36.0	29.3	19.4	20.1	21.1	51.0	78.8
636	33.95	7.3	2.3	8.6	17.0	32.1	23.5	15.5	27.2	35.9	38.8	19.2	31.2	53.0	71.7
637	33.99	8.8	4.3	8.7	9.3	30.6	30.8	22.5	28.5	35.7	29.9	44.2	66.0	33.7	34.5
638	34.04	3.2	2.3	6.2	8.7	31.1	16.7	24.6	22.9	16.7	36.4	27.3	40.4	36.9	42.9
639	34.08	17.4	21.0	29.5	36.4	68.5	33.9	58.6	60.5	35.1	29.6	73.2	56.9	55.4	157.6
640	34.13	2.3	2.7	4.1	3.4	18.3	9.1	7.1	11.9	3.4	9.0	12.8	20.1	21.4	30.6
641	34.17	3.6	2.7	7.7	11.6	24.9	41.9	19.5	14.2	14.2	41.5	43.5	51.4	20.0	56.1
642	34.22	5.1	3.4	6.2	13.5	39.6	8.1	40.3	18.0	35.4	26.4	18.9	35.9	48.5	100.1
643	34.26	3.8	5.1	20.9	27.6	62.9	44.4	48.8	35.7	49.2	39.1	45.8	49.3	47.3	152.7
644	34.30	2.3	4.1	19.9	18.8	39.1	25.6	22.1	17.4	25.8	40.2	45.0	30.2	38.9	70.2
645	34.33	7.8	3.8	4.4	9.9	8.7	17.0	9.8	24.3	19.9	23.6	40.2	43.8	34.6	22.7
646	34.37	1.2	2.1	5.3	9.8	19.5	15.0	27.9	17.3	21.0	27.2	13.2	27.0	21.5	28.0
647	34.41	3.4	1.5	1.8	5.7	9.8	15.7	10.4	18.2	23.5	21.6	30.8	36.1	12.7	32.0
648	34.45	2.9	2.6	6.6	12.1	48.2	30.6	42.1	17.5	36.1	38.9	19.8	46.1	56.6	30.5
649	34.49	11.1	7.4	16.6	25.1	53.3	56.3	19.1	45.4	61.1	43.9	66.4	58.4	62.6	106.2
650	34.53	6.9	7.6	75.7	15.6	47.1	34.2	32.5	22.3	23.8	27.6	45.4	41.4	96.1	99.2
651	34.58	13.6	5.8	14.7	11.7	51.2	27.2	53.4	47.5	43.0	26.5	50.4	25.9	53.2	100.1
652	34.62	10.3	8.6	9.8	28.7	37.1	53.1	32.9	40.0	36.8	54.4	27.3	53.4	62.9	66.4
653	34.67	5.1	3.1	10.7	12.5	45.1	34.5	41.5	24.4	44.2	29.1	50.6	63.8	45.3	82.5
654	34.71	2.7	1.2	2.6	3.1	7.7	9.5	8.3	8.1	11.8	17.7	32.9	48.5	38.3	41.2
655	34.76	8.2	4.1	10.7	20.7	19.3	26.3	36.0	18.1	24.4	35.8	8.9	39.7	17.4	108.2
656	34.80	6.9	3.0	13.9	12.6	45.5	63.4	29.8	28.1	19.5	33.0	50.7	51.9	74.4	40.9
657	34.84	6.7	4.7	18.3	12.8	33.4	21.3	21.5	22.4	38.7	29.8	36.7	46.2	70.1	63.5
658	34.88	4.0	3.3	10.6	7.4	25.0	26.7	32.3	36.2	21.0	25.2	35.5	31.6	65.5	92.3
659	34.93	3.1	2.3	5.3	8.4	13.7	23.4	22.8	9.7	23.7	31.7	28.1	47.0	33.2	38.2
660	34.97	5.9	2.1	7.4	9.2	13.6	23.1	21.3	30.0	20.9	22.8	20.9	18.0	14.9	47.8
661	35.02	5.5	3.6	11.5	11.1	18.9	14.7	16.5	30.4	24.6	25.0	32.8	27.3	88.2	83.4
662	35.06	4.6	2.6	23.2	16.9	38.6	57.5	30.3	35.3	42.0	23.2	41.3	85.7	76.7	94.5
663	35.10	3.6	2.7	6.4	6.8	17.4	35.5	17.7	19.6	29.3	29.6	33.1	33.0	58.7	30.8
664	35.15	5.5	4.2	6.0	7.8	20.5	29.6	8.7	22.0	14.9	28.4	44.7	30.8	15.2	191.7
665	35.19	4.7	3.9	7.3	9.8	16.1	22.5	14.3	19.7	10.3	21.8	17.2	34.0	39.8	36.7

666	35.23	6.6	2.4	7.1	11.6	18.6	23.9	19.0	18.8	13.8	17.4	35.1	33.0	43.3	55.3
667	35.27	4.7	6.2	6.2	9.4	19.4	24.2	12.2	21.7	13.4	8.7	17.6	38.5	31.6	50.0
668	35.31	2.4	4.0	6.8	14.8	18.3	25.5	23.2	33.5	16.1	25.4	16.9	32.7	35.9	30.1
669	35.35	2.5	1.7	5.0	4.1	16.3	17.7	7.6	20.3	18.4	21.8	27.7	29.4	18.7	32.6
670	35.39	4.6	4.9	5.9	13.6	35.8	39.5	30.5	28.0	25.7	29.3	12.7	46.7	25.8	64.4
671	35.43	5.4	3.7	4.5	9.8	25.3	17.6	25.8	23.4	22.6	8.8	31.0	54.5	38.0	74.3
672	35.47	2.3	3.1	17.1	8.1	46.7	55.3	21.8	39.9	33.0	42.2	36.6	36.8	80.4	51.9
673	35.51	6.7	4.3	7.8	16.1	17.2	25.6	31.7	13.9	28.3	33.3	27.1	61.7	13.3	32.5
674	35.55	3.7	2.5	6.1	3.5	11.0	15.1	30.4	28.1	25.7	24.0	23.3	58.8	31.4	33.2
675	35.59	4.0	3.5	7.6	11.9	19.0	24.7	33.1	25.1	18.0	24.1	48.7	54.9	37.8	82.2
676	35.63	4.0	4.6	8.8	8.6	18.6	38.3	14.9	12.9	27.4	16.5	18.1	35.4	35.3	31.7
677	35.67	5.9	4.9	10.7	16.9	24.9	26.6	52.9	39.6	44.0	20.0	67.8	39.3	49.7	52.4
678	35.71	4.1	4.8	9.2	4.3	11.2	21.1	28.3	19.8	36.2	16.2	25.0	45.0	33.7	84.4
679	35.75	5.2	3.6	3.6	11.1	20.5	11.9	14.7	17.1	18.2	19.8	13.2	32.6	35.8	17.8
680	35.78	7.2	4.4	10.3	11.5	27.1	27.5	21.7	46.6	27.8	76.0	17.1	59.0	51.1	75.1
681	35.81	6.1	4.3	23.2	9.3	26.6	43.6	30.0	67.7	28.9	30.4	80.4	60.6	81.6	109.3
682	35.85	3.2	3.7	11.4	14.5	33.8	28.3	28.7	20.2	13.3	24.5	21.3	41.5	69.6	41.4
683	35.88	2.2	2.6	2.4	6.4	13.6	5.7	9.3	18.0	15.8	16.6	32.6	39.5	50.6	31.9
684	35.91	3.8	3.7	3.6	10.1	12.4	17.7	25.8	4.8	14.4	23.4	38.6	25.5	27.7	62.9
685	35.95	3.5	5.4	5.7	6.2	28.0	8.0	14.4	34.7	29.4	30.0	38.2	69.8	76.1	41.4
686	35.98	3.2	1.6	5.5	9.9	10.9	19.4	20.8	25.5	20.3	21.0	26.0	29.9	53.6	58.7
687	36.05	5.2	3.5	12.4	12.4	17.5	35.1	43.0	22.5	27.4	26.7	26.3	27.6	74.7	45.4
688	36.08	7.4	3.5	3.2	8.6	14.9	30.4	25.4	21.4	31.2	18.8	56.4	28.1	41.9	42.3
689	36.12	3.9	3.8	10.7	15.8	19.2	31.2	38.9	27.0	43.6	21.1	24.5	42.1	54.1	54.4
690	36.16	6.6	3.5	4.9	7.5	31.4	22.7	19.9	9.4	23.9	36.1	34.7	47.7	60.3	137.2
691	36.21	5.0	4.3	9.1	13.6	23.4	30.1	20.0	22.8	16.1	15.1	17.3	68.0	42.0	19.0
692	36.25	3.7	4.2	5.5	8.6	13.9	20.1	27.5	16.1	18.9	26.4	23.4	65.0	53.8	39.4
693	36.29	3.4	3.7	6.5	4.8	12.0	37.5	14.4	22.9	13.7	12.0	13.4	27.9	35.3	31.6
694	36.33	10.9	5.9	7.3	13.5	30.5	28.2	46.5	40.9	27.7	14.9	41.8	38.6	37.4	91.5
695	36.37	10.9	3.9	2.1	10.1	34.9	27.1	14.6	26.7	30.8	39.9	32.2	35.2	16.3	50.2
696	36.41	6.0	1.9	7.8	11.9	13.8	35.5	21.3	12.6	33.4	15.3	45.8	37.7	55.6	62.4
697	36.45	6.5	5.5	14.5	15.9	39.9	33.2	42.9	44.8	44.7	37.9	44.3	43.3	76.6	89.6
698	36.49	6.2	3.8	9.5	19.6	18.2	28.2	34.8	38.8	47.0	17.2	58.8	42.9	55.7	90.2
699	36.52	5.6	3.1	13.9	9.8	19.9	37.1	21.6	30.0	29.7	14.2	36.6	53.7	51.3	82.2
700	36.56	4.4	3.3	8.4	5.7	18.9	43.3	48.9	16.8	15.5	18.5	17.8	22.1	38.9	38.2
701	36.60	6.4	5.1	12.6	8.9	30.4	51.3	38.4	22.0	36.0	29.4	30.7	70.5	80.2	109.4
702	36.64	10.1	2.0	11.3	26.1	64.9	35.6	34.1	28.5	37.4	21.0	76.1	91.3	77.1	181.8
703	36.67	9.2	5.2	14.9	10.7	21.5	40.6	60.1	31.9	32.6	41.3	82.0	56.0	58.2	71.6
704	36.71	4.5	5.0	11.4	13.3	29.9	41.8	33.4	23.0	35.2	19.7	45.6	60.9	40.7	82.9
705	36.76	5.5	3.1	10.5	14.9	16.0	29.8	33.4	41.7	29.4	22.1	36.0	42.0	41.9	35.5
706	36.79	3.8	3.5	9.6	16.5	29.9	30.3	11.5	36.4	34.3	21.4	52.2	53.4	26.7	80.3
707	36.83	8.3	3.8	11.3	12.9	12.4	21.1	18.8	31.2	20.4	21.1	22.6	50.3	24.3	78.9
708	36.87	1.8	3.4	9.5	8.0	22.6	23.7	35.4	16.1	24.9	24.2	24.6	25.6	53.1	48.4
709	36.91	8.3	3.9	8.7	10.0	28.8	20.2	21.1	28.2	17.9	33.4	44.5	75.5	36.6	71.2
710	36.95	2.6	4.0	7.3	9.2	28.1	24.4	27.7	27.0	30.2	24.6	25.7	37.5	38.6	45.7
711	37.00	3.9	3.4	5.5	3.9	12.7	23.2	12.2	18.8	20.6	14.8	8.1	36.8	8.7	35.0
712	37.04	5.3	2.8	11.3	8.0	11.2	7.3	25.6	12.5	27.5	20.1	27.2	31.9	32.6	50.8
713	37.08	3.5	3.2	8.9	11.6	14.5	26.2	20.6	22.9	28.9	24.1	11.7	54.8	24.4	28.2
714	37.13	1.5	3.2	7.7	5.5	16.2	31.7	14.1	16.3	18.3	14.4	14.9	38.0	8.7	38.8
715	37.16	3.1	3.3	9.5	8.9	27.3	22.5	23.4	16.6	15.2	29.1	53.5	39.2	27.8	149.4
716	37.20	11.6	8.1	16.0	22.9	22.1	41.3	34.6	23.3	83.3	29.1	41.6	70.2	114.0	217.3
717	37.24	22.0	9.5	26.1	19.2	46.2	38.0	56.9	63.0	64.3	29.6	60.4	62.6	92.9	89.3
718	37.28	10.5	7.1	15.7	22.5	40.7	29.8	50.4	43.4	44.0	88.8	56.3	116.2	100.9	91.9
719	37.32	10.5	150.6	17.9	10.5	60.1	18.2	57.3	44.7	42.2	28.4	137.9	38.0	47.6	118.0
720	37.35	4.8	3.2	10.0	17.6	23.7	31.3	34.1	18.8	38.7	22.2	20.1	53.5	50.7	54.6
721	37.39	14.0	6.2	9.6	11.2	32.7	21.8	20.1	18.0	27.4	15.3	49.0	30.7	26.7	22.1
722	37.43	15.4	3.8	6.9	6.9	23.6	5.1	13.5	20.7	16.3	18.7	19.0	35.7	31.7	50.4
723	37.46	6.0	5.3	4.5	7.0	21.5	23.5	37.3	13.5	18.3	18.2	15.9	26.0	45.7	20.7
724	37.50	4.6	2.8	5.2	7.3	19.1	11.1	9.9	18.1	12.0	17.7	21.0	16.4	19.6	33.5
725	37.54	5.8	2.7	5.2	5.6	20.1	24.9	23.9	20.0	23.3	18.6	26.5	33.2	30.1	71.3
726	37.58	4.0	3.7	9.2	11.5	21.7	26.1	41.1	50.0	43.6	48.6	24.0	58.7	86.3	82.8
727	37.61	6.2	2.9	8.7	19.3	74.2	39.4	52.8	18.1	13.4	45.2	51.6	60.0	43.0	53.2
728	37.65	5.9	2.7	6.4	6.2	23.4	25.6	15.0	33.9	22.0	18.8	18.8	38.5	44.1	41.0
729	37.69	3.9	4.3	5.8	6.1	10.0	7.2	19.7	15.4	18.9	14.9	21.4	49.1	31.7	49.2
730	37.72	5.0	1.8	6.4	2.8	18.8	15.2	13.6	15.5	11.1	17.4	22.8	27.8	33.6	54.6
731	37.76	2.9	2.4	8.0	5.5	14.0	12.5	17.0	18.7	7.2	16.2	14.2	49.8	16.4	43.0
732	37.80	3.9	6.8	16.4	15.9	50.1	31.2	39.1	30.9	56.7	19.6	45.9	69.1	69.7	121.2
733	37.85	7.9	7.5	5.4	17.3	35.3	34.7	51.9	33.7	27.5	39.5	32.7	55.5	44.6	77.7
734	37.89	6.1	6.6	7.1	18.5	18.3	40.0	39.1	40.8	47.9	27.4	72.5	65.9	72.1	103.6
735	37.93	2.6	2.9	11.1	11.4	23.2	15.7	18.8	22.7	49.5	26.6	28.9	25.1	78.8	40.6
736	37.97	3.4	1.3	4.2	8.2	15.3	10.4	19.4	21.2	18.4	7.1	15.4	31.5	24.5	22.9
737	38.01	5.1	2.8	10.3	14.5	21.5	32.1	30.0	16.2	36.6	13.2	45.7	48.3	41.5	86.5
738	38.05	7.8	4.0	7.6	8.2	16.1	14.8	18.6	26.0	18.5	16.1	24.4	39.7	34.7	209.5
739	38.09	5.4	6.4	9.1	13.6	39.5	31.9	20.4	31.2	20.9	35.5	30.1	42.6	39.5	67.7
740	38.13	5.1	3.4	10.3	12.7	31.1	17.4	39.6	18.6	35.0	27.0	53.2	21.5	39.7	133.1
741	38.17	6.3	6.6	19.8	18.8	43.6	26.1	30.9	35.4	14.5	22.0	33.8	54.7	63.6	51.0
742	38.21	4.9	2.2	6.0	8.9	36.3	30.2	28.2	21.6	21.1	30.7	29.2	39.2	17.8	87.5

743	38.25	2.3	3.5	7.8	12.9	7.7	27.1	17.5	18.0	11.6	29.3	35.2	44.0	32.7	21.3
744	38.29	4.7	3.4	4.5	8.7	14.6	11.0	18.2	17.8	17.3	29.2	24.8	26.9	17.6	55.4
745	38.33	2.1	2.0	2.5	6.1	20.9	12.2	4.8	21.2	16.6	15.4	17.3	25.4	33.4	43.6
746	38.37	3.1	1.9	5.3	21.7	10.7	23.2	14.8	11.7	6.8	17.8	10.1	32.2	13.2	47.4
747	38.40	4.0	3.8	5.9	7.1	21.6	22.3	13.3	16.8	15.5	10.7	26.7	29.8	25.7	32.0
748	38.44	6.1	5.8	4.6	6.7	11.6	25.1	19.2	16.3	20.7	20.7	24.7	43.1	26.3	31.8
749	38.48	6.3	4.6	4.4	8.4	30.5	22.4	25.3	39.3	30.7	25.4	37.9	34.9	37.3	94.2
750	38.52	4.6	3.8	10.2	11.2	54.4	25.4	37.3	21.1	17.0	35.5	34.6	51.0	35.8	53.2
751	38.55	20.4	4.8	17.0	28.3	28.6	33.4	36.3	32.8	23.3	30.4	37.4	24.3	59.7	190.6
752	38.59	4.5	4.6	7.4	9.5	39.2	19.7	38.4	26.6	13.4	22.3	38.6	48.5	56.5	37.4
753	38.64	4.3	2.2	6.8	9.3	17.2	16.5	20.8	32.4	29.4	35.1	35.3	52.8	53.8	54.9
754	38.69	11.8	4.4	16.7	22.2	48.8	39.5	52.1	58.0	30.4	16.8	30.0	41.5	16.2	66.0
755	38.74	9.5	4.5	12.9	15.7	35.5	25.9	23.6	15.1	37.5	48.5	59.4	40.0	73.5	155.8
756	38.79	5.2	4.4	9.0	17.4	33.1	47.5	56.2	26.4	26.9	40.6	55.8	57.2	49.3	30.1
757	38.83	6.1	5.4	10.1	9.8	28.5	22.6	13.5	31.7	10.0	32.6	42.1	20.0	62.6	41.3
758	38.86	4.7	3.5	7.9	7.7	8.6	30.9	18.7	30.4	14.4	42.7	38.9	44.7	48.6	199.1
759	38.91	10.6	4.1	14.6	21.3	72.1	27.4	32.5	37.0	39.4	26.6	49.0	51.6	97.5	45.7
760	38.95	4.3	1.6	13.1	8.6	28.4	43.6	23.9	28.3	29.2	32.0	18.0	65.3	52.4	99.2
761	38.99	8.2	2.3	7.4	18.7	36.3	27.2	14.0	32.0	39.5	47.8	36.9	45.9	49.3	70.4
762	39.04	6.7	2.3	7.2	8.5	32.9	35.8	33.9	51.2	22.8	41.7	36.5	23.2	66.7	68.2
763	39.09	6.6	4.4	6.6	13.2	29.7	17.4	32.8	31.0	29.5	22.0	43.5	70.3	32.8	42.5
764	39.13	4.8	4.5	14.4	6.8	32.7	35.8	35.7	31.3	35.2	19.1	27.7	94.6	54.7	35.5
765	39.18	3.8	4.0	7.9	7.3	13.4	29.3	11.5	42.0	28.7	36.1	16.0	36.8	37.5	63.2
766	39.22	3.8	2.4	4.6	13.8	21.5	28.8	23.7	20.4	34.5	43.6	28.0	65.6	55.6	38.3
767	39.26	7.0	2.5	10.6	13.3	15.8	18.7	16.9	34.5	27.9	26.1	21.1	52.8	35.5	89.7
768	39.31	5.9	6.5	15.0	13.6	49.3	37.5	15.7	20.1	48.8	28.6	41.3	61.2	41.7	101.1
769	39.36	9.1	4.5	10.0	15.7	28.5	44.0	31.3	70.5	23.3	35.3	62.4	32.9	26.8	83.2
770	39.40	8.3	5.1	26.7	20.4	34.3	35.3	26.7	34.0	21.7	30.7	32.0	46.3	56.4	22.4
771	39.44	19.5	3.7	10.3	13.4	47.4	37.4	14.4	36.8	48.6	24.9	41.0	26.4	44.1	78.1
772	39.48	7.0	3.5	10.2	18.1	34.8	15.3	21.7	20.0	39.5	34.6	42.7	73.9	48.0	38.0
773	39.52	5.8	3.8	13.7	8.4	12.1	17.3	19.9	20.5	21.3	10.1	22.0	20.8	36.3	43.6
774	39.57	4.3	5.0	13.4	20.6	26.2	45.4	45.8	70.3	49.3	49.4	34.1	71.8	78.2	116.6
775	39.61	9.9	1.8	16.5	35.0	52.8	20.0	19.8	56.2	24.5	55.4	41.6	50.9	14.2	140.1
776	39.65	3.9	3.0	9.8	7.0	13.2	30.8	20.6	30.7	16.3	16.1	27.0	41.3	47.2	60.9
777	39.69	4.3	5.0	11.4	10.2	28.9	27.0	32.0	18.0	33.4	27.2	15.3	60.3	40.6	26.9
778	39.73	3.6	1.3	8.9	6.8	31.9	26.3	35.1	30.4	29.8	26.1	54.5	53.5	57.6	52.9
779	39.77	11.6	3.6	8.1	17.6	26.9	34.9	24.6	34.8	44.2	23.2	31.6	72.3	46.9	68.7
780	39.81	9.0	4.6	14.2	17.6	38.5	42.8	23.4	26.1	45.1	24.8	18.3	41.4	64.7	178.4
781	39.85	12.2	3.1	6.1	17.1	18.6	17.6	42.9	42.0	27.5	37.6	37.4	29.4	84.9	66.8
782	39.88	3.7	2.7	4.0	3.5	7.4	7.2	11.2	11.0	8.5	20.6	14.6	14.4	21.1	24.9
783	39.92	6.3	2.8	12.7	9.4	18.5	34.3	15.6	21.9	17.0	12.9	23.6	37.0	46.1	39.0
784	39.96	3.1	3.7	5.7	9.6	11.8	10.6	16.7	10.4	17.4	15.1	10.5	20.2	24.4	24.3

RICE deep core combined 40m to 320m samples, from the 2013 core processing campaign. Recalibrated using MATLAB 'robustfit' (bisquare) method; analytical blank corrected. All concentrations in pg g^{-1}.

Top Depth (m)	Sample ID	La139	Ce140	Pr141	Nd146	Sm147	Eu153	Gd157	Tb159	Dy163	Ho165	Er166	Tm169	Yb172	Lu175
40.00	RICE_3yr_1	0.228	0.612	0.051	0.200	0.039	0.007	0.032	0.004	0.024	0.005	0.016	0.003	0.004	0.001
40.95	RICE_3yr_2	0.129	0.352	0.026	0.113	0.028	0.005	0.022	0.002	0.016	0.003	0.012	0.001	0.001	<0.001
42.27	RICE_3yr_3	0.123	0.325	0.029	0.107	0.021	0.004	0.020	0.002	0.016	0.004	0.011	0.001	0.001	0.001
43.64	RICE_3yr_4	0.068	0.198	0.015	0.064	0.019	0.003	0.010	0.002	0.012	0.002	0.005	<0.001	0.001	<0.001
44.68	RICE_3yr_5	0.091	0.214	0.016	0.066	0.012	0.001	0.018	0.002	0.008	0.001	0.004	<0.001	0.001	<0.001
45.61	RICE_3yr_6	0.099	0.254	0.020	0.063	0.035	0.003	0.009	0.002	0.009	0.001	0.007	<0.001	0.001	<0.001
46.60	RICE_3yr_7	0.091	0.221	0.021	0.079	0.021	0.003	0.021	0.001	0.013	0.002	0.006	<0.001	0.001	<0.001
47.59	RICE_3yr_8	0.119	0.259	0.022	0.085	0.020	0.003	0.010	0.001	0.008	0.002	0.006	<0.001	0.001	0.002
48.56	RICE_3yr_9	0.092	0.190	0.017	0.065	0.020	0.001	0.012	0.002	0.009	0.001	0.007	<0.001	<0.001	<0.001
49.58	RICE_3yr_10	0.069	0.153	0.012	0.058	0.025	0.001	0.007	0.001	0.003	0.001	0.005	<0.001	0.001	<0.001
50.50	RICE_3yr_11	0.137	0.308	0.034	1.575	0.024	0.005	0.014	0.003	0.018	0.003	0.009	0.001	0.003	0.001
51.41	RICE_3yr_12	0.098	0.202	0.021	0.074	0.012	0.002	0.010	<0.001	0.013	0.003	0.006	0.001	0.001	<0.001
52.34	RICE_3yr_13	0.078	0.192	0.015	0.048	0.015	0.002	0.017	0.001	0.004	0.001	0.005	0.001	0.001	<0.001
53.31	RICE_3yr_14	0.088	1.347	0.016	0.059	0.023	0.003	0.016	<0.001	0.007	0.002	0.003	<0.001	<0.001	<0.001
54.19	RICE_3yr_15	0.084	0.257	0.020	0.058	0.020	0.003	0.008	0.001	0.007	0.001	0.006	0.001	<0.001	<0.001
55.17	RICE_3yr_16	0.069	0.148	0.015	0.046	0.012	<0.001	0.010	0.001	0.006	0.001	0.003	0.001	<0.001	0.001
56.02	RICE_3yr_17	0.104	0.235	0.020	0.070	0.015	0.002	0.016	0.001	0.010	0.002	0.008	<0.001	0.001	<0.001
56.89	RICE_3yr_18	0.068	0.176	0.015	0.059	0.008	0.002	0.007	0.002	0.008	0.001	0.005	-0.001	0.001	<0.001
57.77	RICE_3yr_19	0.068	0.183	0.012	0.045	0.011	0.002	0.013	<0.001	0.005	0.002	0.004	<0.001	<0.001	<0.001
58.69	RICE_3yr_20	0.073	0.192	0.014	0.055	0.012	0.001	0.011	<0.001	0.005	0.002	0.006	<0.001	0.001	<0.001
59.52	RICE_3yr_21	0.086	0.210	0.017	0.068	0.007	0.001	0.009	0.003	0.009	0.001	0.007	<0.001	0.001	<0.001
60.40	RICE_3yr_22	0.095	0.267	0.015	0.074	0.015	0.001	0.012	0.001	0.008	0.002	0.006	<0.001	<0.001	<0.001

61.36	RICE_3yr_23	0.072	0.195	0.014	0.063	0.008	0.003	0.017	<0.001	0.008	<0.001	0.005	<0.001	<0.001	<0.001
62.17	RICE_3yr_24	0.103	0.258	0.020	0.078	0.015	0.002	0.017	0.002	0.007	0.002	0.005	<0.001	0.001	<0.001
63.08	RICE_3yr_25	0.537	1.032	0.116	0.436	0.064	0.011	0.062	0.009	0.054	0.008	0.023	0.001	0.004	0.008
63.92	RICE_3yr_26	0.428	0.766	0.073	0.256	0.045	0.006	0.041	0.004	0.027	0.006	0.020	0.002	0.002	0.007
64.76	RICE_3yr_27	0.101	0.217	0.018	0.065	0.012	0.002	0.009	0.001	0.008	0.002	0.004	<0.001	<0.001	<0.001
65.61	RICE_3yr_28	0.131	0.272	0.022	0.090	0.023	0.003	0.013	0.002	0.014	0.001	0.007	<0.001	<0.001	0.001
66.45	RICE_3yr_29	0.082	0.180	0.016	0.063	0.012	0.001	0.009	0.002	0.005	0.001	0.006	0.001	<0.001	<0.001
67.32	RICE_3yr_30	0.079	0.160	0.015	0.055	0.011	0.002	0.014	<0.001	0.010	0.001	0.005	<0.001	0.001	0.001
68.14	RICE_3yr_31	0.057	0.130	0.013	0.043	0.007	0.002	0.009	0.001	0.004	<0.001	0.003	<0.001	<0.001	0.001
68.97	RICE_3yr_32	0.107	0.378	0.021	0.084	0.007	0.003	0.013	0.001	0.010	<0.001	0.006	<0.001	0.001	<0.001
69.80	RICE_3yr_33	0.073	0.160	0.014	0.053	0.017	0.002	0.006	0.001	0.008	0.002	0.007	<0.001	<0.001	<0.001
70.65	RICE_3yr_34	0.058	0.168	0.009	0.040	0.008	0.001	0.003	0.001	0.005	0.001	0.004	<0.001	<0.001	0.012
71.46	RICE_3yr_35	0.064	0.161	0.015	0.058	0.011	0.001	0.006	0.001	0.010	0.001	0.005	<0.001	<0.001	0.001
72.30	RICE_3yr_36	0.060	0.141	0.012	0.036	0.016	<0.001	0.011	<0.001	0.006	<0.001	0.003	<0.001	<0.001	<0.001
73.15	RICE_3yr_37	0.073	0.162	0.015	0.061	0.008	0.001	0.006	0.002	0.008	0.001	0.004	<0.001	<0.001	<0.001
73.93	RICE_3yr_38	0.084	0.338	0.019	0.065	0.022	0.001	0.012	0.001	0.010	0.001	0.003	<0.001	0.001	<0.001
74.75	RICE_3yr_39	0.072	0.467	0.013	0.053	0.012	0.001	0.006	<0.001	0.005	0.002	0.004	<0.001	<0.001	0.001
75.54	RICE_3yr_40	0.129	0.383	0.028	0.113	0.018	0.002	0.016	0.002	0.018	0.004	0.011	0.001	0.001	0.001
76.31	RICE_3yr_41	0.112	0.276	0.020	0.084	0.022	0.002	0.013	0.001	0.013	0.002	0.007	0.002	0.001	<0.001
77.14	RICE_3yr_42	0.076	0.183	0.014	0.056	0.014	<0.001	0.011	0.001	0.010	0.002	0.002	<0.001	<0.001	<0.001
77.94	RICE_3yr_43	0.122	0.320	0.018	0.073	0.021	0.001	0.010	0.001	0.014	0.002	0.005	<0.001	0.001	0.001
78.75	RICE_3yr_44	0.080	0.381	0.015	0.061	0.008	0.002	0.009	<0.001	0.007	0.002	0.005	<0.001	0.001	0.001
79.51	RICE_3yr_45	0.077	0.413	0.017	0.055	0.015	<0.001	0.009	0.001	0.009	0.003	0.006	<0.001	0.001	<0.001
80.32	RICE_3yr_46	0.094	0.329	0.018	0.066	0.018	0.001	0.015	0.001	0.006	0.001	0.003	<0.001	0.002	0.001
81.06	RICE_3yr_47	0.075	0.256	0.014	0.050	0.007	0.002	0.008	<0.001	0.009	0.001	0.003	<0.001	<0.001	<0.001
81.86	RICE_3yr_48	0.107	0.401	0.020	0.070	0.023	0.001	0.008	0.001	0.011	0.001	0.007	<0.001	0.001	<0.001
82.64	RICE_3yr_49	0.103	0.242	0.019	0.089	0.014	0.004	0.017	0.002	0.010	0.002	0.006	0.001	0.001	<0.001
83.51	RICE_3yr_50	0.099	0.285	0.019	0.065	0.012	0.001	0.009	0.001	0.010	0.002	0.005	<0.001	0.001	<0.001
84.29	RICE_3yr_51	0.112	0.289	0.020	0.079	0.024	0.004	0.011	0.002	0.012	0.001	0.009	<0.001	0.001	0.001
85.01	RICE_3yr_52	0.080	0.215	0.015	0.051	0.008	<0.001	0.011	0.001	0.006	0.002	0.002	0.001	<0.001	<0.001
85.80	RICE_3yr_53	0.131	0.235	0.028	0.114	0.019	0.003	0.016	<0.001	0.015	0.001	0.006	<0.001	0.001	0.001
86.57	RICE_3yr_54	0.091	0.533	0.019	0.065	0.023	0.002	0.015	0.002	0.012	0.002	0.008	<0.001	<0.001	<0.001
87.32	RICE_3yr_55	0.096	1.030	0.018	0.059	0.024	0.002	0.008	0.001	0.005	0.001	0.005	0.001	<0.001	0.001
88.09	RICE_3yr_56	0.083	0.889	0.016	0.054	0.009	0.001	0.010	<0.001	0.008	0.001	0.004	-0.001	<0.001	0.001
88.84	RICE_3yr_57	0.118	0.320	0.025	0.095	0.022	0.003	0.015	0.003	0.016	0.002	0.007	0.001	0.002	<0.001
89.57	RICE_3yr_58	0.132	0.321	0.031	0.105	0.023	0.002	0.020	0.003	0.019	0.004	0.012	0.001	0.002	0.001
90.30	RICE_3yr_59	0.049	0.438	0.010	0.031	0.013	0.001	0.011	<0.001	0.007	0.001	0.004	<0.001	<0.001	<0.001
91.05	RICE_3yr_60	0.079	0.211	0.016	0.057	0.007	0.002	0.006	<0.001	0.009	0.001	0.006	<0.001	<0.001	0.001
91.80	RICE_3yr_61	0.111	0.236	0.021	0.089	0.016	0.002	0.014	0.001	0.012	0.002	0.005	0.001	0.001	0.002
92.56	RICE_3yr_62	0.129	0.391	0.026	0.097	0.019	0.002	0.020	0.001	0.013	0.002	0.005	<0.001	0.002	<0.001
93.30	RICE_3yr_63	0.067	0.182	0.014	0.058	0.012	0.002	0.008	<0.001	0.009	0.001	0.004	0.001	0.001	0.001
93.99	RICE_3yr_64	0.055	0.225	0.011	0.045	0.010	0.001	0.005	0.001	0.002	<0.001	0.003	<0.001	<0.001	<0.001
94.75	RICE_3yr_65	0.065	0.186	0.014	0.052	0.013	0.002	0.007	<0.001	0.008	0.001	0.004	<0.001	<0.001	0.001
95.50	RICE_3yr_66	0.072	0.185	0.017	0.058	0.009	0.001	0.003	0.001	0.005	0.001	0.004	<0.001	0.001	<0.001
96.21	RICE_3yr_67	0.069	0.160	0.012	0.055	0.011	0.001	0.009	<0.001	0.007	0.001	0.005	<0.001	<0.001	<0.001
96.92	RICE_3yr_68	0.078	0.212	0.016	0.066	0.006	0.003	0.009	<0.001	0.007	0.001	0.015	<0.001	<0.001	<0.001
97.67	RICE_3yr_69	0.087	0.205	0.018	0.070	0.009	0.002	0.009	0.001	0.013	0.002	0.005	<0.001	0.001	<0.001
98.40	RICE_3yr_70	0.072	0.155	0.016	0.061	0.008	0.001	0.002	0.001	0.011	0.001	0.003	<0.001	<0.001	<0.001
99.09	RICE_3yr_71	0.070	0.150	0.015	0.059	0.010	0.001	0.013	0.001	0.004	0.001	0.003	<0.001	0.001	0.001
99.78	RICE_3yr_72	0.055	0.293	0.010	0.036	0.008	<0.001	0.004	0.001	0.008	0.001	0.001	0.001	<0.001	<0.001
100.51	RICE_3yr_73	0.092	0.254	0.020	0.070	0.017	0.002	0.012	0.002	0.010	0.001	0.003	0.001	<0.001	0.001
101.23	RICE_3yr_74	0.073	0.167	0.015	0.055	0.015	0.001	0.009	0.001	0.010	0.001	0.005	<0.001	0.001	0.001
101.92	RICE_3yr_75	0.070	0.147	0.014	0.053	0.013	0.002	0.010	0.001	0.013	0.001	0.003	0.001	<0.001	<0.001
102.67	RICE_3yr_76	0.055	0.198	0.010	0.046	0.014	0.001	0.001	<0.001	0.006	<0.001	0.003	<0.001	<0.001	<0.001
103.36	RICE_3yr_77	0.067	0.273	0.014	0.057	0.007	0.001	0.008	0.001	0.008	0.001	0.005	<0.001	<0.001	0.001
104.04	RICE_3yr_78	0.070	0.168	0.014	0.047	0.012	0.001	0.009	0.001	0.011	<0.001	0.005	<0.001	<0.001	<0.001
104.77	RICE_3yr_79	0.077	0.184	0.016	0.090	0.013	0.002	0.008	0.002	0.006	0.001	0.005	<0.001	<0.001	<0.001
105.47	RICE_3yr_80	0.151	0.873	0.031	0.114	0.028	0.004	0.015	0.001	0.009	0.001	0.008	<0.001	0.002	0.001
106.18	RICE_3yr_81	0.115	0.290	0.025	0.096	0.014	0.003	0.014	0.001	0.009	0.002	0.008	0.001	0.002	0.001
106.91	RICE_3yr_82	0.088	0.727	0.018	0.074	0.026	0.003	0.012	0.001	0.008	0.002	0.005	<0.001	0.001	<0.001
107.56	RICE_3yr_83	0.117	0.279	0.023	0.076	0.019	0.003	0.009	0.002	0.010	0.002	0.007	<0.001	0.001	0.034
108.25	RICE_3yr_84	0.146	0.306	0.031	0.094	0.021	0.003	0.023	0.001	0.016	0.003	0.009	0.001	0.002	0.001
108.96	RICE_3yr_85	0.119	0.806	0.021	0.085	0.024	0.004	0.018	0.001	0.011	0.001	0.009	<0.001	0.002	0.001

109.62	RICE_3yr_86	0.108	0.823	0.022	0.088	0.018	0.004	0.013	0.002	0.011	0.003	0.008	0.001	0.001	<0.001
110.31	RICE_3yr_87	0.165	0.391	0.037	0.129	0.018	0.005	0.031	0.002	0.017	0.001	0.009	0.001	0.001	0.001
111.04	RICE_3yr_88	0.082	0.192	0.016	0.071	0.019	0.003	0.007	0.001	0.012	<0.001	0.004	0.001	0.001	0.001
111.71	RICE_3yr_89	0.096	0.233	0.018	0.060	0.014	0.003	0.001	0.001	0.007	0.001	0.007	0.001	0.001	<0.001
112.38	RICE_3yr_90	0.098	0.214	0.019	0.066	0.009	0.002	0.011	0.001	0.007	0.001	0.007	<0.001	<0.001	<0.001
113.06	RICE_3yr_91	0.140	0.322	0.028	0.105	0.020	0.003	0.018	0.003	0.013	0.002	0.007	<0.001	0.001	0.001
113.73	RICE_3yr_92	0.077	0.196	0.015	0.054	0.010	0.001	0.010	<0.001	0.010	0.001	0.004	<0.001	<0.001	0.001
114.39	RICE_3yr_93	0.074	0.329	0.014	0.045	0.008	<0.001	0.005	0.001	0.006	<0.001	0.001	-0.001	<0.001	<0.001
115.11	RICE_3yr_94	0.120	0.334	0.025	0.097	0.020	0.001	0.011	0.001	0.010	0.002	0.005	<0.001	0.002	0.001
115.78	RICE_3yr_95	0.121	0.392	0.024	0.095	0.024	0.002	0.014	0.002	0.013	0.002	0.006	0.001	0.001	0.002
116.44	RICE_3yr_96	0.141	0.331	0.023	0.099	0.012	0.003	0.014	0.002	0.015	0.001	0.008	<0.001	0.002	0.002
117.12	RICE_3yr_97	0.080	0.207	0.017	0.070	0.011	0.002	0.005	<0.001	0.009	0.001	0.004	<0.001	0.001	<0.001
117.76	RICE_3yr_98	0.054	0.170	0.011	0.045	0.010	0.001	0.006	<0.001	0.007	0.001	0.004	0.001	<0.001	0.001
118.41	RICE_3yr_99	0.093	0.552	0.019	0.079	0.011	0.001	0.008	0.001	0.013	0.001	0.007	0.001	0.001	0.001
119.08	RICE_3yr_100	0.090	0.233	0.020	0.076	0.016	0.002	0.011	0.001	0.012	0.001	0.007	<0.001	0.001	0.001
119.75	RICE_3yr_101	0.088	0.214	0.020	0.057	0.016	<0.001	0.010	0.002	0.007	0.001	0.004	0.001	0.002	0.009
120.44	RICE_3yr_102	0.057	0.202	0.014	0.051	0.006	0.001	0.008	0.001	0.006	0.001	0.003	<0.001	<0.001	<0.001
121.05	RICE_3yr_103	0.065	0.164	0.013	0.052	0.012	0.001	0.007	<0.001	0.005	0.001	0.002	0.001	<0.001	0.001
121.74	RICE_3yr_104	0.084	0.233	0.018	0.074	0.023	0.002	0.012	0.002	0.011	0.001	0.005	0.001	0.001	0.001
122.37	RICE_3yr_105	0.084	0.189	0.017	0.059	0.018	<0.001	0.007	0.001	0.007	0.002	0.003	0.001	0.001	<0.001
123.04	RICE_3yr_106	0.069	0.142	0.013	0.041	0.007	<0.001	0.007	0.001	0.004	<0.001	0.004	<0.001	<0.001	0.001
123.69	RICE_3yr_107	0.066	0.237	0.012	0.049	0.014	0.002	0.004	<0.001	0.008	0.001	0.005	<0.001	<0.001	0.001
124.33	RICE_3yr_108	0.071	0.168	0.015	0.051	0.016	0.001	0.003	<0.001	0.004	0.001	0.003	<0.001	<0.001	0.001
124.94	RICE_3yr_109	0.089	0.487	0.017	0.074	0.014	0.002	0.008	<0.001	0.007	0.001	0.004	<0.001	<0.001	0.001
125.59	RICE_3yr_110	0.060	0.161	0.011	0.047	0.005	0.002	0.003	0.001	0.006	0.001	0.005	<0.001	<0.001	<0.001
126.25	RICE_3yr_111	0.075	0.175	0.014	0.059	0.005	0.001	0.008	0.002	0.009	0.001	0.006	0.001	<0.001	0.001
126.89	RICE_3yr_112	0.102	0.702	0.020	0.082	0.015	<0.001	0.008	0.001	0.008	0.001	0.005	0.001	0.001	0.764
127.53	RICE_3yr_113	0.123	0.331	0.022	0.077	0.011	<0.001	0.013	0.002	0.007	0.002	0.006	<0.001	0.001	<0.001
128.17	RICE_3yr_114	0.068	0.173	0.014	0.058	0.004	0.001	0.007	0.001	0.005	0.001	0.007	<0.001	0.001	<0.001
128.81	RICE_3yr_115	0.088	0.835	0.021	0.064	0.009	0.002	0.008	0.002	0.012	0.003	0.006	<0.001	0.002	0.001
129.45	RICE_3yr_116	0.084	0.276	0.016	0.058	0.017	0.003	0.009	0.001	0.008	0.001	0.008	<0.001	0.001	<0.001
130.06	RICE_3yr_117	0.088	0.234	0.018	0.075	0.018	0.003	0.004	0.001	0.005	0.001	0.005	<0.001	0.001	0.001
130.71	RICE_3yr_118	0.101	0.298	0.024	0.077	0.016	0.002	0.011	0.002	0.007	0.002	0.004	<0.001	0.001	<0.001
131.32	RICE_3yr_119	0.115	0.265	0.023	0.082	0.018	0.003	0.014	0.001	0.009	0.002	0.006	<0.001	0.001	<0.001
131.95	RICE_3yr_120	0.109	0.926	0.023	0.073	0.016	0.003	0.012	0.001	0.006	0.002	0.006	0.001	0.001	0.001
132.61	RICE_3yr_121	0.090	0.381	0.016	0.049	0.014	0.002	0.006	0.001	0.006	0.001	0.008	<0.001	0.001	0.001
133.20	RICE_3yr_122	0.077	0.194	0.013	0.055	0.008	0.001	0.010	0.001	0.007	<0.001	0.004	<0.001	<0.001	<0.001
133.83	RICE_3yr_123	0.066	0.186	0.014	0.044	0.011	0.002	0.003	<0.001	0.006	0.001	0.006	<0.001	<0.001	0.001
134.45	RICE_3yr_124	0.073	0.209	0.016	0.054	0.006	0.001	0.009	0.001	0.006	<0.001	0.005	<0.001	0.001	<0.001
135.10	RICE_3yr_125	0.102	0.250	0.020	0.082	0.006	0.001	0.007	0.002	0.010	0.001	0.005	0.001	0.001	0.001
135.69	RICE_3yr_126	0.092	1.034	0.022	0.072	0.015	<0.001	0.015	0.002	0.010	0.002	0.007	<0.001	0.001	0.001
136.33	RICE_3yr_127	0.065	0.224	0.012	0.053	0.013	0.001	0.006	0.001	0.004	0.001	0.004	0.001	<0.001	0.001
136.92	RICE_3yr_128	0.077	0.244	0.016	0.067	0.010	0.002	0.014	0.002	0.015	0.002	0.008	<0.001	0.001	0.001
137.52	RICE_3yr_129	0.073	0.287	0.014	0.064	0.015	0.001	0.011	<0.001	0.007	0.002	0.005	0.001	0.001	<0.001
138.15	RICE_3yr_130	0.072	0.205	0.016	0.065	0.009	0.002	0.013	0.001	0.009	0.001	0.003	<0.001	0.001	<0.001
138.77	RICE_3yr_131	0.083	0.634	0.016	0.057	0.016	0.001	0.010	0.002	0.008	0.002	0.004	0.001	<0.001	<0.001
139.36	RICE_3yr_132	0.063	0.179	0.013	0.049	0.002	0.001	0.006	0.002	0.008	<0.001	0.006	<0.001	0.001	0.001
139.97	RICE_3yr_133	0.089	0.228	0.017	0.068	0.012	0.004	0.013	0.001	0.007	0.001	0.006	<0.001	0.001	0.001
140.59	RICE_3yr_134	0.081	0.240	0.015	0.056	0.014	0.002	0.005	0.001	0.009	0.001	0.006	<0.001	0.001	0.001
141.18	RICE_3yr_135	0.090	0.230	0.020	0.066	0.013	0.002	0.015	0.002	0.007	<0.001	0.003	0.001	0.001	<0.001
141.78	RICE_3yr_136	0.072	1.457	0.013	0.057	0.016	0.001	0.010	0.002	0.012	<0.001	0.004	<0.001	0.001	0.001
142.37	RICE_3yr_137	0.079	0.229	0.018	0.053	0.020	0.001	0.007	<0.001	0.007	0.001	0.006	<0.001	0.001	0.001
142.97	RICE_3yr_138	0.075	0.198	0.015	0.061	0.011	0.002	0.012	0.001	0.007	0.001	0.005	<0.001	0.001	0.001
143.59	RICE_3yr_139	0.082	0.651	0.014	0.048	0.019	<0.001	0.007	0.001	0.006	0.001	0.004	<0.001	0.001	<0.001
144.19	RICE_3yr_140	0.111	0.255	0.024	0.091	0.017	0.003	0.013	0.001	0.011	0.001	0.005	<0.001	0.002	0.001
144.76	RICE_3yr_141	0.087	1.209	0.020	0.063	0.016	0.002	0.012	0.002	0.010	<0.001	0.006	0.001	0.001	<0.001
145.32	RICE_3yr_142	0.062	0.186	0.012	0.052	<0.001	0.002	0.005	<0.001	0.007	0.001	0.005	0.001	0.001	<0.001
145.91	RICE_3yr_143	0.076	0.220	0.014	0.059	0.014	<0.001	0.011	0.001	0.007	0.002	0.008	<0.001	0.001	<0.001
146.48	RICE_3yr_144	0.142	2.322	0.031	0.097	0.025	0.004	0.009	0.002	0.017	0.001	0.011	0.001	0.002	0.002
147.08	RICE_3yr_145	0.098	0.301	0.021	0.080	0.008	0.003	0.011	0.002	0.008	0.001	0.007	0.001	0.001	0.001
147.67	RICE_3yr_146	0.114	0.333	0.021	0.067	0.015	0.003	0.012	0.003	0.010	0.001	0.007	0.001	<0.001	<0.001
148.28	RICE_3yr_147	0.105	0.282	0.019	0.092	0.016	0.002	0.006	0.002	0.013	0.001	0.007	<0.001	0.002	<0.001
148.84	RICE_3yr_148	0.079	0.252	0.014	0.059	0.008	0.002	0.009	<0.001	0.006	0.001	0.004	0.001	0.001	0.001

149.44	RICE_3yr_149	0.081	0.822	0.014	0.063	0.011	0.001	0.002	0.001	0.005	0.001	0.005	0.001	<0.001	<0.001
150.03	RICE_3yr_150	0.090	0.312	0.020	0.074	0.012	0.001	0.016	0.001	0.012	0.001	0.005	0.001	0.002	0.001
150.61	RICE_3yr_151	0.067	0.367	0.014	0.053	0.003	0.002	0.004	<0.001	0.004	0.001	0.002	<0.001	<0.001	<0.001
151.20	RICE_3yr_152	0.060	0.189	0.012	0.040	0.006	-0.001	0.003	<0.001	0.006	0.005	0.002	0.001	0.001	<0.001
151.77	RICE_3yr_153	0.083	0.236	0.016	0.086	0.020	0.001	0.006	0.001	0.009	0.001	0.006	<0.001	0.001	<0.001
152.32	RICE_3yr_154	0.080	0.209	0.015	0.049	0.011	0.001	0.005	<0.001	0.014	0.001	0.005	<0.001	0.001	<0.001
152.91	RICE_3yr_155	0.099	1.505	0.017	0.075	0.029	0.001	0.018	0.002	0.010	0.002	0.007	<0.001	0.001	<0.001
153.49	RICE_3yr_156	0.138	0.530	0.023	0.101	0.021	0.004	0.017	0.002	0.009	0.001	0.006	0.001	0.001	<0.001
154.04	RICE_3yr_157	0.139	0.362	0.025	0.090	0.017	0.003	0.017	0.003	0.013	0.002	0.009	<0.001	0.001	0.001
154.61	RICE_3yr_158	0.227	1.002	0.049	0.215	0.043	0.007	0.027	0.006	0.025	0.004	0.014	0.002	0.003	0.002
155.21	RICE_3yr_159	0.114	0.373	0.025	0.099	0.017	0.003	0.012	0.002	0.010	0.002	0.008	<0.001	0.001	0.001
155.75	RICE_3yr_160	0.105	0.409	0.021	0.071	0.014	0.001	0.013	0.002	0.015	0.003	0.011	0.001	0.002	0.001
156.34	RICE_3yr_161	0.091	0.238	0.017	0.075	0.012	0.003	0.008	0.002	0.012	0.001	0.005	0.001	0.002	0.001
156.90	RICE_3yr_162	0.092	0.360	0.019	0.066	0.017	0.002	0.017	0.002	0.014	0.001	0.005	<0.001	<0.001	0.001
157.45	RICE_3yr_163	0.137	0.411	0.028	0.106	0.019	0.004	0.015	0.002	0.013	0.001	0.007	0.002	0.002	0.001
157.97	RICE_3yr_164	0.109	0.320	0.023	0.071	0.015	0.002	0.009	0.003	0.009	0.002	0.009	<0.001	0.001	0.001
158.54	RICE_3yr_165	0.091	0.417	0.018	0.073	0.013	0.005	0.007	0.002	0.009	0.001	0.007	0.001	0.001	0.001
159.13	RICE_3yr_166	0.123	0.326	0.023	0.090	0.007	0.002	0.008	0.002	0.012	0.001	0.003	0.001	0.001	<0.001
159.67	RICE_3yr_167	0.146	0.471	0.029	0.097	0.023	0.004	0.019	0.003	0.017	0.003	0.011	0.001	0.002	<0.001
160.24	RICE_3yr_168	0.057	0.163	0.012	0.054	0.006	0.001	0.008	0.001	0.007	<0.001	0.004	0.001	<0.001	<0.001
160.79	RICE_3yr_169	0.117	0.352	0.023	0.102	0.017	0.002	0.010	0.003	0.009	0.002	0.007	<0.001	0.001	0.001
161.32	RICE_3yr_170	0.100	0.298	0.024	0.087	0.018	0.003	0.015	0.003	0.011	0.003	0.009	0.001	0.001	<0.001
161.87	RICE_3yr_171	0.402	2.047	0.101	0.429	0.110	0.017	0.086	0.011	0.065	0.012	0.039	0.004	0.006	0.003
162.44	RICE_3yr_172	0.079	0.223	0.016	0.067	0.007	0.003	0.007	0.002	0.009	0.002	0.004	0.001	0.001	0.001
162.97	RICE_3yr_173	0.105	0.269	0.023	0.078	0.021	0.002	0.007	0.003	0.011	0.002	0.006	0.001	0.001	<0.001
163.54	RICE_3yr_174	0.144	0.568	0.032	0.138	0.022	0.002	0.024	0.003	0.019	0.003	0.010	0.002	0.002	0.001
164.06	RICE_3yr_175	0.247	0.722	0.051	0.188	0.040	0.009	0.035	0.003	0.032	0.004	0.015	0.001	0.003	0.001
164.62	RICE_3yr_176	0.161	0.495	0.035	0.103	0.022	0.003	0.015	0.002	0.014	0.003	0.007	0.001	0.003	<0.001
165.14	RICE_3yr_177	0.069	0.187	0.014	0.050	0.010	0.003	0.005	0.002	0.011	0.001	0.002	<0.001	0.001	<0.001
165.68	RICE_3yr_178	0.083	0.242	0.015	0.067	0.012	0.004	0.005	0.002	0.006	0.002	0.002	<0.001	0.001	<0.001
166.26	RICE_3yr_179	0.122	0.316	0.023	0.085	0.010	0.002	0.014	0.002	0.013	0.001	0.005	<0.001	<0.001	<0.001
166.80	RICE_3yr_180	0.087	0.503	0.018	0.057	0.016	0.002	0.012	0.001	0.011	0.001	0.003	0.001	0.001	0.001
167.35	RICE_3yr_181	0.063	0.162	0.013	0.055	0.008	0.001	0.003	0.001	0.007	0.001	0.002	<0.001	0.001	<0.001
167.88	RICE_3yr_182	0.098	0.601	0.020	0.067	0.019	0.002	0.010	0.001	0.011	0.001	0.005	<0.001	0.001	<0.001
168.39	RICE_3yr_183	0.097	0.243	0.020	0.076	0.016	0.003	0.013	0.001	0.010	0.003	0.008	0.001	0.002	0.001
168.94	RICE_3yr_184	0.093	0.271	0.018	0.068	0.007	0.001	0.011	0.002	0.006	0.001	0.003	<0.001	0.001	<0.001
169.45	RICE_3yr_185	0.084	0.592	0.018	0.069	0.020	0.006	0.010	0.001	0.012	<0.001	0.003	0.001	<0.001	0.001
170.02	RICE_3yr_186	0.083	0.566	0.017	0.057	0.007	0.002	0.017	0.001	0.009	0.001	0.007	0.001	<0.001	<0.001
170.55	RICE_3yr_187	0.101	0.520	0.019	0.068	0.015	0.001	0.011	0.002	0.006	0.001	0.006	<0.001	0.001	<0.001
171.07	RICE_3yr_188	0.070	0.831	0.012	0.046	0.009	0.002	0.008	0.001	0.008	0.001	0.004	<0.001	0.001	<0.001
171.59	RICE_3yr_189	0.079	0.260	0.014	0.078	0.008	0.001	0.009	<0.001	0.008	0.001	0.005	<0.001	0.001	0.001
172.10	RICE_3yr_190	0.100	0.274	0.025	0.069	0.014	0.003	0.017	0.002	0.011	0.001	0.006	<0.001	0.001	<0.001
172.63	RICE_3yr_191	0.080	1.175	0.014	0.077	0.012	0.003	0.012	0.001	0.007	<0.001	0.005	<0.001	0.001	<0.001
173.16	RICE_3yr_192	0.062	0.202	0.015	0.060	0.006	0.001	0.002	0.001	0.004	<0.001	0.003	0.001	0.001	<0.001
173.66	RICE_3yr_193	0.075	0.347	0.017	0.066	0.007	0.002	0.010	0.001	0.005	0.001	0.006	<0.001	0.001	<0.001
174.18	RICE_3yr_194	0.105	0.317	0.023	0.098	0.005	0.002	0.009	0.001	0.013	0.003	0.004	0.002	0.001	0.001
174.71	RICE_3yr_195	0.084	0.285	0.019	0.067	0.018	0.002	0.015	0.001	0.006	0.001	0.007	<0.001	0.001	<0.001
175.23	RICE_3yr_196	0.089	0.265	0.019	0.085	0.006	0.001	0.013	0.001	0.010	0.002	0.006	<0.001	0.001	<0.001
175.76	RICE_3yr_197	0.139	0.661	0.022	0.107	0.017	0.002	0.012	0.001	0.009	0.002	0.006	0.001	0.001	0.001
176.26	RICE_3yr_198	0.067	0.190	0.016	0.047	0.012	0.001	0.003	0.001	0.007	<0.001	0.004	<0.001	0.001	<0.001
176.79	RICE_3yr_199	0.121	0.379	0.022	0.101	0.022	0.003	0.013	0.002	0.019	0.003	0.010	<0.001	0.002	<0.001
177.32	RICE_3yr_200	0.092	0.403	0.019	0.062	0.008	0.001	0.013	0.001	0.006	0.001	0.006	<0.001	<0.001	0.001
197.84	RICE_3yr_241	0.081	0.505	0.017	0.064	0.012	<0.001	0.009	0.001	0.011	0.001	0.003	0.001	0.001	<0.001
198.27	RICE_3yr_242	0.125	0.347	0.023	0.093	0.017	0.001	0.012	0.002	0.012	0.001	0.006	0.001	0.001	0.001
198.78	RICE_3yr_243	0.078	0.226	0.018	0.063	0.009	<0.001	0.007	0.001	0.010	<0.001	0.001	0.001	0.001	<0.001
199.25	RICE_3yr_244	0.065	0.200	0.014	0.060	0.010	<0.001	0.004	0.002	0.008	<0.001	0.002	<0.001	0.001	<0.001
199.69	RICE_3yr_245	0.095	0.717	0.020	0.070	0.019	0.001	0.009	0.002	0.008	0.001	0.005	0.001	0.001	0.001
200.15	RICE_3yr_246	0.161	0.347	0.029	0.112	0.016	<0.001	0.012	0.002	0.011	0.002	0.006	0.001	0.001	0.001
200.63	RICE_3yr_247	0.089	0.428	0.017	0.068	0.019	<0.001	0.008	0.001	0.010	0.001	0.004	0.001	0.001	0.001
201.08	RICE_3yr_248	0.113	0.311	0.022	0.080	0.014	0.001	0.013	0.003	0.015	0.002	0.007	0.001	0.001	0.001
201.56	RICE_3yr_249	0.103	0.266	0.020	0.073	0.016	0.001	0.007	0.001	0.010	0.002	0.005	0.001	0.001	0.001
201.99	RICE_3yr_250	0.068	0.185	0.015	0.053	0.008	<0.001	0.007	0.001	0.007	0.001	0.004	0.001	0.001	<0.001
202.45	RICE_3yr_251	0.101	0.202	0.019	0.072	0.011	<0.001	0.008	0.001	0.009	0.001	0.003	<0.001	0.001	<0.001

202.89	RICE_3yr_252	0.107	0.700	0.021	0.080	0.016	<0.001	0.012	0.002	0.011	0.001	0.005	0.001	0.001	0.001
203.34	RICE_3yr_253	0.122	0.356	0.023	0.088	0.012	<0.001	0.010	0.002	0.011	0.002	0.004	0.001	0.001	0.001
203.80	RICE_3yr_254	0.103	0.472	0.020	0.084	0.019	<0.001	0.008	0.002	0.011	0.003	0.005	0.001	0.002	0.001
204.29	RICE_3yr_255	0.144	0.431	0.029	0.116	0.022	0.002	0.016	0.002	0.015	0.002	0.009	0.001	0.001	0.001
204.70	RICE_3yr_256	0.094	0.257	0.019	0.074	0.012	0.001	0.008	0.002	0.013	0.002	0.004	0.001	0.001	0.001
205.19	RICE_3yr_257	0.072	0.188	0.014	0.060	0.011	<0.001	0.006	0.001	0.008	0.001	0.004	0.001	0.001	<0.001
205.62	RICE_3yr_258	0.116	0.311	0.024	0.094	0.014	0.001	0.013	0.002	0.014	0.002	0.006	0.001	0.002	0.001
206.07	RICE_3yr_259	0.120	0.334	0.024	0.097	0.020	0.002	0.013	0.002	0.018	0.003	0.006	0.001	0.002	0.001
206.50	RICE_3yr_260	0.110	0.278	0.021	0.073	0.012	<0.001	0.012	0.002	0.010	0.001	0.004	0.001	0.001	0.001
206.95	RICE_3yr_261	0.077	0.395	0.017	0.055	0.018	0.001	0.008	0.001	0.008	0.002	0.005	0.001	0.001	0.001
207.41	RICE_3yr_262	0.138	0.323	0.027	0.097	0.017	0.001	0.012	0.002	0.014	0.002	0.005	0.001	0.001	0.001
207.85	RICE_3yr_263	0.102	0.233	0.019	0.071	0.015	0.001	0.012	0.002	0.013	0.002	0.006	0.001	0.001	0.001
208.30	RICE_3yr_264	0.116	0.258	0.022	0.078	0.015	0.001	0.011	0.002	0.011	0.002	0.004	0.001	0.001	0.001
208.72	RICE_3yr_265	0.138	0.370	0.026	0.104	0.020	0.002	0.014	0.002	0.015	0.003	0.007	0.002	0.002	0.001
209.19	RICE_3yr_266	0.084	0.221	0.016	0.057	0.013	<0.001	0.007	0.001	0.009	0.001	0.003	0.001	0.001	0.001
209.61	RICE_3yr_267	0.109	0.405	0.023	0.080	0.019	<0.001	0.010	0.002	0.008	0.003	0.006	0.001	0.001	0.001
210.04	RICE_3yr_268	0.068	0.202	0.014	0.051	0.009	<0.001	0.006	0.001	0.008	0.001	0.003	<0.001	<0.001	<0.001
210.49	RICE_3yr_269	0.061	0.172	0.013	0.051	0.010	<0.001	0.006	0.001	0.007	0.001	0.003	0.001	0.001	<0.001
210.93	RICE_3yr_270	0.124	0.381	0.027	0.098	0.020	0.002	0.012	0.002	0.011	0.002	0.006	0.001	0.002	0.001
211.38	RICE_3yr_271	0.105	0.282	0.020	0.084	0.019	0.001	0.012	0.002	0.011	0.003	0.006	0.001	0.001	0.001
211.80	RICE_3yr_272	0.151	0.451	0.028	0.114	0.021	0.001	0.017	0.003	0.017	0.003	0.008	0.001	0.001	0.001
212.25	RICE_3yr_273	0.127	0.325	0.025	0.088	0.020	<0.001	0.014	0.002	0.011	0.002	0.005	0.001	0.001	0.001
212.67	RICE_3yr_274	0.084	0.428	0.017	0.065	0.017	<0.001	0.011	0.002	0.011	0.002	0.005	0.001	0.001	0.001
213.08	RICE_3yr_275	0.111	0.298	0.022	0.083	0.017	0.001	0.011	0.002	0.009	0.002	0.005	0.001	0.002	0.001
213.51	RICE_3yr_276	0.108	0.291	0.021	0.077	0.014	0.002	0.011	0.001	0.011	0.002	0.005	0.001	0.002	0.001
213.94	RICE_3yr_277	0.066	0.154	0.013	0.050	0.007	<0.001	0.007	0.002	0.007	0.002	0.004	0.001	0.001	<0.001
214.39	RICE_3yr_278	0.100	0.232	0.019	0.073	0.013	<0.001	0.009	0.001	0.009	0.002	0.003	0.001	0.001	0.001
214.78	RICE_3yr_279	0.071	0.243	0.014	0.052	0.011	<0.001	0.006	0.001	0.009	0.001	0.003	<0.001	0.001	<0.001
215.23	RICE_3yr_280	0.116	0.248	0.022	0.083	0.014	<0.001	0.011	0.002	0.010	0.003	0.005	0.001	0.001	0.001
215.66	RICE_3yr_281	0.129	0.421	0.024	0.103	0.023	0.001	0.016	0.001	0.014	0.003	0.007	0.001	0.001	<0.001
216.07	RICE_3yr_282	0.104	0.279	0.020	0.084	0.017	0.001	0.011	0.002	0.013	0.002	0.004	0.001	0.001	0.001
216.50	RICE_3yr_283	0.113	0.272	0.023	0.082	0.019	0.001	0.013	0.002	0.012	0.003	0.005	0.001	0.001	0.001
216.92	RICE_3yr_284	0.082	0.192	0.017	0.063	0.013	0.001	0.010	0.001	0.007	0.002	0.005	<0.001	0.001	<0.001
217.32	RICE_3yr_285	0.108	0.267	0.021	0.079	0.018	0.001	0.012	0.002	0.011	0.002	0.006	0.001	0.001	0.001
217.77	RICE_3yr_286	0.084	0.735	0.017	0.066	0.014	0.001	0.011	0.001	0.008	0.002	0.005	<0.001	0.001	<0.001
218.17	RICE_3yr_287	0.079	0.217	0.015	0.055	0.011	<0.001	0.009	0.001	0.008	0.002	0.002	<0.001	0.001	<0.001
218.61	RICE_3yr_288	0.259	0.347	0.080	0.356	0.093	0.017	0.071	0.016	0.090	0.016	0.037	0.005	0.006	0.003
219.00	RICE_3yr_289	0.119	0.302	0.025	0.089	0.021	0.001	0.011	0.002	0.012	0.003	0.005	0.001	0.001	0.001
219.43	RICE_3yr_290	0.095	0.266	0.019	0.075	0.015	<0.001	0.010	0.002	0.011	0.002	0.005	0.001	0.001	0.001
219.85	RICE_3yr_291	0.161	0.406	0.030	0.116	0.026	0.002	0.015	0.003	0.015	0.003	0.008	0.001	0.002	0.001
220.28	RICE_3yr_292	0.087	0.241	0.017	0.060	0.010	0.001	0.010	0.001	0.010	0.002	0.005	0.001	0.001	0.001
220.66	RICE_3yr_293	0.095	0.782	0.018	0.058	0.014	0.001	0.011	0.001	0.007	0.001	0.006	<0.001	0.001	0.001
221.11	RICE_3yr_294	0.080	0.225	0.017	0.063	0.010	<0.001	0.009	0.001	0.010	0.002	0.005	0.001	0.001	0.001
221.52	RICE_3yr_295	0.087	0.241	0.016	0.066	0.015	0.001	0.012	0.002	0.010	0.003	0.007	0.001	0.001	0.001
221.91	RICE_3yr_296	0.128	0.340	0.025	0.095	0.026	0.002	0.012	0.003	0.012	0.003	0.007	0.001	0.002	0.001
222.33	RICE_3yr_297	0.066	0.191	0.016	0.047	0.009	<0.001	0.008	0.001	0.009	0.002	0.005	0.001	0.001	0.001
222.71	RICE_3yr_298	0.143	0.404	0.031	0.108	0.024	0.002	0.017	0.003	0.018	0.004	0.009	0.001	0.002	0.001
223.16	RICE_3yr_299	0.162	0.407	0.031	0.119	0.026	0.002	0.016	0.003	0.015	0.003	0.008	0.001	0.002	0.001
223.54	RICE_3yr_300	0.113	0.289	0.022	0.091	0.017	0.001	0.012	0.002	0.010	0.003	0.006	0.001	0.002	0.001
223.96	RICE_3yr_301	0.108	0.420	0.024	0.092	0.020	0.001	0.014	0.002	0.014	0.003	0.006	0.001	0.001	0.001
224.35	RICE_3yr_302	0.148	0.333	0.027	0.105	0.015	0.002	0.013	0.001	0.013	0.002	0.006	0.001	0.001	0.001
224.76	RICE_3yr_303	0.114	0.286	0.024	0.085	0.021	0.001	0.013	0.002	0.011	0.002	0.005	0.001	0.001	0.001
225.14	RICE_3yr_304	0.096	0.259	0.019	0.071	0.015	0.001	0.011	0.002	0.013	0.003	0.007	0.001	0.001	0.001
225.54	RICE_3yr_305	0.082	0.207	0.015	0.052	0.012	<0.001	0.007	0.001	0.009	0.001	0.004	0.001	<0.001	0.001
225.96	RICE_3yr_306	0.089	0.286	0.019	0.063	0.016	<0.001	0.009	0.001	0.009	0.002	0.005	0.001	0.001	<0.001
226.42	RICE_3yr_307	0.111	0.253	0.021	0.085	0.014	0.002	0.011	0.002	0.009	0.002	0.005	0.001	0.001	0.001
226.79	RICE_3yr_308	0.088	0.430	0.017	0.059	0.013	<0.001	0.007	0.001	0.008	0.002	0.004	<0.001	0.002	<0.001
227.22	RICE_3yr_309	0.331	0.416	0.063	0.223	0.040	0.002	0.021	0.003	0.018	0.003	0.008	0.001	0.001	0.001
227.58	RICE_3yr_310	0.184	0.279	0.033	0.115	0.019	0.001	0.010	0.002	0.012	0.002	0.006	0.001	0.001	0.001
228.00	RICE_3yr_311	0.096	0.208	0.020	0.074	0.014	<0.001	0.010	0.002	0.008	0.002	0.004	<0.001	0.001	<0.001
228.41	RICE_3yr_312	0.095	0.205	0.018	0.061	0.015	<0.001	0.010	0.002	0.008	0.002	0.005	0.001	0.001	0.001
228.77	RICE_3yr_313	0.114	3.552	0.021	0.083	0.021	0.001	0.011	0.002	0.012	0.003	0.006	0.001	0.002	0.001
229.17	RICE_3yr_314	0.134	0.359	0.027	0.102	0.021	0.002	0.014	0.002	0.013	0.002	0.007	0.001	0.002	0.001

229.57	RICE_3yr_315	0.100	0.266	0.019	0.072	0.015	<0.001	0.010	0.001	0.009	0.002	0.006	0.001	0.001	0.001
229.97	RICE_3yr_316	0.165	0.957	0.031	0.108	0.031	0.001	0.012	0.002	0.016	0.004	0.008	0.002	0.002	0.001
230.37	RICE_3yr_317	0.078	0.183	0.016	0.060	0.014	0.001	0.010	0.001	0.014	0.003	0.005	0.001	0.001	0.001
230.76	RICE_3yr_318	0.140	0.334	0.031	0.112	0.030	0.002	0.015	0.003	0.016	0.003	0.009	0.001	0.002	0.001
231.12	RICE_3yr_319	0.085	0.213	0.017	0.067	0.018	0.001	0.010	0.002	0.012	0.002	0.006	0.001	0.002	0.001
231.53	RICE_3yr_320	0.088	0.203	0.016	0.065	0.016	0.001	0.010	0.002	0.010	0.002	0.004	<0.001	0.001	0.001
231.90	RICE_3yr_321	0.117	0.326	0.022	0.087	0.018	<0.001	0.012	0.002	0.013	0.002	0.006	0.001	0.001	0.001
232.33	RICE_3yr_322	0.156	0.389	0.031	0.121	0.023	0.002	0.015	0.003	0.014	0.003	0.009	0.001	0.002	0.001
232.71	RICE_3yr_323	0.143	0.325	0.029	0.108	0.026	0.002	0.013	0.003	0.014	0.002	0.007	0.001	0.002	0.001
233.07	RICE_3yr_324	0.125	0.277	0.023	0.091	0.017	0.001	0.012	0.002	0.012	0.003	0.006	0.001	0.001	0.001
233.45	RICE_3yr_325	0.133	0.322	0.026	0.089	0.019	0.001	0.011	0.002	0.014	0.002	0.006	0.001	0.001	0.001
233.85	RICE_3yr_326	0.108	0.292	0.021	0.082	0.016	0.001	0.013	0.002	0.015	0.002	0.006	0.001	0.001	0.001
234.25	RICE_3yr_327	0.117	0.266	0.024	0.083	0.019	0.002	0.013	0.002	0.013	0.003	0.007	0.001	0.002	0.001
234.63	RICE_3yr_328	0.106	0.311	0.019	0.071	0.020	<0.001	0.009	0.001	0.012	0.002	0.004	0.001	0.001	0.001
235.02	RICE_3yr_329	0.093	0.226	0.016	0.070	0.016	0.001	0.008	0.001	0.008	0.002	0.005	<0.001	0.001	<0.001
235.36	RICE_3yr_330	0.119	0.282	0.022	0.084	0.014	0.001	0.010	0.002	0.010	0.002	0.006	<0.001	0.001	0.001
235.75	RICE_3yr_331	0.077	0.225	0.016	0.060	0.017	<0.001	0.008	0.002	0.009	0.002	0.003	<0.001	0.001	<0.001
236.14	RICE_3yr_332	0.099	0.201	0.019	0.070	0.015	0.001	0.009	0.001	0.010	0.002	0.005	0.001	0.001	0.001
236.49	RICE_3yr_333	0.114	0.252	0.022	0.080	0.019	0.002	0.012	0.002	0.013	0.002	0.006	0.001	0.001	0.001
236.88	RICE_3yr_334	0.469	0.946	0.088	0.333	0.054	0.013	0.034	0.006	0.037	0.007	0.019	0.002	0.005	0.003
237.29	RICE_3yr_335	0.081	0.195	0.014	0.056	0.009	0.001	0.006	0.001	0.008	0.002	0.003	0.001	0.001	<0.001
237.64	RICE_3yr_336	0.132	1.572	0.024	0.079	0.018	0.001	0.009	0.001	0.011	0.002	0.005	0.001	0.001	0.001
238.03	RICE_3yr_337	0.080	0.246	0.014	0.053	0.010	0.001	0.007	0.001	0.008	0.002	0.004	<0.001	0.001	<0.001
238.39	RICE_3yr_338	0.066	0.153	0.014	0.053	0.013	<0.001	0.007	0.001	0.006	0.001	0.003	<0.001	0.001	<0.001
238.78	RICE_3yr_339	0.079	0.276	0.015	0.053	0.013	0.001	0.007	<0.001	0.007	0.002	0.003	0.001	0.001	<0.001
239.15	RICE_3yr_340	0.157	0.347	0.029	0.099	0.025	0.001	0.015	0.002	0.015	0.002	0.006	0.001	0.001	0.001
239.51	RICE_3yr_341	0.065	0.170	0.012	0.047	0.014	<0.001	0.007	0.001	0.008	0.001	0.003	<0.001	0.001	<0.001
239.86	RICE_3yr_342	0.104	0.240	0.020	0.064	0.015	0.001	0.009	0.002	0.010	0.002	0.005	0.001	0.001	0.001
240.23	RICE_3yr_343	0.078	0.188	0.016	0.049	0.012	<0.001	0.008	0.001	0.006	0.001	0.003	<0.001	<0.001	<0.001
240.60	RICE_3yr_344	0.083	0.158	0.015	0.051	0.011	<0.001	0.005	0.001	0.007	0.002	0.004	0.001	0.001	<0.001
240.96	RICE_3yr_345	0.170	0.568	0.034	0.126	0.030	0.004	0.018	0.003	0.021	0.004	0.010	0.002	0.002	0.002
241.37	RICE_3yr_346	0.064	0.148	0.012	0.043	0.009	<0.001	0.005	0.001	0.007	0.001	0.003	<0.001	<0.001	<0.001
241.69	RICE_3yr_347	0.094	1.421	0.017	0.064	0.012	0.001	0.008	0.001	0.008	0.002	0.004	0.001	0.001	<0.001
242.07	RICE_3yr_348	0.060	0.160	0.011	0.045	0.014	-0.001	0.004	0.002	0.006	0.001	0.003	<0.001	0.001	<0.001
242.46	RICE_3yr_349	0.110	0.255	0.022	0.088	0.019	0.002	0.009	0.002	0.015	0.003	0.008	0.001	0.002	0.001
242.79	RICE_3yr_350	0.096	0.209	0.019	0.076	0.014	0.001	0.009	0.001	0.010	0.002	0.003	0.001	0.001	0.001
243.15	RICE_3yr_351	0.074	0.193	0.014	0.050	0.009	<0.001	0.008	0.001	0.007	0.001	0.005	0.001	0.001	<0.001
243.54	RICE_3yr_352	0.104	0.240	0.020	0.072	0.015	0.001	0.009	0.001	0.012	0.002	0.004	<0.001	0.002	<0.001
243.89	RICE_3yr_353	0.113	0.351	0.026	0.097	0.022	0.002	0.010	0.002	0.014	0.002	0.006	0.001	0.001	0.001
244.24	RICE_3yr_354	0.132	0.299	0.026	0.104	0.021	0.001	0.014	0.002	0.011	0.002	0.006	0.001	0.001	0.001
244.63	RICE_3yr_355	0.119	0.269	0.025	0.097	0.023	0.002	0.016	0.003	0.024	0.004	0.011	0.002	0.002	0.001
245.00	RICE_3yr_356	0.096	0.300	0.017	0.069	0.015	0.001	0.009	0.002	0.009	0.002	0.004	<0.001	0.001	0.001
245.35	RICE_3yr_357	0.081	0.208	0.014	0.054	0.009	<0.001	0.006	0.001	0.007	0.001	0.003	<0.001	0.001	<0.001
245.68	RICE_3yr_358	0.087	0.210	0.015	0.053	0.010	<0.001	0.007	0.001	0.007	0.001	0.003	<0.001	0.001	<0.001
246.07	RICE_3yr_359	0.075	0.206	0.016	0.059	0.014	<0.001	0.008	0.001	0.009	0.002	0.005	<0.001	0.001	<0.001
246.40	RICE_3yr_360	0.161	0.425	0.038	0.133	0.022	0.004	0.018	0.002	0.021	0.003	0.010	0.002	0.002	0.001
246.78	RICE_3yr_361	0.147	0.500	0.034	0.115	0.029	0.003	0.023	0.003	0.021	0.003	0.010	0.001	0.002	0.001
247.14	RICE_3yr_362	0.126	0.317	0.025	0.095	0.016	0.003	0.016	0.002	0.012	0.002	0.008	0.001	0.001	0.001
247.48	RICE_3yr_363	0.164	0.415	0.035	0.122	0.024	0.003	0.022	0.003	0.018	0.004	0.009	0.001	0.002	0.001
247.85	RICE_3yr_364	0.093	0.291	0.019	0.065	0.019	0.001	0.011	0.002	0.012	0.003	0.006	0.001	0.001	0.001
248.17	RICE_3yr_365	0.186	0.458	0.042	0.148	0.031	0.005	0.023	0.003	0.023	0.004	0.012	0.002	0.004	0.001
248.54	RICE_3yr_366	0.165	0.439	0.034	0.131	0.027	0.003	0.025	0.003	0.023	0.003	0.014	0.002	0.002	0.002
248.88	RICE_3yr_367	0.126	0.330	0.027	0.103	0.023	0.003	0.019	0.002	0.021	0.003	0.008	0.001	0.002	0.001
249.25	RICE_3yr_368	0.092	0.263	0.017	0.062	0.010	0.001	0.009	0.001	0.007	0.002	0.003	<0.001	0.001	<0.001
249.59	RICE_3yr_369	0.114	0.263	0.022	0.089	0.016	0.002	0.013	0.002	0.016	0.002	0.007	0.001	0.002	0.001
249.97	RICE_3yr_370	0.168	0.414	0.037	0.132	0.025	0.004	0.029	0.004	0.020	0.004	0.012	0.002	0.002	0.001
250.28	RICE_3yr_371	0.589	1.401	0.137	0.506	0.120	0.046	0.058	0.017	0.069	0.017	0.042	0.006	0.007	0.005
250.65	RICE_3yr_372	0.074	0.174	0.012	0.046	0.009	<0.001	0.004	0.001	0.006	0.001	0.004	<0.001	0.001	<0.001
250.97	RICE_3yr_373	0.078	0.190	0.014	0.051	0.009	<0.001	0.009	0.001	0.008	0.002	0.005	<0.001	0.001	<0.001
251.34	RICE_3yr_374	0.070	0.347	0.013	0.048	0.010	<0.001	0.008	0.001	0.006	0.002	0.005	0.001	0.001	<0.001
251.66	RICE_3yr_375	0.061	0.143	0.011	0.041	0.005	-0.001	0.008	0.001	0.006	0.002	0.004	<0.001	0.001	<0.001
252.03	RICE_3yr_376	0.093	0.210	0.016	0.063	0.012	<0.001	0.012	0.001	0.009	0.001	0.005	0.001	0.001	<0.001
252.38	RICE_3yr_377	0.099	0.267	0.021	0.071	0.013	0.002	0.010	0.002	0.010	0.001	0.006	0.001	0.002	0.001

252.76	RICE_3yr_378	0.079	0.598	0.018	0.065	0.015	0.002	0.009	0.001	0.009	0.001	0.006	0.001	0.001	0.001
253.08	RICE_3yr_379	0.128	0.263	0.023	0.071	0.011	-0.001	0.010	0.001	0.009	0.001	0.004	<0.001	0.001	<0.001
253.44	RICE_3yr_380	0.077	0.182	0.015	0.051	0.011	0.001	0.009	0.002	0.007	0.001	0.004	0.001	0.001	0.001
253.77	RICE_3yr_381	0.072	0.449	0.014	0.055	0.010	0.001	0.009	0.001	0.010	0.001	0.004	0.001	0.001	<0.001
254.14	RICE_3yr_382	0.111	0.279	0.022	0.082	0.021	0.001	0.015	0.002	0.016	0.002	0.007	0.001	0.002	0.001
254.46	RICE_3yr_383	0.103	0.241	0.019	0.065	0.017	0.001	0.010	0.002	0.013	0.001	0.006	0.001	0.002	0.001
254.80	RICE_3yr_384	0.153	0.300	0.030	0.104	0.023	0.002	0.016	0.002	0.017	0.002	0.006	0.001	0.001	0.001
255.13	RICE_3yr_385	0.065	0.149	0.014	0.042	0.009	-0.001	0.007	0.001	0.007	0.001	0.003	<0.001	0.001	<0.001
255.47	RICE_3yr_386	0.053	0.129	0.012	0.037	0.008	<0.001	0.007	<0.001	0.007	0.001	0.003	<0.001	0.001	<0.001
255.80	RICE_3yr_387	0.104	0.668	0.023	0.080	0.018	0.002	0.013	0.001	0.013	0.002	0.006	0.001	0.001	0.001
256.13	RICE_3yr_388	0.079	0.192	0.016	0.052	0.007	<0.001	0.010	0.001	0.008	0.001	0.004	0.001	0.001	0.001
256.49	RICE_3yr_389	0.138	0.336	0.026	0.093	0.021	<0.001	0.012	0.002	0.015	0.002	0.006	0.001	0.001	0.001
256.80	RICE_3yr_390	0.098	1.450	0.020	0.071	0.014	0.001	0.012	0.002	0.011	0.001	0.006	0.001	0.002	0.001
257.15	RICE_3yr_391	0.193	0.641	0.044	0.168	0.031	0.003	0.027	0.004	0.031	0.005	0.014	0.002	0.003	0.001
257.49	RICE_3yr_392	0.062	0.203	0.013	0.050	0.008	<0.001	0.008	0.001	0.007	<0.001	0.003	<0.001	<0.001	0.001
257.80	RICE_3yr_393	0.094	0.309	0.020	0.073	0.015	<0.001	0.015	0.002	0.013	0.001	0.006	<0.001	0.002	0.001
258.14	RICE_3yr_394	0.102	0.244	0.021	0.066	0.010	<0.001	0.011	0.001	0.009	0.002	0.005	0.001	0.001	<0.001
258.47	RICE_3yr_395	0.096	0.258	0.018	0.062	0.013	<0.001	0.009	0.002	0.008	0.002	0.005	0.001	0.001	<0.001
258.81	RICE_3yr_396	0.101	0.732	0.020	0.069	0.015	0.001	0.012	0.002	0.010	0.002	0.004	0.001	0.002	0.001
259.14	RICE_3yr_397	0.101	0.259	0.019	0.068	0.015	<0.001	0.010	0.001	0.009	0.002	0.006	<0.001	0.001	<0.001
259.47	RICE_3yr_398	0.277	0.586	0.055	0.179	0.031	0.002	0.019	0.003	0.014	0.002	0.007	0.001	0.001	0.001
259.82	RICE_3yr_399	0.109	0.998	0.021	0.067	0.017	0.001	0.011	0.001	0.011	0.002	0.005	<0.001	0.001	0.001
260.13	RICE_3yr_400	0.150	0.361	0.029	0.104	0.017	0.002	0.013	0.001	0.008	0.001	0.005	0.001	0.001	<0.001
260.44	RICE_3yr_401	0.199	0.460	0.040	0.134	0.022	0.003	0.017	0.002	0.016	0.002	0.008	0.001	0.002	0.001
260.76	RICE_3yr_402	0.109	0.271	0.023	0.085	0.015	0.002	0.017	0.001	0.013	0.001	0.005	0.001	0.001	0.001
261.14	RICE_3yr_403	0.106	0.268	0.023	0.078	0.016	0.002	0.012	0.002	0.012	0.002	0.006	0.001	0.001	0.001
261.47	RICE_3yr_404	0.124	0.280	0.023	0.080	0.015	0.001	0.011	0.001	0.010	0.001	0.005	0.001	0.001	0.001
261.81	RICE_3yr_405	0.193	0.957	0.042	0.159	0.032	0.003	0.027	0.003	0.024	0.005	0.013	0.002	0.003	0.002
262.14	RICE_3yr_406	0.106	0.258	0.022	0.079	0.016	0.002	0.013	0.001	0.009	0.001	0.003	<0.001	0.001	0.001
262.46	RICE_3yr_407	0.113	0.287	0.022	0.085	0.014	0.001	0.009	0.001	0.012	0.001	0.005	0.001	0.001	0.001
262.77	RICE_3yr_408	0.129	0.324	0.025	0.082	0.020	0.001	0.010	0.002	0.013	0.002	0.007	0.001	0.001	0.001
263.09	RICE_3yr_409	0.177	0.412	0.032	0.114	0.022	0.002	0.018	0.002	0.014	0.002	0.008	0.001	0.002	0.001
263.42	RICE_3yr_410	0.103	0.250	0.021	0.072	0.016	<0.001	0.010	0.002	0.011	0.001	0.005	0.001	0.001	0.001
263.75	RICE_3yr_411	0.109	0.260	0.022	0.076	0.013	0.002	0.014	0.002	0.013	0.002	0.006	0.001	0.002	0.001
264.08	RICE_3yr_412	0.113	0.242	0.021	0.074	0.013	0.001	0.008	0.001	0.007	0.001	0.004	<0.001	<0.001	<0.001
264.41	RICE_3yr_413	0.077	0.382	0.016	0.054	0.014	0.001	0.009	0.001	0.006	0.001	0.002	0.001	0.001	<0.001
264.75	RICE_3yr_414	0.109	0.268	0.023	0.075	0.016	0.001	0.011	0.002	0.012	0.002	0.005	<0.001	0.001	<0.001
265.04	RICE_3yr_415	0.118	0.385	0.022	0.074	0.019	0.002	0.009	0.002	0.009	0.002	0.004	0.001	0.001	0.001
265.34	RICE_3yr_416	0.086	0.213	0.018	0.068	0.015	0.001	0.008	0.001	0.008	0.001	0.004	0.001	0.001	<0.001
265.66	RICE_3yr_417	0.093	0.219	0.019	0.063	0.013	0.001	0.010	0.001	0.010	0.002	0.005	0.001	0.001	<0.001
265.98	RICE_3yr_418	0.111	1.148	0.023	0.079	0.017	0.002	0.013	0.002	0.013	0.002	0.006	0.001	0.001	0.001
266.30	RICE_3yr_419	0.109	0.264	0.022	0.070	0.016	0.002	0.010	0.001	0.009	0.001	0.005	0.001	0.001	0.001
266.58	RICE_3yr_420	0.170	0.420	0.034	0.113	0.019	0.002	0.013	0.002	0.016	0.002	0.008	0.001	0.001	0.001
266.91	RICE_3yr_421	0.180	0.494	0.034	0.130	0.030	0.002	0.019	0.003	0.015	0.003	0.008	0.001	0.001	0.001
267.21	RICE_3yr_422	0.133	0.370	0.026	0.093	0.019	0.002	0.013	0.001	0.015	0.002	0.006	0.001	0.001	<0.001
267.54	RICE_3yr_423	0.102	0.261	0.019	0.073	0.015	0.001	0.010	0.001	0.009	0.001	0.004	0.001	0.001	0.001
267.84	RICE_3yr_424	0.159	0.481	0.026	0.103	0.021	0.002	0.014	0.002	0.013	0.003	0.007	0.001	0.002	0.001
268.19	RICE_3yr_425	0.075	0.187	0.015	0.048	0.011	<0.001	0.004	0.001	0.010	0.001	0.003	<0.001	0.001	<0.001
268.47	RICE_3yr_426	0.103	0.278	0.020	0.075	0.015	0.001	0.011	0.002	0.011	0.002	0.006	0.001	0.001	0.001
268.79	RICE_3yr_427	0.167	0.581	0.032	0.121	0.026	0.002	0.014	0.002	0.013	0.002	0.008	0.001	0.001	0.001
269.09	RICE_3yr_428	0.087	0.242	0.019	0.061	0.014	<0.001	0.013	0.001	0.010	0.001	0.005	0.001	0.001	<0.001
269.40	RICE_3yr_429	0.106	0.286	0.021	0.081	0.017	0.001	0.011	0.001	0.012	0.002	0.005	0.001	0.001	0.001
269.72	RICE_3yr_430	0.148	0.347	0.029	0.102	0.019	0.002	0.013	0.002	0.011	0.002	0.007	0.001	0.001	0.001
270.05	RICE_3yr_431	0.101	0.252	0.022	0.077	0.018	0.001	0.010	0.001	0.010	0.001	0.006	0.001	0.001	0.001
270.34	RICE_3yr_432	0.115	0.269	0.023	0.078	0.019	0.001	0.014	0.001	0.010	0.001	0.005	<0.001	0.001	<0.001
270.65	RICE_3yr_433	0.164	0.838	0.034	0.110	0.025	0.003	0.017	0.002	0.017	0.002	0.007	0.001	0.001	0.001
270.96	RICE_3yr_434	0.092	0.404	0.019	0.070	0.012	0.001	0.011	0.002	0.010	0.001	0.007	0.001	0.001	<0.001
271.27	RICE_3yr_435	0.128	0.353	0.026	0.089	0.017	0.002	0.013	0.002	0.012	0.002	0.008	0.001	0.001	<0.001
271.56	RICE_3yr_436	0.067	0.175	0.014	0.045	0.007	-0.001	0.005	0.001	0.008	0.001	0.005	0.001	0.001	<0.001
271.86	RICE_3yr_437	0.094	0.513	0.018	0.060	0.013	0.002	0.007	0.001	0.008	0.001	0.006	<0.001	0.001	0.001
272.20	RICE_3yr_438	0.128	0.257	0.025	0.082	0.016	0.002	0.012	0.002	0.010	0.001	0.004	0.001	0.001	0.001
272.47	RICE_3yr_439	0.121	0.309	0.023	0.084	0.014	0.002	0.012	0.001	0.011	0.002	0.005	0.001	0.001	0.006
272.82	RICE_3yr_440	0.137	0.358	0.027	0.094	0.024	0.002	0.016	0.002	0.015	0.003	0.007	0.001	0.001	0.001

273.10	RICE_3yr_441	0.137	0.349	0.027	0.100	0.021	0.002	0.012	0.002	0.012	0.002	0.006	0.001	0.001	0.001
273.39	RICE_3yr_442	0.138	0.313	0.028	0.096	0.020	0.001	0.014	0.002	0.013	0.002	0.007	0.001	0.001	0.001
273.70	RICE_3yr_443	0.121	0.783	0.025	0.096	0.035	0.002	0.017	0.003	0.016	0.003	0.009	0.001	0.001	0.001
274.01	RICE_3yr_444	0.093	0.256	0.017	0.064	0.013	0.001	0.008	0.002	0.008	0.001	0.004	0.001	0.001	<0.001
274.30	RICE_3yr_445	0.077	0.195	0.018	0.060	0.007	0.001	0.006	0.001	0.008	0.001	0.004	<0.001	0.001	0.001
274.62	RICE_3yr_446	0.109	0.300	0.022	0.077	0.014	0.002	0.008	0.001	0.011	0.002	0.007	0.001	0.001	<0.001
274.88	RICE_3yr_447	0.141	0.516	0.026	0.105	0.023	0.002	0.015	0.003	0.015	0.003	0.009	0.001	0.002	0.001
275.19	RICE_3yr_448	0.143	0.324	0.026	0.087	0.017	0.002	0.015	0.001	0.016	0.003	0.006	0.001	0.002	0.001
275.51	RICE_3yr_449	0.196	0.440	0.037	0.125	0.029	0.003	0.024	0.003	0.018	0.003	0.009	0.002	0.003	0.001
275.82	RICE_3yr_450	2.665	5.076	0.504	1.818	0.331	0.056	0.245	0.040	0.231	0.038	0.107	0.014	0.021	0.010
276.12	RICE_3yr_451	0.263	0.617	0.055	0.192	0.040	0.004	0.026	0.004	0.028	0.005	0.016	0.002	0.002	0.001
276.40	RICE_3yr_452	0.205	0.460	0.040	0.141	0.026	0.004	0.019	0.003	0.023	0.004	0.011	0.001	0.002	0.001
276.72	RICE_3yr_453	0.355	1.110	0.061	0.226	0.039	0.005	0.028	0.005	0.029	0.005	0.018	0.002	0.002	0.001
276.98	RICE_3yr_454	0.285	1.248	0.055	0.178	0.037	0.004	0.026	0.004	0.025	0.006	0.012	0.002	0.002	0.001
277.28	RICE_3yr_455	0.133	0.283	0.023	0.088	0.018	0.001	0.013	0.002	0.011	0.002	0.005	0.001	0.001	0.001
277.60	RICE_3yr_456	0.184	0.402	0.035	0.129	0.029	0.003	0.017	0.003	0.019	0.003	0.009	0.001	0.002	0.001
277.89	RICE_3yr_457	0.179	0.624	0.033	0.113	0.022	0.003	0.022	0.003	0.011	0.003	0.007	0.001	0.001	0.001
278.20	RICE_3yr_458	0.126	0.287	0.025	0.093	0.017	0.002	0.013	0.002	0.013	0.002	0.005	0.001	0.001	0.001
278.48	RICE_3yr_459	0.162	0.354	0.033	0.110	0.025	0.003	0.017	0.003	0.018	0.003	0.008	0.001	0.002	0.001
278.76	RICE_3yr_460	0.200	0.451	0.041	0.138	0.030	0.004	0.023	0.002	0.023	0.003	0.009	0.001	0.002	0.002
279.06	RICE_3yr_461	0.170	0.424	0.036	0.129	0.027	0.003	0.019	0.003	0.017	0.002	0.009	0.001	0.002	0.001
279.35	RICE_3yr_462	0.154	0.344	0.031	0.116	0.022	0.002	0.019	0.003	0.020	0.003	0.010	0.001	0.002	0.001
279.63	RICE_3yr_463	0.098	0.226	0.022	0.069	0.016	0.001	0.012	0.002	0.011	0.002	0.005	0.001	0.001	0.001
279.91	RICE_3yr_464	0.178	0.611	0.036	0.135	0.031	0.003	0.019	0.003	0.018	0.003	0.010	0.001	0.002	0.001
280.21	RICE_3yr_465	0.115	0.265	0.024	0.074	0.017	0.001	0.014	0.001	0.009	0.002	0.005	0.001	0.001	0.001
280.51	RICE_3yr_466	0.093	0.216	0.019	0.064	0.014	<0.001	0.009	0.001	0.009	0.002	0.005	0.001	0.001	<0.001
280.77	RICE_3yr_467	0.148	0.535	0.029	0.106	0.024	0.002	0.015	0.003	0.018	0.002	0.009	0.001	0.001	0.001
281.06	RICE_3yr_468	0.180	0.435	0.135	0.128	0.031	0.002	0.017	0.002	0.020	0.003	0.008	0.001	0.002	0.001
281.35	RICE_3yr_469	0.137	0.307	0.028	0.101	0.018	0.001	0.011	0.002	0.015	0.002	0.007	0.001	0.001	0.001
281.65	RICE_3yr_470	0.098	0.216	0.018	0.066	0.016	0.001	0.009	0.001	0.010	0.001	0.005	0.001	0.001	0.001
281.91	RICE_3yr_471	0.146	0.320	0.029	0.109	0.020	0.002	0.015	0.002	0.012	0.002	0.005	0.001	0.002	0.001
282.23	RICE_3yr_472	0.076	0.167	0.015	0.055	0.009	0.001	0.007	<0.001	0.005	<0.001	0.003	0.001	0.001	<0.001
282.48	RICE_3yr_473	0.116	0.278	0.024	0.092	0.022	0.002	0.011	0.002	0.013	0.001	0.005	<0.001	0.002	0.001
282.79	RICE_3yr_474	0.150	1.132	0.031	0.112	0.027	0.002	0.018	0.002	0.015	0.003	0.007	0.001	0.001	0.001
283.05	RICE_3yr_475	0.133	0.516	0.027	0.108	0.025	0.001	0.015	0.002	0.017	0.001	0.007	0.001	0.002	0.001
283.32	RICE_3yr_476	0.144	0.437	0.029	0.105	0.018	0.002	0.018	0.002	0.013	0.002	0.007	0.001	0.001	0.001
283.64	RICE_3yr_477	0.091	0.290	0.019	0.063	0.015	<0.001	0.009	0.001	0.010	0.001	0.005	0.001	0.001	<0.001
283.89	RICE_3yr_478	0.161	0.678	0.039	0.160	0.044	0.004	0.028	0.004	0.029	0.003	0.012	0.001	0.003	0.002
284.18	RICE_3yr_479	0.138	0.338	0.029	0.096	0.019	0.001	0.014	0.002	0.012	0.001	0.006	0.001	0.001	<0.001
284.45	RICE_3yr_480	0.092	0.224	0.016	0.056	0.018	<0.001	0.010	0.001	0.010	0.001	0.003	0.001	0.001	<0.001
284.74	RICE_3yr_481	0.105	0.267	0.020	0.079	0.015	0.001	0.013	0.002	0.012	0.001	0.005	0.001	0.001	0.001
285.02	RICE_3yr_482	0.108	0.311	0.021	0.075	0.020	<0.001	0.011	0.002	0.010	0.001	0.007	0.001	0.001	0.001
285.32	RICE_3yr_483	0.082	0.214	0.017	0.059	0.010	0.001	0.008	0.001	0.009	0.001	0.004	<0.001	0.001	<0.001
285.57	RICE_3yr_484	0.119	0.345	0.025	0.103	0.018	0.003	0.017	0.001	0.012	0.002	0.008	0.001	0.001	0.001
285.86	RICE_3yr_485	0.165	4.119	0.034	0.133	0.030	0.002	0.022	0.003	0.018	0.002	0.009	0.001	0.003	0.001
286.15	RICE_3yr_486	0.120	0.388	0.025	0.093	0.016	0.002	0.013	0.002	0.012	0.002	0.007	0.001	0.001	<0.001
286.41	RICE_3yr_487	0.118	0.372	0.025	0.096	0.022	0.002	0.015	0.001	0.014	0.002	0.007	0.001	0.001	<0.001
286.68	RICE_3yr_488	0.116	0.346	0.022	0.089	0.017	0.002	0.011	0.002	0.012	0.002	0.009	0.001	0.001	0.001
286.99	RICE_3yr_489	0.143	0.837	0.033	0.113	0.021	0.003	0.020	0.003	0.016	0.003	0.010	0.001	0.002	0.001
287.28	RICE_3yr_490	0.135	0.435	0.028	0.088	0.018	0.002	0.015	0.002	0.014	0.003	0.008	0.001	0.002	0.001
287.55	RICE_3yr_491	0.127	0.338	0.026	0.088	0.018	0.002	0.012	0.002	0.013	0.002	0.006	0.001	0.001	0.001
287.80	RICE_3yr_492	0.144	0.383	0.029	0.111	0.023	0.001	0.015	0.003	0.014	0.002	0.008	0.001	0.002	0.001
288.05	RICE_3yr_493	0.121	0.336	0.023	0.093	0.019	0.001	0.014	0.001	0.014	0.002	0.006	0.001	0.001	0.001
288.36	RICE_3yr_494	0.094	0.249	0.018	0.076	0.015	0.001	0.011	0.001	0.011	0.001	0.006	0.001	0.001	0.001
288.63	RICE_3yr_495	0.110	0.275	0.023	0.081	0.017	0.002	0.012	0.002	0.009	0.001	0.005	0.001	0.001	0.001
288.90	RICE_3yr_496	0.139	0.522	0.027	0.100	0.021	0.002	0.018	0.002	0.014	0.003	0.007	0.001	0.002	0.001
289.19	RICE_3yr_497	0.113	0.352	0.023	0.084	0.017	0.002	0.011	0.002	0.011	0.002	0.005	<0.001	0.001	0.001
289.35	RICE_3yr_498	0.187	0.667	0.036	0.124	0.027	0.003	0.017	0.003	0.017	0.002	0.008	0.002	0.001	0.001
289.70	RICE_3yr_499	0.108	0.372	0.020	0.079	0.013	0.001	0.013	0.002	0.010	0.001	0.004	0.001	0.001	0.002
289.98	RICE_3yr_500	0.071	0.464	0.013	0.056	0.010	<0.001	0.007	0.001	0.008	0.001	0.004	<0.001	0.001	<0.001
290.25	RICE_3yr_501	0.083	0.248	0.017	0.067	0.014	0.001	0.010	0.001	0.007	0.001	0.003	<0.001	0.001	0.001
290.51	RICE_3yr_502	0.140	0.391	0.027	0.101	0.028	0.002	0.018	0.002	0.015	0.002	0.006	0.001	0.001	0.001
290.78	RICE_3yr_503	0.185	0.476	0.036	0.128	0.025	0.002	0.017	0.003	0.019	0.003	0.010	0.001	0.002	0.001

291.06	RICE_3yr_504	0.181	0.429	0.034	0.129	0.023	0.002	0.015	0.002	0.017	0.003	0.007	0.001	0.002	0.001
291.32	RICE_3yr_505	0.107	0.255	0.021	0.082	0.013	0.001	0.010	0.002	0.009	0.001	0.004	0.001	0.001	0.001
291.57	RICE_3yr_506	0.108	0.264	0.021	0.077	0.014	0.001	0.014	0.002	0.012	0.001	0.005	0.001	0.001	0.001
291.86	RICE_3yr_507	0.091	0.913	0.016	0.070	0.012	0.002	0.013	0.001	0.008	0.001	0.005	0.001	<0.001	0.001
292.12	RICE_3yr_508	0.129	0.349	0.025	0.097	0.017	0.002	0.014	0.002	0.012	0.002	0.006	0.001	0.001	0.001
292.38	RICE_3yr_509	0.087	0.219	0.016	0.062	0.009	<0.001	0.009	0.001	0.008	0.001	0.004	<0.001	0.001	0.001
292.63	RICE_3yr_510	0.115	0.298	0.021	0.079	0.016	0.002	0.015	0.002	0.013	0.002	0.006	0.001	0.001	0.001
292.94	RICE_3yr_511	0.105	0.340	0.022	0.081	0.015	0.001	0.012	0.002	0.011	0.002	0.006	0.001	0.001	<0.001
293.17	RICE_3yr_512	0.170	0.336	0.033	0.114	0.019	0.004	0.016	0.003	0.016	0.003	0.009	0.001	0.002	0.001
293.42	RICE_3yr_513	0.089	0.234	0.019	0.078	0.017	0.001	0.006	0.002	0.010	0.001	0.005	0.001	<0.001	0.001
293.71	RICE_3yr_514	0.093	0.247	0.018	0.065	0.011	<0.001	0.009	0.001	0.006	0.001	0.003	0.001	0.001	<0.001
293.97	RICE_3yr_515	0.086	0.221	0.018	0.062	0.014	0.001	0.008	0.002	0.008	0.001	0.006	0.001	0.001	0.001
294.25	RICE_3yr_516	0.078	0.185	0.015	0.056	0.011	<0.001	0.010	0.001	0.010	0.001	0.004	<0.001	0.001	0.001
294.50	RICE_3yr_517	0.076	0.193	0.016	0.056	0.007	0.001	0.007	0.001	0.009	0.001	0.004	<0.001	0.001	<0.001
294.76	RICE_3yr_518	0.109	1.045	0.021	0.075	0.017	0.001	0.014	0.002	0.008	0.001	0.006	0.001	0.001	<0.001
295.02	RICE_3yr_519	0.131	0.349	0.024	0.089	0.014	0.001	0.011	0.002	0.011	0.001	0.006	0.001	0.001	0.001
295.29	RICE_3yr_520	0.172	0.411	0.033	0.109	0.021	0.002	0.014	0.003	0.014	0.002	0.008	0.001	0.001	0.001
295.57	RICE_3yr_521	0.138	0.302	0.024	0.101	0.019	0.002	0.014	0.002	0.013	0.002	0.007	0.001	0.001	0.001
295.85	RICE_3yr_522	0.221	1.605	0.032	0.114	0.024	0.002	0.017	0.003	0.017	0.002	0.010	0.002	0.002	0.001
296.07	RICE_3yr_523	0.154	0.399	0.029	0.109	0.019	0.003	0.019	0.002	0.013	0.002	0.007	0.001	0.002	0.001
296.33	RICE_3yr_524	0.135	0.394	0.028	0.099	0.021	0.002	0.014	0.002	0.017	0.002	0.006	0.001	0.001	0.001
296.59	RICE_3yr_525	0.102	0.285	0.021	0.080	0.014	0.001	0.013	0.001	0.011	0.001	0.005	<0.001	0.001	0.001
296.85	RICE_3yr_526	0.131	0.339	0.025	0.098	0.019	0.001	0.015	0.002	0.012	0.002	0.005	0.001	0.001	<0.001
297.11	RICE_3yr_527	0.131	0.360	0.028	0.101	0.018	0.002	0.015	0.002	0.013	0.001	0.006	0.001	0.001	<0.001
297.40	RICE_3yr_528	0.093	0.238	0.019	0.079	0.012	0.001	0.014	0.002	0.011	0.001	0.005	<0.001	0.001	<0.001
297.61	RICE_3yr_529	0.094	0.256	0.018	0.065	0.013	0.001	0.009	0.001	0.012	0.001	0.006	0.001	0.001	<0.001
297.89	RICE_3yr_530	0.121	1.469	0.024	0.100	0.024	0.003	0.017	0.002	0.013	0.002	0.007	0.001	0.002	0.001
298.12	RICE_3yr_531	0.153	0.413	0.029	0.105	0.022	0.002	0.019	0.002	0.019	0.002	0.009	0.001	0.001	0.001
298.40	RICE_3yr_532	0.102	0.317	0.021	0.076	0.019	0.001	0.011	0.003	0.009	0.002	0.005	0.001	0.001	0.002
298.61	RICE_3yr_533	0.214	0.625	0.046	0.157	0.037	0.003	0.028	0.003	0.021	0.003	0.010	0.001	0.001	0.001
298.92	RICE_3yr_534	0.164	2.416	0.034	0.137	0.028	0.003	0.019	0.003	0.022	0.003	0.010	0.001	0.002	0.001
299.14	RICE_3yr_535	0.172	0.507	0.033	0.116	0.023	0.002	0.017	0.002	0.019	0.003	0.009	0.001	0.001	0.001
299.43	RICE_3yr_536	0.072	0.211	0.016	0.057	0.010	<0.001	0.010	0.002	0.011	0.002	0.006	0.001	0.001	0.001
299.67	RICE_3yr_537	0.173	0.515	0.036	0.130	0.030	0.002	0.015	0.003	0.014	0.002	0.007	0.001	0.001	0.001
299.90	RICE_3yr_538	0.123	0.340	0.023	0.090	0.016	<0.001	0.015	0.002	0.011	0.002	0.007	0.001	0.001	0.001
300.17	RICE_3yr_539	0.083	0.232	0.017	0.070	0.009	<0.001	0.009	0.001	0.010	0.002	0.004	<0.001	<0.001	0.001
300.44	RICE_3yr_540	0.219	0.473	0.039	0.138	0.026	0.003	0.019	0.003	0.017	0.004	0.010	0.001	0.002	0.001
300.69	RICE_3yr_541	0.161	0.379	0.031	0.114	0.024	0.002	0.016	0.002	0.013	0.003	0.010	0.001	0.001	0.001
300.95	RICE_3yr_542	0.167	1.290	0.034	0.131	0.026	0.002	0.016	0.002	0.014	0.002	0.006	0.001	0.001	0.001
301.19	RICE_3yr_543	0.111	0.323	0.022	0.082	0.009	0.001	0.014	0.002	0.010	0.001	0.007	0.001	0.001	<0.001
301.40	RICE_3yr_544	0.109	0.289	0.020	0.070	0.016	0.001	0.011	0.002	0.010	0.001	0.006	0.001	0.001	<0.001
301.65	RICE_3yr_545	0.114	0.283	0.023	0.080	0.016	0.001	0.009	0.001	0.009	0.001	0.004	0.001	0.001	0.001
301.94	RICE_3yr_546	0.153	0.540	0.030	0.107	0.021	0.002	0.019	0.003	0.016	0.001	0.008	0.001	0.001	0.001
302.17	RICE_3yr_547	0.132	0.328	0.026	0.091	0.019	0.001	0.015	0.002	0.012	0.002	0.006	<0.001	0.001	0.001
302.42	RICE_3yr_548	0.163	0.374	0.029	0.108	0.022	0.002	0.018	0.003	0.016	0.003	0.008	0.001	0.001	0.001
302.66	RICE_3yr_549	0.194	0.475	0.038	0.147	0.028	0.005	0.019	0.004	0.021	0.003	0.009	0.002	0.002	0.001
302.93	RICE_3yr_550	0.431	1.189	0.095	0.369	0.075	0.015	0.060	0.008	0.046	0.007	0.023	0.003	0.004	0.002
303.20	RICE_3yr_551	-0.002	-0.003	-0.001	-0.003	-0.001	0.004	<0.001	-0.001	-0.001	-0.001	<0.001	<0.001	<0.001	<0.001
303.48	RICE_3yr_552	0.547	1.848	0.119	0.443	0.094	0.017	0.075	0.012	0.068	0.010	0.033	0.005	0.007	0.003
303.67	RICE_3yr_553	0.473	1.492	0.104	0.375	0.077	0.013	0.062	0.009	0.058	0.009	0.025	0.004	0.006	0.003
303.90	RICE_3yr_554	0.370	1.090	0.066	0.231	0.050	0.007	0.034	0.005	0.035	0.005	0.016	0.002	0.004	0.002
304.16	RICE_3yr_555	0.285	0.654	0.052	0.199	0.037	0.005	0.029	0.004	0.024	0.004	0.012	0.002	0.002	0.001
304.42	RICE_3yr_556	0.173	0.453	0.033	0.117	0.024	0.003	0.017	0.003	0.020	0.002	0.008	0.001	0.002	0.001
304.65	RICE_3yr_557	0.150	0.403	0.031	0.115	0.019	0.003	0.017	0.002	0.016	0.001	0.007	0.001	0.001	0.001
304.89	RICE_3yr_558	0.210	1.351	0.043	0.163	0.036	0.004	0.026	0.003	0.026	0.002	0.011	0.002	0.003	0.001
305.16	RICE_3yr_559	0.171	0.496	0.037	0.141	0.029	0.004	0.019	0.003	0.020	0.002	0.009	0.001	0.002	0.001
305.40	RICE_3yr_560	0.127	0.364	0.026	0.102	0.016	0.002	0.018	0.002	0.014	0.002	0.006	0.001	0.001	0.001
305.62	RICE_3yr_561	0.116	0.306	0.024	0.078	0.015	0.001	0.013	0.002	0.012	0.001	0.005	0.001	0.001	0.001
305.85	RICE_3yr_562	0.220	0.463	0.042	0.161	0.029	0.004	0.021	0.003	0.019	0.003	0.013	0.001	0.002	0.001
306.13	RICE_3yr_563	0.133	0.345	0.027	0.090	0.021	0.003	0.015	0.002	0.013	0.001	0.005	0.001	0.002	0.001
306.37	RICE_3yr_564	0.155	0.395	0.030	0.108	0.024	0.002	0.015	0.003	0.013	0.002	0.008	0.001	0.002	0.001
306.61	RICE_3yr_565	0.103	0.241	0.020	0.070	0.015	0.001	0.009	0.002	0.010	0.001	0.006	0.001	0.001	<0.001
306.83	RICE_3yr_566	0.183	0.941	0.041	0.148	0.030	0.003	0.025	0.003	0.022	0.003	0.009	0.001	0.002	0.001

307.10	RICE_3yr_567	0.109	0.292	0.022	0.069	0.015	0.001	0.012	0.002	0.009	0.002	0.005	0.001	0.001	0.001
307.31	RICE_3yr_568	0.166	0.413	0.030	0.108	0.018	0.002	0.017	0.002	0.014	0.002	0.006	0.001	0.001	0.001
307.56	RICE_3yr_569	0.146	0.358	0.028	0.104	0.017	0.002	0.013	0.002	0.013	0.002	0.007	0.001	0.002	0.001
307.79	RICE_3yr_570	1.307	3.340	0.392	1.600	0.258	0.048	0.154	0.014	0.053	0.005	0.015	0.001	0.002	0.001
308.04	RICE_3yr_571	0.169	0.363	0.032	0.107	0.019	0.001	0.011	0.002	0.011	0.002	0.007	0.001	0.001	0.001
308.25	RICE_3yr_572	0.140	0.334	0.028	0.100	0.022	0.002	0.015	0.002	0.013	0.002	0.007	0.001	0.002	0.001
308.50	RICE_3yr_573	0.143	0.340	0.028	0.104	0.020	0.003	0.014	0.002	0.013	0.001	0.006	0.001	0.001	<0.001
308.75	RICE_3yr_574	0.148	0.312	0.026	0.090	0.015	0.002	0.013	0.002	0.010	0.001	0.006	0.001	0.001	0.001
308.98	RICE_3yr_575	0.095	0.225	0.020	0.065	0.015	0.001	0.008	<0.001	0.008	0.001	0.005	0.001	0.001	<0.001
309.19	RICE_3yr_576	0.078	0.201	0.016	0.054	0.008	0.001	0.012	0.001	0.007	0.001	0.005	0.001	0.001	<0.001
309.44	RICE_3yr_577	0.075	0.196	0.017	0.061	0.013	0.001	0.009	0.001	0.008	0.001	0.004	0.001	0.001	<0.001
309.69	RICE_3yr_578	0.138	0.735	0.027	0.087	0.029	0.003	0.015	0.002	0.017	0.001	0.005	0.001	0.002	0.001
309.93	RICE_3yr_579	0.129	0.354	0.026	0.085	0.018	0.001	0.013	0.001	0.011	0.002	0.005	0.001	0.001	0.001
310.15	RICE_3yr_580	0.088	0.225	0.020	0.065	0.011	0.001	0.005	0.001	0.010	0.001	0.004	0.001	0.001	<0.001
310.36	RICE_3yr_581	0.157	0.346	0.028	0.089	0.018	0.001	0.011	0.002	0.010	0.002	0.005	0.001	0.001	<0.001
310.60	RICE_3yr_582	0.194	1.955	0.036	0.129	0.026	0.003	0.019	0.002	0.020	0.002	0.010	0.001	0.002	<0.001
310.84	RICE_3yr_583	0.166	0.435	0.033	0.121	0.024	0.003	0.018	0.002	0.016	0.003	0.010	0.001	0.002	0.002
311.09	RICE_3yr_584	0.133	0.309	0.024	0.074	0.015	0.002	0.013	0.001	0.010	0.002	0.005	0.001	0.002	0.001
311.29	RICE_3yr_585	0.087	0.210	0.018	0.058	0.010	0.001	0.005	0.001	0.008	0.001	0.005	0.001	0.001	<0.001
311.55	RICE_3yr_586	0.140	0.357	0.031	0.096	0.020	0.003	0.013	0.002	0.012	0.002	0.007	0.001	0.001	0.001
311.79	RICE_3yr_587	0.186	0.472	0.038	0.134	0.026	0.003	0.019	0.002	0.019	0.002	0.006	0.002	0.002	0.001
312.02	RICE_3yr_588	0.142	0.322	0.027	0.100	0.023	0.001	0.013	0.002	0.014	0.002	0.005	<0.001	0.001	0.001
312.26	RICE_3yr_589	0.088	0.231	0.019	0.064	0.012	0.001	0.011	0.001	0.011	0.001	0.004	0.001	0.001	0.001
312.45	RICE_3yr_590	0.136	0.317	0.026	0.088	0.019	0.002	0.015	0.002	0.013	0.002	0.005	0.001	0.001	0.001
312.68	RICE_3yr_591	0.073	0.482	0.015	0.053	0.010	0.002	0.010	0.001	0.006	0.001	0.004	<0.001	0.001	<0.001
312.96	RICE_3yr_592	0.080	0.210	0.017	0.054	0.012	<0.001	0.007	0.001	0.008	0.001	0.003	0.001	0.001	<0.001
313.15	RICE_3yr_593	0.494	0.977	0.097	0.498	0.101	0.020	0.041	0.008	0.051	0.008	0.020	0.005	0.019	0.005
313.41	RICE_3yr_594	0.474	0.953	0.095	0.470	0.089	0.019	0.051	0.009	0.047	0.007	0.017	0.005	0.020	0.004
313.60	RICE_3yr_595	0.110	0.246	0.020	0.075	0.016	0.001	0.011	0.002	0.013	0.002	0.005	<0.001	0.001	<0.001
313.82	RICE_3yr_596	0.155	1.787	0.030	0.114	0.021	0.003	0.016	0.003	0.019	0.024	0.007	0.001	0.002	0.001
314.09	RICE_3yr_597	0.141	0.434	0.026	0.102	0.014	0.001	0.013	0.003	0.012	0.002	0.005	0.001	0.001	<0.001
314.31	RICE_3yr_598	0.132	0.351	0.026	0.093	0.016	0.002	0.012	0.002	0.010	0.001	0.005	0.001	0.002	0.001
314.51	RICE_3yr_599	0.080	0.233	0.016	0.058	0.011	0.001	0.010	0.002	0.008	0.001	0.003	<0.001	0.001	<0.001
314.74	RICE_3yr_600	0.113	0.294	0.022	0.077	0.017	0.001	0.011	0.002	0.008	0.002	0.006	0.001	0.001	<0.001
314.97	RICE_3yr_601	0.111	0.271	0.024	0.082	0.020	0.002	0.015	0.002	0.013	0.002	0.006	0.001	0.001	0.001
315.18	RICE_3yr_602	0.111	0.258	0.022	0.075	0.014	0.002	0.010	0.002	0.010	0.001	0.006	0.001	0.001	0.001
315.43	RICE_3yr_603	0.181	0.408	0.039	0.137	0.028	0.004	0.014	0.003	0.013	0.002	0.004	0.001	0.001	<0.001
315.63	RICE_3yr_604	0.080	0.181	0.014	0.050	0.006	0.001	0.007	0.001	0.007	<0.001	0.003	0.001	<0.001	<0.001
315.85	RICE_3yr_605	0.085	1.784	0.017	0.055	0.014	0.002	0.008	0.001	0.007	0.001	0.004	<0.001	0.001	<0.001
316.07	RICE_3yr_606	0.080	0.223	0.017	0.056	0.011	0.001	0.009	0.001	0.009	0.001	0.004	0.001	0.001	0.001
316.29	RICE_3yr_607	0.084	0.248	0.017	0.064	0.009	0.001	0.010	0.001	0.009	0.001	0.004	0.001	0.001	<0.001
316.56	RICE_3yr_608	0.095	0.264	0.022	0.083	0.016	0.002	0.012	0.001	0.010	0.001	0.008	0.001	0.001	0.001
316.75	RICE_3yr_609	0.148	0.397	0.030	0.108	0.018	0.003	0.018	0.002	0.013	0.002	0.006	0.001	0.002	0.001
316.96	RICE_3yr_610	0.126	1.563	0.025	0.091	0.020	0.002	0.015	0.002	0.012	0.002	0.006	0.001	0.001	0.001
317.22	RICE_3yr_611	0.113	0.318	0.023	0.077	0.015	0.001	0.012	0.001	0.008	0.002	0.005	0.001	0.001	<0.001
317.43	RICE_3yr_612	0.106	0.292	0.021	0.084	0.011	0.001	0.011	0.002	0.009	0.001	0.005	0.001	0.001	<0.001
317.67	RICE_3yr_613	0.065	0.177	0.014	0.045	0.007	0.001	0.005	0.001	0.006	<0.001	0.003	0.001	0.001	<0.001
317.88	RICE_3yr_614	0.156	0.361	0.031	0.098	0.019	0.002	0.014	0.001	0.011	0.001	0.005	0.001	0.001	<0.001
318.13	RICE_3yr_615	0.093	0.217	0.020	0.065	0.008	0.001	0.012	0.001	0.007	0.001	0.003	0.001	<0.001	<0.001
318.33	RICE_3yr_616	0.097	0.228	0.019	0.066	0.010	0.002	0.010	0.001	0.010	0.001	0.003	<0.001	0.001	<0.001
318.57	RICE_3yr_617	0.081	0.202	0.016	0.059	0.009	0.001	0.010	0.001	0.008	0.001	0.004	0.001	0.001	0.001
318.75	RICE_3yr_618	0.097	5.495	0.018	0.062	0.013	0.001	0.008	0.002	0.009	0.001	0.005	0.001	0.001	0.001
319.02	RICE_3yr_619	0.072	0.932	0.017	0.048	0.011	0.001	0.010	0.001	0.007	0.001	0.004	0.001	0.001	<0.001
319.23	RICE_3yr_620	0.101	0.411	0.020	0.072	0.016	0.002	0.010	0.002	0.011	0.001	0.005	0.001	0.001	<0.001

RICE deep core combined 40m to 320m samples, relative standard deviation (RSD, %).

Top Depth (m)	Sample ID	La139	Ce140	Pr141	Nd146	Sm147	Eu153	Gd157	Tb159	Dy163	Ho165	Er166	Tm169	Yb172	Lu175
40.00	RICE_3yr_1	9.1	3.2	8.6	11.5	41.7	42.0	28.1	41.5	17.3	18.3	37.0	42.3	52.3	74.3
40.95	RICE_3yr_2	5.6	3.2	12.0	25.6	30.5	32.2	38.9	18.8	23.3	50.8	45.8	42.8	59.7	60.8
42.27	RICE_3yr_3	6.8	4.5	21.9	15.1	18.3	42.2	28.5	44.5	52.0	40.3	56.6	28.8	31.7	52.6
43.64	RICE_3yr_4	5.9	5.8	12.1	22.1	47.6	26.7	27.0	29.8	49.5	39.1	58.0	45.9	90.4	45.8

44.68	RICE_3yr_5	4.4	6.1	23.4	31.8	55.4	29.5	35.3	23.6	42.8	89.6	112.9	38.9	92.6	71.9
45.61	RICE_3yr_6	6.1	2.1	21.2	24.1	33.5	44.9	32.7	19.5	27.1	36.9	46.8	49.4	84.8	63.1
46.60	RICE_3yr_7	9.3	6.5	9.0	16.7	25.1	36.2	27.4	32.7	26.5	42.3	70.5	65.6	83.8	68.9
47.59	RICE_3yr_8	10.3	3.6	15.4	28.8	27.7	41.7	43.7	70.6	26.7	40.5	55.9	46.2	33.2	98.1
48.56	RICE_3yr_9	7.4	6.4	14.7	35.2	59.1	48.5	45.4	36.8	36.6	26.7	48.7	65.6	76.6	85.5
49.58	RICE_3yr_10	8.1	5.1	17.8	31.8	39.5	27.5	46.8	34.7	39.3	56.0	30.1	73.4	82.2	86.9
50.50	RICE_3yr_11	5.5	6.5	21.1	7.8	21.9	41.8	32.5	27.9	29.1	30.3	58.9	39.9	63.0	73.5
51.41	RICE_3yr_12	5.1	3.7	20.9	24.0	63.3	44.9	23.7	37.4	31.7	101.3	27.3	42.9	132.7	73.7
52.34	RICE_3yr_13	14.9	4.9	14.3	20.9	34.8	24.9	35.1	38.9	37.4	45.0	41.4	55.0	40.0	93.0
53.31	RICE_3yr_14	11.3	2.1	12.3	24.1	25.9	50.5	38.5	56.3	38.3	20.5	100.7	46.2	79.3	84.0
54.19	RICE_3yr_15	2.9	6.4	24.5	16.7	35.8	63.1	43.8	52.8	51.6	56.4	64.0	77.5	52.0	117.4
55.17	RICE_3yr_16	5.5	8.2	24.4	24.4	74.8	52.0	54.9	46.0	48.1	38.4	90.8	43.8	73.2	74.2
56.02	RICE_3yr_17	5.9	4.0	12.8	17.3	50.5	25.5	53.4	36.8	50.1	21.2	51.1	82.1	61.0	107.0
56.89	RICE_3yr_18	4.6	7.5	29.7	8.7	52.9	22.4	49.9	30.6	30.4	64.1	67.6	133.1	71.3	104.2
57.77	RICE_3yr_19	6.1	10.2	18.8	22.3	37.0	27.0	47.1	51.3	63.8	56.4	53.6	84.0	123.7	65.7
58.69	RICE_3yr_20	8.8	5.4	21.3	19.3	45.4	89.9	48.2	44.2	70.9	57.4	16.0	73.8	92.9	126.3
59.52	RICE_3yr_21	8.3	1.4	14.9	14.8	49.9	40.0	44.7	15.0	24.5	48.3	49.0	92.7	85.0	100.3
60.40	RICE_3yr_22	6.4	6.2	20.1	21.3	37.3	50.4	41.2	52.7	49.7	59.8	43.9	56.4	101.1	74.7
61.36	RICE_3yr_23	7.8	5.6	16.5	18.6	67.0	43.1	26.5	64.2	36.6	62.1	94.2	67.0	99.1	88.5
62.17	RICE_3yr_24	7.3	3.5	8.2	20.5	40.7	35.2	47.4	38.8	46.0	39.7	44.7	83.4	84.1	90.6
63.08	RICE_3yr_25	13.8	3.7	8.1	6.4	21.3	22.4	25.8	36.5	36.0	14.8	39.8	66.0	25.0	208.6
63.92	RICE_3yr_26	7.7	6.3	5.0	13.9	29.2	32.6	16.4	22.1	23.1	34.7	21.5	36.2	51.3	191.4
64.76	RICE_3yr_27	7.6	5.4	12.6	15.1	43.0	23.2	50.8	38.0	58.5	64.6	42.4	62.6	63.3	44.7
65.61	RICE_3yr_28	8.2	5.7	16.6	21.3	42.6	40.6	51.2	29.5	22.3	64.3	26.5	70.3	82.9	65.0
66.45	RICE_3yr_29	2.4	5.8	14.1	26.7	31.2	64.5	55.6	36.4	82.0	62.7	65.1	97.0	55.7	69.7
67.32	RICE_3yr_30	14.6	6.5	19.2	36.0	41.0	49.1	71.0	63.4	75.5	49.6	52.4	66.6	64.0	74.2
68.14	RICE_3yr_31	6.5	4.0	19.9	24.1	64.1	73.3	48.0	82.9	29.3	21.4	37.9	72.9	111.0	70.4
68.97	RICE_3yr_32	14.4	5.6	9.8	11.7	45.2	38.5	30.6	55.4	32.5	80.5	85.2	57.5	78.0	30.1
69.80	RICE_3yr_33	9.9	9.4	18.6	26.0	30.4	41.3	13.8	76.7	45.9	29.4	77.3	41.0	55.4	216.9
70.65	RICE_3yr_34	12.9	4.9	9.2	23.2	38.4	53.7	49.4	40.2	58.3	38.5	73.1	75.1	73.5	237.4
71.46	RICE_3yr_35	14.9	5.4	15.4	29.4	53.2	30.3	52.2	33.2	53.4	54.8	57.7	95.4	76.4	73.8
72.30	RICE_3yr_36	12.0	5.3	18.3	30.6	48.1	51.0	47.9	64.3	83.2	35.9	68.5	63.9	102.8	99.6
73.15	RICE_3yr_37	6.3	6.4	29.2	26.0	38.5	41.0	45.8	33.4	28.3	54.6	39.5	67.3	97.2	90.2
73.93	RICE_3yr_38	7.7	6.4	12.6	29.4	39.4	44.2	35.8	60.2	51.8	64.4	53.5	67.2	88.6	102.7
74.75	RICE_3yr_39	9.0	3.6	19.3	15.3	37.6	45.7	52.9	53.4	63.5	30.4	35.9	61.0	70.6	117.5
75.54	RICE_3yr_40	6.2	4.0	17.2	22.8	45.8	52.3	23.9	43.1	20.6	19.8	26.5	58.9	53.4	30.5
76.31	RICE_3yr_41	7.7	2.7	12.8	24.6	25.5	56.2	27.4	28.6	31.3	35.1	57.7	43.4	66.2	109.3
77.14	RICE_3yr_42	6.7	6.8	16.7	26.4	34.8	37.7	31.2	27.4	38.4	28.6	44.3	50.0	131.5	114.4
77.94	RICE_3yr_43	53.5	4.2	14.9	19.5	34.3	29.3	43.9	51.7	32.5	46.1	63.9	52.7	83.9	64.1
78.75	RICE_3yr_44	10.9	12.4	17.0	19.4	47.5	56.1	38.9	65.2	36.6	65.2	65.1	32.6	69.7	69.3
79.51	RICE_3yr_45	11.7	3.8	7.5	19.7	69.8	40.4	46.8	63.5	51.9	27.0	37.2	64.3	85.1	140.4
80.32	RICE_3yr_46	8.1	3.9	19.2	25.5	31.4	45.9	39.5	44.2	62.6	50.6	85.7	48.3	37.4	71.5
81.06	RICE_3yr_47	13.2	5.1	23.9	18.3	36.5	61.1	37.0	45.9	39.9	54.4	59.7	58.0	4.3	139.6
81.86	RICE_3yr_48	4.2	3.3	16.8	29.2	34.3	27.5	69.6	38.2	27.2	43.1	21.7	41.8	53.0	118.2
82.64	RICE_3yr_49	6.4	5.5	26.3	10.1	49.5	56.5	39.6	25.6	54.7	30.1	40.6	56.1	79.3	91.0
83.51	RICE_3yr_50	11.7	1.8	9.1	14.4	27.4	40.1	40.8	59.4	36.3	39.1	42.0	57.8	137.5	92.2
84.29	RICE_3yr_51	12.9	4.6	9.1	16.5	25.6	51.4	52.1	25.4	42.4	51.8	23.7	39.6	61.6	58.8
85.01	RICE_3yr_52	11.6	4.5	22.3	20.4	56.0	64.0	42.7	97.0	62.2	41.7	82.0	43.7	76.5	117.6
85.80	RICE_3yr_53	7.1	7.2	5.8	18.4	30.6	39.8	25.3	69.2	45.3	76.1	60.5	63.6	41.1	78.3
86.57	RICE_3yr_54	7.6	4.6	10.0	15.5	36.0	81.6	44.2	46.6	41.4	26.1	53.9	32.0	81.8	91.5
87.32	RICE_3yr_55	7.0	2.1	23.2	16.6	32.5	23.2	27.1	62.9	30.0	24.1	82.5	75.3	82.1	71.7
88.09	RICE_3yr_56	10.5	175.4	20.9	22.9	62.4	39.5	30.0	35.2	57.1	66.6	44.5	116.5	80.8	82.5
88.84	RICE_3yr_57	5.5	6.0	12.7	9.3	53.6	58.1	50.1	30.4	18.3	31.4	24.8	86.0	67.6	64.1
89.57	RICE_3yr_58	7.7	5.4	10.0	16.4	41.1	23.7	36.8	38.5	22.6	53.6	25.4	59.3	60.0	51.2
90.30	RICE_3yr_59	7.9	2.7	35.1	28.2	36.3	54.0	27.9	47.2	85.8	69.2	75.9	76.3	70.8	112.4
91.05	RICE_3yr_60	7.8	4.2	14.1	23.7	47.3	50.2	34.6	37.7	47.6	33.2	69.8	101.7	131.5	111.2
91.80	RICE_3yr_61	7.7	3.6	14.5	13.7	37.0	55.9	40.4	68.2	38.0	40.5	98.7	59.0	42.8	115.2
92.56	RICE_3yr_62	4.9	3.0	11.9	21.2	26.9	19.4	50.7	44.6	41.2	28.8	28.4	41.0	52.1	49.6
93.30	RICE_3yr_63	3.9	7.8	13.0	33.5	28.7	34.0	37.5	62.2	57.6	60.8	90.4	84.7	105.7	68.9
93.99	RICE_3yr_64	13.2	4.5	18.9	27.4	54.0	55.7	34.8	22.9	113.1	49.9	48.7	128.1	101.1	136.8
94.75	RICE_3yr_65	14.2	7.4	24.3	14.3	46.8	29.5	40.4	88.7	45.4	62.6	45.8	41.3	55.7	80.7
95.50	RICE_3yr_66	10.7	4.8	10.5	29.6	34.8	68.2	40.0	37.1	48.2	84.8	44.0	108.1	102.1	113.4
96.21	RICE_3yr_67	6.1	7.0	27.9	19.3	52.3	39.2	39.9	41.8	38.0	38.5	50.6	67.9	54.2	76.1

96.92	RICE_3yr_68	7.6	3.5	14.5	19.5	23.7	45.6	32.6	64.6	20.8	52.4	156.0	59.6	99.2	181.9
97.67	RICE_3yr_69	9.1	3.5	21.5	25.4	46.1	42.7	59.8	56.6	33.3	53.7	43.9	86.5	87.5	89.2
98.40	RICE_3yr_70	10.2	5.6	40.4	43.2	46.4	50.8	86.8	70.4	48.9	48.1	98.5	53.5	139.9	83.5
99.09	RICE_3yr_71	4.6	3.5	14.8	23.5	67.3	65.7	61.2	22.1	44.2	46.8	106.2	59.2	97.2	80.1
99.78	RICE_3yr_72	13.7	6.0	19.2	25.6	54.4	23.6	74.3	80.4	52.4	66.6	65.9	80.0	63.0	127.3
100.51	RICE_3yr_73	9.9	6.5	19.4	13.8	34.9	53.5	39.8	60.4	14.0	73.1	75.4	70.1	94.9	62.7
101.23	RICE_3yr_74	17.1	4.6	20.5	35.7	48.7	30.4	33.6	38.8	43.7	59.3	70.7	89.7	98.8	109.2
101.92	RICE_3yr_75	9.4	2.8	18.4	22.5	75.1	45.6	63.3	55.3	129.0	43.6	79.1	48.1	81.4	102.7
102.67	RICE_3yr_76	7.5	2.6	19.5	34.7	42.2	31.1	58.2	46.5	73.2	62.1	81.8	66.1	108.4	111.4
103.36	RICE_3yr_77	13.5	3.9	22.8	25.7	68.1	48.2	47.1	66.6	43.7	36.6	61.9	78.1	51.7	62.6
104.04	RICE_3yr_78	10.4	8.2	22.4	16.2	29.7	31.4	50.0	31.4	46.9	54.7	86.1	35.7	122.5	245.0
104.77	RICE_3yr_79	11.4	7.4	9.1	48.5	67.7	47.5	60.4	54.2	93.5	27.9	45.5	46.3	90.1	90.7
105.47	RICE_3yr_80	10.6	5.8	23.2	15.3	46.4	33.7	35.9	29.6	30.4	40.7	42.0	84.8	77.5	63.6
106.18	RICE_3yr_81	7.2	7.2	17.5	17.3	55.7	24.0	38.2	41.0	60.2	59.3	49.1	31.3	68.0	61.8
106.91	RICE_3yr_82	9.9	3.3	16.4	14.2	22.8	44.6	41.3	49.5	15.6	36.2	17.5	57.6	92.2	148.8
107.56	RICE_3yr_83	8.0	3.5	15.7	16.7	38.8	58.0	45.0	55.5	61.7	32.5	44.5	42.8	23.2	232.2
108.25	RICE_3yr_84	6.6	4.6	10.0	13.0	54.4	11.6	46.6	40.1	43.2	36.1	27.3	36.8	36.5	34.5
108.96	RICE_3yr_85	5.5	3.1	19.5	10.0	59.9	25.6	36.9	82.3	43.7	42.1	59.0	41.7	56.0	47.0
109.62	RICE_3yr_86	9.4	2.7	16.6	19.3	33.3	19.0	31.8	42.9	67.3	35.8	46.0	41.1	69.6	89.2
110.31	RICE_3yr_87	8.4	5.6	14.1	11.8	32.3	23.2	38.8	40.8	34.7	37.6	39.5	77.6	96.6	86.2
111.04	RICE_3yr_88	9.2	9.1	12.0	59.4	24.2	29.9	37.5	33.6	33.0	46.6	42.3	34.5	69.2	68.6
111.71	RICE_3yr_89	6.6	4.3	9.8	21.6	53.3	39.6	72.9	32.2	49.0	53.9	28.3	90.5	54.5	91.6
112.38	RICE_3yr_90	6.4	3.2	19.5	11.5	37.6	23.9	23.9	35.4	58.0	28.9	67.2	87.0	88.0	64.7
113.06	RICE_3yr_91	4.6	5.2	16.4	20.0	37.7	52.7	39.0	51.5	41.3	46.7	28.3	43.1	72.5	52.3
113.73	RICE_3yr_92	6.1	6.8	23.9	18.3	46.7	65.6	47.2	39.4	49.4	56.6	75.1	64.7	108.5	190.4
114.39	RICE_3yr_93	16.6	9.1	14.4	14.1	66.3	35.2	47.7	59.2	64.7	27.8	89.6	90.6	100.8	159.8
115.11	RICE_3yr_94	8.8	1.3	16.8	9.6	31.6	48.8	35.1	32.4	19.1	46.2	46.9	44.6	63.4	63.0
115.78	RICE_3yr_95	9.1	4.2	9.4	13.6	41.9	43.3	21.3	26.7	24.3	43.3	63.6	59.6	69.8	47.7
116.44	RICE_3yr_96	8.5	5.2	16.9	25.6	42.9	25.3	40.2	39.7	20.2	61.9	40.8	68.1	62.6	175.2
117.12	RICE_3yr_97	8.8	3.8	15.5	20.4	40.5	42.7	61.2	73.8	37.5	39.1	62.2	49.5	51.7	72.8
117.76	RICE_3yr_98	6.1	9.5	15.2	18.8	62.3	64.3	72.1	85.3	48.8	28.8	56.6	70.8	95.2	143.1
118.41	RICE_3yr_99	7.3	3.4	6.8	18.0	50.3	52.3	35.7	57.8	45.8	31.5	37.4	63.1	66.9	91.8
119.08	RICE_3yr_100	4.3	3.8	19.2	26.5	45.8	46.0	43.8	63.1	60.9	42.1	35.1	31.6	70.2	62.3
119.75	RICE_3yr_101	4.6	4.8	19.1	11.3	29.2	55.9	27.4	31.5	55.1	45.8	63.9	53.2	42.4	215.8
120.44	RICE_3yr_102	12.9	9.4	7.7	15.6	41.2	54.4	72.4	47.8	69.5	39.8	115.8	91.3	103.3	93.1
121.05	RICE_3yr_103	12.3	6.3	12.3	32.7	50.0	41.5	84.1	45.5	56.1	60.4	83.1	48.2	113.4	44.8
121.74	RICE_3yr_104	10.0	5.9	17.6	23.4	26.3	44.5	31.4	61.7	55.8	40.2	53.6	44.3	70.9	98.5
122.37	RICE_3yr_105	7.3	7.1	24.2	19.7	36.3	51.9	80.4	46.4	44.2	60.1	77.2	51.5	84.1	126.2
123.04	RICE_3yr_106	10.2	8.1	18.4	27.9	47.2	70.2	65.6	18.9	44.7	76.9	85.0	69.5	64.5	106.3
123.69	RICE_3yr_107	8.4	5.9	28.4	23.2	47.7	56.9	48.0	52.0	44.5	57.3	48.1	110.8	92.0	140.2
124.33	RICE_3yr_108	6.2	3.3	17.7	33.2	23.2	71.7	76.2	59.9	77.5	63.0	64.9	136.3	63.5	83.3
124.94	RICE_3yr_109	5.4	3.1	11.0	18.2	45.6	41.0	49.3	50.9	69.0	46.4	56.4	63.6	90.5	75.4
125.59	RICE_3yr_110	9.6	5.3	12.0	24.1	51.7	18.2	42.5	40.2	64.8	39.1	95.2	79.3	78.4	126.6
126.25	RICE_3yr_111	12.9	6.7	10.1	19.1	50.3	33.1	70.3	29.3	63.2	42.8	37.7	32.0	110.0	120.5
126.89	RICE_3yr_112	11.8	3.3	17.1	22.6	37.7	48.5	46.1	38.0	49.0	63.6	40.1	79.5	55.2	244.6
127.53	RICE_3yr_113	4.0	4.9	9.1	20.2	70.6	78.6	36.1	23.1	38.6	36.5	54.9	47.0	64.5	64.9
128.17	RICE_3yr_114	7.8	7.3	10.3	12.5	53.5	48.3	18.7	41.9	27.9	32.3	37.0	36.0	61.5	122.0
128.81	RICE_3yr_115	11.2	3.7	21.3	5.4	56.7	62.2	58.3	29.1	44.3	15.5	62.5	87.2	85.0	81.8
129.45	RICE_3yr_116	3.7	1.6	15.1	23.7	43.3	41.8	48.5	35.5	31.6	59.0	50.2	75.9	70.5	118.1
130.06	RICE_3yr_117	4.4	8.9	22.3	16.7	33.1	23.5	42.9	40.8	72.9	64.8	50.3	64.7	70.2	141.4
130.71	RICE_3yr_118	8.6	5.0	14.8	13.0	59.7	19.6	41.6	24.3	50.6	52.3	76.6	70.1	40.5	100.7
131.32	RICE_3yr_119	8.1	6.4	14.1	9.9	45.3	55.3	10.6	45.4	47.0	45.8	45.6	63.4	67.3	113.7
131.95	RICE_3yr_120	2.9	3.4	17.9	24.4	52.1	57.5	39.9	36.1	25.1	27.5	76.1	42.6	68.6	72.8
132.61	RICE_3yr_121	22.7	3.9	21.7	33.4	40.9	72.7	79.4	66.1	39.3	60.4	33.2	102.1	64.0	98.8
133.20	RICE_3yr_122	9.9	3.1	23.8	21.9	59.1	26.0	36.2	26.9	33.7	55.0	70.5	107.7	112.3	119.7
133.83	RICE_3yr_123	7.4	5.5	31.7	23.6	50.4	43.3	62.4	21.3	46.6	56.6	80.8	95.3	90.8	79.8
134.45	RICE_3yr_124	12.8	7.5	17.4	31.0	60.9	42.7	60.6	25.6	58.8	94.2	76.2	55.3	137.6	141.3
135.10	RICE_3yr_125	11.3	4.8	12.9	22.9	79.4	60.7	64.7	43.9	36.8	70.4	58.9	37.1	82.3	99.5
135.69	RICE_3yr_126	7.4	2.7	10.3	14.1	42.8	53.5	44.8	22.5	34.5	48.7	40.9	66.4	62.9	100.0
136.33	RICE_3yr_127	7.5	5.2	22.8	26.6	54.3	24.8	29.8	62.0	60.1	57.6	60.1	83.2	131.6	140.7
136.92	RICE_3yr_128	12.3	6.9	24.9	23.1	49.7	25.9	25.5	66.0	48.0	29.8	39.7	81.4	63.8	63.6
137.52	RICE_3yr_129	4.6	5.9	16.3	26.4	48.9	44.0	68.1	49.9	45.7	31.0	93.0	55.5	62.2	70.8
138.15	RICE_3yr_130	13.9	5.0	16.2	21.2	47.1	55.7	55.7	42.6	92.6	54.2	31.0	48.7	95.6	168.3

138.77	RICE_3yr_131	10.5	2.0	18.4	27.9	35.7	31.9	25.7	35.3	25.4	52.6	52.6	64.4	84.2	113.1
139.36	RICE_3yr_132	9.4	6.5	27.3	29.6	83.2	74.5	57.4	20.3	43.0	45.3	50.3	116.7	54.6	41.3
139.97	RICE_3yr_133	10.1	3.7	18.6	12.9	49.8	19.0	43.1	42.2	60.3	26.5	68.8	74.6	103.5	68.4
140.59	RICE_3yr_134	7.0	7.4	21.4	18.1	37.5	35.7	46.6	47.4	65.2	41.6	54.2	75.2	52.9	87.4
141.18	RICE_3yr_135	7.1	4.2	7.6	31.6	40.4	56.0	39.6	77.5	82.3	71.9	93.1	85.8	70.6	91.9
141.78	RICE_3yr_136	11.7	2.5	31.7	23.2	36.4	30.2	39.3	36.3	47.3	54.2	84.4	63.3	103.9	103.1
142.37	RICE_3yr_137	10.6	3.4	21.2	24.6	47.5	67.5	46.6	41.2	23.0	45.2	39.0	46.4	84.9	83.7
142.97	RICE_3yr_138	13.6	4.7	15.4	12.4	36.0	49.9	68.6	59.4	50.3	66.1	60.2	97.6	67.7	80.1
143.59	RICE_3yr_139	12.5	3.8	13.5	27.7	36.6	93.8	50.1	60.3	69.3	34.7	41.0	106.8	67.8	121.4
144.19	RICE_3yr_140	8.9	7.0	9.8	23.1	65.7	51.9	30.5	51.7	32.1	48.9	89.9	63.5	29.8	115.2
144.76	RICE_3yr_141	8.0	4.3	24.0	20.6	60.1	57.2	46.7	59.5	34.7	69.1	42.5	83.0	70.3	167.2
145.32	RICE_3yr_142	14.4	7.2	31.6	27.8	88.2	47.0	47.0	88.6	43.7	37.8	98.5	57.7	69.3	182.2
145.91	RICE_3yr_143	11.6	5.4	25.0	27.9	67.9	56.4	39.2	46.5	61.4	36.1	42.8	84.5	42.0	55.7
146.48	RICE_3yr_144	7.7	3.9	19.5	8.7	28.7	59.8	85.4	29.6	18.2	40.2	38.1	77.5	75.1	44.8
147.08	RICE_3yr_145	10.9	4.2	13.0	20.7	34.3	35.4	45.9	49.5	55.2	57.1	25.6	54.9	89.3	85.4
147.67	RICE_3yr_146	8.6	5.4	9.6	22.6	29.2	19.6	29.7	25.6	58.9	31.7	74.4	54.6	74.0	126.1
148.28	RICE_3yr_147	13.4	2.6	24.3	23.5	48.3	49.4	32.0	23.2	63.2	40.3	76.0	120.0	35.9	124.5
148.84	RICE_3yr_148	5.6	3.8	15.5	21.9	141.1	9.8	33.1	46.8	49.7	51.1	73.1	78.9	70.2	83.5
149.44	RICE_3yr_149	12.0	3.2	15.0	12.3	34.8	71.0	67.5	41.5	69.8	41.4	98.4	65.4	111.5	92.4
150.03	RICE_3yr_150	7.1	3.0	14.7	6.5	32.1	64.4	25.5	38.6	37.2	54.6	33.0	64.3	91.6	92.2
150.61	RICE_3yr_151	10.1	4.0	19.2	21.7	41.5	62.1	48.8	46.3	58.6	53.9	159.3	72.2	63.3	49.0
151.20	RICE_3yr_152	10.4	6.2	30.6	16.8	78.2	75.0	38.2	51.9	37.1	149.6	112.0	50.5	155.1	111.4
151.77	RICE_3yr_153	6.9	5.9	21.6	18.3	60.8	81.3	50.8	39.7	20.8	66.2	57.3	63.8	78.2	81.4
152.32	RICE_3yr_154	9.9	4.2	22.5	31.4	54.5	44.0	48.0	93.6	37.4	58.6	63.8	72.5	55.2	100.6
152.91	RICE_3yr_155	13.3	1.3	7.5	25.3	39.0	28.7	35.7	48.7	35.6	51.5	52.3	41.3	88.7	102.4
153.49	RICE_3yr_156	2.9	6.1	28.4	10.0	43.0	64.7	31.9	22.3	58.4	41.1	73.3	23.7	53.6	182.1
154.04	RICE_3yr_157	4.8	3.8	10.4	19.0	43.4	27.4	29.0	26.8	45.9	39.3	50.0	68.0	94.4	87.8
154.61	RICE_3yr_158	5.2	3.0	13.8	10.0	38.2	28.5	32.3	10.5	27.9	35.5	57.3	40.7	57.7	73.2
155.21	RICE_3yr_159	12.5	5.5	7.7	13.0	87.4	38.0	30.8	40.1	31.3	38.6	40.2	47.2	118.1	69.1
155.75	RICE_3yr_160	5.3	4.1	19.6	27.0	61.4	44.6	29.9	42.3	37.3	54.1	46.4	65.8	61.3	78.7
156.34	RICE_3yr_161	6.4	7.3	20.6	20.9	39.0	45.3	64.8	62.1	33.0	59.5	34.4	60.6	72.3	129.3
156.90	RICE_3yr_162	10.3	6.1	9.0	20.2	41.0	39.9	35.1	39.6	25.7	50.2	71.5	95.6	122.5	70.1
157.45	RICE_3yr_163	4.5	5.4	10.0	21.6	53.0	35.1	61.6	17.0	34.2	56.5	41.2	42.0	32.6	62.2
157.97	RICE_3yr_164	10.6	4.0	16.6	4.8	37.7	43.4	70.8	9.5	32.0	40.8	55.8	56.0	65.9	139.6
158.54	RICE_3yr_165	1.7	4.3	17.8	21.7	35.8	17.6	32.4	36.0	45.9	29.1	38.8	27.2	87.1	72.0
159.13	RICE_3yr_166	4.7	5.5	12.0	17.4	49.9	41.1	47.6	33.4	41.6	48.3	63.5	47.8	128.7	159.8
159.67	RICE_3yr_167	6.3	4.9	12.8	18.4	46.1	47.5	48.6	47.5	26.9	51.6	43.8	53.7	68.6	60.7
160.24	RICE_3yr_168	10.2	4.6	17.8	28.1	61.9	49.7	63.9	58.6	57.0	60.8	49.6	61.0	245.0	63.7
160.79	RICE_3yr_169	14.4	4.2	31.7	15.2	20.8	29.3	59.6	23.1	39.4	31.9	34.8	34.1	41.4	130.2
161.32	RICE_3yr_170	7.0	3.5	24.9	21.6	56.0	53.9	32.5	49.8	50.9	35.9	22.1	50.0	49.6	102.5
161.87	RICE_3yr_171	6.6	2.3	13.9	13.7	26.3	30.3	13.7	15.8	30.4	28.4	17.7	39.3	46.3	27.4
162.44	RICE_3yr_172	4.7	5.2	38.1	30.0	41.6	28.7	44.7	47.6	48.6	17.1	40.5	42.3	40.7	41.9
162.97	RICE_3yr_173	7.3	6.5	14.0	15.0	37.4	62.1	49.7	77.5	66.5	46.3	69.0	34.3	82.9	91.4
163.54	RICE_3yr_174	10.2	4.4	18.5	13.4	43.6	45.3	25.8	36.9	18.0	26.8	54.6	65.3	82.1	60.5
164.06	RICE_3yr_175	8.9	4.5	7.8	22.0	43.7	25.7	24.1	26.5	21.7	36.6	47.1	26.5	41.1	81.4
164.62	RICE_3yr_176	6.5	4.4	10.0	16.0	32.9	37.9	56.5	25.7	19.1	34.8	28.7	60.3	68.4	90.6
165.14	RICE_3yr_177	13.6	11.8	26.7	34.3	60.6	70.5	36.6	35.4	61.8	53.6	81.7	62.3	55.2	84.0
165.68	RICE_3yr_178	6.2	5.7	16.3	15.8	50.5	33.6	44.5	61.5	51.4	55.9	86.7	83.0	81.5	91.1
166.26	RICE_3yr_179	7.6	2.4	15.9	21.3	25.1	62.0	51.8	35.6	42.3	66.8	53.9	104.9	73.4	113.1
166.80	RICE_3yr_180	6.7	3.8	6.6	38.2	43.8	52.4	41.6	20.4	70.0	49.1	50.6	37.1	108.8	82.4
167.35	RICE_3yr_181	15.4	7.8	21.5	16.6	72.5	76.2	104.6	59.3	67.3	66.4	90.1	59.9	99.3	77.5
167.88	RICE_3yr_182	15.1	4.0	11.0	38.8	29.3	86.8	40.1	32.7	62.8	60.3	95.8	84.9	73.6	76.2
168.39	RICE_3yr_183	13.1	6.1	23.7	27.3	73.7	30.8	54.1	49.5	47.7	36.0	43.4	98.3	79.4	87.8
168.94	RICE_3yr_184	6.9	8.1	18.8	19.0	42.9	31.6	50.8	36.2	58.8	61.3	99.0	80.2	36.9	159.7
169.45	RICE_3yr_185	7.4	2.5	18.3	22.8	50.0	27.0	42.6	59.2	23.9	38.8	58.0	88.2	90.8	118.0
170.02	RICE_3yr_186	3.5	2.9	16.2	19.8	44.6	62.8	36.9	84.0	19.2	37.5	26.3	61.0	76.6	113.6
170.55	RICE_3yr_187	7.6	4.7	16.4	25.8	20.3	56.3	32.4	55.7	57.5	42.2	65.9	75.3	66.7	64.7
171.07	RICE_3yr_188	7.3	3.3	11.3	21.0	55.9	69.0	54.1	52.2	47.8	44.5	74.4	75.2	79.3	109.5
171.59	RICE_3yr_189	9.1	4.4	21.1	19.2	39.9	41.2	35.5	44.8	36.0	27.8	64.6	66.4	102.7	63.7
172.10	RICE_3yr_190	5.4	3.4	26.3	27.4	49.5	52.5	31.1	59.4	47.0	45.8	52.6	100.6	113.2	97.8
172.63	RICE_3yr_191	7.5	1.7	14.7	21.7	67.1	22.4	47.4	35.5	39.7	52.6	69.3	80.0	100.2	89.2
173.16	RICE_3yr_192	13.8	5.3	17.5	35.2	55.1	54.1	25.2	74.3	66.1	52.7	125.1	29.2	80.4	81.2
173.66	RICE_3yr_193	6.4	3.1	20.0	20.8	69.4	55.2	39.3	52.2	58.1	48.6	64.2	59.8	98.6	72.2

174.18	RICE_3yr_194	5.3	6.9	9.6	6.8	39.0	39.4	36.5	22.0	39.9	56.1	78.6	25.8	32.8	31.8
174.71	RICE_3yr_195	4.4	6.3	8.2	34.7	47.1	51.4	58.7	26.4	51.7	51.2	72.5	81.4	57.8	82.0
175.23	RICE_3yr_196	12.2	4.6	7.4	19.3	49.2	44.9	23.4	44.6	9.5	50.1	62.9	80.4	75.0	122.7
175.76	RICE_3yr_197	7.3	5.2	16.7	16.3	59.5	47.6	36.4	53.5	29.4	54.1	82.9	81.6	96.4	128.7
176.26	RICE_3yr_198	6.6	5.6	14.8	24.2	34.4	43.4	45.8	57.4	35.0	72.0	68.7	68.8	64.3	118.0
176.79	RICE_3yr_199	11.3	3.9	18.6	15.4	39.1	50.9	44.5	33.1	18.8	40.9	34.3	61.3	45.6	68.9
177.32	RICE_3yr_200	8.7	52.6	19.2	28.0	46.6	46.4	34.1	43.3	72.7	44.3	76.0	93.3	117.6	86.9
197.84	RICE_3yr_241	2.3	2.5	2.8	8.2	14.0	20.4	30.2	47.0	27.5	17.7	32.8	43.5	44.3	48.6
198.27	RICE_3yr_242	1.6	5.5	3.9	11.0	16.0	30.0	31.9	26.6	17.8	35.0	30.4	30.1	32.6	52.5
198.78	RICE_3yr_243	1.0	9.2	2.0	13.7	17.6	21.2	15.8	40.3	45.8	28.2	25.5	27.4	70.1	64.8
199.25	RICE_3yr_244	2.4	4.1	5.9	10.6	18.8	39.1	31.6	23.5	35.4	19.0	29.5	20.6	69.7	58.8
199.69	RICE_3yr_245	1.4	5.4	4.4	9.8	11.8	15.3	24.3	28.6	31.7	29.2	21.1	20.1	39.2	38.4
200.15	RICE_3yr_246	1.6	4.1	3.3	8.4	8.5	21.5	24.9	25.4	26.3	6.9	16.1	31.7	22.6	32.9
200.63	RICE_3yr_247	1.8	4.4	2.8	12.1	11.6	9.8	28.1	35.1	35.5	31.5	14.5	27.2	30.8	24.5
201.08	RICE_3yr_248	1.3	2.7	3.9	11.2	10.6	25.7	23.4	27.5	17.5	12.1	22.0	35.0	54.3	7.3
201.56	RICE_3yr_249	3.2	7.8	4.0	6.8	9.4	28.0	23.5	17.5	38.3	14.8	20.8	29.5	33.3	32.7
201.99	RICE_3yr_250	1.4	9.5	7.0	15.6	8.4	35.7	18.5	20.3	24.9	46.5	12.8	24.8	53.4	31.9
202.45	RICE_3yr_251	0.7	3.8	3.4	11.1	13.1	26.8	28.5	26.3	19.9	17.1	25.7	62.4	46.5	32.3
202.89	RICE_3yr_252	1.2	3.9	2.2	4.3	11.1	18.5	32.0	23.3	20.2	16.7	17.2	32.2	56.5	24.3
203.34	RICE_3yr_253	1.8	4.1	3.2	6.9	7.4	33.0	43.5	25.2	15.8	20.1	8.4	18.3	43.8	29.4
203.80	RICE_3yr_254	2.7	9.7	3.2	4.9	12.0	28.1	22.8	34.0	12.9	35.2	14.4	31.0	37.9	53.4
204.29	RICE_3yr_255	2.6	4.9	4.8	11.7	9.7	20.5	14.7	14.1	24.6	27.8	29.2	13.0	25.5	65.3
204.70	RICE_3yr_256	2.5	7.7	4.6	6.2	16.2	24.6	24.1	29.6	29.8	34.9	29.2	31.3	48.1	43.3
205.19	RICE_3yr_257	3.1	4.2	4.3	9.9	14.3	45.0	22.4	25.7	47.1	44.4	18.7	30.0	40.4	58.3
205.62	RICE_3yr_258	1.7	2.9	3.9	11.5	7.9	19.9	43.6	13.0	19.5	25.6	15.8	27.2	37.0	35.9
206.07	RICE_3yr_259	2.6	3.8	2.5	6.3	10.1	38.8	11.5	17.8	28.5	21.2	29.4	16.9	36.7	27.9
206.50	RICE_3yr_260	1.8	3.9	4.7	3.5	9.6	10.1	22.1	49.9	10.4	33.7	23.5	26.5	55.9	25.8
206.95	RICE_3yr_261	7.9	15.5	11.0	20.9	17.7	32.9	20.8	33.3	29.5	24.1	41.2	14.9	45.4	47.7
207.41	RICE_3yr_262	0.9	6.7	2.7	5.0	14.4	29.9	17.1	16.8	24.0	32.5	24.2	24.8	41.0	25.0
207.85	RICE_3yr_263	2.6	6.1	3.6	7.5	17.6	23.5	25.1	31.3	26.4	19.1	44.1	17.6	37.8	30.0
208.30	RICE_3yr_264	1.9	6.7	4.1	14.2	14.5	15.5	29.8	30.3	16.1	23.4	19.9	24.4	47.1	43.5
208.72	RICE_3yr_265	2.3	3.3	3.3	10.3	9.9	14.4	14.7	30.0	13.1	27.1	25.3	23.1	39.6	39.6
209.19	RICE_3yr_266	2.5	6.1	4.7	13.8	18.5	22.7	21.4	42.5	21.6	16.6	21.7	37.1	31.4	22.9
209.61	RICE_3yr_267	2.1	4.3	3.1	11.6	7.5	16.1	28.6	34.9	29.0	34.6	29.5	49.3	35.0	40.1
210.04	RICE_3yr_268	1.9	3.6	2.3	11.2	21.7	51.6	22.3	35.2	26.7	25.4	29.6	51.4	45.5	51.1
210.49	RICE_3yr_269	1.3	5.3	2.6	6.2	17.0	33.4	23.9	37.8	20.4	31.4	26.1	32.6	50.8	29.7
210.93	RICE_3yr_270	1.6	3.2	2.9	8.4	5.9	20.3	26.3	22.9	32.2	30.7	29.2	31.6	61.5	66.1
211.38	RICE_3yr_271	1.5	5.2	2.8	11.8	6.5	15.8	28.7	58.6	32.2	39.7	13.4	39.4	44.0	34.5
211.80	RICE_3yr_272	2.5	4.3	3.8	8.8	9.1	16.1	22.1	16.7	26.9	27.4	27.7	16.3	69.1	47.4
212.25	RICE_3yr_273	1.5	5.0	3.6	7.0	10.1	21.7	21.8	30.5	20.6	33.5	36.3	48.8	44.2	28.9
212.67	RICE_3yr_274	3.2	5.5	3.0	8.6	15.9	22.4	23.9	30.5	34.0	27.4	23.6	30.5	53.1	32.7
213.08	RICE_3yr_275	1.8	5.2	3.7	6.9	14.7	16.0	31.1	22.9	25.3	17.7	20.8	19.7	58.9	41.4
213.51	RICE_3yr_276	1.3	5.5	4.2	5.7	20.9	22.5	21.3	49.3	38.1	22.7	33.5	28.9	43.3	29.2
213.94	RICE_3yr_277	1.4	6.2	3.7	7.9	13.9	39.9	38.0	28.2	23.7	39.0	18.0	16.3	53.9	34.8
214.39	RICE_3yr_278	2.6	7.7	4.9	10.8	18.9	34.9	21.8	33.2	11.4	18.5	20.6	44.6	45.0	35.7
214.78	RICE_3yr_279	3.4	3.7	2.7	12.3	11.2	21.1	44.6	33.8	27.7	23.6	25.8	39.5	59.8	35.4
215.23	RICE_3yr_280	1.3	2.7	5.2	13.0	8.1	41.0	20.1	31.5	31.1	39.0	13.8	16.7	31.2	62.9
215.66	RICE_3yr_281	1.6	3.0	3.2	11.0	4.3	17.7	12.8	10.3	24.1	31.1	16.0	23.2	17.8	49.6
216.07	RICE_3yr_282	1.8	3.6	2.9	9.7	17.4	29.3	41.9	21.7	32.6	24.4	19.1	30.8	55.8	44.5
216.50	RICE_3yr_283	0.4	3.6	6.0	7.8	6.1	30.5	25.2	23.6	20.8	22.9	17.3	24.8	58.2	47.7
216.92	RICE_3yr_284	3.0	7.4	6.8	8.8	3.9	24.1	32.9	16.3	32.8	37.4	29.3	42.1	56.8	61.2
217.32	RICE_3yr_285	1.7	5.1	5.5	11.5	12.4	24.4	18.3	19.4	18.7	28.6	21.7	34.1	38.5	61.6
217.77	RICE_3yr_286	1.4	8.2	2.8	7.4	8.7	32.7	29.3	25.4	43.6	10.4	7.1	52.8	78.5	21.5
218.17	RICE_3yr_287	1.5	4.5	2.4	14.0	14.4	38.6	36.7	23.6	26.0	17.7	38.4	19.6	48.2	37.3
218.61	RICE_3yr_288	1.4	1.0	4.2	7.7	8.2	8.8	4.5	10.0	8.8	14.8	9.9	14.1	23.5	21.9
219.00	RICE_3yr_289	3.6	5.2	6.6	6.0	11.7	33.7	16.0	42.5	16.1	20.8	15.8	42.2	46.4	44.0
219.43	RICE_3yr_290	0.9	4.9	2.8	6.1	6.0	22.5	37.9	30.7	31.9	33.7	14.8	32.5	37.8	24.2
219.85	RICE_3yr_291	4.6	6.8	5.2	5.1	11.1	29.3	31.1	22.3	21.7	13.8	11.1	14.5	51.0	20.2
220.28	RICE_3yr_292	1.9	8.4	6.5	15.3	10.1	29.1	25.5	16.6	26.6	32.0	19.9	33.2	63.6	39.7
220.66	RICE_3yr_293	1.9	7.4	4.5	8.2	8.5	19.4	36.7	16.3	27.5	28.9	34.5	26.0	46.5	33.3
221.11	RICE_3yr_294	1.3	5.5	2.6	8.4	15.1	30.4	17.5	25.8	17.3	30.4	19.7	55.4	45.5	46.3
221.52	RICE_3yr_295	2.2	4.4	1.8	13.2	7.3	38.4	13.8	15.8	20.0	23.0	32.0	18.1	31.7	44.3
221.91	RICE_3yr_296	1.7	6.7	2.5	9.5	7.4	18.6	27.0	21.6	11.5	13.3	15.7	18.8	59.0	47.3

222.33	RICE_3yr_297	1.9	6.3	5.0	10.6	3.9	21.6	20.7	9.4	12.0	15.4	28.3	23.9	26.4	52.8
222.71	RICE_3yr_298	2.4	5.4	2.2	10.4	11.9	23.2	19.1	21.3	15.9	14.0	11.6	10.6	34.1	27.3
223.16	RICE_3yr_299	1.4	1.8	3.2	6.5	11.9	33.3	33.4	30.1	19.0	30.6	33.7	25.6	30.4	26.8
223.54	RICE_3yr_300	4.5	3.2	3.4	9.7	11.6	36.1	13.6	16.7	19.5	24.5	22.4	30.8	46.2	47.4
223.96	RICE_3yr_301	0.9	5.5	2.2	9.5	9.3	18.6	16.6	14.1	18.7	10.2	17.5	20.3	20.8	33.4
224.35	RICE_3yr_302	3.3	8.3	5.5	6.6	9.6	18.4	16.4	26.3	9.0	23.7	17.6	32.9	46.2	17.6
224.76	RICE_3yr_303	1.1	5.4	1.8	6.7	15.5	27.6	21.4	30.3	29.1	35.9	30.7	35.2	56.9	13.0
225.14	RICE_3yr_304	2.0	4.0	2.7	13.9	6.7	20.0	21.4	20.7	26.8	11.7	12.4	25.3	40.7	35.5
225.54	RICE_3yr_305	1.6	2.4	3.9	11.6	16.4	38.0	37.1	18.8	26.4	16.7	22.3	41.8	81.4	44.9
225.96	RICE_3yr_306	1.5	5.6	6.0	5.4	16.4	33.8	24.0	53.1	30.0	20.5	17.8	29.8	80.1	32.0
226.42	RICE_3yr_307	1.1	5.5	3.4	6.7	9.3	21.6	17.8	13.9	27.2	35.0	17.9	37.7	67.9	32.4
226.79	RICE_3yr_308	1.1	6.9	4.6	9.7	11.7	18.8	29.4	39.1	22.9	23.5	31.8	30.9	34.0	46.2
227.22	RICE_3yr_309	2.9	3.6	2.7	2.1	6.8	11.4	19.1	18.6	22.6	13.9	10.2	29.2	31.5	49.0
227.58	RICE_3yr_310	3.5	6.0	3.2	5.8	8.9	37.3	23.5	16.1	39.1	9.6	22.3	25.9	60.7	39.0
228.00	RICE_3yr_311	1.4	6.7	4.2	6.4	8.3	25.8	34.2	26.7	14.4	29.8	16.6	22.2	61.1	41.8
228.41	RICE_3yr_312	2.6	9.3	6.0	6.2	10.7	35.6	31.8	21.8	15.4	28.1	24.4	21.9	43.6	30.4
228.77	RICE_3yr_313	3.1	8.8	1.8	11.5	13.0	24.5	21.5	27.7	20.1	23.4	28.3	29.4	30.9	34.2
229.17	RICE_3yr_314	2.8	6.6	4.6	10.1	4.5	34.1	24.6	22.9	23.7	15.6	22.5	24.1	51.5	19.8
229.57	RICE_3yr_315	5.8	13.5	8.5	16.5	13.9	20.7	23.0	17.3	23.8	10.4	26.3	33.7	45.4	35.2
229.97	RICE_3yr_316	2.5	6.2	6.0	7.4	15.6	14.8	25.6	4.8	10.9	16.9	37.0	22.8	51.1	21.7
230.37	RICE_3yr_317	2.4	14.8	9.8	10.4	13.3	20.1	28.5	14.3	28.1	27.0	20.3	36.9	45.7	59.8
230.76	RICE_3yr_318	1.2	3.6	5.9	5.1	13.6	16.6	14.7	26.1	16.5	13.5	15.5	28.0	43.6	24.6
231.12	RICE_3yr_319	4.1	6.3	2.8	8.2	13.9	19.7	22.1	20.0	15.4	18.4	16.5	25.4	38.9	31.7
231.53	RICE_3yr_320	1.6	3.5	4.9	10.7	17.1	21.7	19.1	28.3	25.4	27.0	28.3	17.0	41.0	26.7
231.90	RICE_3yr_321	0.8	7.9	4.3	13.6	8.2	16.9	29.0	22.0	26.5	20.0	25.1	27.8	51.4	42.1
232.33	RICE_3yr_322	2.8	2.8	4.6	3.8	6.4	10.8	30.1	18.6	24.6	11.6	13.7	20.3	71.1	38.3
232.71	RICE_3yr_323	2.2	3.0	2.1	5.1	5.2	12.4	29.2	27.8	15.7	21.8	34.9	31.5	46.9	47.8
233.07	RICE_3yr_324	1.3	8.2	4.2	7.7	11.9	38.6	25.1	30.3	20.1	27.2	25.3	20.7	65.5	36.4
233.45	RICE_3yr_325	1.1	7.1	2.9	5.3	11.2	10.2	37.1	35.3	15.8	17.4	11.4	21.9	40.3	22.7
233.85	RICE_3yr_326	2.6	7.2	7.0	16.3	15.7	19.9	20.1	33.9	23.7	22.8	30.1	27.3	12.3	39.7
234.25	RICE_3yr_327	3.4	11.0	7.5	9.5	10.9	18.2	21.8	10.0	12.4	20.8	29.8	30.9	36.7	48.0
234.63	RICE_3yr_328	0.6	6.2	5.9	13.3	8.3	30.4	21.0	26.0	22.2	16.8	28.7	21.5	46.1	30.6
235.02	RICE_3yr_329	3.8	5.0	5.8	14.1	12.9	46.1	14.8	14.0	29.1	28.4	16.8	21.7	56.4	53.9
235.36	RICE_3yr_330	2.5	4.6	6.3	9.9	9.0	21.0	33.0	16.9	26.8	21.3	19.3	20.0	26.1	42.2
235.75	RICE_3yr_331	1.5	5.9	5.3	3.9	13.9	24.3	35.3	32.3	46.1	37.1	28.8	46.4	35.2	54.8
236.14	RICE_3yr_332	1.8	5.0	3.2	8.4	12.3	25.2	24.2	34.4	38.4	34.3	25.1	20.8	66.7	57.9
236.49	RICE_3yr_333	1.8	9.2	6.8	9.8	11.5	26.5	31.3	15.5	14.7	22.6	13.7	30.2	49.3	21.1
236.88	RICE_3yr_334	2.9	2.3	3.5	2.6	5.1	18.3	17.8	13.7	13.8	8.4	13.9	14.6	12.2	24.8
237.29	RICE_3yr_335	2.8	9.6	11.9	8.7	26.1	31.6	22.1	36.8	15.3	23.2	25.7	39.5	42.2	30.2
237.64	RICE_3yr_336	3.1	8.6	3.4	5.0	8.6	25.6	25.8	9.6	31.4	23.3	28.4	16.7	45.2	56.1
238.03	RICE_3yr_337	2.0	3.9	4.4	11.6	10.9	24.8	13.7	18.9	31.0	29.9	24.2	25.2	34.1	44.7
238.39	RICE_3yr_338	1.1	6.5	3.8	15.9	7.0	22.1	28.5	31.5	19.1	30.9	35.2	39.0	75.7	43.9
238.78	RICE_3yr_339	2.3	4.6	3.6	8.9	15.0	18.2	21.9	30.7	19.5	35.3	27.0	23.9	40.8	41.3
239.15	RICE_3yr_340	2.1	13.3	8.6	9.4	10.6	19.2	24.0	31.5	29.9	27.0	17.4	20.4	17.9	23.1
239.51	RICE_3yr_341	2.7	9.9	4.5	12.3	19.0	16.1	27.1	35.7	38.8	33.9	25.0	45.6	55.7	60.5
239.86	RICE_3yr_342	1.7	5.8	3.2	5.2	7.7	25.1	16.5	23.2	13.6	27.8	28.3	28.5	38.1	79.5
240.23	RICE_3yr_343	1.6	6.0	8.9	15.2	18.4	24.3	36.7	18.8	26.6	29.5	26.0	33.8	76.8	35.2
240.60	RICE_3yr_344	2.0	1.5	4.7	15.9	17.6	28.2	37.1	37.3	24.4	33.3	26.3	24.3	31.9	63.8
240.96	RICE_3yr_345	2.3	9.2	5.8	6.6	10.8	20.2	13.1	10.6	17.8	11.0	17.1	10.7	21.4	31.3
241.37	RICE_3yr_346	1.2	9.6	4.6	15.3	18.4	49.1	32.1	22.3	19.8	22.4	16.6	29.3	68.8	50.7
241.69	RICE_3yr_347	1.5	4.2	8.4	14.3	10.5	43.8	33.3	24.6	30.2	32.9	10.3	18.5	79.4	40.0
242.07	RICE_3yr_348	3.3	7.4	8.4	6.4	18.6	29.0	39.6	41.2	17.6	34.7	34.2	22.4	49.4	42.3
242.46	RICE_3yr_349	1.7	8.2	10.6	16.3	21.6	24.2	20.1	26.4	25.9	25.9	12.6	33.1	29.7	23.1
242.79	RICE_3yr_350	2.0	14.4	13.7	15.2	10.2	34.1	31.2	24.0	20.7	14.0	42.4	30.6	18.1	34.1
243.15	RICE_3yr_351	4.1	6.1	3.3	14.6	14.9	26.4	25.8	33.7	40.5	14.5	25.2	43.2	74.1	51.4
243.54	RICE_3yr_352	1.2	9.8	7.9	4.1	12.4	29.2	25.9	19.8	15.1	25.2	30.6	38.5	42.3	58.6
243.89	RICE_3yr_353	2.1	6.5	6.6	9.6	9.1	24.5	29.3	37.9	27.3	15.0	23.4	30.2	27.6	57.0
244.24	RICE_3yr_354	1.2	5.8	4.7	9.2	8.5	22.9	28.4	21.4	15.3	18.4	21.1	15.9	17.8	46.3
244.63	RICE_3yr_355	1.1	8.8	6.7	11.6	6.4	45.5	18.0	19.9	16.9	13.5	17.1	19.7	28.1	30.1
245.00	RICE_3yr_356	2.5	11.1	11.3	10.0	21.0	38.1	28.5	20.6	33.2	24.5	28.7	15.2	83.7	34.0
245.35	RICE_3yr_357	2.2	8.6	4.1	7.7	14.6	25.6	31.3	14.3	26.4	19.9	29.6	28.7	72.5	48.6
245.68	RICE_3yr_358	1.3	4.9	5.6	9.1	9.0	14.5	23.7	22.4	23.3	21.9	31.6	56.0	36.4	40.5
246.07	RICE_3yr_359	2.1	2.9	3.9	12.3	24.2	25.1	21.6	32.3	44.1	16.9	22.5	28.5	54.8	45.8

246.40	RICE_3yr_360	2.3	5.4	6.2	7.7	5.5	26.9	19.5	22.8	18.4	21.4	15.0	14.8	13.5	39.5
246.78	RICE_3yr_361	1.8	2.9	2.2	5.9	9.2	17.4	19.1	14.8	22.9	20.2	17.3	16.5	15.6	10.3
247.14	RICE_3yr_362	2.9	5.9	3.2	8.4	12.4	31.0	25.5	26.3	17.6	30.8	24.3	21.7	21.6	30.3
247.48	RICE_3yr_363	3.7	4.2	3.7	8.5	11.8	16.0	11.3	13.0	19.1	14.3	22.8	27.7	32.4	31.5
247.85	RICE_3yr_364	1.8	4.9	4.3	7.7	12.9	31.8	30.9	33.4	27.1	23.8	17.9	24.1	38.6	34.4
248.17	RICE_3yr_365	2.4	4.3	3.4	6.3	9.5	16.8	15.9	26.8	20.2	21.8	12.8	16.2	39.2	17.5
248.54	RICE_3yr_366	1.3	2.8	3.3	7.1	11.0	28.3	15.5	21.6	10.3	19.0	22.7	25.6	35.8	18.2
248.88	RICE_3yr_367	1.2	4.6	4.1	4.8	12.6	9.3	23.9	11.9	33.7	18.3	11.2	22.8	19.8	26.1
249.25	RICE_3yr_368	3.0	8.9	4.9	11.9	10.1	42.9	30.1	39.4	37.2	49.6	22.5	50.4	44.8	28.2
249.59	RICE_3yr_369	1.6	4.3	6.7	12.9	16.4	30.1	19.9	19.5	25.7	18.9	21.3	32.5	33.5	31.9
249.97	RICE_3yr_370	1.6	4.8	3.6	12.5	10.3	17.6	15.6	19.3	22.4	5.8	17.4	28.1	13.6	24.1
250.28	RICE_3yr_371	10.9	17.8	3.5	10.9	3.7	13.5	7.7	13.3	10.5	11.9	10.1	6.6	18.2	11.9
250.65	RICE_3yr_372	6.6	8.4	3.6	7.6	8.3	45.0	32.3	36.6	19.2	24.7	26.0	23.7	63.4	73.6
250.97	RICE_3yr_373	3.8	3.9	5.5	8.5	17.7	25.4	29.5	26.9	30.4	16.2	20.5	43.3	34.0	75.2
251.34	RICE_3yr_374	3.7	8.1	5.7	15.8	16.1	35.3	44.4	39.4	18.9	19.5	15.5	34.8	47.6	48.4
251.66	RICE_3yr_375	3.1	7.5	5.9	11.9	14.4	31.2	16.2	35.9	25.5	18.8	23.8	34.9	33.2	57.1
252.03	RICE_3yr_376	0.5	6.7	6.8	12.3	9.5	24.4	20.1	28.2	24.1	16.6	17.3	30.0	29.4	64.4
252.38	RICE_3yr_377	1.7	6.4	2.3	8.2	6.8	37.5	39.3	25.6	15.5	35.8	14.0	19.5	43.8	30.8
252.76	RICE_3yr_378	1.6	2.2	3.2	7.8	13.6	33.6	13.8	7.2	38.3	19.2	23.4	49.8	35.7	29.7
253.08	RICE_3yr_379	3.1	3.6	5.4	11.1	16.5	24.1	22.0	32.4	49.9	32.9	25.5	55.3	48.8	41.5
253.44	RICE_3yr_380	1.6	5.5	5.2	19.9	15.8	25.0	44.2	37.6	21.3	23.0	33.9	17.2	57.7	47.6
253.77	RICE_3yr_381	3.9	7.3	3.2	16.4	12.1	26.7	30.8	30.1	24.7	17.1	20.7	47.8	66.1	24.0
254.14	RICE_3yr_382	3.3	3.1	3.2	4.0	17.8	18.8	18.6	21.4	23.0	14.3	29.1	21.5	23.4	24.3
254.46	RICE_3yr_383	0.8	3.1	3.0	4.1	11.0	20.8	28.7	18.7	25.4	20.5	17.1	26.0	58.6	30.5
254.80	RICE_3yr_384	2.6	7.0	4.9	9.4	11.7	32.8	30.3	28.1	15.9	33.2	32.6	23.4	28.5	36.3
255.13	RICE_3yr_385	3.1	3.5	2.8	10.2	15.6	28.1	46.3	25.8	16.5	35.5	20.5	26.7	46.0	61.9
255.47	RICE_3yr_386	3.3	2.6	7.7	11.0	17.0	30.9	47.3	31.8	16.8	36.8	25.5	56.3	48.0	29.1
255.80	RICE_3yr_387	3.6	4.8	3.8	10.9	7.5	17.9	11.8	31.9	20.1	26.8	28.2	33.4	55.5	37.4
256.13	RICE_3yr_388	3.3	6.9	7.5	9.1	7.1	37.9	20.6	26.1	11.3	13.3	10.1	34.8	33.0	45.6
256.49	RICE_3yr_389	2.9	5.9	6.1	8.0	10.1	19.7	26.6	17.8	19.6	19.7	20.4	35.3	53.7	39.2
256.80	RICE_3yr_390	2.0	3.1	1.4	13.0	7.2	13.2	26.1	23.0	15.9	32.8	26.7	41.0	64.2	24.0
257.15	RICE_3yr_391	1.4	3.4	1.9	4.1	4.5	15.0	21.2	21.6	26.8	12.4	10.4	23.2	34.3	23.4
257.49	RICE_3yr_392	3.6	13.9	5.3	4.0	7.5	21.4	27.6	23.5	34.2	36.5	28.3	31.1	40.0	53.5
257.80	RICE_3yr_393	2.1	6.9	6.6	5.6	6.1	27.9	23.8	26.0	19.1	36.6	24.5	31.7	52.6	42.8
258.14	RICE_3yr_394	1.5	5.2	4.0	8.9	4.7	32.9	13.2	13.5	27.2	31.1	19.7	40.4	27.7	39.3
258.47	RICE_3yr_395	2.4	4.9	3.4	7.2	14.2	32.1	34.9	21.6	9.4	35.1	19.1	24.6	22.3	44.4
258.81	RICE_3yr_396	4.2	6.8	4.4	6.2	10.5	22.5	24.6	15.3	24.3	32.8	24.8	15.1	64.8	28.8
259.14	RICE_3yr_397	4.1	7.4	3.1	10.0	14.2	29.0	23.9	24.6	31.4	25.5	27.0	21.9	98.4	33.2
259.47	RICE_3yr_398	1.8	5.5	4.5	5.4	6.5	17.4	40.8	22.6	18.1	31.7	14.0	28.2	26.8	35.9
259.82	RICE_3yr_399	2.0	8.3	5.5	14.3	7.2	17.6	34.8	22.1	30.0	31.4	17.8	37.6	63.8	39.5
260.13	RICE_3yr_400	1.5	2.1	2.7	10.2	10.5	31.8	21.4	20.8	29.3	21.9	25.1	40.8	32.0	63.7
260.44	RICE_3yr_401	1.4	5.4	3.8	10.8	12.8	20.7	17.9	21.5	22.2	16.9	10.0	23.1	16.7	36.4
260.76	RICE_3yr_402	2.8	6.5	5.4	8.9	12.1	19.7	37.6	14.5	25.1	31.1	18.2	21.2	48.9	46.4
261.14	RICE_3yr_403	2.2	6.3	3.3	6.1	10.5	18.4	17.6	14.5	18.4	21.6	15.0	13.1	23.2	40.3
261.47	RICE_3yr_404	3.2	4.5	7.5	11.1	15.0	32.8	18.5	26.1	32.4	21.7	27.7	25.9	34.8	29.2
261.81	RICE_3yr_405	2.1	3.7	1.5	5.6	7.2	26.7	29.2	15.1	23.3	13.6	12.7	11.8	27.5	25.9
262.14	RICE_3yr_406	2.8	8.8	2.4	10.1	10.0	16.0	19.1	36.0	7.4	27.6	13.8	37.1	63.8	43.2
262.46	RICE_3yr_407	2.1	3.4	3.5	12.8	10.7	19.5	27.2	23.7	34.4	22.2	24.9	29.5	36.6	25.3
262.77	RICE_3yr_408	1.6	3.9	3.1	8.0	8.4	23.8	32.8	11.3	23.4	16.0	23.3	28.9	44.4	51.4
263.09	RICE_3yr_409	3.0	3.8	7.2	17.1	14.3	36.2	34.9	12.8	25.5	27.4	19.3	24.9	33.1	49.2
263.42	RICE_3yr_410	2.7	3.4	2.2	3.4	11.6	25.5	35.1	12.8	27.1	36.3	23.5	22.0	55.7	30.2
263.75	RICE_3yr_411	1.5	4.3	2.4	10.2	12.3	11.9	38.8	28.7	18.0	9.8	15.0	25.1	55.3	30.4
264.08	RICE_3yr_412	4.0	7.4	4.9	10.3	10.4	23.6	30.0	34.7	12.6	32.0	19.4	33.4	67.7	48.7
264.41	RICE_3yr_413	2.1	5.2	4.6	11.7	10.3	24.6	22.0	31.8	31.5	25.4	12.0	36.1	51.9	39.3
264.75	RICE_3yr_414	1.2	4.7	2.4	9.2	7.8	20.5	28.0	31.6	22.3	16.9	21.4	16.5	61.2	56.4
265.04	RICE_3yr_415	3.9	4.2	5.5	6.6	5.6	26.0	16.8	28.1	5.8	38.3	23.2	40.3	20.0	40.0
265.34	RICE_3yr_416	1.9	8.0	5.4	11.2	7.8	14.2	18.6	23.1	30.1	27.6	31.4	33.6	42.9	48.5
265.66	RICE_3yr_417	1.7	5.3	4.8	7.1	12.4	36.7	23.1	9.3	34.6	35.2	26.9	43.5	46.8	38.2
265.98	RICE_3yr_418	1.2	4.4	3.2	16.8	13.0	23.0	18.9	30.5	17.5	16.9	9.5	12.9	30.5	24.1
266.30	RICE_3yr_419	1.8	4.8	1.9	6.9	14.0	38.5	14.5	26.8	28.4	30.2	19.1	10.6	27.4	26.9
266.58	RICE_3yr_420	2.5	2.1	2.6	6.6	8.9	19.8	28.6	20.8	20.9	20.4	20.9	34.3	20.6	33.4
266.91	RICE_3yr_421	1.3	2.5	2.0	4.8	4.4	13.7	11.1	16.7	18.2	16.2	14.1	22.2	28.8	16.1
267.21	RICE_3yr_422	3.8	4.4	3.7	15.0	8.4	23.9	29.0	24.1	32.6	17.2	24.4	25.3	74.5	50.3

267.54	RICE_3yr_423	2.7	7.3	4.6	16.6	8.4	24.1	32.6	31.4	17.8	18.0	28.4	17.3	65.3	38.9
267.84	RICE_3yr_424	3.2	3.5	3.2	14.1	4.9	16.1	18.2	23.8	19.4	9.3	12.9	19.9	31.0	40.3
268.19	RICE_3yr_425	1.7	5.1	5.6	14.6	10.8	30.5	16.9	41.8	47.4	29.1	8.0	37.6	36.5	46.7
268.47	RICE_3yr_426	0.9	5.9	2.7	9.7	9.0	30.3	27.7	24.9	11.6	27.2	12.8	32.2	19.0	31.0
268.79	RICE_3yr_427	3.7	5.2	4.4	7.5	6.7	24.1	24.6	38.1	20.6	22.7	19.0	18.8	68.6	17.9
269.09	RICE_3yr_428	1.1	3.2	3.0	10.2	7.1	34.3	17.2	25.2	33.9	16.1	15.9	30.3	52.5	18.8
269.40	RICE_3yr_429	1.9	4.4	2.7	12.0	15.7	24.4	24.8	37.9	23.4	21.4	21.4	36.0	66.4	29.9
269.72	RICE_3yr_430	3.1	3.1	3.4	9.9	8.7	24.8	30.1	32.1	20.8	24.8	18.7	14.2	59.2	32.2
270.05	RICE_3yr_431	1.1	6.1	2.5	5.2	8.8	21.8	30.6	28.4	13.0	29.0	29.0	26.1	33.3	34.1
270.34	RICE_3yr_432	2.9	4.9	5.7	9.1	9.9	16.1	24.7	23.9	22.1	23.2	23.0	33.3	52.4	43.3
270.65	RICE_3yr_433	2.9	5.7	5.8	8.3	13.3	17.0	26.6	9.8	20.1	11.1	6.2	21.1	32.1	55.1
270.96	RICE_3yr_434	3.0	4.1	5.4	6.8	9.9	17.9	38.0	29.5	29.7	30.3	22.5	16.8	77.0	49.2
271.27	RICE_3yr_435	1.0	5.8	4.0	9.1	3.7	25.3	21.9	20.4	24.0	32.4	24.3	21.5	42.9	22.5
271.56	RICE_3yr_436	1.8	4.5	6.7	11.8	20.0	31.2	23.1	29.2	31.2	22.1	9.9	35.4	68.7	57.1
271.86	RICE_3yr_437	2.1	6.4	4.3	7.0	15.7	50.1	18.8	24.0	16.2	39.7	14.6	35.6	50.7	61.1
272.20	RICE_3yr_438	2.1	2.6	3.9	11.6	10.0	19.5	26.0	46.2	34.8	34.9	27.4	31.5	42.2	17.7
272.47	RICE_3yr_439	2.4	4.0	6.2	6.7	5.2	22.2	19.8	4.7	23.0	14.3	36.4	33.1	60.0	38.2
272.82	RICE_3yr_440	1.8	6.0	5.1	6.0	10.5	13.4	14.3	41.1	19.8	17.1	19.9	25.2	33.7	37.7
273.10	RICE_3yr_441	0.9	3.0	5.4	8.8	5.2	28.6	33.7	19.0	30.5	37.6	10.7	24.4	17.7	50.0
273.39	RICE_3yr_442	2.2	6.4	4.4	8.9	11.1	21.4	30.6	24.0	40.2	26.0	25.5	35.2	51.7	32.0
273.70	RICE_3yr_443	2.4	10.1	8.8	6.9	10.5	14.6	13.0	17.3	33.3	21.9	17.6	26.1	50.3	45.7
274.01	RICE_3yr_444	1.4	8.7	7.7	11.6	12.0	32.7	17.4	47.0	21.6	33.5	20.8	12.7	16.0	16.9
274.30	RICE_3yr_445	2.4	9.2	10.2	16.1	10.2	40.6	18.0	32.1	25.4	40.1	23.9	41.6	74.4	50.0
274.62	RICE_3yr_446	1.9	4.5	2.8	5.8	10.9	29.0	24.2	29.3	20.0	13.8	14.8	21.4	66.3	42.5
274.88	RICE_3yr_447	3.5	7.4	6.3	6.4	7.9	23.2	27.4	22.8	17.2	16.1	12.1	43.0	23.3	26.5
275.19	RICE_3yr_448	2.5	5.0	5.4	7.1	10.0	39.7	32.8	32.5	28.9	16.1	20.9	35.9	26.9	21.0
275.51	RICE_3yr_449	2.7	6.4	1.7	7.3	9.3	24.2	25.4	9.8	17.8	19.8	25.4	38.0	41.5	36.4
275.82	RICE_3yr_450	1.5	2.5	1.9	3.0	5.2	7.0	6.0	5.2	7.1	6.8	9.2	6.8	6.4	13.6
276.12	RICE_3yr_451	1.8	2.5	3.3	4.9	8.1	17.5	8.6	18.4	5.8	23.9	13.5	23.9	42.5	14.2
276.40	RICE_3yr_452	1.4	5.4	2.9	9.2	11.6	27.4	19.2	20.4	17.4	22.0	24.3	22.7	34.3	26.3
276.72	RICE_3yr_453	4.4	5.9	5.7	4.7	4.9	16.5	15.2	10.1	20.6	14.8	13.6	8.7	30.0	27.9
276.98	RICE_3yr_454	4.0	6.9	4.0	8.5	8.4	11.9	34.9	8.0	16.4	9.7	14.8	25.7	21.7	20.6
277.28	RICE_3yr_455	2.4	6.7	2.8	11.4	22.0	24.7	32.4	24.2	17.5	11.9	25.6	38.2	28.4	24.1
277.60	RICE_3yr_456	2.1	4.6	4.6	3.4	12.8	18.7	31.9	29.8	20.1	19.8	13.8	23.0	42.3	29.5
277.89	RICE_3yr_457	2.0	4.3	3.6	7.7	5.7	33.3	23.8	24.2	23.2	12.0	13.0	36.4	50.5	31.9
278.20	RICE_3yr_458	3.1	6.4	4.2	6.8	13.7	19.9	7.6	27.7	14.5	14.0	23.1	44.8	56.6	37.1
278.48	RICE_3yr_459	4.0	8.4	5.8	4.9	10.0	13.4	17.6	24.9	21.6	28.4	23.6	19.0	41.0	36.8
278.76	RICE_3yr_460	2.2	14.9	6.8	16.8	5.5	14.6	20.3	30.6	22.0	22.3	18.2	22.4	71.7	34.6
279.06	RICE_3yr_461	2.3	3.3	1.9	5.6	8.9	12.1	25.9	15.2	10.7	15.9	14.0	26.3	34.0	31.4
279.35	RICE_3yr_462	2.2	3.9	2.9	3.9	5.2	26.8	22.6	18.9	20.1	16.9	12.5	22.9	33.4	19.6
279.63	RICE_3yr_463	2.2	9.1	6.8	11.2	13.1	24.3	38.9	21.9	17.0	16.9	15.7	28.0	34.3	31.4
279.91	RICE_3yr_464	1.1	5.1	4.8	3.6	16.1	14.4	32.3	18.8	12.1	23.5	15.8	28.4	26.4	14.6
280.21	RICE_3yr_465	3.5	5.5	4.1	15.0	11.8	22.9	22.0	28.0	42.4	33.3	27.9	53.2	49.1	61.9
280.51	RICE_3yr_466	3.7	6.5	5.6	6.2	9.4	35.8	37.7	12.5	31.8	15.7	20.2	25.5	38.1	84.2
280.77	RICE_3yr_467	2.2	6.2	4.4	8.0	11.5	31.9	21.4	20.1	28.6	15.7	24.6	18.5	56.3	30.5
281.06	RICE_3yr_468	2.6	6.2	7.9	160.2	11.3	11.2	26.8	27.5	24.5	17.3	11.0	21.7	26.1	50.6
281.35	RICE_3yr_469	2.4	7.0	6.8	9.6	12.4	21.1	21.8	18.4	28.8	16.4	29.1	23.0	31.5	37.5
281.65	RICE_3yr_470	0.8	10.1	4.1	8.4	11.4	20.5	57.8	33.0	17.8	19.0	40.8	39.7	50.5	43.3
281.91	RICE_3yr_471	2.3	4.3	3.2	7.6	12.7	28.0	29.3	22.3	22.5	25.1	18.5	27.1	63.2	40.9
282.23	RICE_3yr_472	15.4	93.3	93.4	90.7	88.3	81.6	49.6	88.3	77.9	86.6	82.9	100.4	91.0	90.0
282.48	RICE_3yr_473	3.0	9.0	8.3	14.0	8.5	27.0	18.5	26.1	25.4	20.2	21.8	19.1	60.9	49.9
282.79	RICE_3yr_474	2.0	4.2	5.2	6.5	5.9	28.1	20.7	21.0	35.3	17.9	29.6	26.8	28.3	41.7
283.05	RICE_3yr_475	2.4	5.0	4.0	8.1	10.6	24.9	32.0	21.9	21.1	19.7	14.7	34.2	43.6	35.6
283.32	RICE_3yr_476	3.3	5.7	6.8	7.1	17.2	20.3	11.7	17.7	18.2	23.5	25.9	26.1	34.4	27.3
283.64	RICE_3yr_477	3.2	6.4	5.6	7.0	19.1	14.8	37.7	35.6	44.9	17.3	35.2	24.8	79.1	55.1
283.89	RICE_3yr_478	3.4	5.5	6.0	10.2	11.8	19.4	20.7	16.3	19.0	17.6	18.6	23.4	17.0	43.7
284.18	RICE_3yr_479	2.8	4.7	5.1	7.3	14.7	17.1	30.1	19.5	31.1	19.5	22.1	41.6	43.2	33.7
284.45	RICE_3yr_480	3.1	5.3	3.7	9.7	9.8	17.6	16.6	32.8	21.7	40.7	24.1	21.7	73.7	27.0
284.74	RICE_3yr_481	1.9	5.2	6.2	5.8	13.2	22.7	40.6	19.2	31.3	38.0	12.3	16.8	51.4	38.1
285.02	RICE_3yr_482	1.2	3.0	3.4	10.9	6.9	22.9	25.1	43.0	34.8	19.3	15.1	19.4	54.7	41.7
285.32	RICE_3yr_483	2.2	4.7	2.9	9.5	6.2	25.2	28.3	36.0	23.8	42.5	23.7	36.7	41.4	50.7
285.57	RICE_3yr_484	4.0	4.8	3.2	9.1	10.4	20.1	20.6	21.0	15.4	24.2	15.0	24.2	21.7	40.2
285.86	RICE_3yr_485	1.8	8.1	3.5	4.3	9.2	16.8	20.6	17.5	32.9	21.9	26.4	41.6	47.1	16.0

286.15	RICE_3yr_486	1.6	3.5	3.9	11.3	9.7	36.4	34.7	26.9	27.0	19.2	29.8	23.1	28.2	39.2
286.41	RICE_3yr_487	1.8	3.8	5.3	13.0	13.8	21.6	33.6	14.7	20.0	25.3	20.5	25.5	44.2	41.6
286.68	RICE_3yr_488	2.3	6.2	3.7	6.2	19.4	28.4	26.6	22.4	33.0	22.5	32.8	18.3	37.3	57.9
286.99	RICE_3yr_489	2.8	1.1	2.4	11.3	5.8	21.1	27.5	18.8	27.7	24.3	22.3	28.0	57.0	28.2
287.28	RICE_3yr_490	2.6	5.4	2.6	9.9	3.6	25.1	21.2	32.0	13.7	15.2	14.7	23.7	44.3	30.1
287.55	RICE_3yr_491	1.6	2.7	4.5	8.9	9.5	22.8	30.3	28.1	42.9	12.7	20.0	36.5	37.8	27.3
287.80	RICE_3yr_492	2.9	5.9	4.6	8.9	10.9	24.1	30.2	19.5	16.4	28.1	19.3	40.2	48.2	22.8
288.05	RICE_3yr_493	3.0	5.9	4.7	12.3	5.3	24.1	11.4	20.2	25.3	11.2	13.2	20.3	44.5	35.3
288.36	RICE_3yr_494	2.1	6.2	7.1	16.3	12.0	18.9	32.2	15.1	25.9	20.8	24.9	21.8	42.9	33.1
288.63	RICE_3yr_495	2.4	3.5	3.8	10.6	11.5	19.0	28.5	23.3	27.7	34.2	17.9	29.6	54.7	49.4
288.90	RICE_3yr_496	2.5	3.7	1.8	7.1	12.0	20.5	22.9	24.0	44.3	25.8	10.7	37.6	50.6	25.3
289.19	RICE_3yr_497	1.3	3.3	4.6	10.0	12.9	17.1	46.6	23.9	32.1	15.0	10.9	22.9	44.1	38.1
289.35	RICE_3yr_498	1.4	9.2	8.7	11.0	10.0	37.8	22.1	19.7	14.3	32.6	14.9	29.9	18.7	28.3
289.70	RICE_3yr_499	1.5	9.4	4.0	7.2	4.4	22.7	26.7	14.3	26.3	24.8	26.8	42.3	35.3	26.4
289.98	RICE_3yr_500	3.2	5.8	4.6	9.8	15.2	30.4	16.4	17.1	24.9	27.8	30.4	28.8	28.4	49.4
290.25	RICE_3yr_501	1.7	3.9	4.7	10.5	10.0	23.9	25.1	32.7	25.7	26.3	18.9	28.6	52.8	41.8
290.51	RICE_3yr_502	2.4	2.3	4.9	9.9	9.3	20.7	24.4	30.3	23.8	19.3	21.2	26.1	35.7	46.4
290.78	RICE_3yr_503	2.9	4.9	7.2	10.0	14.6	20.0	20.7	21.1	30.5	15.6	22.6	51.0	42.0	33.1
291.06	RICE_3yr_504	2.8	4.9	3.6	9.3	11.8	15.6	15.2	23.9	16.8	29.5	12.5	14.8	54.0	17.3
291.32	RICE_3yr_505	1.1	3.8	4.7	11.5	10.6	27.3	19.4	17.2	47.0	20.3	21.4	29.5	46.3	26.1
291.57	RICE_3yr_506	2.8	5.4	3.0	4.9	6.7	22.8	30.9	28.3	29.0	17.1	26.0	29.9	45.8	45.0
291.86	RICE_3yr_507	3.6	28.8	6.8	16.6	16.0	26.9	50.4	37.3	33.2	28.4	15.1	16.4	48.0	46.5
292.12	RICE_3yr_508	2.1	9.1	8.0	5.2	18.2	21.2	23.8	13.0	22.8	25.2	24.8	35.2	39.9	61.6
292.38	RICE_3yr_509	3.6	12.0	12.9	10.8	21.1	10.7	19.0	35.6	38.0	21.9	12.4	25.4	25.9	59.4
292.63	RICE_3yr_510	2.0	7.3	5.6	16.4	8.2	19.2	18.7	18.3	29.7	34.4	26.1	43.7	41.8	55.0
292.94	RICE_3yr_511	2.5	5.0	3.7	10.2	6.4	26.7	26.5	27.2	25.5	14.9	18.7	21.2	47.3	52.5
293.17	RICE_3yr_512	3.1	9.1	9.3	12.1	12.7	19.2	23.8	24.0	23.1	18.2	14.4	18.3	29.1	34.7
293.42	RICE_3yr_513	2.7	4.5	4.8	15.8	9.8	25.0	39.6	27.4	35.6	37.3	11.6	32.4	54.8	52.7
293.71	RICE_3yr_514	2.3	6.6	4.3	6.9	19.7	27.9	24.0	16.4	12.1	12.0	24.6	35.3	68.2	46.5
293.97	RICE_3yr_515	2.0	6.2	5.7	10.9	11.8	25.4	18.1	22.5	33.5	31.0	19.1	22.5	31.3	33.6
294.25	RICE_3yr_516	2.5	6.5	7.1	20.1	18.1	54.8	29.4	30.4	31.7	28.5	19.5	44.5	93.8	34.6
294.50	RICE_3yr_517	2.2	6.0	6.8	11.7	11.6	27.4	29.8	19.2	32.7	20.4	22.5	60.7	51.6	64.5
294.76	RICE_3yr_518	2.0	5.0	4.8	11.1	11.6	28.0	27.3	37.7	32.9	23.6	20.8	20.0	59.1	48.1
295.02	RICE_3yr_519	2.3	6.7	4.5	10.0	5.7	23.9	35.1	10.3	28.5	27.1	22.8	35.7	65.5	18.8
295.29	RICE_3yr_520	3.0	5.6	5.1	8.5	6.0	23.5	30.4	23.6	11.3	21.0	13.5	27.0	52.8	39.7
295.57	RICE_3yr_521	3.3	2.1	3.4	3.3	6.1	25.5	35.7	28.9	12.4	30.5	14.8	33.2	65.8	42.2
295.85	RICE_3yr_522	4.1	8.1	7.8	11.6	6.3	26.8	25.6	26.9	32.0	20.0	27.9	27.4	40.7	38.8
296.07	RICE_3yr_523	2.1	10.4	4.4	12.5	16.3	8.4	32.2	17.6	24.2	9.9	24.5	37.7	32.3	44.9
296.33	RICE_3yr_524	2.2	6.3	6.0	9.6	11.9	41.6	20.7	35.4	23.7	28.2	15.1	25.5	28.5	12.1
296.59	RICE_3yr_525	3.4	12.8	6.1	13.8	21.2	22.2	41.9	25.5	19.5	36.9	17.9	39.1	58.4	56.7
296.85	RICE_3yr_526	3.8	9.2	3.0	5.6	7.4	16.2	27.9	18.6	28.9	28.6	28.8	20.7	36.4	58.5
297.11	RICE_3yr_527	2.6	6.3	3.8	14.1	8.2	34.3	21.6	25.9	18.0	18.5	31.9	13.7	36.1	55.5
297.40	RICE_3yr_528	1.7	6.9	2.8	6.3	17.6	22.5	40.3	19.1	30.6	27.9	23.9	24.8	76.9	29.1
297.61	RICE_3yr_529	1.9	2.2	4.4	10.9	14.6	19.3	39.7	35.7	16.3	32.2	25.4	21.5	30.9	41.1
297.89	RICE_3yr_530	2.2	5.2	4.5	12.6	10.3	24.9	36.3	29.2	36.2	22.6	19.4	30.8	52.2	28.2
298.12	RICE_3yr_531	1.2	3.9	2.0	6.6	9.2	20.2	17.6	21.0	32.0	17.7	48.4	17.6	49.5	55.7
298.40	RICE_3yr_532	4.4	7.4	2.8	9.4	11.2	10.0	41.3	16.5	27.7	37.9	15.2	29.9	56.6	43.1
298.61	RICE_3yr_533	2.7	3.1	6.2	9.4	14.5	29.5	37.1	18.6	24.6	21.2	14.8	11.5	48.8	46.6
298.92	RICE_3yr_534	4.2	5.3	2.4	10.8	5.5	11.4	31.4	17.9	27.5	22.5	20.4	37.0	47.9	33.8
299.14	RICE_3yr_535	2.0	4.9	4.7	8.6	12.5	10.0	24.4	24.4	47.7	19.3	28.4	30.8	57.2	38.4
299.43	RICE_3yr_536	3.4	4.0	3.9	8.0	16.7	35.2	25.9	33.2	21.3	27.9	26.4	24.0	34.5	54.6
299.67	RICE_3yr_537	1.8	3.9	3.9	7.9	6.3	24.7	24.4	17.0	21.1	28.9	12.3	11.9	36.4	41.8
299.90	RICE_3yr_538	2.4	3.8	3.9	8.8	10.0	18.2	29.2	32.7	34.1	14.5	9.5	30.5	38.7	31.3
300.17	RICE_3yr_539	2.2	4.0	3.0	9.2	10.8	36.0	33.5	40.5	27.6	23.1	15.5	25.6	25.4	57.4
300.44	RICE_3yr_540	1.0	7.0	4.7	10.0	17.4	10.4	9.0	26.6	16.8	11.7	5.1	18.2	28.2	45.5
300.69	RICE_3yr_541	1.9	6.8	2.4	6.2	10.3	15.4	24.3	25.0	12.5	18.1	27.5	22.1	41.3	39.2
300.95	RICE_3yr_542	15.4	15.3	11.8	15.2	14.1	19.9	10.0	19.3	27.9	23.8	25.6	31.6	44.3	27.6
301.19	RICE_3yr_543	2.1	5.6	7.3	8.5	9.4	28.5	33.3	24.7	23.8	21.4	20.9	33.4	54.5	34.8
301.40	RICE_3yr_544	2.8	7.8	5.3	13.4	10.3	30.9	38.7	30.2	30.9	18.1	36.7	49.3	30.1	29.5
301.65	RICE_3yr_545	3.4	7.8	6.9	5.9	13.4	29.5	27.5	22.0	36.5	35.7	30.5	14.2	34.7	28.3
301.94	RICE_3yr_546	1.8	10.0	8.7	3.9	10.9	14.7	25.3	17.1	18.4	21.2	22.3	25.4	72.2	46.3
302.17	RICE_3yr_547	4.1	7.1	8.0	11.4	13.7	27.8	29.9	39.8	17.1	24.8	14.4	21.6	29.4	36.8
302.42	RICE_3yr_548	3.3	6.0	2.5	9.6	11.3	19.2	14.7	19.5	36.3	14.3	34.4	26.6	35.4	50.0

302.66	RICE_3yr_549	2.3	6.3	3.1	7.2	8.7	23.6	10.3	29.0	17.0	20.9	24.1	24.9	49.5	19.5
302.93	RICE_3yr_550	1.9	4.7	1.1	5.4	3.0	18.2	24.9	15.1	7.5	9.9	10.3	24.1	26.9	8.2
303.20	RICE_3yr_551	44.5	33.5	62.4	38.6	39.6	113.9	86.2	48.9	63.1	50.5	73.2	96.5	105.4	92.7
303.48	RICE_3yr_552	3.8	3.2	2.7	3.8	8.7	10.9	6.0	16.8	9.8	14.6	13.0	19.3	21.3	14.2
303.67	RICE_3yr_553	1.6	3.1	2.2	3.8	5.9	10.3	19.3	11.0	12.6	9.5	14.6	15.4	18.7	25.8
303.90	RICE_3yr_554	2.3	5.0	2.8	8.8	7.6	30.2	15.3	16.0	16.5	13.2	17.2	24.1	20.3	19.6
304.16	RICE_3yr_555	1.9	4.7	2.6	4.6	13.9	19.0	9.0	22.4	20.8	22.5	16.7	19.0	28.8	52.2
304.42	RICE_3yr_556	2.9	2.7	3.4	9.6	8.9	24.0	33.9	25.8	17.9	9.9	15.2	27.0	73.5	28.6
304.65	RICE_3yr_557	3.3	4.2	4.3	9.3	14.8	23.5	11.9	14.6	21.4	30.5	17.8	19.0	28.8	23.9
304.89	RICE_3yr_558	3.5	6.9	5.5	8.9	13.9	12.1	27.9	15.9	23.1	24.5	24.3	27.8	21.7	14.2
305.16	RICE_3yr_559	2.0	6.4	8.4	12.2	13.4	22.1	17.6	17.1	21.7	11.9	22.3	39.3	20.4	29.5
305.40	RICE_3yr_560	1.5	6.9	4.5	9.4	2.6	32.9	19.3	23.7	22.1	31.4	24.7	35.2	36.2	32.9
305.62	RICE_3yr_561	1.6	4.9	4.2	6.2	7.0	27.1	26.9	9.2	29.9	16.6	20.4	21.9	44.6	26.1
305.85	RICE_3yr_562	3.5	5.9	3.2	4.5	7.7	24.5	31.5	15.2	16.5	19.2	10.2	25.8	38.4	13.5
306.13	RICE_3yr_563	2.0	6.0	2.5	8.8	12.3	30.1	20.5	24.8	22.9	19.6	18.6	31.0	41.9	49.8
306.37	RICE_3yr_564	2.0	3.0	4.2	10.5	9.5	23.7	31.3	25.9	34.4	17.1	24.1	40.2	26.6	24.2
306.61	RICE_3yr_565	4.8	4.0	8.7	7.6	14.4	16.4	40.2	21.1	27.0	32.6	36.3	27.2	29.2	36.1
306.83	RICE_3yr_566	2.0	5.5	7.4	6.4	9.7	34.6	19.6	8.3	28.6	16.7	15.6	35.3	20.5	39.2
307.10	RICE_3yr_567	2.3	4.2	3.0	6.7	14.5	26.5	37.0	24.0	27.1	17.8	29.9	57.7	52.2	45.1
307.31	RICE_3yr_568	2.3	4.2	4.2	5.9	9.1	24.2	33.3	19.4	22.7	37.7	23.9	26.9	61.5	56.4
307.56	RICE_3yr_569	4.5	5.8	3.8	8.2	9.0	22.6	13.0	23.9	19.0	23.3	25.8	44.6	22.5	54.4
307.79	RICE_3yr_570	1.4	4.1	3.2	3.9	6.0	5.8	5.8	9.4	12.8	15.0	14.6	19.3	41.4	31.2
308.04	RICE_3yr_571	1.4	3.5	2.9	10.4	8.4	33.3	48.3	37.0	32.7	34.7	24.6	28.9	38.5	38.1
308.25	RICE_3yr_572	2.2	3.1	3.1	5.4	8.9	19.6	23.2	36.0	17.9	21.7	25.1	41.3	61.7	49.7
308.50	RICE_3yr_573	2.8	6.6	6.1	10.7	4.8	16.8	32.5	25.3	29.7	21.5	32.7	18.9	51.6	31.1
308.75	RICE_3yr_574	1.2	9.1	9.0	11.4	12.6	39.0	34.8	35.5	29.9	39.0	46.0	24.8	31.8	27.0
308.98	RICE_3yr_575	2.3	4.7	8.7	9.1	7.2	36.7	26.2	25.2	29.0	42.8	27.2	33.2	42.2	52.0
309.19	RICE_3yr_576	1.8	5.7	5.1	8.0	20.4	33.2	10.4	29.5	32.0	15.7	18.7	62.7	57.2	41.3
309.44	RICE_3yr_577	1.1	3.7	3.2	8.7	9.5	28.5	18.6	31.8	14.6	36.0	28.7	34.7	57.3	29.9
309.69	RICE_3yr_578	11.1	8.2	6.5	8.0	5.1	27.1	36.4	25.9	23.8	26.7	19.1	36.2	62.5	31.4
309.93	RICE_3yr_579	1.1	4.9	4.2	7.3	24.0	24.2	32.5	10.7	14.7	11.6	22.9	30.6	29.9	54.6
310.15	RICE_3yr_580	1.6	7.1	6.0	9.2	13.4	27.2	30.4	66.5	46.9	28.1	20.7	33.3	68.8	28.8
310.36	RICE_3yr_581	2.6	5.1	4.8	12.5	13.6	18.9	27.4	19.4	23.5	22.9	11.6	37.0	68.9	28.8
310.60	RICE_3yr_582	1.5	9.2	7.2	13.5	7.7	17.1	17.1	31.7	24.3	20.2	21.8	24.0	48.4	46.2
310.84	RICE_3yr_583	2.2	5.0	4.1	4.7	16.7	23.6	32.1	26.4	26.0	17.1	14.3	27.1	23.7	41.2
311.09	RICE_3yr_584	1.8	5.7	3.4	8.8	10.7	17.6	42.6	31.6	22.8	14.2	25.4	33.5	34.6	52.7
311.29	RICE_3yr_585	2.3	6.6	4.3	7.8	14.4	42.0	48.9	17.3	28.1	42.9	37.5	15.7	83.6	34.1
311.55	RICE_3yr_586	2.1	5.0	2.8	9.0	9.7	13.5	5.8	23.3	29.1	24.7	13.3	31.6	50.8	45.8
311.79	RICE_3yr_587	2.5	3.8	2.8	7.9	5.8	19.4	23.3	18.2	39.1	14.3	20.5	37.4	38.5	11.7
312.02	RICE_3yr_588	3.9	7.7	4.5	7.1	14.1	29.1	16.0	15.4	28.3	35.5	21.5	45.9	54.3	17.0
312.26	RICE_3yr_589	1.0	4.3	3.4	10.3	12.8	35.3	33.7	33.9	18.0	27.0	24.1	44.9	27.5	30.8
312.45	RICE_3yr_590	2.2	3.9	3.6	9.1	12.3	23.1	23.4	38.4	25.9	20.3	22.4	45.8	64.2	28.6
312.68	RICE_3yr_591	1.7	3.8	3.9	12.6	10.1	41.7	34.8	24.4	8.7	40.2	33.1	17.4	93.2	41.8
312.96	RICE_3yr_592	3.3	10.2	2.6	18.1	21.6	28.6	36.5	42.1	33.1	28.2	27.0	27.7	45.6	74.7
313.15	RICE_3yr_593	1.3	2.3	1.9	6.2	4.1	16.3	20.2	21.4	10.4	20.9	17.9	31.4	32.0	18.8
313.41	RICE_3yr_594	2.3	4.6	2.2	6.4	1.5	19.4	11.6	20.6	10.3	9.4	20.4	23.0	16.9	9.7
313.60	RICE_3yr_595	0.9	3.2	4.2	8.9	14.0	13.6	36.3	33.9	32.6	37.9	13.0	22.5	71.8	40.9
313.82	RICE_3yr_596	1.1	4.1	2.3	8.0	15.6	15.4	19.0	34.4	12.6	28.3	204.2	39.0	29.3	26.4
314.09	RICE_3yr_597	0.9	5.5	2.9	13.9	9.5	45.1	29.9	26.1	39.9	15.7	27.7	16.2	23.2	72.9
314.31	RICE_3yr_598	2.1	12.0	4.6	10.7	8.1	26.8	21.8	22.7	17.2	42.0	18.8	24.2	43.7	32.0
314.51	RICE_3yr_599	1.6	8.4	5.2	17.1	13.2	49.1	32.8	41.2	28.3	18.1	28.3	42.1	40.3	42.2
314.74	RICE_3yr_600	3.9	6.4	4.4	11.9	16.9	20.4	15.1	23.5	27.4	32.4	23.9	37.2	48.8	28.3
314.97	RICE_3yr_601	2.4	5.4	6.1	7.7	8.9	7.4	16.9	12.9	31.8	20.3	26.8	20.2	70.4	53.4
315.18	RICE_3yr_602	2.4	6.9	7.2	6.9	13.4	39.3	35.7	25.7	26.5	21.2	15.0	28.0	41.6	51.6
315.43	RICE_3yr_603	7.0	8.2	9.0	10.4	10.9	18.1	15.7	49.0	21.6	20.2	40.6	30.1	40.7	33.5
315.63	RICE_3yr_604	2.9	3.8	5.5	11.8	23.0	67.8	37.0	43.8	35.6	41.7	41.0	33.4	41.2	39.6
315.85	RICE_3yr_605	1.8	6.0	3.3	15.4	17.5	30.0	18.1	32.1	16.7	38.2	21.7	31.2	87.0	63.1
316.07	RICE_3yr_606	3.9	14.6	4.6	15.6	25.7	21.5	32.1	32.6	20.9	31.3	24.7	72.0	64.5	55.3
316.29	RICE_3yr_607	2.7	8.1	7.0	7.9	8.2	17.9	37.7	49.3	23.0	38.5	32.8	30.1	78.2	59.6
316.56	RICE_3yr_608	4.3	5.1	3.5	5.9	12.9	17.5	18.2	20.7	51.1	16.2	17.7	28.6	49.8	57.6
316.75	RICE_3yr_609	2.1	9.6	4.0	7.9	11.1	27.8	37.6	16.8	26.4	14.8	18.7	37.8	54.5	34.0
316.96	RICE_3yr_610	2.1	9.5	7.3	9.5	12.6	13.0	18.1	22.0	12.8	28.1	22.8	29.8	41.8	65.2
317.22	RICE_3yr_611	3.5	7.1	5.8	12.1	9.2	9.7	22.1	21.5	48.0	20.0	29.4	20.6	46.1	44.7

317.43	RICE_3yr_612	5.2	5.3	2.1	3.8	11.8	16.3	29.8	20.9	38.8	44.1	16.6	19.1	48.9	27.7
317.67	RICE_3yr_613	0.8	9.8	5.5	12.3	18.7	15.8	32.7	24.5	30.2	39.5	45.1	42.8	46.4	46.8
317.88	RICE_3yr_614	1.6	3.0	3.5	7.7	19.3	21.9	35.5	25.7	24.0	25.0	18.9	27.1	33.4	36.3
318.13	RICE_3yr_615	1.7	6.3	3.3	7.6	11.4	32.2	13.8	50.6	29.5	36.5	45.8	44.2	48.6	66.8
318.33	RICE_3yr_616	2.5	5.6	7.4	10.0	6.0	21.8	27.1	41.7	29.0	38.9	34.7	36.6	88.8	42.3
318.57	RICE_3yr_617	1.8	5.8	2.8	8.2	12.2	31.8	36.5	35.9	23.5	34.3	27.0	25.5	63.2	60.8
318.75	RICE_3yr_618	1.2	2.1	1.5	8.2	14.7	22.5	43.3	32.6	24.0	30.4	15.6	20.5	53.8	29.4
319.02	RICE_3yr_619	2.3	6.2	2.7	11.8	20.6	24.3	10.1	39.9	28.7	30.9	30.7	46.4	60.7	48.5
319.23	RICE_3yr_620	2.2	4.8	4.8	8.1	9.7	14.9	25.6	17.1	13.4	28.9	27.4	30.8	74.5	44.7